REPORT SERIES IN AEROSOL SCIENCE

N:o 107 (2010)

Proceedings of 2009 EUCAARI Annual Meeting Stockholm 17.–20.11.2009

Editors: Hanna K. Lappalainen, Ari Asmi, Tuomo Nieminen, and Markku Kulmala

ISSN 0784-3496
ISBN 978-952-5822-13-7 (PDF)
http://www.atm.helsinki.fi/FAAR/

CONTENTS

3. Climate and Air Quality Effects Element

5. Impacts Element

EUCAARI SCIENCE ABSTRACTS

EUCAARI progress in third year (2009) – A short overview

Ari Asmi[1], Markku Kulmala[1], Hanna Lappalainen[1] and the EUCAARI team[2]

[1]Division of Atmospheric Sciences, University of Helsinki, Helsinki, Finland

[2]http://www.atm.helsinki.fi/eucaari

Keywords: EUCAARI, integration, overview

INTRODUCTION

European Integrated Project on Aerosol, Cloud, Climate and Air Quality Interactions (EUCAARI) is a project of the 6th Framework programme of the European Commission. The project has been active from beginning of 2007 and it will continue until end of 2010. The objectives of EUCAARI are

(I) Reduction of the current uncertainty of the impact of aerosol particles on climate by 50% and quantification of the relationship between anthropogenic aerosol particles and regional air quality, and

(II) Quantification of the side effects of European air quality directives on global and regional climate**,** and provide tools for future quantifications for different stakeholders.

The project approach for achieving these goals has been using wide array of methods from molecular simulations to global circulation models, from laboratory experiments of nucleation to world-spanning field experiment campaigns (Kulmala et al, 2009a and 2009b). The overall philosophy of the project has been using all the available tools of the atmospheric sciences and to facilitate successful communication and co-operation between the communities of scientists in these fields. The EUCAARI consortium believes that only by combining the excellence of different European atmospheric sciences, the complex interactions between atmospheric aerosols, clouds, climate and air quality can be investigated.

METHODS AND RESULTS

As the year 2008 was the year of measurement for EUCAARI, the year 2009 concentrated on the data analysis, publication and on combining measurements with large scale modelling efforts. The results of the EUCAARI studies have started to be disseminated to end-users and the first parts of the project have been successfully completed. The work on the final results, to be disseminated at the end of the project, has started. Figure 1 summarizes some of the main aspects work done in 2009 in EUCAARI.

The goals of EUCAARI can only be achieved with large amount of new experimental knowledge. The project includes large contributions on European and developing countries long-term atmospheric monitoring, several shorter campaign-type experiments, laboratory studies and special aircraft-based measurement campaigns. Although the main year of measurement was 2008, many of the measurements were continued in 2009. More importantly, the analysis and results of the field and laboratory experiments have started to come available to the EUCAARI community.

The EUCAARI European network of measurements is based on another EU-funded project, EUSAAR. The network of stations had significant extra equipment installed (e.g. ion or neutral cluster measurements using newly developed instrumentation) and the data delivery was accelerated for the use in EUCAARI uses. The continuing measurements provide excellent framework and background for the more specialized campaigns and they provide necessary long-term data for statistical and data-mining studies (Costabile et al, 2009, Hussein et al, 2009, Lappalainen et al, 2009, Mazon et al, 2009). The main achievement of the field experiments in 2009 has been the inclusion of the EUCAARI field experiment

data from Intensive Observational Period and long term measurements to the EBAS database. This data provides the most comprehensive dataset of quality-controlled, calibrated and reliable sub-micron aerosol data in Europe. The dataset includes many additional measurements aside from traditional size-distribution information, such as information of particle composition, hygroscopicity and information on the concentrations of sub 3 nanometre clusters (Asmi et al, 2009, Lehtipalo et al, 2009, Manninen et al 2009). This dataset provides excellent tool for use in comparison with different modelling studies. The results are further augmented by extensive analysis of aerosol sources using a combination of special measurements of organic tracers, C_{14} analysis and aerosol and precursor composition (Petäjä et al, 2009, Riipinen et al, 2009).

The EUCAARI field experiments were not limited to the long-term measurements. Several special campaigns were done and the results of these experiments were also included in the database. The special campaigns in Cabauw (the main IOP campaign in Netherlands), Mace Head (Ireland), San Pietro Capofiume (Italy), K-Puzta (Hungary), and Finokalia (Greece) provided very important new information in a set of detailed experiments (Bougiatioti et al, 2009, Järvi et al, 2009,). The EUCAARI IOP also included set of comprehensive aircraft measurements. The EUCAARI-LONGREX was a very successful study of European aerosol characterization and aging experiment. EUCAARI-IMPACT was a combined multiple-aircraft and field station (Cabauw) study of aerosol-cloud interactions together with detailed Large Eddy Simulations (Schaap et al, 2009). The results of both of these studies have been under intense evaluation during 2009 and the data has been made available to the EUCAARI community.

The European aerosol is well characterized in the EUCAARI studies, but aerosol-climate-AQ interactions are not limited to Europe. The EUCAARI consortium has augmented the European stations by building new stations in four developing countries sites to provide more global approach, and to gain knowledge of long-term behaviour of atmospheric processes. Due to their rapid development, China, India, South-Africa, and Brazil are main contributors to air pollution in the corresponding regions. Good quality long-term data sets of physical, chemical, and optical characteristics are rare, and these are urgently needed to underpin policy making. Intensive field studies by the international community brought some insights, but not enough to understand quantitatively the impact on regional climate and air quality. Four measurement stations were established outside Europe in beginning of 2008. To reach the goal of representative measurements, sampling sites for regionally aerosol measurements were be established in cooperation with selected local partners. The total measurement period for the in-situ measurements was planned to be two years, while for the filter sampling and lidar measurements is foreseen only for a period of one year. The data from 2008 was not completely continuous due several delays with site building and operation. Even not complete for the 2008, the data from 2009 has been much more successful (e.g. Meier et al, 2009). The data from these experiments were also made available to the modelling community via EUCAARI data archive.

The field experiments provide the main part of the experimental data in the project in terms of volume. However, controlled studies of different processes are a key aspect of any scientific study. The results of such laboratory studies can be more directly used in different process models and thus they form one of the cornerstones of process-based knowledge which can then be used to understand the field experiments and generalize them to larger scale solutions. The laboratory work of aerosol formation (nucleation) and on the secondary organic aerosol processes (SOA) has been doing well. Homogeneous nucleation experiments were done, and as a highlight, new laboratory experiments resolved the existing discrepancies between earlier H_2SO_4–H_2O measurements, as well as the differences in nucleation rates between laboratory measurement and atmospheric observations. The laboratory studies of secondary organic aerosol formation identified marker compounds and the will make possible to determine the photochemical age (i.e. the “age spectrum”) of biogenic SOA (Mentel et al, 2009). As one of the main results, the studies showed that isoprene emissions could actually inhibit new particle formation (Kiendler-Scharr et al, 2009). Furthermore, studies of aerosol-cloud interactions and the ability of different particles to act as either cloud-condensation nuclei or ice-cloud nuclei have been investigated in the laboratory, in the field and on modelling basis (Reutter et al, 2009, Sandu et al, 2009, Welti et al,

2009). The results of the laboratory experiments of such systems have then been used together with field experiments.

The laboratory and field experiments are very important, but without comprehensive modelling effort to combine and generalize them the synthesis of such studies is hard to make. The modelling and theoretical work on aerosol nucleation and the first steps of growth of these particles were done in 2009, providing physical and chemical backbone for the analysis and use of the new experimental results (Hienola et al, 2009, Kurtén et al, 2009, Sihto et al, 2009). Simulations using master chemical mechanism made possible to find out generic model compounds of organics and furthermore generalize the organic species studies for the modelling in larger scale models. The process modelling was also integral for many field experiment work packages, providing immediate feedback for the experimentalists.

The emission database work of EUCAARI has been partly successful. The main results have been the improved work on the European organic aerosol emission inventory, which has been delivered to the partners in 2009. The work on the number emission inventory has been intense (e.g. Birmili et al, 2009), but the delivery of the number emission inventory was problematical, as the information on different source categories are often inconsistent with each other. The work on this critical task is being done in co-operation with modelling community to produce the emission inventory directly to internal project users. The experiments and modelling efforts were also augmented by new satellite products, which provided partners possibility to use larger scale experimental remote-sensing information in basis of their analysis of experimental or modelled information.

The large scale modelling work in EUCAARI has been very active in 2009. The first simulations using new parameterizations have been made and compared to the field experiments. The database access for the modellers have started to be used and as such the main tasks have been concentrated on the availability of the experimental results and parameterizations to the modelling community. Large scale models can not usually directly use the new findings of the process models, thus several layers of parameterization are needed. Most of these parameterizations have been directly made in EUCAARI workpackages related to the processes themselves, but some specific processes, such as aerosol-cloud interaction, boundary layer meteorology and microphysics parameterizations have been specifically done in a separate parameterization work package, which has been very active in the 2009 year.

Difference between anthropogenic and biogenic aerosol formation is a complex issue, which is impossible to study without good combination of experimental, theoretical and modelling tools. The studies of these processes for the global and regional particle number studies have successfully used all these methods and are a good showcase of the EUCAARI integration in practise. The combination of detailed CTMs together with aircraft and field data has shown the importance of this kind of projects to achieve scientific excellence in this field (Manktelow et al, 2009). Similar studies have then already been combined with CCN studies and are then implemented also in climate community. The improvements in emission inventories and the effect of new parameterizations to the air quality in European scale have been successfully implemented and tested against the field experiments. Climate models have been using some of the products developed in EUCAARI and other sources during 2009. The inclusion of biogenic organics, secondary organics modules and new nucleation parameterizations produce excellent opportunities to study feedbacks from the climate change to the global aerosol properties and thus back to the climate system (e.g. Makkonen et al, 2009).. The use of new modules in the Earth system models will provide in the future even more information on the aerosol-climate interactions. The work on the evaluation of the climate and CTM models has started in 2009 and will continue in 2010 in co-operation with AEROCOM initiative.

An integrated project like EUCAARI requires a database that integrates all data collected within the project as well as relevant data from other sources. It furthermore requires that the data are made accessible to the project partners via a common platform. By month 30 of the project 33 users have signed the data protocol. All data available (incl. aircraft data and data from other platforms) are stored at a common area located at the NADIR data centre at NILU. The EBAS interface has dynamic web pages

that allows searching for aerosol data from any ground based instrument or location. Currently 54 datasets with 2008 data (e.g. AMS and H-TDMA data) from EUSAAR stations are stored in EBAS.

The integration activities of the project has been concentrated on the data delivery and advertisement inside the consortium. Speedy delivery of the data and maintaining the communication networks has been of utmost importance to the project. The project has also been active disseminating the results of the project into different end-user groups and this work will be one of the main goals of the project Steering Committee in the 2010.

CONCLUSIONS

The EUCAARI has been very active in 2009. The main aspects of the work has been on the analysis of experimental work, preparation of data for further use and on starting up the large scale modelling work. The integration activities have been successful this far, but care must be taken to make sure that the EUCAARI results are well disseminated both inside the consortium and to the end-user communities.

ACKNOWLEDGEMENTS

This work was partly funded by the Sixth Framework Programme of the European Commission project EUCAARI (contract 36833).

REFERENCES

Asmi E., M. Sipilä, H. E. Manninen, J. Vanhanen, K. Lehtipalo, S. Gagné, K. Neitola, A. Mirme, S. Mirme, E. Tamm, J. Uin, K. Komsaare, M. Attoui, and M. Kulmala. Results of the first air ion spectrometer calibration and intercomparison workshop Atmos. Chem. Phys., 9, 141-154, 2009

Birmili W., B. Alaviippola, D. Hinneburg, O. Knoth, T. Tuch, J. Borken-Kleefeld, and A. Schacht Dispersion of traffic-related exhaust particles near the Berlin urban motorway – estimation of fleet emission factors. Atmos. Chem. Phys., 9, 2355-2374, 2009

Bougiatioti A. , C. Fountoukis, N. Kalivitis, S. N. Pandis, A. Nenes, and N. Mihalopoulos. Cloud condensation nuclei measurements in the marine boundary layer of the Eastern Mediterranean: CCN closure and droplet growth kinetics. Atmos. Chem. Phys., 9, 7053-7066, 2009

Costabile F. , W. Birmili, S. Klose, T. Tuch, B. Wehner, A. Wiedensohler, U. Franck, K. König, and A. Sonntag. Spatio-temporal variability and principal components of the particle number size distribution in an urban atmosphere. Atmos. Chem. Phys., 9, 3163-3195, 2009

Hienola A. I. , H. Vehkamäki, I. Riipinen, and M. Kulmala Homogeneous vs. heterogeneous nucleation in water-dicarboxylic acid systems. Atmos. Chem. Phys., 9, 1873-1881, 2009

Hussein T. , H. Junninen, P. Tunved, A. Kristensson, M. Dal Maso, I. Riipinen, P. P. Aalto, H.-C. Hansson, E. Swietlicki, and M. Kulmala. Time span and spatial scale of regional new particle formation events over Finland and Southern Sweden. Atmos. Chem. Phys., 9, 4699-4716, 2009

Järvi L, Ü. Rannik, I. Mammarella, A. Sogachev, P. P. Aalto, P. Keronen, E. Siivola, M. Kulmala, and T. Vesala. Annual particle flux observations over a heterogeneous urban area. Atmos. Chem. Phys., 9, 7847-7856, 2009

Kiendler-Scharr A., J Wildt, M Dal Maso, T Hohaus, E Kleist,T.F. Mentel, R Tillmann, R Uerlings, U Schurr and A Wahner. New particle formation in forests inhibited by isoprene emissions. Nature 461, 381-384, 2009

Kulmala M, A. Asmi, H. K. Lappalainen, K. S. Carslaw, U. Pöschl, U. Baltensperger, Ø. Hov, J.-L. Brenquier, S. N. Pandis, M. C. Facchini, H.-C. Hansson, A. Wiedensohler, and C. D. O'Dowd. Introduction: European Integrated Project on Aerosol Cloud Climate and Air Quality interactions (EUCAARI) – integrating aerosol research from nano to global scales.
Atmos. Chem. Phys., 9, 2825-2841, 2009

Kulmala M. , A. Asmi, H. K. Lappalainen, K. S. Carslaw, U. Pöschl, U. Baltensperger, Ø. Hov, J.-L. Brenguier, S. N. Pandis, M. C. Facchini, H.-C. Hansson, A. Wiedensohler, and C. D. O'Dowd. Corrigendum to "Introduction: European Integrated Project on Aerosol Cloud Climate and Air Quality interactions (EUCAARI) – integrating aerosol research from nano to global scales" published in Atmos. Chem. Phys., 9, 2825–2841, 2009. Atmos. Chem. Phys., 9, 3443-3444, 2009

Kurtén T. , T. Berndt, and F. Stratmann . Hydration increases the lifetime of HSO_5 and enhances its ability to act as a nucleation precursor – a computational study. Atmos. Chem. Phys., 9, 3357-3369, 2009

Lappalainen H. K. , S. Sevanto, J. Bäck, T. M. Ruuskanen, P. Kolari, R. Taipale, J. Rinne, M. Kulmala, and P. Hari. Day-time concentrations of biogenic volatile organic compounds in a boreal forest canopy and their relation to environmental and biological factors. Atmos. Chem. Phys., 9, 5447-5459, 2009

Lehtipalo K. , M. Sipilä, I. Riipinen, T. Nieminen, and M. Kulmala. Analysis of atmospheric neutral and charged molecular clusters in boreal forest using pulse-height CPC. Atmos. Chem. Phys., 9, 4177-4184, 2009

Makkonen R, A. Asmi, H. Korhonen, H. Kokkola, S. Järvenoja, P. Räisänen, K. E. J. Lehtinen, A. Laaksonen, V.-M. Kerminen, H. Järvinen, U. Lohmann, R. Bennartz, J. Feichter, and M. Kulmala Sensitivity of aerosol concentrations and cloud properties to nucleation and secondary organic distribution in ECHAM5-HAM global circulation model. Atmos. Chem. Phys., 9, 1747-1766, 2009

Manktelow P. T. , K. S. Carslaw, G. W. Mann, and D. V. Spracklen .Variable CCN formation potential of regional sulfur emissions. Atmos. Chem. Phys., 9, 3253-3259, 2009

Manninen H. E. , T. Nieminen, I. Riipinen, T. Yli-Juuti, S. Gagné, E. Asmi, P. P. Aalto, T. Petäjä, V.-M. Kerminen, and M. Kulmala Charged and total particle formation and growth rates during EUCAARI 2007 campaign in Hyytiälä. Atmos. Chem. Phys., 9, 4077-4089, 2009

Mazon S. Buenrostro , I. Riipinen, D. M. Schultz, M. Valtanen, M. Dal Maso, L. Sogacheva, H. Junninen, T. Nieminen, V.-M. Kerminen, and M. Kulmala. Classifying previously undefined days from eleven years of aerosol-particle-size distribution data from the SMEAR II station, Hyytiälä, Finland. Atmos. Chem. Phys., 9, 667-676, 2009

Meier J. , B. Wehner, A. Massling, W. Birmili, A. Nowak, T. Gnauk, E. Brüggemann, H. Herrmann, H. Min, and A. Wiedensohler . Hygroscopic growth of urban aerosol particles in Beijing (China) during wintertime: a comparison of three experimental methods. Atmos. Chem. Phys., 9, 6865-6880, 2009

Mentel Th. F. , J. Wildt, A. Kiendler-Scharr, E. Kleist, R. Tillmann, M. Dal Maso, R. Fisseha, Th. Hohaus, H. Spahn, R. Uerlings, R. Wegener, P. T. Griffiths, E. Dinar, Y. Rudich, and A. Wahner. Photochemical production of aerosols from real plant emissions. Atmos. Chem. Phys., 9, 4387-4406, 2009

Petäjä T. , R. L. Mauldin, III, E. Kosciuch, J. McGrath, T. Nieminen, P. Paasonen, M. Boy, A. Adamov, T. Kotiaho, and M. Kulmala. Sulfuric acid and OH concentrations in a boreal forest site. Atmos. Chem. Phys., 9, 7435-7448, 2009

Reutter P. , H. Su, J. Trentmann, M. Simmel, D. Rose, S. S. Gunthe, H. Wernli, M. O. Andreae, and U. Pöschl. Aerosol- and updraft-limited regimes of cloud droplet formation: influence of particle number, size and hygroscopicity on the activation of cloud condensation nuclei (CCN). Atmos. Chem. Phys., 9, 7067-7080, 2009

Riipinen I. , H. E. Manninen, T. Yli-Juuti, M. Boy, M. Sipilä, M. Ehn, H. Junninen, T. Petäjä, and M. Kulmala. Applying the Condensation Particle Counter Battery (CPCB) to study the water-affinity of freshly-formed 2–9 nm particles in boreal forest. Atmos. Chem. Phys., 9, 3317-3330, 2009

Sandu I. , J.-L. Brenguier, O. Thouron, and B. Stevens . How important is the vertical structure for the representation of aerosol impacts on the diurnal cycle of marine stratocumulus? Atmos. Chem. Phys., 9, 4039-4052, 2009

Schaap M. , A. Apituley, R. M. A. Timmermans, R. B. A. Koelemeijer, and G. de Leeuw. Exploring the relation between aerosol optical depth and $PM_{2.5}$ at Cabauw, the Netherlands Atmos. Chem. Phys., 9, 909-925, 2009

Sihto S.-L. , H. Vuollekoski, J. Leppä, I. Riipinen, V.-M. Kerminen, H. Korhonen, K. E. J. Lehtinen, M. Boy, and M. Kulmala. Aerosol dynamics simulations on the connection of sulphuric acid and new particle formation. Atmos. Chem. Phys., 9, 2933-2947, 2009

Welti A, F. Lüönd, O. Stetzer, and U. Lohmann. Influence of particle size on the ice nucleating ability of mineral dusts. Atmos. Chem. Phys., 9, 6705-6715, 2009

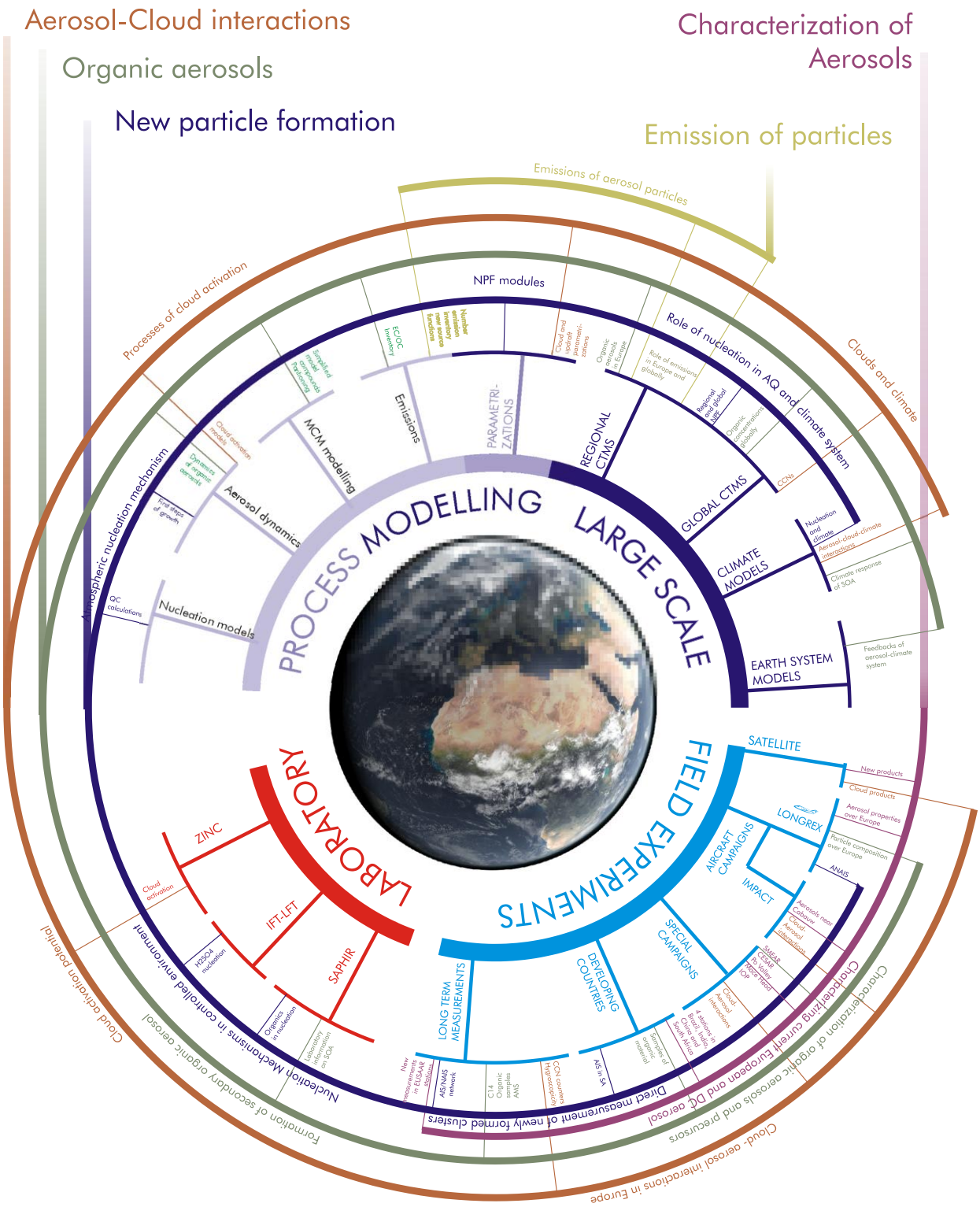

Figure 1. A schematic view of several main activities of EUCAARI

WP1.1: NUCLEATION

Veli-Matti Kerminen[1,2], David Brus[1], Antti Hyvärinen[1], Mikko Sipilä[2], Hanna Manninen[2], Tuomo Nieminen[2], Pauli Paasonen[2], Theo Kurten[2], Hanna Vehkamäki[2], Aadu Mirme[3], Sander Mirme[3], Urmas Horrak[3], Torsten Berndt[4], Frank Stratmann[4], Wolfram Birmili[4], Andreas Minikin[5], Andreas Petzold[5], Christian Plass-Dülmer[6], and Markku Kulmala[2,7]

[1]Finnish Meteorological Institute, Erik Palmenin Aukio 1, FI-00101 Helsinki, Finland
[2]University of Helsinki, Dept. Physical Sciences, P.O. Box 64, FI-00014 University of Helsinki, Finland
[3]University of Tartu, Institute of Physics, Ülikooli 18, EE-50090, Tartu, Estonia
[4]Leibniz-Institute für Troposfärenforchung e.V., Permoserstrasse 15, D-04318, Leipzig, Germany
[5]Deutches Zentrum für Luft- und Raumfahrt (DLR), Wessling, Germany
[6]Meteorologische Observatorium Hohenpeissenberg, Deutscher Wetterdients (DWD), Germany
[7]Department of Applied Environmental Science, Stockholm University, S-10691 Stockholm, Sweden

Keywords: Atmospheric nucleation, air ions, cluster spectrometers, modelling, parameterization.

INTRODUCTION

Work package 1.1 aims at improving our ability to predict the number concentration of new aerosol particles produced via atmospheric nucleation processes. Nucleation is a very non-linear process linked closely to different feedback processes. In large-scale models, nucleation has either not been described at all or is described very crudely. Producing realistic parameterisations of nucleation rates and implementing the parameterisations in large-scale models will considerably improve the present calculations of aerosol impacts on climate and regional air quality. The development and test of cluster spectrometers (ion and neutral clusters) will improve significantly our ability to measure atmospheric nucleation processes. The overall goal of WP 1.1 is to produce parameterized representations of nucleation processes for sulphuric acid – ammonia – water, organic and iodine oxide systems based on combined information from classical nucleation theory (CNT), modelling and experimental studies, to be used in regional and global scale models.

The specific objectives of Work package 1.1 at the beginning of Year 3 were:

- to publish final results from nucleation experiments for systems involving sulphuric acid, water, ammonia and organic vapours (Task 1.1.2)
- to complete the continuous operation of different type of cluster spectrometers associated with the EUCAARI Intensive observation period, and to construct a data set based on these (Task 1.1.3)
- to develop a new modelling tool that assists the interpretation of cluster spectrometer measurements, and to apply it to the conducted measurements (Tasks 1.1.3 and 1.1.4)
- to publish final results of quantum chemical calculations regarding various organo-sulfate-water-ammonia/amine cluster systems (task 1.1.4)

MAIN RESULTS

Task 1.1.1 Development and testing of cluster spectrometers

This task was already completed before Year 3.

Task 1.1.2 Homogeneous nucleation experiments for sulphate and organic systems

During 2009, homogeneous nucleation experiments were carried out in IFT and FMI. Both sulphuric acid-water (H_2SO_4–H_2O) and sulphuric acid-water-ammonia (H_2SO_4–H_2O-NH_3) systems were considered. The results from these experiments have been submitted for publication or are in preparation (Brus et al., 2009; Sipilä et al., 2009).

The most important findings from these nucleation experiments are summarized in Figure 1. The new laboratory experiments resolve the existing discrepancies between earlier H_2SO_4–H_2O measurements, as well as the differences in nucleation rates between laboratory measurement and atmospheric observations.

Task 1.1.3 Atmospheric nucleation mechanism

Field measurements using different type of cluster spectrometers at 13 field sites associated with the EUCAARI Intensive Observation Period were completed, and a data set associated with these measurements was constructed. The used spectrometers were calibrated and inter-compared both before and after the Intensive Observation Period in two workshops held in Helsinki. Results from the first of these workshops were published (Asmi et al., 2009).

Results from field experiments demonstrate that the new prototype cluster spectrometer (Neutral cluster and Air Ion Spectrometer, NAIS), developed as part of EUCAARI, is capable of measuring accurately the time evolution of both neutral and charge particles/clusters in the size range 2-40 nm during atmospheric new particle formation events (Manninen et al., 2009a; Figure 2).

From NAIS data, one may calculate the formation rate of both charged and neutral 2-nm particles (Manninen et al., 2009b) Comparison of these formation rates with other measured quantities, such as gaseous sulphuric acid concentrations, provides valuable new information on atmospheric nucleation mechanisms (Nieminen et al., 2009). Preliminary results of the NAIS data from various EUCAARI ground sites suggest that the contribution of ion-meditated nucleation to total atmospheric nucleation is usually minor in the continental boundary layer (Figure 3).

The NAIS was successfully operated in an aircraft during the EUCAARI long range experiment EUCAARI LONGREX 2008 (Mirme et al., 2009, Figures 4 and 5). This was the first time when sub-3 nm neutral clusters were measured throughout the tropospheric column. The measurements indicate that new particle formation takes place actively from ground level up to the tropopause. Particles were found to be formed mainly via neutral pathways in the boundary layer, and there was no sighn of an increasing role by ion-induced nucleation toward the upper troposphere. Clouds, while acting as a source of sub-10 nm ions, did not affect the overall budget of atmospheric clusters and particles.

Task 1.1.4 Nucleation theory, modelling and parametrisations (UHEL, UKU, FMI)

Final results from quantum chemical calculations regarding various organo-sulfate-water-ammonia/amine cluster systems were published (Kurtén et al., 2009a, 2009b; Salonen et al., 2009).

A new modelling tool, called Ion-UHMA, that assists the interpretation of cluster spectrometer measurements, was developed (Leppä et al., 2009). Ion-UHMA is a zero-dimensional sectional box model, which simulates the dynamics of neutral and electrically charged aerosol particles in atmospheric conditions. It builds on the aerosol dynamical model UHMA (Korhonen *et al.*, 2004) and model AEROION (Laakso *et al.*, 2002). An example on how to apply the model into measurement data is shown in Figure 6. In this example, the formation rates of charged and neutral 2-nm particles are taken from measurements used as model input. Similarly, particle growth rates as well as the background aerosol size distribution above 20 nm are taken from measurements. Based on these inputs, the evolution of charged and neutral particles number size distributions between 2 and 20 nm are then simulated (Figure 6, left panel) and compared with observations (Figure 6, right panel). The good agreement between simulations and observations demonstrates that model is able to capture the dynamics of the system in cases when measured air masses are sufficiently homogenous in their horizontal extent and when vertical exchange processes do not seriously affect the charging state of newly-formed particles

FUTURE PLANS

There are no research activities for WP1.1 during Year 4. However, some of the results related to this WP, including a synthesis of all the results, will be published in Year 4.

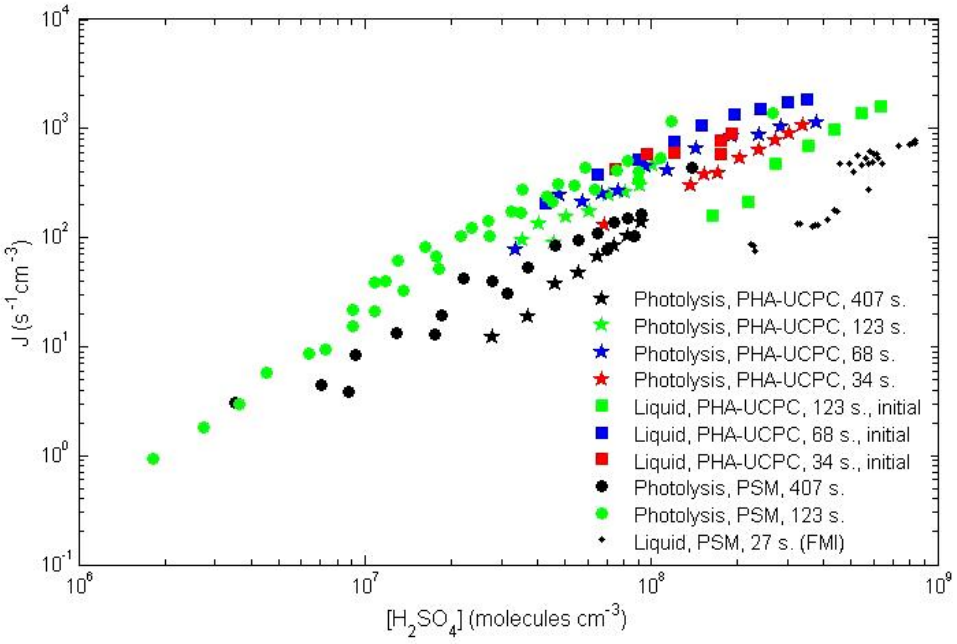

Figure 1. Nucleation rates as a function of sulphuric acid concentration, [H_2SO_4]. Fittings to different data series yield the slopes of nucleation rate vs. [H_2SO_4] that range between 1.0 and 2.1 with an average of 1.5. The sulfuric acid concentration shown in the figure is the average concentration in photolysis experiment and initial (maximum) concentration in experiments with sulfuric acid from a liquid sample. Experiments in FMI laminar flow tube (black dots) were performed at 25°C and relative humidity of 30%, whereas the data from IfT-LFT were made at 20°C and relative humidity of 22% (Sipilä et al., 2009).

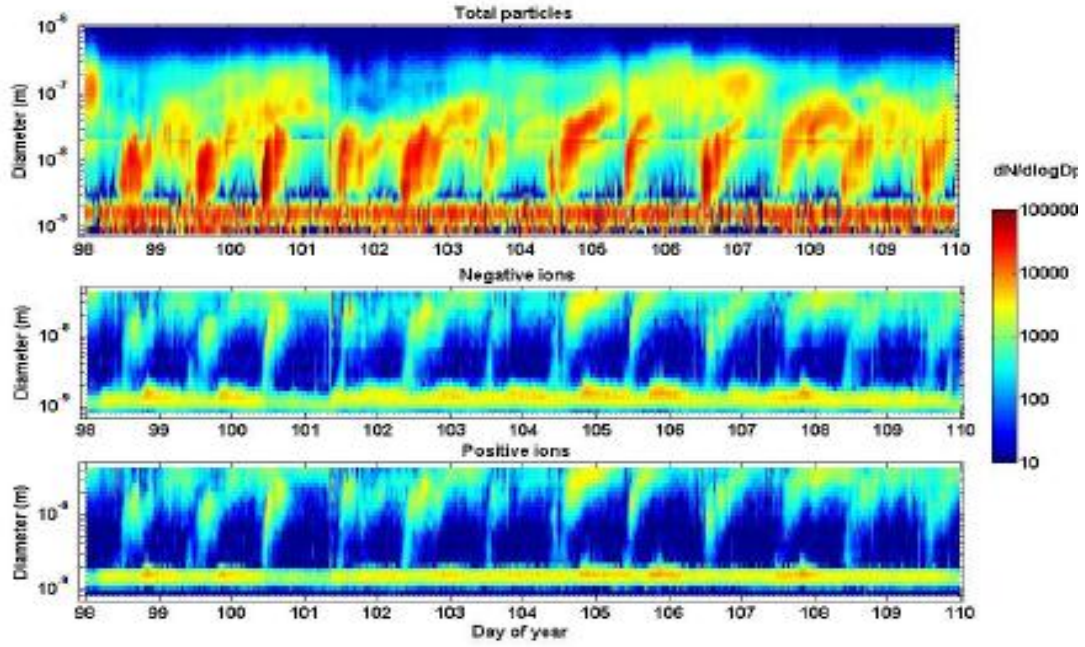

Figure 2. Example of NAIS measurements on 12 consecutive particle formation event days between 8 and 19 April 2007 carried out in Hyytiälä, Finland (Manninen et al., 2009a). Total particle size distribution measured with the NAIS in the size range 0.8–20 nm and with the DMPS in the size range 20–1000 nm (top). Negative (middle) and positive (bottom) air-ion distributions were measured with the NAIS ion mode (0.8–40 nm).

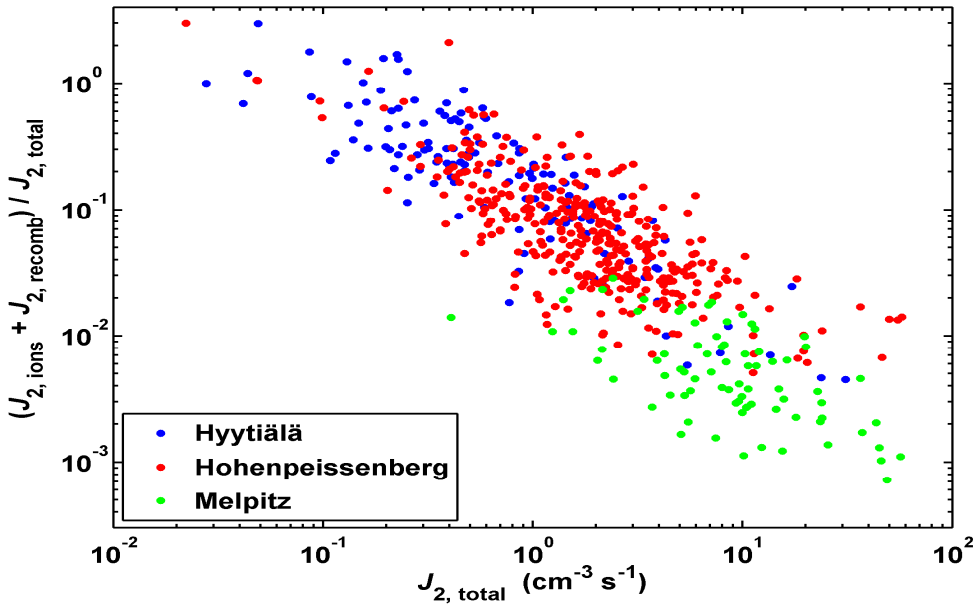

Figure 3. Contribution of ion-mediated nucleation to the total formation rate of 2 nm particles ($J_{2,\,total}$) as a function of $J_{2,total}$ at three EUCAARI measurement sites (Kulmala et al., 2009).

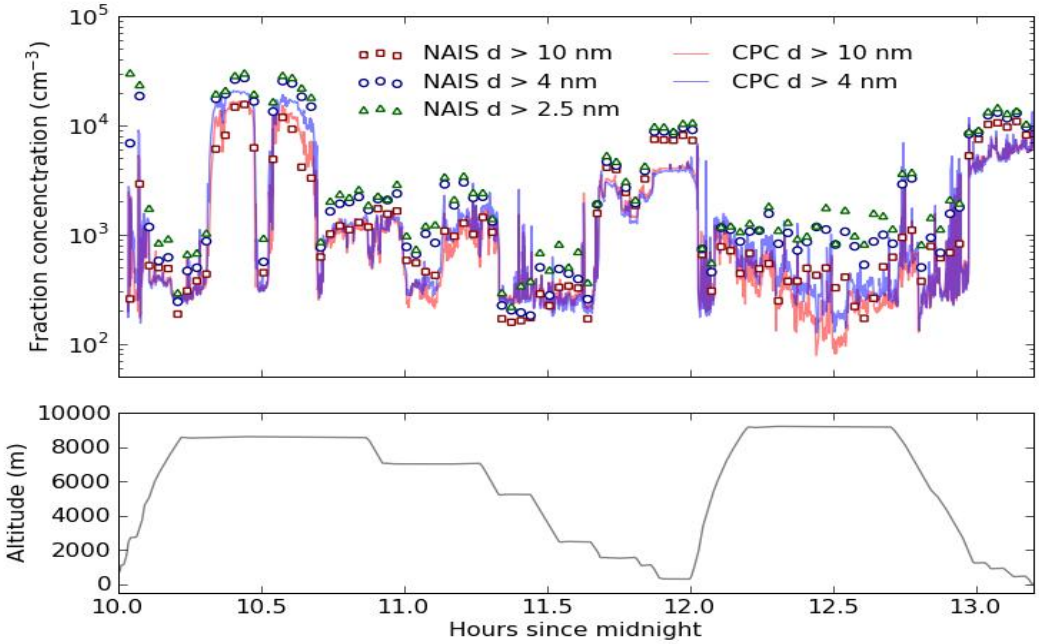

Figure 4. Time-altitude profiles particle number concentrations measured by NAIS and the CPC system between 10:00 and 13:15 on May 21, 2008. From the CPC data, number concentrations of particles >4 and >10 nm in diameter are obtained (Mirme et al., 2009).

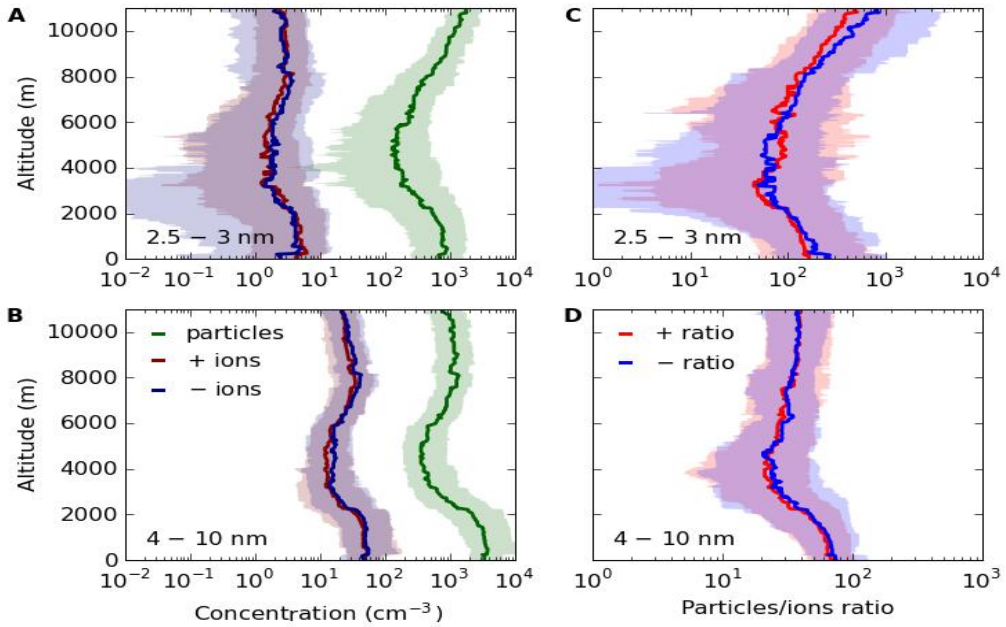

Figure 5. Median concentration profiles total (green) and charged (red and blue) clusters and particles in size ranges 2.5-3 nm (A) and 4-10 nm (B), as well as the corresponding concentration ratios between total and charged cluster/particles (C and D), derived from measurements from all flights in May 2008 over Central Europe. Solid line shows the median over all measurement flights, while the shading represents 25 and 75 % percentiles of the data (Mirme et al., 2009).

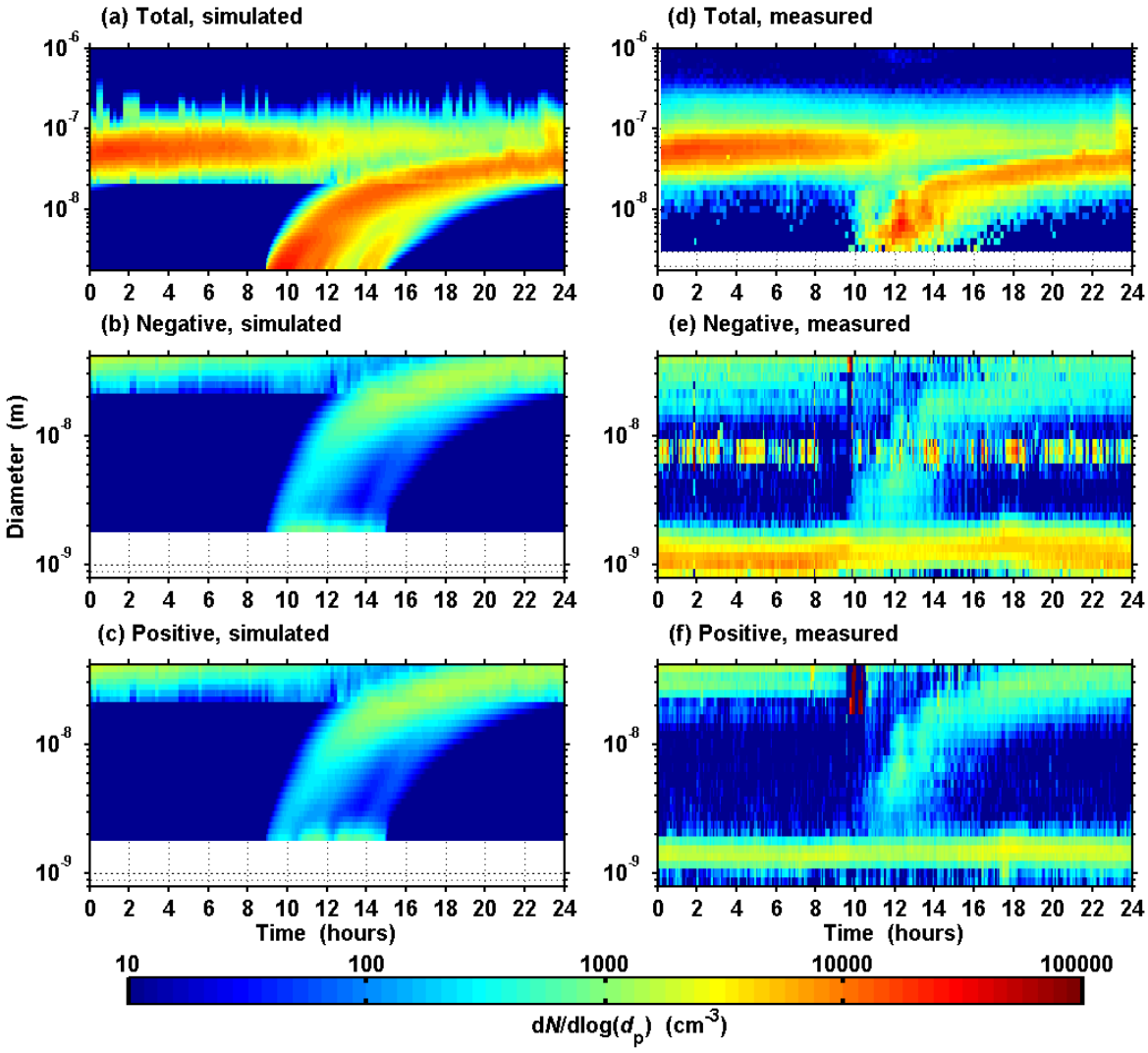

Figure 6. Simulated (panels a, b and c) and measured (panels d, e and f) evolution of the particle number size distribution for 15 September 2006. The evolution is shown for total (panels a and d), negatively charged (panels b and e) and positively charged particles (panels c and f). The color denotes the particle number concentration ($dN/d\log d_p$) as a function of time and diameter. The new particle formation rate, the growth rate of the particles and concentrations of particles larger than 20 nm in diameter were taken from measurements and used as input for the simulation (Leppä et al., 2009).

REFERENCES

Asmi E, Sipilä M, Manninen H E, Vanhanen J, Lehtipalo K, Gagné S, Neitola K, Mirme A, Mirme S, Tamm E, Uin J, Komsaare K, Attoui M, Kulmala M (2009) Results of the first air ion spectrometer calibration and intercomparison workshop. *Atmos. Chem. Phys.*, **9**, 141-154.

Brus D., Hyvärinen A.-P., Viisanen Y., Kulmala M. and Lihavainen H. (2009) Homogeneous Nucleation of Sulfuric Acid and Water Mixture: Experimental Setup and First Results. *Atmos. Chem. Phys.* (submitted).

Korhonen H., Lehtinen K. E. J. and Kulmala M. (2004) Multicomponent aerosol dynamics model UHMA: model development and validation. *Atmos. Chem. Phys*. **4**, 757-771.

Kulmala M., Riipinen I., Nieminen T., Hulkkonen M., Sagacheva L., Manninen H. E., Paasonen P., Petäjä T., Dal Maso M., Aalto P. P., Viljanen A., Isoskin I., Vainio R., Mirme S., Mirme A, Minikin A., Petzold A, Horrak U., Plass-Dülmer C., Birmili W., and Kerminen V.-M. (2009) Atmospheric data over a solar cycle: no connection between galactic cosmic rays and new particle formation. *Atmos. Chem. Phys. Discuss.* **9**, 21525-21560

Kurtén T., Berndt T. and Stratmann F. (2009a) Hydration increases the lifetime of HSO5 and enhances its ability to act as a nucleation precursor - a computational study. *J. Molec. Structure-Theorem* **901**, 169-173.

Kurtén T., Ortega I. K., Vehkamäki H. (2009b) The sign preference in sulfuric acid nucleation. *Atmos. Chem. Phys.* **8**, 4095-4103.

Laakso L., Mäkelä J. M., Pirjola L. & Kulmala M. 2002. Model studies on ion-induced nucleation in the atmosphere. *J. Geophys. Res.* **107**(D20), 4427, doi:10.1029/2002JD002140.

Leppä J., Kerminen V.-M., Laakso L., Korhonen H., Lehtinen K. E. J., Gagne S., Manninen H. E., Nieminen T. and Kulmala M. (2009) Ion-UHMA: a model for simulating the dynamics of neutral and charged aerosol particles. *Boreal Env. Res.* **14**, 559-575.

Manninen H. E., Petäjä T., Asmi E., Riipinen I., Nieminen T., Mikkilä J., Hõrrak U., Mirme A., Mirme S., Laakso L., Kerminen V.-M. and Kulmala M. (2009a) Long-term field measurements of charged and neutral clusters using Neutral cluster and Air Ion Spectrometer (NAIS) *Boreal Env. Res.* **14**, 591-605.

Manninen H. E., Nieminen T., Riipinen I., Yli-Juuti T., Gagne S., Asmi. E., Aalto P. P., Petäjä T., Kerminen V.-M. and Kulmala M. (2009b) Charged and total particle formation and growth rates during EUCAARI 2007 campaign in Hyytiälä. *Atmos. Chem. Phys.* **9**, 4077-4089.

Mirme S., Mirme A., Minikin A., Petzold A., Horrak U., Kerminen V.-M. and Kulmala M. (2009) Atmospheric sub-3nm particles at high latitudes. *Atmos. Chem. Phys. Discuss.* **9**, 19435-19470.

Nieminen T., Manninen H. E., Sihto S.-L., Yli-Juuti T., Mauldin III R. L., Petäjä T., Riipinen I., Kerminen V.-M. and Kulmala M. (2009) Connection of sulfuric acid to atmospheric nucleation in boreal forest. *Environ. Sci. Technol*. **43**, 4715-4721.

Salonen M., Kurtén T., Vehkamäki H., Berndt T. and Kulmala M. (2009) Computational investigation of the possible role of some intermediate products of SO_2 oxidation in sulfuric acid-water nucleation. *Atmos. Res.* **91**, 47-52.

Sipilä M., Berndt T., Petäjä T., Brus D., Vanhanen J., Stratmann F., Patokoski J., Mauldin L., Hyvärinen A.-P., Lihavainen H. and Kulmala M.(2009) Resolving the Mystery of Sulphuric Acid in Atmospheric Nucleation (manuscript in preparation).

WP1.2 FORMATION AND GROWTH OF ORGANIC PARTICLES

WP1.2 Team* and Thomas F. Mentel

Forschungszentrum Juelich, ICG-2, 52425 Juelich, FZJ (24)

*A. Kiendler-Scharr, J. Wildt, R. Tillmann, E. Kleist, B. Bohn, Th. Brauers, A. Buchholz, H.P. Dorn, R. Fisseha, R. Häseler, Th. Hohaus, A. Mensah, K.P. Müller, E. Schlosser, Ch. Spindler, R. Wegener, R. Uerlings, FZJ (24), Th. Hoffmann, Ch. Reinnig, L. Müller, JGUM (42) , Y. Iinuma, A. Kahnt, Olaf Böge, IfT (4) , M.C. Facchini, S. Decesari, E. Finessi, ISAC (5), G. Kiss, A. Hofer, ACUV (12), M. Kulmala, M. Dal Maso, UHEL(1), Ch. George, B. D'Anna,CNRS (2), M. Ammann, PSI (19), U. Poeschl, MPIC (9)
Guest contributions: M. Hallquist, E. Emanuelsson, U Gothenburg, N. Lang, Y.Rudich, Weizmann Institute

Keywords: SOA formation, SOA yields, SOA markers, ageing process

INTRODUCTION

Biogenic secondary organic aerosols (BSOA) may play an increasing role in a warming climate. Vegetation models predict an about 50% increase in emissions of biogenic volatile compounds (BVOC) (Lathiere et al., 2005) and possibly a more than twofold increase of the BSOA burden (Tsigaridis and Kanakidou, 2007). From the current point of view, such an increase in SOA could have a cooling potential of the order of 1 W/m^2, thus constituting a considerable negative feedback between vegetation and climate (Kulmala et al. 2004, Spracklen et al., 2008). Moreover, organics play a pivotal role in new particle formation (Laaksonen et al., 2008), thus contribute to not only to size but *also* to the number concentration of atmospheric particles. However, despite of this potential importance, today's SOA sources are highly uncertain and in predicting SOA mass models often fall short by more than an order of magnitude. (Kanakidou et al., 2005, Heald et al., 2005, Goldstein and Galbally, 2007). The discrepancy could be due to missing precursors (e.g. Heald et al. 2005, Robinson et al. 2007) or missing long term chemistry in the laboratory studies. WP.1.2. addressed SOA formation by using real plants as VOC emission sources (Task.1.2.1), making long term photochemical simulation studies (Task 1.2.2) and searching for new chemical pathways and mechanisms of multi-phase oxidation (Task 1.2.3). The synthesis of the results of the Tasks 1.2.1.- 1.2.3 will be accomplished by the modelling Task .1.2.4.

EXPERIMENTS

Experiments were performed in the plant chamber JPAC (Task 1.2.1) and the SAPHIR chamber (Task 1.2.2) at FZJ (24). In these simulation experiments we applied a multi-methodological approach in gas-phase (including measurement of OH radicals) and particulate-phase measurements. This included on-site cooperation between the partners comprising aerosol microphysical characterization, aerosol mass spectrometry, and chemical analysis of filter samples. Three plant chamber campaigns (total of 6 month) and two SAPHIR chamber campaigns under autumn and summer conditions (total of 2.5 month) were successfully accomplished. Besides particle formation and ageing also hygroscopic properties of the particles were determined.
Recently, we studied the relative role of organic compounds and sulphuric acid in early stages of particle formation. Partners FZJ and UHEL performed these measurements in the JPAC plant chamber in Sept. 2009 using Boreal trees from Hyytiälä. The data are currently under evaluation.
The partners in Task 1.2.3 provided detailed studies of ageing processes applying an aerosol chamber (IfT (4)), flow tubes, and contact angle measurements (PSI (19), CNRS (2)). Partners PSI and CNRS focussed in detailed experiments i) on the effect of the photosensitized uptake of O_3 to organic films on the

substrate's hydrophilicity; ii) the quenching kinetics of a model photosensitizer in aqueous solutions; and iii) the extent of photosensitized polymerization of dicarboxylic acids in an aerosol.

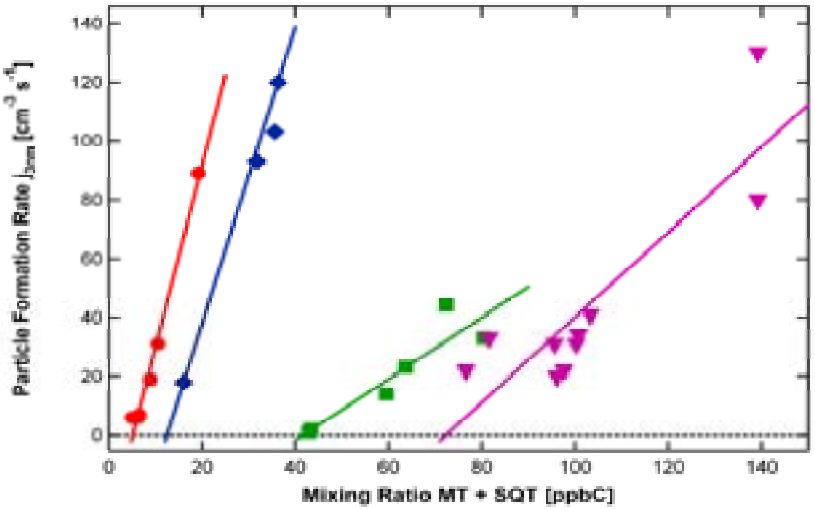

Figure1. Particle formation rates as a function of the terpene concentration. Particle formation rates depend linearly on available Carbon concentration (solid lines).

RESULTS

The plant chamber experiments in Task 1.2.3 with species of the Boreal forest, we observed simple linear relationships between the carbon mixing ratio of monoterpenes & sesquiterpenes and formation rate of 3 nm particles (Fig. 1), condensational growth rate, and SOA mass. The slope of the latter agrees with the analysis of field observations in the Boreal forest by Tunved et al. 2008 (Mentel et al., 2009). In experiments with holm oak and a small Mediterranean stand we demonstrated that linearity and slope (6% incremental mass yield) of the SOA mass as f(VOC[ppbC] consumed) holds in a similar way in Mediterranean stands as for Boreal stands (in prep.).

In studies of particle formation in stands including strong isoprene emitter new particle formation was strongly suppressed. In systematic studies we added different amounts of isoprene to tree emissions and to α-pinene in reference experiments. We could demonstrate that in the presence of isoprene the OH radical concentrations were lowered (Fig 2a) and that 3-4 OH radicals are needed to induce nucleation. Model considerations showed that competition of isoprene for the OH radicals lowered the concentration of potential nucleating species of the MT oxidation and thus the nucleation rates (Fig 2b). If future climate conditions shift the relative emission strength of BVOC in favour of isoprene this could lead to a relative reduction of new particle formation, thus isoprene emissions could damp the expected negative vegetation-climate feedback described in the Introduction section (Kiendler-Scharr et al., Nature 2009).

In the campaigns in the SAPHIR chamber in Task 1.2.2 the partners investigated a mix of those MT and SQT which are main components of tree emissions of Boreal species. The experiments were performed under low NOX regime and at various actinic fluxes (autumn - summer, cloudy - sunny). Particles were formed during the first day and than aged over a second day. OH radicals and ozone served as oxidants; experiments at low actinic fluxes were dominated by ozone oxidation, whereas oxidation by OH radicals dominated at high actinic fluxes. As key quantities the particle composition, the particle size and mass distribution, hygroscopic growth, CCN activity, and volatility were measured. Moreover, OH radical concentration was measured in most cases. Data analysis showed that the condensation growth rates at the second day are linearly related to the OH concentration while the O/C ratio increases nearly linear with the OH dose.

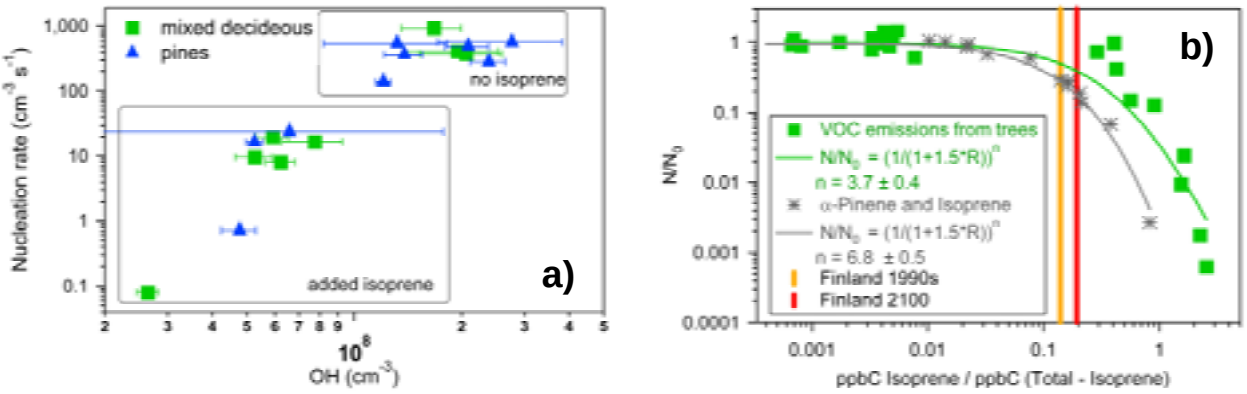

Figure 2. a) Particle formation rate as f([OH]). OH concentrations were lower in the presence of isoprene resulting in decreased nucleation rates. b) Inhibition of particle number concentration as a function of the carbon based ratio of isoprene to other VOC concentrations. Data are shown for all plant emissions studied (filled squares) and a-pinene (asterisks). Vertical bars indicate modelled concentration ratios of isoprene and monoterpenes for Finland in the 1990s (orange) and in 2100 (red).

Chemical ageing of particles was detected by on-line APCI mass spectrometry and in the analysis of filter samples by H-NMR spectroscopy and various LC-MS techniques. Marker compounds for chemical ageing were detected by APCI-MS, CE-MS, LC-ESI-MS as well as GC-MS. Figure 3 compares APCI-MS results of partner UGUM of fresh SAPHIR, PSI chamber, aged SAPHIR, and Hyytiälä data. The marker composition of the aged aerosol approaches the pattern observed in Hyytiälä, however with an excess of ozonolysis products. The analysis showed that the tricarboxylic acid detected at m/z 203 is a key marker for higher generation products in according with observations of Szmigielski et al. 2007. Moreover, the ratio of m/z 203 to m/z 185 (Pinonic acid, a first generation product) evolves in time and increased only when OH radicals were available. From that we concluded that we indeed detected photo-chemical ageing and that the ratio of m/z 203/185 may serve as a measure of the progress of the ageing process.
C15H24O4 (MW 268) was determined in the particle phase by partner IfT. The signal was assigned to sesquiterpene originating monoaldehyde based on the derivatisation reaction of this compound and a number of carbon atoms.The intensity of this aldehyde decreased dramatically after the photo-chemical aging process. This is different to monoterpene originating aldehyde such as endolim and pinonaldehyde that showed a small change or higher concentrations after photochemical aging.

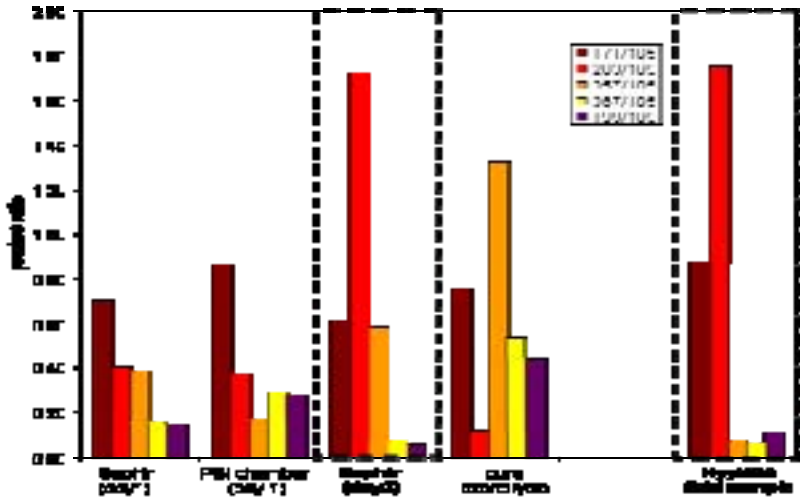

Figure 3. Comparison of the concentration ratios of characteristic products in particle phase samples from different chamber experiments and from Hyytiälä

HNMR analysis of partner ISAS-CNR shows the decrease in content of first-generation degradation products such as pinonic acid in aged SOA samples. The bands of the more complex mixtures (which represents > 90% of the signal) change to a much lesser extent. On the basis of the main functional group distributions, ageing is not reflected by an actual change of the functionalization degree although oxidation may occur through conversion of the functional groups into more oxidized forms: e.g., C=O to COOH (Fig. 4). Distinct NMR fingerprints can be found for SOA formed by biogenic (MT+SQT, MT, α-pinene alone) compared to anthropogenic (toluene, 1,3,5-TMB) reactive VOCs, providing confirmation that the chemical composition of SOA (even its more complex and oxidized fraction) retains information on the original chemical structure of precursors. Such NMR fingerprints can be used for organic source apportionment of ambient samples.

Filter samples were extracted and investigated by partner ACUV using ESI/MS. UV absorption and fluorescence measurements of the filter extracts were also performed. On the basis of these results (Fig. 5) it can be concluded that in the chamber experiments a complex mixture of oxidation products is formed from monoterpenes and sesquiterpenes that resembled in mass spectrometric signatures, in UV and fluorescence properties humic-like substances isolated from rural aerosol. Thus terpene emission can be an important source of humic-like substances which often account for 60% of the water-soluble organic carbon content of ambient aerosol.

The microphysical properties of particles generally spoken reflected the changes in particle composition by the ageing processes, but dramatic changes were not observed. The most important parameter influencing microphysical properties was actinic flux / OH oxidation, whereby sunny days favour the formation of more hygroscopic particles and OH radicals seem to be needed to make chemical ageing manifest in hygroscopic properties. Volatility measurements show the same trend. Here in addition volatility decreased stronger than expected from the chemical analysis of the same particles by Q-AMS. This could indicate an influence of morphological effects (compaction, layering) in the ageing process.

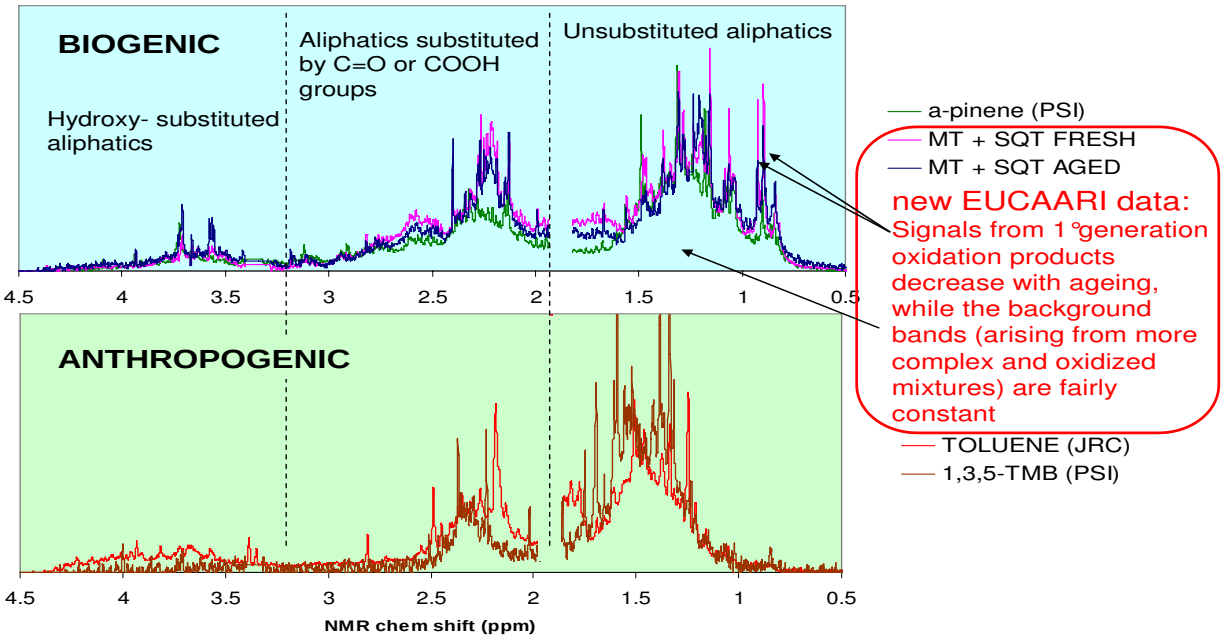

Figure 4. NMR analysis of biogenic, fresh and aged biogenic SOA in the SAPHIR chamber compared to pure α-pinene SOA and 1,3,5,-TMB SOA in the PSI chamber and Toluene SOA in JRC chamber.

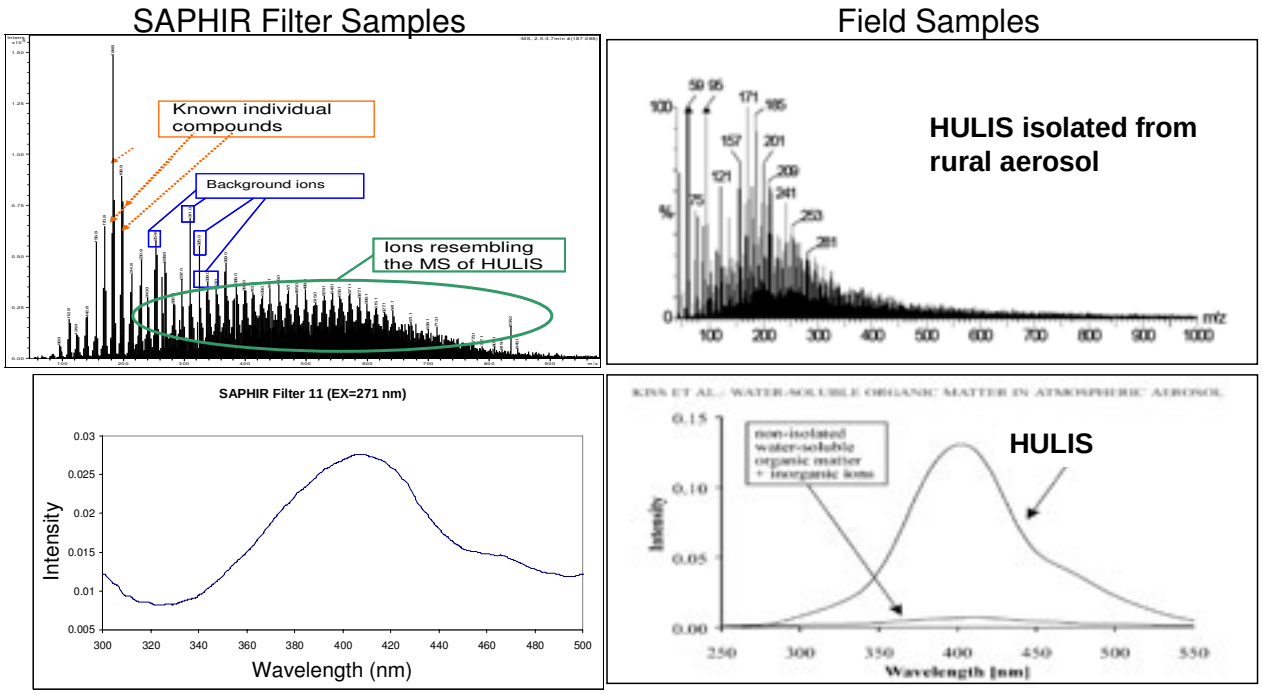

Figure 5. Comparison of aged BSOA generated from a monoterpene mix in the SAPHIR chamber to a sample of rural HULIS fraction. Upper panel: ESI/MS spectra, bottom panel: wavelength-resolved fluorescence.

In Task 1.2.3 heterogeneous reactions were studied. Laser flash photolysis work indicated that simple organic acids such as adipic and succinic acids efficiently quench the excited benzophenone triplet in aqueous solution. Longer term exposure of such solutions to simulated sunlight leads to the build up of new absorption features extending into the visible, indicative of polymerisation processes. Experiments in aerosol and coated flow tubes indicate effective removal of these acids driven by light, and in some cases indicate the build-up of secondary organic material in the aerosol phase. X-ray microspectroscopy work was devoted to the development of a microreactor system and its application to a first test system. The results with mixed ammonium sulphate / adipic acid particles indicate complex microstructure and its evolution, when part of the material forms a solution. This provides a proof of concept that this method can be used to follow oxidative and photochemical processing in situ and in real time in the future.

SUMMARY AND STATUS OF WP1.2

According to the planning WP1.2 ended at the end of year two. The experiments needed to achieve the goals were successfully performed in close interaction between the partners. In the first extension year extra experiments were performed in JPAC and in the context of photo-sensitized heterogeneous reactions. The observation of SOA formation from tree emissions was one step generalized as similar relations for Mediterranean trees were found as for the Boreal species. This can possibly lead to simple parameterizations for models in order to predict future SOA formation. New insights in the role of OH radicals and isoprene in nucleation of fresh particles in forested regions were provided.
Evaluation of data measured in SAPHIR experiments made progress and available data indicate that photo-chemical aging of biogenic SOA should occur under natural oxidant and light conditions. The

results of the different analysis of the filter samples, on line APCI-MS, and AMS are now ready to be brought in a common context. Marker compounds were identified and the partners can evaluate their potential to determine the photochemical age *(i.e. the "age spectrum")* of biogenic SOA. Moreover, valuable quantitative information on the time scale of oxidative processing, i.e. kinetic data for implementation into models can be extracted. Photo-chemical aging changes chemical composition and thus the microphysical properties of SOA particles, its manifestation depends on oxidation regime during the formation and ageing process.
All results shown were presented as poster or oral contributions at several conferences and workshops including EGU 2009, Goldschmidt conference 2009, EAC 2009. One final step which needs to be done in the remaining year is to bring together chamber kinetic results, flow tube kinetic results and the model frame-work development in WP 1.2.4.

REFERENCES

Goldstein, A. H., and Galbally, I. E. (2007) Known and unexplored organic constituents in the earth's atmosphere, *Environ. Sci. Technol.,* **41**, 1514-1521

Heald, C. L., D. J. Jacob, R. J. Park, L. M. Russell, B. J. Huebert, J. H. Seinfeld, H. Liao, and R. J. Weber (2005), A large organic aerosol source in the free troposphere missing from current models, *Geophys. Res. Lett.*, *32*(18), L18809, doi:18810.11029/12005GL023831

Kanakidou, M., Seinfeld, J. H., Pandis, S. N., Barnes, I., Dentener, F. J., Facchini, M. C., Van Dingenen, R., Ervens, B., Nenes, A., Nielsen, C. J., Swietlicki, E., Putaud, J. P., Balkanski, Y., Fuzzi, S., Horth, J., Moortgat, G. K., Winterhalter, R., Myhre, C. E. L., Tsigaridis, K., Vignati, E., Stephanou, E. G. and Wilson, J. (2005) Organic aerosol and global climate modelling: a review, *Atmos. Chem. and Phys.,* **5**, 1053-1123

Kiendler-Scharr, A., J. Wildt, M. Dal Maso, T. Hohaus, E. Kleist, T. F. Mentel, R. Tillmann, R. Uerlings, U. Schurr, and A. Wahner (2009), Isoprene emissions inhibit new particle formation in forests., *Nature*, 381 - 384

Kulmala, M., Suni, T., Lehtinen, K. E. J., Dal Maso, M., Boy, M., Reissell, A., Rannik, U., Aalto, P., Keronen, P., Hakola, H., Back, J. B., Hoffmann, T., Vesala, T. and Hari, P. (2004) A new feedback mechanism linking forests, aerosols, and climate, Atmos. Chem. Phys., **4**, 557-562

Laaksonen, A., Kulmala, M., O'Dowd, C. D., Joutsensaari, J., Vaattovaara, P., Mikkonen, S., Lehtinen, K. E. J., Sogacheva, L., Dal Maso, M., Aalto, P., Petaja, T., Sogachev, A., Yoon, Y. J., Lihavainen, H., Nilsson, D., Facchini, M. C., Cavalli, F., Fuzzi, S., Hoffmann, T., Arnold, F., Hanke, M., Sellegri, K., Umann, B., Junkermann, W., Coe, H., Allan, J. D., Alfarra, M. R., Worsnop, D. R., Riekkola, M. L., Hyotylainen, T. and Viisanen, Y. (2008) The role of VOC oxidation products in continental new particle formation, *Atmos. Chem. Phys.,* **8**, 2657-2665, 2008.

Lathiere, J., Hauglustaine, D. A., De Noblet-Ducoudre, N., Krinner, G., and Folberth G. A. (2005) Past and future changes in biogenic volatile organic compound emissions simulated with a global dynamic vegetation model, *Geophysical Research Letters,* **32**, L20818, doi:10.1029/2005GL024164, 2005.

Robinson, A. L., Donahue, N. M., Weitkamp, E. A., Sage, A. M., Grieshop, A. P., Lane, T. E., Pierce, T. E. and Pandis, S (2007) Rethinking Organic Aerosols: Semivolatile Emissions and Photochemical Aging, *Science,* **350**, 1259-1262

Spracklen, D. V., B. Bonn, and K. S. Carslaw (2008), Boreal forests, aerosols and the impacts on clouds and climate, *Philosophical Transactions of the Royal Society a-Mathematical Physical and Engineering Sciences*, *366*(1885), 4613-4626

Szmigielski, R., J. D. Surratt, Y. Gomez-Gonzalez, P. Van der Veken, I. Kourtchev, R. Vermeylen, F. Blockhuys, M. Jaoui, T. E. Kleindienst, M. Lewandowski, J. H. Offenberg, E. O. Edney, J. H. Seinfeld, W. Maenhaut, and M. Claeys (2007), 3-methyl-1,2,3-butanetricarboxylic acid: An atmospheric tracer for terpene secondary organic aerosol, *Geophys. Res. Lett.*, *34*(24)

Tsigaridis, K., and Kanakidou, M. (2007) Secondary organic aerosol importance in the future atmosphere, *Atmospheric Environment,* **41**, 4682-4692

Anthropogenic and biogenic emissions of aerosols and precursors EUCAARI WP 1.3:

Hugo Denier van der Gon on behalf of WP 1.3
TNO, Utrecht, the Netherlands

Keywords: Emissions, aerosols, particle numbers, EC, OC, biomass burning

INTRODUCTION

WP 1.3 focuses on the emissions of particulates and precursors on regional and global scales. Special attention is given to the carbonaceous fraction in particulate emissions and the number of particles emitted in different size classes by various sources. It will provide inventories of aerosols and precursors to be used in regional and global-scale models. The more specific aims of WP 1.3 are to produce a carbonaceous aerosol inventory for the base year 2005, a first European size-resolved particle number (PN) inventory for Europe, algorithms for the translation of the PN emissions for urban, regional and global scales to be used in CTMs and Marine and pyrogenic aerosols emission estimates and/or source functions to be used in models. In this abstract the progress of the various tasks of WP 1.3 in Nov. 2008- Nov. 2009 are discussed. A number of deliverables and objectives have been achieved earlier, these are not discussed here but we refer to previous progress reports and the EUCAARI website for deliverable reports.

Task 1.3.1 First size-resolved Pan-European aerosol emission inventory

Activity data for the major sources like wood combustion and road transport have been compiled by TNO, checked and updated where necessary. For the major sources, based on a key-source inventory of an available PM1 inventory, we have searched for direct PN emission factors. SU has compiled a set of PN emission factors for wood combustion (Johansson et al. 2009), the work by MPI-C for pyrogenic aerosols (see task 1.3.3., Janhall et al., 2009) has been used to estimate PN from agricultural waste burning and UB contributed by complementing the missing PN emission factors for certain road transport categories (Beddows and Harrison, 2008). The remainder of the sources has been covered by TNO using direct emission factors or, if these could not be obtained and/or the source was minor, the PN inventory is based on the fraction of PM0.3 in PM1. The particle number size distribution is derived from literature data for each source category and applied to both the direct estimated PN emissions and the PM0.3 estimates. From the literature about 50 different number size distributions are compiled. However, various source categories can share the same size distribution as this is often related to the fuel type used and burning conditions. The approach as followed for major point sources such as power plants is outlined by Denier van der Gon and Visschedijk (2009) .The number median diameter data is based on mobility diameter as this was most available. In rare occasions where only aerodynamic diameter was available this has been empirically converted to mobility diameter.

Table 1 Size bins of the EUCAARI particle number inventory for Europe in 2005

Bin #	Size class	Bin #	Size class	Bin #	Size class
1	10-13 nm	6	32-41 nm	11	102-129 nm
2	13-16 nm	7	41-51 nm	12	129-162 nm
3	16-20 nm	8	51-65 nm	13	162-205 nm
4	20-26 nm	9	65-81 nm	14	205-258 nm
5	26-32 nm	10	81-102 nm	15	258-300 nm

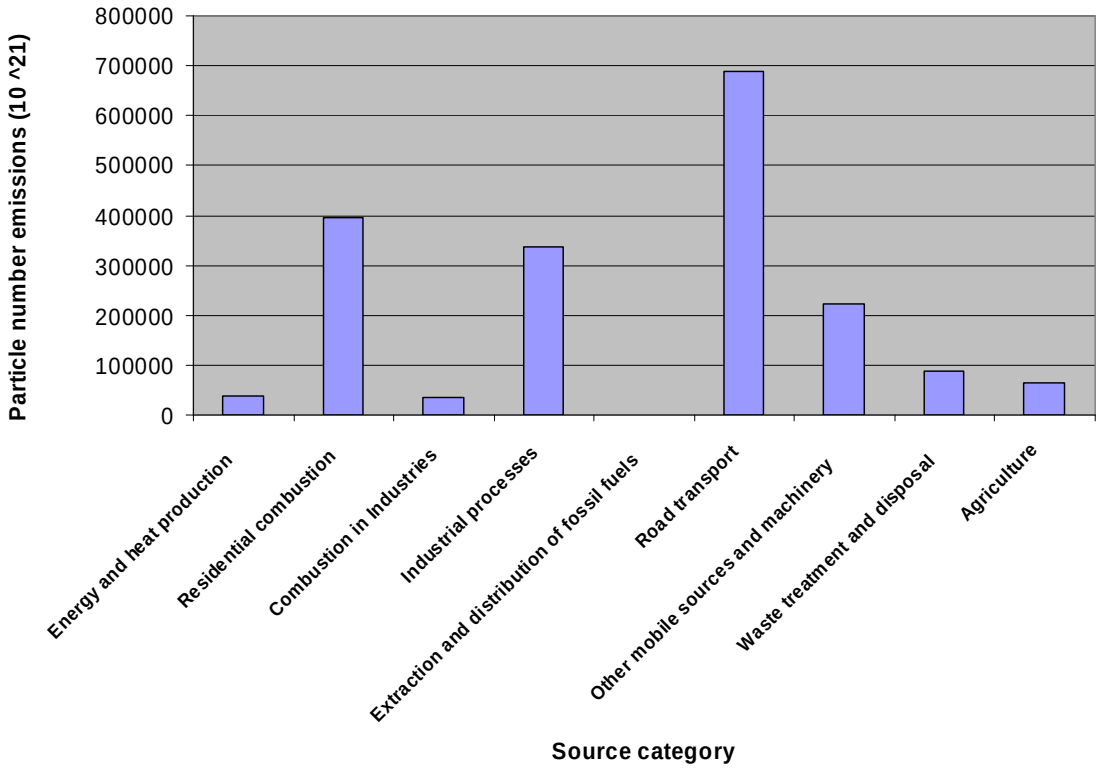

Figure 1. Total particle number emitted by source category in UNECE Europe in 2005.

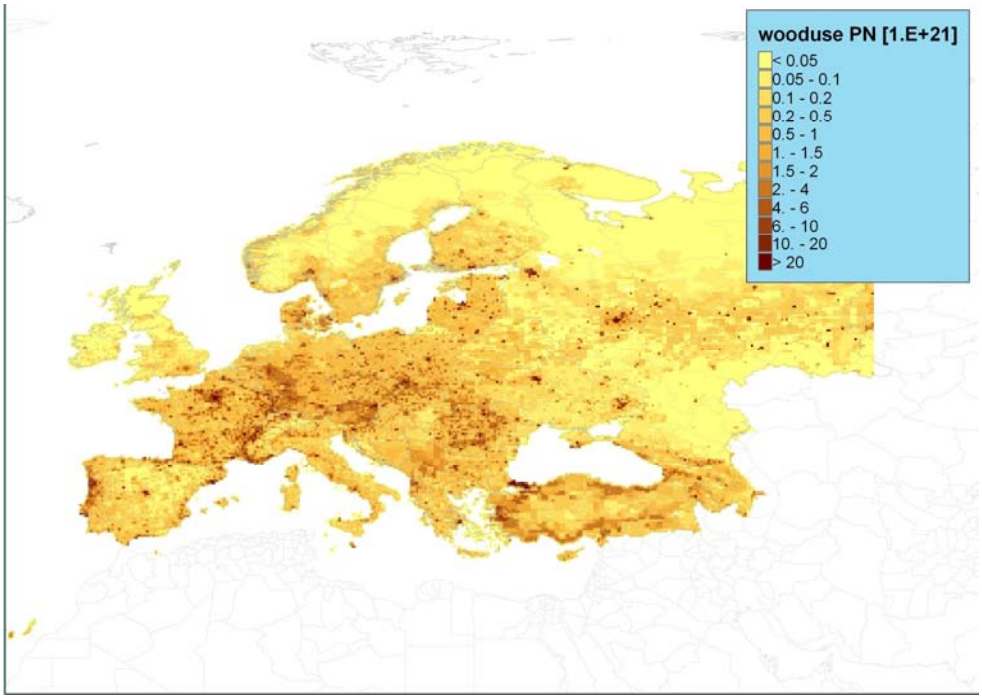

Figure 2. Distribution of total particle number (size range 10-300 nm) due to residential wood combustion in Europe in 2005.

Finally the PN emissions are split into discrete size bins (Table 1). These size bins have been proposed by EUCAARI modelers to optimize implementation of the PN inventory in their models.
The ~70 source categories distinguished in the underlying database are aggregated to the so-called SNAP-level 1 categories (Figure 1) with a detailed split for road transport and residential combustion. The results show that road transport and residential combustion dominate the total PN emissions. The PN inventory covers all particles in the 0-300 nm size range. Thereby it captures the majority of PN by far. The mass of PM > 0.3 um contributes very little to total PN and can be ignored. An example of the total PN emitted from a source category is presented in Figure 2.
The PN inventory was a deliverable within EUCAARI that was delayed and is severely needed by other WPs to make further progress and address EUCAARI questions. As of November 2009 it can be downloaded by EUCAARI partners and used in their research.

Task 1.3.2 Pan-European Carbonaceous aerosol emission inventory

Understanding the role of aerosols on human health and climate requires chemically speciated emission inventories. Among the needed speciation is a split in the carbonaceous and non-carbonaceous aerosols. The carbonaceous aerosols should at least be further split into elemental carbon (EC) and organic carbon (OC). TNO, SU and IIASA developed an EC and OC inventory for the year 2005 with special emphasis on the role of wood combustion. The emission of anthropogenic particulate elemental carbon (EC) and organic carbon (OC) from Europe is calculated for the year 2005. The inventories are based on previous particulate matter (PM) inventories, especially the IIASA GAINS model.

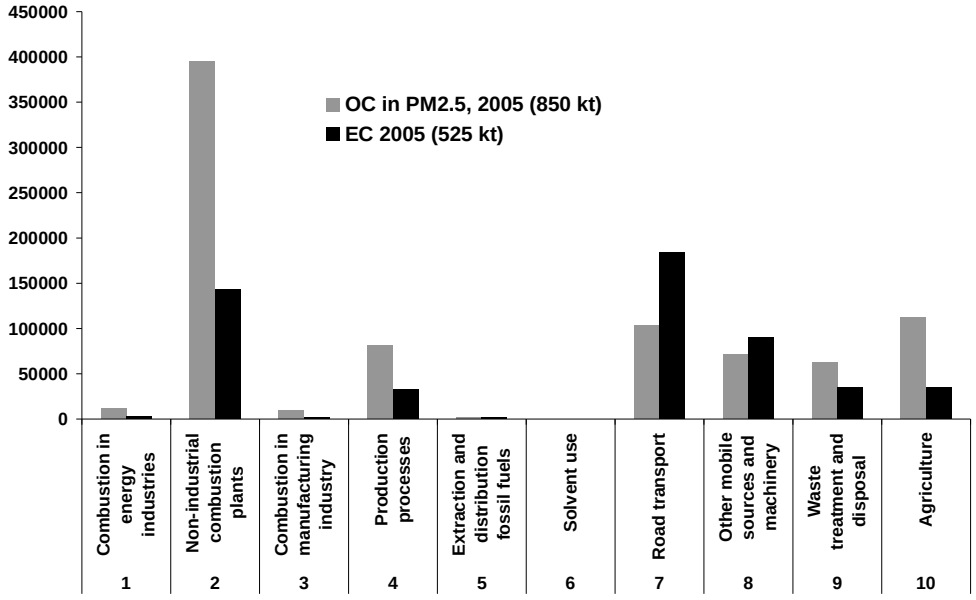

Figure 3 Emission (tonnes) of EC and OC in PM2.5 for Europe in 2005 by source sector (SNAP level 1)

Representative EC and OC fractions are selected and applied to ~200 individual GAINS PM source categories and separated in < 1μm, 1-2.5 μm and 2.5-10 μm size classes. The total EC and OC emission is constrained by the amount of PM emitted which limits uncertainty. Total PM2.5 for UNECE Europe excluding international shipping amounts to 3400 kt and about half of this is carbonaceous aerosol (organic matter). Primary sources of *non*-carbonaceous particles are combustion in industries and residential combustion, comprising fly ash and suspended product particles. The largest OC source in Europe is residential combustion of wood and coal (Figure 3). EC emissions are dominated by road transport (diesel) and non-road transport (diesel and fuel oil). Total carbonaceous aerosol for Europe in 2005 amounts to ~2000 kt/yr of which ~10% is due to international shipping.
The emissions are gridded on a 1/8 º x 1/16 º resolution (or approximately 7x 7 km) using especially prepared distribution maps. The gridded data have been made available to the model WPs in EUCAARI in March 2009 and are currently being used by e.g. the EMEP model and CAMx in e.g EUCAARI WP 3.4.

Task 1.3.3 Size-resolved particle emissions of marine and pyrogenic aerosols
The size resolved marine aerosol emission have been delivered by NIUG and FMI in 2008 (See WP 1.3 abstract 2008). The developed source function is described in more detail by O'Dowd et al. 2008.

For the pyrogenic aerosols from biomass burning emission factors have been developed by MPI-C (Janhäll et al. 2009). Published experimental data and different fitting procedures are used to derive particle number and mass emission factors (EFPN, EFPM) related to fuel category and mass of dry fuel burned as well as characteristic scaling ratios between particle and carbon monoxide emissions (PN/CO, PM/CO). Moreover, the variability of the smoke particle size distribution is characterized. The particle size distribution is typically dominated by a lognormal accumulation mode with count median diameters in the range of 100-150 nm (depending on age, fuel and combustion efficiency). The emissions of particles are mainly described by linear relations to the modified combustion efficiency, MCE, defined as the ratio between the carbon emitted from the fire as carbon dioxide and the carbon emitted from the fire as carbon dioxide and carbon monoxide as a total. $MCE = (\Delta CCO2) / (\Delta CCO2 + \Delta CCO)$

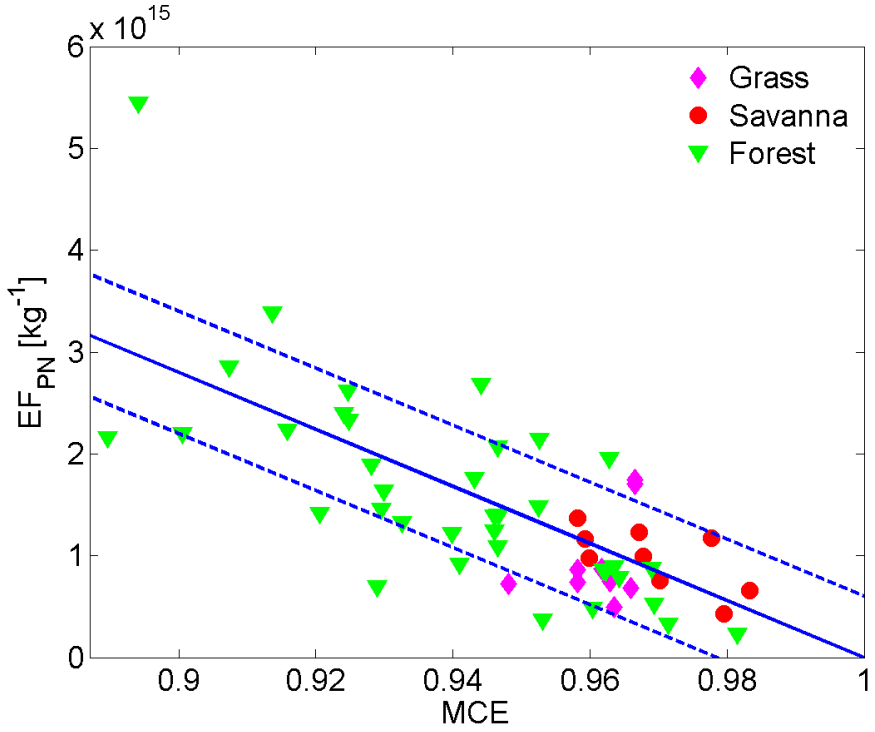

Figure 4. Emission factor of particle number versus modified combustion efficiency (MCE) (Janhäll et al. 2009)

An example of the fittings is shown in Figure 4, for the emission factor for particle number, EFPN, from different fuels. The result of the work done under this task is a description of the particle emissions from biomass burning, relating the variables to modified combustion efficiency and fuel. It describes both the particle number, particle mass and particle size distribution of the emissions.

FUTURE PLANS AND INTEGRATION

Task 1.3.4 Evaluation of the accuracy and optimization of the inventories

This work will mostly be done interactively with the modelers working with the out put of WP 1.3. A recent example has been presented by Simpson and Yttri (2009) where the EC / OC inventory will be used to test new schemes for secondary organic aerosol formation.. Furthermore, Risø (Sorensen et al.) have worked on an evaluation of the sea spray fluxes by comparing the proposed calculation schemes with observations from different cruises. However, within EUCAARI little time (and no budget) is availbel to make major changes in the reusults from WP 1.3. Hence, major shortcomings or potential improvements will be listed as recommendations for future research.

Finally the work done in WP 1.3 should be further documented and published. A preliminary list of submitted and/or planned publications with EUCAARI acknowledgements:

Denier van der Gon, H., A. Visschedijk, R. Droge, M. Mulder, C. Johansson, Z. Klimont, A high resolution emission inventory of particulate elemental carbon and organic carbon for Europe in 2005.

Janhäll, S., M.O. Andreae and U. Pöschl, Biomass burning aerosol emissions from wildfires: particle number and mass emission factors and size distributions

Johansson, C., E. Hedberg, C. Boman, H. Denier van der Gon, A. Visschedijk, Particle number emission factors for residential biomass burning, (in prep.)

Visschedijk, A., Denier van der Gon, H., Emission inventory of ultrafine particles and particle numbers from coal and oil-fired power plants in Europe.

Denier van der Gon et al. A first European size-resolved particle number emissions inventory.

References

Beddows, D., R.M. Harrison (2008) Comparison of average particle number emission factors for heavy and light duty vehicles derived from rolling chassis dynamometer and field studies, Atmos. Environ. 42 7954–7966

Denier van der Gon, H., A. Visschedijk, Emission inventory of ultrafine particles and particle numbers from coal and oil-fired power plants in Europe, EFCA International Symposium, Brussels, Belgium, May 19 and 20, 2009

Denier van der Gon, H., A. Visschedijk, R. Droge, M. Mulder, C. Johansson, Z. Klimont (2009) A high resolution emission inventory of particulate elemental carbon and organic carbon for Europe in 2005, paper presented at 7th International Conference on Air Quality - Science and Application (Air Quality 2009), Istanbul, 24-27 March 2009

Janhäll, S., M.O. Andreae and U. Pöschl, (2009) Parameterization of biomass burning particle emissions from wildfires, European Aerosol Conference 2009, Karlsruhe, Abstract T057A11

O'Dowd, C. D., B. Langmann, S. Vargahese, C. Scannell, D. Ceburnis, and M. C. Facchini, (2008), A combined organic – inorganic sea – spray source function, *Geophys. Res. Letts.*, *35*, L01801, doi:10.1029/2007GL030331.

Simpson D., K.E. Yttri (2009) Source-apportionment and model evaluation: experiences with the EMEP SOA model Geophysical Research Abstracts, Vol. 11, EGU2009-12423, 2009

EUCAARI WP1.4: MULTICOMPONENT AEROSOL PARTITIONING AND THRMODYNAMICS: towards an accurate simplified model for the partitioning of semi-volatile components to a multicomponent condensed phase

WP1.4 Team* and Gordon McFiggans

School of Earth, Atmospheric and Environmental Science, University of Manchester, Manchester, M13 9PL, UK

D. O. Topping, M. Barley, D. Lowe, T. Williams, M. E. Jenkin, UMAN, S. L. Clegg, UEA, A. Zardini, I. K. Koponen, G. P. Frank, M. Bilde, UKBH, C. Facchini, S. Decesari, M. Mircea, ISAC, G. Kiss, ACUV,I. Riipinen, M. Kulmala, UHEL, K. Lehtinen, F, MIT. Mentel, FZJ, U. Baltensperger, PSI, E. Swietlicki, ULUND

Keywords: Thermodynamics, Gas / Particle partitioning, Organic aerosol.

1.INTRODUCTION

The objective of workpackage 1.4 in the EUCAARI project is to provide a traceable, evaluated module for the partitioning of semi-volatile components between the gas phase and multicomponent aerosol particles. The intention is to use the best current knowledge to investigate the variability of molecular distribution of low volatility and semi-volatile organic compounds predicted to be in the condensed phase under equilibrium conditions, to evaluate these predictions against field and / or chamber observations and to derive a simplified representation of the partitioning capable of being used in large scale models. This simplified treatment is to be evaluated against benchmark thermodynamic code developed within the workpackage.

A description of gas to particle mass transfer of semi-volatile components, driven by a difference in equilibrium vapour pressure and actual partial pressures above an aerosol particle, is necessary when determining the evolving chemical composition of the particle and for predicting aerosol loading and composition. Pure component vapour pressures for dominant atmospheric condensable organic compounds are not readily available and activity coefficients of the components in their mixtures are not straightforwardly calculated. Complex numerical representations of the equilibrium particulate loading and composition must be evaluated against atmospheric measurements prior to their simplification and simplified code must be benchmarked against rigorous thermodynamic treatment of the component mixtures.

Task 1.4.1 Generic compound groups representing SOA

A survey of available literature reveals that organic components in ambient particulate exhibit a range of oxygen : carbon (O:C) ratios and molecular weights that can serve as a useful comparator for detailed model predictions (see below). Furthermore, measurements of the change in functionality of the organic fraction of the aerosol as a function of photochemical ageing from a number of locations (as shown in Figure 2) can provide constraint data for simulations of equilibrium partitioning with airmass age. Such data, in addition to broad chemical characterisation of non-refractory aerosol components by Aerosol Mass Spectrometer (AMS) measurements and molecular information from mass spectrometric analyses of filter samples, can be used to assess the skill of any partitioning calculations. The chemical composition measurements provided within WP 2.1 have been assembled to derive simplified representation of SOA by functionality and derived property (e.g. hygroscopicity) as a function of age. As many measurements in as many varied locations and photochemical ages (along with the appropriate hydrocarbon “clock” measurements) have been to inform the lumped organic representation. Solubilities of compounds lumped after the methodology carried out in task 1.4.2 have been described and measurements made of solution water activities and surface tension.

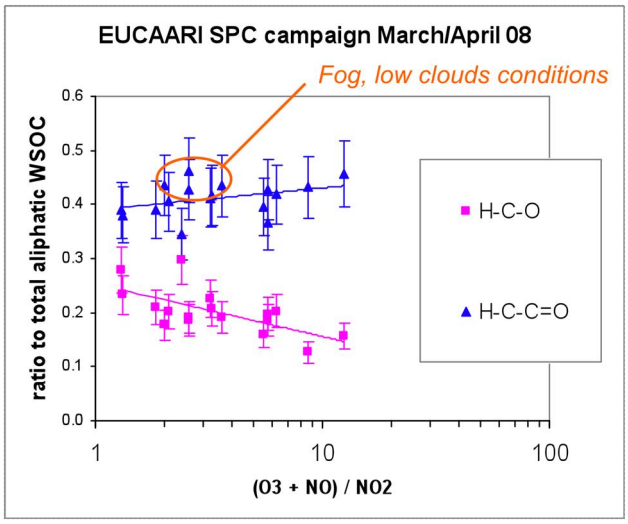

Figure 1. Distribution of O/C ratios and molecular weight (MW) for classes of compounds determined in ambient OOA samples.

1.4.2 VOC oxidation products and their vapour pressures

The Master Chemical Mechanism (MCM) has be used to explicitly simulate the oxidation of atmospheric VOCs in a range of environments. The MCM generates thousands of oxidised organic degradation products that may partition between the gaseous and condensed phase. Equilibrium absorptive partitioning predictions using the model of Barley et al. (2009) of the particulate component loading have been used to inform a series of lumping methodologies for incorporation of a heavily reduced series of

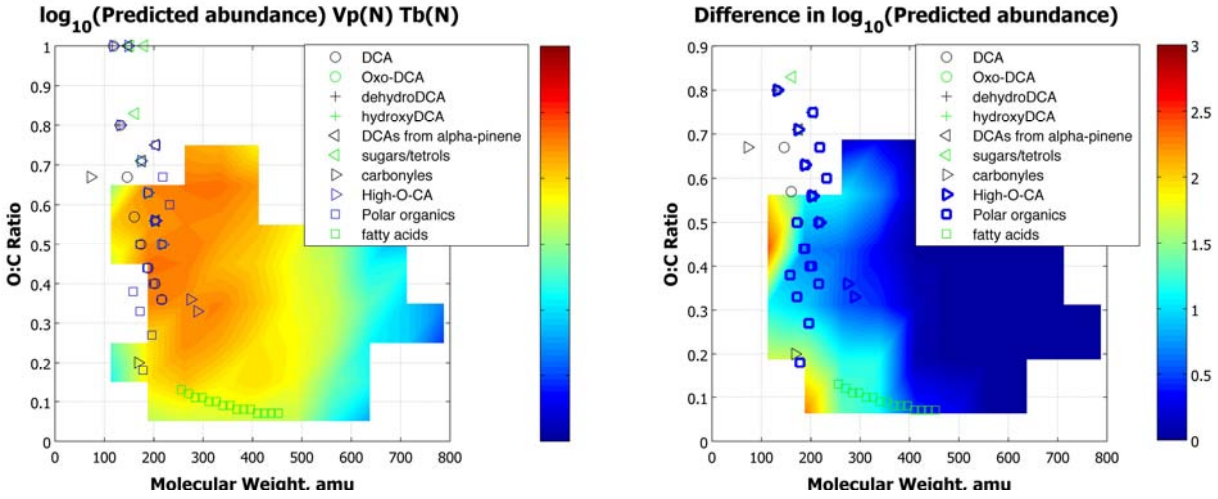

Figure 2: Predicted condensed component O:C ratio and molecular weight. Left panel shows the logarithm of predicted mass concentrations (in μg m^{-3}) using a base case method (overlayed with symbols denoting the values of compounds found in the atmosphere). The right panel shows the difference in the mass concentration logarithm using basing the vapour pressure predictive technique on a widely-used method for boiling point T_b prediction.

representative compounds into a simplified framework in task 1.4.3. This is described more fully in (Topping et al., 2009a, this issue). In order to conduct these simulations, the individual component vapour pressures and their activity coefficients in mixtures are required. These have been calculated in a number of approaches to investigate the sensitivity of the most likely SOA precursor compounds. Figure 2 shows the magnitude of the differences in predicted O:C and molecular weight resulting from use of

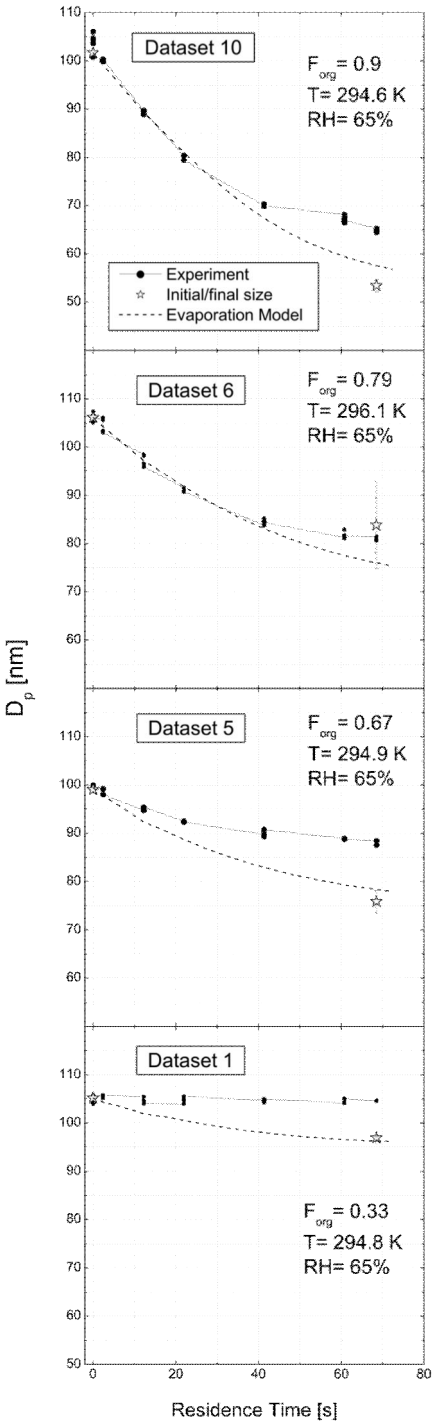

Figure 3 Evaporation measurements of NaCl, succinic acid / water particles performed at ambient T, RH=65%, and different organic mole fraction F_{org} (increasing inorganic salt from top to bottom). The model predicts a faster evaporation for all cases, while the E-AIM model underpredicts the final size except for dataset 6.

two different commonly used vapour pressure predictive techniques. Available vapour pressure techniques have been evaluated in Barley and McFiggans (2009). It is evident that significant variability exists in prediction of vapour pressures to which there is a significant sensitivity.

In order to evaluate and ultimately improve such predictions, two techniques have been employed to provide measurements of vapour pressure. The first is based around evaporation rate measurements using a modified TDMA with a laminar flow system for simplified multi-component aerosols. The measurements have provided experimentally determined evaporation rates and vapour pressure for validation of the predictive techniques and multi-component evaporation models. Figure 3 shows a comparison between experimental evaporation curves and model predictions for ternary droplets made of succinic acid, sodium chloride and water.

The second technique, reported in Booth et al. (2009a, b, this issue), uses a Knudsen Effusion Mass Spectrometer (KEMS) system to measure the solid state vapour pressure of a wide range of multifunctional low volatility components. Sub-cooled liquid corrections are provided by ΔH_{fus} measurements using Differential Scanning Calorimetry (DSC). Vapour pressures of a large number of compounds have been determined and are being used to further evaluate and improve the predictions made by the techniques employed in the absorptive partitioning code.

1.4.3 Model framework for the phase partitioning of organic compounds

The hybrid Partial Derivative Fitted Taylor Expansion (PD-FiTE), reported for inorganic compounds in Topping et al. (2009b), is a reduced complexity thermodynamic model for calculating activity coefficients in solution. This approach uses optimised model parameters describing the interaction between different components resulting in comparable computational performance with existing reduced methods, whilst retaining accuracy of more complete thermodynamic models. PD-FiTE provides a generalised framework for the inclusion of inorganic and organic components. An example of the reduction methodology employed to incorporate organic components is provided in Topping et al. (2009a, this issue). A version of PD-FiTE can be produced for any reduced complexity gaseous VOC degradation scheme, though the skill in reproducing SOA loading will obviously be determined by the ability of the oxidation mechanism to produce the SOA precursors.

Task 1.4.4. Benchmark thermodynamic code adaptation and partitioning model evaluation

The benchmark code, E-AIM, has been developed for the evaluation and improvement of the partitioning code, employing current state-of-the-art thermodynamic models for gas/aerosol partitioning and water uptake. This code is be based upon an assessment of available treatments of multi-component phase equilibrium descriptions applied to atmospherically relevant systems, and their ability to capture measured laboratory behaviour (component activities, vapour pressures etc.). The code has a web interface (http://www.aim.env.uea.ac.uk/aim/aim.php) for interactive use, with user-defined organic compound properties and both vapour pressure and density calculators.
PD-FiTE compares well with E-AIM for inorganic components (H^+-NH_4^+-Na^+-SO_4^{2-}-HSO_4^--NO_3^--Cl^-) at 298.15K and the comparisons are presented in Topping et al. (2009a, this issue). The linear additive framework readily allows inclusion of organic components with the interaction between inorganic / organic components where appropriate data exists. Whilst attempts have been made to formulate detailed coupled thermodynamic models for atmospheric purposes, an interim assessment concluded that a neglective approach which renders the inorganic and organic components uncoupled is preferable (Tong et al 2008).

The partitioning code will be validated against suitable chamber experiments conducted within WP 1.2, and literature data.

Planned publications in the immediate future:

1) McFiggans, Topping, Barley, The sensitivity of Secondary Organic Aerosol component partitioning to the predictions of component properties: part 1; a systematic evaluation of available predictive techniques, in prep.
2) Barley, Topping, Jenkin, Decesari, Kiss, Hamilton, Alfarra, McFiggans, The sensitivity of Secondary Organic Aerosol component partitioning to the predictions of component properties: part 2; an example model-measurement comparison and implications for simplified SOA representation, in prep.
3) Topping, Barley, Kiss, Good, Irwin, McFiggans, The sensitivity of Secondary Organic Aerosol component partitioning to the predictions of component properties: part 3; impacts on predicted aerosol behaviour
4) Booth et al., second paper on comparison of KEMS derived and predicted vapour pressures
5) Booth et al., Large dataset of multifunctional compound solid state vapour pressures with their sub-cooled correction

FUTURE PLANS AND INTEGRATION

Extensive comparison between predictions of SOA mass loading, volatility distribution, functionality, O:C ratio, molecular weight, “mass spectra” and appropriate measurements from EUCAARI field or chamber programmes.

Incorporation of the reduced partitioning code into any host model that wants it and has an appropriate VOC degradation mechanism.

ACKNOWLEDGEMENTS

This work was supported by the National Centre for Atmospheric Science (UK).

REFERENCES (*EUCAARI acknowledged)

*Barley, M. H. and McFiggans, G. (2009), The critical assessment of vapour pressure estimation methods for use in modelling the formation of atmospheric organic aerosol, Atmos. Chem. Phys. Discuss., 9: 18375-18416

*Barley, M.H., Topping, D. O., Jenkin, M.E. and McFiggans, G. (2009), Sensitivities of the absorptive partitioning model of secondary organic aerosol formation to the inclusion of water, Atmospheric Chemistry and Physics, 9:2919-2932

Booth, A. M., Markus, T., McFiggans, G., Percival, C. J., McGillen, M. R. and Topping, D. O. (2009a) Design and construction of a simple Knudsen Effusion Mass Spectrometer (KEMS) system for vapour pressure measurements of low volatility organics, Atmos. Meas. Tech., 2, 355-361

Booth, A. M., Barley, M. H., Topping, D. O. McFiggans, G., Percival, C. J. (2009b) Assessing vapour pressure estimation methods and their impact using Knudsen Effusion Mass Spectromenty (KEMS), this issue

Tong, C. H., S. L. Clegg, and J. H. Seinfeld (2008), Comparison of activity coefficient models for atmospheric aerosols containing mixtures of electrolytes, organics, and water, Atmospheric Environment, 42, 5459-5482

*Topping, D. O., McFiggans, G. B., Barley, M., and Lowe, D. (2009a), Developing reduced complexity parameterisations to calculate gas/particle partitioning in large scale models, this issue

Topping, D., D. Lowe, and G. McFiggans (2009b), Partial Derivative Fitted Taylor Expansion: An efficient method for calculating gas-liquid equilibria in atmospheric aerosol particles: 1. Inorganic compounds, Journal of Geophysical Research-Atmospheres, 114

WP 2.1 Aerosol Transport and Transformation

Leader: P. Laj, CNRS, contributions from K. Sellegri, U. Baltensperger, N. Milahopoulos, S. Decesari, A.-M. Fjaera, G. Kiss, S. Pandis, E. Svietlicki.

WORK PACKAGE OBJECTIVES

WP 2.1 will quantify the evolution of aerosol properties, particularly aerosol mixing state and hygroscopic growth factor upon transport in the Boundary Layer or Lower Free Troposphere. This will be performed by i) direct continuous observation of aerosol mixing state, hygroscopic growth and size segregated chemistry in addition to standard EUSAAR measurements coupled with back-trajectory analyses and ii) intensive observation periods following the evolution of aerosol properties on a temporal scale of 1-3 days. WP 2.1 contributes to EUCAARI objectives 1a and 1b. Simultaneous long-term measurements of the aerosol size distribution, hygroscopic growth and size segregated chemical characterization are theoretically sufficient to estimate the fraction of aerosol particles activated at a given supersaturation, and also the processes responsible for the aerosol evolution. WP2.1 is aimed at providing the experimental data to investigate changes in mixing state and chemistry during transport in the troposphere and analyze results to provide better constrains to Chemistry-Transport modelling.

Work Package 2.1 started at the beginning of the project. The first year has been devoted to the organization of the long-term and intensive observation periods (including intercalibration exercises and instrumental development). The second year is defined as "the measurement year" and includes additional intercalibration exercises and the initiation of the long-term measurement period. In addition, intensive observation campaigns were organized at several sites in Europe at different periods of the year, in close coordination with the EMEP and EUSAAR programs. The third year corresponds to the end of the measurement year (for non-EUSAAR measurements) and the start of data analysis by both WP2.1 groups and the EUCAARI modelling group.

The specific objectives of Work package 2.1 at the beginning of Month 24 and over to month 42 were:

1. To provide a data-base relating long-term observation of aerosol hygroscopic growth, size distribution, size-segregated chemical composition at selected sites over the European continent using a combination of ground-based instruments. **Task 2.1.1 Continuous monitoring of aerosol properties in Europe**
2. To extend monitoring during the intensive observation periods at selected stations to CCN measurements performed at1% supersaturation and to size segregated chemistry in a number of stations performed with Aerosol Mass spectrometers. **Task 2.1.2 Size-segregated chemistry and CCN properties**
3. To monitor the main aerosol variables along aerosol transport corridors identified in WP 4.2 using Airborne Aerosol Mass spectrometers possibly completed by airborne and ground based LIDARs for monitoring aerosol the vertical layering. **Task 2.1.3 Lagrangian experiment**

4. To analyse the continuous data sets describing the evolution of the aerosol size distribution during the transport and the results from the intensive observation periods and to ensure rapid and efficient diffusion of data to the EUCAARI community. **Task 2.1.4 Analysis and processing of Lagragian and continuous measurement data**

The following deliverables related to WP 2.1 were due during the 3rd year of the project:
1- Implementation of long-term observation data base due Month 32
2- Database with HGF from selected stations due Month 32
3- Back-trajectory analysis and HGF evolution for connected flow conditions at selected stations due M36

1- DELIVERABLE 1: IMPLEMENTATION OF LONG-TERM OBSERVATION DATA BASE (JOINT EUSAAR/EUCAARI).

One of the main achievement of the 3rd year of EUCAARI, performed in close cooperation with the I3 EUSAAR is the open access to the data base that now includes 2006 and 2007 data from EUSAAR stations (http://ebas.nilu.no/) and 2008 data from both EUSAAR and EUCAARI (long term and intensive campaign). An unprecedented series of high quality aerosol data is now available to the entire scientific community. it is already the most comprehensive data base regarding in-situ information of advanced aerosol properties in Europe, beside AOD and PM10 information. There is a clear improvement that is expected to continue in the following years.

More specifically, for the 2008 long-term EUCAARI observing period, Table 1 summarizes available measurements for 2008.

Station	Aerosols Properties (Instrument)				
	Scatt. Coeff (Nephelometer)	Size Distribution (DMPS/SMPS)	Abs. Coeff. (MAAP/Aeth./PSAP)	Total Number (CPC)	Org. Carbon / El. Carbon (thermo-optical)
BG0001 BEO Moussala					
CH0001 Jungfraujoch					
CZ0003 Kosetice					
DE0003 Schauinsland					
DE0043 Hohenpeissenberg					
DE0044 Melpitz					
ES0017 Montseny					
FI0050 Hyytiala					
FI0096 Pallas					
FR0030 Puy de Dome					
GB0036 Harwell					
GR0002 Finokalia					
HU0002 K-Pustza					
IN1016 Gual Pahra					
IE0031 Mace Head					
IT0004 JRC Ispra					
IT0009 Monte Cimone					
LT0015 Preila					
NL0011 Cabauw					
NO0001 Birkenes					
NO0042 Zeppelin					
SE0011 Vavihill					
SE0012 Aspvreten					

Table 1: data sets available at http://ebas.nilu.no for 2008. Gree: data available, red: no data sent to EBAS, white: no measurements performed

As shown in the table, reporting of size distribution with SMPS/DMPS data is very good with 19 sites sending their information (as respect to a total of 21 SMPS running in theory). The situation is also very positive for Abs. Coefficients measured using MAAP, PSAP and/or Aethalometers (17 reported for a total of 17 instruments running at EUCAARI sites). Overall, 78 data sets were expected in 2008 and 72 data sets have been reported by EUSAAR/EUCAARI partners. This is a very good score (reporting factor of 92,3%), much higher than in any previous long-term studies. This represents a very substantial improvement as respect to 2006 and 2007 data. The current situation should be compared to pre-EUCAARI / pre-EUSAAR situation where information on aerosol properties was very difficult to obtain. For example, centralized long-term size distribution information was available for 3 sites only in 2003 (see Figure 1). This is a very substantial improvement. However, a challenge ahead will be to maintain the reporting efficiency as high for 2009 data (reporting deadline July 31, 2010).

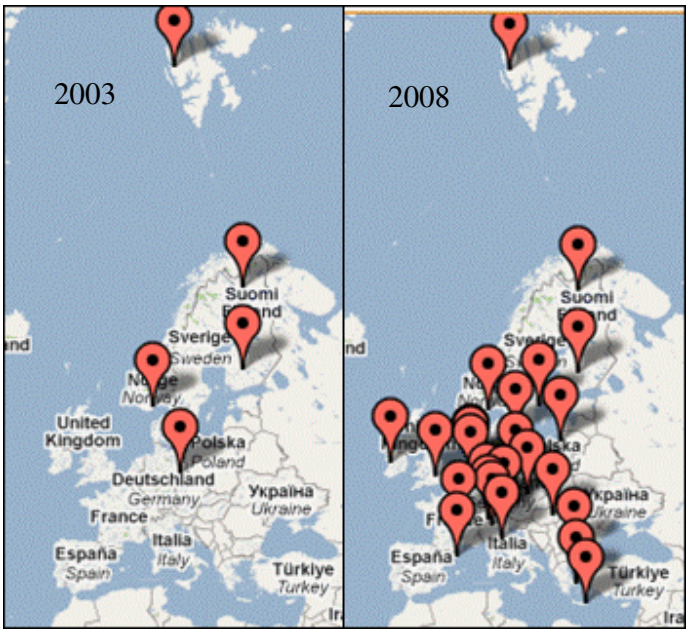

Figure 1: station reporting aerosol variables in 2003 and 2008 over the EUCAARI domain.

Several remarks can be made concerning the data base: the open data policy of EUSAAR/EUCAARI long-term for non-commercial use is a clear encouragement to the whole scientific community to use the information. The data base, and more specifically the SMPS information, has already been used by EUCAARI partners to propose a very complete view of aerosol size distribution world-wide. Recommendation to offer coauthorship to data providers whenever substantial use is made of the data is also a strong incentive to promote collaboration between data providers and users.

It should be noted that data reported to EBAS is also quality controlled and reported under similar format (modified NASA-AMES according to EUSAAR recommendations). Data quality has been achieved by running a series of regular calibration workshops for

size distribution and aerosol optical properties as well as joint Round Robin intercomparison exercises for chemical analysis. Objectives of the intercomparison exercises were to characterize the different instruments and methods, to evaluate their intercomparability, and to develop technical standards intended to form a minimum of measurement requirements. This first series of workshops have already contributed to developing harmonized measurement and analysis procedures for the methods.
Results do show that improvement still is necessary in terms of data quality. For that reason data are reported with the following quality level (Table 2).

	SMPS	Scatt. Coeff.	Abs. Coeff	OC/EC
Level 0: raw information	Never seen by users	Never seen by users	All information in BC is level 0	Level 0 if open filter OC/EC measurements
Level 1: pre-processedinter mediate data in STP	Level 1 provided at most site. Intercomp but not necessarily follow all recommendation (higher uncertainty)	Level 1 data when use neph other than TSI or TSI without additional controls	Not able to provide level 1 data yet for aethalometer	Some level 1 data
Level 2: EUSAAR quality Objectives	Some level 2 data when passed intercomp. Studies and follow Wiedensohler et al., 2008 recommendations	Level 2 data when follow EUSAAR/GAW operational procedures + use TSI neph.	Level 2 when Bond et al., or Weingartner et al , or EUSAAR corrections are used	No level 2 data yet (negative artefact accounted for)

This information is particularly required for OC/EC measurements. The different EUCAARI laboratories involved in OC/EC data provision are still showing a large inter-variability reporting reference filters, despite the use of a standard protocol. Different problem arises for the abs. coeff. data. Here, recommendations are to avoid reporting BC (plagued by substantial uncertainties until correction procedures are not available for all instruments) and to limit reporting to light attenuation and calculated abs. coefficient. For both OC/EC and absorption coefficients, quality level of data is not optimal and shall be considered only level 0 or level 1 data. Instead, data quality for scattering coefficient and size distribution is much better and most data are reported in level 2.

2- DELIVERABLE 2: DATABASE WITH HGF FROM SELECTED STATIONS (DUE MONTH 32)

In the framework of EUCAARI/EUSAAR activities and complementary to long-term regular aerosol observations at EUSAAR sites, a long-term monitoring of aerosol hygroscopic growth has been performed within the framework of EUCAARI. The work has been made possible by the common development of monitoring HTDMAs (Hygroscopic Tandem Differential Mobility Analyzers) by 11 participating institutions in EUCAARI. Several workshops and intercomparison exercises were performed to ensure

intercomparibility of measurements and data retrievals. The performance of custom-built H-TDMA systems was harmonize and recommendations for atmospheric measurements and their data evaluation proposed. The H-TDMA systems have been compared in terms of particle dry sizing, RH (relative humidity) uncertainty, and consistency in determination of number fractions of different hygroscopic particle groups. To obtain harmonization, all systems were intercompared in air conditioned laboratory and and standard calibration procedures applied. Subsequently, data from H-TDMA running at EUCAARI sites were processed using the individual data evaluation procedure and an independent data evaluation procedure. Particle dry sizing of the six H-TDMA systems was within 0.2 to 4.2% (external data evaluation) and within 0.2 to 4.1% (internal data evaluation) in relative uncertainty depending on investigated size and individual system. Results for individual systems differed at most 4% comparing external and internal data evaluation. With regard to RH uncertainty, the H-TDMA systems showed deviations up to 4.5% RH (external data evaluation) and up to 4.5% RH (internal data evaluation) from the set point at RH = 90% investigating the hygroscopic growth of ammonium sulfate particles. Results from the use of the different data evaluation procedures showed a difference of up to 1.9% RH determined for one and the same system. The evaluation of number fractions investigating an externally mixed aerosol delivered differences up to +/- 8% (external data evaluation) and +/- 7% (internal data evaluation) in calculated number fraction for one and the same aerosol type. A comparison of the use of the external and internal data evaluation procedures resulted in slightly different values +/- 9% for individual H-TDMA instruments. A series of running recommendations have also been issued by EUSAAR/EUCAARI teams involved. Measurements have been performed from May 2008 to May 2009 at 11 EUCAARI sites. Due to technical problems, not all sites are reporting a full year of measurements. Figure 2 summarizes the status of HTDMA measurements within the project.

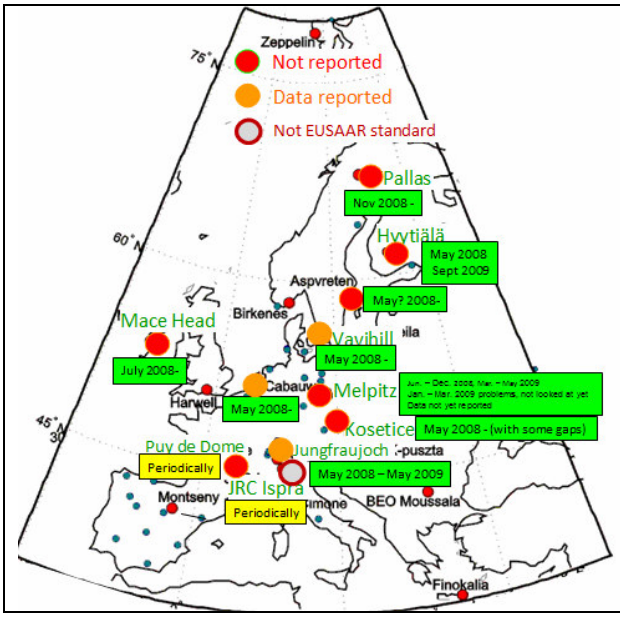

Figure 2: status of H-TDMA measurements and reporting as of October 2009.

Due to difficulties inverting data sets, not all information is currently included in EBAS. So far, data from Vavihill (May-Dec 2008), Jungfraujoch (May 2008 - May 2009) and Cabauw (May 2008) are in the data base. However, we expect additional data to be downloaded in EBAS before the end of the reporting period (Month 36 instead of Month 32). In any case, measurements performed within the EUCAARI measurement year by far exceed what was expected from the EUCAARI DoW.

3- DELIVERABLE 3: BACK-TRAJECTORY ANALYSIS AND HGF EVOLUTION FOR CONNECTED FLOW CONDITIONS AT SELECTED STATIONS DUE M36

Analysis of HTDMA measurements proceed at the different institutes involved in the study. So far, HTDMA measurements from Vavihill, Jungfrajoch and Puy de Dôme stations have been connected to back-trajectory analysis. However, different strategies were chosen by the different research groups to proceed with the data analysis.

3.1. Preliminary Results from Puy de Dôme station

Results from the puy de Dôme station are preliminary but still, differentiation of hygroscopic growth factors can be made in the basis of air mass origins. Results for 3 intensive observation periods are presented in Figure 3.

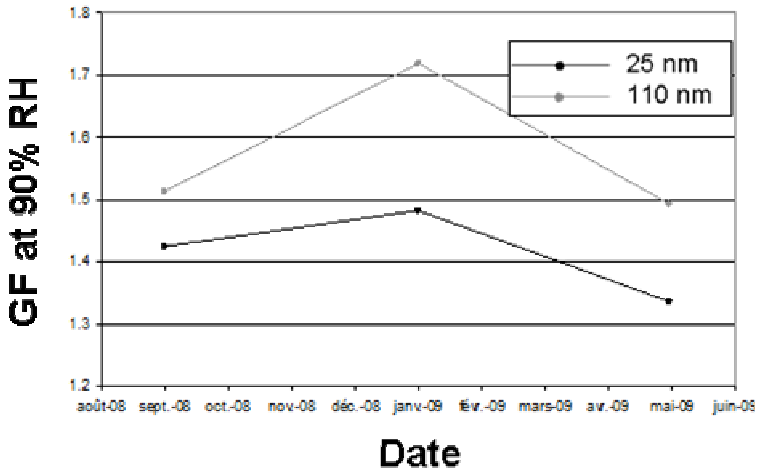

Figure 3: average GF at 90%RH for 25nm and 110 nm particles for 3 intensive observing periods at Puy de Dôme.

The average growth factor is changing according to seasons with higher GF in winter as respect to summer. This is likely linked to origin of the sampled air masses mostly from regional background in summer (short lifetime) and from long-range transport in winter. Aging of the air mass, especially for the Aitken mode particles is likely responsible for the evolution of GF towards higher values.
Presenting the average GF is somewhat misleading since 2 or more hygroscopic modes are usually found. The number fraction of the less hygroscopic mode (GF= 1.1±0.1) is relatively low (2%<FN1<18% at 25nm and 8%<FN1<17% at 110nm) and is not seen in wintertime. The more hygroscopic mode (1.3<GF<1.5) is extremely numerous for 25nm particles (46%<FN2<68%) much less 110nm particles (9%<FN2<25%). Finally, the very hygroscopic GF>1.6±0.1 is mostly found amongst 110 nm particles (FN4=40%) while

being much less present at 25 nm (FN4=8%). Additional work is needed to further analyse seasonal variability of GF at puy de Dôme.

3.2. Preliminary Results from Vavihill station

Vavihill HTDMA has been running on average 62% of the time between May 2008 and May 2009. On some month, data coverage is close to 100% of the time and only 2 months during the period have coverage below 15%.

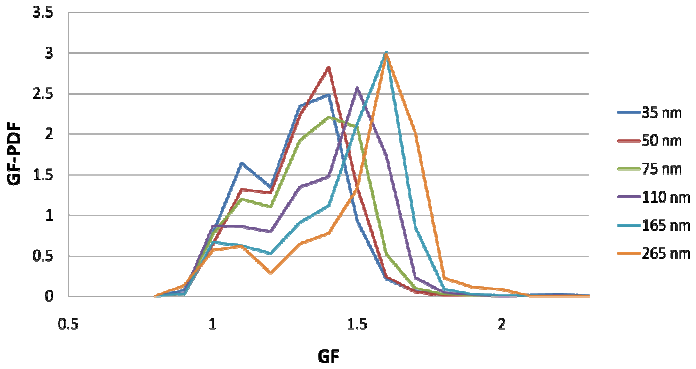

Figure 4: variability of GF 90% at Vavihill for different particle sizes during the May 2008-May 2009 period.

The variability of GF frequencies during the 1-yr measurement at Vavihill is shown in Figure 4. Three different hygroscopic modes can be identified with different frequencies according to particle sizes.
To be completed

3.3. Preliminary Results from Jungfrajoch station

The annual cycle of the hygroscopic growth factor (GF) at Jungfraujoch showed no clear annual trend (Figure 4A). GFs were similar for all sizes, i.e. the size dependence can largely be explained by the Kelvin effect.
The slightly lower GFs during winter (November 08 – February 09) can be attributed to the higher fraction of the less-hygroscopic particles (Figure 4B), while the GF of the particles with GF > 1.25 is in winter not different to other months (Figure 4C).
During summer (June – August 08) the lower GFs can be attributed to the lower GF of the more hygroscopic particles (Figure 4C). This is explained by the higher fraction of organics that condensed on the particles due to higher photochemical activity.
Analyses of diurnal cycles clustered by alpine weather classes revealed the GF to be influenced by vertical transport but not so much by wind direction. A possible exception are air masses from south that were shown to have higher BC fractions (BC mass per total particle concentration), compared to other air masses. Trajectory analyses are of interest for such cases but are not possible because aged air masses are disturbed by small-scale turbulences and local sources in the in alpine valleys south of Jungfraujoch.
Saharan dust events typically result in large fractions of the less hygroscopic mode for the larger sizes (larger than about 150 nm).

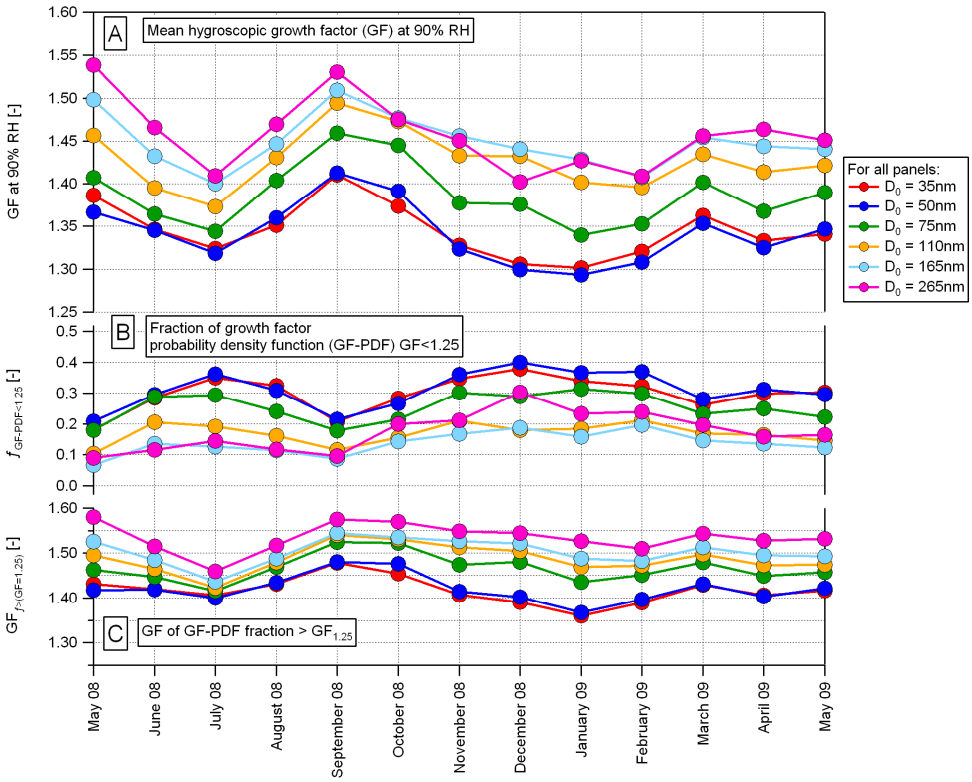

Figure 4: Annual cycles of A) the mean hygroscopic growth factor (GF) at 90% relative humidity (RH), B) of the fraction of the growth factor probability density function (GF-PDF) at GF < 1.25 and C) of the GF of the GF-PDF-fraction > $GF_{1.25}$.

4- OTHER ACTIONS: SUMMARY OF ACTIVITIES DURING GROUND BASED INTENSIVE CAMPAIGNS (EMEP).

4.1. Highlight from Finokalia Experiment (N. Mihalopoulos)

A Quadrupole Aerosol Mass Spectrometer (Q-AMS) was employed at Finokalia during the EUCAARI intensive campaign of May 2008 to measure the size-resolved chemical composition of non-refractory submicron aerosol (NR-PM_1) at ambient relative humidity, and to quantify the extent of oxidation of the organic aerosol. The largest fraction of the NR-PM_1 sampled was ammonium sulfate and ammonium bisulfate, followed by organics, water, and a small amount of nitrate (see Figure 5) . The particles were internally mixed and liquid. There was no statistically significant diurnal variation in the bulk composition of NR-PM_1; however, the extent of organic oxidation exhibited statistically significant diurnal variation. The organic aerosol was highly oxidized, regardless of the source region. Total organic aerosol concentrations also varied little with source region, suggesting that the sources of organic aerosol were mostly regional. These effects of atmospheric processing on organic aerosol will need to be included in air-quality models to accurately represent organic aerosol concentrations, processing and fate in the

atmosphere. All these results are presented in Hildebrandt et al. Aged Organic Aerosol in the Eastern Mediterranean: The Finokalia Aerosol Measurement Experiment – 2008, to be submitted to ACP.

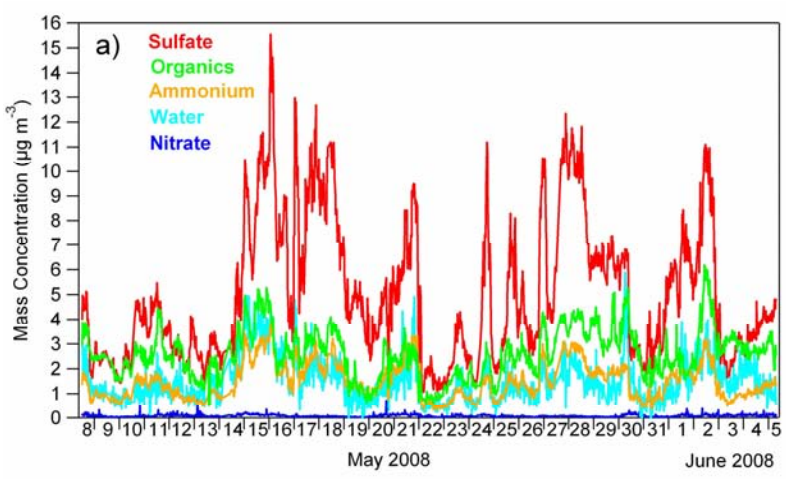

Figure 5: AMS-derived aerosol chemical composition during the Finokalia campaign 08.

4.2. Highlight from San Pietro Capofiume Experiment (S. Decesari)

An intensive field campaign was held in San Pietro Capofiume from 29 June to 12 July 2009 with the aim of investigating the photochemical formation of secondary aerosols at a European polluted rural site. The EUCAARI groups participating to the campaign were: CNR-ISAC, UHEL, NUIG, UKU, UNIMAN, UNIBHAM, DWD, Aerodyne Res.. All the instrumentation performed well. The analysis of the data is still underway. Preliminary findings include: A) new-particle formation can be described as a function of sulphuric acid concentration through a simple kinetic model; B) an increase of the concentrations of sulphate and oxidized organic particles is typically observed in the middle of the day pointing to either a photochemical origin or to the result of entrainment of aged pollution air travelling in residual layers between 500 and 3000 m above the ground (based on lidar profiles); C) the new soot-photometer (SP) - AMS provided first ambient measurements of BC mass concentrations, showing a good correlation with the optical measurement of BC (PSAP) (see Figure6).

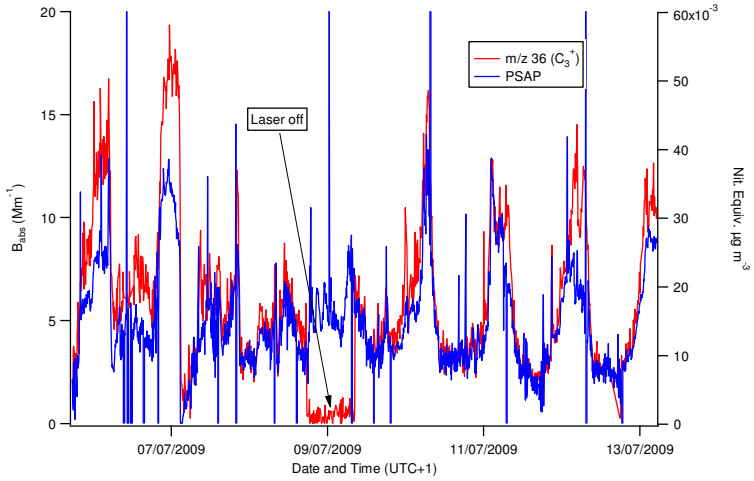

Figure 6: comparison between PSAP and AMS-derived BC during the Po Valley experiment 08.

4.3. Highlight from K-Puszta Experiment (G. Kiss)

Not received yet

5- FUTURE PLAN AND INTEGRATION

Del. no.	Deliverable name	WP	Date due	Actual/ Forecast delivery date	Estimated indicative person-months *)	Used indicative person-months *)	Lead contractor
DXX	Implementation of long-term observation data base for 2009	2.1	M48	M48			CNRS/NILU/Lund
DXX	Scientific publications related to EMEP and airborne intensive campaigns	2.1	M48	M48			All WP2.1 partners
DXX	Analysis of HGF evolution at selected stations	2.1	M48	M48			SU/CNRS

6- ADDITIONAL REFERENCES

- Venzac, H., Sellegri, K. & Laj, P, Seasonal variation of aerosol size distribution at puy de Dôme (1465 m asl, Central France), Atmospheric Chemistry and Physics, Vol.9, n°4, p. 1465-1478, 2009.
- Cristofanelli, P., A. Marinoni, J. Arduini, U. Bonafè, F. Calzolari, T. Colombo, S. Decesari, R. Duchi, M. C. Facchini, F. Fierli, E. Finessi, M. Maione, M. Chiari, G. Calzolai, P. Messina, E. Orlandi, F. Roccato, and P. Bonasoni. Significant variations of trace gas composition and aerosol properties at Mt. Cimone during

air mass transport from North Africa - contributions from wildfire emissions and mineral dust. Atmos. Chem. Phys., 9, 4603-4619, 2009.

- Dall'Osto et al., Characterization of aerosol properties under different air masses influences at the Mace Head Global Atmosphere Watch (GAW) station during the summer EUCAARI 2008 campaign, submitted to Atmos. Chem. Phys. Discuss.
- Saarikoski et al., Chemical characterization of springtime aerosol in the Po Valley, Italy. Paper to be submitted to ACPD within 2009.
- Lea Hildebrandt, Gabriella J. Engelhart, Claudia Mohr, Evangelia Kostenidou, A. Bougiatioti, Peter F. DeCarlo, Andre S.H. Prevot, Urs Baltensperger, Nikos Mihalopoulos, Neil M. Donahue, Spyros N. Pandis Aged Organic Aerosol in the Eastern Mediterranean: The Finokalia Aerosol Measurement Experiment – 2008 Atmos. Chem. Phys., to be submitted.

- Lee B. H., E. Kostenidou, L. Hildebrandt, I. Riipinen, G. J. Engelhart, N. Mihalopoulos, A. S. H. Prevot, U. Baltensperger, and S. N. Pandis (2009) Measurement of the Ambient Organic Aerosol Volatility Distribution: Application during the Finokalia Aerosol Measurement Experiment (FAME-2008), Atmos. Chem. Phys., to be submitted.
- Pikridas M., K. Bougiatioti, G. J. Engelhart, L. Hildebrandt, E. Kostenidou, C. Mohr, G. Kouvarakis, P. Zarmpas, M. Psichoudaki, S. Gagne, N. Mihalopoulos, C. Pilinis, A. S. H. Prevot, U. Baltensperger, M. Kulmala, S. N. Pandis (2009) The Finokalia Aerosol Measurement Experiment 2008 (FAME-08): An Overview, Atmos. Chem. Phys., to be submitted.

GROUND SITE DEVELOPMENT AND AEROSOL CHARACTERIZATION IS DEVELOPING COUNTRIES

Alfred Wiedensohler on behalf of WP 2.2 and WP 4.1

Leibniz Institute for Tropospheric Research, Leipzig, Germany

Studies that have investigated number size distributions or concentrations of aerosol particles in Asia, Latin America or Africa are very few even though the air pollution problem is particularly serious in the mega cities of South and East Asia. Especially, cities like Delhi, Kolkata (Calcutta), Mumbai (Bombay), Dhaka, Karachi, Bangkok, Beijing, Shanghai, Jakarta, and Manila are concerned to be one of the most polluted cities. The major source of particulate matter (PM) and air pollution in the above mentioned megacities is due to rapid urbanization and increasing energy production, vehicle density, and industrialisation. The emissions from internal combustion engines have been regulated solely on the basis of total PM emission even though ambient particulate matter can also be characterized by other parameters like number concentration, mass size distribution, number size distribution and modality of size distribution.

Due to their rapid development, China, India, South-Africa, and Brazil are main contributors to air pollution in the corresponding regions. China and India will become more and more significant players in the global economy with all the accompanying problems of water, soil, and air pollution. Large regions in these countries are strongly influenced by particulate emissions, a fact visible due to satellite observations. Brazil is a main contributor to the haze over South- America mainly due to biomass burning. South Africa is one of the main producers of electric power in the southern part of Africa and contributes significantly hereby to regional aerosol formation. The atmospheric aerosol and its regional and global impacts are much less investigated and understood in such rapidly economically developing countries than in Europe or North America. Furthermore, regional air quality is rapidly changing and short-term measurements cannot reflect the actual situation. Good quality long-term data sets of physical, chemical, and optical characteristics are rare, and these are urgently needed to underpin policy making. Intensive field studies by the international community brought some insights, but not enough to understand quantitatively the impact on regional climate and air quality.

Four measurement stations were established outside Europe in beginning of 2008. Their locations were chosen to represent major regional pollution sources in four different countries in three continents. In Asia measurement sites are close to two mega cities, Peking and New Delhi. In South-Africa the site is in a heavily industrialized area and in South-America the site was chosen so that particulate matter from forest fires and continental Amazonian background can be monitored. To reach the goal of representative measurements, sampling sites for regionally aerosol measurements were be established in cooperation with selected local partners. To obtain a useful data set for climate and air quality issues, in-situ aerosol parameters measured on ground should be combined with vertical aerosol information. The in-situ parameters measured are the light scattering coefficient (nephelometer), light absorption coefficient (absorption photometer) and number size distribution (mobility size spectrometer). Chemical characterization of particles will be by filter sampling with size ranges, P10 and PM1. For the vertical aerosol information, Raman lidars will be used along with sun photometers. A Raman lidar provides the vertical profile of the extinction coefficient and additionally information about the boundary evolution and possible aerosol layers in different altitudes. The total measurement period for the in-situ measurements was planned to be two years, while for the filter sampling and lidar measurements is foreseen only for a period of one year.

China: Shangdianzi

Measurements of particle number size distribution (3nm~10µm) were conducted from March, 2008 to August, 2009 at Shangdianzi Regional Background station in northern China. The data coverage was approximately 80%. Presently, the size spectrometers are back to Germany because of custom reason and for maintenance. The measurements will then be continued until end of 2010.

	Nnuc (cm-3) 3-25nm	NAit (cm-3) 25-100nm	Nacc (cm-3) 100-1000nm	Ncoa (cm-3) 1-10µm	Ntot (cm-3)	Stot (µm2cm-3)	Vtot (µm3cm-3)
Min	4	19	49	<1	424	11	<1
25%	511	2107	1104	<1	6391	214	11
Median	1212	3644	2772	1	9780	519	28
75%	2846	5790	5182	3	13646	1013	61
Max	118770	54196	34070	198	124725	4564	1560
mean	3606	4429	3468	2	11505	690	46
std	7948	3376	2825	4	9232	601	64

Table 1: Statistic of the number size distribution of Shangdianzi, China

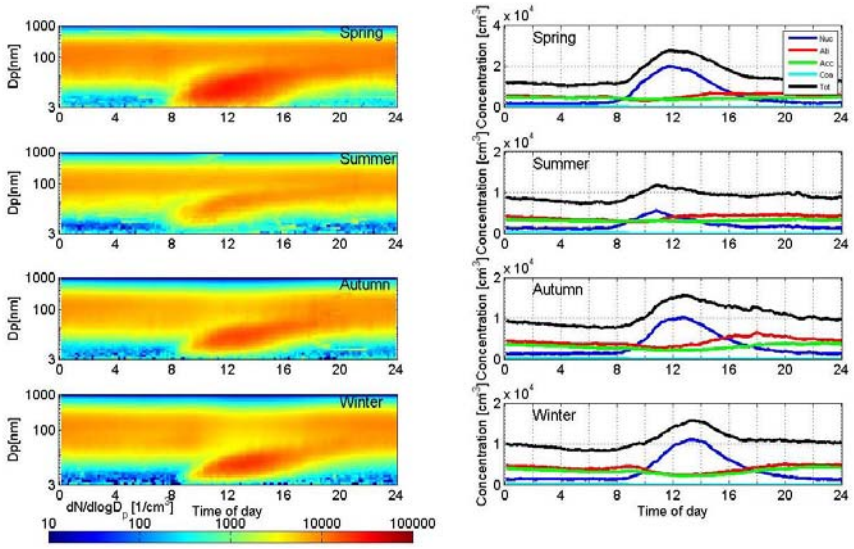

Figure 1: Diurnal behavior of the number size distribution and concentration

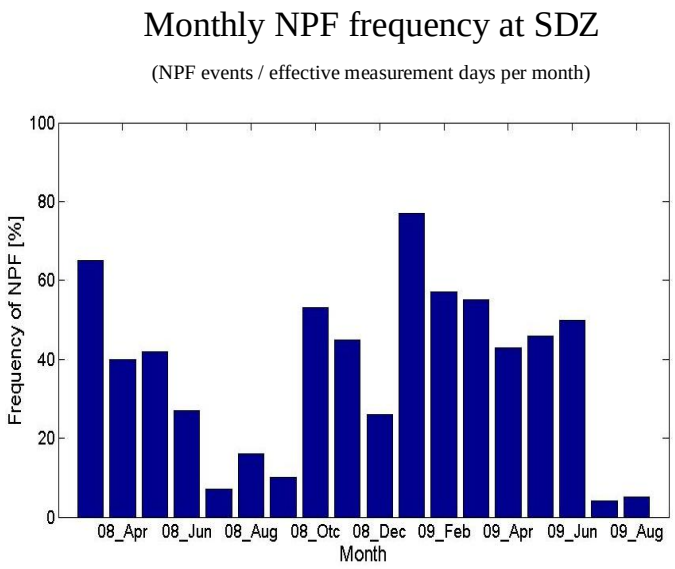

Figure 2: Frequency of the new particle formation event

In Table 1, the statics of the number size distribution observed are listed. Since the station is on the border between rather clean continental air masses and the polluted air, the variation is rather high. In Figure 1, the diurnal behavior of the number distribution and number concentration is shown a contour plots and time series, respectively. One can clearly see, the seasonal trend of new particle formation, which is maximum in winter and spring and minimum in summer. This fact is also related to the condensational sink or the air mass origin (clean from North, polluted from South). The frequency of the particle formation events is shown in Figure 2. The seasonal variations of the calculated formation and the growth rate are plotted in Figure 3 and 4.

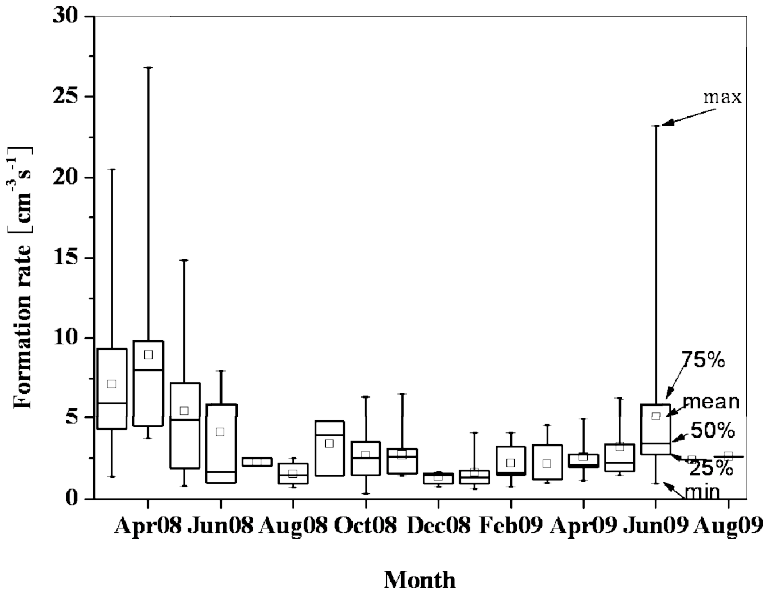

Figure 3: Seasonal variation of the ne particle formation rate

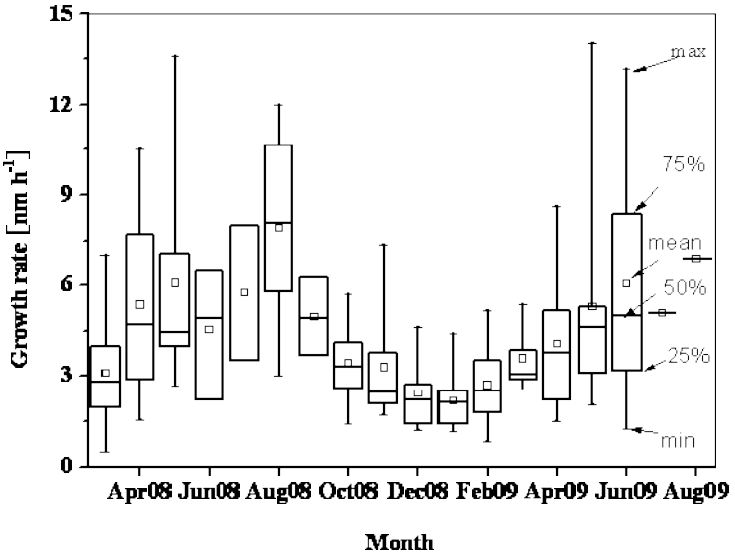

Figure 4: Seasonal variation of the growth rate

India: Gual Pahari

FMI has set up a station for measuring atmospheric aerosols in a heavily polluted urban background environment in Gual Pahari, close to New Delhi in India, together with the The Energy and Resources Institute (TERI). This station was partly operational from December 2007 and fully operational from March 2008. The in-situ instrumentation at Gual Pahari include $PM_{2.5}$ and PM_{10} monitors, a MAAP (absorption photometer) for black carbon, an Ecotech Nephelometer for the scattering coefficient at 520 nm, and a dual mobility size spectrometer and an aerodynamic particle counter for particle number size distributions.

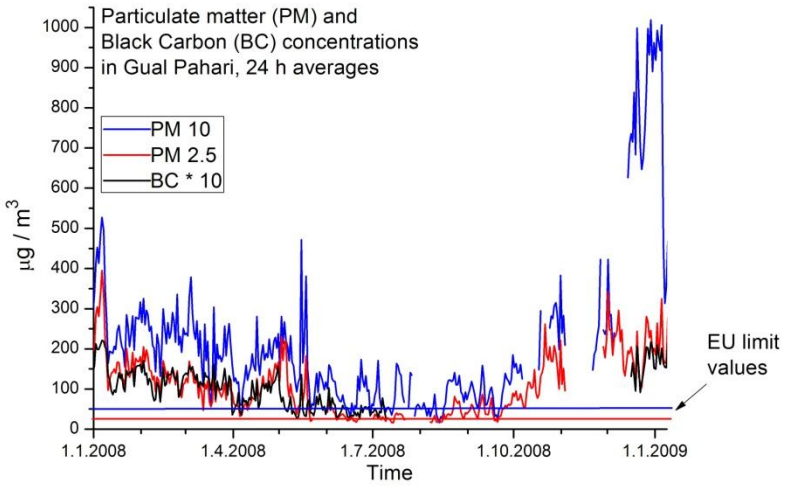

Figure 5: Time series of $PM_{2.5}$, PM_{10} and BC concentrations in 2008.

The PM-monitors are located under separate heated inlets and all the other instruments under a molecular sieve dryer unit. Condensational sink, several nucleation events were observed from the size distribution data. The 24 hour average $PM_{2.5}$ and PM_{10} concentrations vary from the rainy season low of 20 and 45 μgm^{-3} to a high of 450 and 500 μgm^{-3} observed during the winter (Figure 5). The measured Black carbon concentrations are about 10 % of respective $PM_{2.5}$ and 6 % from PM_{10} (Figure 5). The scattering coefficient varies from < 100 Mm^{-1} observed during the rainy season to > 2500 Mm^{-1} measured during

December-January. Particle number concentrations varies mostly between 10 000 – 60 000 cm^{-3}. Even though the obviously high condensational sink, several nucleation events were observed from the size distribution data.

South-Africa:

The South African measurement site is located on the eastern part of Highveld, approximately 200 km east of Johannesburg at a hilltop approximately 1750 meter asl. The NE-E-SE sector of the measurement site contains a limited number of pollution sources; whereas the other sectors have significant anthropogenic emissions especially from coal-based power production, petrochemical industry and further away, the megacity of Johannesburg. The location of the measurement site gives an opportunity to study the plumes from the western sector and clean air from the east side and thus is an excellent observation site with great variability.

Due to technical and logistical problems, full measurements only started in February 2009. In this paper some preliminary results from 9-days period in June 2009 are presented. Figure 6 represent the 10-870 nm particle size distribution during the same period. Clearly, new particle formation takes place during the six first days. During the three last days, wind was from the east and clouds reduce solar radiation (Figure 7). The limited radiation prevented the formation of nucleating vapours. Larger particles above 100 nm were almost non-existent due to cloud processing of the air masses during their path over the Drakensberg Mountains, and limited number of anthropogenic sources in the easterly direction.

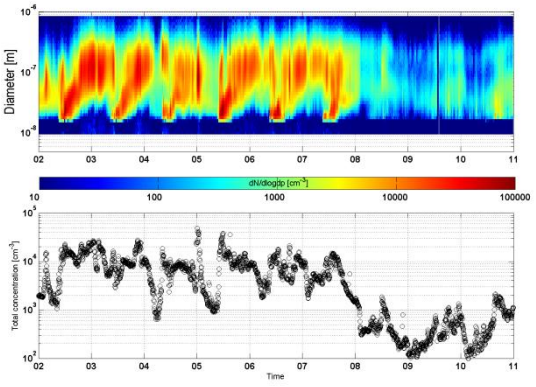

Figure 6: 10-870 nm aerosol number size distributions on 2-10 June 2009 at Elandsfontein measurement station

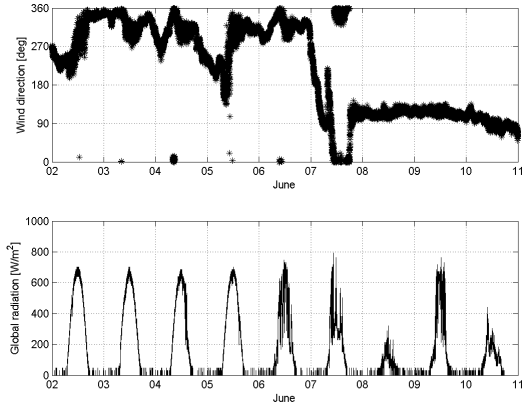

Figure 7: Wind direction and solar radiation on 2-10 June 2009 at Elandsfontein measurement station

Within the scope of this abstract, two different days, i.e. the June 2 and 8, 2009 can further be considered in detail, since they overlap with the Partisol aerosol samples. The chemical composition of the PM2.5 and PM2.5-10 for these two days was significantly different. OM, sulfate and ammonium were the main components of the fine mass during both the days. On June 2 nitrate and EC showed a larger contribution to the fine mass: 3% and 10 %, respectively. The largest contribution of nitrate overlaps with the peaks of NO and NO_2 concentrations, and the EC concentration correlates with the BC time series. Sodium and chloride showed higher concentrations on June 8, which may be related to the transport of marine aerosol from the Indian Ocean. The differences in fine aerosol composition highlight the influence of industrial sources on June 2 and the influence of cleaner (possible marine) air masses on June 8. Biomass combustion emissions were likely responsible for the similar concentrations of EC-fine and EC-coarse on June 2.

Currently, the first observational results are being processed. After the first full year of measurements is completed, we will quantify the direct aerosol radiative forcing of the Highveld area. This includes the estimation of vertical aerosol profiles, chemical composition of particles and closure between the particle size distributions and direct absorption and scattering mechanisms. These results will be utilized in conjunction with satellite observations, as well as regional and global climate and air pollution models, in an attempt to improve their accuracy with regards to southern Africa.

Brazil

Aerosol physical and chemical properties were measured at a pristine Amazonian forest site from January 2008 to October 2009. Measurements were taken at the Cuieiras forest site, tower TT34, above the canopy (45m), under dry conditions. Aerosol number concentrations ranged between 400 and 3000 cm-3. Although the forest site is preserved, it was occasionally affected by regional transport of polluted air masses, either from biomass burning or urban plumes. Only a few nucleation events were observed during the whole experiment. However, the Aitken mode has been present in most of observed aerosol size distributions, suggesting that new particle formation may be occurring somewhere else above or below the canopy. Coarse mode particles, possibly from biogenic origin, dominate the volume size spectra, either at dry or wet season (Figure 8). The volume ratio between coarse and fine mode increases greatly at night (Figure 9). On reason might be a nocturnal release of biogenic particles as a result of the ecosystem natural metabolism. As shown in Figure 10, time series of aerosol scattering and absorption coefficients show a clear seasonal pattern, with higher extinction coefficients observed during the dry season (Jul-Oct), at the onset of the biomass burning period, in comparison to the wet season (Nov-Jun). From the wet to the dry season, average aerosol scattering coefficients increased from 10 Mm-1 to 100 Mm-1.

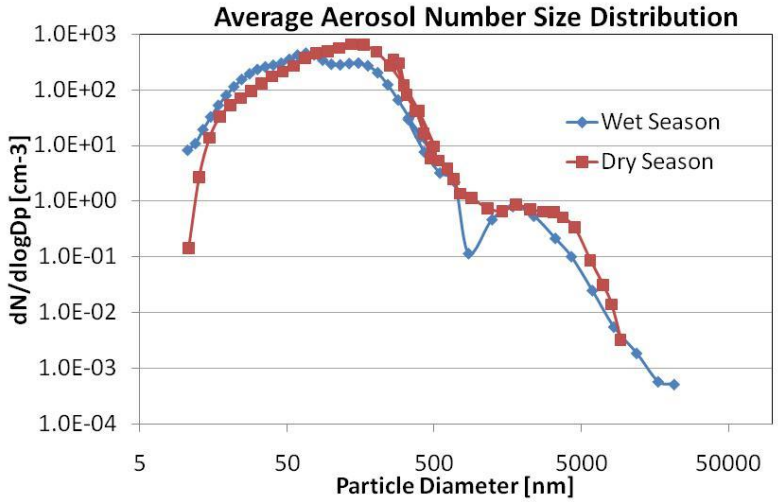

Figure 8: Number size distributions in the Amazonian rain forest during wet and dry season

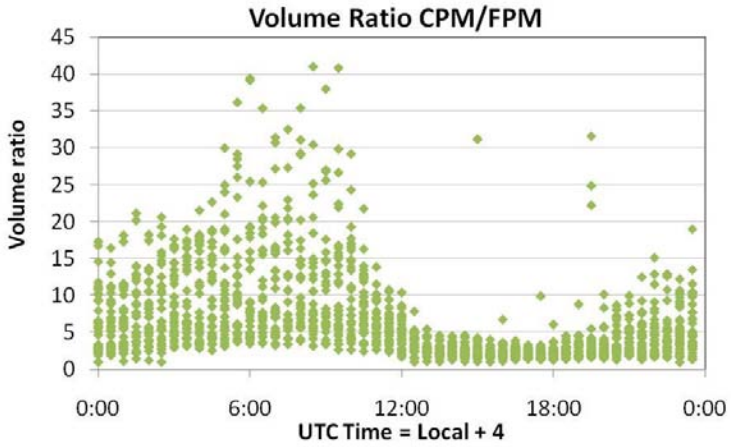

Figure 9: Ratio volume concentration coarse to fine mode in the Amazonian rain forest

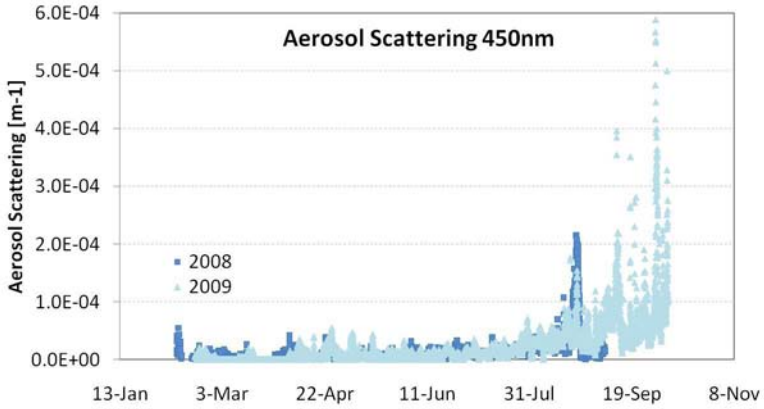

Figure 10: Scattering coefficient at 450 nm – transition from wet to dry season

Lidar:

After 11 months, lidar measurements in Brazil were stopped in November 2008 and the lidar was shipped back to Germany for maintenance. The analysis of these data is still going on, but some results have already been published.

In April 2009 a Raman lidar was installed at the EUCAARI site SDZ in China. Since that time measurements are performed daily. Due to air conditions problems no lidar observations were made June/July 2009. After maintenance end of July measurements could be continued. It is planned to run the measurements in China until March 2010.

In India, the measurements were conducted for one year from March 2008 until March 2009. However, we had to deal with several longer interruptions due to laser damages.

In October 2009, the Raman lidar, which was in India before, was installed in South-Africa.

In Figure 11, an example of the vertical aerosol structure over the Amazonian rain forest is shown. In general, the boundary layer is approximately 2.5 km. Another example is plotted in Figure 12 showing the complex vertical aerosol structure over the Northern India.

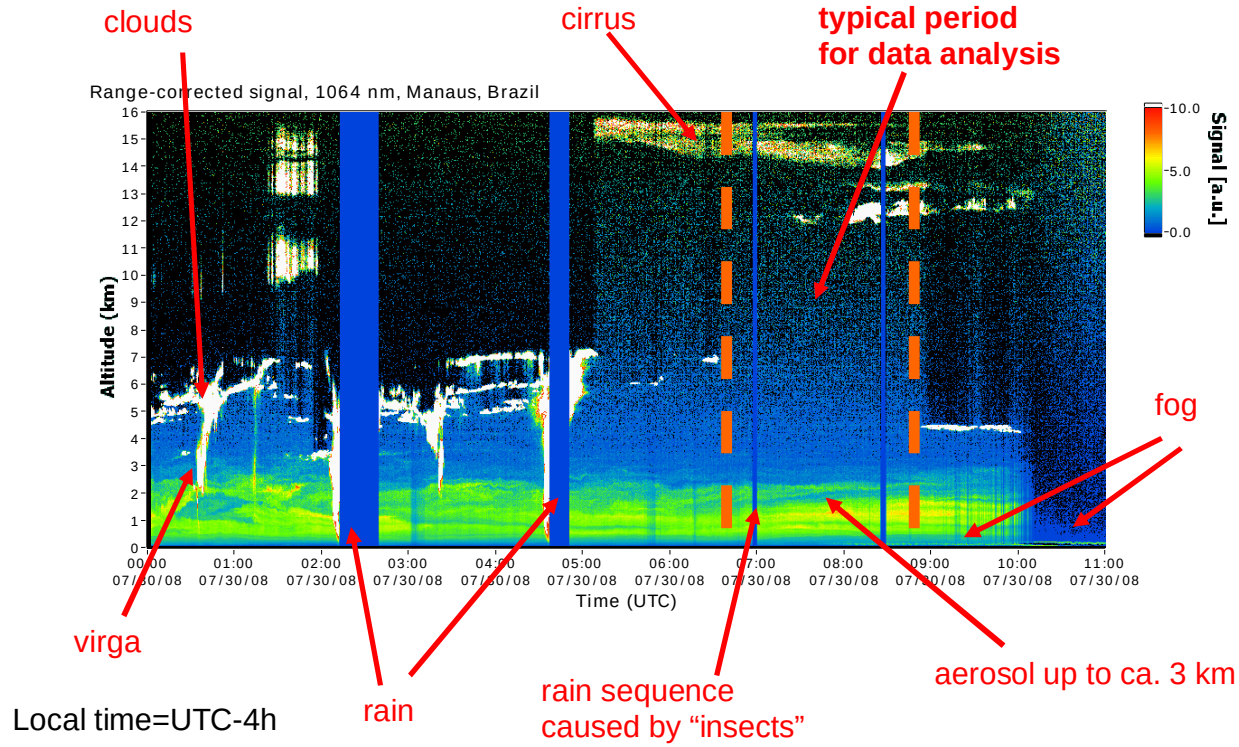

Figure 11: Example of the vertical aerosol structure over the Amazonian forest

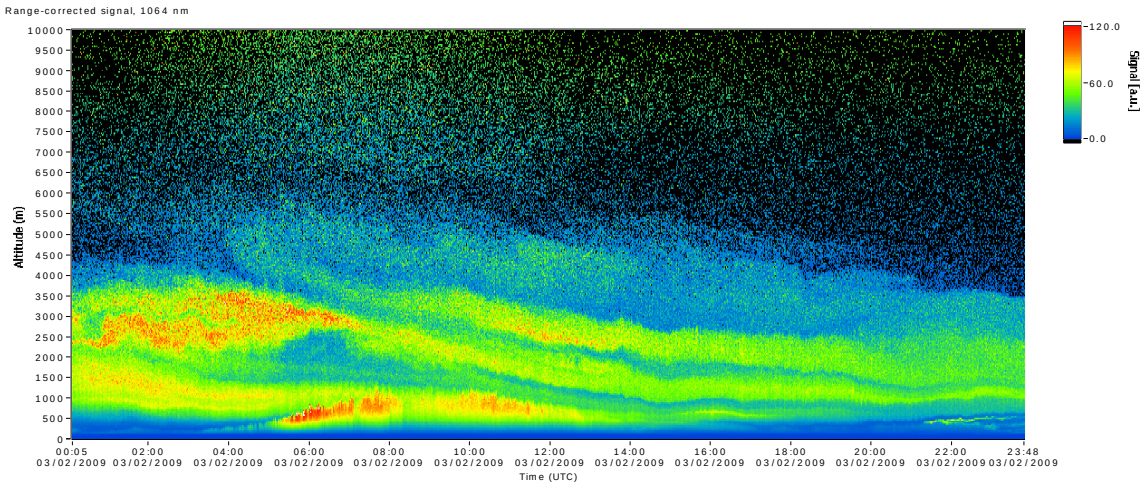

Figure 12: Example of the vertical aerosol structure in Northern India

Sampling for Chemical Analysis

Aerosol collection was performed with a Dichotomous Partisol sampler (Rupprecht & Patashnick Co., Inc). Fine particles (aerodynamic diameter below 2.5 µm) and coarse particles (aerodynamic diameter between 2.5 and 10 µm) were collected simultaneously on quartz filters. Aerosol masses were obtained from gravimetric analysis (relative humidity 20%). Water soluble ion concentrations (chloride, sulfate, nitrate, ammonium, sodium, calcium, potassium, and magnesium) were measured by ion chromatography. Elemental carbon (EC) and organic carbon (OC) were characterized using an EC/OC thermo-optical analyzer (Sunset Laboratory) (Birch and Cary, 1996). Equivalent black carbon (EBC) in Brazil was measured with a Smoke Stain Reflectometer (Diffusion System) that quantifies EBC deposited on filters from the reflectance of broad-band visible light.

The data here reported refers to the entire campaign in Brazil (10/02/2008-17/9/2008) and to the first part of the campaign in South Africa (13/3/2009 – 26/9/2009). The average fine and coarse aerosol mass at Manaus and Elandsfontein are reported in Table 1. In Manaus the chemical species identified during the present studies (carbonaceous aerosol and water soluble ions) reconstruct almost completely fine and coarse mass. In Elandsfontein the percentage of reconstructed mass is 74% and 22% of fine and coarse aerosol, respectively. The lower value in the coarse mode is likely due to the contribution of dust; to assess the contribution of this source additional aerosol samples will be collected on polycarbonate filters and analyzed by X-ray fluorescence (XRF).

	Fine - wet season	Coarse – wet season	Fine – dry season	Coarse – dry season
Manaus	2.5 (1.3)	8.0 (2.7)	4.2 (1.8)	6.9 (2.8)
Elandsfontein			18.8 (11.6)	21.7 (12.5)

Table 2. Fine and coarse aerosol mass concentration in μg m^{-3} (standard deviation between brackets).

In Manaus higher concentrations of sodium and chloride are observed in the coarse mode, likely due to marine sources. Sulfate, nitrate and ammonium are more abundant in the fine aerosols, where the ammonium concentration is usually enough to fully neutralize sulfate and nitrate. The higher concentration of sulfate in the fine fraction indicates gas-phase condensation processes. OC represents more than 50% of the fine mass and more than 75% of the coarse mass. The source of OC is mostly biogenic as confirmed by results of absolute principal component analysis and analysis of EC/OC thermo-optical data.

In Elandsfontein, ammonium sulfate and nitrate represent about 50% of fine mass. Aerosol masses affected by industrial sources are characterized by higher concentrations of nitrate and elemental carbon, while clean sector air masses show higher concentrations of sodium and chloride, indicating the influence of marine aerosol.

SATELLITE RETRIEVALS

Gerrit de Leeuw[1,2,3], Jean-Louis Brenguier[4], Stefan Kinne[5], Pekka Kolmonen[1], Andreas Minikin[6], Laurent Labonnotte[6], Jean-Francois Léon[6], Jerome Riédi[6], Daniel Rosenfeld[7], Larisa Sogacheva[2], Deborah Stein-Zweers[8], Anu-Maija Sundström[2], Pepeijn Veefkind[8], Ben Veihelmann[8]

[1]FMI, Helsinki, Finland
[2]University of Helsinki, Finland
[3]TNO, Utrecht, The Netherlands
[4]CNRM, Toulouse, France
[5]MPI-Meteorology, Hamburg, Germany
[6]LOA, Lilli, France
[7]HUJ, Jerusalem, Israel
[8]KNMI, De Bilt, The Netherlands

Keywords : aerosols, clouds, satellite remote sensing

INTRODUCTION

Optical instruments on satellites, i.e. radiometers and spectrometers, are used to retrieve aerosol and cloud properties over large spatial scales. Most of the satellites used are in a polar orbit (MODIS, POLDER, OMI, AATSR) and provide daily snapshots during the time of overpass. The area observed depends on the swath. Instruments such as OMI, POLDER and MODIS provide (near) global coverage, AATSR has a revisit time of three days at mid-latitudes. SEVIRI, on the other hand, flies on MSG in a geostationary orbit and provides data every 15 minutes.

In the second year of EUCAARI, the satellite retrieval work in WP2.3 has focused on the further development and improvement of algorithms, the provision of satellite aerosol and cloud products using these algorithms, comparison of products from different sensors, merging of these and development of Level 3 products. Integrative studies used satellite products to obtain more information on aerosol cloud interactions and underlying processes.

AEROSOL PRODUCTS

Task 2.3.1: Satellite aerosol observations (CNRS, FMI, KNMI, MPI, DLR)

Aerosol products include the total aerosol optical depth (AOD) from MODIS, OMI and AATSR, and fine mode AOD from POLDER. In the presence of clouds, aerosol retrieval is not possible. The daily products have been used to provide monthly composite aerosol fields. In addition CALIPSO L1 and L2 products are available.

POLDER, MODIS, OMI and CALIPSO products
In Year3 the MODIS and POLDER level 2 and level 3 products availability has been extended up to June 2009 covering the entire EUCAARI observational period.

For the production of gridded POLDER, MODIS and OMI aerosol products, a tool has been developed to project on a regular latitude/longitude grid the POLDER (total AOD, FMF AOD, coarse AOD and NS AOD), OMI (OMAERUV AOD) and MODIS (total and FMF AOD) aerosol products. The outputs are stored in a HDF4 file structure. An initial dataset at 0.5x0.5 resolution at the global scale will be produced in the next weeks and will be available on request.

For the determination of the aerosol altitude using data from a passive sensor, a new approach has been developed that uses the oxygen A-band of POLDER. The method was recently published in RSE by Dubuisson et al (2009). This new method gives a new insight in the vertical distribution of aerosol at the global scale. This product won't be available operationally and was developed as a side-project.

A new approach has recently been developed for the retrieval of aerosol optical thickness above clouds from merged POLDER and MODIS observations. The method has been published recently in JAS by Waquet et al (2009) and provides new perspective for studying aerosols properties and radiative forcing in presence of underlying clouds. This product won't be available operationally and was developed as a side-project.

The production of a 4D data set by merging Cloudsat/Calipso/MODIS/POLDER cloud and aerosol products is described in Task 2.3.2.

OMAERO Operational Product

The OMI data record (2004-2009) has been reprocessed with v1.1.1 of the OMAERO algorithm. The main improvement over previous versions is the use of the surface albedo climatology from OMI over land [Kleipool et al., 2008], which replaces the previous one, which was based on GOME.
Figure 1 shows a comparison with collocated MODIS and PARASOL data over the ocean for June 2006.

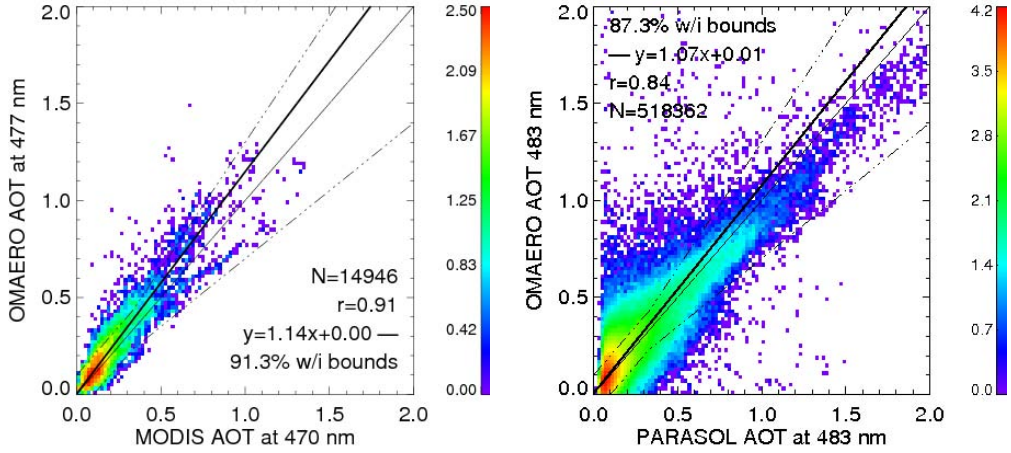

Figure 1: AOD from the OMAERO product compared with quality assured data from the MODIS standard product (left) and with quality parameter filtered data from POLDER (right) over ocean in June 2006.

The main shortcoming of the OMAERO product is the cloud clearing. The cloud clearing is difficult because of the relatively large size of the pixels, in combination with the absence of near infrared and thermal infrared channels.

Apart from the aerosol optical thickness and the aerosol type retrieval, the OMAERO product also produces the Aerosol Absorbing Index (AAI). The AAI is not a geophysical parameter, but an indicator of the presence of elevated layers of absorbing aerosol, such as desert dust or biomass burning plumes.

Figure 2 show the mean AAI for 2007, which is dominated by the signature of the Saharan dust. However, also several other dust sources as well as biomass burning regions show up in this map.

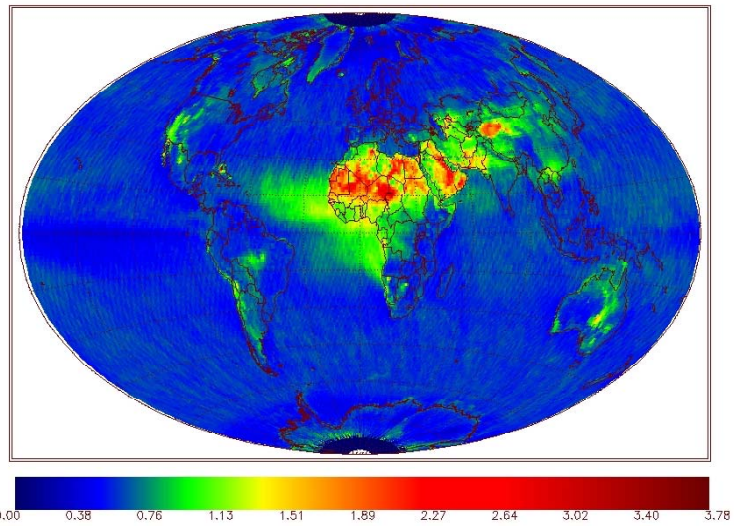

Figure 2. Mean AAI for 2007, which is dominated by the signature of Saharan dust. Several other dust sources as well as biomass burning regions are visible.

OMAERO Algorithm Development

In addition to the operational OMAERO algorithm, research versions have been developed to test further improvements of the algorithm. The main focus has been to combine the MODIS-AQUA cloud screening with the OMI data, in order to improve the cloud screening for OMAERO. MODIS-AQUA and OMI are both part of the A-Train satellite constellation and the two sensors observe the same area within 10 minutes. An algorithm has been delivered that regrids the finer scale MODIS-AQUA data on clouds and aerosols on the OMI ground pixel grid. The OMAERO algorithm has been adapted such that it can ingest these regridded MODIS data and use as additional information on clouds and/or to constrain the aerosol optical thickness. The aerosol optical thickness constraint has been explored to improve the information derived from OMI on aerosol type and absorption.

The MODIS regridder will be converted to an operational algorithm. When this data set has been produced for the full OMI period, a larger test data set of OMAERO with the MODIS cloud mask will be generated.

AATSR products

The AATSR dual view (ADV) algorithm has been further developed and validated vs AERONET data. ADV products are the AOD at wavelengths of 555nm, 685nm and 1600nm. These are determined by minimization of the error function, i.e the difference between computed and measured TOA reflectances, for a series of aerosol models. Hence, in addition to AOD (λ), also an estimate for the aerosol model is provided. The Ångström coefficient describes the wavelength dependence of the AOD.

AATSR data have been produced over Europe for the EUCAARI years 2006 and 2008. Data are available on a 10x10 km^2 grid or can be made available on 1x1 km^2 for a regional focus. Annual averages for these years are shown in Figure 3a. It is noted that this is an aggregate of individual data for the whole year 2008. Figure 3 shows high AOD over, e.g., Ireland, which is believed to be a, thus far unresolved, artefact.

In addition the ADV algorithm has been optimized for use over other regions which contribute to EUCAARO WP 2.2 on development countries. The first focus was on China. An example is shown in Figure 3b. A publication on the application has been submitted (Sundström et al., 2009).

A website has recently been constructed to make these data available (http://aatsraerosol.fmi.fi/).

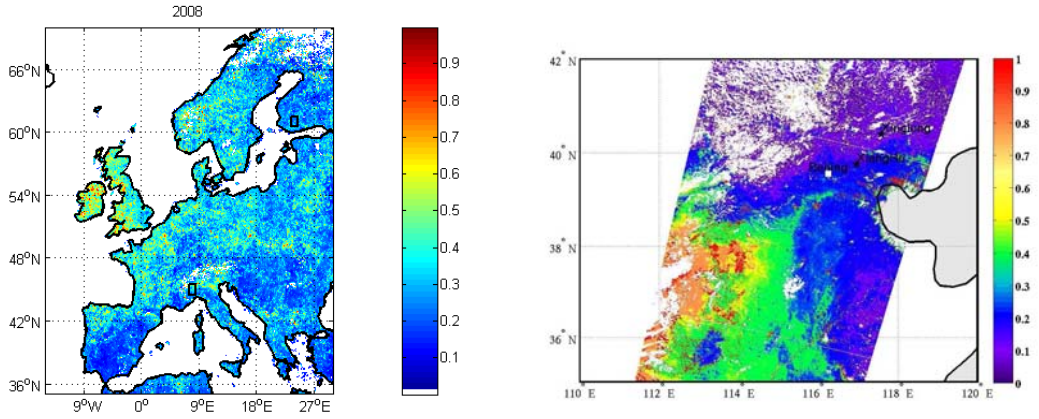

a b

Figure 3.a) AOD at 555nm over Europe, as an aggregate of the individual data for the whole year 2008.White areas (e.g. over the Alps) indicate the absence of data.
b) AOD pattern at 555 nm retrieved from AATSR data during an overpass over the Beijing area on 7.3.2008. Low AODs are observed over the Beijing area, bercause the air flow was from north, bringing clean air; further to the south the AOD increases. Resolution is 1x1 km^2 . White areas designate clouds.

CLOUD PRODUCTS

Task 2.3.2: Satellite cloud observations (CNRS, CNRM, HUJ, KNMI)

Cloud properties are available from MODIS (TERRA: 10:30 local; AQUA (14:30 local), POLDER, OMI and SEVIRI. OMI cloud products include the effective cloud fraction and the cloud pressure retrieved using the oxygen dimer (O_2-O_2) absorption band around 475 nm. The products available from MODIS and POLDER pixel level retrievals and daily, weekly or monthly gridded level 3 products. The most relevant cloud properties from these instruments are cloud fraction, cloud phase, optical depth, effective radius, liquid water path, cloud top pressure and short wave albedo.

During year 3, work has been focussed on the production of a merged dataset from instruments that are part of the A-Train and comparison of cloud products from the POLDER and MODIS datasets.

1) Production of MODIS and POLDER level 2 and level 3 products

Availability of products has been extended up to June 2009 covering the entire EUCAARI period.

2) Production of merged POLDER/MODIS level 2 products

Merged level 2 products have been created from POLDER and MODIS datasets. One set of products has been created by combining level 1 observations from POLDER and MODIS to create new products with a dedicated synergistic algorithm. Of particular interest is the combined « cloud thermodynamic phase » product (Riedi et al, 2007). This product is referenced in ICARE database as PM02_L2 and available under MODIS_POLDER directory.
A second dataset has been created to facilitate the use, comparison and exploration of POLDER and MODIS level 2 official products. This new dataset is provided in individual swath corresponding to POLDER orbit, reprojected to a integerized sinusoidal grid centered on POLDER/PARASOL ascending node longitude. All POLDER and MODIS official level 2 cloud products are reformatted and reprojected to this common grid at 6kmx6km resolution. When multiple MODIS pixels fall into a single grid cell, cloud products are averaged and the mean value is provided along with standard deviation.

This product is referenced in ICARE database as PM03_L2 and available under MODIS_POLDER directory.

3) Comparison between MODIS and POLDER cloud products (cloud fraction, cloud optical thickness and cloud phase).
Thanks to the above mentioned reformatted products, studies have been done to compare MODIS and POLDER products (Figures 4 and 5). In particular, cloud fractions from both datasets have been thoroughly investigated. Seasonal variations and spatial distribution of high, middle and low, ice/liquid cloud fractions have been compared and analysed. Main differences and reasons for those have been identified and quantified. A paper is in preparation (Zeng et al, 2009) and will document the cloud fraction and cloud phase products from MODIS and POLDER. A statistical comparison of cloud optical thickness products from both instruments is underway.
Also, the framework for merged processing of POLDER and MODIS level1 and level2 data has been used in a study by Zhang et al (2009) to investigate differences in ice cloud optical thickness retrieved from POLDER and MODIS. This paper can serve as a reference document to understand the impact of microphysical model uncertainties on cloud optical thickness retrievals and subsequent errors on the estimate of ice cloud radiative forcing.

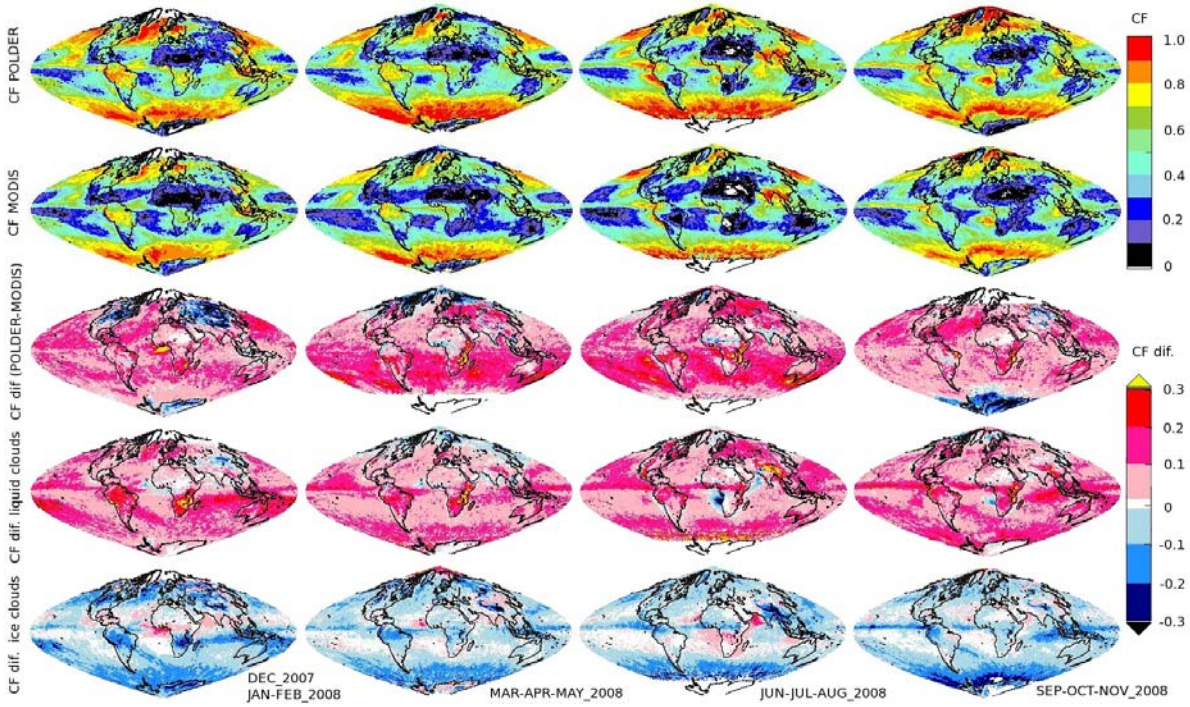

Figure 4. Comparison of MODIS and POLDER cloud fractions (Zeng et al, 2009 to be submitted).

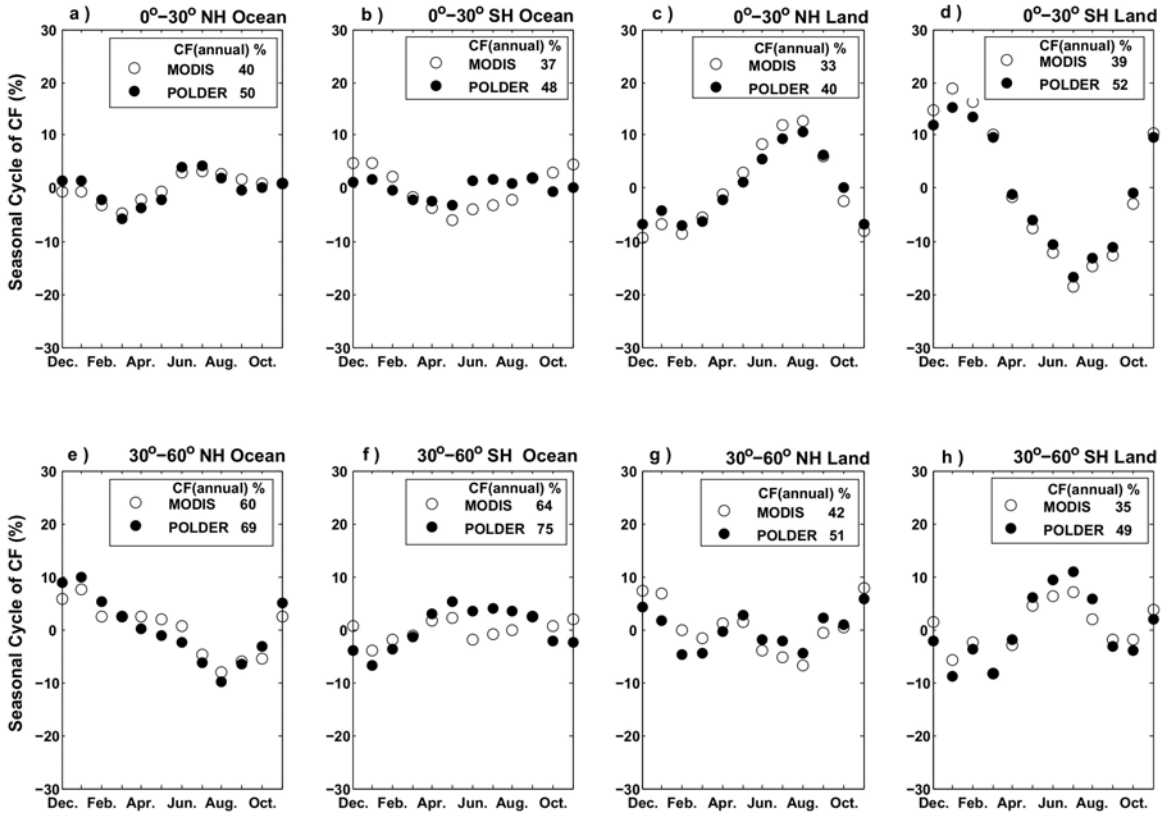

Figure 5. Seasonal cycle of the MODIS and POLDER cloud fractions for different regions (Zeng et al, 2009 to be submitted).

4) Production of reformatted POLDER level 3 statistics

As part of a joint effort for the intercomparison of various cloud datasets, in the framework of the GEWEX project, a reformatted POLDER level 3 dataset has been created to provide monthly statistics of total, low, middle and high cloud fractions, for either liquid or ice clouds, or both. Also joint histograms of cloud optical thickness against cloud top pressure have been created again for either liquid or ice clouds.
This dataset is available for 2006, 2007 and 2008 and provided at 1degx1deg resolution in Netcdf format which is common in the modelling community. These data are currently available on request to the EUCAARI partners and will eventually be made available through the ICARE database.

5) Production of 4D dataset : merged Cloudsat/Calipso/MODIS/POLDER cloud and aerosol products

A merged « A-Train » 4D dataset is now available through ICARE. CloudSat, POLDER and MODIS main aerosols and clouds products have been collocated along the CALIPSO orbital track and are provided at CALIPSO horizontal resolution. Two sets of files are available depending on the desired level of merging. First, data are provided individually for each instrument and only sampled/reformatted to allow easy collocation with CALIPSO. Each file contains various products from one instrument only but in a format that is directly consistent/comparable with CALIPSO. These products are referenced in the ICARE database as CALTRACK_L2_*SENSOR_NAME* and available under directory MULTI_SENSOR/CALTRACK_UNIT.
A second level of merging has been operated from those files and provides selected CALIPSO, MODIS, POLDER and CLOUDSAT products all merged into a single orbit file. This provides the user with smaller files containing most products of interest though selection may be limited for specific use.
These products are referred to in the ICARE database as CALTRACK_ and available under directory MULTI_SENSOR/CALTRACK.

Note that ICARE can reprocess the merged dataset (both CALTRACK_UNIT and/or CALTRACK) in order to include more products if necessary. This reprocessing can be requested either through the usual ICARE proposal call mechanism or through LOA/CNRS partner in the framework of EUCAARI project.

EVALUATION

Task 2.3.3: Evaluation of the use of satellite products (CNRM, CNRS, KNMI, FMI, MPI)

A new scoring system is introduced to quantify the performance of MISR and MODIS satellite sensor retrieval products for aerosol optical depth (AOD). Based on comparisons to highly accurate ground-based sun-photometer data of AERONET here stratified into 25 regions and 12 months, scores for bias and variability are assigned. These regional and temporal sub-scores are then combined into single annual global overall scores. MODIS (.61) and MISR (.58) global annual scores are at the top of available multi-annual AOD data-sets. Both data-sets (based on multi-annual statistics) score even better than the usually well behaved multi-model median (.58). MODIS scores better over oceans and MISR scores better over land. Another aspect of this new scoring is the diagnostics, which allows tracing poor retrieval performance back to failure at temporal and spatial sub-scales. Such analysis for instance suggests that MODIS suffers from retrieval issues over continents in mid-latitudes during winter (possibly due to sub-pixel snow) and that MISR suffers from retrieval issue at high latitudes (certainly related to MISR's relatively poor temporal sampling). Differences in scores at these sub-scales allow the identification of regional and seasonal retrieval strengths and help in making more objective choices when picking one retrieval over another.

APPLICATIONS

OMAERO AAI Trend Analysis

With five years of OMI data available (2004-2009), studies on inter annual variations in biomass burning and desert dust are performed, using the OMAERO AAI. An example of inter annual variations in the Saharan desert dust plume is shown in Figure 6, which shows the mean positive AAI for January. This month has the weakest biomass burning signal and thus the clearest signal of the desert dust. Figure 6 shows much higher average positive AAI in January 2005 and January 2007, as compared to 2006 and 2008.

Since the AAI is an indicator for biomass burning events the trend analysis should include more statistics than just the average value. Sporadic will probably not change the average significantly but will have an impact on for example the maximum value. For this reason we are deriving more advanced statistical information computing histograms of the observed monthly AAI distribution on 1x1 degree grids.

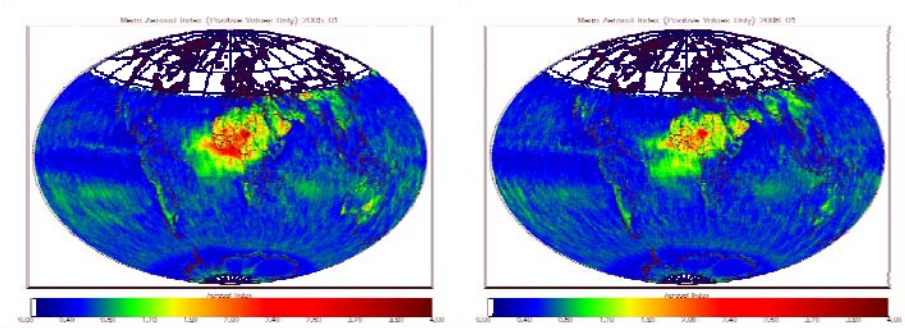

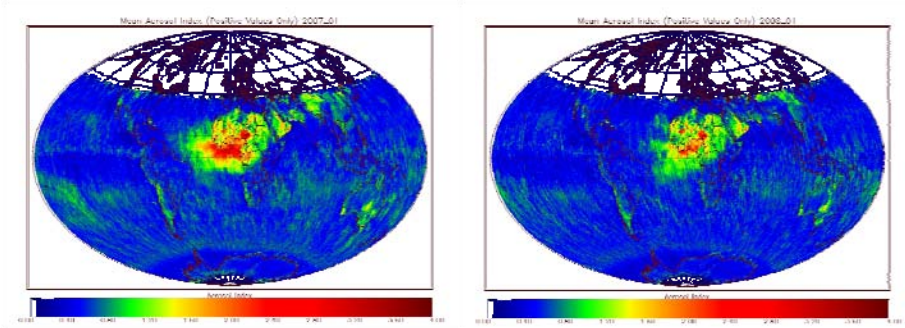

Figure 6. Average positive AAI for the month of January for 2005-2008.

Satellite and aircraft measurements of aerosol impacts on vertical cloud microphysical profiles during the EUCAARI IOP in May 2008.

During the EUCAARI IOP over the Netherlands and adjacent sea in May 2008, 25 flights were conducted with the SAFIRE ATR-42 research aircraft, on which aerosol and cloud microphysics probes were mounted. Due to the lack of clouds during most of the IOP and the specific aims of the a/c missions, which concentrated mostly on aerosol and radiation measurements, cloud data was collected only in 6 flights out of the 25. From these 6 flights, 8 different (rather shallow) vertical profiles of cloud droplet properties, in particular cloud droplet effective diameter, were constructed that covered both pristine and polluted conditions.
The shape of the vertical evolution of the droplet size distribution in convective cloud elements (including in layer clouds) was used to parameterize the impacts of aerosols. Similar characterization was done by satellite retrieval of the vertical profiles of cloud top particle effective radius. These satellite inferences were validated by the aircraft measurements.
To study the aerosol effects on the cloud microphysical properties, for the clouds sampled during EUCAAPI IOP, existing analysis methods were used. For polar orbiting satellite retrieval of cloud top particle effective radius the method of Rosenfeld and Lensky(1998) was applied. The validity of this method was reinforced after the launch of the geostationary EUMETSAT MSG. A special sequence of 3-minute rapid scans allowed to track with time the growing tops of individual convective cells and produce similar Temperature-Cloud top particle effective radius (henceforth T-Re) profiles as those produced from snapshots of the same scenes (Lensky and Rosenfeld, 2006).

Aerosol and CCN concentrations are not always representative for the profiled clouds, and because there are different types of clouds with potentially different mixing processes, a new parameter was introduced which is not directly measured, namely: adiabatic droplet concentration normalized to cloud base air-density (in short: "$N_{adi\text{-}cb}$").Because $N_{adi\text{-}cb}$ is dependent on the calculated adiabatic water, it was important to try to estimate the cloud base altitude carefully, which was not always a simple task. This also affects the calculation of the cloud depth parameter, which is vital for comparing the growth of cloud droplets of clouds with bases at different altitudes. Figure 7 shows the mean Re for all penetrations (defined as more than 5 subsequent 1Hz measurements with cloud droplet concentration > 20 cm^{-3}) versus the distance above cloud base. The colour of each data point is defined by $N_{adi\text{-}cb}$ for the containing profile. It can be clearly seen that profiles with smaller $N_{adi\text{-}cb}$ have larger Re for any given cloud depth, and that the differences are more evident further away from the cloud bases. This pinpoints the importance of sampling clouds far from their bases when studying the effects of the aerosols on the cloud droplet size spectra and its evolution with altitude.
The cloud top particle effective diameter derived from MSG (the circles in Figure 7) for the corresponding location and time of the aircraft measurements, shows in general good agreement the aircraft profile top Re, and also shows Re sensitivity to cloud depth and droplet concentration, but at least in two cases is taken from a cloud top which is significantly higher than the top of the profile and may represent a higher layer cloud. MODIS derived Re (triangles in Figure 7) has the advantage of higher resolution than MSG, and it is easier to identify the cloud that the a/c had actually penetrated, unless it is covered by a higher

layer of clouds, but on the down side, the timing of the satellite overpass is 1 to 3 hours from the a/c measurement. Anyway, MODIS derived Re also shows dependence on $N_{adi\text{-}cb}$ and on cloud depth, but tends to be smaller than MSG derived Re.

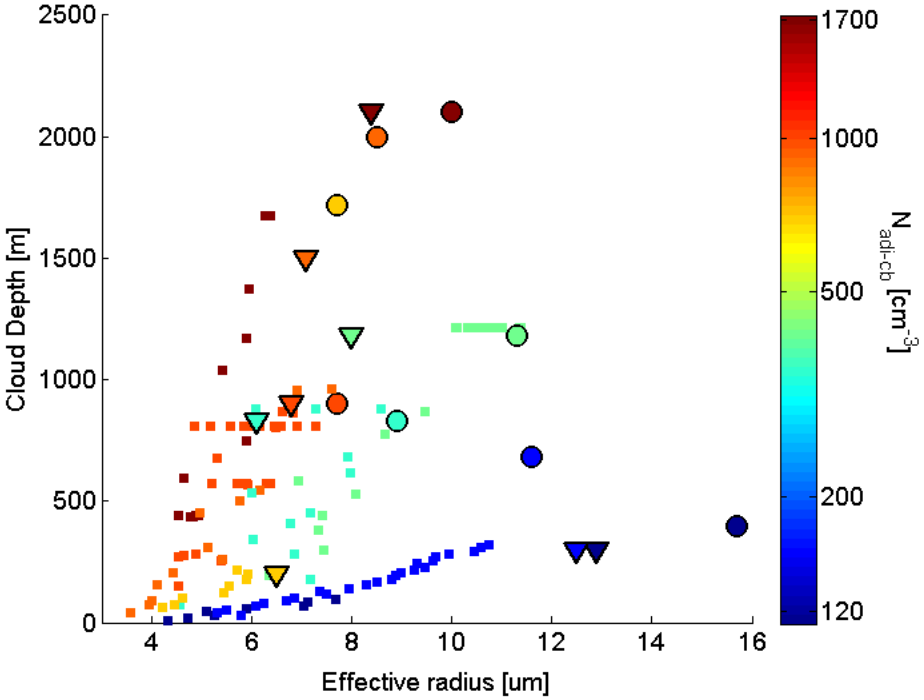

Figure 7. Mean penetration Re vs. Cloud Depth for all profiles. Colour coding represents the $N_{adi\text{-}cb}$ and its scale is logarithmic. The outlined circles show the MSG derived cloud top Re for the corresponding profiles, but in some cases the profiled cloud could not be "seen" by the satellite because higher cloud. Outlined triangles show the MODIS derived cloud top Re from closest overpass

Figure 8 shows data for the same penetrations, but instead Re, another parameter is used to relate to the droplet sizes. Here we use the mode of the cloud droplet mass density ("D_L"), which indicates the droplet diameter that contributes most to the cloud liquid water content for each measurement. D_L and Re are highly correlative, but D_L is used here so the results from the current dataset could be directly compared to measurements taken from other parts of the world. This allows to see whether it is reasonable to extrapolate EUCAARI fairly shallow measurements to greater cloud depths, which were not sampled, and to conclude something with regard to the aerosol effect on precipitation forming processes. The typical threshold of D_L for the onset of precipitation at 24µm, was not reached during EUCAARI IOP, but it seems reasonable to conclude that the more "polluted" clouds, shown in figure 2 (left panel) in warmer colours, are much further from precipitating compared to the clouds with smaller droplet concentrations. The D_L profile of the convective cloud sampled on May 14, 2008 over Eindhoven area, which formed in continental south-easterly flow in well mixed area, shows similarity with lower parts of the "Argentina-Hail" and "Amazon-Smoky" profiles. On the other hand, the *StCu* sampled a day later above the North Sea just off Newcastle in maritime airmass, has a D_L profile similar to the lower part of the "California-Pristine" profile, which crossed the 24µm precipitation threshold already at a depth of 500m.
Although we were able to clearly identify the aerosol signal, as is represented by $N_{adi\text{-}cb}$, on the Re or D_L profiles in different clouds over The Netherlands and the North Sea, we would like to emphasize that good quantification of the aerosol effects on the cloud microphysical processes is not achievable without penetrating through the clouds all the way to their tops or at least to the precipitation onset height, as well as without measuring the aerosols right below the profiled cloud's base.

More detail can be found in the abstract by Freud and Rosenfeld (EUCAARI 3rd GA in Stockholm).

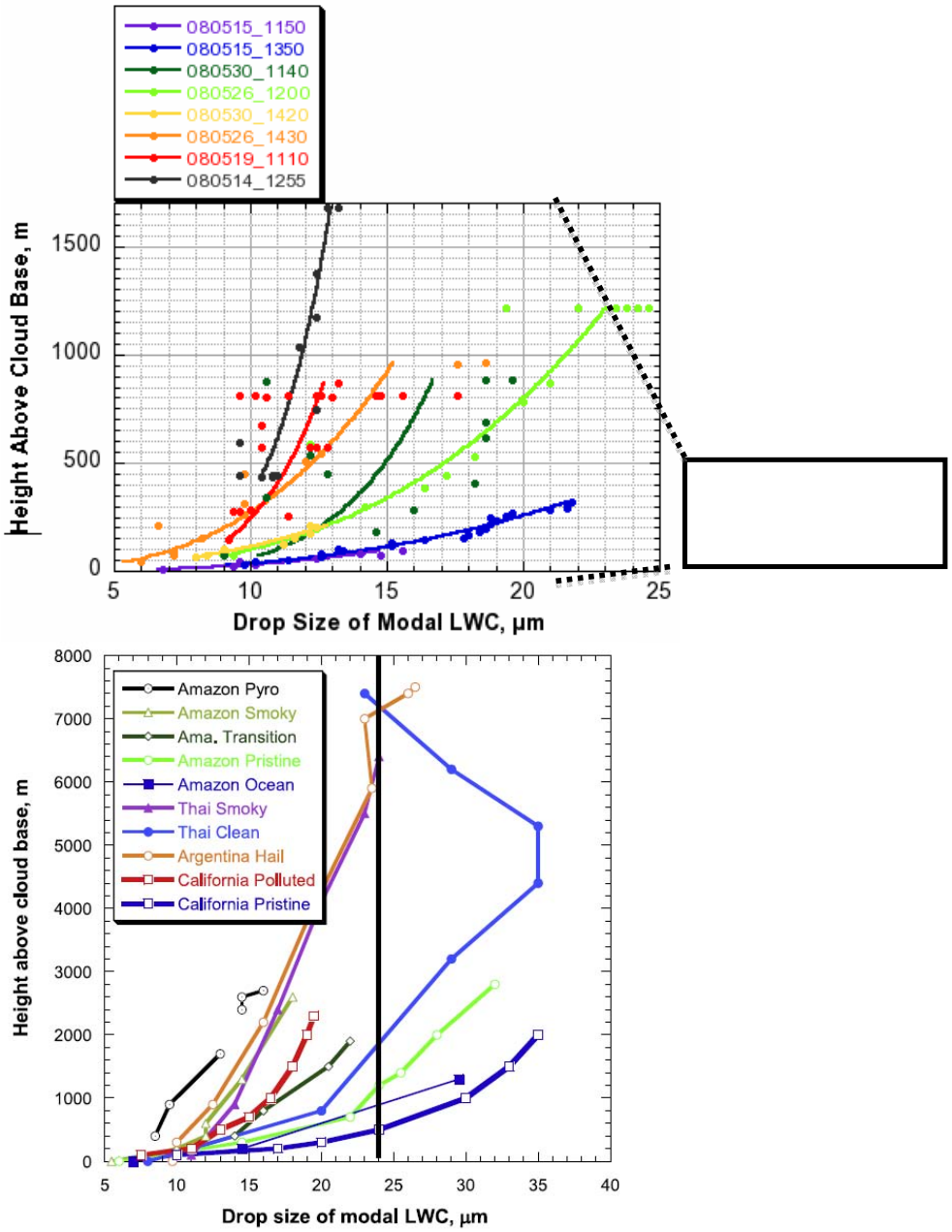

Figure 8. The mode of the droplet mass distribution in each penetration vs. cloud depth. Profiles in left panel are from EUCAARI IOP and their colours, from cold to warm, are sorted after $N_{adi\text{-}cb}$. Right panel is figure 14 from Rosenfeld et al. 2008. Black rectangle corresponds to axis limits of left panel.

Comparison between modeled and SEVIRI retrieved cloud optical thickness: 15.05.2008

Modeled and satellite retrieved cloud optical thickness, for a stratocumulus case on 15.05.2008, are compared. The modeling part was large eddy simulations (LES) with the nonhydrostatic model Meso-NH (Lafore et al. 1998), initialized with the results obtained in a uniform stratocumulus cloud over the North Sea by the aircraft in the EUCAARI campaign (on 15. May 2008) (WP3.2). The simulation provides a connection between in situ measurements from the aircraft during the EUCAARI campaign to the model spatial resolutions.

Satellite observations are available from MODIS (on board polar-satellite, TERRA and AQUA) and SEVIRI (on board geostationary MSG). SEVIRI has the advantage that we can choose the same time as the simulation and the in situ measurements, however the spatial resolution are less good compared to MODIS, which have the overpasses at 11:00 (TERRA) and 13:00 (AQUA).

The distribution of the cloud optical thickness of the simulation and the satellite observation (SEVIRI) at 09:00 in the morning have been compared. The cloud optical thickness for the model domain and from satellite in Figure 9 illustrate the cloud inhomogeneities and typical cellular pattern of the stratocumulus cloud. The track of the flight is included in Figure 9c. The distribution of the cloud optical thickness from SEVIRI is given for two domains for diversity.

We are facing the difficulties of different spatial resolutions. The SEVIRI resolution over the North Sea for one pixel is 7km x 7km. We chose a domain of 100km x 100km for the satellite observation, where as the model domain is one tenth of it 10km x 10km (Figure 9a). This exercise gives us the possibility to compare the modeled distribution of the cloud optical thickness with the distribution of the cloud optical thickness for a greater area. The results of the comparison shows that the simulated cloud optical thickness are in good agreement with observation and presenting a part of the diversity.

Figure 9. a) Scheme of the relation between model spatial resolution and satellite observations
b) Cot from the model domain at 09:00
c) FUB-COT from SEVIRI at 09:00 with two domain and flight track
d) Frequency of the COT meso-NH (black) and FUB-COT SEVIRI (blue and red)

Diurnal cycle of marine stratocumulus clouds from SEVIRI

Further studies included the analysis of the diurnal cycle using SEVIRI data. All cases show a pronounced diurnal cycle in the radiances. The comparison with simulated radiances shows that the diurnal cycle is not caused only by the sun. The diurnal cycle is also depending on the diurnal cycle of the LWP. A pronounced diurnal cycle of LWP has been found. The maximum of the LWP are in the morning, which agrees with the climatology and other observations. The minimum of the LWP are not distinct and general in the afternoon.

A preliminary algorithm for LWP has been developed for the day and night. The performance of the algorithm would be improved by using for the day time the UWM-algorithm of the cloud optical thickness and effective radius. The assumptions for the night retrieval are not accurate enough. It has been shown that we should consider also the temperature profile changes with the surface temperature (SST) and with the sunset. To study this dependency I would propose a sensitivity study or comparison with independent data.

Method developed to separate drizzling and non drizzling clouds are promising and should be compared with independent measurements. For example use the rain data from J. Tournadre who apparently is able to estimate oceanic rainfall rates from the TOPEX/POSEIDON or JASON altimeter for comparison.

For more detail, see Huenerbein (2009)

CONCLUSION

Aerosol and cloud products have been processed for the period covering June 2006 to December 2008 and available through the ICARE data and services center (http://www.icare.univ-lille1.fr).
The merged and reformatted products are all being distributed in self-describing hdf4 format. Though tools and libraries for reading hdf files can be found throughout the web, ICARE has also developed high

level functions libraries and tools for accessing HDF files produced at ICARE. The tools and libraries can be found at : http://www.icare.univ-lille1.fr/tools/

The main portal for the OMAERO data is the NASA DISC: http://disc.sci.gsfc.nasa.gov/Aura/data-holdings/OMI/omaero_v003.shtml. From this site the Level 2 orbit data can be obtained, as well as daily gridded datasets. In addition, overpass data over the AERONET stations are available for the Aura Validation Data Centre (AVDC) http://avdc.gsfc.nasa.gov. Data in near-real-time (available within three hours of observation) can be obtained from the http://www.temis.nl.

AATSR retrieved AOD is available at (http://aatsraerosol.fmi.fi/)

REFERENCES

Dubuisson, P., Frouin, R., Dessailly, D., Duforêt, L., Léon, J.-F., Moss, K., & Antoine, D. (2008). Estimation of aerosol altitude from reflectance ratio measurements in the O2 A-band. *Remote Sens. Environ., 113*, 1899-1911

Freud E. and D. Rosenfeld (2009). Satellite and aircraft measurements of vertical cloud microphysical profiles and teir relations to aerosols during EUCAARI IOP of May 2009. (Abstract EUCAARI GA 2009, Stockholm.

Huenerbein, A. (2009). Diurnal cycle of marine stratocumulus clouds from SEVIRI. Visiting Scientist Report at Meteo-France.

Kleipool, Q. L.; Dobber, M. R.; de Haan, J. F.; Levelt, P. F. (2008): Earth surface reflectance climatology from 3 years of OMI data, J. Geophys. Res., Vol. 113 (D18), DOI: 10.1029/2008JD010290.

Lafore, J. and Coauthors, 1998: The Meso-NH Atmospheric Simulation System. Part I: Adiabatic formulation and control and control simulations. Ann. Geophys., 16, 90-109.

Lensky, I.M. and D. Rosenfeld (2006). The time-space exchangeability of satellite retrieved relations between cloud top temperature and particle effective radius. *Atmos. Chem. Phys.*, **6**, 2887-2894.

Riédi, J., B. Marchant, S. Platnick, B. Baum, F. Thieuleux, C. Oudard, F. Parol, J-M. Nicolas, and P. Dubuisson, "Cloud thermodynamic phase inferred from merged POLDER and MODIS data", 2007, *Atmos. Chem. Phys. Discuss.* , 7,14103-14137.

Rosenfeld, D. and I.M. Lensky (1998). Satellite-based insights into precipitation formation processes in continental and maritime convective clouds. *The Bulletin of American Meteorological Society*, **79**, 2457-2476.

Sundström, A.-M., P. Kolmonen, L. Sogacheva and G. de Leeuw(2009). Aerosol retrievals over China with the AATSR Dual-View Algorithm. *Submitted for publication in RSE (AATSR special issue)*

Waquet F., Riedi J., C-Labonnote L., Goloub P., Cairns B., Deuze J-L., Tanre D., “Aerosol remote sensing over clouds using the A-Train observations”, 2009, *Journal of the Atmospheric Sciences*: In Press

Zhang, Z., P. Yang, G. W. Kattawar, J. Riedi, L. C. Labonnote, B. A. Baum, S. Platnick, and H. L. Huang, “Influence of ice particle model on satellite ice cloud retrieval: Lessons learned from MODIS and POLDER cloud product comparison”, 2009, *Atmos. Chem. Phys. Discuss*., 9, 1757-1796.

REGIONAL AEROSOL SOURCE APPORTIONMENT AND LONG RANGE TRANSPORT: WORK PACKAGE 2.4

Erik Swietlicki[1], Urs Baltensperger[2], Maria Kanakidou[3], Maria Cristina Facchini[4], Gyula Kiss[5], Casimiro Pio[6], Andreas Stohl[7], and David Simpson[8]

[1]Lund University, Lund, Sweden
[2]Paul Scherrer Institut PSI, Villigen, Switzerland
[3]University of Crete, Heraklion, Greece
[4]Institute of Atmospheric Sciences and Climate CNR-ISAC, Bologna, Italy
[5]University of Veszprém, Veszprém, Hungary
[6]University of Aveiro, Aveiro, Portugal
[7]Norwegian Institute for Air Research NILU, Oslo, Norway
[8]EMEP MSC-W, Oslo, Norway

Keywords: Organic aerosol, source apportionment, regional and global models, air quality, climate

INTRODUCTION

WP 2.4 aims at improving our ability to accurately apportion the European aerosol to its various sources. The focus is apportionment of aerosol mass (PM), with special attention to the development and implementation of new methodologies for source apportionment of the organic aerosol components. The aerosol source apportionment will distinguish between anthropogenic and natural, as well as primary and secondary aerosol components. WP 2.4 will develop tools that will enable a quantitative estimate of the influence of various sources to the AQ and PM levels within Europe, in particular regarding the organic aerosol. WP 2.4 contributes to the EUCAARI objective 1a.

More specific objectives in WP 2.4 are to produce

- Source apportionments of the organic aerosol at European sites (Task 2.4.1)
- Determine the geographical source region (Task 2.4.2)
- Updated EMEP model for the concentration fields of mineral dust and sea salt (Task 2.4.3)
- Organic aerosol (OA) process description and parameterization (Task 2.4.4)

ONGOING AND FUTURE WORK

The activities of WP 2.4 are still ongoing.

Task 2.4.1
The aim of this Task is to perform a source apportionment of the organic aerosol at selected European sites by means of source-specific tracer compounds quantified using various analytical techniques:

- GC-MS Molecular tracers (Task 2.4.1a, Partners UAV and ACUV)
- H-NMR spectral fingerprints (Task 2.4.1b, Partner CNR-ISAC)
- AMS spectral fingerprints (Task 2.4.1b, Partners LU and PSI)
- ^{14}C (Task 2.4.1c, Partners LU and PSI)

Details on the various analytical techniques can be found in EUCAARI Deliverable 9 (Initial implementation strategy and prioritize tasks in the workplan for WP2.4).

At the AMS (Aerosol Mass Spectrometry) User´s Meeting in Manchester (UMAN) in September 2008, eight AMS users agreed on a coordinated effort to deploy their AMS instruments at various background sites in Europe during the two EMEP intensive OA campaigns in September-October 2008 and February-March 2009. At PSI in May 2009, the first results of the various AMS campaigns were discussed, and a common AMS data format was decided. The AMS turnout within the community is certainly excellent considering the limited number of AMS instruments available in Europe. The AMS instruments are capable of quantitative analysis of oxygenated OA (OOA) and hydrocarbon-like OA (HOA), as well as tracer m/z peaks that are characteristic for biomass combustion (e.g. levoglucosan). EUSAAR/EUCAARI background sites operating AMS instruments include Harwell, Hyytiälä, K-puszta, Mace Head, Melpitz, Puy de Dôme, Vavihill, Cabauw and Montseny. Data processing workshops are arranged within the EUCAARI-AMS community to ensure data quality and intercomparability between sites.

An intercalibration (round-robin test) was carried out within the European ^{14}C analytical community, including WP2.4 partners PSI-ETHZ and LU. Results are still pending. Samples from the EUCAARI/EMEP campaigns are analyzed for ^{14}C by PSI-ETHZ and LU. At LU, the separation and graphitization scheme of OC/EC for subsequent ^{14}C analysis has been developed in cooperation with PSI-ETHZ, and intercomparison tests will be performed.

OA source apportionments are performed at six background sites. Five of these are EUCAARI-EUSAAR sites, while one site (San Pietro Capofiume) is operated by one of the EUCAARI-EUSAAR partners (CNR-ISAC). Three of the sites participated in the Lagrangian experiments (Hyytiälä, Melpitz, K-puszta). Additional background sites are San Pietro Capofiume, Finokalia and Montseny. Urban sites where OA source apportionment will be performed are Zürich and Barcelona. More details on the selection of sampling sites can be found in EUCAARI Deliverable 32 (Selection of sampling sites, coordinated with WP 2.1, 4.2 and EUSAAR).

Since funding is very limited within EUCAARI for the source apportionment task, we were forced to focus on shorter and more intensive campaigns rather than long-term measurements, which would have otherwise been beneficial for OA model validation. This is however compensated by the use of a several source apportionment methodologies which, when combined in time and space, will provide deeper insight regarding the sources contributing to the OA concentrations.

The analysis of OA samples using GC-MS, H-NMR and ^{14}C is still ongoing, but nearly finished.

More information and results from Task 2.4.1a are given in the abstract by Alves et al (2009, these proceedings).

The summer 2008 K-puszta campaign will serve here as an example of such a combination of OA data. At this Central European (ACUV) sampling site, PM2.5 aerosol samples were collected on pre-heated quartz filters by a high-volume sampler. For the tracer analysis the samples were extraced in dichloromethane and the extracts were fractionated (5 fractions) based on polarity by flash chromatography (by UAV). The less polar compounds were analysed directly by GC-MS (EI, 70eV), whereas the polar compounds were measured after derivatisation by BSTFA. The concentration of levoglucosan was measured directly from the filter after several extraction steps in methanol:dichloromethane and aceton:methanol solvent mixtures after derivatisation with BSTFA. For the H-NMR measurements the samples were extracted in water and the filtered and afterwards dried extracts were redissolved in D2O and measured by at 400 MHz in a Varian Mercury 400 spectrometer (by CNR-ISAC). The TC and OC/EC were determined by a thermal-optical method using the EUSAAR-2 protocol. Analysis of ^{14}C in TC was performed using accelerator mass spectrometry (by LU).

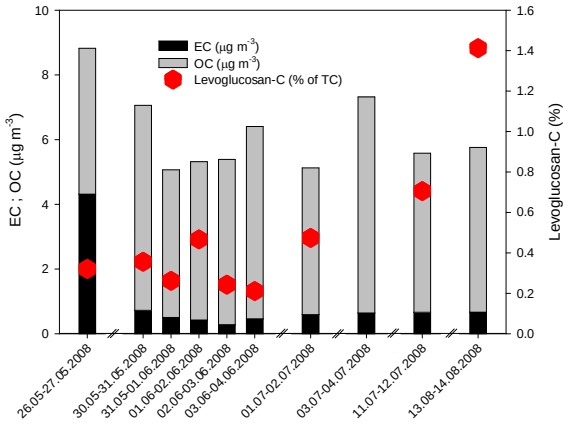

Figure 1. Concentration of OC, EC and the relative concentration of levoglucosan in the samples.

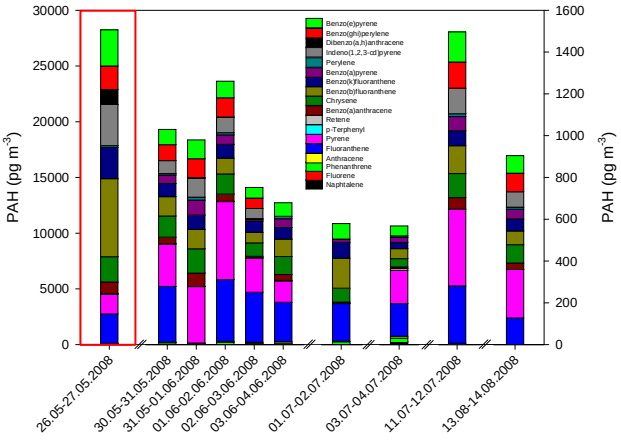

Figure 2. Concentration of PAHs in the samples collected at K-puszta

The contribution of EC to TC (TC mean concentration 6.2 µg m^{-3}) is on average 9.4% except the first sample (48.9%), which can be considered as a polluted sample, since wood-cutting were performed at the close vicinity of the site during the sampling (Figure 1). Note, that the concentration of levoglucosan remained average, indicating that wood combustion did not take place. Based on the levoglucosan concentration (mean 65.7 ng m^{-3}) it can be established that the contribution of biomass burning to the OC is on average 8.7%, indicating the importance of the natural sources.

The total concentration of PAHs in the polluted sample is about 30 times higher than the average of that in the other samples (Figure 2). This also indicates the strong anthropogenic input in this sample. The average total concentration of PAHs in the more clean period is about twice as much that measured for San Pietro Capofiume, an urban background site. The low value of the PAH ratio Flu/(Flu+Pyr) in the last sample indicates the contribution of biomass burning, in agreement with the elevated levoglucosan concentrations.

Total concentration of *n*-alkanes varied between 6.5 and 84.6 ng m^{-3}. The predominant *n*-alkane congeners (C27 and C29) reflect a significant incorporation of higher plant waxes. This biogenic origin is also pointed out by an average CPI of 7.67±3.9, which is in the range of values reported for other rural area. The contribution of natural wax alkanes (WNA%) to the total alkanes is on average 64.7%.

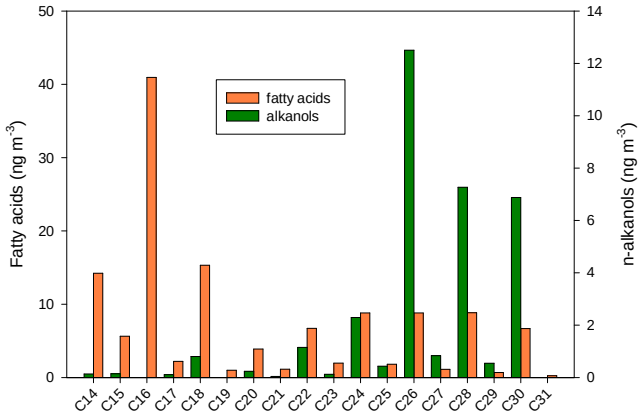

Figure 3. Distribution of n-alcohols and fatty acids in the K-puszta samples.

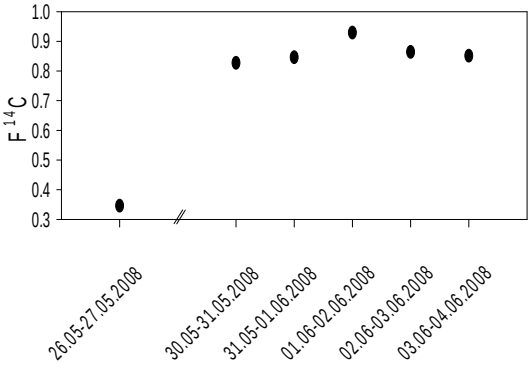

Figure 4. $F^{14}C$ values of samples colleted at K-puszta.

Fatty acids (Figure 3) show a clear even carbon number predominance (the average global CPI=8.1±1.7), with a bimodal distribution presenting maxima at C16 and C24-C28. The homologues <C20 may represent a microbial component. The release of n-alkanoic acids from fossil fuel combustion is another important source of the lower molecular weight n-alkanoic acids, peaking at C16:0. The higher molecular weight homologues are typical of composited terrestrial vegetation wax. The values of ≥C22/<C20 is on average 0.56. This ratio is only 0.1 at the polluted sample indicating the elevated contribution of the anthropogenic sources. The C18/C16 ratio is also indicative of source type. Ratios lower than 0.25 have been obtained in atmospheric PM2.5 resulting from foliar vegetation combustion, waxy leaf surface abrasions, and wood smoke; values between 0.25 and 0.5 were registered for car and diesel trucks exhausts. At K-puszta this rato varies between 0.23 and 0.57, indicating the contribution of these sources. The n-alkanols also show even carbon number predominance (CPI=13.1±1.6) the Cmax is at C26. These parameters indicate biogenic origin. The n-alkanol homologues <C20 are derived from microbial sources. The long chain linear alcohols are characteristic of the vegetation waxes. The contribution of the natural sources (WNAL%) to the n-alkanol concentration in the measured carbon number range is on average 85.1%.

The K-puszta H-NMR spectra (Task 2.4.1b, by CNR-ISAC) of the water soluble fraction show sharp peaks from individual compounds superimposed on a broad background signal attributable to a more complex mixture of products (not shown here). All spectra overlap quite nicely, and no appreciable changes in their general features can be found among the different samples. The collected samples present a chemical composition prevalently aliphatic accounting partly for species containing aromatic groups. Oxygenated groups, e.g. ketone, carboxyl and hydroxyl, contribute significantly together with alkyl moieties, the latter showing prominent bands in the right side of the spectrum. The functional group composition pattern found for these samples is typical of rural ambient oxidized organic aerosols. Moreover the substantial contribution of hydroxyl groups along with the detection of signals belonging to levoglucosan, a well-known biomass burning tracer, suggest that the collected aerosol was impacted by biomass burning.

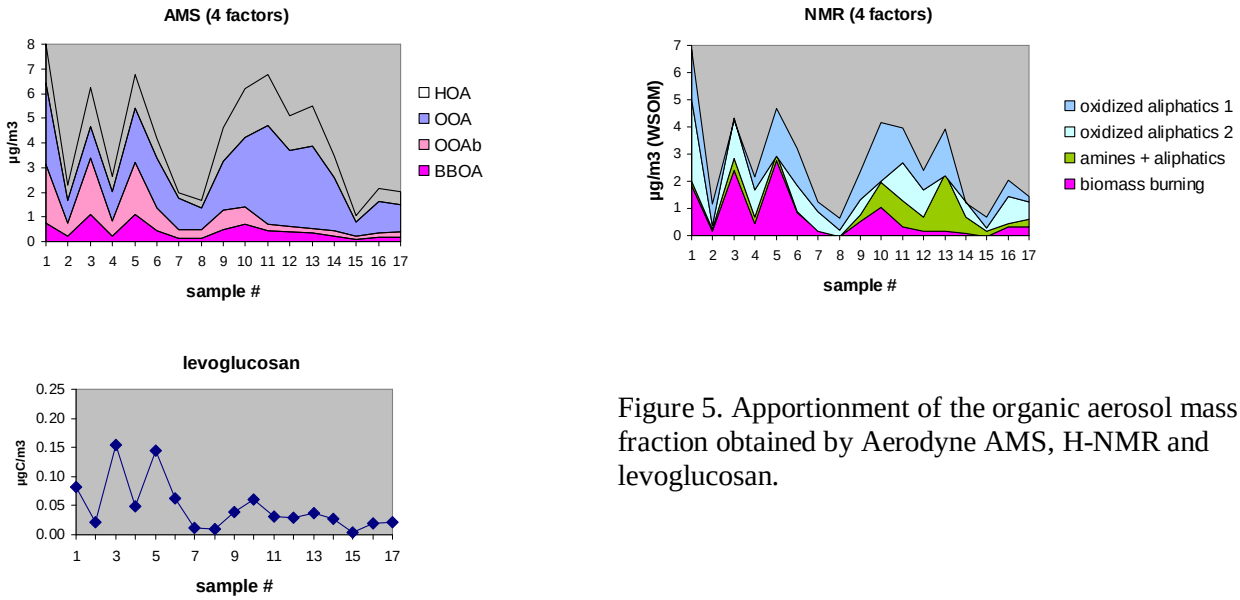

Figure 5. Apportionment of the organic aerosol mass fraction obtained by Aerodyne AMS, H-NMR and levoglucosan.

The ^{14}C measurements of the samples (Task 2.4.1c, by LU) indicates that the contribution of recent carbon to the samples is 10-15%, except at the first sample, where the low value of $F^{14}C$ (fraction modern carbon) indicates the contribution of fossil fuel combustion (Figure 4).

The 2008 campaign at San Pietro Capofiume, Italy, can serve as an example of the combination of organic tracers (Task 2.4.1a) and spectral fingerprints using H-NMR and an Aerodyne Aerosol Mass Spectrometer (AMS, Task 2.4.1b). At this site, organic source apportionment was performed by applying the PMF multivariate statistical technique (Positive Matrix Factorization) to the time series of AMS and 1H-NMR spectra.

The time-averaged AMS factors (derived from a PMF analysis of the original AMS mass spectra) and the 1H-NMR factors correlate well in tracing the contribution of wood burning (Figure 5).

Task 2.4.2
FLEXPART calculations have been performed by NILU for all EUCAARI/EUSAAR sites and are continuously being updated. These will be used to determine the geographical source regions. The FLEXPART output data are presented at http://transport.nilu.no/projects/eucaari.

Task 2.4.3
Updates of the EMEP model for the concentration fields of mineral dust and sea salt is carried out within EMEP MSC-W, and ongoing.

The Unified EMEP model version rv3 is now available as open source together with a full input data set for 2005 (http://www.emep.int/OpenSource/index.html).

The release of the model is intended to facilitate insight in the model assumptions, the parametrizations used, the requirements for input data and the actual model code; encourage dialogue and collaboration with modeling community; and to allow individual model runs and insight on how to run different scenarios. The parameterizations used for mineral dust and sea salt are described in an EMEP report (http://emep.int/UniDoc/report.html).

Task 2.4.4
This task aims to evaluate the uncertainties in the formation and fate of secondary organic aerosol (SOA) in regional and global models, and develop improved parameterizations. These uncertainties in the SOA component simulations are associated with a number of adopted simplifications in order to reduce the computational requirements of the modules. The evaluation of the simulations is performed by comparison with observational data.

The EMEP and the ECPL model parameterizations of secondary organic aerosol (SOA) formation in the troposphere were compared, differences have been identified and critical gaps in knowledge have been pointed out.

The EMEP EC/OC model involves two versions of a gas-particle scheme for secondary organic aerosol (SOA) and was previously compared with measurements from the EMEP EC/OC campaign and the EU CARBOSOL project. The two schemes were Kam-2 and a modification, Kam-2X. The EMEP SOA scheme was able to predict observed levels of OC in Northern Europe quite well, but that we underestimated significantly in southern Europe. In wintertime, the underprediction was explained by problems with wood-burning emissions (possibly local). In summer the problems were shown to arise from an underprediction of the SOA components. This study also demonstrated that the model results were very sensitive to assumptions concerning the vapour pressure of the model compounds.

In order to improve the EMEP SOA model, a new version is under construction incorporating some of the recent ideas inherent in the so-called volatility-basis set (VBS) approach, which was introduced to help models cope with both the wide range of aerosol concentrations (COA) in the atmosphere and the ongoing

oxidation of semi-volatile organics in both the gas and particle phases. The VBS based model results are very sensitive to assumptions regarding the (semi)volatility of anthropogenic VOC-emissions and chemical aging of SOA. Further validation against larger observational data sets will be needed before firm conclusions can be drawn. The VBS models are computationally efficient and they are interesting candidates for 3D modelling.

GLOBAL/REGIONAL-SCALE PARTICLE NUMBER – PRIMARY VS. SECONDARY, NATURAL VS. ANTHROPOGENIC: WORK PACKAGE 2.5

Ilona Riipinen on behalf of WP 2.5

University of Helsinki, Department of Physics, Helsinki, Finland

Keywords: Models, global, regional, particle number, primary, secondary, natural, anthropogenic

INTRODUCTION

Work Package 2.5 aims to quantify the relative contribution of natural and anthropogenic as well as primary and secondary sources to particle number concentrations at climate-relevant sizes. The budget of particle number concentration is essentially unknown except in specific environments with a few dominant sources (such as urban areas). Directly emitted (primary) particles contribute directly to particle number, and natural and anthropogenic emissions of gases, such as SO2 and organics, can lead to formation of new (secondary) particles through their nucleation and condensation. We need to know what fraction of particles comes from primary particles and what fraction is formed through nucleation in different environments. Without such fundamental information, long-term changes in aerosol abundance, and hence the effects of aerosol and climate, will remain uncertain in models.

Work Package 2.5 started at the beginning of Month 18, in the second half of Year 2. The specific objectives of Work package 2.5 at the beginning of Month 18 were:

- to assess the relative contribution of primary and secondary particle emissions to total particle number in different size ranges and environments (Task 2.5.1);
- to assess the relative contribution of natural and anthropogenic particle emissions to total particle number in different size ranges and environments (Task 2.5.2);
- to evaluate long-term changes in particle concentrations in different environments (Task 2.5.3).

To achvieve these goals, this WP implements the latest emission inventories and formation mechanisms in both global and regional aerosol microphysics models, along with detailed process models, evaluates them against observations, and determines how different particle sources shape the particle size distribution and number. The models that are used within the framework of WP 2.5 include global CTM GLOMAP, regional 3-D model PMCAMx-UF, modified box model UHMA and a modification of the GCM ECHAM5-HAM.

RESULTS AND ONGOING WORK

Task 2.5.1

First model runs on the global impact of secondary particle formation on CN and CCN numbers have been conducted conducted with a global CTM GLOMAP and published (Spracklen et al., 2006, 2007, Merikanto et al., 2009a). The latest model results suggest that 31–49 % of the low-level CCN are derived from nucleation, 35 % being originally formed in upper and free troposphere. Recently, CN numbers produced by GLOMAP have been evaluated against a number of global field sites as in the earlier studies comparison was concentrated on stations in Finland and central Europe.

In the global analysis, observations of total particle concentration (CN) at 32 sites worldwide are used to quantify the global sources of particle number concentration (Fig. 1). It is found that emissions of primary particles can reasonably reproduce the spatial pattern of observed CN (R^2=0.54) but not the observed

annual cycle (R^2=0.1). In the continental boundary layer (BL) the modeled CN concentration is biased low (normalized mean bias, NMB=-73%) unless anthropogenic primary particles are emitted at small sizes or an empirical boundary layer (BL) particle formation mechanism based on sulfuric acid is included (input from WP 1.1). Using sensitivity tests we derive optimum nucleation rate coefficients for this mechanism, which agree with values derived from detailed case studies at individual sites. We find that the annual CN cycle observed at continental BL sites is best explained including this BL nucleation mechanism (R^2=0.3). At free tropospheric sites a combination of primary emissions and binary homogeneous nucleation in the free and upper troposphere can reasonably explain the magnitude (NMB=-25%) and seasonal cycle (R^2=0.26) of observed CN.

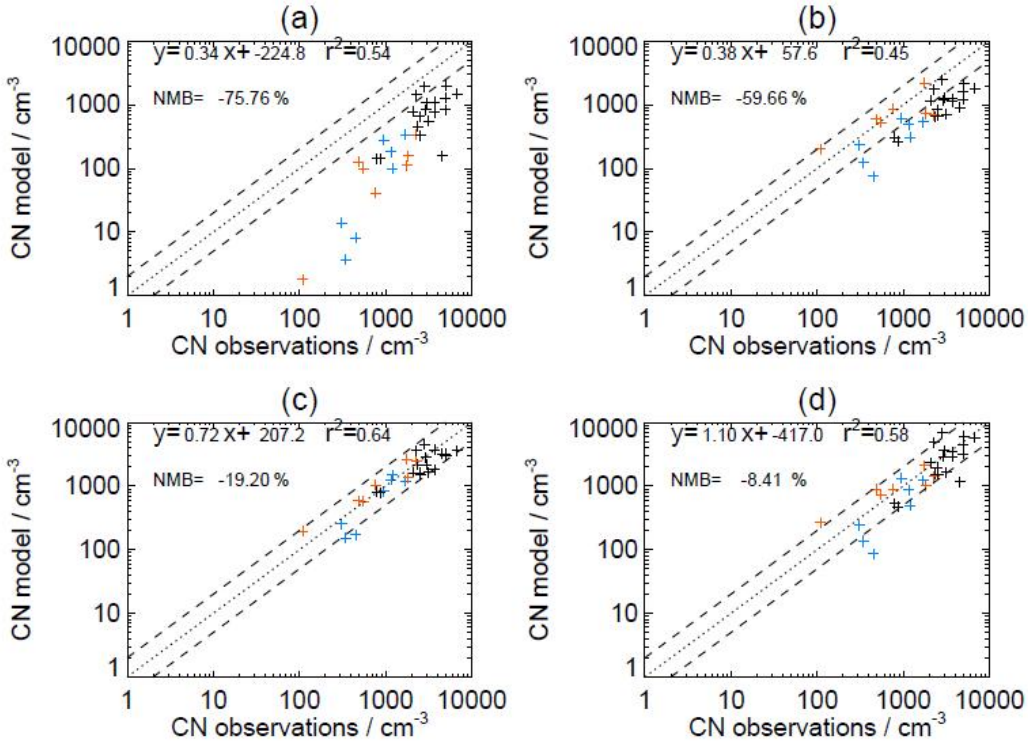

Figure 1. Comparison of modelled and observed CN on a global scale. a) primary emissions only, b) primary emissions + binary homogeneous nucleation in the FT, c) as b but with boundary layer nucleation; d) as b but with primary emissions of particle number * 8. Results from Spracklen et al., in prep (2009).

In our analysis of particle concentrations over Europe we used observations from the Long Range Experiment (LONGREX) during which ambient aerosol was sampled over Europe by the DLR Falcon research aircraft providing particle number size distribution measurements from 14 separate flights. The CN number concentration data used in this study were obtained by the Condensation Particle Size Analyzer (CPSA) and Passive Cavity Aerosol Spectrometer Probe (PCASP) instruments onboard the aircraft. Observations of primary aerosol were also obtained by the Falcon aircraft by measuring the non-volatile particle fraction with a cut-off particle diameter (Dp) of 14 nm.

Work is at an early stage and is reported in detail in Reddington et al. (this volume). So far, the results show that even with boundary layer nucleation the model underpredicts particle number in the European boundary layer (Fig. 2). Analysis of involatile particles suggests the underprediction is in both volatile (presumably nucleated) particles and involatile (presumably primary) particles. This is in contrast to previous analyses, which showed reasonable agreement.

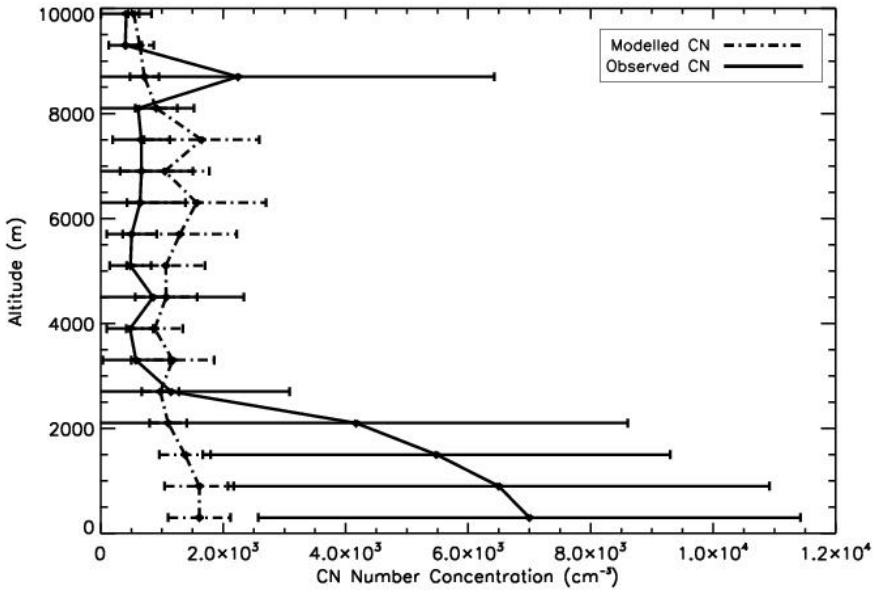

Figure 2. Campaign average vertical profile of modelled and observed CN number concentrations (Dp > 10nm). The modelled CN concentration was interpolated to the flight path of the Falcon aircraft and sectioned into altitude bins of 600 m. The mean CN concentration of each bin has been plotted with error bars showing the standard deviation of the mean. From Reddington et al. (this volume).

Regional 3D-model PMCAMx-UF has been developed (Jung et al., 2008; Jung 2008). The model simulates the aerosol number (from 1 nm to 10 μm) and mass distributions for a variety of chemical components, and first applications and tests were conducted for the Eastern United States for which input data such as emission inventories were readily available (Jung et al., 2009). To test the impact of boundary layer nucleation on aerosol number, the model allows the user to user can select among several different nucleation parameterizations, one of which being the parameterization developed in WP 1.1. Specifically, it was found in these first studies that model runs using scaled ternary water – sulphuric acid – ammonia nucleation parameterisation (Napari et al., 2002) served well in predicting the particle formation and growth events observed in Pittsburgh, USA. Recently, a version of PMCAMx-UF simulating the European domain has been developed (see Fig. 3), and first comparisons between the predicted particle composition, mass and number against observations at the EUCAARI sites have been conducted (Figs. 4 and 5).

The global climate model ECHAM5-HAM (Stier et al., 2005) has been modified to improve the representation of new particle formation in the boundary layer. The effect of nucleation on cloud droplet number was studied with the modified version of the model (Makkonen et al., 2008). In these runs the simple particle formation scheme introduced in WP 1.1 (see also e.g. Sihto et al., 2006) was used to model boundary layer nucleation, and the particle growth was accounted for with the condensation of organics. Comparisons to observations indicate that simple nucleation scheme used in the study is a promising way to improve the ECHAM5-HAM model closer towards the average values observed over different locations.

a)

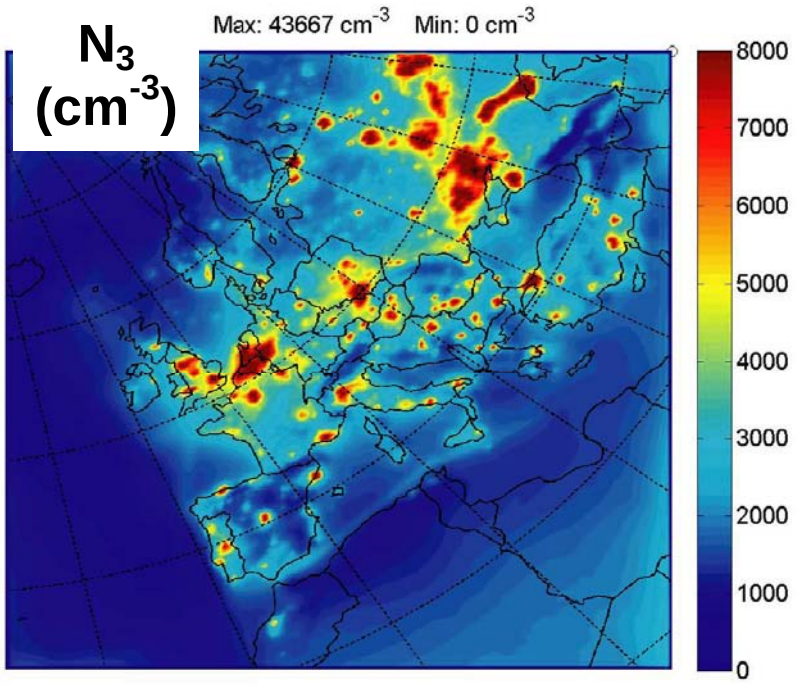

b)

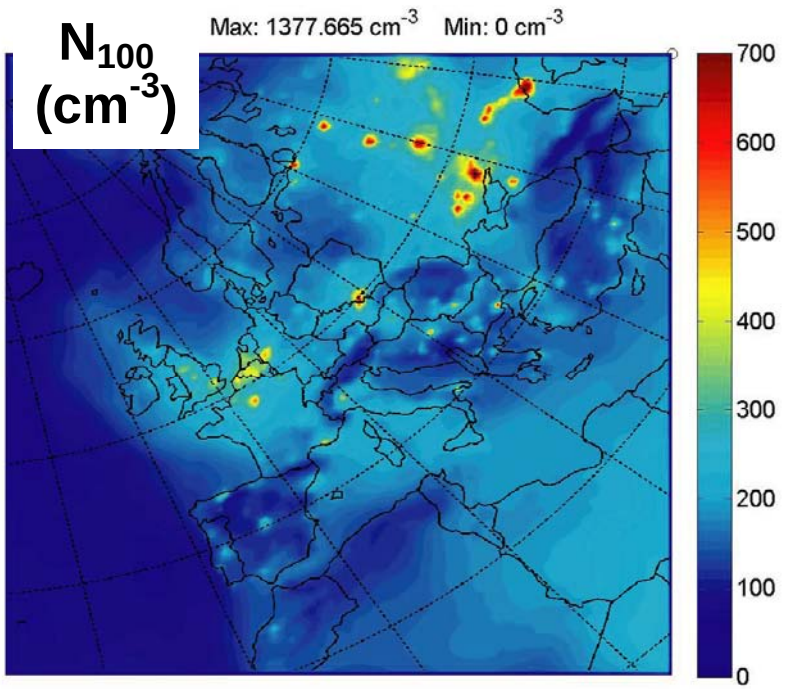

Figure 3. Larger than a) 3 nm and b) 100 nm number concentrations in Europe as predicted with the 3-D regional model PMCAMx-UF.

a)

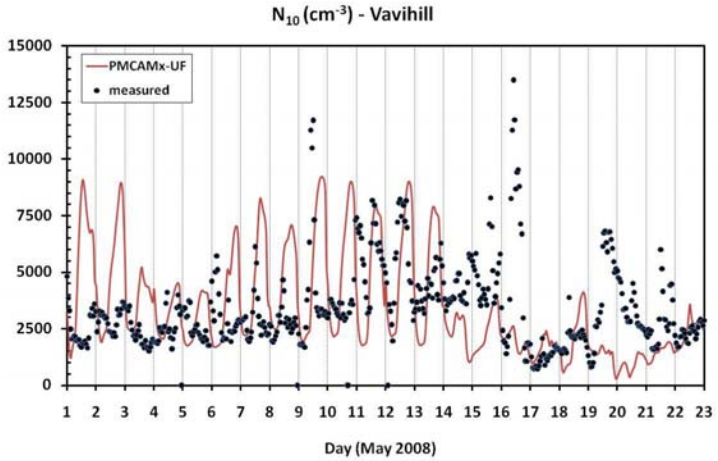

b)

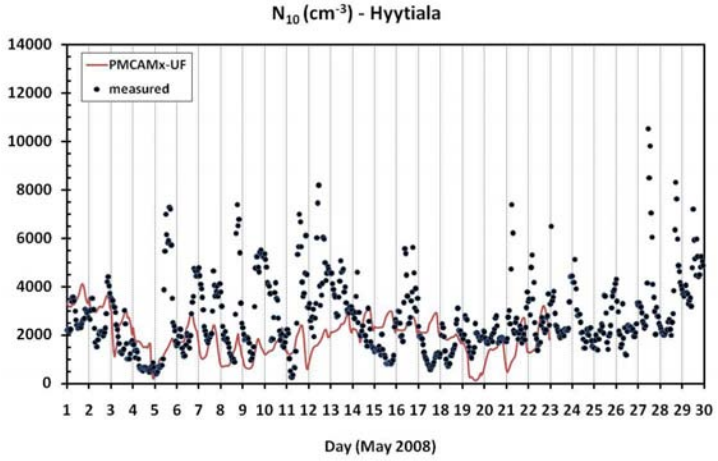

c)

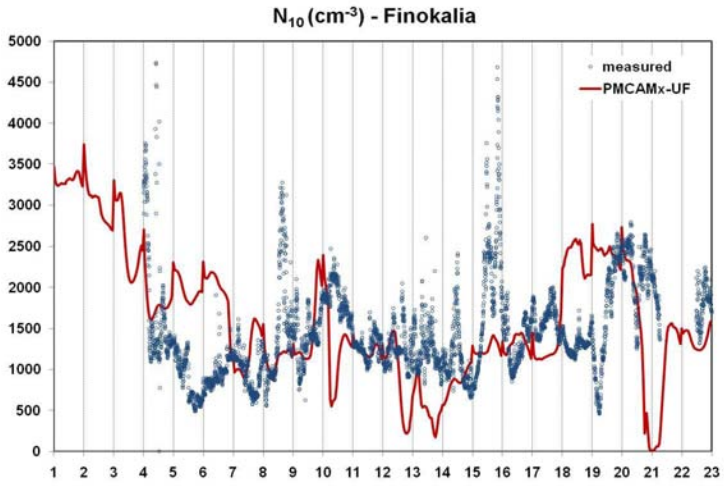

Figure 4. A comparison between the measured and modeled number concentrations of particles larger than 10 nm at a) Vavihill b) Hyytiälä c) Finokalia.

Task 2.5.2

First global model runs studying the effect of anthtropogenic and biogenic emissions on particle formation have been conducted with GLOMAP (Spracklen et al., 2008). It was observed that boundary layer nucleation and emissions of biogenic organics are coupled, when looking at their effect on CCN numbers, and that on average the forest emissions increase boreal CCN with about 100%. However, in a run without nucleation the forest emissions increase CCN by only 50%. Thus, forest terpene emissions are twice as effective at producing CCN if nucleation occurs.

The contribution of biogenic SOA formation on total aerosol mass has been estimated using a physico-chemical box model applied in a Lagrangian manner over Scandinavia (Tunved et al., 2008). A recently-developed parameterization for the aerosol mass yield from biogenic terpenes was used (see also Tunved et al., 2006). It was concluded that the needle-leaved forest above 58ºN alone is capable of producing aerosol mass concentrations corresponding to 12-50% of today's total values in the boundary layer – giving the minimum estimate for the biogenic influence on particle mass. It was also demonstrated that the forest itself could produce up to 200 CCN per cubic centimetre on average over Scandinavia.

Task 5.2.3

Model runs comparing global CCN, cloud droplet numbers (CDN) and cloud reflectivity in 1850 and 2000 have been conducted with GLOMAP (Merikanto et al., 2009b). The results indicate that the global impact of nucleation on the 1850-to-2000 change in cloud reflectivity is small (few percent) but regionally it may be as high as 50% and can be either positive or negative. These early results suggest that boundary layer nucleation will be important in indirect forcing calculations on a regional scale.

FUTURE WORK AND INTEGRATION

In the upcoming 18 months more global and regional model experiments with GLOMAP and PMCAMx-UF will be carried out to quantify the relative contribution of particle formation and primary emissions to observed particle number concentrations in different size ranges and in different environments. The sensitivity of the results to varying biogenic and anthropogenic emissions will be tested as well. We will continue the effort to evaluate the models against existing observations from ground stations and against new observations made during the EUCAARI field phase and airborne measurements in 2008 (WPs 2.1, 2.2, 4.2, 4.3), and a model intercomparison will be undertaken to better understand the model processes that are important for a realistic simulation of nucleation events and growth to CCN sizes. The latest particle formation schemes from WP 1.1 and 1.2 and new size-resolved primary particle emission inventories from WP 1.3 will be implemented in the models.

REFERENCES

Jung J.-G., Pandis S.N. and Adams P.J., 2008. Evaluation of nucleation theories in a sulfur-rich environment. Aerosol Sci. Technol., 42, 495-504.

Jung J.-G., 2008. Regional Air Quality-Atmospheric Nucleation Interactions, Ph.D. thesis, Carnegie Mellon University, Pittsburgh, Pennsylvania.

Jung J.-G., Fountoukis C., Adams P. J., and Pandis S. N., 2009. Simulation of in-Situ Ultrafine Particle Formation in the Eastern United States Using PMCAMx-UF, J. Geophys. Res., in review.

Kulmala M., Lehtinen K. and Laaksonen A., 2006. Cluster activation theory as an explanation of the linear dependence between formation rate of 3 nm particles and sulphuric acid concentrations. Atmos. Chem. Phys., 6, 787-793.

Makkonen R., Asmi A., Korhonen H., Kokkola H., Järvenoja S., Räisänen P., Lehtinen K.E.J., Laaksonen A., Kerminen V.-M., Järvinen H., Lohmann U., Feichter J. and Kulmala, M., 2008. Sensitivity of aerosol concentrations and cloud properties to nucleation and secondary organic distribution in ECHAM5-HAM global circulation model. Atmos. Chem. Phys. Discuss., 8, 10955-10998.

Merikanto J., Spracklen D. V., Mann G. W., Pickering S. J., and Carslaw K. S., 2009a. Impact of nucleation on global CCN, Atmos. Chem. Phys. Discuss., 9, 12999-13037.

Merikanto J., Spracklen D. V., Pringle K. J., and Carslaw K. S., 2009b. Effects of boundary layer particle formation on cloud droplet number and changes in cloud albedo from 1850 to 2000, Atmos. Chem. Phys. Discuss., 9, 5263-5287.

Napari I., Noppel M., Vehkamäki, H. and Kulmala M., 2002. Parameterization of ternary nucleation rates for H2SO4-NH3-H2O vapors. J. Geophys. Res., 107(D19), 4381, doi:10.1029/2002JD002132.

Sihto S.-L., Kulmala M., Kerminen V.-M., Dal Maso M., Petäjä T., Riipinen I., Korhonen H., Arnold F., Janson R., Boy M., Laaksonen A. and Lehtinen K. E. J., 2006. Atmospheric sulphuric acid and aerosol formation: implications from atmospheric measurements for nucleation and early growth mechanisms. Atmos. Chem. Phys., 6, 4079-4091.

Spracklen D., Carslaw K., Kulmala M., Kerminen V.-M., Mann G. and Sihto S.- L., 2006. The contribution of boundary layer nucleation events to total particle concentrations on regional and global scales. Atmos. Chem. Phys., 6, 5631–5648.

Spracklen D.V., Carslaw K.S., Kulmala M., Kerminen V.-M., Sihto S.-L., Riipinen, I., Merikanto J., Mann, G.W., Chipperfield M.P., Wiedensohler, A., Birmili, W. and Lihavainen H., 2007. Contribution of particle formation to global cloud condensation nuclei concentrations. Geophys. Res. Lett., 35, L06808, doi:10.1029/2007GL033038.

Spracklen, D.V., Carslaw K.S. and Bonn, B., 2008. Boreal forests, aerosols and the impacts on clouds and climate, Philosophical Transactions, A., accepted.

Stier, P., Feichter, J., Kinne, S., Kloster, S., Vignati, E., Wilson, J., Ganzeveld, L., Tegen,
I., Werner, M., Balkanski, Y., Schulz, M. and Boucher, O., 2005. The aerosol-climate model ECHAM5-HAM, Atmos. Chem. Phys., 5, 1125–1156.

Tunved P., Hansson H.-C., Kerminen V.-M., Ström J.M.D., Lihavainen H., Viisanen Y., Aalto P., Komppula M. and Kulmala M., 2006. High natural aerosol loading over boreal forests. Science, 312, 261-263.

Tunved P., Ström J., Kulmala M., Kerminen V.-M., Dal Maso M., Svennignsson B., Lunder C and Hansson H.-C., 2008. The natural aerosol over Northern Europe and its relation to anthropogenic emissions – Implications of important climate feedbacks Tellus, 60B, 473-484.
.

CCN/IN activation and optical properties

Ulrike Lohmann on behalf of WP3.1

Institute for Atmospheric and Climate Science, ETH Zurich, Switzerland

Keywords: CCN, IN, optical properties

INTRODUCTION

Anthropogenic aerosol particles such as sulphate and carbonaceous aerosols have substantially increased the global mean burden of aerosol particles from pre-industrial times to the present-day. One of the biggest unknowns is the role of aerosols acting as cloud condensation nuclei (CCN) and as ice nuclei (IN). The increase in cloud droplet number due to an increase in anthropogenic aerosols for a given cloud water content increases the cloud albedo. In addition, the precipitation efficiency of warm clouds is reduced, possibly increasing cloud lifetime (aerosol cloud lifetime effect). Both effects remain to be very uncertain (Denman et al., 2007). Here, laboratory studies are used to evaluate the ability of aerosols to act as CCN and IN.

Task 3.1.1 Laboratory studies of the ability of aerosols to act as CCN:

Organic compounds with surfactant properties are commonly found in atmospheric aerosol particles and can significantly affect their ability to activate as cloud droplets.
Prisle et al. (2009) confirm previous results for single-component organic surfactant particles, that experimental critical supersaturations are greatly underpredicted, if reduced surface tension is applied in Köhler theory while ignoring the effects of surface partitioning in droplets. We further show that assuming the constant surface tension of pure water can also lead to significant underpredictions of experimental critical supersaturations. The full account for surfactant partitioning in activating droplets generally predicts experimental critical supersaturations well. In addition, for mixed particles comprising less than 50% by mass of surfactant, ignoring surfactant properties and simply using the constant surface tension of pure water also provides a good first-order approximation of the observed activation (Figure 1).

Results: mixed SDS + NaCl particles

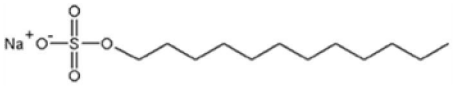

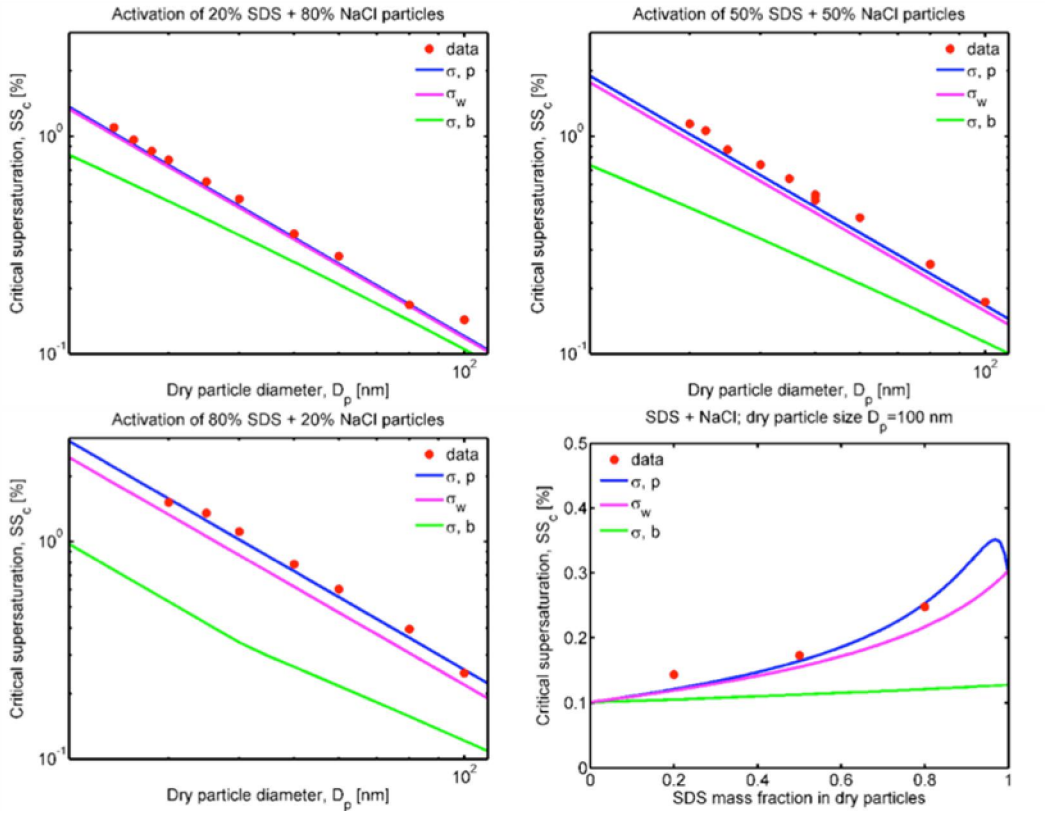

Figure 1. Experimental results and model predictions for mixed particles of SDS and NaCl (from Prisle et al., 2009).

In addition to the laboratory measurements, the group at PSI (Juranyi et al.) now has more than a full year of CCN data from the Jungfraujoch, which includes May 2008. They also have a large data set of complementary data, which allow for a closure between size distribution, hygroscopic growth and CCN number concentration (Figure 2). They will be able to provide a simple parameterization for CCNC concentration for the Jungfraujoch.

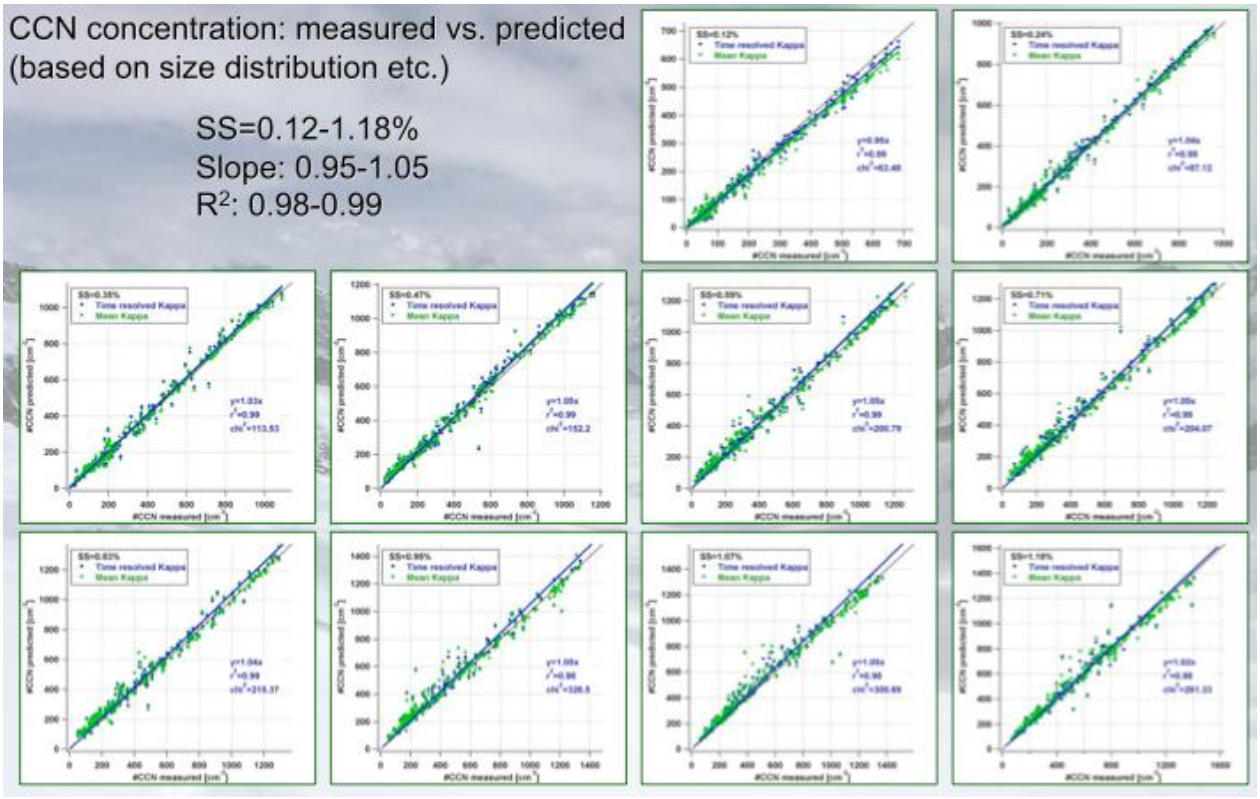

Figure 2: Measured vs. predicted CCN concentrations from one year of continuous data at the Jungfraujoch.

Task 3.1.2 Laboratory studies of the ability of aerosols to act as IN:

The recently developed Immersion Mode Cooling Chamber (IMCA) has been used as an extension of the Zurich Ice Nucleation Chamber (ZINC; Stetzer et al., 2008) in order to measure the ice nucleation efficiency of size selected kaolinite particles in the immersion mode. Particles with selected sizes of 200 nm, 400 nm and 800 nm have been activated as cloud condensation nuclei (CCN) in order to obtain droplets with single immersed particles. After continuous cooling of the droplets to the experimental temperature in ZINC, the frozen fraction of the droplets was measured with the newly developed depolarisation detector IODE (Ice Optical Detector; Nicolet et al., 2008). In the investigated size range, kaolinite particles do not appear to be particularly efficient ice nuclei (IN). Although not very strong, a size dependence of the freezing efficiency has been observed. The median freezing temperature increases from −35◦C for 200 nm kaolinite particles to −33◦C for 800 nm particles (Figure 3). The temperature dependent frozen fraction of droplets has been fitted with functions derived with different theoretical models. Best fits of the data are obtained with two models: One is based on classical nucleation theory (CNT) in combination with a surface distribution of active sites of various quality (represented by a contact angle α), and the other is a deterministic model attributing a distinct freezing temperature to each potential nucleating site. In contrast, a fit function based on CNT with one constant contact angle for all IN (stochastic hypothesis) cannot be used to describe immersion freezing with kaolinite particles.

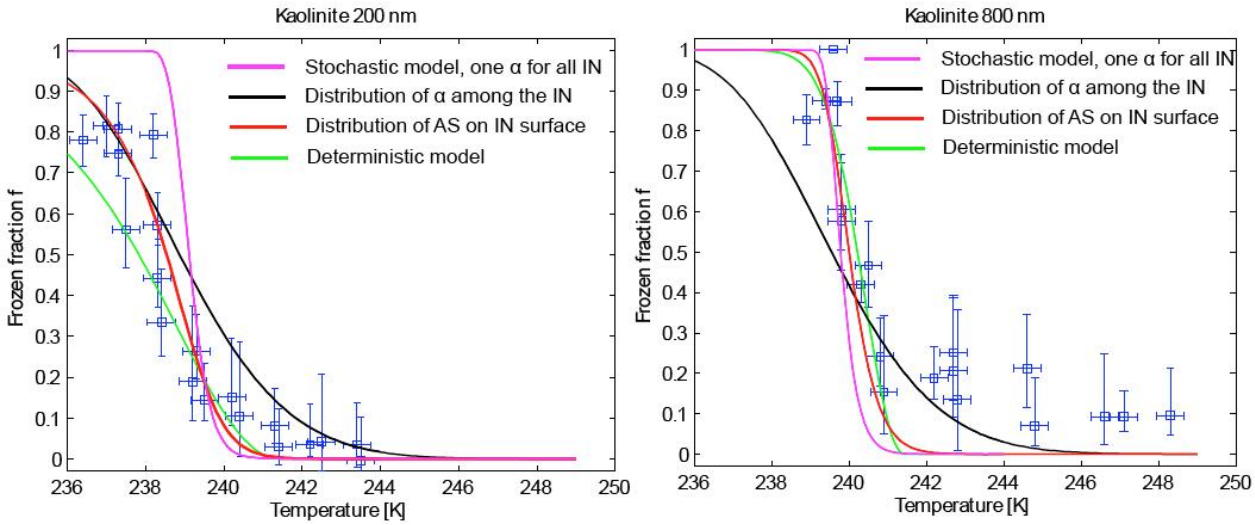

Figure 3: Frozen fraction *f* of droplets as a function of temperature for immersed 200 nm and 800 nm kaolinite particles. Solid lines show fit curves obtained with different functions for *f* derived from nucleation theory with different assumptions concerning the stochastic or deterministic nature of the ice nucleation process. (Lüönd et al., subm. to JGR).

In a next step, "ageing" of IN and CCN will be investigated from measurements at the PSI smog chamber.

Task 3.1.3 Analysis of airborne data

Aerosol-cloud interactions should be studied at the cloud level; yet, aerosols (and particularly cloud condensation nuclei) are often measured at ground-based sites owing to high costs and demanding infrastructure associated with routine airborne observations. To reduce the uncertainty of the impact of aerosol particles on the climate, the European Integrated project on Aerosol Cloud Climate and Air Quality Interactions (EUCAARI) intensive integrated multiple aircraft and ground stations to quantify the sources and sinks of regional aerosol and their physical and chemical transformations with respect to their cloud-forming potential. During EUCAARI, simultaneous observations of cloud condensation nuclei (CCN) and lidar aerosol extinction profiles provide a unique opportunity to quantify the vertical distribution of CCN and relate the in-situ measurements to remote sensing observations. In-situ observations of CCN concentrations between the ground-based measurements and the airborne measurements on indicate that CCN measurements on the ground often over-estimate the concentrations at levels where clouds form. During the clean background conditions when the air masses originate from the North Sea and cloud bases are relatively low, the boundary layer is well mixed and CCN concentrations at the ground resemble those at cloud base. The difference between ground-based and airborne measurements is especially important at higher concentrations associated with local pollution, when boundary layer mixing timescales are greater than the timescales for transport. In addition, multiple layers of aerosols with different origins related to long-range transport, especially during a Sahara dust episode, further complicate the relationship between in-situ ground-based and airborne CCN measurements. An order of magnitude difference in CCN spectra between clean period related to northerly winds & Sahara dust episode was observed (European polluted background between the two). Ground-based and airborne lidar observations detect multiple aerosol layers, provide insight to boundary layer mixing and are useful tools to investigate the relationships between ground-based and airborne measurements (Roberts et al., 2009).

The IMPACT campaign covered multi-instrument aircraft measurements of in-cloud vertical wind velocity as well as cloud-droplet size spectrometry. Results of these in-situ measurements are the basis for deriving statistics of cloud-microphysical parameters such as liquid water content, cloud droplet concentration and other statistical moments of the droplet size spectrum by Pawlowska et al. The key datasets employed in the analysis are the data obtained by the PVM-100 and FSSP-100 optical cloud-

droplet sensors. The cloud-droplet size spectrum features are to be compared on different levels above the cloud base. By using the data from the aircraft gust probe, the droplet-spectrum features are to be analyzed separately for the updraft and downdraft regions in the cloud. The analysis is to be carried out separately for the case of marine stratocumulus deck probed along the Scottish coast of the North Sea on May 15th 2008, and for the several cases where continental cumuli were probed above The Netherlands, e.g. on May 13th, 14th, 19th and 28th.

Task 3.1.4 Lagrangian parcel model simulations:

Due to changes in personal, no one has worked on this task and will work on that in future.

Task 3.1.5 Large-eddy-simulation model simulations for investigating cloud radiative properties (Horn and Knoth, Leipzig)

A simple one moment microphysical scheme with explicit handling of the condensation process was implemented into the model ASAM by Stefan Horn (IfT, Leipzig) to reproduce marine stratocumulus and cumulus cloud structures. In parallel a strong reduction of computation time could be reached by writing a new 3D-LES model with the same physical parametrisations but using the enormous computation power of modern GPU's. The scheme and also the new GPU-Model was tested against the DYCOMS (Stevens et al., 2005) and BOMEX (Siebesma et al., 2003) cases, and produced quite promising results (Fig. 4).

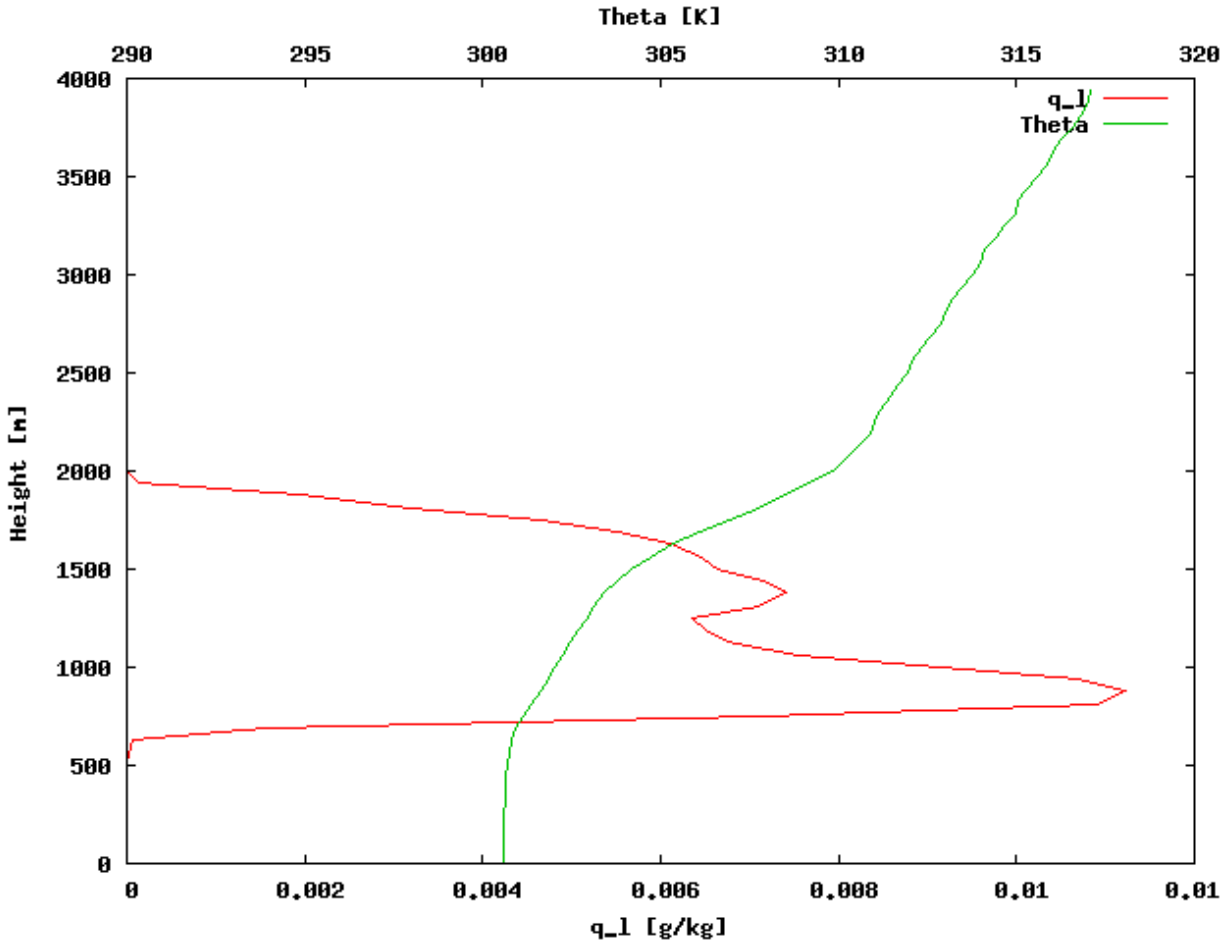

Figure 4: Mean profiles for the 4th hour of the BOMEX-Case for cloud water (red) and potential temperature (green)

The next step to study aerosol effects on cloud structures and after that radiation effects in such cloud structures, was the further development to a two moment microphysical scheme with explicit treatment of nucleation and cloud condensation nuclei. So a parametrization containing warm processes (based on the work of Seifert and Beheng, 2006) was implemented.
At the moment this two moment scheme is still under development and testing, using the RICO case, which is the 9th case study of the GCSS boundary layer cloud working group. But first results from the GPU-Model for this case are also available (Fig. 5).

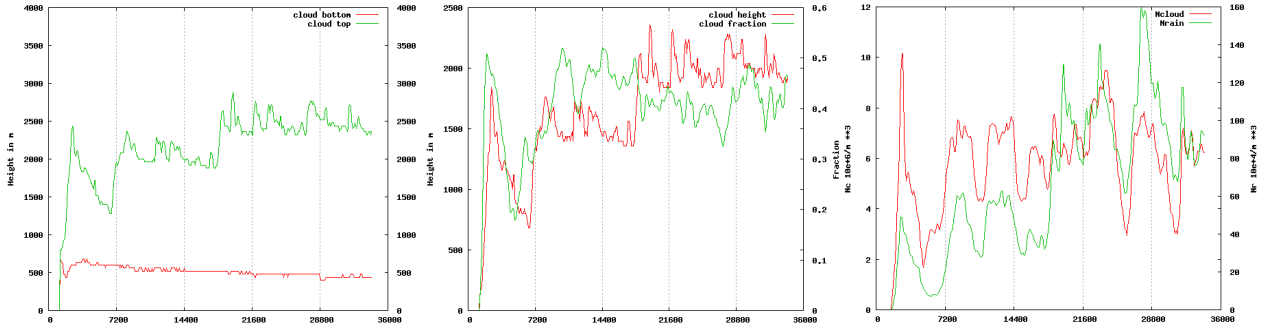

Figure 5: First results from the RICO test case; x-axis: time in seconds; left: cloud-top and base; middle: cloud height and fraction; right: number concentration cloud droplets and rain droplets;

In Fig. 5 it is noticeable that there are still problems with the number concentrations for cloud- and rain droplets, which are too low for the cloud- and too high for the rain droplets. After fixing the problems and further testing of the new microphysical scheme, comparisons using Cabauw boundary conditions to the measurements and other model runs are planned. If the microphysical implementation for the warm processes will be done, the next challenge is a simple radiation code. In the GPU-model there are already routines for ray casting, which are currently used for the visualisation, but should be applicable to simple radiation parametrisations in three-dimensional space as well.

Submitted publications with EUCAARI acknowledgements in 2009:

1) Prisle, N. L., T. Raatikainen, A. Laaksonen, and M. Bilde, Surfactants in cloud droplet activation: mixed organic-inorganic particles, submitted to Atmospheric Chemistry and Physics Discussions, Oct 2009
2) Lüönd, F., O. Stetzer, and U. Lohmann, Experimental study on the ice nucleation ability of size selected kaolinite particles in the immersion mode, submitted to J. Geophys. Res., 2009.

Planned publications:

1) Frosch et al., Thermodynamic properties and cloud droplet activation of a series of oxo-acids
2) Varga et al., Joint effect of organic acids and inorganic salts on cloud droplet activation
3) Urs Baltensperger's group: Paper on CCN data at the Jungfraujoch
4) Roberts G.C., L. Gomes, J.-L. Brenguier, A. Apituley, K.Wilson, R. Boers, D.P. Donovan, J. Pelon, D.B. Josset, M. Boquet, H. Coe, J. Trembath, Assessing aerosol-cloud interactions linking multi-platform observations and remote sensing, ACPD, in preparation.

The planned publication by Frosch et al. has overlap with WP 1.4

Additional References

Denman, K., Brasseur, G., Chidthaisong, A., Ciais, P., Cox, P., Dickinson, R., Hauglustaine, D., Heinze, C., Holland, E., Jacob, D., Lohmann, U., Ramachandran, S., Silva Dias, P., Wofsy, S., and Zhang, X. (2007), Couplings between changes in the climate system and biogeochemistry, in Climate Change 2007: The Physical Science Basis. Contribution of Working Group I to the Fourth Assessment Report of the Intergovernmental Panel on Climate Change, edited by S. Solomon, D. Qin, M. Manning, Z. Chen, M. Marquis, K. B. Averyt, M. Tignor, and H. L. 5 Miller, pp. 499–588, Cambridge Univ. Press, Cambridge, United Kingdom and New York, NY, USA, 2007.

Nicolet, M., Stetzer, O., and Lohmann, U.: Single ice crystal measurements during nucleation experiments with the depolarization detector IODE, Atmos. Chem. Phys. Discuss., 8, 20 965–21 000, 2008.

Stetzer, O., B. Baschek, F. Lüönd and U. Lohmann, The Zurich Ice Nucleation Chamber (ZINC) - A new instrument to investigate atmospheric ice formation, Aerosol Sci. Tech. 42, 64-74, 2008.

Seifert A., and K. D. Beheng, A two-moment cloud microphysics parameterization for mixed-phase clouds. Part I: Model description. *Meteor. Atmos. Phys.*, **92**, 45–66, 2006.

Siebesma, A. P., C. S. Bretherton, A. Brown, A. Chlond, J. Cuxart, P. G. Duynkerke, H. Jiang, M. Khairoutdinov, D. C. Lewellen, C.-H. Moeng, E. Sanchez, Stevens, and D. E. Stevens, A large eddy simulation intercomparison study of shallow cumulus convection. J. Atmos. Sci., 60, 1201-1219, 2003.

Stevens, B., C.H. Moeng, A.S. Ackerman, C.S. Bretherton, A. Chlond, S. de Roode, J. Edwards, J.C. Golaz, H. Jiang, M. Khairoutdinov, M.P. Kirkpatrick, D.C. Lewellen, A. Lock, F. Müller, D.E. Stevens, E. Whelan, and P. Zhu, Evaluation of Large-Eddy Simulations via Observations of Nocturnal Marine Stratocumulus. Mon. Wea. Rev., 133, 1443–1462, 2005.

WP3.2: Observational and modelling activities carried out to study the link between aerosols and clouds over the Netherlands and the North Sea

R. BOERS[1], M. SAVENIJE[1], G.-J. VAN ZADELHOFF[1], J. L. BRENGUIER[2], L. GOMEZ[2], V. PUYGRENIER[2], G. ROBERTS[2], J. PELON[2], H. PAWLOWSKA[3], S. ARABAS[3], D. JARECKA[3], H. SIEBERT[4], B. WEHNER[4], A. MENSAH[5], A. KIENDLER-SCHARR[5], A. TRIMBORN[5], T. MENTEL[5], H. TEN BRINK[6], G. KOS[6], G.-J. ROELOFS[7], R. HOLZINGER[7], C. UNAL[8], Y. DUFOURNET[8], H. RUSCCHENBERG[8], P. WANG[1], W. KNAP[1], A. P. SIEBESMA[1], R. NEGGERS[1], T. HEUS[9], I. SANDU[9], A. APITULEY[10]

[1]KNMI, De Bilt, Netherlands, [2]Metéo-France, Toulouse, France, [3]Institute of Geophysics, Warsaw, Poland, [4]Leipnitz Institute for Tropospheric Research, Leipzig, Germany, [5]Julich Research Centre, Germany, [6]Energy Centre, Netherlands, [7]University of Utrecht, Utrecht, Netherlands, [8]Technical University of Delft, Delft, Netherlands, [9]MPI, Hamburg, Germany, [10]RIVM, Bilthoven, Netherlands

Keywords: aerosol, clouds, indirect aerosol effect

INTRODUCTION

Present reporting is an inventory of substantial work performed by many people directly or indirectly involved in the WP3.2 work package. It encompasses work funded directly under EUCAARI, but also work funded by the individual institutes. The overall aim of WP3.2 was to improve our understanding of, and quantification of the indirect aerosol effect. This year, the 12 month record of data taking at The Cabauw Experimental Site for Atmospheric Research (CESAR) was completed. Considerable attention has been given to analysis of data and to setting up of modelling studies to interpret a number of case studies, both at Cabauw and at other locations off shore.

12 MONTH CONTINUOUS OBSERVATION PERIOD AND IMPACT DATA BASE (KNMI)

After the IMPACT campaign of May 2008 a select set of cloud and aerosol instruments continued to be operated at Cabauw, together with the standard operational set of tower, remote sensing and radiation instruments. This continuous observation period ended May 31 2009. The data are collected in the website annex data centre which was set up ahead of the IMPACT campaign (see http://www.knmi.nl/eucaari). This website has evolved over time; At first, emphasis was at preparations for the measuring campaign: Although initially used as a website, it has evolved to a full data centre. It supplies information on instruments that participated in the campaign, quick looks, data and utilities. Inventories can be derived from the web site. Additionally, the data are stored at the EUCAARI nilu web site / data base.

GROUNDBASED OBSERVATIONS

a) AMS (Julich)

Due to the success of employment of the High-Resolution Time of Flight Aerosol Mass Spectrometer (HR-ToF AMS) during IMPACT, the same instrument was deployed at Cabauw tower from 24th of February to 25th of March 2009. The instrument was located in the basement and connected to the common sampling line. The inlet of the sampling line was at 60 m and the aerosol was dried by two naphion dryers. The average mass loading was about 6 μgm^{-3}. 4 events with mass loadings exceeding 15 μgm^{-3} were recorded, each about 12 h to 24 h in duration. The average particle composition is dominated by nitrate (42%) and organics (22%). The fractional abundances of nitrate and organics are interchanged compared to May 2008. The average fractional abundance of sulfate (17%), ammonium (16%), and chloride (2%) are similar to the results from May 2008.

b) CCN – COUNTER

1) Back calibration of KNMI CCN counter (KNMI)

Effort is under way to perform a back calibration on the KNMI CCN counter. During the 2008 – 2009 period it was found that several CCN counter filters did not perform to their optimal standards. As a result it was decided to assess the filter quality and perform an in-depth study on the effect of filter quality on counter performance. This study is presently under way at ECN, Netherlands. Early results indicate that some of the CCN counter data will need to be corrected by a fixed reduction factor [to be decided later].

2) Integration of CCN data and airborne observations (Metéo-France)

Aerosol-cloud interactions should be studied at the cloud level; yet, aerosols (and particularly cloud condensation nuclei) are often measured at ground-based sites owing to high costs and demanding infrastructure associated with routine airborne observations. During EUCAARI, simultaneous observations of cloud condensation nuclei (CCN) and lidar aerosol extinction profiles provide a unique opportunity to quantify the vertical distribution of CCN and relate the in-situ measurements to remote sensing observations. In-situ observations of CCN concentrations between the ground-based measurements and the airborne measurements on indicate that CCN measurements on the ground often over-estimate the concentrations at levels where clouds form. During the clean background conditions when the air masses originate from the North Sea and cloud bases are relatively low, the boundary layer is well mixed and CCN concentrations at the ground resemble those at cloud base. The difference between ground-based and airborne measurements is especially important at higher concentrations associated with local pollution, when boundary layer mixing timescales are greater than the timescales for transport. In addition, multiple layers of aerosols with different origins related to long-range transport, especially during a Sahara dust episode, further complicate the relationship between in-situ ground-based and airborne CCN measurements. An order of magnitude difference in CCN spectra between clean period related to northerly winds & Sahara dust episode was observed (European polluted background between the two). Ground-based and airborne lidar observations detect multiple aerosol layers, provide insight to boundary layer mixing and are useful tools to investigate the relationships between ground-based and airborne measurements.

c) PRT-MS (University of Utrecht)

After successful measurements with the prototype aerosol-PTR-MS instrument during the EUCAARI-IOP campaign at Cabauw in May 2008 we successfully developed the new instrument featuring a time-of-flight mass spectrometer with a high mass resolution of >5000 and improved aerosol sampling units. The new instrument was operated at the Cabauw site in May 2009. We were able to detect several hundreds different molecules in the aerosol burden at Cabauw and the detection limit foe individual compounds has been shown to be below 50 pg/m3.

d) VERTICAL RADAR WIND MEASUREMENTS (Technical University of Delft)

One problematic aspect of CCN concentration observations at cloud base is that they are dependent upon the vertical wind speed there. At Cabauw such vertical wind speed observations are to be obtained from remote sensing data. During May 2008, there were several instruments independently operated to obtain vertical wind speed: namely KNMI tower-mounted sonic anemometers (high time resolution, at heights 2, 60, 100 and 180 m), KNMI UHF radar wind profiler LAP3000 (height resolutions 100 m/400 m, hourly-averaged profiles in routine mode, for comparison in EUCAARI: time resolution 6 min), and a new candidate the TU-Delft TARA S-band Doppler polarimetric FMCW radar with 3 beams (height resolutions 3-30 m, time resolutions 3-18 s). Furthermore a commercial lidar was operated during a short period. Good results were evident for the mean vertical wind intercomparison (24 min resolution) between four different sensors (radars, lidar, and sonic anemometer): RMS of 0.3 m s-1 and 0.2 m s-1 High resolution TARA can complement the Cabauw sensors, sonic anemometers (first 200 m) and radar wind profiler (hourly-averaged profiles) for the vertical wind measurement

AIRBORNE HELICOPTER OBSERVATIONS (IFT)

Aerosol particle measurements in the atmospheric boundary layer were performed by a helicopter-borne measurement payload and by a lidar system from a case study in Cabauw. Layers of increased number concentrations of ultrafine particles were observed in the residual layer which is supposed to be an

indication of new particle formation. These layers were characterized by increased turbulence. Turbulent mixing is likely to lead to local supersaturation of possible precursor gases which are essential for new-particle formation. Observed peaks in the number concentrations of ultrafine particles at ground level are connected to the new particle formation in the residual layer by boundary layer development and vertical mixing.

INTEGRATION OF AIRBORNE OBSERVATION AND MODELLING: THE LES – IMPACT CASE STUDIES

a) CABAUW (KNMI, MPI)

The LES model used at KNMI is the Dutch Atmospheric LES model version 3.1 (DALES), as described by Heus et al. (in preparation). The model is relatively modular in structure, meaning that new components can easily be attached to DALES. To drive the LES, the analysis of the KNMI regional atmospheric climate model (RACMO) is used. The advantage of ding so is that the boundary conditions will be internally consistent, and it leaves the extensive set of measurements of EUCAARI as an almost completely independent source for comparison. To compare LES with observations and single column models, the LES is embedded in the KNMI Parameterization Test bed (KPT), which can be found at www.knmi.nl/~neggers/KPT. In this test bed, data streams of observations (including most observations from the EUCAARI-IOP) can be compared with Single Column Model SCM output, and with LES simulations. Various fields of measurements and model statistics can be plotted against each other, and plots can be generated in interactively. The LES was run for 2 May 2008. it was demonstrated that the LES perform better than the SCM. In comparison with the tower measurements, the agreement between LES and observations was remarkable, given the slightly erroneous forcings that drive the LES. Although LES performs less perfect in capturing all cloud cover, it performs still much better than the single column models. The combination of LES and SCM is now being used to analyze to pinpoint the exact components of the SCM that are underperforming in cases like the EUCAARI-IOP.

b) NORTH SEA (Metéo-France, U. Warsaw)

A LES simulation was performed on a case study observed the 15th of May over the North Sea during the EUCAARI campaign. The measurements of the ATR-42 research aircraft, carried out twice during that day on the morning and the afternoon above the same area, were used to compare the simulated cloud fields to the observed ones. Meso-NH is a non-hydrostatic model which has been developed to simulate various atmospheric processes from the synoptic scale to turbulent eddies. The LES configuration chosen here uses a 3D turbulence scheme with a one and a half order closure, which is based on the prognostic turbulent kinetic energy and a diagnostic mixing length. The comparison of the LES simulation to these two datasets shows that the model is able to retrieve realistic cloud fields. In the morning, the simulated cloud thermodynamic and microphysical structure corresponds to the observed one. The midday comparison exhibits that the model can not retrieve the observed weaker cloud due to large-scale phenomenon which were not taking into account in the simulation. The first outgoing of this works would be to confirm this hypothesis testing model sensitivity to observed changes of large-scale forcings. For instance, airborne measurements can be used to analyze the thermodynamic properties of the free troposphere. An observed drying and/or warming of the air above the cloud top would provide a quantitative indication whose impact on the cloud boundary layer can be assessed with the model.

INTEGRATION OF GROUND-BASED OBSERVATIONS AND CHEMICAL MODELLING (University of Utrecht)

A coupled aerosol-climate model ECHAM5/HAM to simulate aerosol optical properties for the IMPACT measurement campaign conducted in May 2008 in Cabauw (The Netherlands). The meteorology of the model is nudged and synoptic scale variability is represented adequately. The aerosol mass and chemical composition is simulated realistically except for nitrate and ammonium. The average aerosol optical thickness (AOT) from the model is 0.33, about 20% larger than observed. For selected periods of the month with relatively dry and moist conditions discrepancies are approximately –30% and +15%, respectively, and +80% when transport of desert dust from the Sahara plays a role. The simulated day-to-day variability of AOT follows the synoptic scale advection of humidity, rather than particle

concentration and aerosol hygroscopicity. Under relatively dry conditions, the observed hourly scale variability of AOT appears to be driven predominantly by RH in the lower boundary layer and is further amplified by simultaneous uptake and release of nitrate and ammonium by the aerosol. This is not adequately simulated, due to neglect of the chemical processes and due to inaccuracies in aerosol and humidity profiles caused by a misrepresentation of the mixing efficiency between the surface, the boundary layer and the free troposphere.

CLEAR SKY RADIATIVE TRANSFER (KNMI)

A clear-sky shortwave closure analysis was performed for the Baseline Surface Radiation Network (BSRN) site of Cabauw, Netherlands (51.97_N, 4.93_E). The analysis is based on an exceptional period of fine weather during the first half of May 2008, resulting in a selection of 72 comparisons, on 6 days, between BSRN measurements and Doubling Adding KNMI (DAK) model simulations of direct, diffuse, and global irradiances. The data span a wide range of aerosol properties, water vapor columns, and solar zenith angles. The model input consisted of operational Aerosol Robotic Network (AERONET) aerosol products and radiosonde data. The wavelength dependence of the aerosol optical thickness, single scattering albedo, and asymmetry parameter was taken into account. On the basis of these data, excellent closure was obtained: the mean differences between model and measurements are 2 W/m2 (+0.2%) for the direct irradiance, 1 W/m2 (+0.8%) for the diffuse irradiance, and 2 W/m2 (+0.3%) for the global irradiance. The good results were obtained because of proper specification of the DAK model input and the high quality of the AERONET and BSRN measurements. The sensitivity of the achieved closure to uncertainties in the aerosol optical thickness, single scattering albedo, and asymmetry parameter was examined. Furthermore, several sensitivity experiments related to the wavelength dependence of the aerosol optical properties and the treatment of water vapor were performed. It appeared that a correct description of the wavelength dependence of the aerosol optical properties is important for achieving broadband closure. However, broadband closure can also be obtained by means of using spectrally averaged values of the single scattering albedo and the asymmetry parameter. Cancellation of errors in different parts of the solar spectrum also contributes to the achieved closure.

ACKNOWLEDGEMENTS

This work was supported in part by the FP7 EUCAARI program. Investigators not funded under EUCAARI were supported by their own institutes. They include: ECN, University of Delft, University of Utrecht, RIVM.

REFERENCES

Apituley, A., K. M. Wilson, C. Potma, M. de Graaf and H. Volten (2009) Performance assessment of CAELI – a high performance Raman lidar for water vapor, aerosol and clouds (*ISTP8 conference Delft*)

Heus, T.; van Heerwaarden, C. C.; Jonker, H. J. J.; Siebesma, A. P.; Axelsen, S.; van den Dries, K.; Geoffroy, O.; Moene, A.; Pino, D.; de Roode, S. R. & de Arellano, J. V.-G. (2009) Description and Application of the Dutch Atmospheric Large-Eddy Simulation (DALES). *in preparation for Geosci. Model. Dev.*

Heus, T., A. P. Siebesma, R. Neggers and R. Boers (2009), Automatic large-eddy simulations of realistic atmospheric boundary layers (*ISTP8 conference Delft*)

Holzinger, R. (2009).: EUCAARRI were presented at a seminar at the Berkeley Atmospheric Science Center. (http://www.atmos.berkeley.edu/seminars/seminars-sp09.html)

Mensah, A. A., H. M. ten Brink, J. S. Henzing, R. Holzinger, Th. F. Mentel, M. Moerman, R. P. Otjes, G.-J. van Zadelhoff and A. Kiendler-Scharr. (2009) Aerosol Mass Spectrometric Measurements at Cabauw Tower during IMPACT May 2008, *EGU 2009 (Poster EGU2009-4591)*

Mensah, A. A., H. M. ten Brink, J. S. Henzing, R. Holzinger, Th. F. Mentel, M. Moerman, R. P. Otjes, G.-J. van Zadelhoff, and A. Kiendler-Scharr. (2009) AMS measurements of aerosol composition at Cabauw tower during IMPACT 2008. *EAC 2009 (Poster T170A07)*

Roberts, G.C., et al., (2009) Assessing aerosol-cloud interactions linking multi-platform observations and remote sensing, *33rd International Symposium for Remote Sensing of the Environment, Stresa, Italy, 2009 (poster).*

Roberts G.C., L. Gomes, J.-L. Brenguier, A. Apituley, K.Wilson, R. Boers, D.P. Donovan, J. Pelon, D.B. Josset, M. Boquet, H. Coe, J. Trembath, (2009) Assessing aerosol-cloud interactions linking multi-platform observations and remote sensing, *American Geophysical Union, San Francisco, 2009 (poster).*

Roelofs. G.-J. e.a. (2009) Simulation of IMPACT (MAY 2008, The Netherlands) with ECHAM/HAM. *To be submitted to J. Geophys. Res.*

Sandu, I., J.-L. Brenguier, O. Thouron and B. Stevens (2009) Parameterization of aerosol cloud interactions in general circulation models: on the importance of vertical structure. *Atmos. Chem. Phys., 9, 4039-4052, Special Issue: European Integrated Project on Aerosol-Cloud-Climate and Air Quality Interactions (EUCAARI)*

Unal, C., S. Arabas, Y. Dufournet and H. Russchenberg (2009) Vertical wind radar measurements at high temporal and spatial resolution (*ISTP8 conference, Delft*)

Wang, P., W. Knap, P. Kuipers Munneke, and . Stammes. (2009) Clear-sky shortwave radiative closure for the Cabauw Baseline Surface Radiation Network site, Netherlands, *accepted for publication in J. Geophys. Res.*

Wehner, B., F. Ditas, A. Wiedensohler, A. Apituley, R.A. Shaw, and H. Siebert (2009): New particle formation in elevated heights above continental Europe. *European Aerosol Conference 2009, Karlsruhe.*

Wehner, B., H. Siebert, A. Ansmann, F. Ditas, P. Seifert, F. Stratmann, A. Wiedensohler1, A. Apituley, R. A. Shaw H. E. Manninen, and M. Kulmala, (2009) New particle formation in the residual layer over central Europe characterized by helicopter and lidar measurements. *To be submitted to ACP.*

The preparation of the papers mentioned above is well under way. However, there are other papers under consideration or at the early stages of preparation:

- a paper is in preparation about new particle formation events measured by the ATR-42 during the Eucaari campaign (lead by Suzanne Crumeyrolle, collaboration CNRS/LAMP-Meteo France/CNRM). A poster will be presented in Stockholm.
- a study is in progress about the dust event over Northern Europe during EUCAARI; the model simulations have just been made (lead L. Gomes, CNRM).
- a paper by G. Roberts et al. about aerosol-cloud interactions using multi-platform analysis and remote sensing is in preparation (lead G. Roberts, CNRM). A poster will be presented in Stockholm.
- A collaborative paper (CNRS/LAMP, UNIMAN, and CNRM) on Airborne in-situ measurements with a C-ToF aerosol mass spectrometer during EUCAARI/IMPACT (lead by Ralf Weigel). A poster will be presented in Stockholm.
- LES simulation of a stratocumulus diurnal cycle (lead by Vincent Puygrenier, CNRM).

PARAMETERISATIONS FOR GLOBAL AND REGIONAL MODELS: WORK PACKAGE 3.3

Elisabetta Vignati[1], Ken Carslaw[2], Jean Louis Brenguier[3], Jon Egill Kristjansson[4], Corinna.Hoose[4], Ulrike Lohmann[5], Colombe Siegenthaler-Ledrian[5], Martijn Schaap[6], and H-C Hansson[7]

[1]Joint Research Centre, Institute for Environment and Sustainability Climate Change, Ispra (VA), Italy
[2]University of Leeds, School of Earth and Environment, Leeds UK
[3]Centre National de Recherches Météorologiques, Groupe de Météorologie Expérimentale et Instrumentale, France
[4]Department of Geosciences, University of Oslo, Norway
[5]ETH Zurich, Institute for Atmospheric and Climate Science, Zurich, Switzerland
[6]TNO-Apeldoorn, Environmental Quality Department, Netherlands
[7]Department of Applied Environmental Science, Stockholm University, Sweden

Keywords: Model, parameterization, global, regional, air quality, climate

INTRODUCTION

WP 3.3 aims to develop and test new parameterizations for global and regional scale models based on the results of detailed process studies and new mechanistic developments in other work packages. The WP also tackles a major problem that limits the accuracy of indirect forcing calculations: modelling the sub-grid scale properties of the clouds and the structure of the boundary layer. The complex chemical and physical properties of the aerosol (particle size distribution, chemical properties, mixing state, chemical transformation, etc.) must be represented efficiently, but any scheme must be capable of capturing the properties important for direct radiative forcing and changes in CCN.Furthermore, model schemes are required to calculate the number of cloud drops as a function of aerosol properties and the microphysical evolution of cloud drop number in different clouds. In order to better represent boundary layer clouds, which are responsible for the majority of the indirect aerosol effect, the representation of the boundary layer needs to be improved such that the magnitude of the temperature and humidity inversions can be captured. Traditionally boundary layer clouds are underestimated in GCMs, which suggests that the indirect aerosol effect is underestimated.

RESULTS

Task 3.3.1Aerosol-cloud interaction and cloud drop number scheme development

Over the last year, the CAM-Oslo model has been extended and improved with respect to both warm and cold cloud indirect effects. In preparation for submission of CAM-Oslo results to the Aerocom Indirect Effect Intercomparison Initiative (now published in Quaas et al., 2009), the updraft and detrainment formulations were revised, resulting in a better agreement with observed cloud droplet number concentrations. The common practice of prescribing a lower bound on the droplet number concentration is avoided in CAM-Oslo. In a publication earlier this year (Hoose et al., 2009), we showed that unphysical lower bounds on the droplet concentration leads to suppression of the simulated indirect effect (from -1.9 W/m2 up to -0.6 W/m2), especially over oceans (see Figure 1). Constraining aerosol concentration instead of droplet concentration has a weaker effect on the change in short-wave cloud forcing and can be considered physically more correct, because global aerosol-cloud models lack some aerosol species like primary biological particles or non-desert dust.

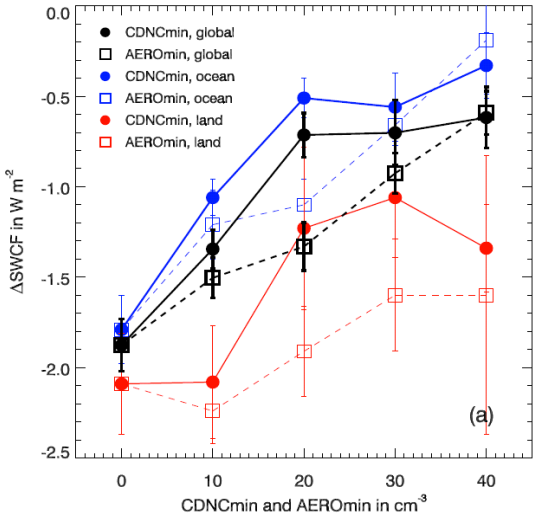

Figure1: Change in short-wave cloud forcing between simulations with present-day and preindustrial aerosol emissions (a measure of the aerosol indirect effect), with different lower bounds on cloud droplet number concentration (CDNCmin) and aerosol number concentration (AEROmin).

CCN activation is among the shortest time scale processes in cloud physics and effective prediction of the number of activated CCN in a numerical model requires times steps of less than 0.01 s that are not feasible in LES, CRM or GCM simulations. In these models, the LWC is adjusted at each time step for the water vapor to be saturated in cloudy grids and the CCN activation process relies on a diagnostic of the supersaturation. At cloud base however, it takes about 10 s for the supersaturation to reach its maximum that determines the number of activated CCNs. The saturation approximation is thus no longer suited when time steps are shorter than 10 s, as in LES or CRM simulations. Theoretically, prediction of heat and moisture is sufficient to derive supersaturation, but practically it is not feasible because supersaturation is a second order parameter compared to these two conservative variables.

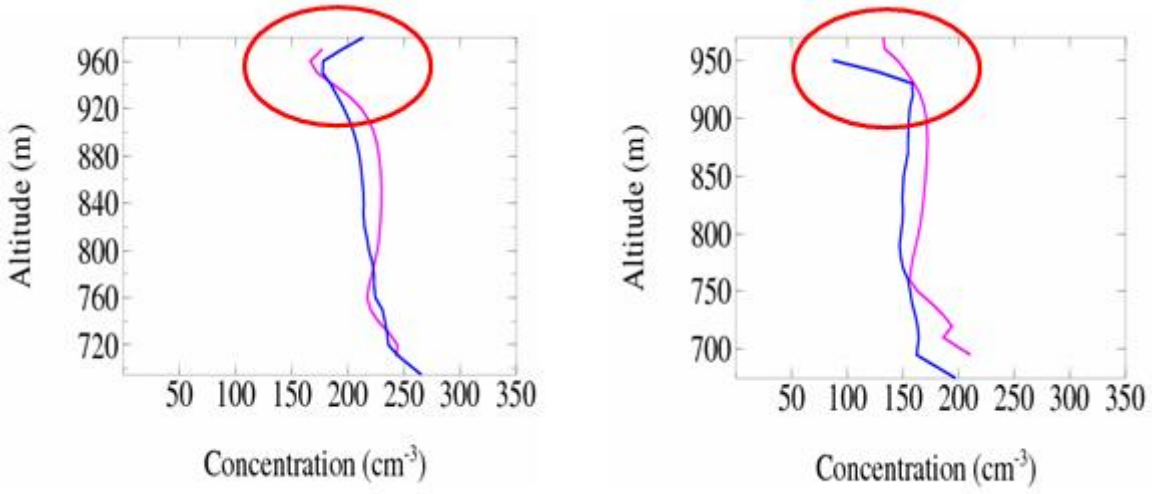

Figure 2: Mean vertical profile of the concentration for two stratocumulus cases (blue and Magenta). Left: obtained with a diagnostic of the saturation. Right: obtained with a prognostic of the saturation. With a prognosticated saturation, the concentration decreases at the cloud top whereas it increases with a saturation diagnostic

Supersaturation prognostic schemes thus show spurious peaks leading to unrealistic activation because of numerical artefacts, especially at cloud boundary when moist air is advected in clear air grids (spurious

activation at cloud top). A new scheme has been developed at CNRM, based on advection of supersaturation, even thought supersaturation is not a conservative variable. Combined with the supersaturation prognostic derived from heat and moisture, the scheme allows to filter numerical artifacts and it provides an accurate prediction of CCN activation. The scheme has been extensively tested in a parcel model against explicit calculation of supersaturation at a 0.01 s time resolution. Implemented in a 3D LES framework to simulate cumulus and stratocumulus clouds, it appears very efficient at suppressing spurious CCN activation at cloud boundaries (Fig.2)

Task 3.3.3 Meteorology of boundary layer clouds in GCMs

ECHAM5 uses a turbulent kinetic energy (TKE)-scheme, which simulates the cloud top fluxes in function of the local turbulence. It reproduces relatively well the clear convective and stratocumulus topped boundary layers in a quite high resolution model (e.g. Duynkerke and Driedonks, 1987). Nevertheless, Lenderink et al. (2000) by studying the turbulent scheme of ECHAM4, showed that its performance diminishes when the resolution decreases, the different fluxes and TKE being not represented satisfactory in the resolution L31 (31 vertical levels). Thus the TKE diffusion was replaced by an explicit entrainment closure at the top of the boundary layer clouds. The new version of the boundary layer in ECHAM5 which includes a parametrisation of cloud-top entrainment in the stratocumulus regions is called ENTR. The version with diffusion on moist conserved variables (CMO) is considered as a reference version. The standard version (with turbulent diffusion on non-conserved variables) is called STD.
The highest values of TKE in ENTR are more in the range of measurements (between 0.1 and 0.5 ms^{-1} than the huge values in STD and CMO. Moreover the highest values of TKE in STD are in a narrow time interval before midnight, thought the values are more constant during the night for ENTR. Moreover the strong increase of TKE during night takes place at the base of the cloud in STD, but it should be at the top of the cloud due to radiative cooling in typical stratocumulus. This feature is reproduced nicely in ENTR. Finally the diurnal cycle simulated in cloud cover or equivalently in cloud water is much more representative of observed subtropical stratocumulus in ENTR than in STD.

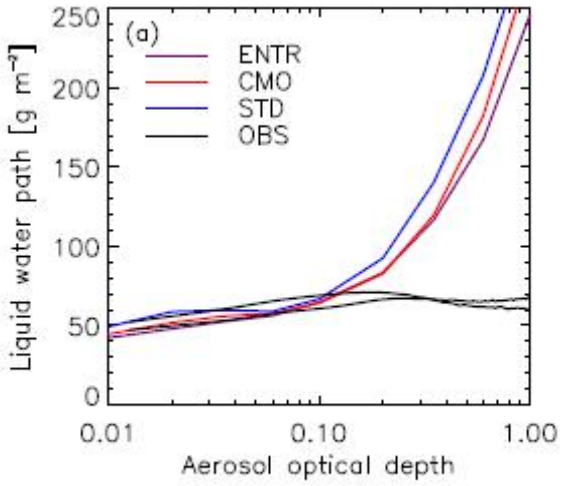

Figure 3: Relationship between aerosol optical depth with LWP from the 3 simulations STD, CMO and ENTR, compared with observations from the MODIS instruments on board of TERRA and AQUA satellites (Mhyre et al., 2007).

On the other hand, the TKE is not well distributed vertically, probably due to a deficiency in turbulent transport of TKE. Figure 3 show the relationship between the LWP and AOD between 50◦ N and 50◦ as seen by MODIS satellites for two full years (2001 from Terra and 2003 from Aqua) and the three model versions. CMO and then ENTR decrease the high LWP simulated for the high AOD, which is going in the right direction compared to the observations. It is still not enough as the observations show a negative

slope of all the variables for AOD > 0.2. Nevertheless, the explicit entrainment reduces the sensitivity of LWP to AOD on a global scale as well.

It has been observed that the stratocumulus are too shallow to be well represented in the standard vertical grid of ECHAM5. To better simulate these low clouds without increasing the vertical resolution tremendously, two levels are added dynamically wherever a stratocumulus could form. More precisely, the thickness of the stratocumulus is found following the approach presented in Grenier and Bretherton (2001), and a new grid containing 2 more levels based on it is defined. It is represented in Figure 4, where the representation of the virtual liquid temperature (θ_{vl} profile produced by the model is in green, and in blue is the extrapolated profile. The new interfaces are following the inversion at the cloud top and the lifting condensation level (LCL) at the bottom of the cloud. The algorithm, which computes the cloud top and the vertical thickness of the stratocumulus-topped boundary layer in ECHAM5, and defines the new grid has been implemented.

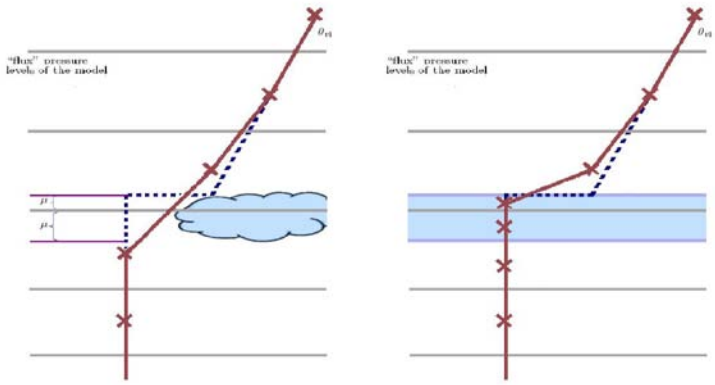

Figure 4: Left: sketch of the approach to extrapolate the virtual potential temperature (θ_{vl}) across the inversion at the top of the boundary layer in our model. Right: new grid.

This method seems to work quite well as one can see in Figure 5, where the thickness of the cloud is represented. Indeed, the method finds stratocumuli in the right place in the GCM with a reasonable pressure for the inversion (cloud top). The implementation of the interaction between this new grid and the cloud microphysics, radiation and the other physical processes in ECHAM5 is still work in progress.

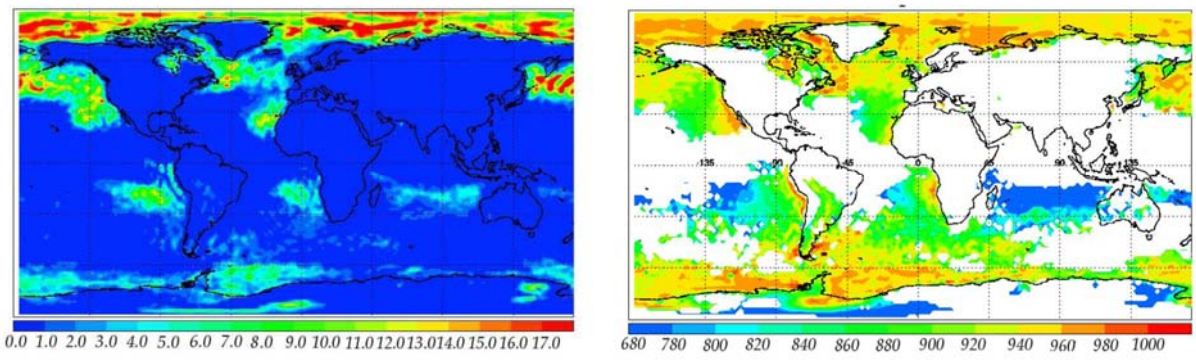

Figure 5: Left: JJA mean of the percentage thickness of the cloud (with respect to the initial thickness of the respective levels, μ_t of Figure 1. Right: JJA mean of the pressure [hPa] of the boundary layer inversion (cloud top).

Task 3.3.4 Aerosol size distribution and microphysics parameterisation

Work at Leeds in WP3.3 has focused on evaluating a modal aerosol model against a more comprehensive section or "bin" model. The GLOMAP model (http://researchpages.net/glomap) was used. GLOMAP is a global chemical transport model with two alternative aerosol microphysics modules. GLOMAP-mode simulates the aerosol size distribution using several log-normal modes while GLOMAP-bin uses 20 size sections. GLOMAP-mode is also used within the UK climate model and runs approximately 10 times faster than GLOMAP-bin.

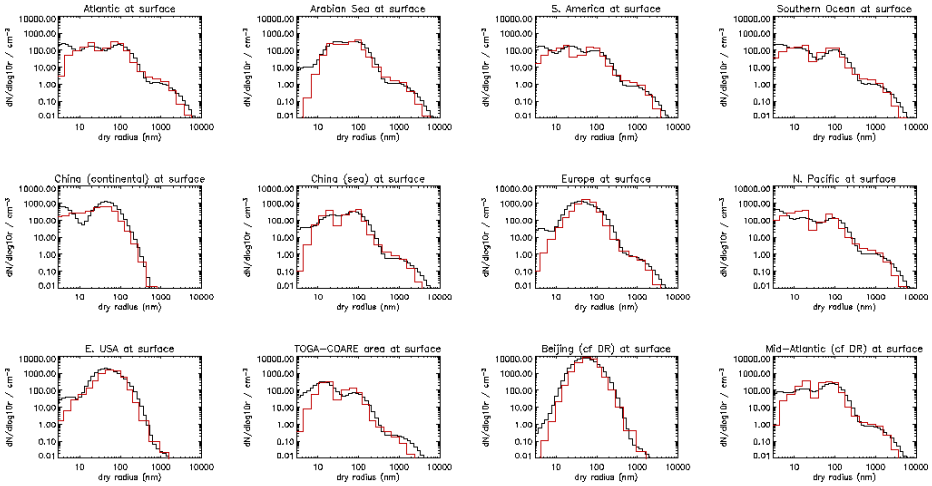

Figure 6. Comparison of modal (black) and bin (red) models for 12 global regions

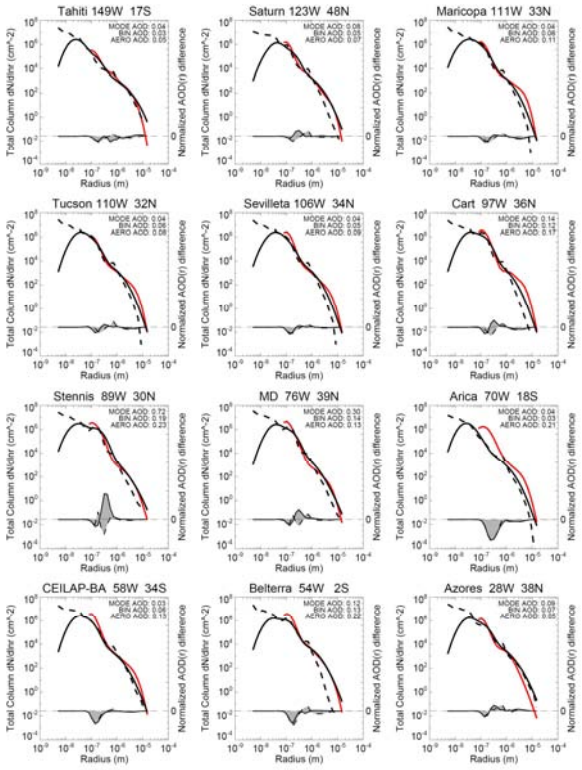

Figure 7: Comparison of modal (black solid) and bin (black dashed) models against AERONET-retrieved particle size distributions (red) at 12 worldwide sites.

The strategy within EUCAARI has been to use the bin model to test the modal model, and thereby understand the weaknesses of the modal model when running in the climate model.GLOMAP was run at

T42 resolution (approx 2.8 degrees) for 1 year using both mode and bin schemes. Particle size distributions have been compared for 12 distinct regions around the world (Fig. 6). The modal and bin schemes agree very well at most sizes, although there tends to be some overprediction of particle concentrations in the nucleation mode of the modal model. Aerosol optical depth has also been evaluated against MODIS and AERONET observations. Both models are in close agreement but differ by approximately the same amount from the retrieved size distributions (Fig. 7). It was therefore concluded that there are general adjustments to make to the aerosol model, rather than a specific issue with the simpler modal model.
Global cloud condensation nuclei have been evaluated against a collection of CCN measurements compiled from several field campaigns (Figure 8). There is reasonable agreement in the model versus observations (with a lot of scatter). But again the difference between the bin and modal schemes is smaller than the difference between either model and the observations. The conclusion is from this study that modal aerosol schemes are a computationally efficient but nonetheless accurate way of simulating the aerosol size distribution, optical properties and CCN concentrations on a global scale.

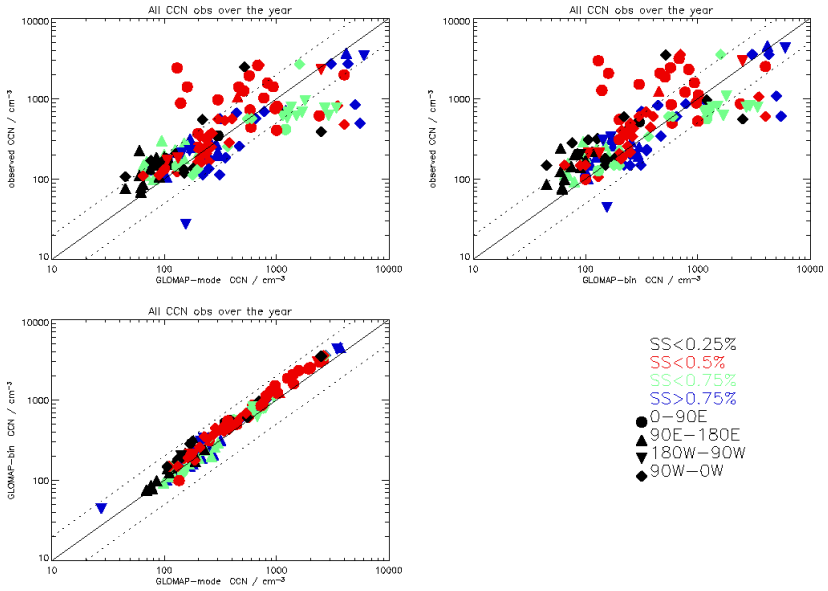

Figure 8: Comparison of modelled CCN concentration at several worldwide locations. The upper panels compare bin and mode models against the observations and the lower panel compares mode and bin predictions.

SENT DELIVERABLES

D110 A tested and validated prognostic cloud water and ice crystal scheme in CAM-Oslo
D118 A sub-grid scale parameterization of cloud updraught using non-symmetric pdf
D123 Quantifying the role of changes in cloud cover for the overall aerosol indirect forcing, using the CAM-Oslo global climate model
D134 A study of aerosol-cloud interaction using a new high resolution stratocumulus model in a GCM

FUTURE WORK

At temperatures between 0 and about -40°C, cloud droplets do not freeze spontaneously, but require aerosol particles as ice nuclei to initiate freezing. Mineral dust, soot and in particular some biological particles (certain species of bacteria, fungal spores and pollen) are efficient ice nucleators. A new ice nucleation parameterization, with a thorough theoretical basis in classical nucleation theory, has been implemented into CAM-Oslo and is currently being evaluated. This new treatment allows us to assess the global importance of biological ice nucleators for the first time in a global model (Hoose et al, 2009c). This work is ongoing. A manuscript submission is planned before the end of this year.

The IMPACT campaign covered multi-instrument aircraft measurements of in-cloud vertical wind velocity as well as cloud-droplet size spectrometry. Results of these in-situ measurements are the basis for deriving statistics of cloud-microphysical parameters such as liquid water content, cloud droplet concentration and other statistical moments of the droplet size spectrum. The key datasets employed in the analysis are the data obtained by the PVM-100 and FSSP-100 optical cloud-droplet sensors. The cloud-droplet size spectrum features are to be compared on different levels above the cloud base. By using the data from the aircraft gust probe, the droplet-spectrum features are to be analysed separately for the updraft and downdraft regions in the cloud. The analysis is to be carried out separately for the case of marine stratocumulus deck probed along the Scottish coast of the North Sea on May 15th 2008, and for the several cases where continental cumuli were probed above The Netherlands, e.g. on May 13th, 14th, 19th and 28th.

An inter-comparison and sensitivity tests, including measured data, with a Lagrangian type box model based on the UHMA model will be done with the GLOMAP model to evaluate the aerosol and cloud representation

The effect of model spatial resolution on microphysics and development of the size distribution will be examined using a hierarchy of models, including the global CTM TM5 and the mesoscale model LOTOS, coupled to M7.

PUBLICATIONS

Hoose, C., J. E. Kristjánsson, T. Iversen, A. Kirkevåg, Ø. Seland and A. Gettelman (2009a): Constraining cloud droplet number concentration in GCMs suppresses the aerosol indirect effect. Geophys. Res. Lett. 36, L12807, doi:10.1029/2009GL038568.

Lohmann, U. and C. Hoose (2009): Sensitivity studies of different aerosol indirect effects in mixed-phase clouds. Atmos. Chem. Phys. Discuss. 9, 15045-15081.

Quaas, J., Y. Ming, S. Menon, T. Takemura, M. Wang, J. E. Penner, A. Gettelman, U. Lohmann, N. Bellouin, O. Boucher, A. M. Sayer, G. E. Thomas, A. McComiskey, G. Feingold, C. Hoose, J. E. Kristjánsson, X. Liu, Y. Balkanski, L. J. Donner, P. A. Ginoux, P. Stier, J. Feichter, I. Sednev, S. E. Bauer, D. Koch, R. G. Grainger, A. Kirkevåg, T. Iversen, Ø. Seland, R. Easter, S. J. Ghan, P. J. Rasch, H. Morrison, J.-F. Lamarque, M. J. Iacono, S. Kinne, and M. Schulz (2009): Aerosol indirect effects - general circulation model intercomparison and evaluation with satellite data. Atmos. Chem. Phys. Discuss. 9, 12731-12779.

PLANNED PUBLICATIONS

Hoose, C., J. E. Kristjánsson, A. Hazra, and J.-P. Chen: Ice nucleation by mineral dust, soot, bacteria, fungal spores and pollen: GCM studies with new freezing parameterizations. In preparation.

Hoose, C., J. E. Kristjánsson, S. Arabas, and H. Pawlowska: Vertical velocity probability distributions simulated in the CAM-Oslo GCM and observed during the EUCAARI-IMPACT campaign. In preparation.

Colombe Siegenthaler - Le Drian, P. Spichtinger and U. Lohmann. Explicit Entrainment parametrisation in the global climate model ECHAM5-HAM. In preparation

O. Touron and J-L Berenguier. A paper on the supersaturation prognostic scheme. In preparation

K. Carslaw's group. A paper on the evaluation of a modal aerosol model against a more comprehensive section or "bin" model

REFERENCES

Duynkerke, P. G. and Driedonks, A. G. M. (1987). A model for the turbulent structure of the stratocumulus topped atmospheric boundary layer. *J. Atmos. Sci*, 44:43–64.

Hoose, C., J. E. Kristjánsson, T. Iversen, A. Kirkevåg, Ø. Seland and A. Gettelman (2009): Constraining cloud droplet number concentration in GCMs suppresses the aerosol indirect effect. *Geophys. Res. Lett*. 36, L12807, doi:10.1029/2009GL038568.

Lenderink, G., Van Meijgaard, E., and Holtslag, A. M. (2000). Evaluation of the ECHAM4 cloud turbulence scheme for stratocumulus. Meteorologische Zeitschrift, 9(1):0041–47.

Mhyre, G., Stordal, F., Johnsrud, M. et al. (2007). Aerosol-cloud interaction inferred from MODIS satellite data and global aerosol models. *Atm. Chem. Phys*., 7:3081–3101.
Quaas, J., Y. Ming, S. Menon, T. Takemura, M. Wang, J. E. Penner, A. Gettelman, U. Lohmann, N. Bellouin, O. Boucher, A. M. Sayer, G. E. Thomas, A. McComiskey, G. Feingold, C. Hoose, J. E. Kristjánsson, X. Liu, Y. Balkanski, L. J. Donner, P. A. Ginoux, P. Stier, J. Feichter, I. Sednev, S. E. Bauer, D. Koch, R. G. Grainger, A. Kirkevåg, T. Iversen, Ø. Seland, R. Easter, S. J. Ghan, P. J. Rasch, H. Morrison, J.-F. Lamarque, M. J. Iacono, S. Kinne, and M. Schulz (2009): Aerosol indirect effects - general circulation model intercomparison and evaluation with satellite data. *Atmos. Chem. Phys. Discuss*. 9, 12731-12779.

Regional and global Air Quality

Christodoulos Pilinis on behalf of WP3.4

University of the Aegean, Mytilene, Greece, GR-81100

Keywords: regional models, global models, air quality

INTRODUCTION

The processes affecting air quality, i.e. the concentrations of ozone, NO2 or atmospheric particulate matter are closely linked to weather and climate. In addition changes of concentrations on a global scale are likely to affect concentrations on regional and urban scales. In this work package an attempt is being made to predict pollution levels in Europe in a continuously changing climate and how air pollution will affect climate change. To achieve this goal a number of state of the art models are used for the period of May 2008.

Task 3.4.1 Continued CTM Development and Evaluation

During the second year of the EUCAARI project the regional Chemical Transport Model PMCAMx was improved with the addition of a new thermodynamics model (ISORROPIA-II) and a new primary and secondary aerosol module using the volatility basis set. The development of this model (called PMCAMx-2008) and its evaluation with data from North America and Mexico City were described in our previous annual report. During the second year of the EUCAARI project COSMO-MUSCAT was also improved so that it has the following features: Extension of the used modal aerosol model M7 by incorporating nitrate, ammonia and selected organics, improvement of the sea salt emission module, computation of extinction coefficients from simulated aerosol distributions, development of a preprocessor for the generation of lateral boundary values from global CTM simulations (implemented for ECHAM5 data) and tools for the comparison between model simulations and measurements.

During the third year of the project the evaluation of these improved CTM models developed in the previous year, took place. To do so a detailed gridded emissions

inventory was developed for both anthropogenic and non-anthropogenic sources. For the anthropogenic emissions of gases we used GEMS, while for particulate matter we used the anthropogenic emissions by size, developed as part of WP1.3 of EUCAARI. For the biogenic emissions we used MEGAN vs. 2.04 for NO, NMVOC, CO. The combined organic-inorganic sea-spray source function was developed as part of WP 1.3. It combines 10 m wind speed, chlorophyll-a concentrations and a sea-spray source function to produce a size resolved emission of number, mass and water insoluble organic matter enrichment. Since non-anthropogenic emissions strongly depend on the meteorological conditions we extracted meteorological fields by applying WRF for the period of May 2008, while chlorophyll_a concentrations were provided from MODIS SeaWiFS (http://oceandata.sci.gsfc.nasa.gov/). An example of the gridded emissions inventory, specifically the SO2 emissions, developed as part of WP3.4, is presented in Figure 1.

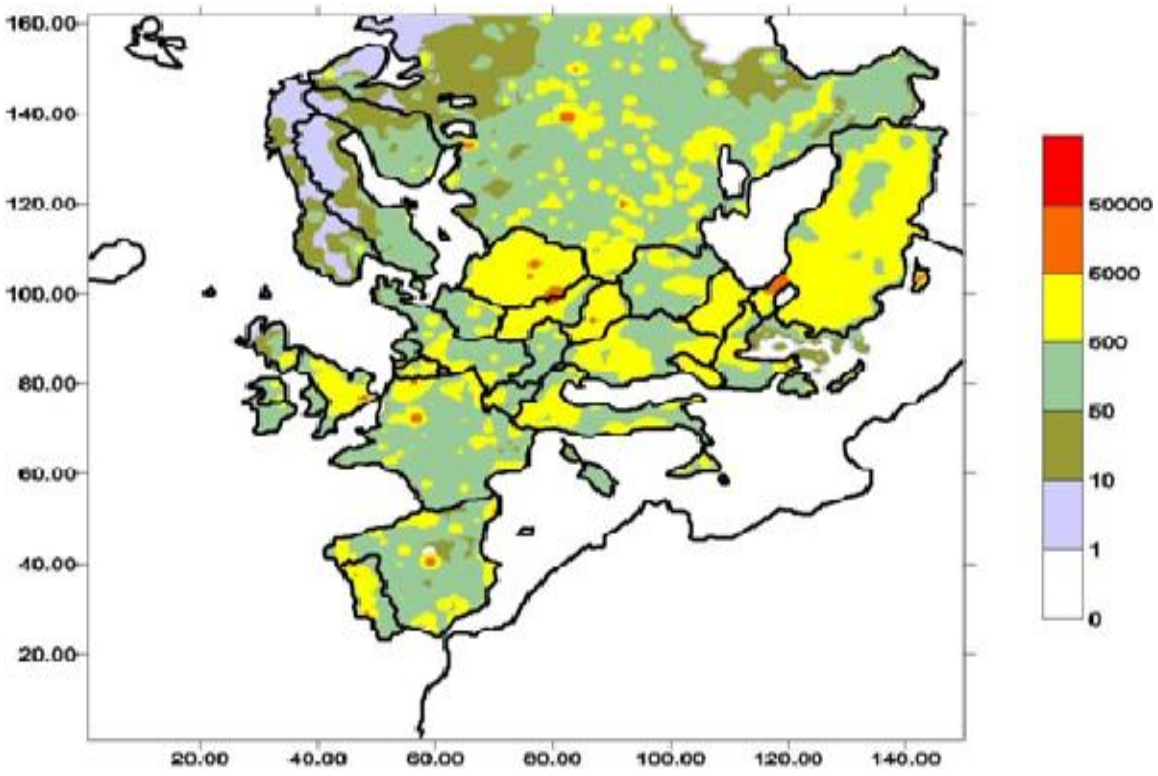

Figure 1. Spatial distribution of anthropogenic, excluding shipping, SO2 annual emissions (metric tonnes/year/cell)

Using this gridded inventory, during the third year of the project, our emphasis was on the evaluation of the models for the European domain using the data collected during the May-2008 EUCAARI intensive campaign. The processed organic aerosol emission inventory has been extended so the organic emissions are a function of compound volatility and are compatible with the volatility basis set framework in PMCAMx-2008. Results of the simulations are shown in Figure 2.

The model predicts that during that period the highest fine particulate matter concentrations existed in Northeast Europe (Netherlands, Belgium, England, Ireland, and northern France) due to the high pressure system that was in that area for the first half of the month.

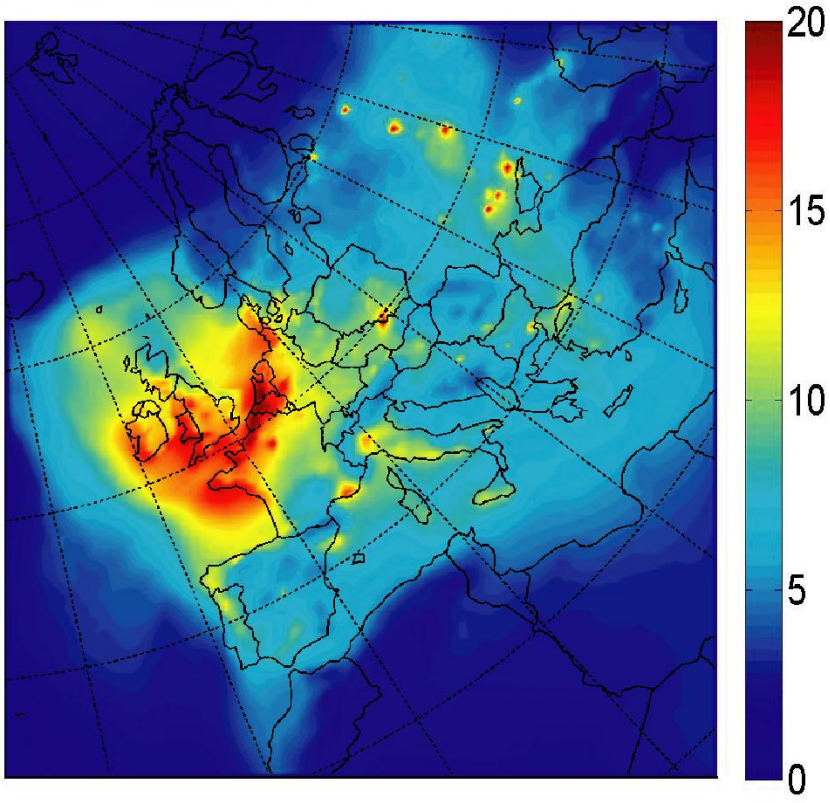

Figure 2. Predicted average ground level $PM_{2.5}$ concentrations for May 2008 (EUCAARI intensive) by PMCAMx-2008.

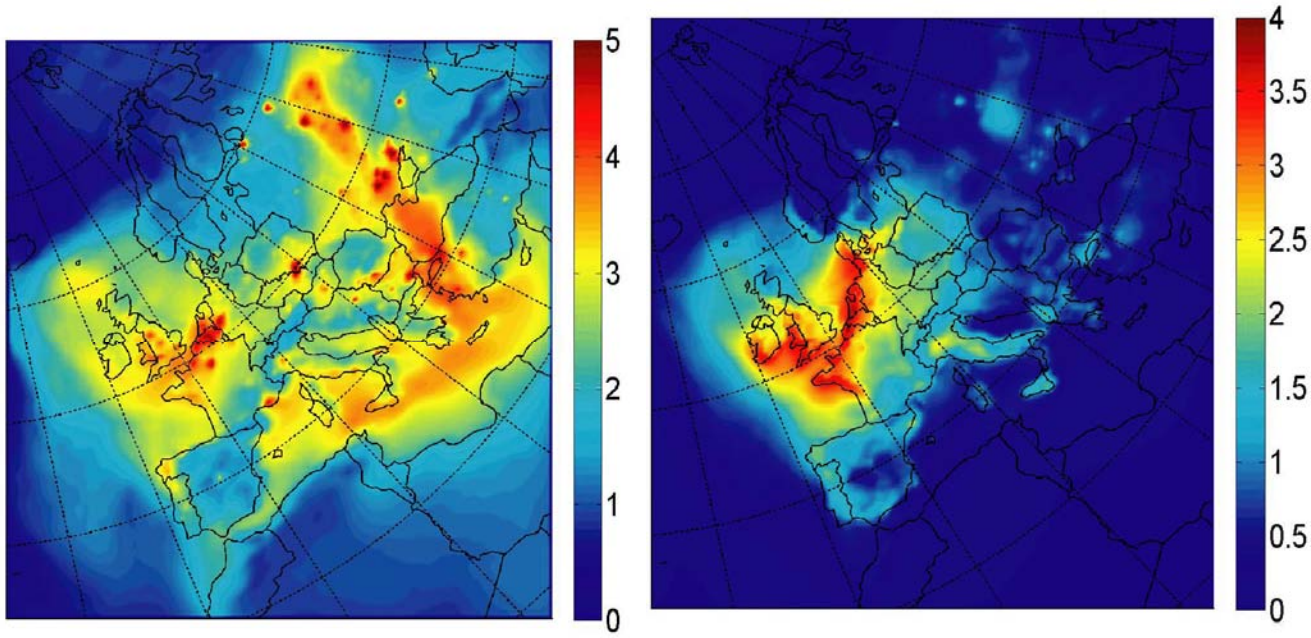

Figure 3. Predicted average ground level $PM_{2.5}$ sulfate (left panel) and nitrate (right) panel concentrations for May 2008.

As shown in Figure 3, the model predicts that Eastern and South-Eastern Europe had high sulfate concentrations whereas ammonium nitrate was at high levels in the northwest contributing significantly to the high concentrations in that area.

The model predictions were first compared against the data collected in Finokalia, Greece. The observed and diurnal profiles of the sulfate concentrations are shown in Figure 4. The comparison is quite encouraging both for absolute magnitude and diurnal profile. PMCAMx-2008 has a small tendency to underpredict and this appears to be related to an underestimation of the Greek sulphur emissions. Both the model predicted and observed fine PM nitrate levels (not shown) were close to zero.

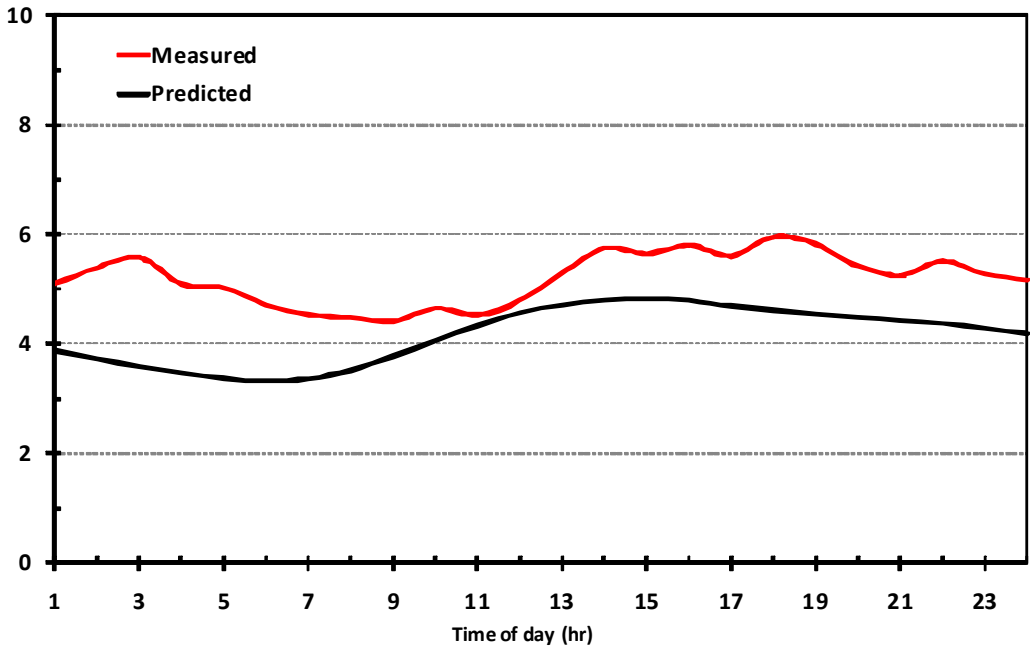

Figure 4. Predicted and observed diurnal PM_1 sulfate (μg m^{-3}) concentrations in Finokalia, Greece during May 2008.

One of the biggest challenges in European PM modelling has been the reproduction of the observed organic aerosol levels. PMCAMx-2008 does an excellent job of reproducing the Finokalia observations (Figure 5) of organic aerosol. This is a major improvement overall previous organic aerosol modelling efforts in Europe. We also compared the predicted oxygenated OA (OOA) and hydrocarbon-like organic aerosol levels (HOA) and the results are very encouraging. Both the model and the measurements suggest that less than 0.1 μg m^{-3} of the observed aerosol was fresh primary (HOA) while the rest was oxygenated OA. This is a good indication that the model reproduces that rapid chemical aging of organic aerosol in that area of Europe.

For another of the EUCAARI sites, Cabauw, where composition measurements are available thanks to the Julich group the performance of PMCAMx-2008 is also very encouraging. The measured OA concentration was roughly 4 μg m^{-3} while the predicted value was 4.6 μg m^{-3}.

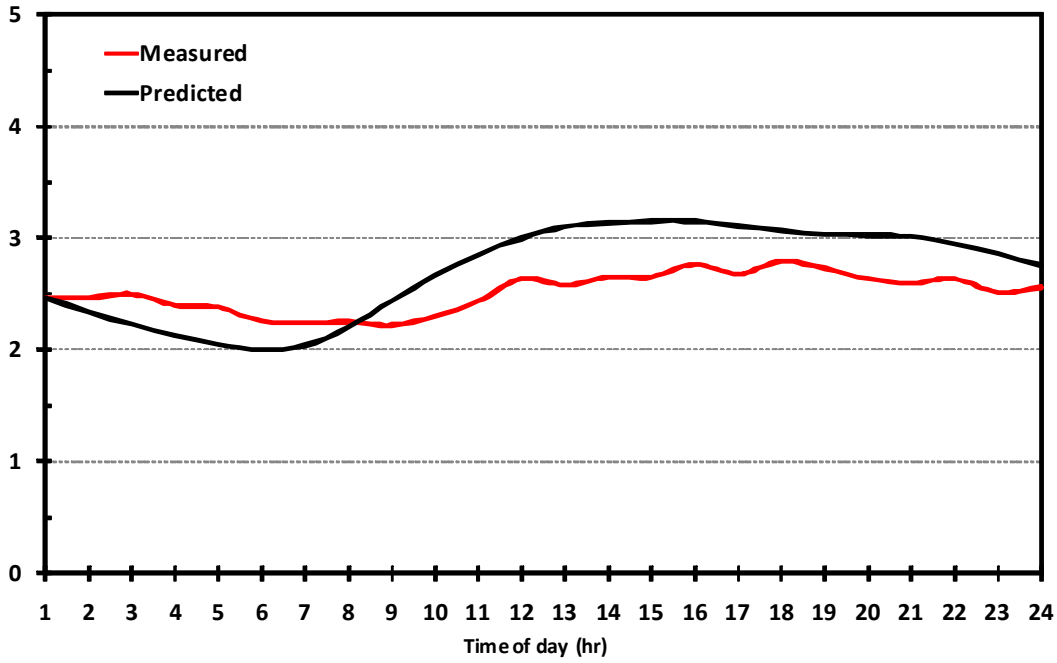

Figure 5. Predicted and observed diurnal PM_1 organic aerosol ($\mu g\ m^{-3}$) concentrations in Finokalia, Greece during May 2008.

Further evaluation of these May-2008 results is currently underway, using the rest of the EUCAARI field campaign measurements (including the airborne platform measurements) as they are becoming available. We are also in the process of completing the simulations for February-March 2009 that will be evaluated against the winter campaign results. The corresponding results will also be compared with satellite observations from WP 2.3

During this period the COSMO-MUSCAT model was setup from the European to the urban scale with Eastern Germany as region of interest (around Berlin and Saxony including the Melpitz station). The developed nesting capabilities of the model were used with the Berlin area being resolved with grid sizes of 2.8 km, as shown in Figure 6.

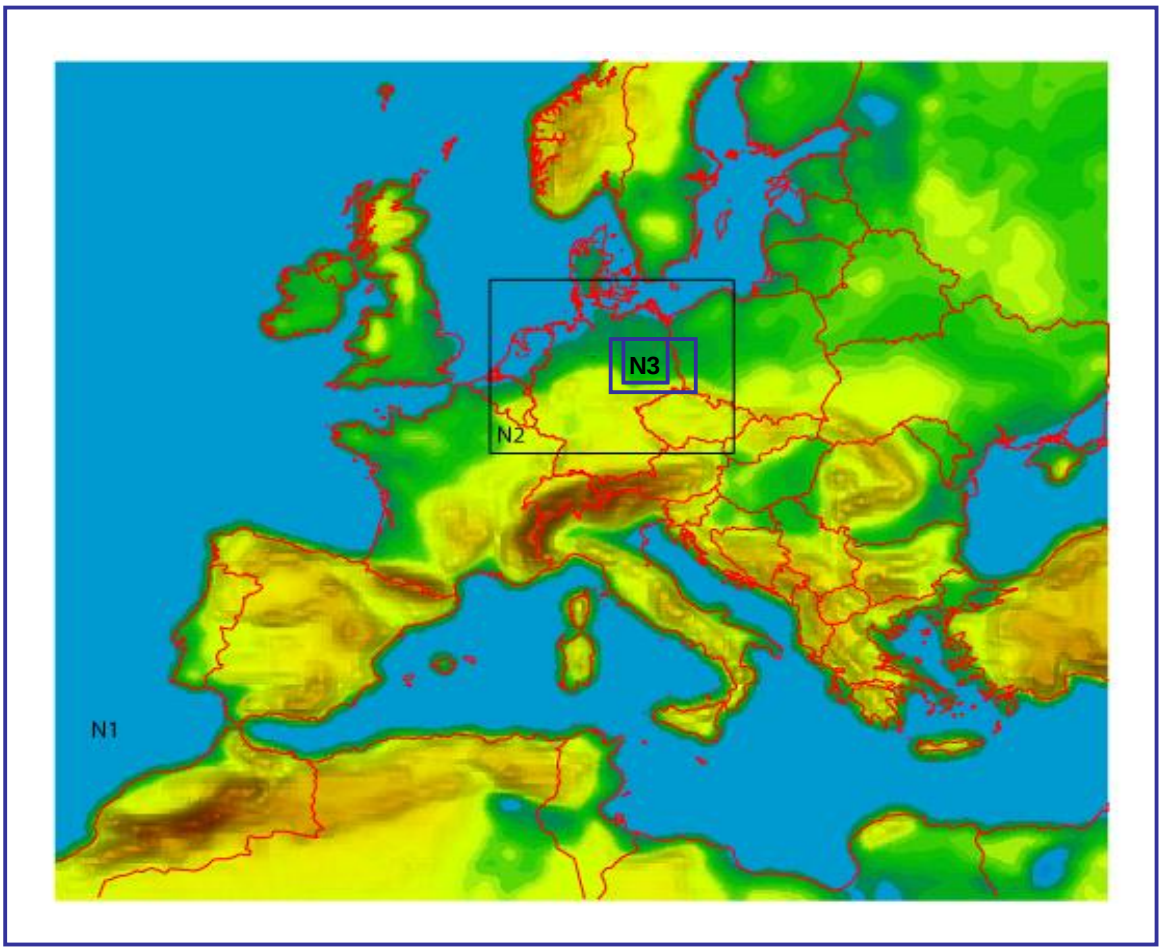

Figure 6. Size resolution N1: 16 km x 16 km - 40 vertical layers, N2: 8 km x 8 km - 50 vertical layers and N3: 2.8 km x 2.8 km - 50 vertical layers.

The comparison of the predictions of the model with the measurements, both for gases and species in the particulate phase is encouraging both for absolute magnitude and diurnal profile, as shown in Figure 7.

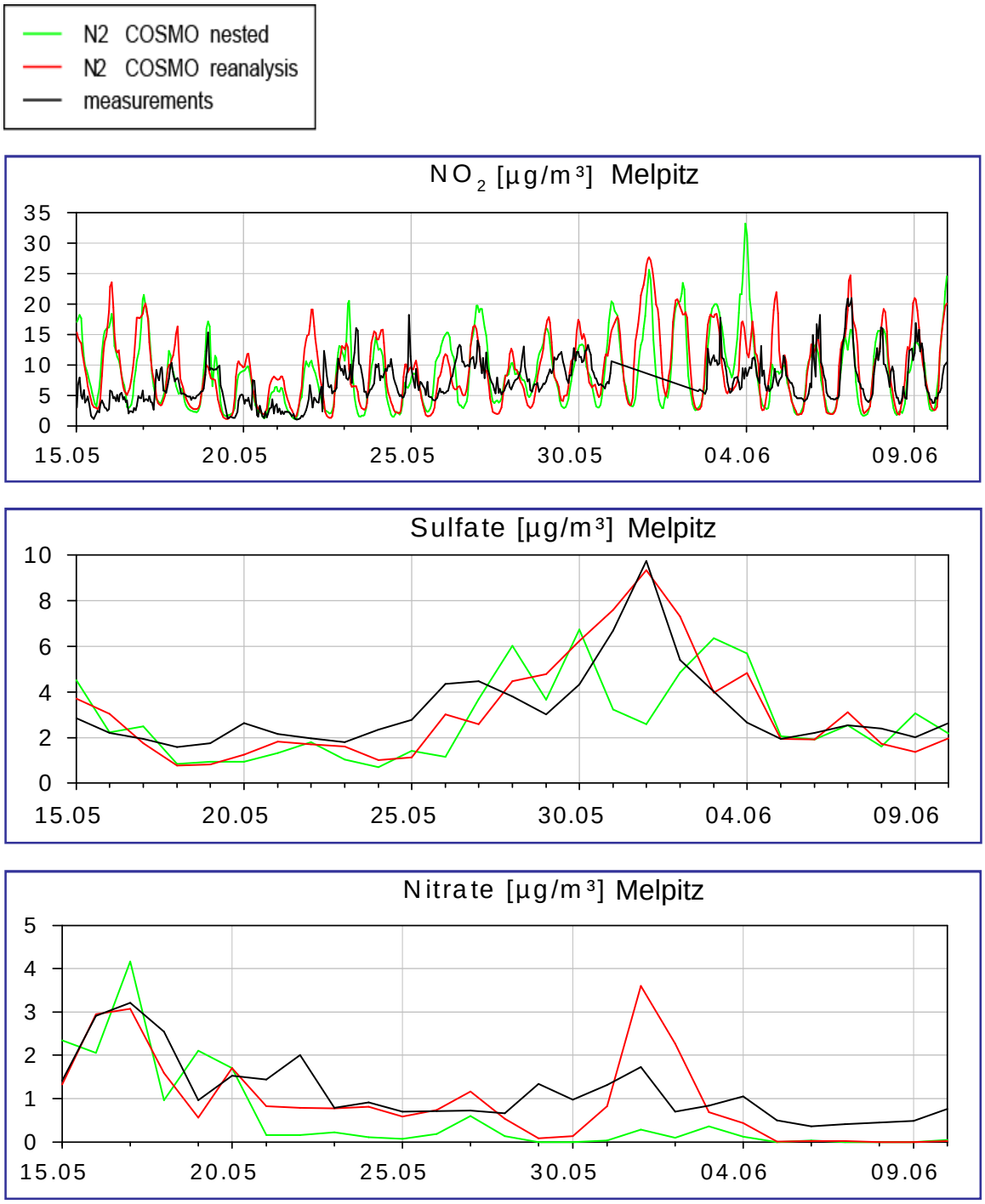

Figure 7. Predicted by COSMO-MUSCAT and observed diurnal NO2, Sulfate and Nitrate (µg m^{-3}) concentrations in Melpitz.

Task 3.4.2 Urban-regional scale air pollution interaction

After the end of the evaluation of the model results the Particle Source Apportionment Technology approach of Wagstrom and Pandis (2008) will be used to explicitly track the primary and secondary pollutants from all major urban areas in Europe. In these simulations the predicted pollutant concentrations will be assigned the European urban areas, rest of Europe, and long range transport. The resulting concentrations will be used not only to look at the contributions of these three different sources but also of the changes that occur as the urban pollutants are transported over long distances or vice versa.

We are also planning to perform a series of emissions sensitivity runs to look at the responses of the concentrations to the changes of emissions of sulfur dioxide, oxides of nitrogen, anthropogenic VOCs, and ammonia. In these tests we will look at the effects of reductions of emissions by 25% and 50%.

Task 3.4.3 Urban and regional pollution in a changing environment

Our next step in this task is to use the models to investigate the sensitivity of air quality over Europe to the most important meteorological parameters (temperature, wind speed, mixing height, cloudiness, etc.) following the approach of Dawson et al. (2007).

PLANNED PAPERS

We are in the process of preparing one manuscript with the results of the evaluation of PMCAMx in Europe for May 2008 with emphasis on the organic aerosol concentration levels. Additional publications are planned for the comparison with the satellite retrievals during both May and February, the urban-regional interactions and the sensitivity of pollution to climate.

REFERENCES

Dawson J. P., P. J. Adams, and S. N. Pandis (2007) Sensitivity of PM2.5 to climate in the Eastern US: a modelling case study, *Atmos. Chem. Phys.*, **7**, 4295-4309.

Wagstrom K. M., S. N. Pandis, G. Yarwood, G. M. Wilson, and R. E. Morris (2008) Development and application of a computationally efficient particulate matter apportionment algorithm in a three-dimensional Chemical Transport Model, *Atmos. Environ.*, **42**, 5650-5659.

AEROSOL FORCING and CLIMATE RESPONSE: WORK PACKAGE 3.5

Johann Feichter[1], Olivier Boucher[2], Michael Schulz[3], Jon-Egill Kristjansson[4], Gerd Folberth[2], Trond Iversen[5], Stefan Kinne[1], Declan O'Donnell[1], Raffaella Vuolo[3], Kai Zhang[1]

[1]Max Planck Institute for Meteorology, Hamburg, Germany
[2]MetOffice, Exeter, UK
[3]CEA-Laboratoire des Sciences du Climat et de l'Environnement, Gif-sur-Yvette, France
[4] University of Oslo, Norway
[5]Norwegian Meteorological Institute, Oslo, Norway

Keywords: Model development, BVOC, global, biosphere-climate interactions, aerosol-climate

INTRODUCTION

WP 3.5 aims to improve our understanding of the role of aerosol particles in the climate system by developing and applying numerical climate models including parameterizations of aerosol and aerosol-cloud processes. Model simulations are carried out to assess the performance and sensitivity of current model versions and new model approaches, as well as the importance of specific processes and their contribution to radiative forcing.

Contributing aims to this general objective in the period 25-36 months are:
- Testing and evaluating new parameterizations
- Assessing the models´ sensitivity to model approaches
- Assess direct radiative forcing DRF and compare to observations
- Statistical analyses of extreme events – results

ACHIEVEMENTS in 2009

Parameterizations simulating secondary organic aerosols

A prime motivation for developing highly complex Earth-System Models is their ability to address urgent questions about the impacts of human activities on the natural environment in a coherent, integrated manner which takes into account the various feedback cycles that exist in the Earth System. To this purpose interactively coupled biogenic volatile organic compound (BVOC) emission model has been included in the global atmosphere models to be used for climate simulations.

The MetOffice **HadGEM2** model:

This new model computes BVOC (at the current stage isoprene) emission fluxes from the terrestrial vegetation. Through this approach BVOC surface fluxes become sensitive to and impact on the climate and its variation over time (e.g., increased emissions activity as a consequence of higher temperatures). The impact of changes in the atmosphere's chemical composition (e.g., damage to the vegetation by ozone) is also taken into account in the most recent model version.

The BVOC emission model has been integrated into the plant physiology module of the HadGEM2 land surface scheme MOSES. It applies the process-based approach as described by Arneth et al. (2007) which links isoprene formation at leaf level to photosynthetic activity. Information on vegetation distribution and leaf area index (LAI, essentially the total area over which BVOC emissions can occur per unit area) is obtained from the dynamic global vegetation model TRIFFID (Cox et al.,) which is also part of the HadGEM2 model. In this way changes in the global vegetation distribution in response to climate change are automatically accounted for. This allows the model to prognosticate the evolution of BVOC emissions in the future climate. The BVOC surface fluxes are provided to the tropospheric chemistry model in HadGEM2, the **U**nited **K**ingdom **C**hemistry and **A**erosol model UKCA, at every time step. Consequently, the model chemistry is tightly coupled to changes in the biosphere.

Figure 1 shows an example of the surface emission fluxes computed by the interactive scheme. The fluxes shown are representative of summertime conditions and are classified according to plant functional types (PFTs) included in the model. The figure shows that isoprene emissions from broadleaf tress (PFT1) and shrubs (PFT5) are the dominant contributions.

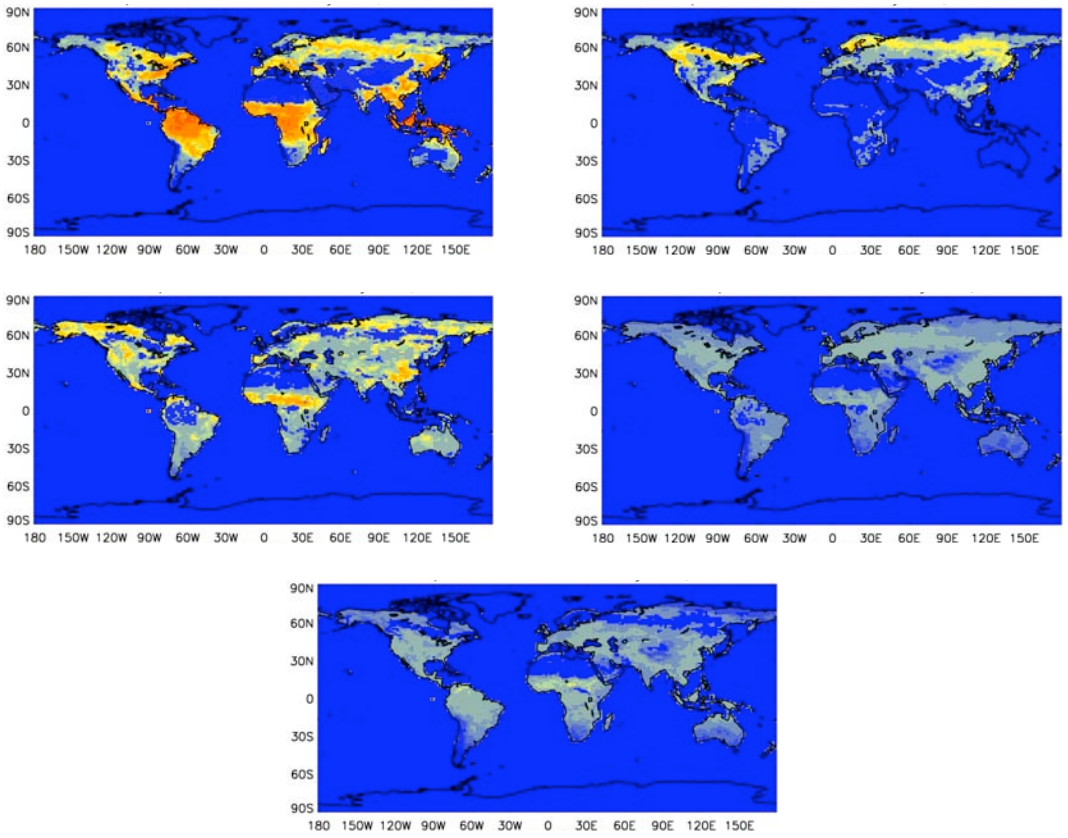

Figure 1: *Global distribution of monthly mean isoprene surface fluxes in mg m^{-2} day^{-1} for the summer season. The individual maps show emissions for each of the five plant functional types (PFTs) currently included in the HadGEM2 land surface scheme, clockwise from the top left: PFT 1: broadleaf trees; PFT 2: needle-leaf trees; PFT 3: C3-grasses; PFT 4: C4-grasses; PFT 5: shrubs.*

Most recently, the efforts of accounting for the predominant feedbacks between the biosphere and the atmosphere in the framework of HadGEM2 have included the fully coupled implementation of ozone leaf damage using the formulation described by Sitch et al (2007) where the ozone surface concentration is provided at every timestep by the atmospheric chemistry model UKCA. Furthermore, a process-based emission model for (mono)terpenes developed by Schurges et al. (2009) has been integrated into HadGEM2 and coupled to the chemistry in the same interactive as the isoprene emission model. Future developments will extend the interactive BVOC model to include emissions for other important biogenic VOC species such as methanol and acetone.

The MPI-Hamburg model **ECHAM5-HAM:**

Secondary organic aerosol (SOA) has been introduced into the global aerosol climate model ECHAM5-HAM. The SOA submodel treats both anthropogenic and biogenic sources of SOA. SOA is formed in the atmosphere from gas-phase oxidation reactions of precursor gases. Anthropogenic precursor gases
include toluene, xylene and benzene. Emissions of anthropogenic precursors are prescribed. Biogenic precursor gases included in the model are isoprene and monoterpenes. Individual monoterpene species are not distinguished from one another, but treated as a single species using the properties of α-pinene as a surrogate. Biogenic emissions are calculated online,

depending on temperature and leaf area index (for both isoprene and monoterpenes) and photosynthetically active radiation (for isoprene), following the widely used parameterisations of Guenther et al., (2006) and Guenther et al., (1995). The model calculates SOA formation from the precursor gases using a highly simplified chemistry scheme, which uses the two-product model of SOA formation developed by Odum et al. (1996).
Prescribed monthly values for the concentrations of the atmospheric oxidants OH, O3 and NO3 are used. Only the major SOA production for each precursor is considered to form SOA (ozonolysis of monoterpenes, and OH oxidation for all other species). Other oxidation reactions serve to consume precursor gas, but not to produce SOA.
SOA may be either semi-volatile or non-volatile (fixed per species): for semi-volatile species the gas-aerosol partitioning is calculated at each timestep using the equilibrium partitioning model of Pankow (1994a, 1994b). This method only describes the partitioning of SOA into gas and aerosol, whereas the SOA model requires partitioning into several size modes. A simple theory of how to extend the Pankow model to describe size-resolved partitioning has been developed and it has further been shown that the Pankow model describes a unique gas-aerosol equilibrium among multiple organic compounds. This theory predicts that SOA condenses preferentially on large particles.

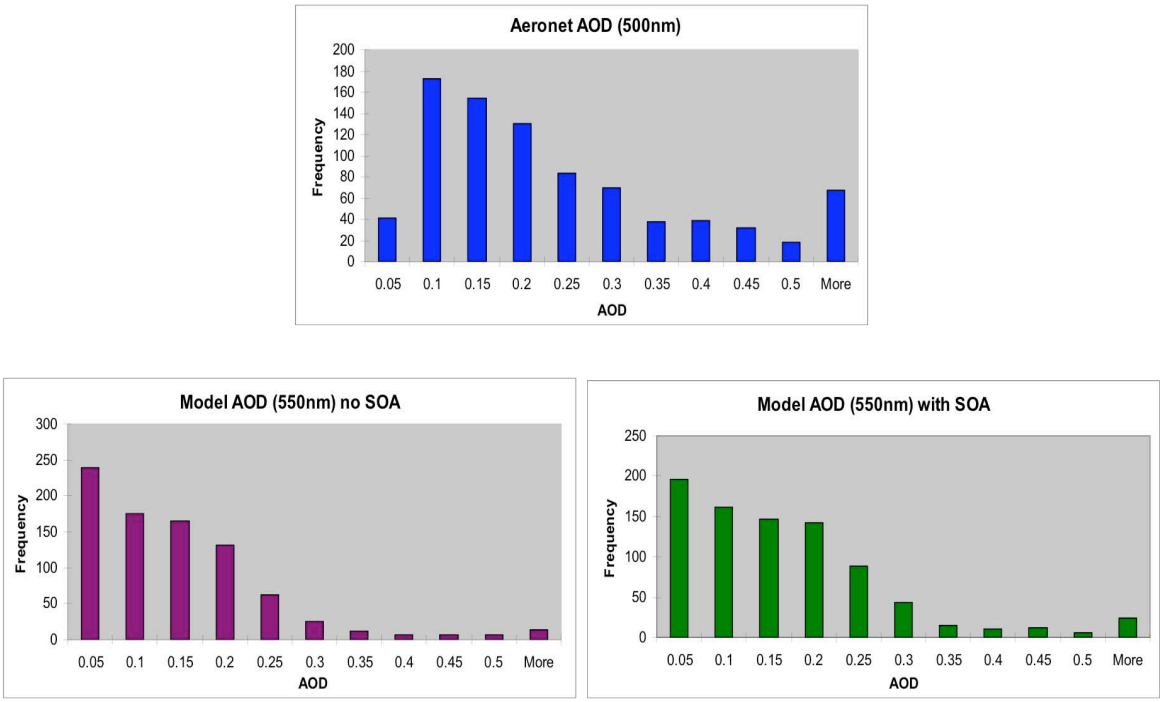

Figure 2: *Distribution of measured and modelled AOD in the mid-visible.*

The distribution of measured and modelled mid-visible AOD at the aeronet sites is shown in figure 2 (note that the scales on the *y*-axes differ). The incidence of very low (less that 0.05) mid-visible AOD in the model is reduced by about 20% in the simulation with SOA compared to that without SOA, but low AOD remains much more common in the model than in the aeronet observations. Otherwise, the distribution is moved slightly in the direction of higher AOD. Overall, the relevant mean (median) values are 0.225 (0.169) observed, 0.125 (0.103) for the model without SOA, and 0.149 (0.120) for the model with SOA.

The CEA-LSCE model **LMDzT-INCA:**

The model has been prepared to be able to simulate three hindcast simulations (agreed upon

under the AeroCom protocol) that are intended to better differentiate the causes of trends on aerosols and radiative fluxes reaching the surface (dimming and brightening) in the last three decades. New IPCC and AeroCom emissions have been prepared to be read into the model version for that purpose. A new higher horizontal and vertical resolution (96x95x19/39) has been introduced and input fields had to be prepared for the new resolutions. The radiative forcing diagnostics have been significantly augmented to properly differentiate the components of radiative flux interactions between clouds and aerosols. Simulations are underway to simulate first with emissions and nudged meteorology the years 1980-2009. Secondly we aim to simulate with emissions fixed and and finally we aim to force the model only by sea surface temperatures to differentiate the origins of simulated trends. All simulations are complemented by simulations of the preindustrial state. First tests have demonstrated that these simulations will be useful to establish the aerosol anthropogenic loads, their optical thickness and radiative effects. Additional sensitivity tests are carried out to provide further analysis through prescription of optical properties of aerosols, fixed albedo experiments and dedicated aerosol radiative flux perturbations due to absorbing aerosols below and above clouds. The vertical distribution of black carbon has been shown to be highly uncertain and thus prone to errors in the black carbon radiative forcing estimate (Koch et al., 2009). Indirect effect diagnostics have been implemented for better comparison to satellite measurements (Quaas et al. 2009). Systematic assessment of the recent evolution of the INCA model with respect to clear sky forcing, aerosol optical properties and surface concentrations, wet deposition and has been done continuously in conjunction with activities under WP53.

References:

Arneth, A., Ü. Niinemets, S. Pressley, J. Bäck, P. Hari, T. Karl, S. Noe, I. C. Prentice, D. Serça, T. Hickler, A.Wolf, and B. Smith, (2007):*Process-based estimates of terrestrial ecosystem isoprene emissions: incorporating the effects of a direct CO₂-isoprene interaction*. Atmospheric Chemistry and Physics, **7,** pp. 31–53.

Guenther, A., C. Hewitt, D. Erickson, R. Fall, C. Geron, T. Graedel, P. Harley, L. Klinger, M. Lerdau, W. McKay, T. Pierce, B. Scholes, R. Steinbrecher, R. Tallamraju, J. Taylor and L. Torres (1995): *A global model of natural volatile organic compound emissions,* J. Geophys. Res., **100**, 8873-8892

Guenther, A., T. Karl, P. Harley, C. Wiedinmyer, P. Palmer and C. Geron (2006): *Estimates of global terrestrial isoprene emissions using MEGAN (Model of emissions of gases and aerosols from nature),* Atmos. Chem. Phys. **6**, 3181-3210.

Odum, J. R., T. Hoffman, F. Bowman, D. Collins, R. C. Flagan and J. H. Seinfeld (1996): *Gas/Particle Partitioning and Secondary Organic Aerosol Yields*, Environ. Sci. Technol. **80**, 2580-2585.

Pankow, J. F. (1994a): *An absorption model of gas/particle partitioning of organic compounds in the atmosphere*, Atmos.Env. **28(2)**, 185-188

Pankow, J. F. (1994b): *An absorption model of the gas/particle partitioning involved in the formation of secondary organic aerosol*, Atmos. Env. **28(2)**, 189-193.

Quaas et al. (2009): Aerosol indirect effects - general circulation model intercomparison and evaluation with satellite data (2009): Atmos. Chem. Phys. Discuss., 9, 12731-12779.

Sitch, S., P. M. Cox, W. J. Collins, and C. Huntingford, *Indirect radiative forcing of climate change through ozone effects on the land-carbon sink*, Nature, **448**, pp. 791-794, 2007.

Schurgers, G., A. Arneth, R. Holzinger, and A. H. Goldstein (2009): *Process-based modelling of biogenic monoterpene emissions combining production and release from storage*. Atmospheric Chemistry and Physics, **9,** pp. 3409–3423.

Evaluation:

Different aspects of the direct aerosol radiative forcing will be investigated to better understand differences between the EUCAARI models. This includes dedicated experiments such as proposed in the framework of AeroCom with eg prescribed aerosol optical properties. Decomposition of direct aerosol forcing in cloudy regions will be attempted to investigate different components of the radiative budget in the simultaneous presence of aerosol and cloud.

Applications:

Joint effort to contribute to **IPCC AR5** by the use of complex climate models:

Discussion initiated by the chair of IPCC after AR4 suggests that IPCC will continue its assessment process and produce another comprehensive report in 2012/13. One of the areas where the next assessment should demonstrate progress with respect to AR4 is the integration of Earth system components including complex feedback processes between climate and chemistry, aerosols and gas-phase compounds, and the exchange of compounds between the terrestrial and marine biosphere and the atmosphere. Including stratospheric dynamics and chemistry are essential elements of the simulations and constitute a major advancement with respect to the simulations discussed in IPCC AR4.

Scope and extent of the planned simulations

The model experiments shall cover a multi-decadal period in the past and explore two or three different scenarios with significant impacts on air quality and climate for the "near term" future. Each experiment shall be run as an ensemble of 4-5 realizations spinning off a unified baseline control simulation which spans several centuries in order to obtain a reasonable dynamic equilibrium for the ocean dynamics, sea ice and carbon cycle components. Stratospheric chemistry will require approximately 20 years of spin-up, while tropospheric chemistry and aerosols generally adjust within about 1 year (provided that methane boundary conditions are prescribed).
The ensemble simulations will start either in 1960 or 1970. There will be one set of ensemble runs covering the recent past (up to 2005), and two or three ensembles will be run for future scenarios (2005 to 2040 or 2050). The scenarios shall encompass at least a "worst case" (some variant of the SRES A2 scenario) and a "best case" (also termed "maximum feasible reduction") scenario. If possible, one intermediate scenario ("current legislation") shall also be run. Number and exact definition of these scenarios will depend on CPU time availability and on the availability of emission data prior to the start of the simulations.

Biosphere-climate interactions:

All EUCAARI models run now modules for the treatment of secondary organic aerosols and thus are able to perform sensitivity simulations to explore the role of biogenic VOC emissions in different climate states.

EUCAARI publications

O'Donnell D. (2009): *Towards the Assessment of the Climate Effects of Secondary Organic Aerosols,* PhD Thesis, submitted to the University of Hamburg, Oct. 2009.

D. Koch, M. Schulz, S. Kinne, T. C. Bond, Y. Balkanski, S. Bauer, T. Berntsen, O. Boucher, M. Chin, A. Clarke, N. De Luca, F. Dentener, T. Diehl, O. Dubovik, R. Easter, D. W. Fahey, J. Feichter, D. Fillmore, S. Freitag, S. Ghan, P. Ginoux, S. Gong, L. Horowitz, T. Iversen, A. Kirkevåg, Z. Klimont, Y. Kondo, M. Krol, X. Liu, C. McNaughton, R. Miller, V. Montanaro, N. Moteki, G. Myhre, J. E. Penner, Ja. Perlwitz, G. Pitari, S. Reddy, L. Sahu, H. Sakamoto, G. Schuster, J. P. Schwarz, Ø. Seland, J. R. Spackman, P. Stier, N. Takegawa, T. Takemura, C. Textor, J. A. van Aardenne, and Y. Zhao, Evaluation of black carbon estimations in global aerosol models Atmos. Chem. Phys. Discuss., 9, 15769-15825, 2009.

Quaas, J., Ming, Y., Menon, S., Takemura, T., Wang, M., Penner, J. E., Gettelman, A., Lohmann, U., Bellouin, N., Boucher, O., Sayer, A. M., Thomas, G. E., McComiskey, A., Feingold, G., Hoose, C., Kristjansson, J. E., Liu, X., Balkanski, Y., Donner, L. J., Ginoux, P. A., Stier, P., Feichter, J., Sednev, I., Bauer, S. E., Koch, D., Grainger, R. G., Kirkevåg, A., Iversen, T., Seland, Ø., Easter, R., Ghan, S. J., Rasch, P. J., Morrison, H., Lamarque, J.-F., Iacono, M. J., Kinne, S., and Schulz, M.: Aerosol indirect effects - general circulation model intercomparison and evaluation with satellite data, Atmos. Chem. Phys. Discuss., 9, 12731-12779, 2009.

Schulz, M., Chin, M., Kinne S., The Aerosol Model Comparison Project, AeroCom, Phase II: Clearing Up Diversity, IGAC Newsletter, No 41, May 2009

In preparation

Kazil et al., New nucleation scheme in ECHAM6-HAM

Stier et al., Implementation of an explicit activation scheme in ECHAM6

Zhang et al., Evaluation of microphysical properties as simulated by ECHAM5-HAM

EUCAARI WP3.6

Olivier Boucher, Met Office Hadley Centre
Hans Feichter, MPI & Michael Schulz, IPSL

November 2009

Contents

This presentation covers the following areas

Improvements made to models

Preparing for CMIP5 / EUCAARI simulations

This year's deliverables and what's next?

New features (M7, ECHAM)

1. New nucleation scheme which considers the charged nucleation induced by cosmic ray
2. New below-cloud scavenging scheme
3. Kappa-Köhler theory based water-uptake scheme
4. New explicit treatment of SOA
5. Two-moment cloud microphysics, CDNC predicted, allow modeling the interaction between aerosol and cloud in a more consistent way

1. T63L31 resolution (~2ºx2º)
2. Nudged with year-2000 ERA40 reanalysis data
3. 1st group: standard cloud microphysics, CDNC prescribed
4. 2nd group: two-moment cloud microphysics, CDNC predicted

lognormal modes – M7 module

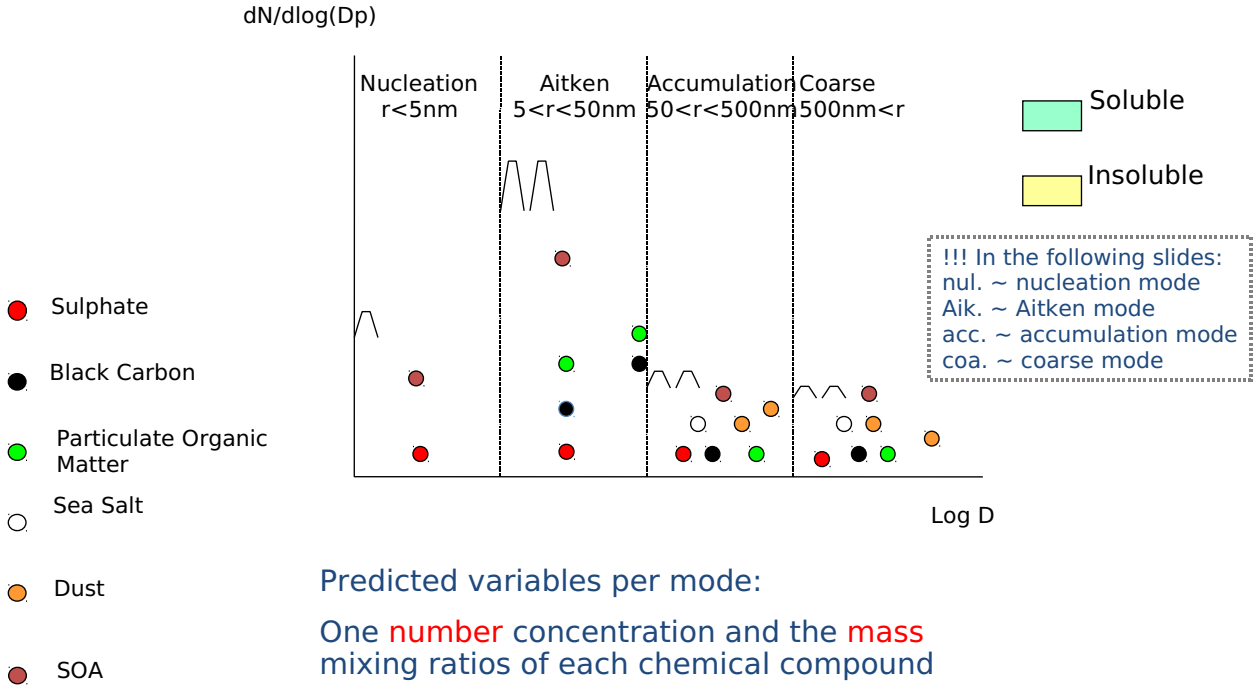

Predicted variables per mode:

One number concentration and the mass mixing ratios of each chemical compound

Courtesy of Declan O'Donnell

Vertical profile of fine mode particles

Comparison between the simulated and observed Aitken and accumulation mode number concentrations over Europe.

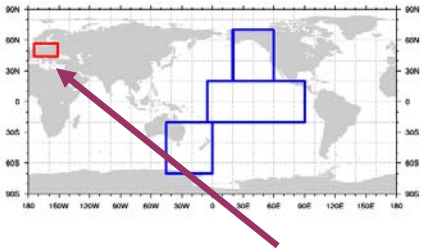

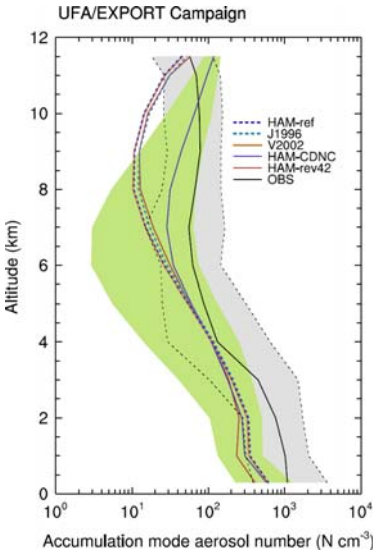

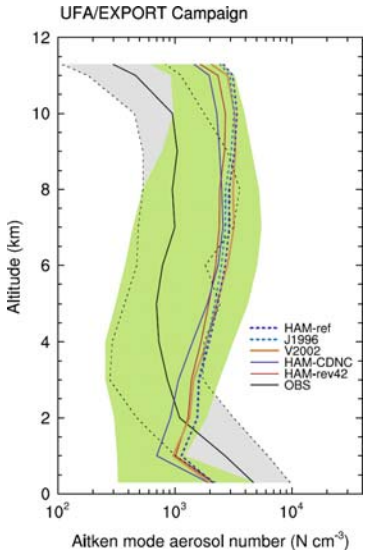

The simulated profiles are July and August averages. Observations were compiled by Minikin et al. (2003) using the measurements obtained in July and August 2000 during the UFA/EXPORT campaign. The boundaries of the shaded areas indicate the 10- and 90-percentiles of the observational data

accumulation mode (0.1–3 µm)

Aitken mode (0.014–0.1 µm)

Vertical profile of ultra-fine particles
(Dp>3nm)

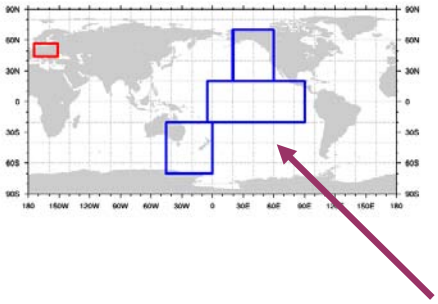

Data from Clarke and Kapustin (2002)

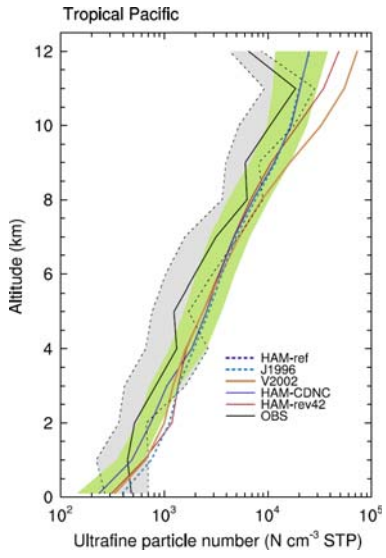

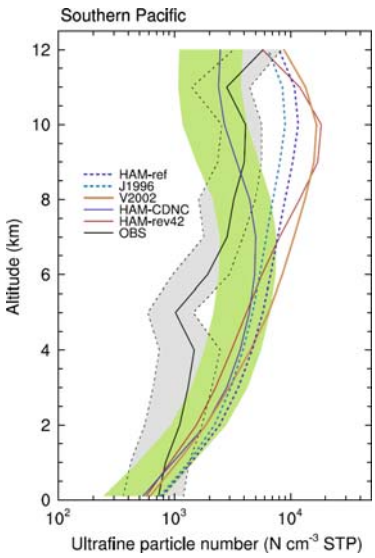

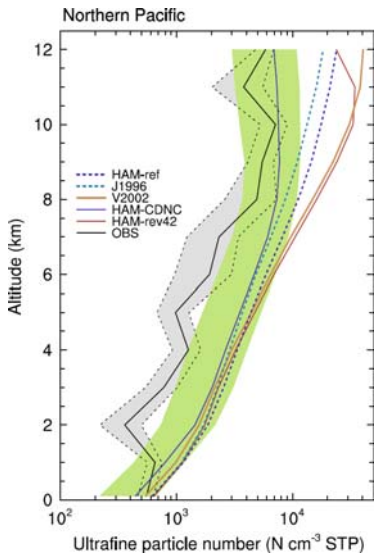

sol size distribution (M7, ECHAM)

in the offshore regions of polluted area

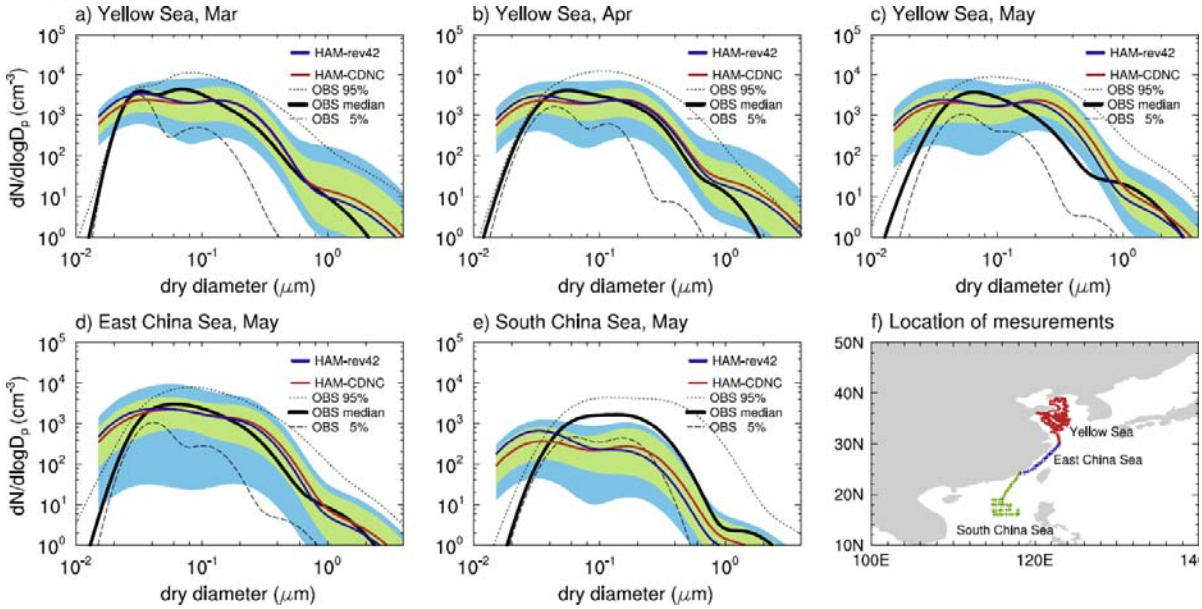

fect of new nucleation scheme

number concentration of soluble nucl. mode particles (r<5nm, N cm-3 STP)

Vehkamaeki et al. *Kazil et al.* *Difference (K - V)*

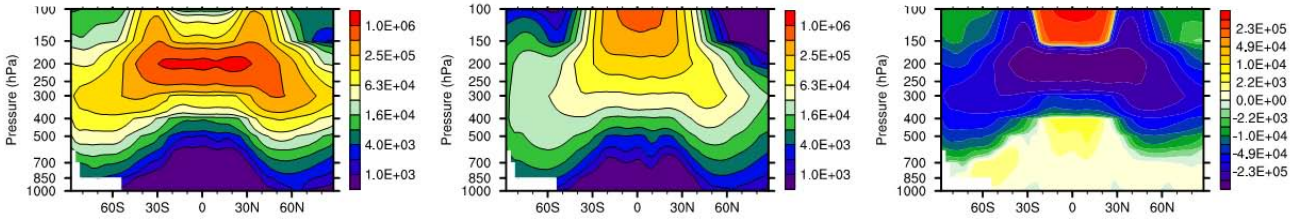

Difference in the simulated AOD

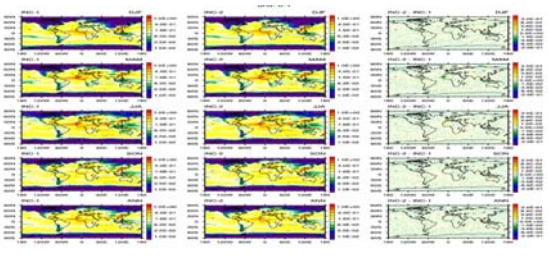

Difference in the simulated SWCF

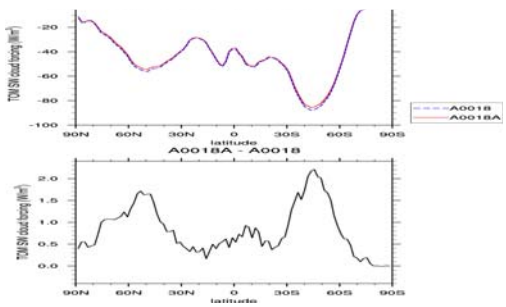

Contribution of SOA to total aerosol mass (M7)

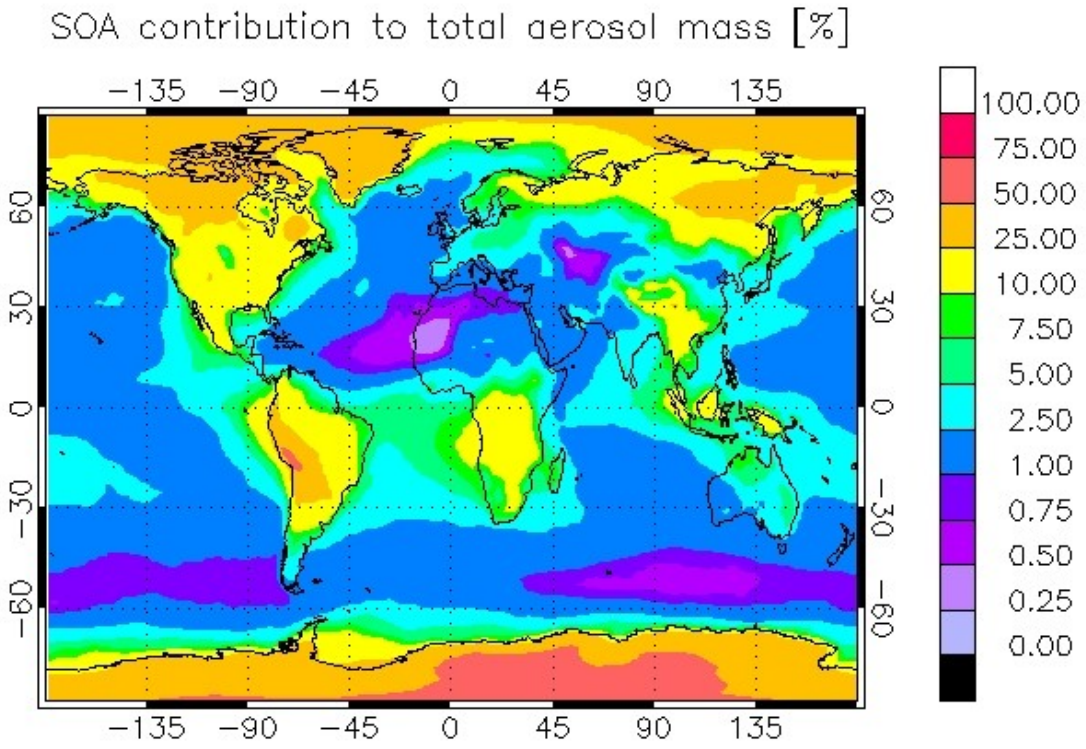

- SOA is globally important in the sense that the aerosol mass is significant compared to e.g. SO4 and POM

New UKCA-MODE aerosol scheme

Nucleation

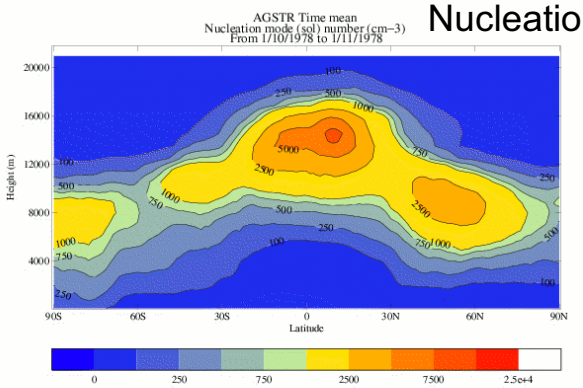

Accumulation

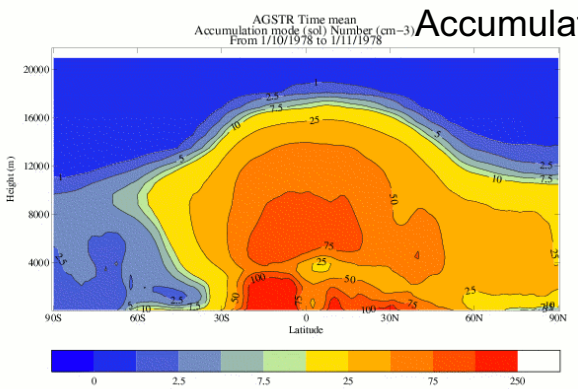

Aitken

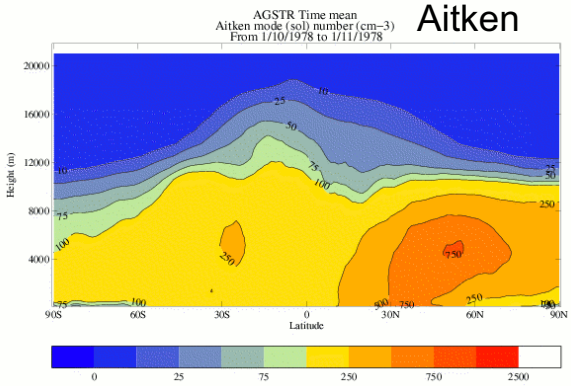

Coarse

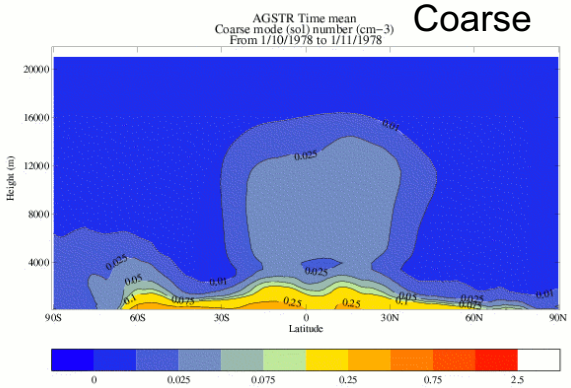

HadGEM2 ES-components
interactive BVOC emissions – iBVOC

interactively coupled to land surface model

uses two ***selectable*** emission models

process based **(Almut Arneth et al., ACP, 2007)**

- **net photosynthesis, dark respiration, leaf temperature, atmospheric CO2 levels (isoprene inhibition)**

empirical (MEGAN; Guenther et al., ACP, 2006)

- temperature, PPFD (photosynthetic photon flux density), PCEEA (parameterized canopy environment emission activity), soil moisture

outputs: instant. C5H8 emission (total, per PFT)

HadGEM2 – iBVOC model
Flux Map for each PFT – JJA

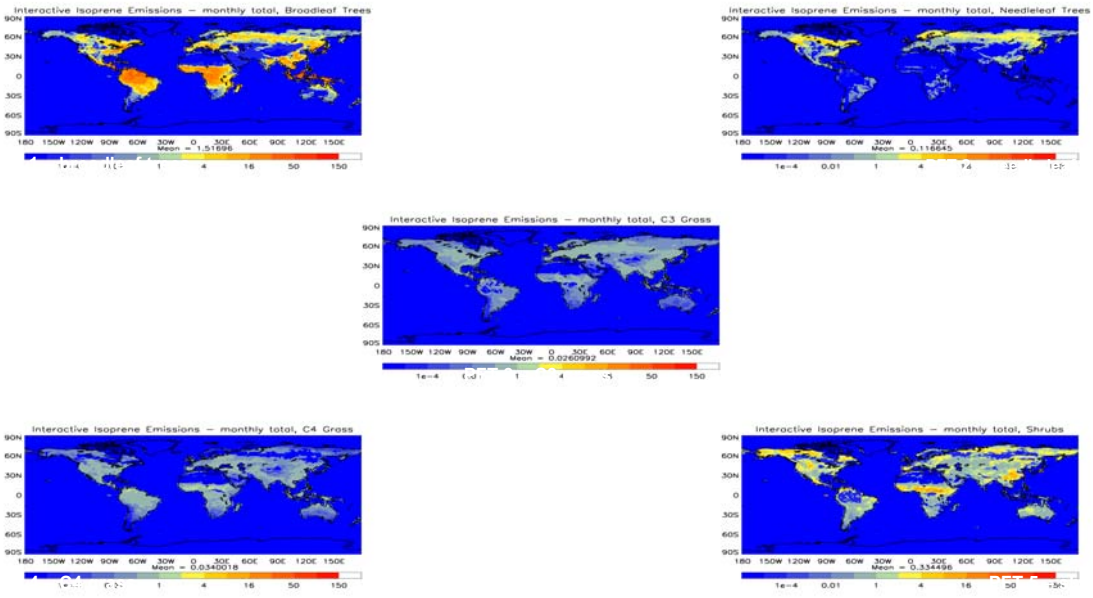

Validation of IPSL Coupled model with aerosol mass fields read in

Additional New Forcing Diagnostics, Annual Average, W m-2

Aerosol Surface forcing

Anthropogenic	swsrfas_ant = -1.58
Natural	swsrfas_nat = -2.58
Anthro, clear sky	swsrfcs_ant = -2.09
Natural, clear csky	swsrfcs_nat = -3.59

Aerosol TOA forcing

Total All-sky	swtoaas_aer = -1.55
Clear-sky	swtoacs_aer = -2.74
Anthro All-sky	swtoaas_ant = -0.48
Anthro Clear-sky	swtoacs_ant = -0.89
Natural All-sky	swtoaas_nat = -1.06
Natural Clear-sky	swtoacs_nat = -1.85

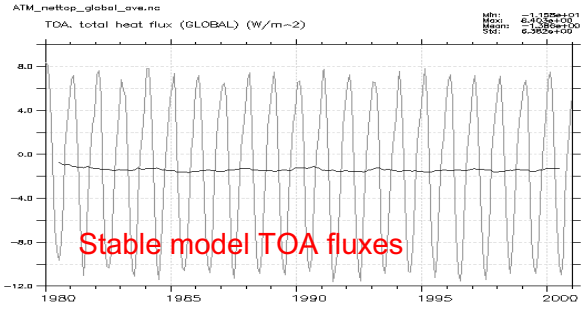

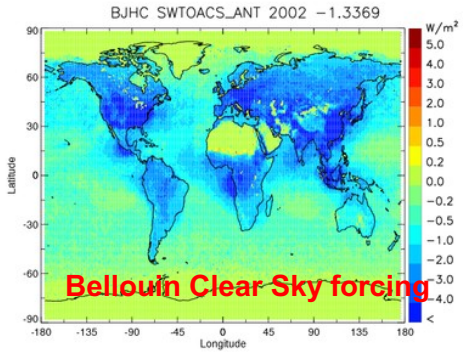

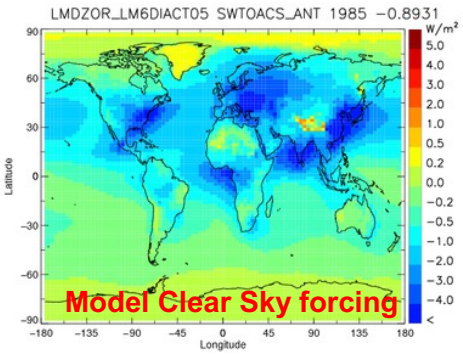

WP3.6: Deliverables

Met Office Hadley Centre

Deliverables

D1 Review paper on how aerosols contribute to climate change feedbacks (METO/Leeds) M24

D2 Report on the relevance of BVOC database for climate change experiments (met.no) M28

D3 Report describing new ESMs and aerosol schemes (METO/CEA/MPI) M36

Milestones and expected result

M1 ESMs ready for 21st experiments (METO, CEA-LSCE, MPI) M30

M2 Common design and aerosol emissions for 21st century simulations agreed M30

M3 ESMs simulations completed (METO, CEA-LSCE, MPI) M42

Being at the end of the EUCAARI chain, this WP will essentially deliver to the EUCAARI annual reports, the European Commission, and the open literature in time for inclusion in the IPCC 5th Assessment Report.

WP3.6: Deliverables

Deliverables

D1 Review paper on how aerosols contribute to climate change feedbacks (METO/Leeds) M24 ✓

D2 Report on the relevance of BVOC database for climate change experiments (met.no) M28 ✗

D3 Report describing new ESMs and aerosol schemes (METO/CEA/MPI) M36

Milestones and expected result

M1 ESMs ready for 21st experiments (METO, CEA-LSCE, MPI) M30 ✓

M2 Common design and aerosol emissions for 21st century simulations agreed M30 ✓

M3 ESMs simulations completed (METO, CEA-LSCE, MPI) M42

Being at the end of the EUCAARI chain, this WP will essentially deliver to the EUCAARI annual reports, the European Commission, and the open literature in time for inclusion in the IPCC 5th Assessment Report.

CMIP5/AR5 experiments

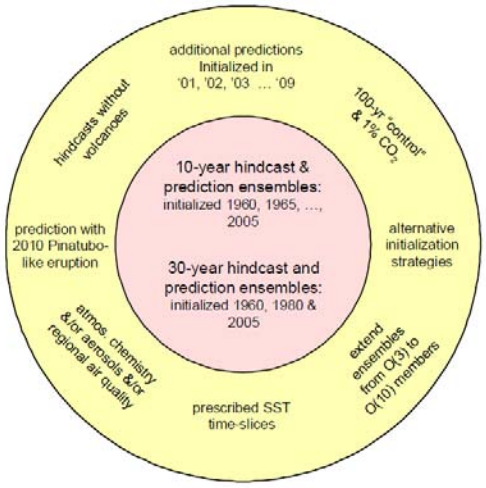

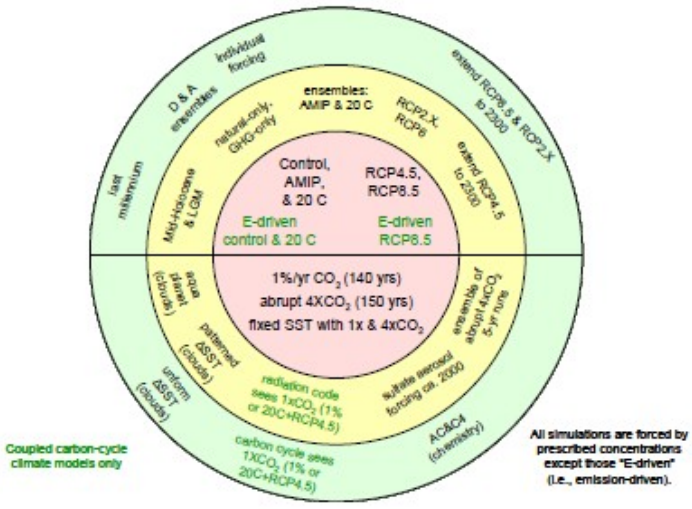

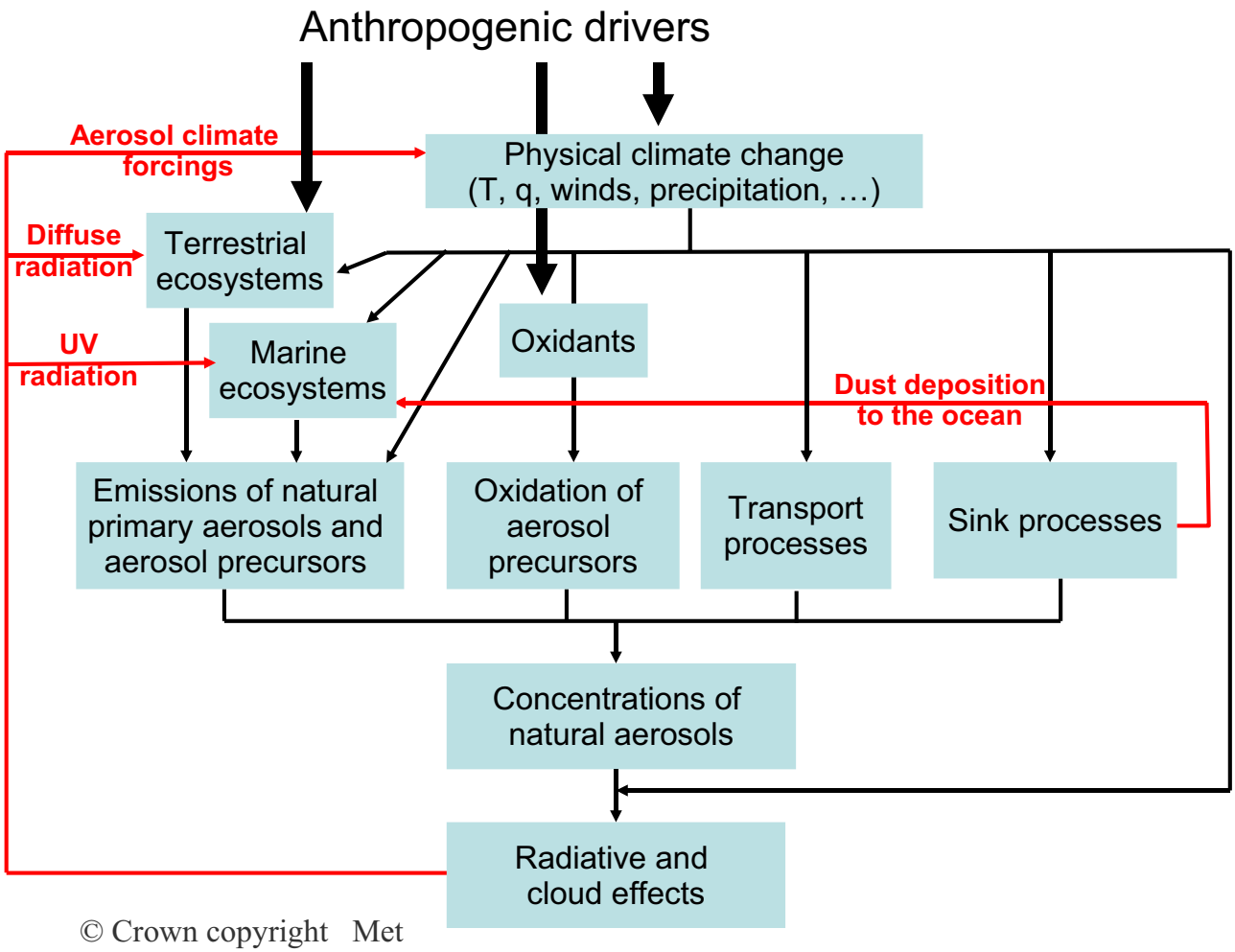

AR5 centennial experiments

Met Office
Hadley Centre

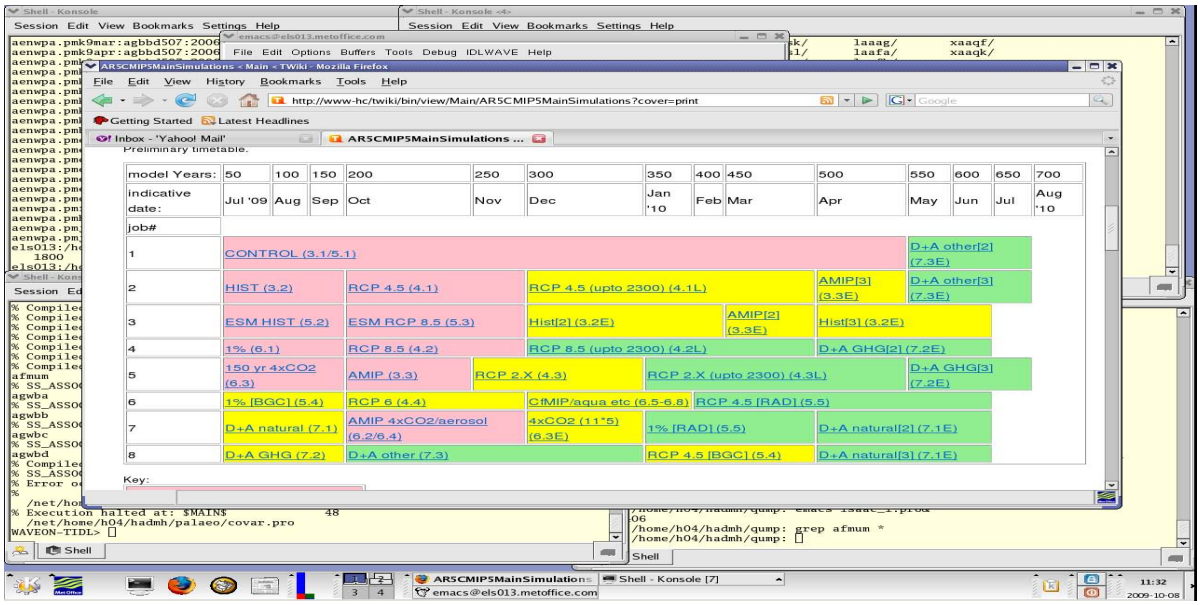

Overview ESM-IPSL-INCA aerosol model configurations for 5th IPCC report

Preindustrial Control Climate state

Is used to start coupled aerosol-climate simulations 1850

144x142 ESM CMIP5

96x95x19/39 ESM-aerosol

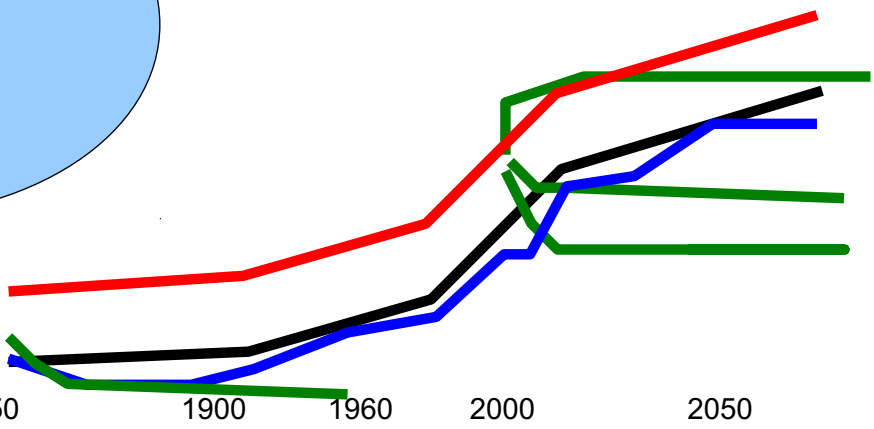

OFFLINE coupled ESM runs

Reading in every 10-20 years precalculated aerosol mass IPCC emissions, INCA-NMHC-AER

ONLINE coupled ESM-INCA

Transient aerosol-climate simulation

Snapshot simulations with different emissions

Hindcast run with SST forcing

AR5 Time Scale Guestimates

Met Office Hadley Centre

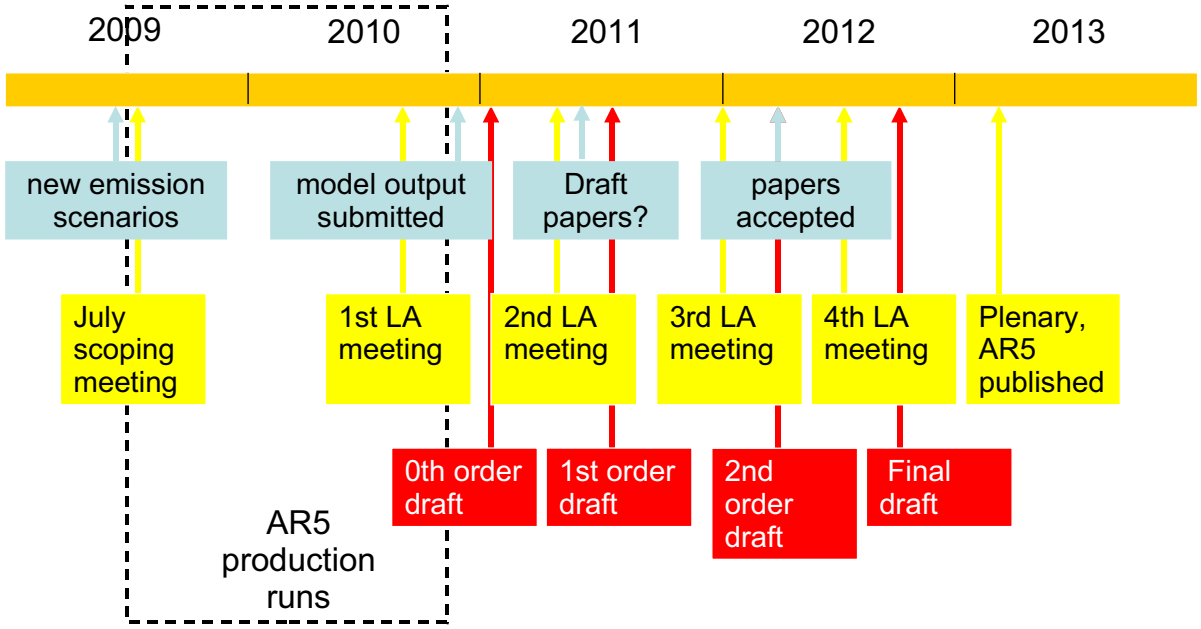

CMIP5

List of aerosol diagnostics now frozen.

CMIP5 runs have started or will soon start and first results will be delivered to by month 42 of the project.

CMIP5 data will archived and made available.

Unfortunately it was not feasible to provide 6-hourly forcing data for regional air quality models in WP5.1 (not planned neither in CMIP5 protocol nor in EUCAARI plans).

Impact on AR5 within and beyond the EUCAARI project.

Description of Work WP3.6 Months 37-48

Met Office
Hadley Centre

Questions

Thanks to Ken!!

HadGEM2-ES aerosol feedbacks

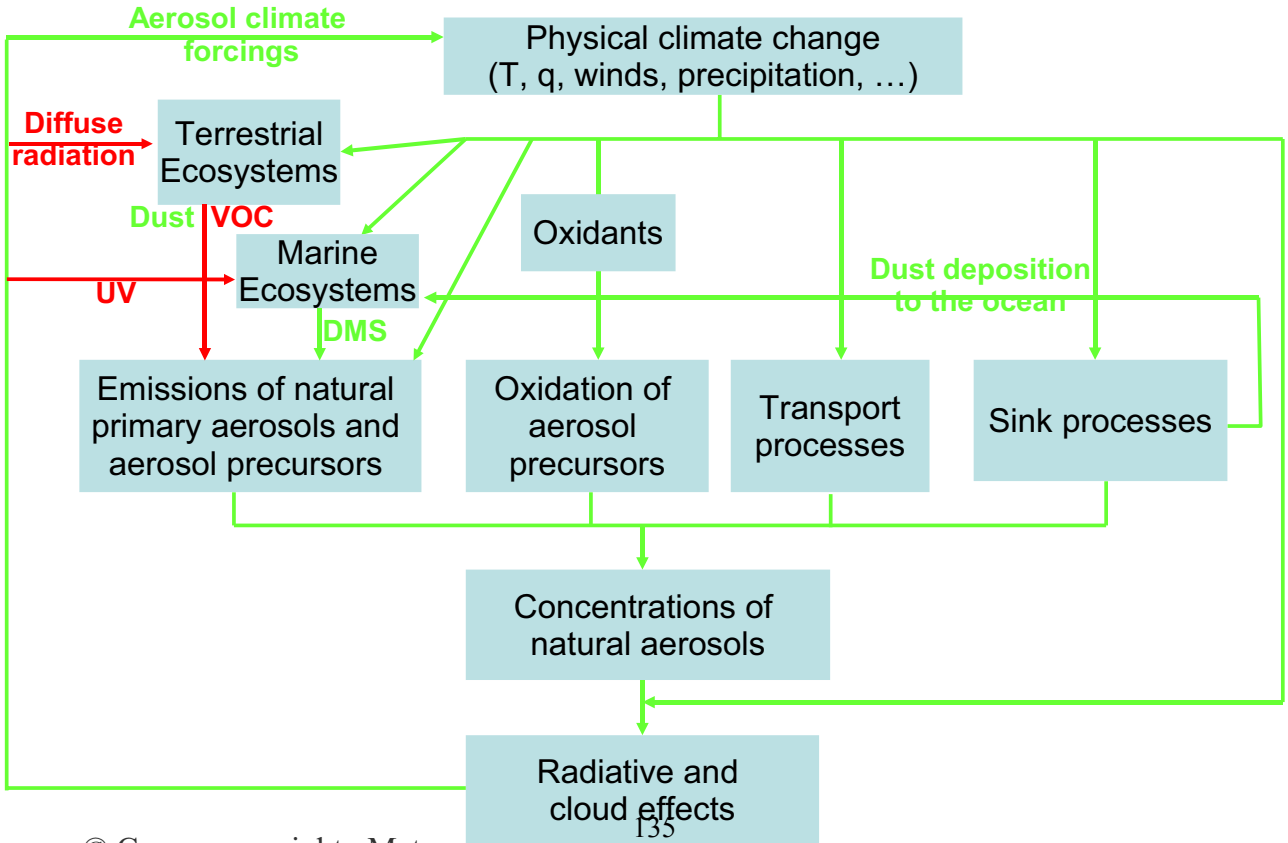

IPSL aerosol feedbacks

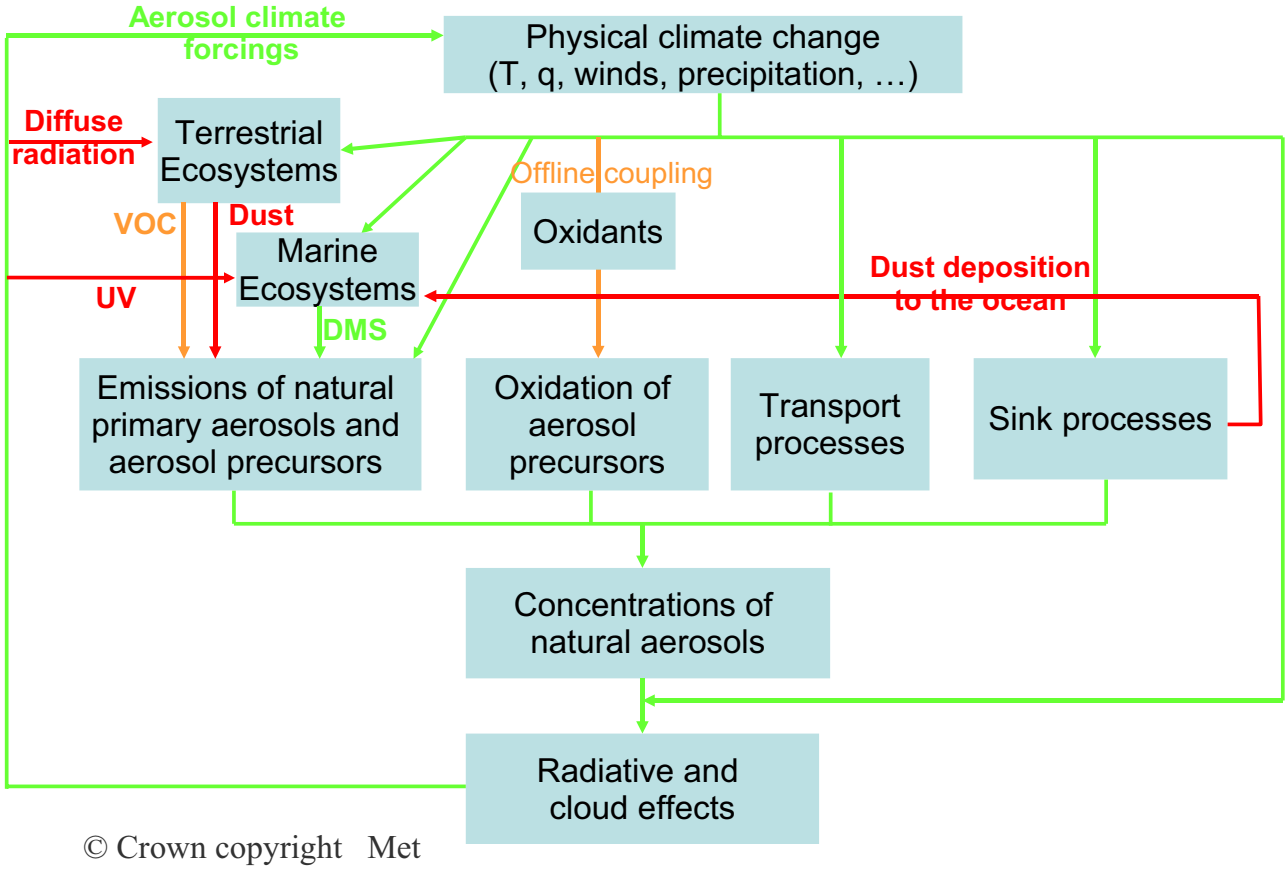

ECHAM5-HAM aerosol feedbacks

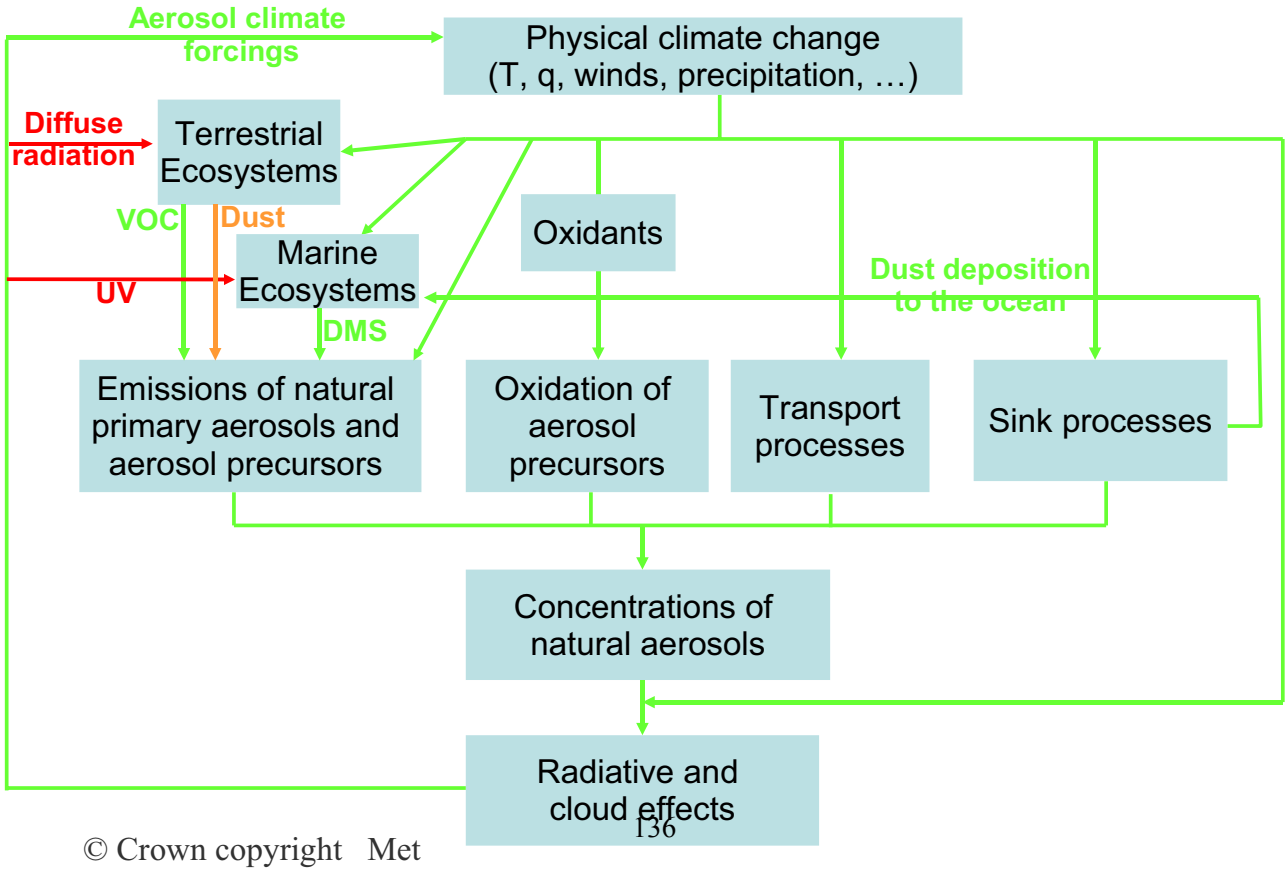

Kappa-Köhler theory based water-uptake scheme

Original: ZSR based scheme

- take aerosol as a solution of mixed electrolytes
- extremely sensitive to higher RH

Jacobson et al. JGR-1996

New: Kappa-Köhler theory based scheme

- can easily be applied for non-electrolytes (e.g. organic specie)
- a hygroscopicity parameter κ for each chemical component

Petters and Kreidenweis ACP-2007

Growth factor of an aerosol particle can be expressed as a function of temperature, relative humidity, aerosol dry diameter and kappa

Implemented by D. O'Donnell

Effect of new water-uptake scheme (M7, ECHAM)

Surf. aerosol water in the soluble acc. mode particles (50<r<500nm, kg kg-1)
Less acc. aerosol water

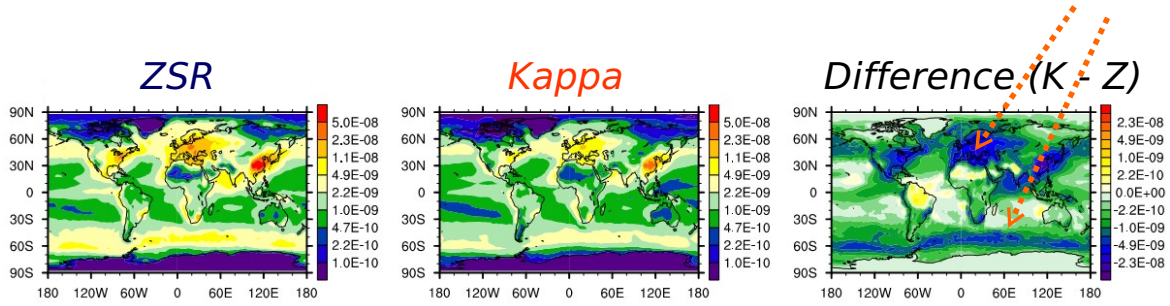

Number concentration of soluble acc. mode particles (50<r<500nm, N cm-3 STP)
Less acc. particles, more smaller particles (nul. Ait.)

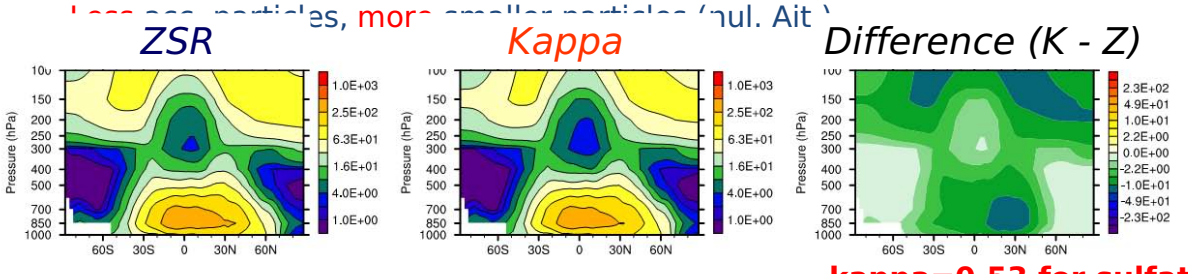

kappa=0.53 for sulfate

Cloud microphysics

Two-moment cloud microphysics:

Lohmann et al. (2007), Lohmann (2008)

Activation: Lin & Leaitch, 1997

$$Q_{\text{nucl}} = \max\left[\frac{1}{\Delta t}\left(0.1\left(\frac{N_a w}{w + \alpha N_a}\right)^{1.27} - N_{l,\text{old}}\right), 0\right]$$

Auto-conversion: Khairoutdinov & Kogan, 2000

$$Q_{\text{aut}} = 1350 \times q_l^{2.47} N_l^{-1.79}$$

Processes that not considered in current simulations:

1. Cloud processing of aerosols
currently smaller particles in cloud droplets can be "re-evaporated" again
2. Microphysics of convective cloud
... ...

Effect of aerosol on cloud and water vapor

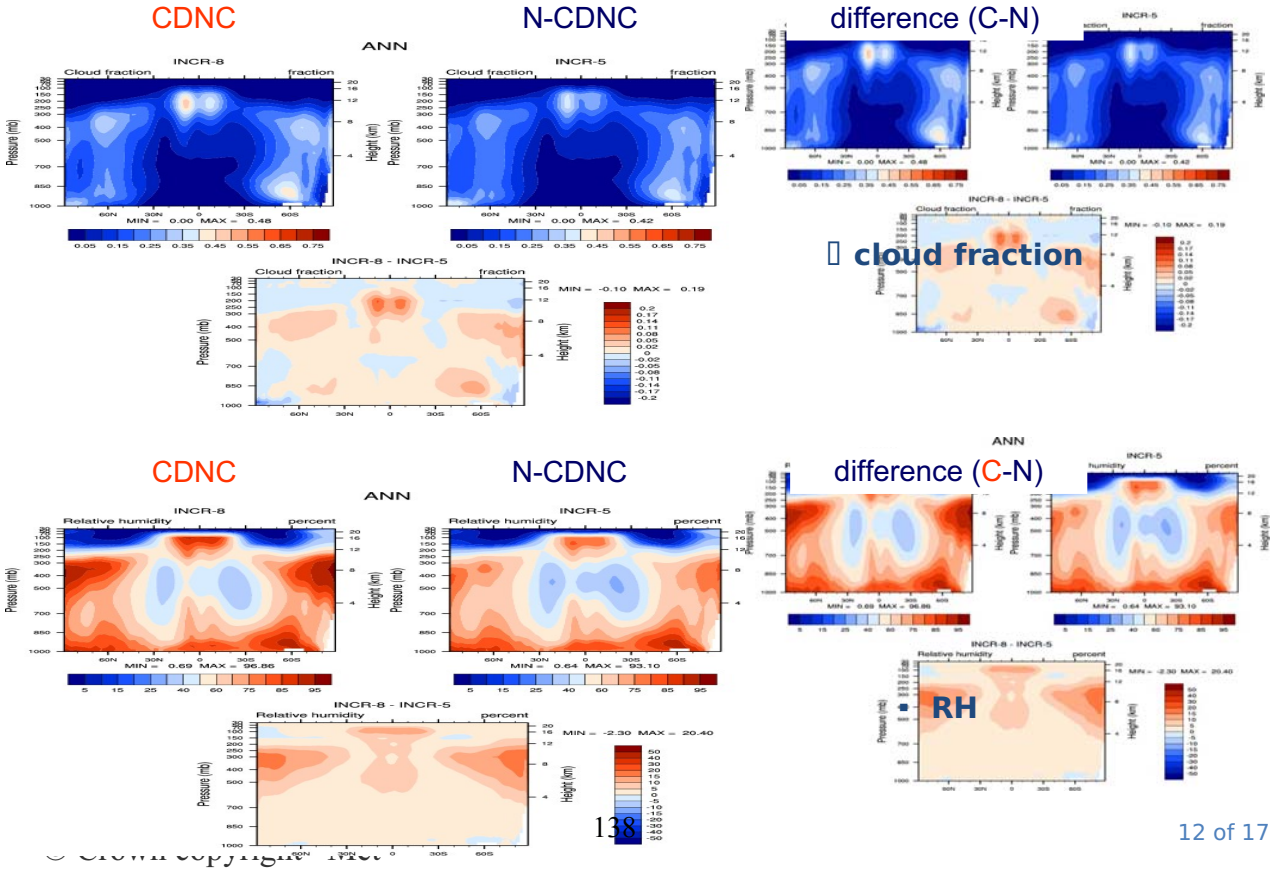

Shortwave cloud forcing

Net shortwave flux at TOA: total sky – clear sky

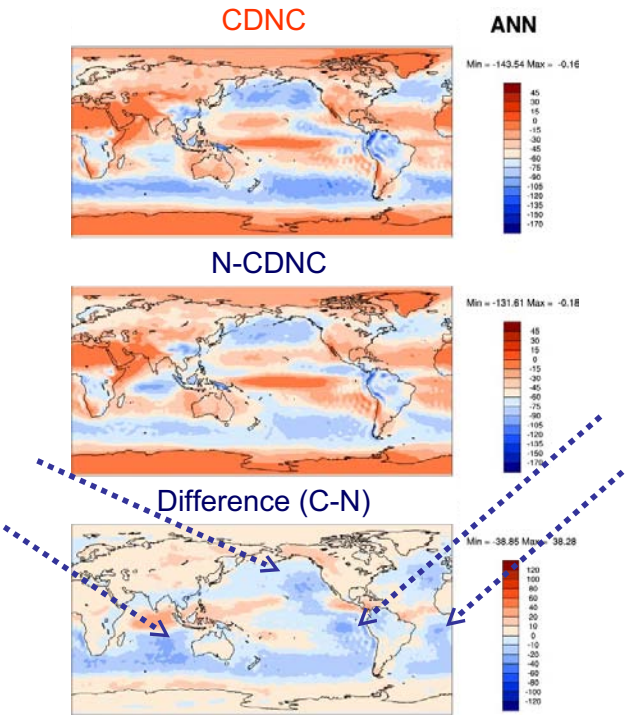

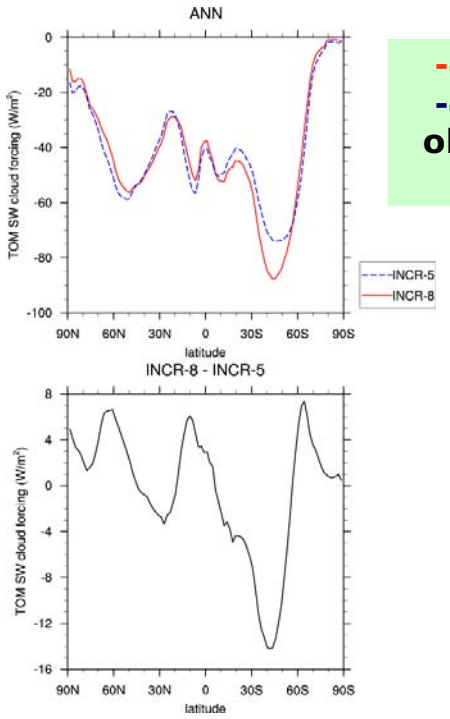

-47.9
-46.6
obs: ~ 50

Longwave cloud forcing

Net longwave flux at TOA: total sky – clear sky

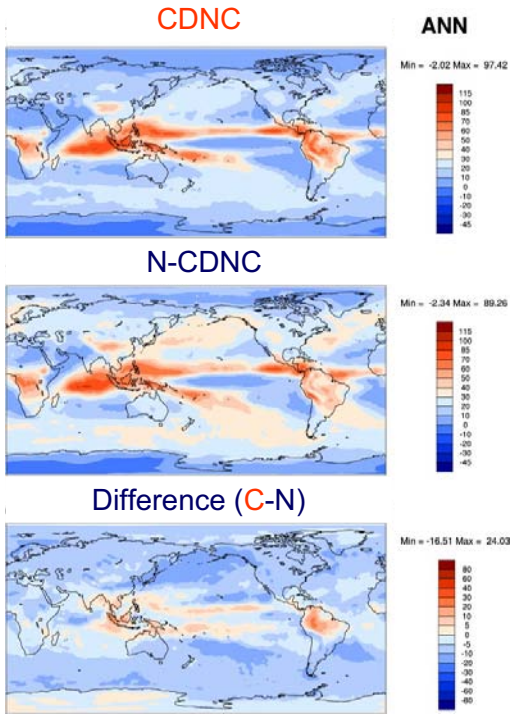

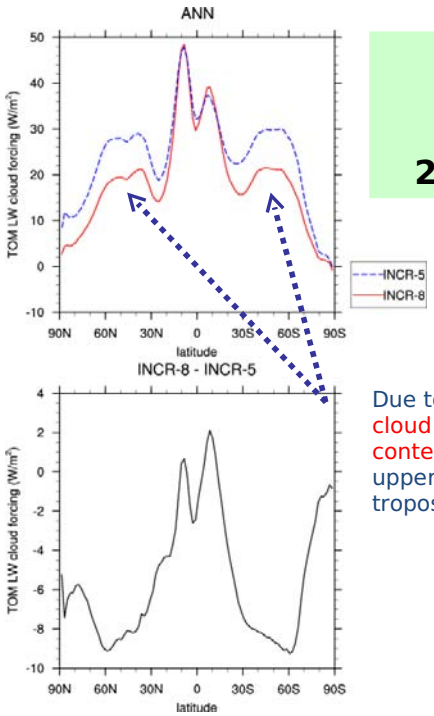

22.8
27.9
obs: 22~30

Due to smaller cloud ice content in the upper troposphere

Feedbacks of clouds on aerosols

Number conc. of soluble acc. mode particles (50<rp<500nm, N cm-3 STP)
More aerosol particles in the upper troposphere
Less aerosol particles in below 700 hPa over the tropical region

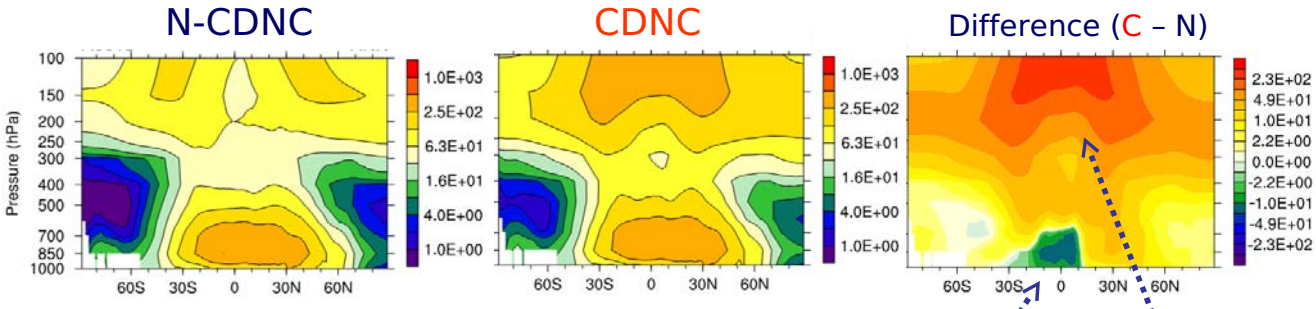

Sulfate burden (Tg)	0.98	1.20
Sulfate lifetime (day)	3.7	4.5
Total AOD	0.11	0.13

Larger rainfall over tropical forest

Less in-cloud scavenging and vertical transport

Why longer aerosol lifetime & larger AOD?

prognostic CDNC

more, smaller cloud droplets → cloud albedo effect (1st)

longer cloud lifetime (2nd)

less in-cloud wet scavenging

larger RH (evaporation of cloud droplet)

longer aerosol lifetime, larger burden and AOD

larger aerosol water-uptake, larger AOD

larger absorption of long-wave radiation

... ...

WP5.1: Aerosol impacts on climate and air quality: Integration with policy

Øystein Hov and David Simpson on behalf of WP5.1, with contributions from Olivier Bouchier, Zbignieuw Klimont, and Elisabetta Vignati

INTRODUCTION

The objective of WP5.1 is to integrate the new results coming out of WP1.1-WP3.6 to address the science questions in EUCAARI in the policy framework of change in climate, air quality and ecosystems. In WP5.1 the focus is on future changes. Historical data will mainly be used for validation of models and to assess the understanding of the relationships between changes in earth-atmosphere fluxes of trace species, and changes in climate, air quality and ecosystem impact.

Much of the work in this WP depends on the completion of emission inventories and other tasks from other parts of EUCAARI, but during 2009 the models were able to start new runs with updated emissions, and the studies on relationships between atmospheric aerosols and carbon allocation are progressing.

Task 5.1.1 a) Emissions (IIASA)

The challenge faced by several modeling efforts is to compile an emission inventory input set that is inherently consistent. Unfortunately, at the present time, no emission inventory covers all species, sectors and years of interest for environmental impact studies. Therefore, a collection of inventories and projections of different origin and quality are used in atmospheric models including climate models where a similar problem of consistency between emissions of greenhouse gases and air pollutants exists.

Key existing emission inventories and major emission projection efforts have been reviewed. The reviewed material refers to either regional or global studies of air pollutants, particularly SO2, NOx, NMVOC, NH3, CO, PM and greenhouse gases CO2, CH4, N2O; however, the primary goal was to assess the state of the knowledge at the global level, i.e., data needed for global modeling exercises. It is by no means a complete review but rather a focused effort to review the mostly used sets of data and attempt to specify the areas that might need either further work or special attention when the set of projections for use in EUCAARI is developed.

Specific attention has been paid to particulate matter (PM) emissions. Although, total PM has been reported for years, speciated PM emission estimates have only been published recently and are still incomplete. As a matter of fact, more work went into establishing and verifying BC and OC inventories than total primary PM10 or PM2.5. We have developed such a global inventory of primary PM with the GAINS model (http://gains.iiasa.ac.at) and it is being prepared for use in the EUCAARI work.

The recent work of the remote sensing community added another edge to the discussion of the emission development in Asia (Richter et al., 2005). The discussion has concentrated on the unprecedented growth in the last decade and mostly on NOx but more recently also SO2 retrievals were shown and compared (Richter et al., 2007). Although, initial comparisons with emission inventories indicated they underestimated the growth, more recent work (e.g., Klimont et al., 2009; Zhang et al., 2007) show very similar pattern (see Figure 1 for NOx).

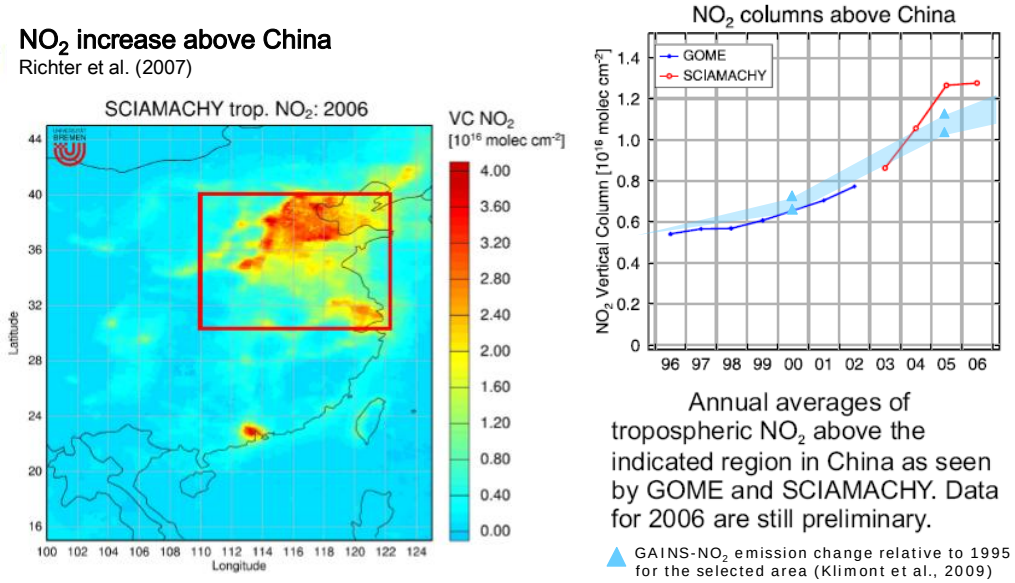

Figure 1. Comparison of remote sensing data on NO2 changes over China with GAINS model calculation

Understanding of the past developments in emissions and the driving forces behind the changes in strength of specific sources is crucial for understanding and modeling of the changing atmosphere as well as for the development of future policies. For that purpose we have been developing with the GAINS model a consistent set of scenarios (the same set of assumptions on growth and control policies to estimate various emitted compounds) for use in EUCAARI. This process has been taking a bit more time than anticipated leading to delays in delivering reports within EUCAARI, however, not hampering the other tasks of the project. One of the reasons for delays was a consideration of using in EUCAARI the scenarios that are harmonized with the work towards the IPPC AR5 assessment discussed below.

Recently, the RCP (Representative Concentration Pathways) emissions have been developed for the IPPC AR5 http://www.igac.noaa.gov/newsletter, IGAC Newsletter 41, May 2009). The RCPs are meant to serve as input for climate and atmospheric chemistry modeling as part of the preparatory phase for the development of new scenarios for the IPCC's Fifth Assessment Report and beyond, and are based on selected scenarios from four modeling teams/models. The scenarios have been published on-line in May 2009 but are not the final versions yet. At IIASA the RCP8.5 scenario has been developed in collaboration between two IIASA groups running GAINS and MESSAGE models.

The RCP scenarios extend to 2100; IIASA has contributed with the medium term perspective (consistent with the goals of EUCAARI) on the impact of currently committed air pollution legislation on the development of the future emissions until 2030. These results have been translated into the larger scale and aggregation model MESSAGE to generate also the spatial pattern of emissions.

The Global Energy Assessment (GEA) is a major initiative established by IIASA to help decision makers address the challenges of providing energy services for sustainable development, whilst ameliorating existing and emerging threats associated with: security of supply; access to modern forms of energy for development and poverty alleviation; local, regional and global environmental impacts; and securing sufficient investment. GEA is not part of EUCAARI activities but we are contributing with our emission scenario work (similar to RCP) and benefit from the access to consistent global energy scenarios as well as an independent peer review process. Within GEA we have contributed to the development of alternative 'high' and 'low' variants of the current legislation scenarios. These are envisaged for use within EUCAARI as they share a number of key common assumptions and parameters to the RCP scenario but provide alternative views on possible future development of air pollution legislation.

The consolidated results of the above described inventories and scenarios are (GEA related will be at the end of the 2009) available for greenhouse gases and air pollutants, including BC and OC at a spatial resolution of 0.5 x0.5 degrees longitude-latitude.

Task 5.1 b) SOA modelling (MET.NO)

In cooperation with the Swedish SCARP project. several different box-model chemistries have been implemented, as a first step towards an updated SOA scheme for use in the EMEP model. Adapted versions of schemes by Kamens et al. (Andersson-Sköld and Simpson, 1999, Kamens et al., 2001, Li et al., 2007, Simpson et al., 2007), and a number of different so called volatility basis set (VBS) models (e.g., Pathak et al., 2007) have been implemented as well as a recently parameterised 2-parameter (αK) model by Svendby et al. (2008). Results from these different model schemes have been compared to SOA yield data from a large number of published smog chamber studies (Fig. 2 gives one example). The results from the comparison were presented at the general assembly of the European Geosciences Union (EGU) in 2009 (Bergström & Simpson, 2009). The parameterised VBS (and 2-product) models seem superior to the semi-explicit chemical models when compared to smog chamber data for the "dark" reactions studied so far, but studies in daytime conditions are needed for a proper evaluation.

For regional scale modelling, several versions of the VBS methods have also been implemented in the 3D-EMEP model and some first tests of these models (as well as the older Kam2X α-pinene model) have been performed on the European scale, comparing the results with detailed observational data from measurement campaigns (e.g., SORGA, Yttri et al., in preparation). The first results were presented at the general assembly of the

EGU in 2009 and in EMEP Status Report 4/2009 (Simpson et al., 2009a,b). The VBS based model results are very sensitive to assumptions regarding the (semi-)volatility of anthropogenic VOC-emissions and chemical aging of SOA. Further validation against larger observational data sets will be needed before firm conclusions can be drawn. The VBS models are computationally efficient and they are interesting candidates for 3D modelling.

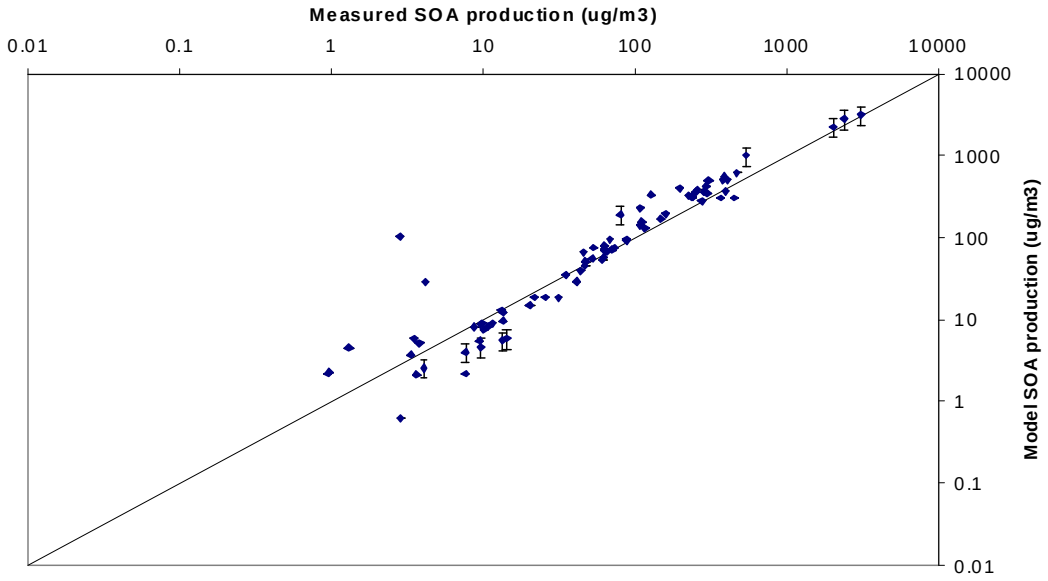

Figure 2. Comparison of results from one set of SOA yield parameters (Svendby et al., 2007) against a large number of smog-chamber data. Results from dark-reactions, ongoing work with alternative algorithms (from Bergström and Simpson, 2009)

Finally, a number of the lessons from the above studies, as well as a review of recent SOA literature survey were reported in two recent review articles, Hallquist et al. (2009) and Monks et al. (2009).

Task 5.1.2 Aerosols, ecosystem impact, air quality and climate (JRC/MPI/METO)

The results from two accurate hindcast simulations for the period 1980-2005 with the chemistry-aerosol-climate fully coupled model, ECHAM5-HAMMOZ. A reference simulation (Ref Run) with changing meteorology and emissions was compared to a second simulation (Fix Emi) where anthropogenic emissions were kept constant at the level of year 1980 (Fig. 3). The comparison between the two simulations permits us to analyze the chemical variability (trace gases and aerosols) due to changes in meteorology vs changes in emissions. Particular attention was given to four regions of the world, North America (NA), Europe (EU), East Asia (EA), and South Asia (SA) where the emissions significantly changed in the last decades. We focused on past changes of sulfate (SO4) as this species has been object of air quality policies in the recent past,

furthermore SO4 is one of the main components of aerosol fine particles that also contribute to climate change trough different processes. The sulfur emissions between 1980 and 2005 decreased by 50% and 35% over Europe and North America, respectively. The annual mean surface concentration of SO4 consequently decreased by 40% and 30%. In East Asia sulfur concentrations increased by 50% and the SO4 surface concentrations only by 20%. In South Asia an increase by a factor of 3 in sulfur concentrations produced only a 40% increase in SO4 concentrations. The relationships between sulfur emissions and SO4 surface concentrations are different in different parts of the world depending on different SO2 oxidation regimes. The variability in SO4 surface concentrations due to meteorology is small, up to 10% over Europe and North America, and 5% in the Asia.

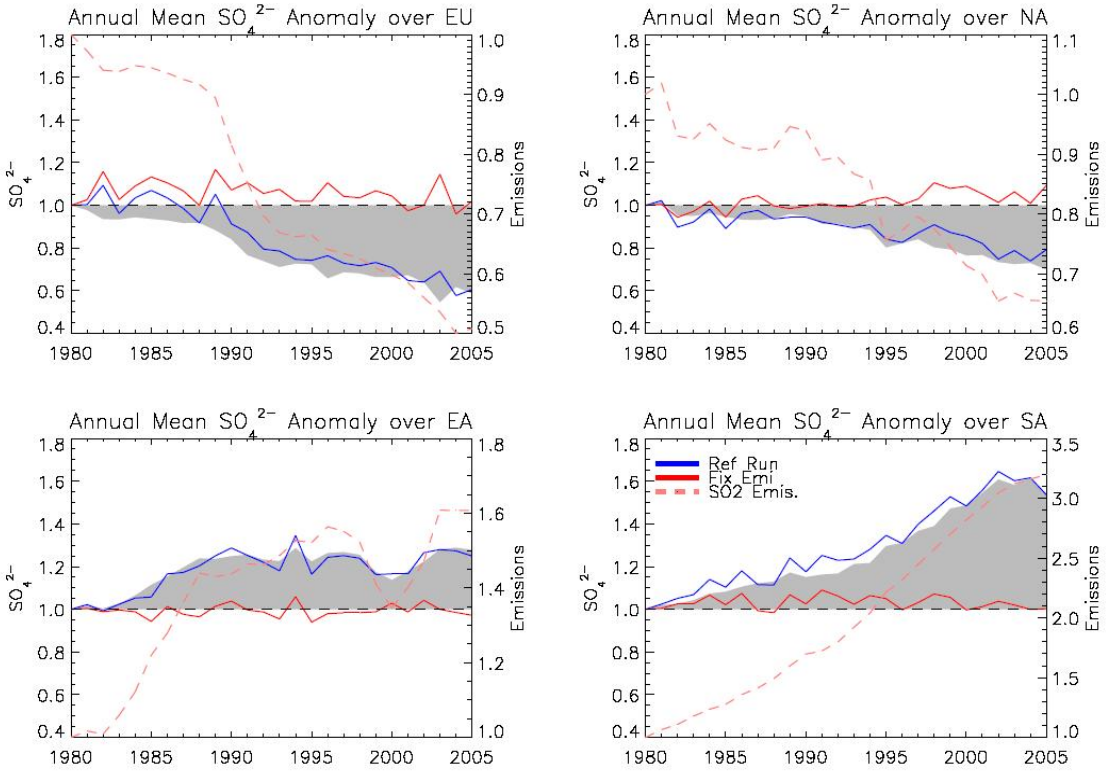

Figure 3: Trends of annual mean surface concentrations of SO4 and annual emissions between year 1980 and 2005 expressed as ratios over year 1980. On the left axis, the blue lines correspond to the the changes in SO4 surface concentrations in the reference simulation with changing meteorology and changing emissions, the red lines correspond to the changes in SO4 surface concentrations in the simulation with anthropogenic emissions fixed at the year 1980, and the gray areas are the difference between the Ref Run and Fix Emi. On the right axis the pink dashed lines corresponds to the changes in total sulfur emissions. Top left panel corresponds to averages over Europe (EU), top right panel over North America (NA), bottom left panel over East Asia (EA), and bottom right panel over South Asia (SA).

Increased aerosol loading and cloud cover decrease incoming shortwave radiation at the surface, thus reducing plant productivity. This effect is included in current climate models. At the same time however, the diffuse fraction of the incoming radiation is increased, which increases plant productivity. While this effect is well known to plant physiologists, climate models do not include that effect. METO performed a study in collaboration with the Centre of Ecology and Hydrology to investigate the effect of changes in diffuse radiation due to aerosols on plant productivity at the global scale and the global carbon sink. The study (see Fig. 4) finds that the diffuse fraction effect increased the land carbon sink by 24% over the period 1960-2000, more than compensating the impact of decreased incoming radiation (16% decrease in sink). Decreasing aerosol concentrations in the future because of air quality control is expected to reverse this effect and reduce the strength of the terrestrial carbon sink. This study is relevant for crop productivity as well which are impacted positively by large aerosol loadings.

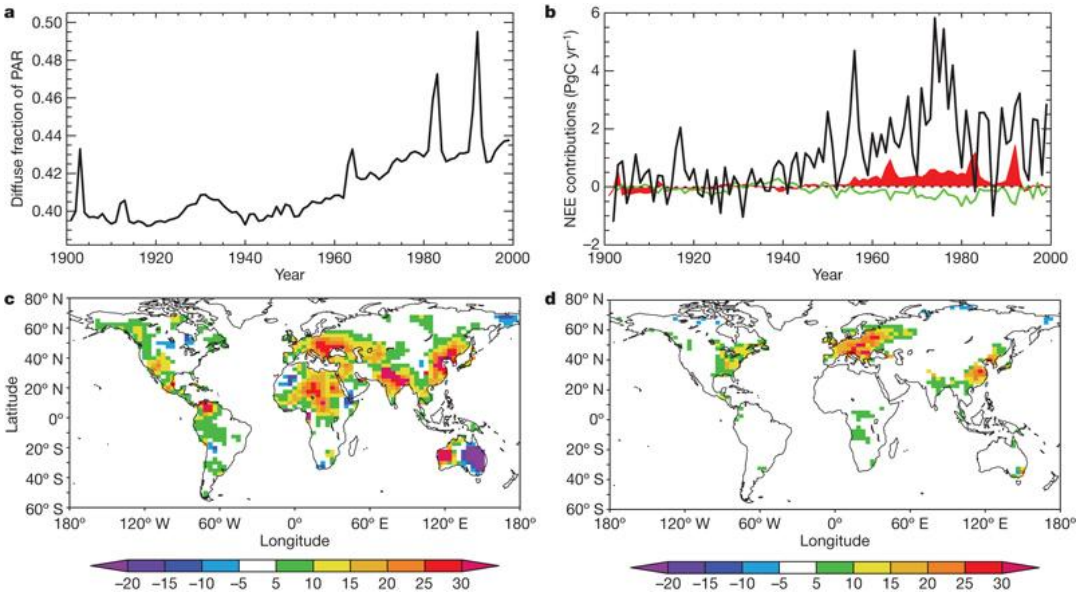

Figure: 4 a, Simulated global mean annual diffuse fraction of the Photosynthetically Available Radiation (PAR), based on aerosol optical depth from volcanic and anthropogenic sources, as simulated by HadGEM2-A, and observed Climate Research Unit cloudiness. b, Simulated contribution of diffuse fraction to simulated land Net Ecosystem Exchange (NEE, red), calculated as the difference between simulated NEE under varying diffuse fraction (black, total NEE) minus simulated NEE under constant diffuse fraction (not shown) and simulated contribution of the total PAR to simulated land NEE (green). c, Simulated percentage change (colour scale) in diffuse fraction between 1950 and 1980. d, Simulated change (colour scale, grams carbon per square metre per year) in diffuse-fraction contribution to land carbon accumulation between 1950 and 1980.

Integration and Synthesis

Emissions:

Consistent sets of global emission data for use in atmospheric models are being finalized. While the base year inventory and historical estimates consistency has received a lot of attention in the last years there are still important gaps and uncertainties. The recent work towards the IPPC AR5 initiated a process into which some EUCCAARI teams both contribute and benefit from. IIASA complemented the other datasets providing the GAINS model global estimates for several pollutants. The GAINS work is fully consistent within itself as estimation of all pollutants' emissions uses the same databases and interpretation of environmental policies. Finally, the same approach is used for projections. The results are used within the RCP and GEA processes and in collaboration with the MESSAGE group at IIASA allowed for development of spatially resolved (0.5 x 0.5 degrees long-lat) emission data sets including projections until 2030.

Although, the above scenarios represent an invaluable input for modeling community, its temporal resolution and lack of national data as well as detailed sectors will not allow for policy analysis in the mid-term and therefore supplementary information is needed, or involvement of some of the more detailed models that have been used to prepare the data for the process. This is especially relevant for regional analysis where additional information from EMEP, TNO and IIASA (GAINS) models will be used.

The work on documentation of the emission scenarios in the peer reviewed journals is under way.

Modelling:

Concerning SOA modelling, the main task now is to compare model results against the new data arising from the EUCAARI and EMEP field campaigns, as well as continued assessment against smog-chamber data. Only after models show satisfactory agreement with such data can we begin to give confident policy advice wit respect to SOA formation.

Concerning the global scale modelling, the remaining tasks for the next 12 months include estimating how changes in specific economic sectors and/or source regions that emit climate relevant gases and particles influence climate and air quality (ECHAM), and how potential changes of emissions up to 2030 influence health and ecosystem impacts on a scale covering Europe and beyond calculated (using the Chemistry Transport model TM5).

Publications and presentations with EUCAARI acknowledgements in 2009:

Bergström, R., and D. Simpson (2009), Evaluation of gas/particle SOA mechanisms for α-pinene for the EMEP model. Poster at the EGU annual meeting 2009, Wien. (abstract: http://meetingorganizer.copernicus.org/EGU2009/EGU2009-12114.pdf)

Hallquist, M.; Wenger, J. C.; Baltensperger, U.; Rudich, Y.; Simpson, D.; Claeys, M.; Dommen, J.; Donahue, N. M.; George, C.; Goldstein, A. H.; Hamilton, J. F.; Herrmann, H.; Hoffmann, T.; Iinuma, Y.; Jang, M.; Jenkin, M. E.; Jimenez, J. L.; Kiendler-Scharr, A.; Maenhaut, W.; McFiggans, G.; Mentel, T. F.; Monod, A.; Prevot, A. S. H.; Seinfeld, J. H.; Surratt, J. D.; Szmigielski, R. & Wildt, J. The formation, properties and impact of secondary organic aerosol: current and emerging issues *Atmos. Chem. and Physics*, 2009, 9, 5155-5236

Simpson, D., K.-E. Yttri, R. Bergström and H. van den Dernier (2009a), Source-apportionment and Model Evaluation: Experiences with the EMEP SOA model. Presentation at the EGU annual meeting 2009a, Wien. (abstract: http://meetingorganizer.copernicus.org/EGU2009/EGU2009-12423.pdf)

Simpson, D., K.-E. Yttri, R. Bergström and H. van den Dernier and S. Tsyro (2009b): Improvements in modeling Secondary Organic Aerosols: Experiments with the VBS Approach, EMEP Status Report 4/2009, pp58-63.

Szidat, S.; Ruff, M.; Wacker, L.; Synal, H.-A.; Hallquist, M.; Shannigrahi, A. S.; Yttri, K. E.; Dye, C. & Simpson, D., Fossil and non-fossil sources of organic carbon (OC) and elemental carbon (EC) in Göteborg, Sweden, *Atmos. Chem. and Physics*, 2009, 9, 1521-1535

Yttri, K.; Dye, C.; Braathen, O.-A.; Steinnes, E. & Simpson, D., Carbonaceous aerosols at urban influenced sites in Norway, *Atmos. Chem. and Physics*, 2009, 9, 2007-2020

Other References

Andersson-Sköld, Y. & Simpson, D., Secondary organic aerosol formation in Northern Europe: a model study, J. Geophys. Res., 2001, 106, 7357-7374

Kamens, R.M. & Jaoui, M. (2001), Modeling Aerosol Formation from a-Pinene + NOx in the Presence of Natural Sunlight Using Gas-Phase Kinetics and Gas-Particle Partitioning Theory, Environ. Sci. Technol., 35, 1394-1405.

Klimont, Z., J. Cofala, J. Xing, W. Wei, C. Zhang, S. Wang, J. Kejun, P. Bhandari, R. Mathur, P. Purohit, P. Rafaj, A. Chambers, M. Amann and J. Hao (2009). Projections of SO2, NOx, and carbonaceous aerosols emissions in Asia. Tellus 61B(4): 602-617.

Kloster, S.; Dentener, F.; Feichter, J.; Raes, F.; van Aardenne, J.; Roeckner, E.; Lohmann, U.; Stier, P. & Swart, R., Influence of future air pollution mitigation strategies on total aerosol radiative forcing, Atmos. Chem. and Physics, 2008, 8, 6405-6437

Li, Q.; Hu, D.; Leungsakul, S. & Kamens, R. M.
Large outdoor chamber experiments and computer simulations: (I) Secondary organic aerosol formation from the oxidation of a mixture of d-limonene and [alpha]-pinene Atmos. Environ., 2007, 41, 9341-9352

Mercado, L. M., N. Bellouin, S. Sitch, O. Boucher, C. Huntingford, and P. Cox, Changing contribution of diffuse radiation to the global land carbon sink, *Nature*, 458, 1014-1017, doi:10.1038/nature07949, 2009.

Monks, P., et al., Atmospheric Composition Change - Global and Regional Air Quality Atmos. Environ., 2009, 43, 5268-5350

Pathak, R. K.; Presto, A. A.; Lane, T. E.; Stanier, C. O.; Donahue, N. M. & Pandis, S. N. Ozonolysis of alpha-pinene: parameterization of secondary organic aerosol mass fraction Atmos. Chem. and Physics, 2007, 7, 3811-3821

Richter, A., J. P. Burrows, H. Nuss, C. Granier and U. Niemeier (2005). Increase in tropospheric nitrogen dioxide over China observed from space. Nature 437(7055): 129-132.

Richter, A., A. Heckel, M. Lee, M. Vrekoussis, F. Wittrock, A. Rozanov and J. P. Burrows (2007). Tropospheric Composition Change observed from Space. 2nd ACCENT Symposium. Urbino, Italy.

Svendby, T.; Lazaridis, M. & Tørseth, K., Temperature dependent secondary organic aerosol formation from terpenes and aromatics, J. Atmos. Chem., 2007

Zhang, Q., D. G. Streets, K. He, Y. Wang, A. Richter, J. P. Burrows, I. Uno, C. J. Jang, D. Chen, Z. Yao and Y. Lei (2007). NOx emission trends for China, 1995–2004: The view from the ground and the view from space. J. Geophys. Res. 112(D22): 1-18.

EUCAARI database and atmospheric transport modelling tools WP5.2

A.M FJAERAA[1], A. STOHL[1] and J.F. BURKHART[1]

[1]Norwegian Institute for Air Research,
PB. 100, 2027 Kjeller, Norway

Keywords: Database, Aerosols, FLEXPART

INTRODUCTION

An integrated project like EUCAARI requires a database that integrates all data collected within the project as well as relevant data from other sources. It furthermore requires that the data are made accessible to the project partners via a common platform. Interpretation of transport processes and identification of source regions was, until now, based mostly on trajectories calculated backwards from the locations measurements were made. This is a rather qualitative approach and can be very misleading especially for surface sites where boundary-layer turbulence influences the arriving air. For EUCAARI, a state-of-the-art Langrangian particle dispersion model is run backward in time to derive emission sensitivities and potential source contributions.

METHODS

The database is a password protected system, and access to data from specific projects or programmes is guaranteed upon submission of signed protocols that regulate the rights to use and distribute data. One user may have access to data from one or several projects (e.g. EUSAAR and/or EUCAARI). The EMEP database 'EBAS' has dynamic web pages that allow searching for aerosol data from any instrument or location. The web interface furthermore provides online visualization of data. All data available (incl. aircraft data and data from other platforms) are stored at a common area located at the NADIR data center at NILU, on the machine zardoz.nilu.no, in subfolders of the parent directory /viper/nadir/projects/other/eucaari/. All EUSAAR and EMEP aerosol data provided for EUCAARI are, in addition, provided to the EUCAARI partners via the EBAS web interface http://ebas.nilu.no The Langrangian particle dispersion model FELXPART are be run backwards in time for 20 days from all EUCAARI measurement sites, including mobile platforms. The version used for EUCAARI uses the European Centre for Medium-Range Weather Forecasts (ECMWF) model output. FLEXPART, using 40.000 particles per backward run, produces a four-dimensional (space and time) emission sensitivity function and potential source contributions for selected aerosol species (e.g., black carbon), precursors (e.g., sulphur dioxide) and tracers (e.g., carbon monoxide). The calculations are based on the assumption of transport alone, i.e., secondary aerosol formation or removal processes are not considered. The source contributions will be summarized in monthly "age spectra" time series giving a quick overview of the variation of various transport tracers, including information on their age.

CONCLUSIONS

The data directory on zardoz.nilu.no currently contain aerosol data from 20 EUSAAR stations, a large number of data from IMPACT (i.e. data from cnrs, imau, juelich, knmi, lamp, meteofrance, safire, tno, tropos, tudelft) and LONGREX (i.e. bae-146, falcon and nais). Plots of all the FLEXTRA modelled results are made accessible via the internt, through a web based interface providing various transport model products for every EUCAARI measurement.

Figure 1. The database web interface; dynamic web pages that allows searching for aerosol data from any ground based instrument or location. The web pages also provide on-line visualisation of time series of data for station comparisition.

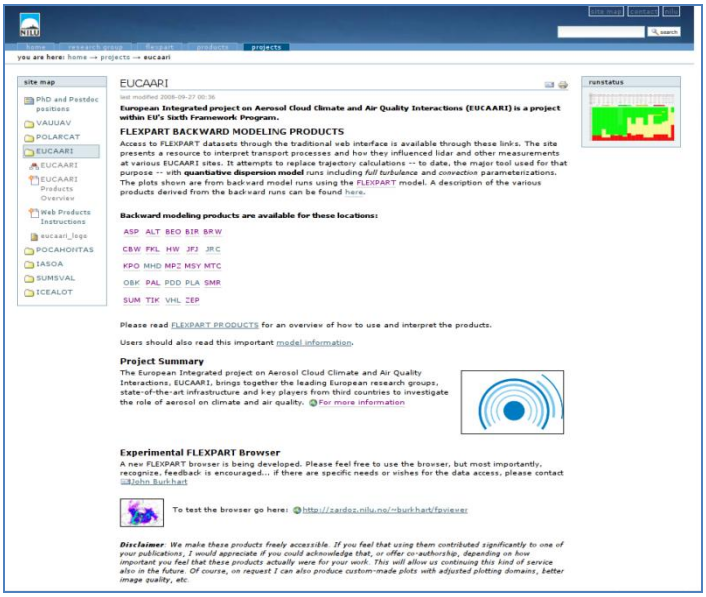

Figure 2. NILU's EUCAARI Project launch pad portal providing links to the FLEXPART model products and other relevant resources. This web portal serves as a starting page for individuals associated with EUCAARI looking for FLEXPART transport product resources.

.

ACKNOWLEDGEMENTS

The EBAS web interface, that provides some of the EUCAARI data, and is a common web portal for all EMEP measurements hosted at the EMEP-CCC (Chemical Coordinating Centre) is developed and maintained at NILU through the EU-funded I3 project EUSAAR.

EUCAARI platform - models

Michael Schulz on behalf of WP53

[1]Laboratoire des Sciences du Climat et de l'Environnement, Gif-sur-Yvette, France

Keywords: Model, evaluation, global, regional, air quality, climate

INTRODUCTION

The aim of the EUCAARI 5.3 work package is to significantly improve the evaluation process of regional and global aerosol models and to document modeling progress made during EUCAARI. The evaluation will allow a quantification of actual uncertainties in our prediction of aerosol impact on climate and air quality. This will be achieved by evaluating not only the end product, but also important sub-steps in modeling. In this work package benchmark test tools shall be developed and applied, which allow analyzing model biases with respect to processes that govern aerosol concentrations and physico-chemical properties of the aerosol. The work package aims at developing a platform, which helps constructing successful modeling studies within EUCAARI and outside of the consortium. A subgoal of the work package is to achieve a link to the international AeroCom model intercomparison initiative (http://nansen.ipsl.jussieu.fr/AEROCOM).

ONGOING AND FUTURE WORK

Task 5.3.1 "Assessment of observational data base"

Data assessment involves that useful existing observational data are applied for model evaluation in cooperation with the scientists which have been preparing these data. This process is dependent on the type of data in question. In practical terms we call here the 'observational data base' those data which are and will be available for common model evaluation within EUCAARI in this work package. This means that they can be used directly with the AeroCom tools on the AeroCom data server at the LSCE. To this date available data comprise sun photometer data from Aeronet, Skynet and GAW (1996-2007); satellite AOD and fine fraction of AOD from MODIS/CERES, MISR and POLDER/PARASOL (1996-2006); and Earlinet lidar data (2000+2001). Further work has been done recently to integrate a large extract from the EBAS database, which contains EUCAARI and other database data. The major task initially was to understand the database in order to obtain all station output from the stored datasets. Wet deposition of sulfate for example requires to combine the right instruments at a given station for precipitation amount and species concentration. The work has been successful and a much larger datasets from N-America, Europe and East Asia is now used to benchmark the models, which have been submitted to the AeroCom dataserver. (See the Aerocom surfobs web interface for the actual state http://nansen.ipsl.jussieu.fr/AEROCOM/surfobs.html).

Task 5.3.2 "Development of pilot benchmark tests".

The benchmark test which had been developed in a pilot version on "Clear sky and all sky forcing", has been augmented considerably over the year. Four reference data sets have been assembled now which are intended to serve as a benchmarks to judge new model results with respect to the direct radiative effect. The first reference are median fields of AeroCom Modeling (*AeroCom Median Model*), the second reference is defined by results of off-line radiative transfer simulations with quality statistics of aerosol column properties by ground-based (sky-photometer) monitoring networks of AERONET and SKYnet (*Aeronet based gridded Aerosol Climatology*), the third comprises of the corresponding aerosol optical

depth measurements, which together with the radiative forcing estimate give a forcing efficiency, which is partly independent from the absolute values of AOD and forcing. The fourth dataset corresponds to the observational based clear sky forcing estimate derived from MODIS and CERES measurements by the Hadley Center (courtesy Nicolas Bellouin for the netcdf files).

Figure 1 shows an example of the resulting clear sky forcing from Aeronet, the Hadley Center for an example station, Hamburg, as compared to the new LMDzT-INCA simulation. The forcing curves do not resemble the aerosol optical depth curves and as such are a new test for the models. At first glance the comparison reveals considerable differences both between the two observational based estimates (Bellouin and Aeronet) and the model and Aeronet derived clear-sky forcing.

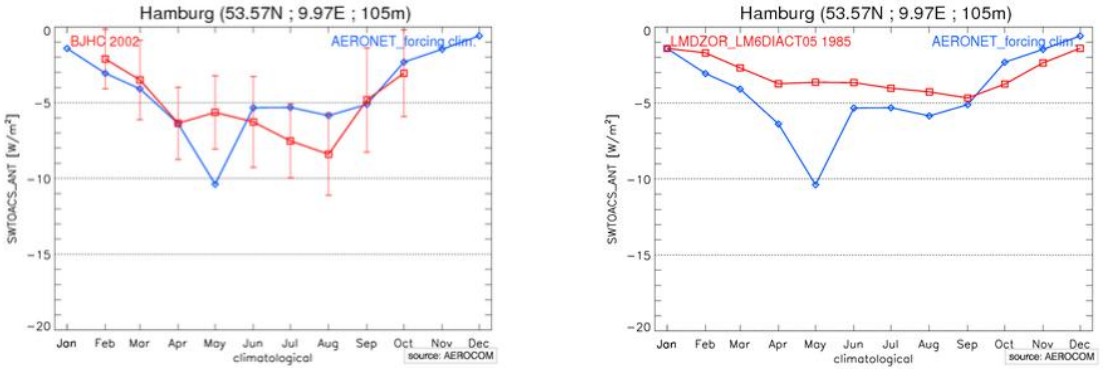

Figure 1: Comparison of the clear sky forcing estimate from MODIS/CERES, (BJHC, data from Nicolas Bellouin) and the new LMDzT-INCA version (LMDZOR_LM6DIACT05, climatological run) against an independent estimate from S. Kinne, based on sky-mode derived Aeronet optical parameters and MODIS surface albedo.

Task 5.3.3 Evaluation, Documentation and Analysis of model experiments

A majr part of the EUCAARI global model experiments has been defined under the framework of Aerocom for better international comparability. In order to better document aerosol size in AeroCom phase II we propose storing the complete output of all aerosol tracer mixing ratios at selected super sites with a higher frequency (hourly, at a set of predefined super site stations as well as daily in the form of a vertical profile for the period 2006-2008). In addition, we propose storing a monthly 3D distribution of all aerosol tracer mixing ratios for the control year 2006. Together with a description of the size class or mode information it should be possible to pursue more complete comparisons of the actual size distributions in the different models. A representative global list of 50 super sites has been selected through consultation with the GAW aerosol committee. By limiting the model output to those sites where intensive aerosol observations exist and to 3D distributions with only monthly resolution we believe to have found a promising compromise between detail and data storage limitations.

The complex dynamics controlling aerosol distributions necessitate further “switch-off-a-process” experiments to differentiate between the role of coagulation, nucleation and condensation for the aerosol number budget in a global atmosphere. Such experiments have therefore been added in cooperation with Graham Mann, University of Leeds, to the newest planned AeroCom experiments. It is hoped that these experiments better elucidate how much detailed microphysics is needed in aerosol-climate models.

Aerosol vertical distributions observed from aircraft, from satellite-based lidar (i.e. CALIOP) or ground-based lidar (*Ferrare et al., 2006*) have the potential to constrain models with respect to aerosol residence time. For example, low black carbon concentrations observed with the SP2 instrument in high altitude aircraft have challenged our model

understanding of vertical mixing (*Schwarz et al, 2007, Koch et al. 2009*), with many models being too diffusive in the upper troposphere or not having efficient enough wet removal of black carbon. Under Phase II, AeroCom is taking advantage of these additional diagnostics. For the years 2006-2008 models are requested to provide daily 3D aerosol extinction as well as 3D monthly wet removal rates, allowing us to better understand the full vertical mass budget. New observations are also available for secondary aerosols such as nitrate and organics. Distinguishing between primary and secondary organic aerosols requires the provision of adequate detail. Thus, model groups are requested to output full mass mixing ratio documentation of all aerosol tracers, as described in the microphysics section of the Phase II AeroCom runs. This will also help us to understand the aerosol mass budget in the models.

A better constraint on aerosol residence times would have direct consequences for the uncertainty estimate of aerosol forcing and regional climate effects. It would allow better long-range transport estimates and improve chances of verifying emission inventories with inversion techniques.

In addition to uncertainties in aerosol distributions and properties, representation of cloudy sky direct radiative forcing by aerosols may be responsible for a significant portion of model diversity in aerosol radiative forcing. Cloud field documentation will therefore be emphasized in AeroCom's phase II. However, because of the co-variance of clouds and aerosols it is suggested to store explicitly the cloudy sky radiative fluxes in control and pre-industrial simulations. A second pathway will be the 3D prescription of the aerosol optical properties in a specific 1-year experiment, which would be dedicated to understanding the role of the host model environment for aerosol perturbed radiative fluxes.

Finally, it should be noted that aerosol radiative forcing has been evolving, due to both anthropogenic aerosol concentration trends and variations in the natural aerosol background. Dimming and brightening, regional aerosol effects and emission changes in different regions of the world should be evident in historic aerosol simulations. 20-25 year "hindcast" experiment are thus planned to investigate recent evolution of aerosols. These aerosol runs will be compared against observational data sets, providing a test of model skill. Complementing the Hindcast runs will be a set of runs simulating future scenarios which will provide "best-guess" aerosol (and other trace species') distributions, using emissions which are consistent with those used in the climate model runs. These "Scenarios" runs will also allow better understanding of sources of sensitivity and uncertainty in the simulation of climatically important short-lived species. Unlike the long-live greenhouse gases, climate is expected to respond rapidly to aerosol perturbations and it is important that we understand how changes in concentrations will feed back with climate. The CMIP5[1] time-slice experiments are foreseen to obtain a quasi forcing, which includes all fast feedbacks of the climate system to aerosols. It is hoped that model versions employed there can be traced back to the more complete documentation within AeroCom.

The AeroCom phase II model experiments are proposed to be submitted by end of 2009. Based on a reference and control simulation for the year 2006 it is suggested to provide additional simulations with new diagnostics. Modelers are asked to choose experiments according to their capabilities, resources and interests. New aspects of these runs have been explained above and are summarized below at a glance. Details of the diagnostics required can be found via the AeroCom website (http://nansen.ipsl.jussieu.fr/AEROCOM/protocol.html).

A difficulty in the interpretation of the climate model runs for the last IPCC report has been the incomplete or altogether missing documentation of the aerosol representation in a given climate model. Adding to this, the model versions used to compute the aerosol radiative forcing (e.g. as reported in *Schulz et al., 2006*) often were different from the model version used to simulate transient climate evolution. In preparation for the next Assessment Report, a small and thus manageable subset of aerosol diagnostics from the AeroCom set is being submitted to the CMIP protocol for inclusion in the next IPCC climate runs. Together with a dedicated experiment to document the fast response due to sulfate (CMIP protocol experiment 6.4), perhaps done also with a total aerosol perturbation, the ability to interpret the role of aerosols in the climate runs will significantly improve for the next IPCC assessment. However, understanding model diversity with respect to the aerosol effect will also require that individual groups link in-house the climate model version to a better documented AeroCom aerosol model run.

AeroCom Infrastructure

As mentioned above the cooperation within AeroCom builds on yearly scientific workshops to report and discuss joint analysis, recent model developments and new observational datasets. The 8th AeroCom workshop was held 5-7 October 2009 in New Jersey, by invitation of the University of Princeton and organized by Paul Ginoux and

[1] CMIP = "Coupled Model Intercomparison Project", for global coupled ocean-atmosphere general circulation models (http://www-pcmdi.llnl.gov/projects/cmip/)

colleagues, with special emphasis on contributions to the next IPCC report. The 2010 AeroCom workshop will probably be hosted by Oxford University, U.K., Philip Stier. An AeroCom email list is updated and used for distribution of relevant news, and interested parties can be added to the list via the AeroCom web page (http://nansen.ipsl.jussieu.fr/AEROCOM/).
Loosely organized working groups within AeroCom foster joint analysis. Group leaders are as follows:

- Microphysics: Graham Mann (Univ of Leeds) & Xiahong Liu (PNL)
- Direct forcing: Philip Stier (Univ of Oxford), Gunnar Myhre (CICERO) & Cynthia Randles (NASA Goddard)
- Indirect forcing: Johannes Quaas (MPI-M)
- Hindcast simulations: Michael Schulz (LSCE) and Mian Chin (NASA-Goddard)
- Organics: Kostas Tsigaridis (GISS) and Maria Kanakidou (Univ of Crete)
- Observational Data: Stefan Kinne (MPI-H)
- Dust: Paul Ginoux (Univ. of Princeton)
- Black Carbon: Dorothy Koch (GISS)
- Emissions: Thomas Diehl (NASA-Goddard) & Tami Bond (Univ. of Illinois)

A database of currently 5 TBytes of model output is kept at the LSCE in Saclay/France and contains all previous AeroCom and EUCAARI experiments. The LSCE database contains original AeroCom data submissions and reformatted, standardized netCDF data. Basic submissions have been secured by a copy on a second data server. A computing server is accessible from the outside for expert users to work directly with the data. At this point access is based on a “gentleman’s agreement”: users are requested to simply declare their analysis project, contact model and data authors before publication and report back during the AeroCom workshops. As described earlier, model output is visible directly via the public AeroCom web interface. Maps, statistics, histograms, scatter plots and simple scores are produced with an automated idl tool developed at LSCE.

REFERENCES

Ferrare, R.A., E.V. Browell, J.W. Hair, S. Ismail, D.D. Turner, M. Clayton, C.F. Butler, V.G. Brackett, M.A. Fenn, A. Notari, S.A. Kooi, M. Chin, S. Guibert, M. Schulz, C. Chuang, M. Krol, S.E. Bauer, X. Liu, G. Myhre, X. Seland, D. Fillmore, S. Ghan, S. Gong, P. Ginoux, and T. Takemura, The Vertical Distribution of Aerosols: Lidar Measurements vs. Model Simulations, in 23rd International Laser Radar Conference, 24-28 July 2006, edited by N.S. Chikao Nagasawa, Nara, Japan, 2006.

Schwarz, J. P., R. S. Gao, D. W. Fahey, D. S. Thomson, L. A. Watts, J. C. Wilson, J. M. Reeves, D. G. Baumgardner, G. L. Kok, S. H. Chung, M. Schulz, J. Hendricks, A. Lauer, B. Kdrcher, J. G. Slowik, K. H. Rosenlof, T. L. Thompson, A. O. Langford, M. Loewenstein, and K. C. Aikin. 2006. Single-particle measurements of midlatitude black carbon and light-scattering aerosols from the boundary layer to the lower stratosphere. *J. Geophys. Res*. **111**, D16207, doi:16210.11029/12006JD007076, 2006.

Schulz, M., C. Textor, S. Kinne, Y. Balkanski, S. Bauer, T. Berntsen, T. Berglen, O. Boucher, F. Dentener, A. Grini, S. Guibert, T. Iversen, D. Koch, A. Kirkeveg, X. Liu, V. Montanaro, G. Myhre, J. Penner, G. Pitari, S. Reddy, X. Seland, P. Stier, and T. Takemura. 2006. Radiative forcing by aerosols as derived from the AeroCom present-day and pre-industrial simulations. *Atmos Chem Phys*, **6**, 5225-5246 .

Quaas, J., Ming, Y., Menon, S., Takemura, T., Wang, M., Penner, J. E., Gettelman, A., Lohmann, U., Bellouin, N., Boucher, O., Sayer, A. M., Thomas, G. E., McComiskey, A., Feingold, G., Hoose, C., Kristjansson, J. E., Liu, X., Balkanski, Y., Donner, L. J., Ginoux, P. A., Stier, P., Feichter, J., Sednev, I., Bauer, S. E., Koch, D., Grainger, R. G., Kirkevåg, A., Iversen, T., Seland, Ø., Easter, R., Ghan, S. J., Rasch, P. J., Morrison, H., Lamarque, J.-F., Iacono, M. J., Kinne, S., and Schulz, M.: Aerosol indirect effects - general circulation model intercomparison and evaluation with satellite data, Atmos. Chem. Phys. Discuss., 9, 12731-12779, 2009.

D. Koch, M. Schulz, S. Kinne, T. C. Bond, Y. Balkanski, S. Bauer, T. Berntsen, O. Boucher, M. Chin, A. Clarke, N. De Luca, F. Dentener, T. Diehl, O. Dubovik, R. Easter, D. W. Fahey, J. Feichter, D. Fillmore, S. Freitag, S. Ghan, P. Ginoux, S. Gong, L. Horowitz, T. Iversen, A. Kirkevåg, Z. Klimont, Y. Kondo, M. Krol, X. Liu, C. McNaughton, R. Miller, V. Montanaro, N. Moteki, G. Myhre, J. E. Penner, Ja. Perlwitz, G. Pitari, S. Reddy, L. Sahu, H. Sakamoto, G. Schuster, J. P. Schwarz, Ø. Seland, J. R. Spackman, P. Stier, N. Takegawa, T. Takemura, C. Textor, J. A. van Aardenne, and Y. Zhao,Evaluation of black carbon estimations in global aerosol models Atmos. Chem. Phys. Discuss., 9, 15769-15825, 2009.

Schulz, M., Chin, M., Kinne S., The Aerosol Model Comparison Project, AeroCom, Phase II: Clearing Up Diversity, IGAC Newsletter, No 41, May 2009

AEROSOL CLASSIFICATION BY AIRBORNE IN-SITU AND HIGH SPECTRAL RESOLUTION LIDAR MEASUREMENTS DURING EUCAARI

F. ABICHT[1], M. ESSELBORN[1], T. HAMBURGER[1], B. Y. LIU[1, 2], A. MINIKIN[1], and A. PETZOLD[1]

[1]Institut für Physik der Atmosphäre, DLR, Oberpfaffenhofen, 82234 Wessling, Germany.

[2]Ocean Remote Sensing Institute, Ocean University of China (OUC), Qingdao, 266003, China.

Keywords: optical properties, extinction, optical depth, lidar, lidar ratio.

INTRODUCTION

In the framework of the EUCAARI-LONGREX (European integrated project on Aerosol Cloud Climate and Air Quality Interactions - LONG Range EXperiment) flight campaign high spectral resolution lidar (HSRL; Esselborn et al., 2008) measurements were performed onboard DLR Falcon 20 over several regions of Europe. Based on the HSRL measurements aerosol-specific quantities at λ = 532 nm were deduced including the aerosol backscatter coefficient, aerosol extinction coefficient, aerosol optical depth, the lidar ratio and aerosol depolarisation ratio.

METHODS

Simultaneous to the HSRL measurements, airborne in-situ aerosol measurements were performed, including aerosol number size distribution, aerosol absorption, and aerosol volatility analyses. For selected aerosol layers, in situ data were used to deduce characteristic aerosol microphysical properties and link them to HSRL aerosol properties like lidar ratio and depolarisation.

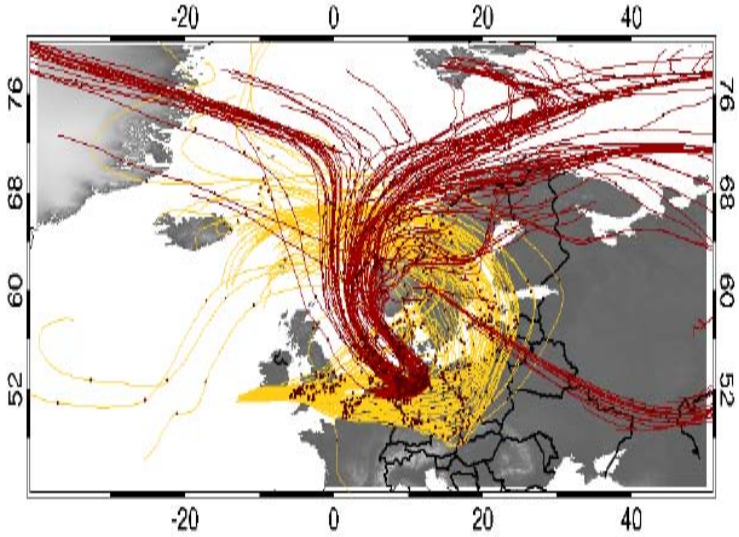

Figure 1. Air mass back trajectories for two key days during EUCAARI-LONGREX: 14 May 2008 (yellow) and 21 May 2008 (brown).

Figure 1 shows examples of back-trajectories for air mass which were probed in-situ and by HSRL: On 14 May 2008 air masses were probed which circulated for several days over Central Europe during a stagnant high pressure system situation, collecting anthropogenic pollution from various source regions. On 21 May, air masses were probed which moved into Central Europe across the North Sea, being considered as relatively clean compared to the previous weather situation.

CONCLUSIONS

Aerosol properties accessible by HSRL cluster in characteristic patterns for different aerosol classes as shown in Figure 2. Aerosol in-situ microphysical data will be used to further investigate the HSRL aerosol classification capabilities and limitations. The favourable synoptic situation during the first part (06 – 14 May) of EUCAARI-LONGREX with an almost stationary anticyclone over Europe enables us to study aerosol transformation and aging over an anthropogenic source region from in-situ observations collocated with active remote sensing studies of the same aerosol.
The presented results serve as an important first step towards the assessment of future spaceborne active remote sensing instruments for the large-scale monitoring of the tropospheric aerosol.

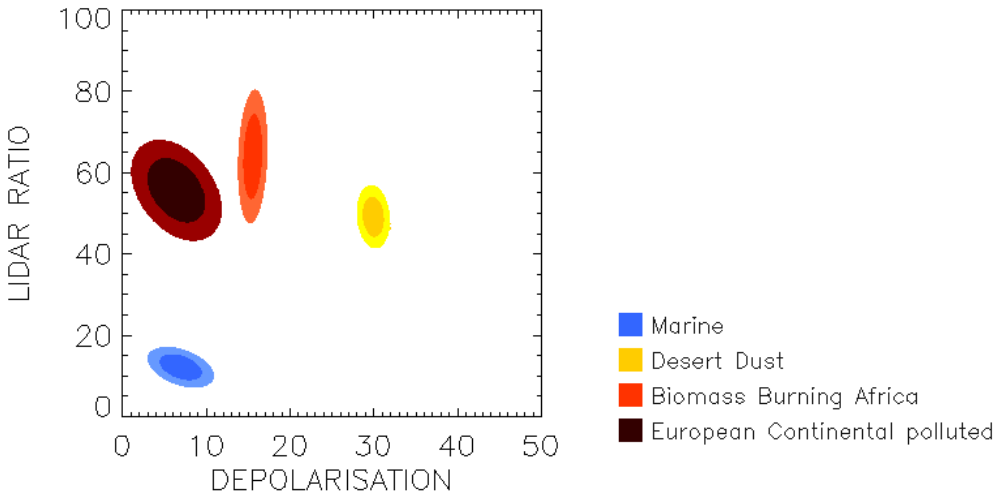

Figure 1. Lidar properties for different aerosol types measured during EUCAARI-LONGREX and SAMUM (desert dust, biomass burning).

ACKNOWLEDGEMENTS

This work has been partly funded by EUCAARI (European Integrated Project on Aerosol Cloud Climate and Air Quality Interactions) No 036833-2.

REFERENCES

Esselborn, M., M. Wirth, A. Fix, M. Tesche, and G. Ehret (2008). Airborne high spectral resolution lidar for measuring aerosol extinction and backscatter coefficients, *Applied Optics*, 47, 346-358.

LIPOPHILIC ORGANIC COMPOUNDS IN AEROSOLS FROM SELECTED EUCAARI SITES

C.A. Alves[1], A. Vicente[1], M. Evtyugina[1], C. Pio[1], A. Hoffer[2], G. Kiss[2], S. Decesari[3], G. Spindler[4], R. Hillamo[5] and E. Swietlicki[6]

[1]Centre for Environmental and Marine Studies (CESAM), University of Aveiro, 3810-193 Aveiro, Portugal

[2]Air Chemistry Group, Hungarian Academy of Sciences, University of Pannonia, 8200 Veszprém, Hungary

[3]Istituto di Scienze dell'Atmosfera e del Clima - CNR, Via P. Gobetti, 101, Bologna 40129, Italy

[4]Leibniz-Institut für Troposphärenforschung e.V., 04318 Leipzig, Germany

[5]Air Quality Research, Finnish Meteorological Institute, Erik Palmenin Aukio 1, FIN-00560 Helsinki, Finland

[6]Department of Physics, Lund University, S-221 00 Lund, Sweden

Keywords: AEROSOL, PAH, BaPE, RURAL SITES, SOURCE RECONCILIATION.

INTRODUCTION

Aerosol particles are ubiquitous, but a highly variable component, in the troposphere. It is now recognised that atmospheric aerosols play a far more complex role in the climate system than previously thought (Ming and Ramaswamy, 2009). Exposure to fine-particulate air pollution has also been associated with increased morbidity and mortality (Pope *et al*., 2009).

Although organic compounds are generally the most important constituents of atmospheric aerosols, their inventory is far from being comprehensive. Hydrocarbons constitute an important group among them. Natural aliphatic and aromatic hydrocarbons are produced by continental and marine plants, with typical components or distributions revealing their origin. Anthropogenic hydrocarbons are widely spread, deriving from the combustion of fuels, like crude or refined petroleum derivatives, coal, wood, etc. Aliphatic hydrocarbons are present in all atmospheric aerosol types regardless of whether they are from urban, rural or marine environments (Alves, 2008). In spite of representing a small fraction of the total organic matter in aerosols, they are regarded as good candidates for source apportionment studies (Gelencsér *et al*., 1998). Polycyclic aromatic hydrocarbons (PAH) derive almost exclusively from incomplete combustion processes, and are also useful organic indicator species, especially for vehicular emissions (Shad *et al*., 2005; Zielinka *et al*., 2004; Zou and Atkinson, 2003). Some of them are among the strongest recognised carcinogens (Armstrong *et al*., 2004; Fang *et al*., 2002; Lin *et al*., 2008; Gerde *et al*., 2001). Atmospheric PAH are partitioned between the gaseous and the particulate phases, but the carcinogenic 5- and 6- ring constituents are chiefly linked to particles (Chirico *et al*., 2007; Tasdemir and Esen, 2007). The European Directive 2008/50/EC stipulates several air pollutants to be taken into consideration in the assessment and management of ambient air quality, defining a target concentration for benzo(a)pyrene, which is used as a marker substance for PAH generally.

The main objectives are to characterise and trace the origin of aliphatic and aromatic hydrocarbons, as well of some carbonyl compounds, in atmospheric aerosol particles from 4 non-urban sites throughout Europe and to reveal the relative share of biogenic *versus* anthropogenic sources for these compounds.

METHODS

One of the sampling sites was located in Hyytiälä (61º51' N, 24º17' E, 181 m above sea level), at the Finnish Station for Measuring Forest Ecosystem–Atmosphere Relations (SMEAR II). The terrain around

the station is representative of the boreal coniferous forest. The daily sampling program, in 2007, occurred from April 5th to 15th under "clean" atmospheric conditions. In the period 15-17 of April, the sampling site was under the influence of long range transport of atmospheric pollution. High volume equipment running at 0.85 m^3 min^{-1} was used to collect $PM_{2.5}$ samples. The Italian sampling site was located in San Pietro Capofiume (44º39' 17'' N, 11º 37' 25'' E, 11 m above sea level), in a flat rural area in the north-eastern part of the Po Valley. The sampling campaign took place between April 8th and 14th, 2008. A high volume (300 L min^{-1}) dichotomous sampler was employed to collect nocturnal and diurnal samples. The submicron fraction (PM_1) was used for the organic characterisation. Aerosols from K-Puszta (46º 58'N, 19º 35'E) were collected at the station run by the Hungarian Meteorological Service and the University of Veszprém, as part of the EMEP network. The site is in the middle of the Hungarian Plain, 60 km southeast from Budapest (1.9 million inhabitants). The sampling site is surrounded by forests (62% coniferous trees) interspersed with clearings. Aerosol was sampled at a flow rate of 0.6 m^3 min^{-1} (Sierra-Andersen impactor) on quartz fiber filters (Whatman QM-A) of 20×25 cm size. The sampler was located at 7 m above ground and was configured to remove particles larger than 2.5 µm. Daily sampling was carried out from May 5th to June 4th and from July 1st and July 12th, in 2008. The German station was situated near the village of Melpitz (51°32' N, 12°54' E, 87 m above sea level). The station was located on a flat meadow surrounded by agricultural land. Digitel PM_{10} and $PM_{2.5}$ samplers operating at 30 m^3 h^{-1} have been used from May 1st to May 3th, 2008, for daily aerosol collection.

Pieces of the filters were extracted by refluxing dichloromethane for 24 h. The total organic extract was vacuum concentrated and dried under a gentle ultra pure nitrogen stream. Aliphatic compounds, PAH and carbonyls were separated from this total extract by flash chromatography with silica gel (230-400 mesh, 60 Å Merck Grade 9385) using, respectively, 15 mL of *n*-hexane, 15 mL of toluene–*n*-hexane (5.6:9.4) and *n*-hexane-dichloromethane (7.5:7.5) (Merck SupraSolv®). After each elution, the different fractions were vacuum concentrated (25-30ºC under reduced pressure) and evaporated under a nitrogen stream. Hydrocarbons were analysed by gas chromatography–mass spectrometry (GC-MS). The quadrupolar analytical equipment was from Hewlett-Packard (GC 9890 and MS 7883), operating with a TRB-5MS 60 m × 0.25 mm × 0.25 µm column. Data were acquired in the electron impact (EI) mode (70 eV). The oven temperature program was as follows: 60ºC (1 min); 60-150ºC (10ºC min^{-1}), 150-290ºC (5ºC min^{-1}), 290ºC (30 min) and using helium as carrier gas at 1 mL min^{-1}. Calibration for GC-MS analysis was based on a total of about 90 standards (Sigma-Aldrich, TSI and Chiron) in five different concentration levels with relative response factors determined individually to the majority of compounds. For those with no authentic standards available, relative response factors were calculated as an average of the relative response factors from the overall homologous series or from compounds of similar chemical structure and retention time. Both aliphatic and carbonyl standards and samples were co-injected with chlorohexadecane (Merck 802339) as an internal standard. In the case of PAHs, a mixture of deuterated internal standards was used: acenaphthene-D10, chrysene-D12, naphtalene-D8, perylene-D12, phenanthrene-D10, 1,4-dichlorobenzene-D4 (Sigma-Aldrich). Compound identification was based on comparison of resulting mass spectra with the Wiley spectral library, co-injection with authentic standards and analysis of fragmentation patterns. A detailed description of the analytical methodology, including recovery efficiency tests for several compounds, can be found in Alves and Pio (2005) and Oliveira et al. (2007). This methodology was previously tested in our laboratory (Alves, 2001; Carvalho, 2003) and elsewhere (Gogou et al., 1998).

RESULTS AND DISCUSSION

The aliphatic fraction of particulate matter comprised *n*-alkanes (Figure 1), *n*-alkenes with a carbon chain length between C_{13} and C_{23}, the unresolved complex mixture of cyclic branched and unsaturated hydrocarbons and acyclic isoprenoids (pristane and phytane). *n*-Alkanes represented the most abundant group of compounds. In general, the *n*-alkanes from C_{19} to C_{32} from fossil fuel are dominated by the C_{20} and C_{25} homologues for gasoline vehicles and by the C_{20} for heavy (Rogge *et al.*, 1993) and medium (Schauer *et al.*, 1999) duty diesel trucks. Unburned heating oil is another source for *n*-alkanes with

carbon number between 14 and 25, presenting maximum concentrations for the C_{19}-C_{25} homologues (Rogge *et al*., 1997). While the *n*-alkanes with a carbon number around C_{20} mostly derive from unburned fuel (Brandenberger et al., 2005), the homologues around C_{25} are largely originated from lubricating oil (Sakurai *et al*., 2003). *n*-Alkanes from these anthropogenic sources show no significant odd or even carbon number predominance. Another important source of atmospheric *n*-alkanes are higher plant waxes, which are released due to abrasion from leaves (Rogge *et al*., 1993b) or as products of incomplete biomass combustion (Simoneit, 2002). These inputs contribute with homologues in the C_{24}-C_{35} range, maximising at C_{27}, C_{29} or C_{31}. The carbon preference index (CPI), which is defined as the sum of the concentrations of the odd carbon number *n*-alkanes divided by the sum of the concentrations of the even carbon number *n*-alkanes, can be used as a qualitative tool to assess the influence of biogenic and anthropogenic inputs (Alves, 2008). The CPI typically ranges from 1.1 to 2.0 in urban environments, while a CPI higher than 2.0 is characteristic of rural environments, where the biogenic influence is more important. Total concentrations of *n*-alkanes in the Finnish samples (3.6-8.2 ng m^{-3}) were of the same order as those previously reported for the same site, which in turn were 10 to 100 times lower than in particulate matter samples collected in the city of Helsinki in July 2002 (Antilla *et al*., 2005). The CPI values in our study (Table 1) are lower than values for other forest environments (Cheng *et al*., 2006; Alves and Pio, 2008). According to Antilla *et al*. (2005), this may be partially due to the weak emission of plant waxes at the low temperatures prevailing in boreal forests. As observed for *n*-alkanes, the envelope of unresolved hydrocarbons was twice higher for the polluted episode than the corresponding hump for the clean period. Ratios between the unresolved and the chromatographically resolved aliphatics (U/R) much higher than 1 and the FLEXTRA back trajectories (not shown) highlight the impact in forest aerosol of long-range transport of anthropogenic pollution from western and central Europe. Besides the CPI and the U/R ratios, the carbon number of the most abundant *n*-alkanes (C_{max}) and a low biogenic contribution of wax *n*-alkanes from plants ($WNA=C_n-[C_{n+1}+C_{n-1})/2]$) are indicative of a petrogenic signature. Total levels of *n*-alkanes in $PM_{2.5}$ from K-puszta varied between 7.3 and 83 ng m^{-3}. The predominant *n*-alkane congeners (C_{27} and C_{29}) reflect a significant incorporation of higher plant waxes. This biogenic origin is also pointed out by an average CPI of 6.7, which is in the range of values reported for other rural areas (Table 1). In San Pietro Capofiume, the total *n*-alkane levels ranged from 2.6 to 18 ng m^{-3}, showing a diurnal pattern with highest values in the daytime and lowest during the night. This may be due to the reduction in the traffic flow rate at night and unfavorable dispersion conditions. A substantial decrease in global concentrations during the "clean" period was observed. The diagnostic ratios (Table 1) indicate a strong influence of anthropogenic emissions. Aliphatics in samples from Melpitz ranged from *n*-C_{10} to *n*-C_{33}, showing a clear dominance of plant wax constituents, especially in $PM_{2.5}$. The contribution of an unresolved complex mixture of petrogenic hydrocarbons is lower than those observed in San Pietro Capofiume and in Hyytiälä, when the former was under the influence of long range transport of anthropogenic pollution.

A series of even carbon numbered *n*-alkanoic acid methyl esters ranging from C_{14} to C_{24} have been detected with global concentrations up to 16 ng m^{-3}, but only in samples from San Pietro Capofiume. Information concerning concentrations and emission sources or formation processes of these particulate constituents is rather sparse. Fine et al. (2004) have detected methyl alkanoates from C_{17} to C_{27} in emissions from wood combustion. Schnelle-Kreis *et al*. (2007) found *n*-alkanoic acid methyl esters in the $PM_{2.5}$ fraction of Augsburg, Germany. They attributed the presence of these constituents to variable influences of wood and coal combustion.

PAH concentrations measured at the four sites are lower than those reported for different urban environments throughout Europe (Fon *et al*., 2007; Mazquiarán and Pinedo, 2007; and references therein). A Hungarian sample strongly impacted by biomass burning deserves attention, in view of the fact that its PAH concentrations were 20 to 50-fold higher that levels measured for the other samples. For the most part of PAH, concentrations obtained during the "clean" periods in Hyytiälä and San Pietro Capofiume are significantly lower than during the "polluted" events (Table 2). The atmospheric concentrations of PAH depends greatly on the meteorological conditions under which emissions are released. The gas/particle partitioning is influenced by the ambient temperature, whereas photo-degradation is affected by solar radiation. PAH, such as fluoranthene and benzo(a)anthracene, decay

rapidly upon exposure to sunlight (Fon *et al.*, 2007). This might partly explain the higher nighttime concentrations observed for some PAH in San Pietro Capofiume. It should be stated that, during the campaign, the polluted conditions were due to emission sources within the Po Valley. Possible sources of particulates in an area of ca. 70-100 km of radius around San Pietro Capofiume are the intense traffic, power plants and other industries. Other potential source includes the maritime traffic in the Adriatic Sea (Hamed *et al.*, 2007).

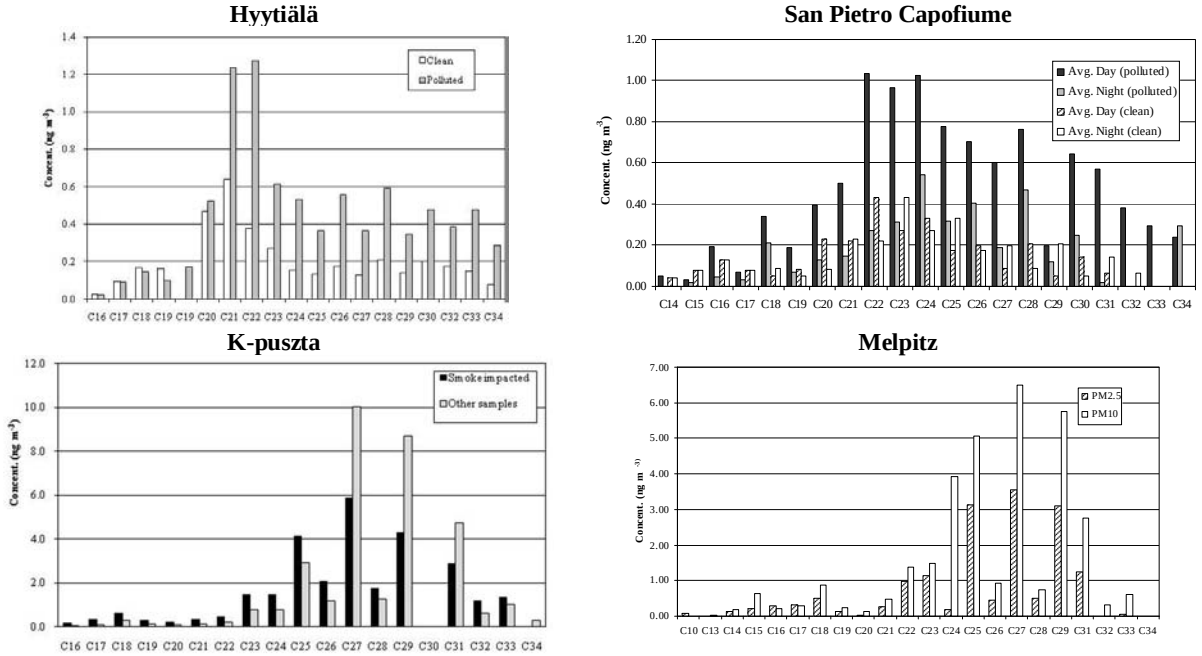

Figure 1. *n*-Alkanes distribution in aerosols from the 4 EUCAARI sites.

Table 1. Comparison of diagnostic ratios for the aerosol aliphatic fraction from different environments.

Location	Period	Particles	C_{max}	CPI	U/R	%WNA	Ref.
Hyytiälä, Finland	Apr 2007	$PM_{2.5}$	C_{22}, C_{23}	1.2±0.03	9.0±5.4	14.5±3.6	This study
K-puszta, Hungary	Spring/Summer 2008	$PM_{2.5}$	C_{27}, C_{29}	6.7±2.2	1.4±0.7	66.3±21.0	This study
San Pietro Capofiume, Italy	Apr 2008	PM_1	C_{22}, C_{24}	0.54±0.41	9.4±4.8	27.5±12.3	This study
Melpitz, Germany	May 2008	$PM_{2.5}$	C_{25}, C_{27}, C_{29}	4.3±2.4	3.3±1.3	58.3±12.8	This study
		PM_{10}	C_{25}, C_{27}, C_{29}	2.8±1.6	3.7±2.2	45.3±13.8	
Terceira island, Azores, Portugal	Jul 2002-Sept 2003 (Summer-Winter averages)	$PM_{2.5}$	C_{27}, C_{29}, C_{31}	5.1-2.5	1.0-1.7	57.8-42.8	Oliveira *et al.* (2007)
Aveiro, coastal rural, Portugal	Jul 2002-Sept 2003 (Summer-Winter averages)	$PM_{2.5}$	C_{22}, C_{27}, C_{29}, C_{31}	2.5-1.5	2.9-7.8	44.8-22.5	Oliveira *et al.* (2007)
Puy de Dôme, rural highlands, France	Jul 2002-Sept 2003 (Summer-Winter averages)	PM_{10}	C_{21}, C_{27}, C_{29}, C_{31}	5.5-2.2	1.2-2.1	66.2-36.9	Oliveira *et al.* (2007)
Schauinsland, forested highlands, Germany	Jul 2002-Sept 2003 (Summer-Winter averages)	PM_{10}	C_{24}, C_{25}, C_{27}, C_{29}, C_{31}	8.2-2.1	0.9-2.4	71.5-31.0	Oliveira *et al.* (2007)
Sonnblick, mountain, Austria	Jul 2002-Sept 2003 (Summer-Winter averages)	$PM_{2.5}$	C_{27}, C_{29}, C_{31}	3.2-1.5	5.0-3.8	46.8-18.8	Oliveira *et al.* (2007)
Athens, roadside, Greece	Aug 2003	$PM_{2.5}$	C_{27}	1.84	25.25	25.15	Andreou *et al.* (2008)
Nanjing, urban, China	2001-2002	$PM_{2.5}$	C_{23}, C_{25}, C_{27}, C_{29}, C_{31}	1.29-1.54		10.8-15.6	Wang *et al.* (2006)
Vienna, urban, Austria	Jan-Dec 2004	PM_{10}	C_{27}, C_{29}, C_{31}	1.23		13.1	Kotianová *et al.* (2008)
Chapinería, rural, Spain	Apr 2004 – Apr 2005	$PM_{2.5}$	C_{25}	1.3		14	Pindado *et al.* (2009)
Beijing, China	Aug 2001 – Jul 2002	$PM_{2.5}$	C_{25}	1.6		20.0	Huang *et al.* (2006)

Table 2. PAH concentrations (pg m^{-3}).

	Hyytiälä		K-puszta		San Pietro Capofiume				Melpitz	
	$PM_{2.5}$		$PM_{2.5}$		PM_1				$PM_{2.5}$	PM_{10}
	Clean	Polluted	Smoke impacted	Other samples	Polluted Day	Polluted Night	Clean Day	Clean Night		
Fluorene			1.4	0.806				3.28	3.54	0.36
Phenanthrene	2.16	2.86	98.1	6.94				1.34	1.35	3.81
Anthracene	2.51	1.53	13.7	3.86			0.707			
Fluoranthene	144	306	2637	192	14.7	17.7				11.02
Pyrene	121	243	1767	208	9.51			32.9	2.95	10.17
Benzo(a)anthracene			1032	29.1	32.7	43.6	5.12	10.6	4.08	10.28
Chrysene	28.8	86.9	2264	86	80.2	124	15.4	37.0	14.82	88.29
Terphenyl			66.4					27.1		
Retene	7.41	3.57	4.19	2.14	7.57	2.09	0.795	0.981	1.48	9.29
Benzo(b)fluoranthene	13.5	52.6	7005	87.2	41.9	89.0		50.2	15.48	52.03
Benzo(k)fluoranthene	13.5	47.8	2803	60.2	72.7	92.7	207	27.6	30.67	58.56
Benzo(a)pyrene	2.75	4.78		40.2	49.5	53.4	5.64	14.3	20.65	41.88
Benzo(e)pyrene	14.7	58.0	3250	78.7	83.7	107	17.5	37.8	73.11	70.80
Perylene			159	8.75	3.77	8.77		4.57		
Indeno(1,2,3-cd)pyrene		55.9	3698	52.3	39.6			274		
Benzo(ghi)perylene		51.1	2104	58.1	30.4				12.34	
Dibenzo(a,h)anthracene		1.64	1344	0.397	5.64	1.52	0.602			

Note: Cells in white represent non-detected PAH or concentrations below the detection limit.

To further assess the different sources of PAH present in the aerosol samples, a comparison among diagnostic ratios was made (Table 3). The IcdP/(BghiP+IcdP) and Flu/(Flu+Pyr) ratios for Hyytiälä, San Pietro Capofiume and K-puszta fell in the range of PAH emitted by diesel vehicles. The Flu/(Flu+Pyr) average ratios obtained in samples from Melpitz are indicative of mixed combustion processes (Alves, 2008). The Flu/(Flu+Pyr) ratio suggests a predominant input from biomass burning in Hyytiälä during the "clean" period. The BghiP/BeP is indicator for traffic, with higher ratios suggesting higher vehicular emissions. This ratio was far below the characteristic value for traffic emission, but more close to that of non-traffic sources. The BeP/(BeP+BaP) ratio is affected by the strong reactivity in the atmosphere since BaP is easily decomposed by light and oxidants. Most of the fresh exhausts have similar contents of BeP and BaP, thus the increasing of the ratio can be regarded as an index of the aging of particles. This diagnosis ratio suggests that vehicular emissions are the major source of the particulate PAH in San Pietro Capofiume, K-puszta and Melpitz, while a more aged aerosol was collected in Hyytiälä. The high Bghi/BaP ratio obtained for the boreal forest reflects, once again, some atmospheric processing of aerosol, suggesting the occurrence of decomposition of BaP during air mass transport. The average Bghi/BaP ratio for the Hungarian samples is in the range of values reported for vehicular emissions. The low values found for San Pietro Capofiume in the polluted period reveals a mixed influence associated with both traffic and industrial processes. The BFs/BghiP ratios suggest again contributions from industrial activities in the Po Valley, impact of biomass burning in K-puszta and a mixed input from both wood combustion and vehicular emissions in Hyytiälä.

Table 3. Concentration ratios between PAH.

	Hyytiälä		San Pietro Capofiume				K-puszta	Melpitz		Source/Interpretation
	$PM_{2.5}$		PM_1				$PM_{2.5}$	$PM_{2.5}$	PM_{10}	
	Clean	Polluted	Polluted Day	Polluted Night	Clean Day	Clean Night				
IcdP/(BghiP+IcdP)	-	0.521	0.566	-	-	-	0.496	-	-	~ 0.2 gasoline emissions (Alves, 2008); 0.35-0.70 diesel cars (Wang *et al*., 2006); 0.51 coal burning (Bi *et al*., 2008); 0.44 biomass burning (Kalaitzoglou *et al*., 2004)
BeP/(BeP+BaP)	0.842	0.924	0.651	0.706	0.757	0.725	0.712	0.620	0.674	0.34 wood; 0.6-0.8 vehicle emissions (Alves, 2008)
Flu/(Flu+Pyr)	0.543	0.557	0.607	-	-	-	0.569	1.0	0.852	0.26 biomass burning (Kalaitzoglou et al., 2004); ~ 0.40 gasoline cars (Alves, 2008); 0.6-0.70 diesel engines (Wang *et al.*, 2006); > 0.50 coal burning (Yunker et al., 2002)
BghiP/BeP	-	0.885	0.360	-	-	-	0.965	0.319	-	2.02 vehicle emissions; 0.80 non-traffic sources (Xie *et al.*, 2009)
BghiP/BaP	-	11.7	0.614	-	-	-	2.31	-	-	0.02–0.06 industrial furnaces; 1.2-2.2 diesel cars; 2.5-3.3 gasoline cars (Alves, 2008)
BFs/BghiP	-	1.96	-	-	-	-	2.16	-	-	0.33 gasoline cars; 1.6 diesel cars; 2.18 wood; >4 industrial processes (Alves, 2008)

IcdP – Indeno(1,2,3-cd)pyrene; BghiP – Benzo(ghi)perylene; BeP – Benzo(e)pyrene; BaP – Benzo(a)pyrene; Flu – Fluoranthene; Pyr – Pyrene; BFs = Benzofluoranthenes

Benzo(a)pyrene is considered a classical carcinogen and one of the most powerful mutagens. The benzo(a)pyrene equivalent concentration (BaPE) has been introduced instead of the sole benzo(a)pyrene since the later is easily decomposed in reactive air. It tries to parameterise the health risk for humans related to ambient PAH exposure and is calculated by adding weighted concentrations of each carcinogenic congener. According to the European Union air quality standards, the maximum permissible risk level is 1 ng m^{-3} (annual average). The average BaPE concentrations obtained for every EUCAARI sites (Figure 2) are much lower than those in urban areas around the world, where the target value is frequently exceeded (Wang *et al.*, 2006). Benzo(a)pyrene is the highest carcinogenic contributor in San Pietro Capofiume and Melpitz, while benzofluoranthenes and dibenzo(a,h)nathracene predominate in K-puzsta. Concentrations of carcinogenic compounds represented 2.5%, 6.5%, 27% and 37% of total PAH in Hyytiälä, K-puszta, San Pietro Capofiume and Melpitz, respectively.

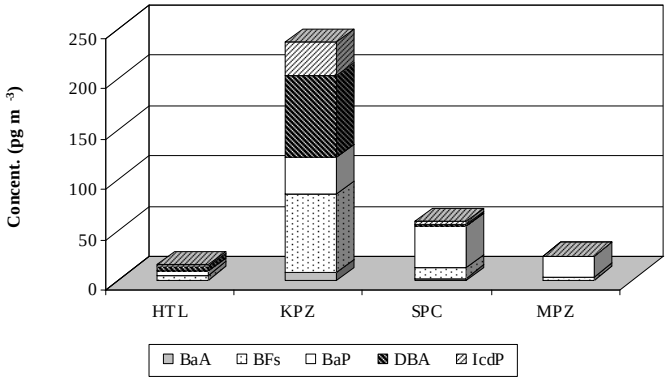

Figure 2. Average benzo(a)pyrene equivalent concentrations in fine or submicrom particulate matter (Benzo(a)pyrene equivalent concentration = BaPE = BaA×0.06+BFs×0.07+BaP+DBA×0.6+ IcdP×0.08; BaA – Benzo(a)anthracene; DBA = Dibenzo(a,h)anthracene)

Other anthropogenic compound identified was 2,6-di-tert-butyl-p-benzoquinone. This quinone was present in samples from Hyytiälä at levels up to 520 pg m^{-3}, while in K-puszta, San Pietro Capofiume and Melpitz concentrations reached values of 9.7, 1.1 and 1.8 ng m^{-3}, respectively. Most of the samples from all sites contained urs-12-en-one. This ketone is a mild oxidation product of amyrins, which are pentacyclic triterpenes used as tracers for biomass burning. The urs-12-en-one concentrations ranged from trace levels to 25.3 pg m^{-3} (SPC), 89.5 pg m^{-3} (K-puszta) and 49.3 pg m^{-3} (Melpitz). In aerosols from Hyytiälä, concentrations varied between 1.24 pg m^{-3}, during the "clean" period, and 6.37 pg m^{-3} under the influence of atmospheric pollution transport. Nopinone, an ozonolysis product of β-pinene, was sporadically detected in samples from Italy, Finland and Germany, at low levels. Contrarily, almost all the Hungarian samples contained the secondary organic aerosol product with concentrations up to 180 pg m^{-3}.

CONCLUSIONS

n-Alkanes and PAH in aerosols from four rural European sites were chemically characterised, along with source reconciliation based on CPI, U/R, %WNA and diagnostic ratios of PAH. The presence of petroleum residues was confirmed by the low CPI values and high ratio of resolved to unresolved aliphatic components, particularly in Hyytiälä and San Pietro Capofiume. The input of biogenic sources was significant in K-puszta and Melpitz, where 60% and about 50%, respectively, of the total *n*-alkanes were attributable to plant waxes. This biogenic contribution represented only 15 and 23% of the total *n*-alkanes found in the boreal and Mediterranean aerosol, respectively. Diagnostic ratios between PAH suggest that vehicular emissions and biomass burning also influence the aerosol constitution in the Hungarian site. Long range transport of air masses contributed with anthropogenic components to the atmospheric aerosol in the boreal forest. In spite of transboundary pollution, Hyytiälä registered the lowest hydrocarbon levels among all locations. Aliphatic and aromatic hydrocarbons in samples from San Pietro Capofiume reveal that both vehicular and industrial emissions are major sources influencing

the diel pattern of concentrations. The average BaPE concentrations obtained for every EUCAARI sites were far lower than the mandatory limit value (1 ng m^{-3}).

ACKNOWLEDGEMENTS

This work was supported by the European Integrated Project on Aerosol Cloud Climate and Air Quality Interactions (EUCAARI). Ana Vicente acknowledges the PhD grant SFRH/BD/48535/2008 from the Portuguese Science Foundation.

REFERENCES

Alves, C. (2001). *Origin and composition of organic matter present in atmospheric aerosols*, PhD Thesis, University of Aveiro, Portugal.

Alves, C. (2008). Characterisation of solvent extractable organic constituents in atmospheric particulate matter: an overview. *Ann. Brazil. Acad. Sci*. 80, 21.

Alves, C., Pio, C. (2005). Secondary organic compounds in atmospheric aerosols: speciation and formation mechanisms. *J. Brazil. Chem. Soc*. 16, 1017.

Alves, C. and C. Pio (2008). Molecular markers, essential oils and diagnostic parameters as indicators for assessing the origin and constitution of organic matter in atmospheric aerosols. *Int. J. Environ. Poll.* 32, 362.

Andreou, G., S.D.Alexiou, G.Loupa and S. Rapsomanikis (2008). Identification, Abundance and Origin of Aliphatic Hydrocarbons in the Fine Atmospheric Particulate Matter of Athens, Greece. *Water, Air, Soil Poll.* 8, 99.

Anttila, P., T. Rissanen, M. Shimmo, M. Kallio, T. Hyötyläinen, M. Kulmala, M.L. Riekkola (2005). Organic compounds in atmospheric aerosols from a Finnish coniferous forest. *Boreal Environ. Res*. 10, 371.

Armstrong, B., E.Hutchinson, J. Unwin, T. Fletcher, (2004). Lung cancer risk after exposure to polycyclic aromatic hydrocarbons: a review and meta-analysis. *Environ. Health Perspect*. 112, 970.

Bi, X., B.R.T. Simoneit, G. Sheng and J. Fu (2008). Characterization of molecular markers in smoke from residential coal combustion in China. *Fuel* 87, 112.

Brandenberger, S., M. Mohr, K. Grob and H.P. Neukom (2005). Contribution of unburned lubricating oil and diesel fuel to particulate emission from passenger cars. *Atmos. Environ.* 39, 6985.

Carvalho, A. (2003). *Characterisation of carbonaceous aerosols in the atmosphere – secondary and* water soluble compounds, PhD Thesis, University of Aveiro, Portugal.

Cheng, Y., S.M. Li, A. Leithead and J.R. Brook (2006). Spatial and diurnal distributions of *n*-alkanes and *n*-alkan-2-ones on $PM_{2.5}$ aerosols in the Lower Fraser Valley, Canada. *Atmos. Environ*. 40, 2706.

Chirico, R., P. Spezzano and D. Cataldi (2007). Gas-particle partitioning of polycyclic aromatic hydrocarbons during the spring and the summer in a suburban site near major traffic arteries. *Polycycl. Aromat. Comp.* 27,401.

Fang, G.C., K.F. Chang, C. Lu and H. Bai (2002). Toxic equivalency factors study of polycyclic aromatic hydrocarbons (PAHs) in Taichung City, Taiwan. *Toxicol. Ind. Health* 18, 279.

Fine, P.M., G.R. Cass and B.R.T. Simoneit (2004). Chemical characterization of fine particle emissions from the fireplace combustion of wood types grown in the Midwestern and Western United States. *Environ. Eng. Sci.* 21, 387.

Fon, T.Y.W., O. Noriatsu and S. Hiroshi (2007). Polycyclic aromatic hydrocarbons (PAHs) in the aerosol of Higashi Hiroshima, Japan: Pollution scenario and source identification. *Water Air Soil Pollut.* 182, 235.

Gelencsér, A., T. Barcza, G. Kiss, Á. Molnár, J. Hlavay and E. Mészáros (1998). Distribution of *n*-alkanes and PAHs in atmospheric aerosols. *Atmos. Res.* 46, 223.

Gerde, P., B.A. Muggenburg, M.L., Lundborg and A.R. Dahl (2001). The rapid alveolar absorption of diesel soot-adsorbed benzo(a)pyrene: bioavailability, metabolism and dosimetry of an inhaled particle-carcinogen. *Carcinogenesis* 22, 741.

Gogou, A., M. Apostolaki and E. Stephanou (1998). Determination of organic molecular markers in marine aerosols and sediments: one- step flash chromatography compound class fractionation and capillary gas chromatographic analysis. *J. Chromatogr. A*, 799, 215.

Hamed, A., J. Joutsensaari, S. Mikkonen, L. Sogacheva, M. Dal Maso, M. Kulmala, F. Cavalli, S. Fuzzi, M.C. Facchini, S. Decesari, M. Mircea, K.E.J. Lehtinen and A. Laaksonen (2007). Nucleation and growth of new particles in Po Valley, Italy. *Atmos. Chem. Phys.* 7, 355.

Huang, X.F., L.Y. He, M. Hu and Y.H. Zhang (2006). Annual variation of particulate organic compounds in $PM_{2.5}$ in the urban atmosphere of Beijing. *Atmos. Environ.* 40, 2449.

Kotianová, P., H. Puxbaum, H. Bauer, A. Caseiro, I.L. Marr and G. Čík (2008). Temporal patterns of *n*-alkanes at traffic exposed and suburban sites in Vienna. *Atmos. Environ.* 42, 2993.

Lin, C.C., S.J. Chen, K.L. Huang, W.J. Lee, W.Y. Lin, J.H. Tsai and H.C. Chaung (2008). PAHs, PAH-induced carcinogenic potency, and particle-extract-induced cytotoxicity of traffic-related nano/ultrafine particles. *Environ. Sci. Technol*, 42, 4229.

Mazquiáran, M.A.B. and L.C.O. Pinedo (2007). Organic composition of atmospheric urban aerosol: Variations and sources of aliphatic and polycyclic aromatic hydrocarbons. *Atmos. Environ.* 85, 288.

Ming, Y. and V. Ramaswamy (2009). Nonlinear climate and hydrological responses to aerosol effects. *J. Climate* 22, 1329.

Oliveira, T.S., C.A. Pio, C.A. Alves, A.J.D. Silvestre, M. Evtyugina, J.V. Afonso, P. Fialho, M. Legrand, H. Puxbaum and A. Gelencsér (2007). Seasonal variation of particulate lipophilic organic compounds at non-urban sites in Europe. *J. Geophys. Res.* 112, D23S09.

Pindado, O., R. Pérez, S. García, M. Sánchez, P. Galán and M. Fernández (2009). Characterization and sources assignation of $PM_{2.5}$ organic aerosol in a rural area of Spain. *Atmos. Environ.* 43, 2796.

Pope III, C.A., M. Ezzati and D.W. Dockery (2009). Fine-particulate air pollution and life expectancy in the United States. *New Engl. J. Med*. 360, 376.

Rogge, W.F., L.M. Hildemann and M.A. Mazurek (1997). Cass, G. R. Sources of fine organic aerosol. 8. Boilers burning no. 2 distillate fuel oil. *Environ. Sci. Technol*. 31, 2731.

Rogge, W.F., L.M. Hildemann, M.A. Mazurek and G.R. Cass (1993a). Sources of fine organic aerosol. 2. Noncatalyst and catalyst-equipped automobiles and heavy-duty diesel trucks. *Environ. Sci. Technol.* 27, 636.

Rogge, W.F., L.M. Hildemann, M.A. Mazurek, G.R. Cass and B.R.T. Simoneit (1993b). Sources of fine organic aerosol. 4. Particulate abrasion products from leaf surfaces of urban plants. *Environ. Sci. Technol*. 27, 2700.

Sakurai, H., H.J. Tobias, K. Park, D. Zarling, K.S. Docherty, D.B. Kittelson, P.H. McMurry and P.J. Ziemann (2003). On-line measurements of diesel nanoparticle composition and volatility. *Atmos. Environ*. 37, 1199.

Schauer, J.J., M.J. Kleeman, G.R. Cass and B.R.T. Simoneit (1999). Measurement of emissions from air pollution sources. 2. C-1 through C-30 organic compounds from medium duty diesel trucks. *Environ. Sci. Technol*. 33, 1578.

Schnelle-Kreis, J., M. Sklorz, J. Orasche, M. Stölzel, A. Peters and R. Zimmermann (2007). Semi volatile organic compounds in ambient $PM_{2.5}$. seasonal trends and daily resolved source contributions. *Environ. Sci. Technol.* 41, 3821.

Shah, S.D., T.A. Ogunyoku, J.W. Miller and D.R. Cocker 3rd (2005). On-road emission rates of PAH and *n*-alkane compounds from heavy-duty diesel vehicles. *Environ. Sci Technol.* 39, 5276.

Simoneit, B.R.T. (2002). Biomass burning: a review of organic tracers for smoke from incomplete combustion. *Appl. Geochem*. 17, 129.

Tasdemir, Y. and F. Esen (2007). Urban air PAHs: Concentrations, temporal changes and gas/particle partitioning at a traffic site in Turkey. *Atmos Res*. 84, 1.

Wang, G., L. Huang, X. Zhao, H. Niu and Z. Dai (2006). Aliphatic and polycylic aromatic hydrocarbons of atmospheric aerosols in five locations of Nanjing urban area, China. *Atmos. Res*. 81, 54.

Xie, M., G. Wang, S. Hu, Q. Han, Y. Xu and Z. Gao (2009). Aliphatic alkanes and polycyclic aromatic hydrocarbons in atmospheric PM_{10} aerosols from Baoji, China: Implications for coal burning. *Atmos. Res*. 93, 840.

Yunker, M.B., R.W. McDonald, R. Vingarzan, R.H. Mitchel, D. Goyette and S. Sylvestre (2002). PAHs in the Fraser River basin: a critical appraisal of PAH ratios as indicators of PAH source and composition. *Org. Geochem.* 33, 489.

Zielinska, B., J. Sagebiel, J.D. McDonald, K. Whitney and D.R. Lawson D.R. (2004). Emission rates and comparative chemical composition from selected in-use diesel and gasoline-fueled vehicles. *J. Air Waste Manag. Assoc.* 54, 1138.

Zou, L. and S. Atkinson (2003). Characterising vehicle emissions from the burning of biodiesel made from vegetable oil. *Environ. Technol.* 24, 1253.

PHOTOCHEMISTRY AND MICROSTRUCTURE OF ORGANIC PARTICLES

M. AMMANN[1], A. ROUVIERE[1], Y. SOSEDOVA[1], C. GEORGE[2], B. D'ANNA[2], V. ZELENAY[1], A. KREPELOVA[1], T. HUTHWELKER[3]

[1]Laboratory of Radiochemistry and Environmental Chemistry, Paul Scherrer Institut, Villigen, Switzerland.
[2]IRCELYON, Institut de Recherches sur la Catalyse et l'Environnement de Lyon UMR 5256 CNRS/Université Lyon1 2, avenue Albert Einstein F-69629 Villeurbanne Cedex.
[3]Swiss Light Source, Paul Scherrer Institut, Villigen, Switzerland

Keywords: organic aerosol, photochemistry, photosensitizer, secondary organic aerosol.

INTRODUCTION

We have recently established that condensed phase photochemical processes can be driven by organic material present in the aerosol phase that is able to absorb light and photosensitise reduction and oxidation of trace gases interacting with the particles (D'Anna et al., 2009; George et al., 2005; Jammoul et al., 2008; Stemmler et al., 2006; Stemmler et al., 2007). While this on one hand leads to important feedbacks to the oxidant budget of the gas phase, these processes may also lead to comparable effects on the organic fraction of the particle phase with the potential of leading to increased fixation of volatile organic compounds through routes not considered so far. We therefore investigated the photochemical aging of proxy organic compounds, such as simple carboxylic acids, in presence of aromatic ketones as photosensitizers. Because complete processing of often viscous organic material is strongly limited by condensed phase diffusion, we invested into the development of an in situ tool to follow chemical processing online using X-ray microspectroscopy. This technique allows following functional group composition with a spatial resolution of down to 20nm. In a first test case, we looked at the microstructure of mixed ammonium sulphate / adipic acid particles particles as a function of humidity.

METHODS

Basic photochemistry experiments were first performed in solution using laser flash photolysis and UV-Vis spectrometry. Experiments with respect to photosensitized uptake of ozone and other small organic molecules were carried out in coated wall flow tubes. Selected experiments with mixtures of different organic acids with benzophenone and benzoylbenzoic acid were also investigated with an aerosol flow reactor coupled to an aerosol mass spectrometer. X-ray microspectroscopy experiments were performed at the PolLux beamline at the Swiss Light Source at Paul Scherrer Institut. We developed a microreactor that allows imaging particles deposited on a 50 nm thick silicon nitride membrane while being exposed to a defined temperature and humidity.

CONCLUSIONS

The laser flash photolysis work indicated that simple organic acids such as adipic and succinic acids efficiently quench the excited benzophenone triplet in aqueous solution (Figure 1). Longer term exposure of such solutions to simulated sunlight leads to the build up of new absorption features extending into the visible, indicative of polymerisation processes. Experiments in aerosol and coated flow tubes indicate effective removal of these acids driven by light, and in some cases indicate the build-up of secondary organic material in the aerosol phase (Figure 2).

The X-ray microspectroscopy work was devoted to the development of the microreactor system and its application to a first test system. The results with mixed ammonium sulphate / adipic acid particles indicate complex microstructure and its evolution, when part of the material forms a solution (Figure 3). This provides a proof of concept that this method can be used to follow oxidative and photochemical processing in situ and in real time in the future.

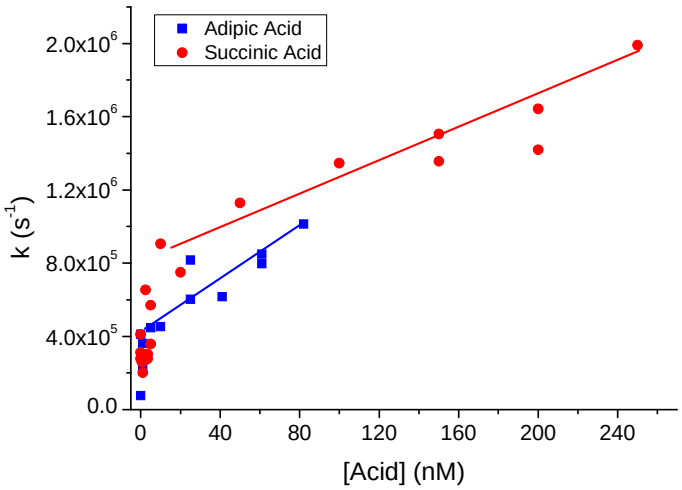

Figure 1.Benzophenone triplet quenching kinetics in succinic and adipic acid solutions.

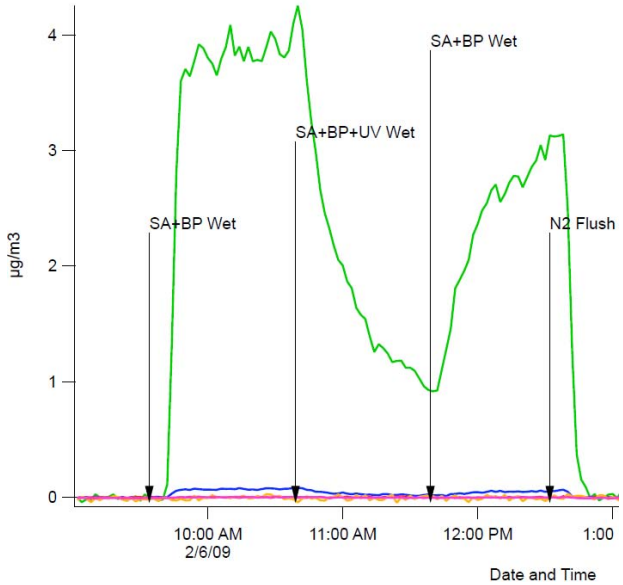

Figure 2. Results from the AMS measurements of the time evolution of the organics (succinic acid and benzophenone) in presence of UV

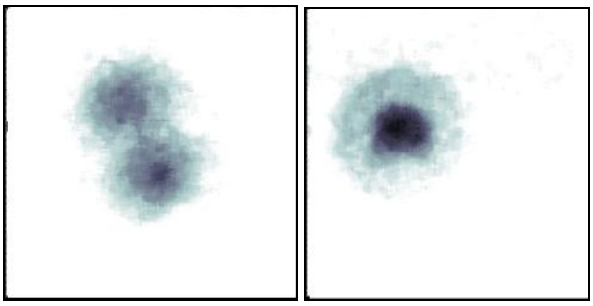

Figure 3. These images were taken with a scanning transmission X-ray microscope, left, the mixed ammonium sulphate / adipic acid particle under dry conditions, right, during exposure to about 80% relative humidity. The grey scale indicates the amount of carbon measured at 288.6 eV, after subtraction of the background at 270 eV.

ACKNOWLEDGEMENTS

This work was supported by EU FP-6 EUCAARI, European Science Foundation INTROP, Swiss National Science Foundation, the Center of Excellence in Energy and Mobility (CCEM-CH) of the Swiss ETH Domain.

REFERENCES

D'Anna, B., Jammoul A., George, C., Stemmler, K., Fahrni, S., Ammann, and M., Wisthaler, A. (2009). Light-induced ozone depletion by humic acid films and submicron aerosol particles. J. Geophys. Res., 114.

George, C., Strekowski, R.S., Kleffmann, J., Stemmler, K. and Ammann, M. (2005). Photoenhanced uptake of gaseous NO2 on solid organic compounds: A photochemical source of HONO? Faraday Discuss., 130: 195-210.

Jammoul, A., Gligorovski, S., George, C. and D'Anna, B. (2008). Photosensitized Heterogeneous Chemistry of Ozone on Organic Films. J. Phys. Chem. A, 112(6): 1268-1276.

Stemmler, K., Ammann, M., Donders, C., Kleffmann, J. and George, C. (2006). Photosensitized reduction of nitrogen dioxide on humic acid as a source of nitrous acid. Nature, 440(7081): 195-198.

Stemmler, K., Ammann, M., Elshorbany, Y., Kleffmann, J., Ndour, M., D'Anna, B., George, C., and Bohn, B. (2007). Light induced conversion of nitrogen dioxide into nitrous acid on submicron humic acid aerosol. Atmos. Chem. Phys. Discuss., 7(2): 4035-4064.

INVESTIGATION ON CLOUD-DROPLET ACTIVATION PROCESS DURING EUCAARI-IMPACT, A CASE STUDY

S. ARABAS[1], H. PAWŁOWSKA[1]

[1] Institute of Geophysics, Faculty of Physics, University of Warsaw,
Pasteura 7, 02-093 Warszawa, Poland.

Keywords: EUCAARI-IMPACT, cloud-droplet activation.

The EUCAARI IMPACT field campaign encompassed a range of ground-based and airborne atmospheric measurements including aerosol and cloud-droplet sizing as well as vertical wind measurements. The resulting dataset is used here to study cloud-droplet activation process. The goal of this ongoing research is to assess the closure between the measured physicochemical aerosol properties and the measured cloud-droplet size distributions in convective clouds probed during the IMPACT experiment.

The considered in-situ aerosol and cloud-droplet measurements were carried out onboard the SAFIRE ATR-42 research aircraft. The aerosol instrumentation of the aircraft included externally-mounted PCASP spectrometer, and a chain of internally-mounted instruments hooked up to two switchable aerosol inlets. When flying through clouds, the counterflow virtual impactor (CVI) was used as an inlet thus enabling the instruments to sample the non-volatile particles contained in the cloud droplets. When the aircraft was not penetrating clouds, the Community Aerosol Inlet (CAI) was used providing the instruments with a constant-velocity, laminar flow of air regardless of the aircraft speed and orientation with regard to the external air flow. The data collected by the following instruments connected to the inlets will be used in our study:

- two pairs of optical (GRIMM OPC) and scanning mobility (SMPS) aerosol size spectrometers (one pair connected through a heater set at $280°C$),
- a Cloud Condensation Nuclei Counter (CCNC) (DMT CCN spectrometer operated at a single supersaturation),
- the TSI 3025 and TSI 3010 Condensation Particle Counters (CPC) and
- an Aerosol Mass Spectrometer.

The considered cloud-droplet measurements were made using the PVM-100 optical liquid water content probe and FSSP-100 optical spectrometer. The air velocity was measured using a 5-hole gust probe integrated in the radome of the aircraft. The ground-based aerosol instrumentation at the Cabauw observatory was a superset of the instruments used inside the SAFIRE ATR-42 aircraft, and was supplied with the air through the inlets mounted $60m$ above ground on the Cabauw tower.

Two flights were chosen for the case study: the RF49 that took place on May 13^{th} over The Netherlands (in the vicinity of the Cabauw observatory, see figure 1), and the RF51 flown on May 15^{th} over the North Sea. The RF49 included about 5 minutes of penetrations of cumulus clouds, while during RF51 the aircraft spent about 50 minutes penetrating a deck of stratocumulus clouds. The two contrasting aerosol characteristics (see fig. 2) of polluted continental air-mass (RF49) and relatively pristine marine air (RF51), and consequently the contrasting cloud-droplet spectra, are used as test cases for a model of cloud-droplet activation process.

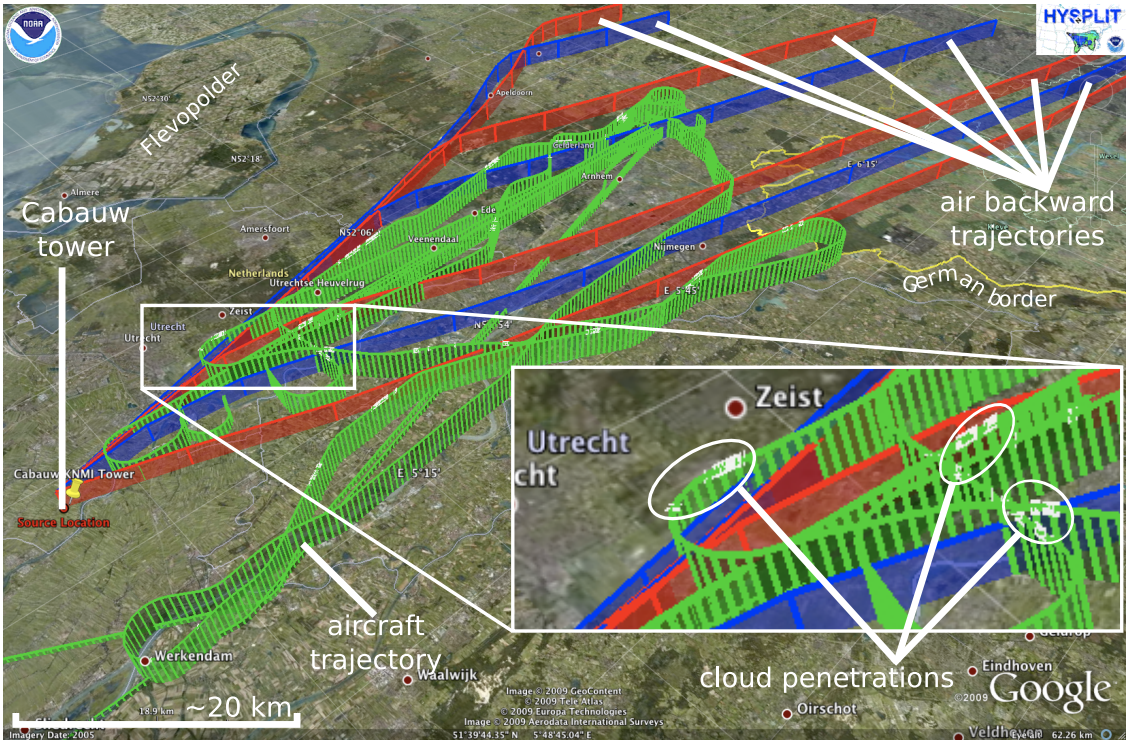

Figure 1: An overview of the RF49 flight scenario. The green ribbon-like path marks the aircraft trajectory with cloud-penetrations highlighted with white marks. The blue and red paths are the air backward trajectories arriving at Cabauw at the time of the flight and several hours earlier (trajectories calculated using the NOAA Hysplit model).

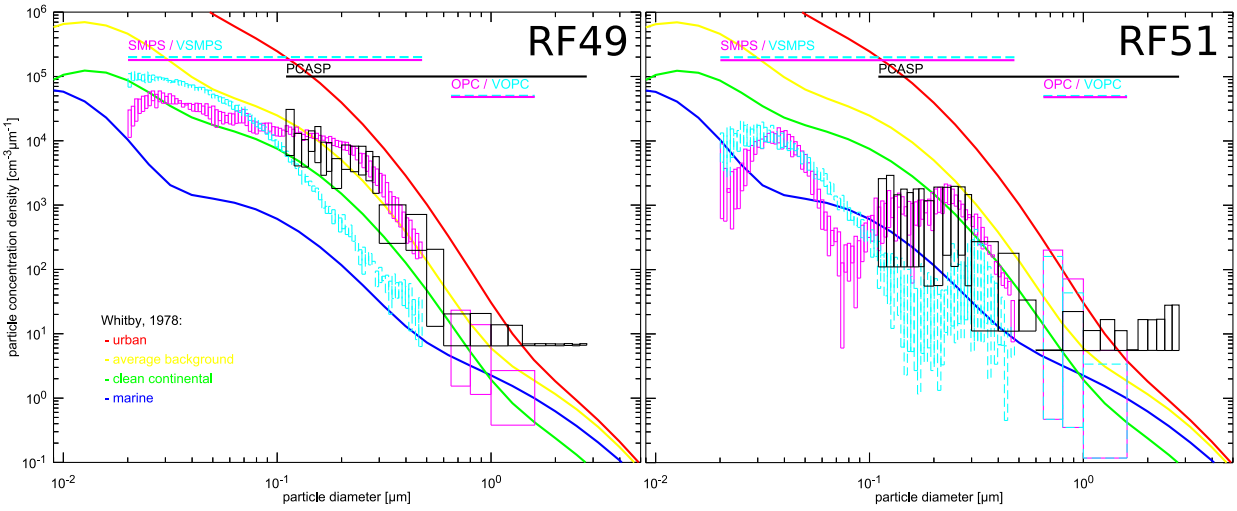

Figure 2: Aerosol size spectra measured in-situ near cloud-base during RF49 (1900-2000 m a.m.s.l.) and RF51 (450-550 m a.m.s.l., longitude $1°W - 0.5°E$) using PCASP and two pairs of SMPS/OPC spectrometers. For each size bin of an instrument a box indicating minimal-maximal values of concentration is plotted with a width corresponding to the bin width. Dashed lines represent measurements done on air-samples heated to $280°C$ (denoted as VSMPS and VOPC). Curves plotted for reference in the background are trimodal lognormal distributions representing examples of urban, clean continental, average background and marine aerosol spectra (as used in Nenes et al., 2001, following Whitby, 1978)

The model considered in this study is built upon the concept of an adiabatic air parcel rising at a constant vertical velocity. The particle size spectrum for a given aerosol chemical composition is divided into classes containing a constant-in-time particle number. The class size (radius) evolution is governed by the drop growth equation. At present, the soluble fraction of aerosol particles is assumed to be composed solely of ammonium sulfate following the description of Johnson (1980). The aim of the ongoing model development is to match the aerosol-composition representation in the model with the range of aerosol parameters measured during IMPACT. The model constitutes a system of ordinary differential equations which is numerically integrated in time using the CVODES sensitivity-analysis enabled solver of Serban and Hindmarsh (2005). A tri-modal (nuclei, accumulation & coarse modes) lognormal distribution is fitted to the experimental data (as used e.g. in Nenes et al., 2001) and used as the model input. Results of multiple simulations performed at different vertical velocities are matched with the measured vertical wind speed spectrum to obtain statistics of droplet-spectrum parameters. The predicted statistics are compared with the in-situ measurements made using the FSSP-100 cloud-droplet size spectrometer.

ACKNOWLEDGEMENTS

Work done within the European Commission's 6. FP IP EUCAARI (European Integrated project on Aerosol Cloud Climate and Air Quality interactions) No 036833-2. SA and HP were supported by the Polish MNiSW grant 396/6/PR UE/2007/7. SA participation in the IMPACT experiment was supported by the ACCENT EU-Network of Excellence "Access to Infrastructures".

REFERENCES

Johnson, D., 1980: The influence of cloud-base temperature and pressure on droplet concentration. *J. Atmos. Sci.*, 37, 2079–2085.

Nenes, A., S. Ghan, H. Abdul-Razzak, P. Chuang, and J. Seinfeld, 2001: Kinetic limitations on cloud droplet formation and impact on cloud albedo. *Tellus B*, 53, 133–149.

Serban, R., and A. C. Hindmarsh, 2005: CVODES, the sensitivity-enabled ODE solver in SUNDIALS. *Proceedings of the 2005 ASME International Design Engineering Technical Conference*, Long Beach, CA, USA. Also published as 2005 LLNL Tech. rep. UCRL-PROC-21030, Lawrence Livermore National Laboratory, USA.

OVERALL PROCESS OF NEW PARTICLE FORMATION INITIATED BY THE REACTION OH + SO_2

T. Berndt[1], M. Sipilä[1,2,4], F. Stratmann[1], J. Vanhanen[2], T. Petäjä[2], A. Grüner[1], G. Spindler[1], R. L. Mauldin III[3], M. Kulmala[2], and J. Heintzenberg[1]

[1]Leibniz-Institut für Troposphärenforschung e.V., Permoserstr. 15, 04318 Leipzig, Germany.
[2]Department of Physics, University of Helsinki, P.O. Box 64, FIN-00014, Finland.
[3]Atmospheric Chemistry Division, Earth and Sun Systems Laboratory, National Center for Atmospheric Research, P.O. Box 3000, Boulder, CO 80307-5000, USA.
[4]Also at: Helsinki Institute of Physics, University of Helsinki, P.O. Box 64, FIN-00014, Finland.

Keywords: Nucleation, Sulphuric Acid, Kinetics.

INTRODUCTION

Simultaneous measurements of newly formed ultra-fine particles and H_2SO_4 in the lower troposphere reveal that new particle formation is strongly connected to the occurrence of H_2SO_4 with concentrations of about 10^5 - 10^7 molecule cm^{-3} and the production rate of new particles can be described by a power law equation for H_2SO_4 with an exponent in the range of 1 - 2 (Weber et al., 1996, Kulmala et al., 2006, Sihto et al., 2006). From our laboratory, using the reaction of OH radicals with SO_2 for H_2SO_4 formation (Berndt et al., 2005), experimental evidence for the formation of new particles was found for H_2SO_4 concentrations of ~10^7 molecule cm^{-3}. The analysis of integral number measurements by means of commercially available UCPCs revealed that measured slopes of log(N) vs. log([H_2SO_4]) were affected by the decreasing size-dependent counting efficiency of the UCPCs used for dp < 3 nm leading to an overestimation of the slopes.
Subject of this study are measurements of the formation rate of freshly nucleated particles by means of high-sensitivity counters with detection limits down to 1.5 nm in diameter. The influence of relative humidity as well as of ammonia on the nucleation rate is investigated.

METHODS

Experiments have been carried out in the atmospheric pressure flow-tube *IfT*-LFT (i.d. 8 cm; length 505 cm) at 293 ± 0.5 K (Berndt et al., 2005). For integral particle measurements commercial UCPCs (TSI 3025 and TSI 3786) as well as a pulse height condensation particle counter (PH-CPC), Sipilä et al., 2008, and a mixing-type CPC (M-CPC), Vanhanen et al., 2009, came into operation. PH-CPC and M-CPC are able counting particles with a diameter of about 1.5 nm.
H_2SO_4 concentrations in the flow tube were calculated using a model according to the following reaction scheme (Berndt et al., 2005):

O_3		$\rightarrow \ldots \rightarrow$	2 OH	(1)
OH	+ scav	$\rightarrow$	products	(2)
OH	+ SO_2	$\rightarrow \ldots \rightarrow$	H_2SO_4	(3)
H_2SO_4		$\rightarrow$	wall	(4)

CO, H_2 or mesitylene (1,3,5-trimethylbenzene) were chosen as OH radical scavenger “scav” in order to adjust atmospheric OH levels in the flow tube. For measuring the H_2SO_4 concentration, the outlet of *IfT*-LFT was directly attached to a Chemical Ionization Mass spectrometer. Measured H_2SO_4 concentrations were found to be in a good agreement with modelling results

CONCLUSIONS

Fig.1 shows experimental findings for different residence times at r.h. = 22%. Nucleation rates are obtained by dividing measured particle numbers by the bulk residence time in the reaction zone. Regression analysis of the whole data set yields for

$$\mathbf{N = k\ (\ [H_2SO_4]/molecule\ cm^{-3}\ )^{\alpha}}$$

the parameters: $\alpha = 1.80$, $k = 1.3 \cdot 10^{-12}$ $cm^{-3}s^{-1}$ (full line in fig.1). Setting $\alpha = 2$ as a fixed parameter, $k = 4.2 \cdot 10^{-14}$ $cm^{-3}s^{-1}$ follows (dashed line in fig.1). The exponents α resulting from the individual measurement series are in the range 1.6 - 2.1. These parameters from the laboratory are very similar to those arising from analysis of ambient nucleation events.

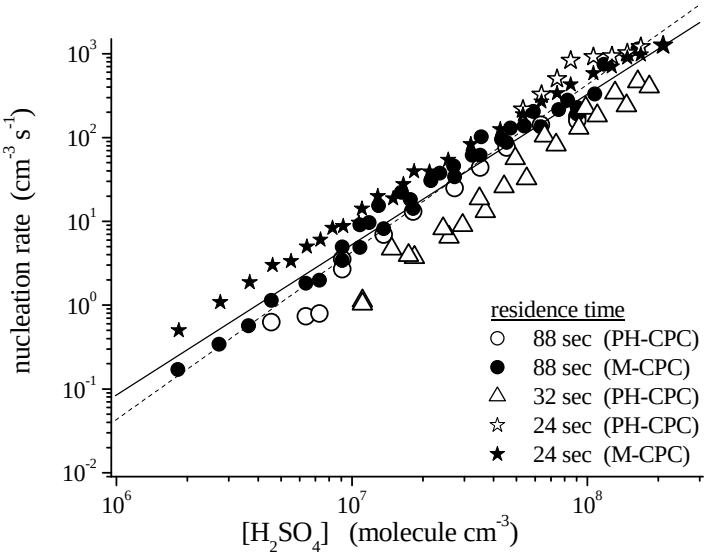

Fig.1. Nucleation rates as a function of sulphuric acid concentration for different residence times, r.h. = 22%.

For a residence time of 88 sec the relative humidity was varied in the range 22 - 61 %. With increasing r.h. there was a distinct increase of particle formation measureable. The overall best fit according to the power equation

$$\mathbf{N = k\ (\ [H_2SO_4]/molecule\ cm^{-3}\ )^{\alpha}\ (\ [H_2O]/\ 10^{15} molecule\ cm^{-3}\ )^{\beta}}$$

results in: $\alpha = 1.86$, $\beta = 3.08$, $k = 9.3 \cdot 10^{-18}$ $cm^{-3}s^{-1}$. It is to be noted, that the exponent for water vapour, $\beta = 3.08$, represents an upper limit caused by experimental difficulties for elevated r.h.
Measurements in the absence ($[NH_3] < 2.5 \cdot 10^9$ molecule cm^{-3}) and presence of ammonia ($[NH_3] = 1.2 \cdot 10^{12}$ molecule cm^{-3}) revealed that ammonia addition has generally a small effect on the nucleation rate. The enhancing effect is more pronounced for relatively dry conditions. A clear increase of particle diameter was observed in experiments with added ammonia.

REFERENCES

Berndt, T., O. Böge, F. Stratmann, J. Heintzenberg, and M. Kulmala (2005), *Science* 307, 698.
Kulmala, M., K. E. J. Lehtinen, and A. Laaksonen (2006), *Atmos. Chem. Phys.* 6, 787.
Sihto, S.-L. et al. (2006), *Atmos. Chem. Phys.* 6, 4079.
Sipilä, M. et al. (2008), *Atmos. Chem. Phys.* 8, 4049.
Weber, R. J., J. J. Marti, P. H. McMurry, F. L. Eisele, D. J. Tanner, and A. Jefferson (1996), *Chem. Eng. Comm.* **151**, 53.
Vanhanen, J. et al. (2009), presented at ICNAA 2009, Praque.

ASSESSING VAPOUR PRESSURE ESTIMATION METHODS AND THEIR IMPACT USING KNUDSEN EFFUSION MASS SPECTROMETRY (KEMS)

A.M. BOOTH[1], M.H. BARLEY[1], D.O. TOPPING[1], G.B. MCFIGGANS[1] and C.J. PERCIVAL[1]

[1]Centre for Atmospheric Science, SEAES, University of Manchester, M13 9PL, Manchester, U.K.

Keywords: VAPOUR PRESSURE, PARTITIONING,

INTRODUCTION

Knowledge of pure component vapour pressures is essential for calculations of gas/particle partitioning. There are many methods of estimating vapour pressures but most of the experimental data collected to date has been for intermediate or high pressure compounds (and often measured at temperatures considerably above ambient) and the proportion of experimental data for low (less than 100Pa) vapour pressure compounds has been very small. Hence the datasets used for developing the estimation methods have reflected this bias in addition to the fact that components studied tend to have one or two functional groups at the most. Hence it is unsurprising that some of the estimation methods can give errors in vapour pressure of several orders of magnitude for multifunctional compounds at ambient temperatures.

METHODS

Knudsen Effusion Mass Spectrometer (KEMS) has been used to measure solid state vapour pressures for dicarboxylic acids (Booth *et al* 2009 (i)) and substituted dicarboxylic acids. In the atmosphere these compounds are likely to exist in the sub-cooled state so Differential Scanning Calorimetry (DSC) was used to obtain thermochemical data (Table 1) to effect the Prausnitz (ref) correction between solid and sub-cooled vapour pressures (Booth *et al* 2009 (ii)).

Table 1. Thermochemical data for dicarboxylic acids.

Acid	Solid State P_{298K} (Pa)	Sub-Cooled P_{298K} (Pa)	T_m (K)	ΔH_{fus} ($kJ.mol^{-1}$)	ΔS_{fus} ($J.mol^{-1}.K^{-1}$)
Malonic	5.73×10^{-4}	3.19×10^{-3}	406	18.7	46.2
Succinic	1.13×10^{-4}	3.86×10^{-3}	458	31.3	68.3
Glutaric	4.21×10^{-4}	1.96×10^{-3}	369	22.0	59.7
Adipic	6.00×10^{-6}	2.14×10^{-4}	423	35.9	84.9

Experimental sub-cooled vapour pressures were compared with two estimation methods (Table 2), identified by Bareley *et al* (2009) as providing the best results for atmospheric compounds; Myrdal and Yalkowsky (1997) vapour pressure curves combined with Stein and Brown (1994) boiling points, and Nannoolal (2008) vapour pressures curves and boiling points. Both methods significantly over-estimate the vapour pressure by one, and in some cases, two orders of magnitude.

Table 2. Estimated vapour pressures and normal boiling points.

Acid	Nannoolal T_b (K)	Nannoolal P_{298K} (Pa)	Stein and Brown T_b (K)	Myrdal and Yalkowsky P_{298K} (Pa)
Malonic	544.6	1.73×10^{-1}	537.3	3.46×10^{-1}
Succinic	559.4	4.71×10^{-2}	553.6	1.50×10^{-1}
Glutaric	573.8	1.30×10^{-2}	570.0	6.51×10^{-2}
Adipic	587.9	3.66×10^{-3}	583.5	2.86×10^{-2}

In order to asses the impact of these vapour pressures on organic aerosol (OA) formation, the partitioning calculation of Barley and McFiggans (2009); Barley *et al.* (2009) was used with each of the C_3–C_6 dicarboxylic acids as part of the ensemble of 45 condensing species which includes glutaric acid. Data for glutaric acid was replaced with data for each diacid in turn. The base case for each diacid used the sub-cooled liquid vapour pressure derived from the KEMS with the abundance of all 45 components set to a value which gave 10.6 µgram.m-3 of OA. Figure 1 shows the effect of substituting alternative vapour pressure values for each diacid on the predicted OA yield. There is a large discrepancy between the KEMS data and that of Riipinen et al. (2007) at Malonic acid (2 µgram.m^{-3}) the difference in OA yield decreases as the chain length increases, reflecting the closure of our vapour pressure values. In spite of the differences in vapour pressures the two estimation methods give a predicted yield within 0.5 µgram.m^{-3} for Malonic and Succinic. This rapidly increases however to a massive 3.5 µgram.m^{-3} difference for Adipic acid, representing a significant under prediction in aerosol mass and far more significant than the difference between the experimental results

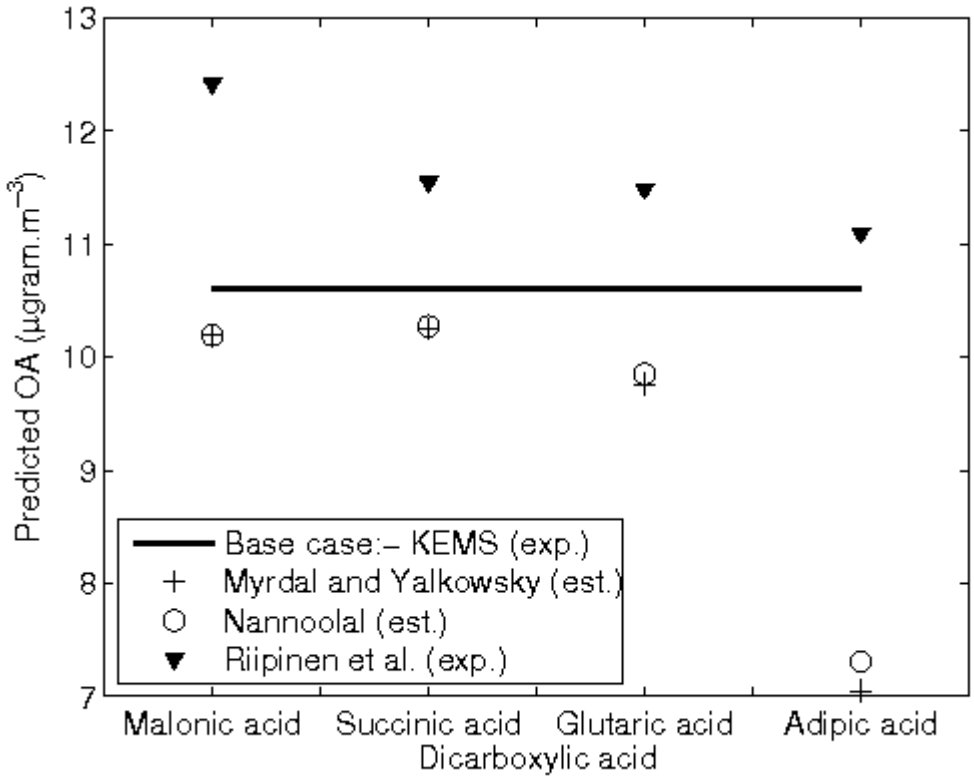

Figure 1. Predicted Organic Aerosol (OA) yield for dicarboxylic acids condensing as part of an ensemble of 45 atmospheric compounds.

CONCLUSIONS

The work shows that with the Prausnitz et al. (1986) correction and DSC obtained thermochemical data it is possible and practical to obtain sub-cooled liquid vapour pressures using Knudsen Effusion Mass Spectrometry. Two of the best estimation methods available have been shown to be in error by orders of magnitude. In partitioning calculations this can result in significant underprediction of OA yields for some compounds. This illustrates the necessity of obtaining more data for low vapour pressure compounds to provide a larger dataset to tailor parameters in group contribution methods.

ACKNOWLEDGEMENTS

This work was supported by NERC under grant NE/E018181/1. We also thank Ilona Riipinen and Merete Bilde for helpful discussions on sub-cooled corrections of vapour pressure.

REFERENCES

Barley, M.H. and McFiggans, G. (2009), The critical assessment of vapour pressure estimation methods for use in modelling the formation of atmospheric organic aerosol, Atmospheric Chemistry and Physics Discussion, 9:18375-18416.

Barley, M.H., Topping, D. O., Jenkin, M.E. and McFiggans, G. (2009), Sensitivities of the absorptive partitioning model of secondary organic aerosol formation to the inclusion of water, Atmospheric Chemistry and Physics, 9:2919-2932.

Booth, A. M., Markus, T., McFiggans, G., Percival, C. J., Mcgillen, M. R. and Topping, D. O. (2009), Design and construction of a simple Knudsen Effusion Mass Spectrometer (KEMS) system for vapour pressure measurements of low volatility organics, Atmospheric Measurement Techniques, 2:355-361.

Booth, A. M., Topping, D. O., McFiggans, G., and Percival, C. J. (2009), Subcooled-liquid vapour pressures of dicarboxylic acids from Knudsen Effusion Mass spectrometry combined with Differential Scanning Calorimetry, Journal of Aerosol Science and Technology, submitted.

Myrdal, P.B. and Yalkowsky, S.H. (1997), Estimating pure component vapour pressures of complex organic molecules, Industrial & Engineering Chemical Research, 36:2494-2499.

Nannoolal, Y., Rarey, J. and Ramjugernath, D. (2008), Part 3. Estimation of the vapor pressure of non-electrolyte organic compounds via group contributions and group interactions, Fluid Phase Equilibria, 269:117-133.

Prausnitz, J.M., Lichtenhaler, R.N. and Azevedo, E.G. de. (1986), Molecular Thermodynamics of Fluid-phase Equilibria, Prentice-Hall Inc, New Jersey,

Riipinen, I., Koponen, I., Frank. G., Hyv'arinen, A-P., Vanhanen, J., Lihavaninen, H., Lehtinen, K., Bilde, M. and Kulmala, M. (2007), Adipic and Malonic Acid Aqueous Solutions: Surface Tensions and Saturation Vapor Pressures, Journal of Physical Chemistry, 111:12995-13002.

Stein, S. E. and Brown, R. L. (1994), Estimation of normal boiling points from group contributions, Journal of Chemical Information and Computer Science, 34,581:587.

NEW PARTICLES FORMATION AND ULTRAFINE AEROSOL CLIMATOLOGY AT A HIGH ALPIN SITE (JUNGFRAUJOCH, 3580m a.s.l.)

J. Boulon[1], H. Venzac[1 *], D. Picard[1], E. Weingartner[2], K. Sellegri[1], P. Laj[3]

[1] Laboratoire de Météorologie Physique CNRS UMR 6016, Observatoire de Physique du Globe de Clermont-Ferrand, Université Blaise Pascal, France.

[2] Paul Scherrer Institute, Villigen PSI, Switzerland.

[3] Laboratoire de Glaciologie et Géophysique de l'Environnement CNRS UMR 5183, Observatoire des Sciences de l'Univers de Grenoble, Université Joseph Fourier, France.

Keywords : New particles formation, NAIS, high altitude, air mass origin, free troposphere.

INTRODUCTION

Number size distributions of particles and ions were measured on a continuous basis during an extended field campaign at a high alpine site (Jungfraujoch, 3580 m a.s.l., Switzerland). Those measurements were performed within EUCAARI program.
High altitude sites allowed long term studies of long range transport and free tropospheric aerosol background. We report aerosol number size distribution related to the air mass origin and new particle formation events analysis over a ten month field experiment (from July 2008 to May 2009).

METHODS

The Sphinx laboratory is located on the southern side of the Jungfraujoch at 3450m a.s.l. (46°32'51" N, 7°59'6" E), 100m below the main crest of the Bernese Alps, Switzerland. Within a horizontal distance of 150m, at the top of the crest (3580m a.s.l.), a station of the Swiss National Monitoring Network for Air Pollution (NABEL) is installed. It measures thirty minute averaged concentrations of NO, NO_2, NO_x and O_3, and daily averaged concentrations of SO_2, aerosol sulfur, and particulate matter with aerodynamic diameter below 10μm (PM10).
Ion and particle number size distributions and concentrations were measured by a Neutral cluster Air Ion Spectrometer (NAIS, Mirme *et al.* (2007), Asmi *et al.* (2009)) in diameter range [0.55nm :49.7nm]. Free tropospheric background (FTB) data are restricted from 0000 to 0800 local time in order to avoid eventual peaks of pollutant concentration due to upslope wind from the valley (Bodhaine *et al.*, 1983). The variability of the FTB and NPF according to the air mass origin is also investigated by the calculation of back-trajectories over a three-day period using the HYSPLIT transport and dispersion model (Draxler and Rolph, 2003).

RESULTS

New particle formation events and parameters (growth rate, formation rate and condensational sink) are presented. The median formation rates of 2nm total and charged particles were 0.25 $cm^{-3}.s^{-1}$ and 0.03 $cm^{-3}.s^{-1}$. The median growth rates of particles in size classes 1.3-3, 3-7 and 7-20 were 5.7, 3.6 and 5.7 $nm.h^{-1}$ respectively. NPF events are classified according to the method proposed by Hirsikko *et al.* (2005). Frequencies of NPF events show a strong dependance with

∗. Now at Weather Measures, Aubière, France.

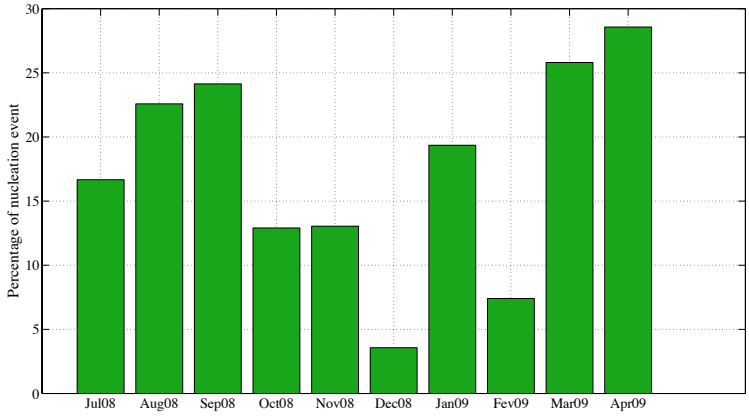

FIGURE 1 – Monthly statistics of nucleation events.

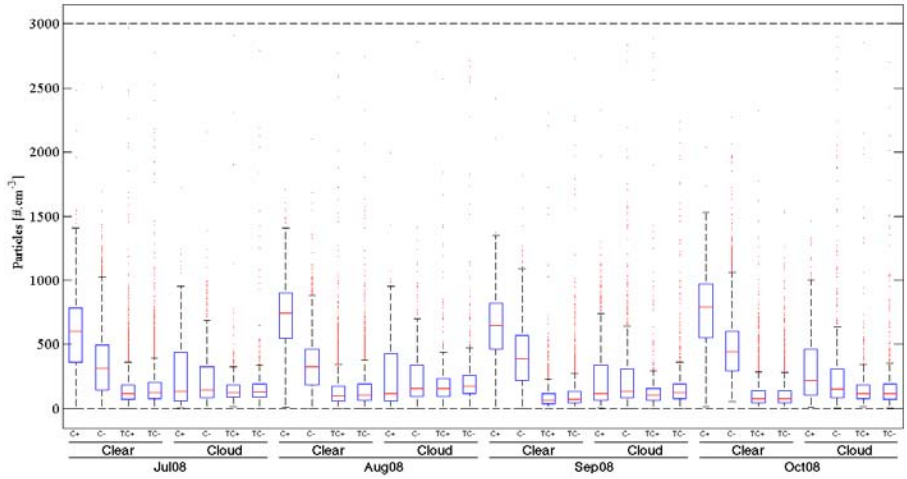

FIGURE 2 – Cloud effect on charged particles. *C+/C- are used for positive/negative clusters and TC+/TC- are used for positive/negative Total ions - Cluster.*

seasons, between 20% and 30% of observed days during summer and spring and less than 15% during autumn and winter present a NPF event (Fig. 1). NPF are negatively correlated with the presence of clouds as reported by Venzac *et al.* (2007) at the Puy de Dôme research station, and may be resulting by scavenging of aerosol precursor. The presence of a cloud provokes a diminution in cluster concentration by a factor 2 to 4 and an increase of intermediate particles and by this way, a modification of the free troposheric aerosol distribution (Fig. 2). This phenomenon was also observed by Venzac *et al.* (2007) at Puy de Dôme. Air mass effects will be also presented.

ACKNOWLEDGEMENTS

We thank organizers of the EUCAARI 2008 campaign at Jungfraujoch and all the researchers, technical staff and students who took part in performing the field measurements used in this study. This work has been partially funded by European Commission 6th Framework program project EUCAARI, contract n°036833-2 (EUCAARI). We thank also the NABEL network for providing gases data and MeteoSwiss for meteorological data at Jungfraujoch.

REFERENCES

Asmi, E., Sipilä, M., Manninen, H.E., Vanhanen, J., Lehtipalo, K., Gagné, S., Neitola, K., Mirme, A., Mirme, S., Tamm, E., Uin, J., Komsaare, K., Attoui, M. and Kulmala, M., 2009. Results of the first air ion spectrometer calibration and intercomparison workshop. *Atmospheric Chemistry and Physics*, **9**, 141–154.

Bodhaine, B.A., 1983. Aerosol measurements at four background sites. *Journal of Geophysical Research*, **88**, 10753–1768.

Draxler, R. R. and Rolph, G. D. (2003). HYSPLIT (Hybrid Single-Particle Langrangian Integrated Trajectory) Model access via NOAA ARL READY website (`http://www.arl.noaa.gov/ready/hysplit4.html`), NOAA Air Resources Laboratory, Silver Spring, MD.

Hirsikko, A., Laakso, L., Hõrrak, U., Aalto, P. P., Kerminen, V.-M. and Kulmala, M. (2005). Annual and size dependent variation of growth rates and ion concentrations in boreal forest. *Boreal Environment Research*, **10**, 357–369.

Mirme, A., Tamm, A., Mordas, G., Vana, M., Uin, J., Mirme, S., Bernotas, T., Laakso, L., Hirsikko, A. and Kulmala, M. , 2007. A wide range multi-channel Air Ion Spectrometer. *Boreal Environment Research*, **12**, 247–264.

Venzac, H., Sellegri, K., Laj, P., 2007 Nucleation events detected at the high altitude site of the Puy de Dôme research station, France. *Boreal Environment Research*, **12**, 345–359.

LONG-TERM COMPARISON OF SULPHURIC ACID, OH AND OTHER COMPOUNDS WITH SOA FORMATION

M. BOY[1], A. SOGACHEV[2], S. SMOLANDER[1], L. ZHOU[1], A. GUENTHER[3] and M. KULMALA[1]

[1]Department of Physics, University of Helsinki, Box 48, 00014 Helsinki, Finland.

[2]Wind Energy Department, Technical University of Denmark, Box 49, Denmark.

[2]ACD/NCAR, Box 3000, 80305 Boulder, Colorado, USA.

Keywords: SOA, Modelling, PBL, Atmospheric Chemistry.

INTRODUCTION

New particle formation has been observed at almost all sites, where both particle number concentrations and size distributions have been measured. Although many field campaigns, laboratory experiments and new modelling approaches have led to increased understanding, detailed mechanisms responsible for the formation of new particles in the troposphere have still not been completely elucidated.

In SOSA (model to simulate the concentrations of organic vapours and sulphuric acid) individually developed codes merged into a one-dimensional model including boundary layer meteorology, biology and chemistry in order to investigate the correlation between different compounds of interest and Secondary Organic Aerosols (SOA). Our knowledge concerning the formation of very small particles or clusters is still limited and the question of which molecules are involved in the atmospheric nucleation processes remains controversial within the aerosol community.

METHODS

SOSA was developed during the last 10 month at the University of Helsinki based on sulphuric acid closure (Boy et al., 2005). The meteorology is based on a 1-D version of the model SCADIS (Sogachev et al., 2002, Sogachev and Panferov, 2006). It is a parallelized model operating on the high-performance supercluster Murska at the CSC - IT Center for Science in Finland, which gives the possibility to run detailed processes in chemistry, meteorology and aerosol dynamic (not operational at this time) within reasonable time. The model uses meteorological, and various other input data (inorganic gas concentrations, aerosol properties and radiation data) measured at the SMEAR II (Station for Measuring Ecosystem Atmosphere Relations) in Hyytiälä, Finland as input to minimize the uncertainty in the simulated variables. The vertical resolution of the model is up to 3 km in 75 levels increasing exponentially from the ground to the model top which provides very detailed information about fluxes inside and above the canopy. Due to the parallelization and the runtime-saving coding, the model only requires 10 hours at the supercluster Murska for a one year simulation with high vertical and temporal resolution which would not be applicable in regional or global models.

SOSA use the Model for Emissions of Gases and Aerosols in Nature (MEGAN, Guenther et al., 2006) to simulate the emission of organic vapours from the biosphere. The gas phase chemistry is solved with the Kinetic PreProcessor (Damian, 2002, and http://people.cs.vt.edu/~asandu/Software/Kpp/) in combination with the Master Chemical Mechanism (MCM, http://mcm.leeds.ac.uk/MCM/) from the University of Leeds.

RESULTS

Hamid and co-workers (2009) observed a decrease in the emissions of sulphur dioxide in Europe during the last decade (Hamid et al., 2009) and a related decrease in nucleation rates for the research station Melpitz, Germany. We will present first results from a long-term comparison (2003-2008) of certain selected simulated compounds like e.g. sulphuric acid and hydroxyl radicals against measured parameters characteristic for the formation of secondary organic aerosols at the SMEAR II in Hyyitälä, Finland. This comparison will show if there is a possibility for different SOA formation mechanisms in rural and more anthropogenic influenced environments.

ACKNOWLEDGEMENTS

This work was supported by the Academy of Finland, the Helsinki University Centre for Environment and the Mai ja Tor Nessling Foundation.

REFERENCES

Boy, M., Kulmala, M., Ruuskanen, T.M., Pihlatie, M., Reisell, A., Aalto, P.P., Keronen, P., Dal Maso, M., Hellen, H., Hakola, H., Jansson, R., Hanke, M., and Arnold, F. 2005. Sulphuric acid closure and contribution to nucleation mode particle growth. *Atmos. Chem. Phys*., **5**, 863-878.

Damian, V., Sandu, A., Damian, M., Potra, F., & Carmichael, G. R. (2002). The Kinetic PreProcessor KPP -- A software environment for solving chemical kinetics. *Computers and Chemica Engineering , 26* (11), 1567-1579.

Guenther, A., Karl, T., Harley, C. W., Palmer, P., & Geron, C. (2006). Estimates of global terrestrial isoprene emissions using MEGAN (Model of Emissions of Gases and Aerosols from Nature). *Atmos. Chem. Phys., 6*, 3181-3210.

Hamed, A., Birmili, W., Joutsensaari, J., Mikkonen, S. Asmi, A., Wehner, B., Spindler, G. Jaatinen, A., Uhse, K., Wiedensohler, A., Lehtinen, K.E.J. and Laaksonen, A.: Changes in the production rate of secondary aerosol particles in central Europe in view of decreasing SO2 emissions between 1996 and 2006, *Atmos. Chem. Phys. Discuss.*, 9, 15083-15123, 2009.

Sogachev, A., & Panferov, O. (2006). Modification of two-equation models to account for plant drag. *Boundary Layer Meteorology , 121*, 229-266.

Sogachev, A., Menzhulin, G. V., Heimann, M., & Lloyd, J. (2002). A simple three-dimensional canopy - planetary boundary layer simulation model for scalar concentrations and fluxes. *Tellus B , 54* (5), 784-819.

Airborne in-situ measurements of physical and chemical aerosol properties during EUCAARI/IMPACT (May 2008)

S. CRUMEYROLLE[1], A. SCHWARZENBOECK[1], R. WEIGEL[1,2], L. GOMES[3], K. SELLEGRI[1], H. MANNINEN[4], G.C. ROBERTS[3] and P. LAJ[5]

[1] Laboratoire de Météorologie-Physique, University of Clermont-Ferrand, France
[2]Institute for Physics of the Atmosphere, University of Mainz, German
[3] CNRS Metéo-France/CNRM/GMEI/MNPCA, Toulouse, France.
[4] University of Helsinky, Finland.
[5]Laboratoire de Glaciologie et Geophysique de l'Environnement, University of Grenoble, France

Keywords: Airborne aerosol measurement, aerosol chemical composition, aerosol size distribution, aerosol particle formation, boundary layer, free troposphere.

INTRODUCTION

Aerosol particle properties were measured during the intensive airborne measurement campaign IMPACT that took place in May 2008 in the Netherlands within the framework of EUCAARI. Measurements on board the French research aircraft ATR-42 involved particle sizing and counting by scanning mobility particle spectrometers SMPS ($20 < Dp < 300$nm), optical particle counters OPC (GRIMM model 1.108, $0.3 < Dp < 2\mu$m), and different condensation particle counters CPC ($Dp>3$nm, $Dp> 10$nm). Particles were introduced into the system through an isokinetic aerosol inlet. Chemical aerosol particle properties have been measured by the aerosol mass spectrometer AMS. During cloudy conditions, cloud residual and interstitial particles were analysed using a counterflow virtual impactor CVI and an interstitial aerosol inlet, respectively. The first objective of the present study is to discuss observations of nucleation mode particles observed with the ATR-42 over the region of Rotterdam and related to events of new particle formation (NPF). The study provides information on the vertical and horizontal extent of the new particle formation phenomenon with good quantitative resolution of ultra-fine particle concentrations. The second more general objective of this study is to show the mean physical and chemical properties of particles sampled during the whole EUCAARI project as a function of the air mass origins and the atmospheric layer sampled by the ATR-42.

RESULTS

New particle formation events :

Considerable amounts of nucleation mode particles, thus related to what we call new particle formation NPF, have been observed during 11 flights (out of 22). The NPF observations could be associated to different types of research flights. Most of the time when NPF has been observed on the aircraft, simultaneously the phenomenon has been observed at the CESAR supersite (Cabauw). As a consequence the new particle formation has not been limited to a local small scale nucleation source, but should have been a spatially widespread phenomenon. Only 1 case (May 29th 2008) is showing a decoupling of the nucleation mode particle observations comparing the Cabauw ground site measurements with aircraft observations. The NPF event is observed with on board instruments over a region of 150km east from CBW.

The measurement results show that nucleation mode particle observations and thus particle production occurrs under the influence of different air mass origins, at different times of the day and over the North Sea as well as over the continent. The ultra-fine particle concentrations varied between 5000 and 75000 part.cm^{-3}. Furthermore, the results highlight that NPF observations were solely detected within the planetary boundary layer. The vertical extension for all nucleation events observed on the ATR-42 never exceeded the top of the planetary boundary layer. The horizontal extent of small particles (in the size range 3-10 μm) could not be delimited due to inflexible flight plans, however, the order of magnitude most of the time reached 100 km and beyond.

Mean physical and chemical properties of aerosol particles :
The air masses study was done using Flexpart results (Sthol et al., 1998) at each position of the ATR-42 of the twenty flights performed during the Eucaari project. Furthermore, the physical and chemical properties of particles were used to improve the first air mass sorting in different groups. About twenty different air mass groups have been identified. Then, the aerosol size distribution and chemical composition have been averaged as a function of air mass origins and as a function of the atmospheric layer (boundary layer to free troposphere) covered by the ATR-42 flight plans, where out of cloud aerosol particles have been analysed. The background size distribution of aerosol particles will be described as well as the chemical composition of each particle. Two cases highlight cloud processing impact, presence of bimodal size distribution of particles, correlate with high concentration of soluble materials (Sulfate, Nitrate…). Few biomass burning events occurred in the eastern part of Europe and were illustrated with high concentration of small particles and high content of non soluble component. At the end of the Eucaari aircraft campaign, the mean diameter of the main particle mode shift from 80nm to 200nm showing evidence of long range transport of desert dust from North Africa to the Netherlands.

ACKNOWLEDGEMENTS

We are thankful to SAFIRE co-workers and the ATR-42 crew. This work was supported by the European Integrated project on Aerosol Cloud Climate and Air Quality Interactions (EUCAARI, N^{o} 036833-2) - a project within EU sixth framework program.

REFERENCES

Stohl, A., Hittenberger, M., and Wotawa, G.: Validation of the Lagrangian particle dispersion model FLEXPART against large scale tracer experiment data, Atmos. Environ., 24, 4245–4264, 1998.Chapman, D.H. (1975). Optical scattering from combustion aerosols, *J. Aerosol Sci.* 36, 3456.

AEROSOL PROPERTIES ASSOCIATED WITH AIR MASSES ARRIVING INTO THE NORTH EAST ATLANTIC DURING THE 2008 MACE HEAD EUCAARI INTENSIVE OBSERVING PERIOD: AN OVERVIEW

M. DALL'OSTO[1], D. CEBURNIS[1], G. MARTUCCI, J. BIALEK[1], R. DUPUY[1], S.G. JENNINGS[1], H. BERRESHEIM[1], J. WENGER[2], R. HEALY[2], M. C. FACCHINI[3], M. RINALDI[3], L. GIULIANELLI[3], E. FINESSI[3], D. WORSNOP[4,5] AND C.D O'DOWD[1*]

[1] School of Physics & Centre for Climate & Air Pollution Studies, Environmental Change Institute, National University of Ireland, Galway, Ireland
[2]Department of Chemistry, University College Cork, Cork. Irelamd
[3] Istituto di Scienze dell'Atmosfera e del Clima Via Gobetti 101, 40129 Bologna, Italy
[4]Aerodyne Inc., Boston, USA,
[5]Department of Physical Sciences, University of Helsinki, Helsinki, Finland.

Keywords: MACE HEAD, MARINE AEROSOL, AEROSOL CHEMISTRY.

INTRODUCTION

As part of the EUCAARI Intensive Observing Period, a 4-week campaign to measure aerosol physical, chemical and optical properties, atmospheric structure, and cloud microphysics was conducted from mid-May to mid-June, 2008 at the Mace Head Atmospheric Research Station, located at the interface of Western Europe and the N.E. Atlantic and centered on the west Irish coastline.

METHODS

During the campaign, continental air masses comprising both young and aged continental plumes were encountered, along with polar, Arctic and tropical air masses. Polluted-continental aerosol concentrations were of the order of 3000 cm^{-3}, while background marine air aerosol concentrations were between 400-600 cm^{-3}. The highest marine air concentrations occurred in polar air masses in which a 15 nm nucleation mode, with concentration of 1100 cm^{-3}, was observed and attributed to open ocean particle formation. Black carbon concentrations in polluted air were between 300-400 ng m^{-3}, and in clean marine air were less than 50 ng m^{-3}. Continental air submicron chemical composition (excluding refractory sea salt) was dominated by organic matter, closely followed by sulphate mass. Although the concentrations and size distribution spectral shape were almost identical for the young and aged continental cases, hygroscopic growth factors (GF) and cloud condensation nuclei (CCN) to total condensation nuclei (CN) concentration ratios were significantly less in the younger pollution plume, indicating a more oxidized organic component to the aged continental plume. The difference in chemical composition and hygroscopic growth factor appear to result in a 40-50% impact on aerosol scattering coefficients and Aerosol Optical Depth, despite almost identical aerosol microphysical properties in both cases, with the higher values been recorded for the more aged case. For the CCN/CN ratio, the highest ratios were seen in the more age plume. In marine air, sulphate mass dominated the sub-micron component, followed by water soluble organic carbon, which, in turn, was dominated by methanesulphonic acid (MSA). Sulphate concentrations were highest in marine tropical air – even higher than in continental air. MSA was present at twice the concentrations of previously-reported concentrations at the same location and the same season. Both continental and marine air exhibited aerosol GFs significantly less than ammonium sulphate and even less in terms of sea salt aerosol pointing to a significant organic contribution to all air mass aerosol properties.

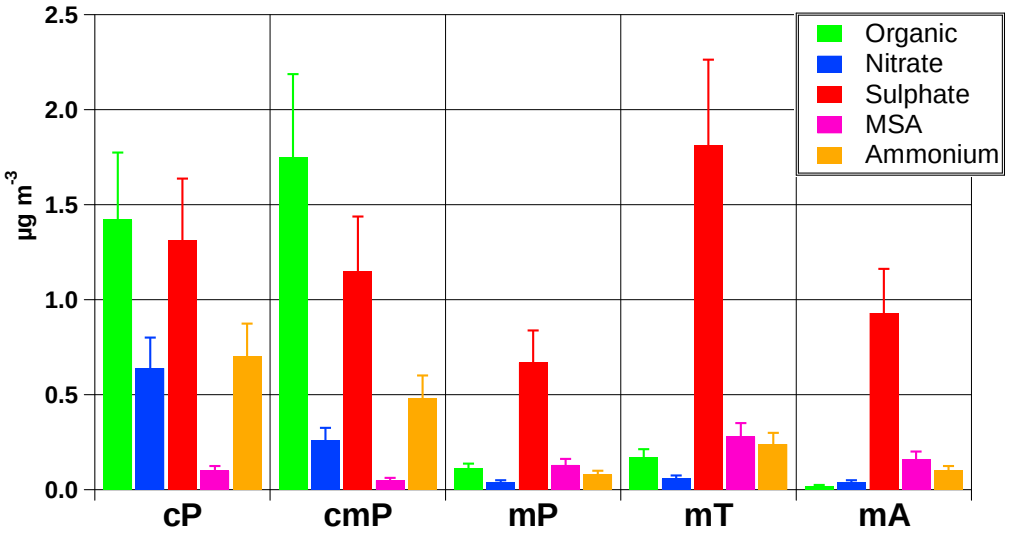

Figure 1: AMS-derived organic, nitrate, sulphate, MSA, and ammonium mass as a function of air mass: Continental Polar (*cP*); Continental Marine Polar (*cmP*); Marine Polar (*mP*); Marine Tropical (*mT*); and Marine Arctic (*mA*)..

CONCLUSIONS

Anthropogenic air advecting out of Europe and into the N.E. Atlantic comprises aerosol concentrations of the order of 3000 cm^{-3} and a size distribution mode of the order of 60 nm. By comparison, marine air entering into Europe via latitudes of 54N, whether tropical, polar or Arctic, exhibit concentrations of the order of 400-600 cm^{-3}, but with concentrations as high as 1100 cm^{-3} occurring in polar air. All marine air size distributions display clear bimodality with an Aitken and accumulation mode. Polar air also exhibited a recently-formed nucleation mode at ~15 nm, indicative of an open ocean source of new particles. The highest organic matter loadings occurred in the two continental cases and dominate submicron mass loadings in both cases. Sulphate contributed less than organics in polluted air, but more so than nitrate. MSA contributed the dominant water soluble organic fraction in marine air masses and contributed up to 30% of the aerosol mass at certain sizes. Water insoluble organic mass contributed significantly less to submicron aerosol mass than previously report, while the MSA fraction was at least double than previously reported (Yoon et al., 2007). All air masses exhibited hygroscopic GFs significantly less than ammonium sulphate and even more so than sea salt. The GF-PDF peaks at 1.35 – 1.4 for the two continental cases and 1.45-1.5 for the marine cases. In both categories, GFs do not reflect GFs for ammonium sulphate and sea salt suggesting significant organic enrichment or coating around inorganic cores.

ACKNOWLEDGEMENTS

This work was funded by the European Commission Framework Programme 6 EUCAARI Integrated Project, Ireland Higher Education Authority Programme for Research in Third Level Institutes – Cycle 5, and the Irish Environmental Protection Agency. NOAA Hysplit and MODIS Ocean Colour website are also acknowledged for providing air mass back trajectories and Chlorophyll map.

REFERENCES

Yoon, Y. J., Ceburnis, D., Cavalli, F., Jourdan, O., Putaud, J. P., Facchini, M. C., Decesari, S. Fuzzi, S., Sellegri, K., Jennings, S. G. and O'Dowd, C. D. , (2007) Seasonal characteristics of the physico-chemical properties of North Atlantic marine atmospheric aerosols. J. Geophys. Res., 112, D04206, doi:10.1029/2005JD007044.

ORGANIC SOURCE APPORTIONMENT BY NMR SPECTROSCOPY DURING THE EUCAARI INTENSIVE FIELD EXPERIMENTS

Stefano Decesari[1], Maria Cristina Facchini[1], Emanuela Finessi[1], Lara Giulianelli[1], Sanna Katriina Saarikoski[2], Samara Carbone[2], Risto Hillamo[2], Doug Wornsop[3], Erik Swietlicki[4]

[1]CNR, Inst. Atmospheric Sciences and Climate, via Gobetti 101, I-40129, Bologna, Italy
[2]Finnish Meteorological Institute, Air Quality Research, P.O. Box 503, FI-00101 Helsinki, Finland
[3]Aerodyne Research, Inc. 45 Manning Rd, Billerica, MA 01821, USA
[4]Dept. of Physics, Lund University, S-221 00 Lund, Sweden

Keywords: organic aerosol, source apportionment, NMR, AMS, PMF, Po Valley.

INTRODUCTION

Despite the recent great advancements in the aerosol measurement technologies, a satisfactory methodology providing both composition and source contributions to the aerosol organic fraction is still elusive. The EUCAARI intensive field experiments provided a unique opportunity to attempt organic source apportionment exploiting a set of complementary techniques, such as molecular tracer analysis, isotopic methods, aerosol mass spectrometry (AMS) and other spectroscopic techniques, which differ with respect to sensitivity, recovery and resolution and specificity to distinct classes of organic compounds. We have developed the original concept of using nuclear magnetic resonance (NMR) spectroscopy for *source attribution* of oxidized organic aerosols (OOA) (Decesari et al., 2007) into an actual organic *source apportionment* method.

METHODS

Proton (^{1}H)-NMR spectroscopy was employed for the off-line analysis of fine (PM1 or PM2.5) aerosol samples collected during the following field experiments: Hyytiälä April 2007, San Pietro Capofiume April 2008, Mace Head May 2008, Cabauw May 2008, K-Puszta June 2008, Melpitz May 2008, San Pietro Capofiume July 2009. AMS measurements were performed during all these experiments and the filter samples for off-line chemical analysis were also distributed to other EUCAARI partners involved in the organic source apportionment exercise.
A new methodology (paper in preparation) was employed for the multivariate statistical analysis of sets of ^{1}H-NMR spectra. The analysis is based on positive matrix factorization (PMF) techniques and on other chemometric methods.

RESULTS AND DISCUSSION

Factor analysis and classification methods (e.g., dendrograms) applied to the whole set of ^{1}H-NMR spectra tend to attribute the samples from the remote sites (Hyytiälä and Mace Head) to distinct groups, while the spectroscopic features for the polluted rural sites show a larger degree of overlap, in agreement with the previous findings based on the functional group distributions (Decesari et al., 2007). For the 2008 San Pietro Capofiume field experiment, we compared the PMF factors emerging from the ^{1}H-NMR analysis with those provided by simultaneous measurements with a HR-Tof-AMS (Ulbrich et al., 2009). To this aim, we averaged the AMS PMF factors over the sampling times of the filters used for ^{1}H-NMR analysis. Results are shown in Figure 1. The organic mass apportioned by NMR corresponds to the water-soluble fraction and can be compared to the oxidized organic fraction determined by AMS, *not* to the hydrocarbon-like compounds (HOA). Clearly, the two techniques based on completely independent methodologies provide the same split between “biomass-burning organic compounds” and other oxidized organics. For both AMS and NMR, the attribution of a factor to biomass burning sources is justified by the occurrence of the peaks of levoglucosan in the profile (spectrum). However, the identification of a specific

factor tracing biomass burning sources and the estimation of its loadings (contributions) in the samples is based not only on the detection of levoglucosan but on all the signals occurring in the spectra. In particular, ^{1}H-NMR analysis shows that the Po Valley samples impacted by biomass burning sources contain a large amount of aromatic compounds beside the polyols. Overall, AMS and ^{1}H-NMR provide a strikingly good agreement in the apportionment of aerosol organic mass to biomass burning sources during the 2008 San Pietro Capofiume experiment. PMF analysis of the ^{1}H-NMR spectra provides also other factors which account for the OOA determined by AMS. Among these, we identified a factor collecting the contribution of low-molecular weight amines, whose origin still needs to be clarified.

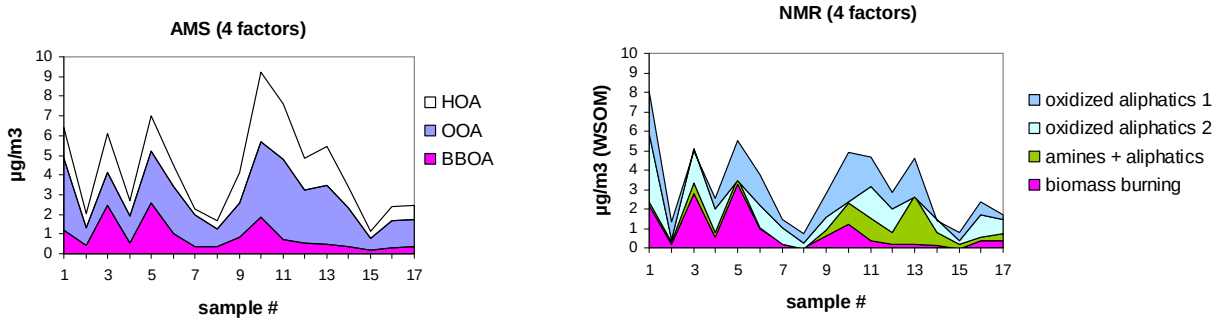

Figure 1. Results of factor analysis (PMF) applied to AMS measurements and to ^{1}H-NMR spectra from the 2008 EUCAARI field experiment in San Pietro Capofiume (Italy).

ACKNOWLEGMENTS

We acknowledge ARPA-Emilia-Romagna for hosting and supporting the field activities at the San Pietro Capofiume research station.

REFERENCES

Decesari, S., M. Mircea, F. Cavalli, S. Fuzzi, F. Moretti, E. Tagliavini, and M. C. Facchini (2007) Source attribution of water-soluble organic aerosol by nuclear magnetic resonance spectroscopy. Environ. Sci. Technol., 41, 2479 – 2484.

Ulbrich, I. M., Canagaratna, M. R., Zhang, Q.,Worsnop, D. R., and Jimenez, J. L. (2009) Interpretation of organic components from positive matrix factorization of aerosol mass spectrometric data. Atmos. Chem. Phys. 9, 2891 – 2918.

A NEW ATMOSPHERIC INTERFACE TIME-OF-FLIGHT MASS SPECTROMETER (API-TOF) TO MEASURE THE COMPOSITION OF SUB-2 NM MOLECULES AND CLUSTERS

M. EHN[1], H. JUNNINEN[1], K. NEITOLA[1], M. SIPILÄ[1], H. MANNINEN[1], T. PETÄJÄ[1], K. FUHRER[2], M. GONIN[2], U. ROHNER[2], S. GRAF[2], M. KULMALA[1], and D.R. WORSNOP[1,3]

[1] Department of Physics, University of Helsinki, P.O.Box 64, 00014, Helsinki, Finland
[2] Tofwerk AG, Switzerland
[3] Aerodyne Research Inc., Billerica, MA, USA

Keywords: Mass spectrometry, clusters, ions

INTRODUCTION

The lower size limit for aerosol particle detection has long been 3 nm. During recent years, new methods of detection and, also indirect composition measurements, have been presented (e.g. Kulmala *et al.*, 2007). Now, a new Atmospheric Pressure Interface Time-of-Flight mass spectrometer (API-TOF) is being developed at Tofwerk AG, Thun, Switzerland. This instrument will give new insight into particle chemical composition in the range 0-3000 Da, which corresponds roughly to a particle size range up to 2.5 nm in diameter. These are the sizes where atmospheric nucleation takes place, and is therefore of great interest.

MEASUREMENTS

The API-TOF has been tested both in the lab and in the field, with promising results. For the calibration and validation measurements, tetraheptyl ammonium bromide (THAB) was electrosprayed and mobility classified with a nano-DMA. The nano-DMA scanned the size range 1.0-2.5 nm, and the output was measured both by an electrometer and the API-TOF. A comparison of electrometer and API-TOF counts yielded transmission values up to 0.5%, meaning that we detect one out of every 200 ions entering the API-TOF.

Ambient positive and negative ion spectra were measured at the SMEAR II station in Hyytiälä, Finland in May 2009. Typical daytime negative ion spectra were dominated by sulfuric acid (97, 195, 293 Da) and it's clusters and SO_5^- (Fig. 1). At night the spectra (not shown) were dominated by nitric acid (63, 125 Da) and malonic acid (103, 207 Da) monomers and dimers, together with a malonic acid/nitric acid cluster (166 Da). There were also large amounts of molecules/clusters above 300 Da with distinct organic patterns.

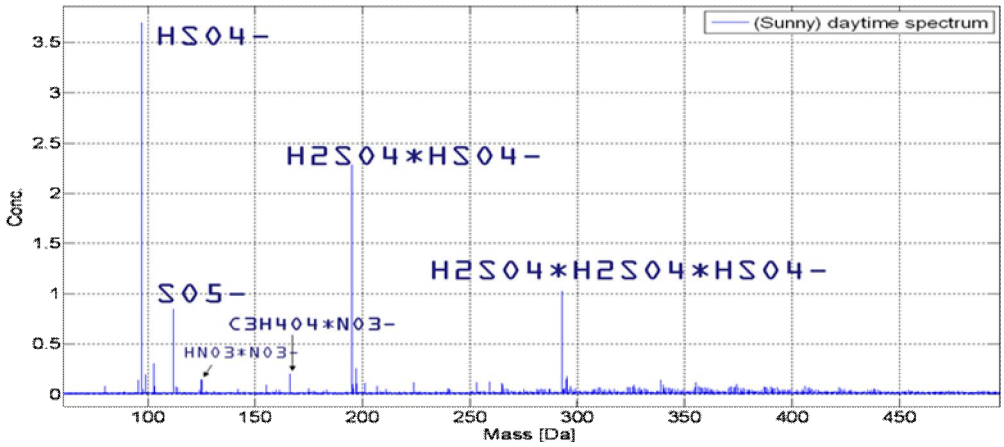

Figure 1. Typical negative ion mass spectrum during a sunny day in Hyytiälä.

FUTURE WORK

It has been shown that the API-TOF can successfully measure high resolution mass spectra even at ambient concentrations of a few hundred ions per cc. The following step is to develop ionization methods to allow charging of neutral molecules and clusters. This process can, however, destroy, produce, and/or modify the sample, and thus the charging methods need to be well characterized before one can select the optimal setup.

REFERENCES

Kulmala, M., Riipinen, I., Sipilä, M., Manninen, H. Petäjä, T., Junninen, H., Dal Maso, M., Mordas, G. Mirme, A., Vana, M., Hirsikko, A., Laakso, L., Harrison, R., Hanson, I., Leung, C., Lehtinen, K., Kerminen, V-M. (2007). *Science*, Vol. 318. No. 5847, pp. 89 - 92.

SATELLITE AND AIRCRAFT MEASUREMENTS OF AEROSOL IMPACTS ON VERTICAL CLOUD MICROPHYSICAL PROFILES DURING EUCAARI IOP OF MAY 2008

E. FREUD[1] and D. ROSENFELD[1]

[1]Institute for Earth Sciences, Department of Atmospheric Sciences, Hebrew University of Jerusalem, Givat Ram, Jerusalem, 91304, Israel.

Keywords: Cloud-Aerosol interactions

INTRODUCTION

During EUCARRI IOP over the Netherlands and adjacent sea, which lasted during the month of May 2008, 25 flights were conducted with the SAFIRE ATR-42 research aircraft, on which aerosol and cloud microphysics probes were mounted. Due to the lack of clouds during most of the IOP and the specific aims of the a/c missions, which concentrated mostly on aerosol and radiation measurements, only in 6 flights out of the 25 some cloud data was collected. From these 6 flights, we were able to construct 8 different (rather shallow) vertical profiles of cloud droplet properties that covered both pristine and polluted conditions.

We used the shape of the vertical evolution of the droplet size distribution in convective cloud elements (including in layer clouds) to parameterize the impacts of aerosols. Similar characterization was done by satellite retrieval of the vertical profiles of cloud top particle effective radius. These satellite inferences were validated by the aircraft measurements.

These results can be better appreciated when compared to our measurements, analyzed with similar methods, that were applied to deep convective clouds in other parts of the world (Andreae *et al.*, 2004; Freud *et al.*, 2008; Rosenfeld *et al.*, 2006 and 2008). Those clouds were sufficiently deep to reach the height of the onset of precipitation, thereby revealing the impacts of aerosols on the precipitation forming processes. The similarity of the EUCAARI dataset with the lower part of the vertical profiles of the deep clouds, allows us to extrapolate the impacts of aerosols in the EUCAARI clouds to the deeper clouds that were quite abundant according to the satellite observations over Western Europe, during parts of the observation period and put the EUCAARI observations it in a global perspective.

METHODS

To study the aerosol effects on the cloud microphysical properties, for the clouds sampled during EUCAAPI IOP, we apply analysis methods that we used in previous studies in other parts of the world in deeper clouds. For polar orbiting satellite retrieval of cloud top particle effective radius, we use the same method as is describe thoroughly by Lensky and Rosenfeld (1998). The validity of this method was reinforced after the launch of the geostationary EUMETSAT MSG. A special sequence of 3-minute rapid scans allowed to track with time the growing tops of individual convective cells and produce similar Temperature-Cloud top particle effective radius (henceforth T-Re) profiles as those produced from snapshots of the same scenes (Lensky and Rosenfeld, 2006). This principle of space-time exchangeability of the cloud temporal and evolutionary structure was also supported by aircraft *in-situ* measurements in the Amazon basin. Freud *et al.* (2008) showed that Re in convective clouds is highly dependent on aerosol properties and cloud depth, but much less on the mixing state of the convective cloud with dry ambient air. Therefore a T-Re profile produced from satellite analysis of cloud tops can represent the T-Re profile of one deep cloud, as long as it has not started precipitating substantially. A detailed description of the aircraft methods we use in searching and quantifying the aerosol effect on cloud vertical development and precipitation formation processes can be found in Rosenfeld et al. (2006 and 2008).

Each of the abovementioned studies may use different parameters to characterize the clouds and aerosols, in the search of their effects on the clouds of interest. Here we use five different parameters as

proxies for aerosols for coupling with the corresponding cloud profile. These are shown in table 1. The CCN counter was set to measure at a constant super-saturation of 0.2%, and the PCASP concentration is the total aerosol concentration integrated over the size range of 0.1 to 3μm. Both can give a first order estimation for the number of activated cloud droplets, which have the most important role in determining the rate of droplet growth as a function of cloud depth and are hence related to cloud radiative properties and precipitation forming processes. Correlation between the CCN or PCASP concentrations with measured cloud droplet concentration (mean or maximum) is far from perfect because coupling aerosol measurement just below the cloud base was not part of the flights' objectives in addition to very heterogeneous conditions in some cases due to stratified atmosphere and local pollution sources. Because the obtained PCASP and CCN values are not always representative for the profiled clouds, and because there are different types of clouds with potentially different mixing processes, we use here a new parameter which is not directly measured, namely: droplet adiabatic concentration normalized to cloud base air-density (in short: "$N_{adi\text{-}cb}$"). Similar parameter was first retrieved for satellite measurements of marine *Sc* by Bennartz (2007). Knowing the cloud base parameters (altitude, pressure and temperature) we can calculate the theoretical adiabatic water. Dividing the FSSP integrated liquid water content by the adiabatic water can derive the adiabatic fraction. If we assume that entrainment of dry ambient air into the cloud leads to rapid droplet evaporation at the edges of the cloud and to the quick saturation of the entrained air (*i.e.* inhomogeneous mixing), then further entrainment of the saturated air deeper into the cloud will only dilute so there will be a proportional reduction in droplet number concentration and LWC, or adiabatic fraction. In this case Re will not be strongly dependent on the adiabatic fraction, except for at the cloud edges where droplets evaporate. This assumption was found to be reasonable in this dataset as in other datasets from earlier studies (*e.g.* Freud *et al.*, 2008). Then to calculate the adiabatic droplet concentration for each measurement, one can just divide the measured droplet concentration by the adiabatic fraction. Normalizing this value to the air density at cloud base prevents the decreasing $N_{adi\text{-}cb}$ with altitude due to parcel expansion. Then we calculate the mean of the 1Hz $N_{adi\text{-}cb}$ values, only for measurements with adiabatic fraction larger than 0.5, to get a single value for each profile, which should represent the mean number of activated aerosols at cloud base, without the need to know the cloud base updrafts or the chemical composition of the aerosols.

Table 1. Aerosol and cloud data for all profiles.

Profile (yymmdd_hhmm)	CCN[1] @ 0.2% (cm^{-3})	PCASP[1] (cm^{-3})	N_{mean}[2] (cm^{-3})	N_{max}[3] (cm^{-3})	$N_{adi\text{-}cb}$[4] (cm^{-3})
090514_1255	1500	3500	430	1600	1738
090515_1150	70	600	75	110	113
090515_1350	70	600	80	110	156
090519_1110	280	3000	280	870	998
090526_1200	1300	3000	100	340	416
090526_1430	850	2500	200	640	917
090530_1140	100	2500	175	440	352
090530_1420	2000	4500	300	530	698

[1] Measured below cloud base before or after the profile, not always in direct vicinity of the profiled cloud
[2] Mean value of FSSP droplet concentration while in cloud (defined as N>20) during profile
[3] Maximum value of FSSP droplet concentration during profile after downsampling the FSSP data from 5Hz to 1Hz
[4] Estimated droplet concentration in adiabatic cloud parcel, normalized for cloud base altitude. See "Methods"

MAIN RESULTS AND CONCLUSIONS

Out of the 26 ATR-42 flights during May 2008, we were able to construct 8 individual and independent vertical profiles of cloud droplet effective diameter vs. altitude, some of them quite shallow. Since $N_{adi\text{-}cb}$ is dependent on the calculated adiabatic water, it was important to try to estimate the cloud base altitude carefully, which was not always a simple task. This also affects the calculation of the cloud depth

parameter, which is vital for comparing the growth of cloud droplets of clouds with bases at different altitudes. Figure 1 shows the mean Re for all penetrations (defined as more than 5 subsequent 1Hz measurements with cloud droplet > 20 cm^{-3}) versus the distance above cloud base. The colour of each data point is defined by the $N_{adi\text{-}cb}$ for the containing profile. It can be clearly seen that profiles with smaller $N_{adi\text{-}cb}$ have larger Re for any given cloud depth, and that the differences are more evident further from the cloud bases. This pinpoints the importance of sampling clouds far from their bases, when studying the effects of the aerosols on the cloud droplet size spectra and its evolution with altitude. The cloud top particle effective diameter derived from MSG for the corresponding location and time of the aircraft measurements, shows in general good agreement the aircraft profile top Re, and also shows Re sensitivity to cloud depth and droplet concentration, but at least in two cases is taken from a cloud top which is significantly higher than the top of the profile and may represent a higher layer cloud.

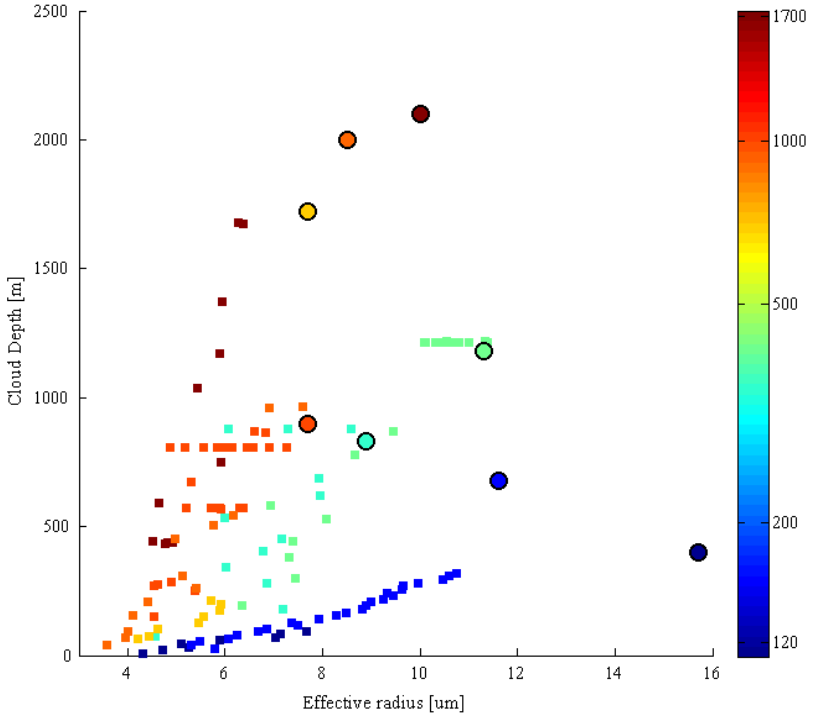

Figure 1. Mean penetration Re vs. Cloud Depth for all profiles. Colour coding represents the $N_{adi\text{-}cb}$ and its scale is logarithmic. The outlined circles show the MSG derived cloud top Re for the corresponding profiles, but in some cases the profiled cloud could not be "seen" by the satellite because higher cloud.

Figure 2 shows data for the same penetration, but instead Re, another parameter is used to relate to the droplet sizes. Here we use the mode of the cloud droplet mass density ("D_L"), which indicates the droplet diameter that contributes the most to the cloud liquid water content for each measurement. D_L and Re are highly correlative, but D_L is used here so the results from the current dataset could be directly compared to measurements taken from other parts of the world, in order to see whether it is reasonable to extrapolate EUCAARI fairly shallow measurements to greater cloud depths, which were not sampled, and to conclude something with regard to the aerosol effect on precipitation forming processes. The typical threshold of D_L for the onset of precipitation at 24µm, was not reached during EUCAARI IOP, but it seems reasonable to conclude that the more "polluted" clouds, shown in figure 2 in warmer colours, are much further from precipitating compared to the clouds with smaller droplet concentrations. The D_L profile of the convective cloud sampled on May 14, 2008 over Eindhoven area, which formed in continental south-easterly flow in well mixed area, shows similarity with lower parts of the "Argentina-Hail" and "Amazon-Smoky" profiles. On the other hand, the *StCu* sampled a day later above the North Sea just off Newcastle in maritime airmass, has a D_L profile similar to the lower part of the "California-Pristine" profile, which crossed the 24µm precipitation threshold already at a depth of 500m.

Although we were able to clearly identify the aerosol signal, as is represented by $N_{adi\text{-}cb}$, on the Re or D_L profiles in different clouds over The Netherlands and the North Sea, we would like to emphasize that good quantification of the aerosol effects on the cloud microphysical processes is not achievable, without penetrating through the clouds all the way to their tops or at least to the precipitation onset height, as well as measuring the aerosols right below the profiled cloud's base.

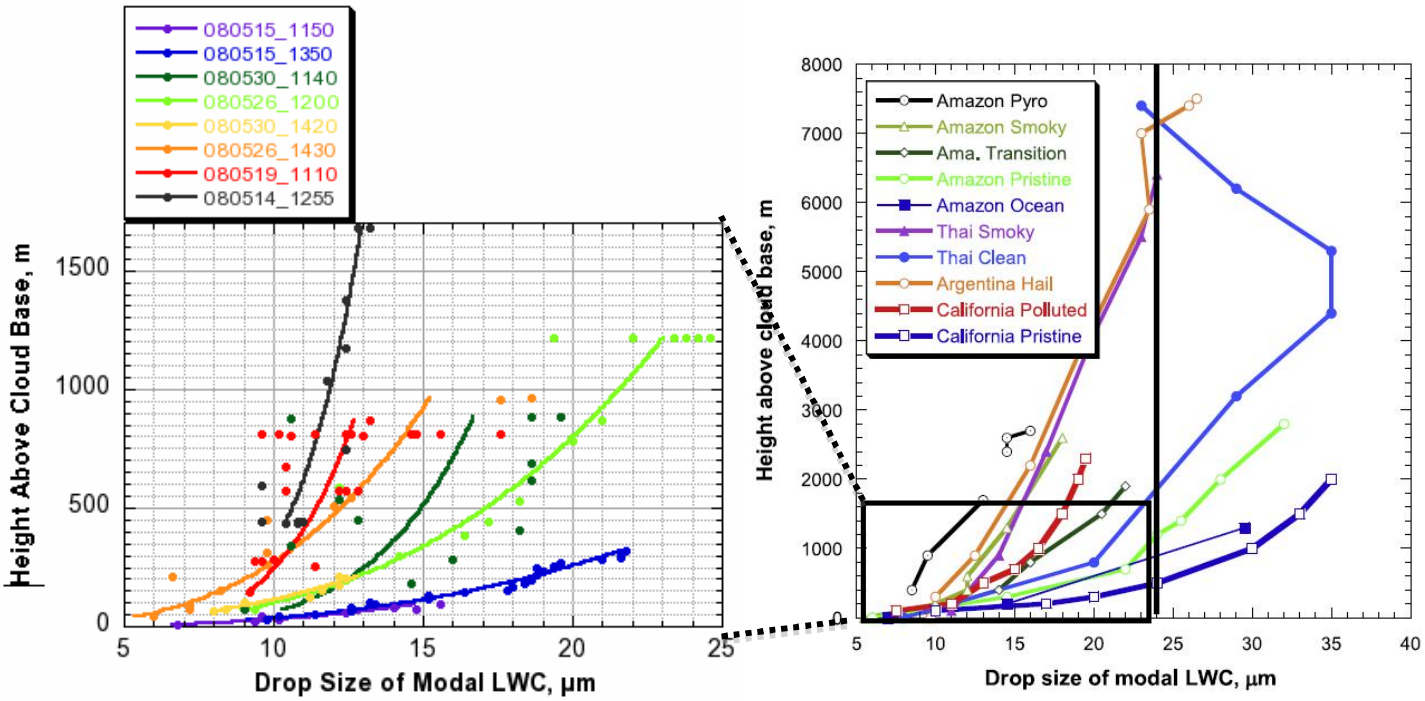

Figure 2. The mode of the droplet mass distribution in each penetration vs. cloud depth. Profiles in left panel are from EUCAARI IOP and their colours, from cold to warm, are sorted after $N_{adi\text{-}cb}$. Right panel is figure 14 from Rosenfeld *et al.* 2008. Black rectangle corresponds to axis limits of left panel.

ACKNOWLEDGEMENTS

Who Should we acknowledge here. Is there a standard EUCAARI acknowlegement?

REFERENCES

Andreae, M.O., Rosenfeld, D., Artaxo, P., Costa, A.A., Frank, G.P., K.M. Longo and M.A.F. Silva-Dias (2004). Smoking rain clouds over the Amazon. *Science*, **303**, 1337-1342.

Bennartz, R. (2007). Global assessment of marine boundary layer cloud droplet number concentration from satellite, *J. Geophys. Res.*, **112**, D02201, doi:10.1029/2006JD007547.

Freud, E., Rosenfeld, D., Andreae, M.O., A.A. Costa and P. Artaxo (2008). Robust relations between CCN and the vertical evolution of cloud drop size distribution in deep convective clouds, *Atmos. Chem. Phys.*, **8**, 1661-1675.

Lensky, I.M. and D. Rosenfeld (2006). The time-space exchangeability of satellite retrieved relations between cloud top temperature and particle effective radius. *Atmos. Chem. Phys.*, **6**, 2887-2894.

Rosenfeld, D. and I.M. Lensky (1998). Satellite-based insights into precipitation formation processes in continental and maritime convective clouds. *The Bulletin of American Meteorological Society,* **79**, 2457-2476.

Rosenfeld, D., Woodley, W.L., T.W. Krauss and V. Makitov (2006). The Structure of Severe Convective Storms in Mendoza, Argentina. *J. Appl. Meteor.,* **45**, 1261–1281.

Rosenfeld, D., Woodley, W.L., Axisa, D., Freud, E., J.G. Hudson and A. Givati, (2008). Aircraft measurements of the impacts of pollution aerosols on clouds and precipitation over the Sierra Nevada. *J. Geophys. Res.*, **113**, D15203, doi:10.1029/2007JD009544.

BLACK CARBON EMISSIONS OVER EUROPE: EMISSIONS, PROCESSES AND UNCERTAINTIES

Maria Grazia Frontoso[1], Kenneth S. Carslaw[1], Graham W. Mann[1], Dominick V. Spracklen[1]
Hugh Coe[2] , Dantong Liu[2], G. McMeeking[2], William Morgan[2]

[1]University of Leeds, Institute for Climate and Atmospheric Science, School of Earth and Environment, Leeds, United Kingdom
[2]University of Manchester, School of Earth, Atmospheric and Environmental Sciences, Manchester, United Kingdom

Keywords: black carbon, global modelling

INTRODUCTION

Atmospheric aerosols play an important role in the global climate system. They modify the global radiation budget directly, by scattering and absorption (Mc Cormic and Ludwig, 1967) and indirectly, by their interaction with clouds (Twomey 1974, Albrecht 1989).
Black carbon (BC) aerosol, a byproduct of incomplete combustion of fossil fuels and biomass, is a strong absorber of the solar radiation and leads to heating of the atmosphere. The current estimates of BC global radiative forcing from fossil fuel and biomass burning are near 0.4 W/m2 and black carbon is likely to be the second leading cause of global warming, after carbon dioxide and comparable to the contribution of methane, the second most important greenhouse gas [Forster et al., 2007]. On regional scales BC forcing estimates can be much higher (> 20 W/m2) [Tripathi et al., 2005; Ramanathan et al., 2001]. Furthermore, regulation of BC emission sources offers potentially important opportunities for short-term mitigation of anthropogenic forcing [Bond and Sun et al., 2005].
The mixing state of BC, namely, the degree to which BC particles are coated with other aerosol components, can affect the impact of BC particles on the radiation [Stier et al., 2006]. BC particles freshly emitted into the atmosphere are generally in the form of bare particles externally mixed with other particles and therefore in a hydrophobic state [Weingartner et al., 1997; Sakurai et al., 2003]. They gradually become internally mixed through condensation, coagulation, and/or photochemical oxidation processes in the atmosphere (aging processes) and eventually become hydrophilic, when they are coated with sufficient water-soluble compounds. Therefore, aging processes increase the wet scavenging efficiency of BC and consequently reduce the amount of BC transported from the PBL to the FT.
In recent years, advanced observation techniques using laser-induced incandescence (single-particle soot photometer, SP2) have been developed, enabling us to obtain mass size resolved measurements and some quantitative information on the mixing states of BC-containing particles [Baumgardner et al., 2004; Schwarz et al., 2006; Gao et al., 2007; Moteki and Kondo, 2007].
In this work BC model simulation have been benchmarked with data from SP2 on board of the BAe-146 aircraft which flew over Europe during the EUCAARI-LONGREX (LONG Range EXperiment) aircraft field campaign in May 2008. Sensitivity to different BC emission schemes and ageing and their impact on optical properties has been tested. A new model setup has been implemented to take into account the mixing state of the BC.

AEROSOL MODELLING: THE GLOMAP MODEL

The GLObal Model of Aerosol Processes (GLOMAP, Spracklen et al., 2005) is an atmospheric aerosol model which runs within the 3D off-line Eulerian chemical transport model, TOMCAT, forced by ECMWF meteorological analyses. The domain of the model is global and the resolution used here is 2.8×2.8 degrees (latitude × longitude) with 31 hybrid levels extending from the surface to 10 hPa. The vertical geometric resolution varies from 60m within the planetary boundary layer to 1 km at the tropopause.

GLOMAP has the unique advantage of having two aerosol schemes: a sectional (bin) scheme (referred as GLOMAP-bin) and a log-normal modal scheme (referred as GLOMAP-mode). GLOMAP-bin uses a sectional scheme (20 bins, spanning a range from 1 nm to 25 um) carrying both mass and number. GLOMAP-mode uses 7 lognormal modes defined in terms of number and masses of each chemical component. Each bin/mode contains internally mixed particles of several components (sulphate, sea salt, organic carbon, secondary organic carbon, black carbon and dust).

GLOMAP-mode has been developed for use in the UK Met Office Unified Model (UM) as part of the new UK Chemistry and Aerosol (UKCA) sub-model. Both models use identical emissions and comparable process descriptions, although the implementation is changed where necessary.

SETUP OF THE SIMULATIONS

The aerosol fields in GLOMAP are generated from an initially aerosol free atmosphere. For the simulations in this work, the model has been 'spun-up' for a 3-month simulation time to allow the processes of emission, processing and removal to produce a realistic aerosol distribution.

Black carbon emissions are based on Bond et al., (2004) inventory for fossil fuel and biofuel and on Van Der Werf (2004) inventory for wildfire sources. BC is emitted as insoluble (in the insoluble distribution for GLOMAP-bin and in the insoluble Aitken mode for GLOMAP-mode) and then microphysically aged, through condensation and coagulation, to modes internally mixed with other aerosol components such as sulphate, organic carbon, sea salt and dust.

For the present work, hourly model outputs were 3D interpolated along the flight-path and cloud coverage from ECMWF fields was used (instead of climatological values from ISCCP, International Satellite Cloud Climatological Project).

RESULTS

Fig.1 shows the averaged (May 2008) BC concentration over Europe during LONGREX campaign predicted by GLOMAP-bin and GLOMAP-mode. The two models agree very well, also proved by the scatter plot in Fig. 2 where BC mass from GLOMAP-mode is plotted against BC from GLOMAP-bin. The slope on the regression fit is 0.995 ± 0.012 and the correlation is 0.98.
This result is very encouraging for the use of GLOMAP-mode as the aerosol module for the Met-Office Unified Model (UM).

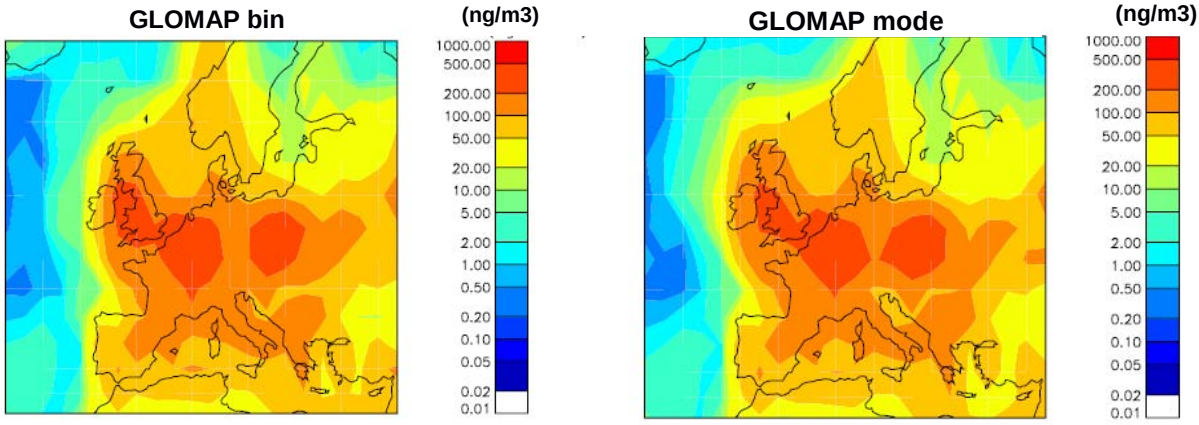

Fig. 1: Total BC mass concentration at ground over Europe during LONGREX campaign predicted by GLOMAP-bin (left) and GLOMAP-mode (right)

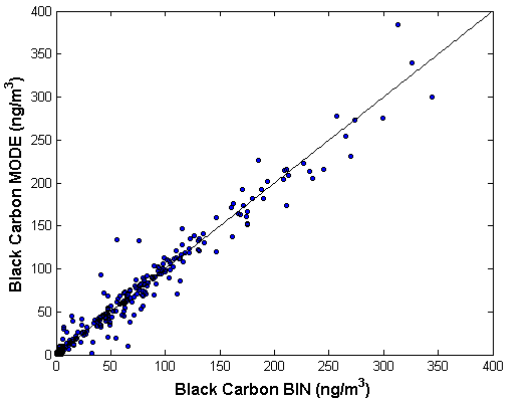

Fig. 2: Scatter plot (GLOMAP-mode vs GLOMAP-bin) for BC mass.

To address uncertainties associated with the BC emissions (mainly associated to the size at which BC should be emitted), a sensitivity simulation was performed. We used two different BC emissions schemes for Bio Fuel (BF) and Fossil Fuel (FF).
In the first scheme (AEROCOM prescribed), BC is emitted as a lognormal mass size distribution with mass median diameter of 80 and 30 nm for BF and FF respectively and geometric standard deviation of 1.8 nm.
In the second scheme (AEROCOM modified by Stier et al., 2005), BC is emitted as a lognormal mass size distribution with mass median diameter of 150 and 60 nm for BF and FF respectively and geometric standard deviation of 1.59 nm.
Fig.3a shows the scatter plots where BC mass from GLOMAP-bin (using the two emissions scheme) is plotted against BC measurements from SP2. The slope on the regression fit is 1.24 ± 0.19 and the normalized mean bias (NMB) is 27.2 % for the first scheme, and 1.01 ± 0.15 and 1.6% for the second scheme.
The second scheme performed better against observations also for the BC mass size distribution as shown in Fig. 3b, where the first scheme predicts more BC mass for smaller particles (less than 70 nm as radius).
For the following simulations the scheme 2 has been used.

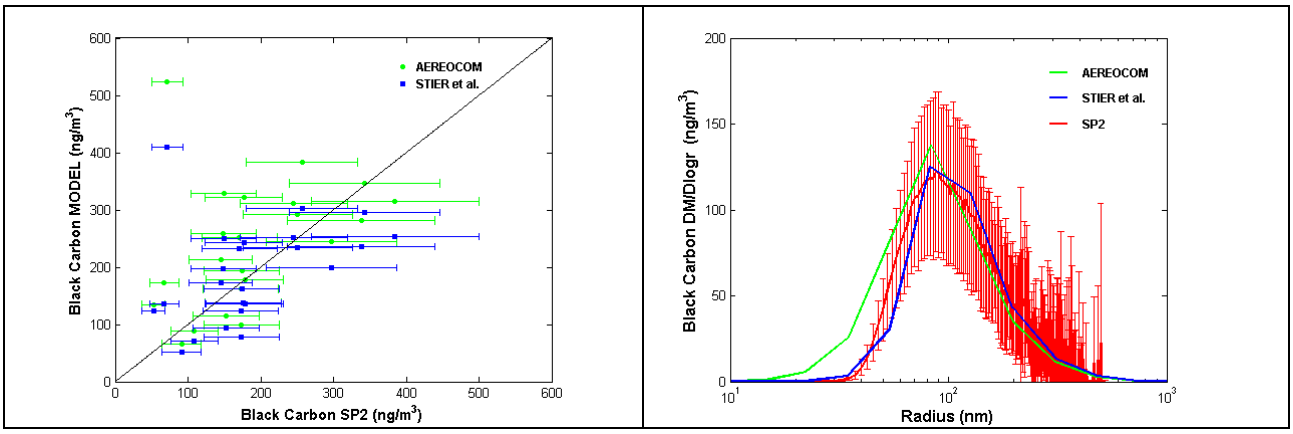

Fig. 4: Scatter plot of the BC mass (model vs SP2 observations) using the two emission schemes (left), and the average BC mass size distribution predicted by the two emission schemes and calculated by SP2.

To address uncertainties associated with the parameterization of BC ageing within GLOMAP, a sensitivity simulation was performed. In GLOMAP BC is microphysically aged through condensation at a rate of 1 molecule (1 layer) of sulphuric acid where both mass and number of insoluble BC is moved to the soluble distribution/modes. We used 10 molecules (10 layers) for the sensitivity study and we refer as “baseline”

the run with 1 molecule. The impact of BC ageing has very little impact on the BC mass, which account for less than 2% overall Europe.

A new setup to take into account the mixing state of the black carbon has been implemented where the sulphate that condenses onto the BC particles is tracked as an additional tracer.

SUMMARY & CONCLUSIONS

Results can be summarized as follows:

- Model simulation of BC during the EUCAARI-LONGREX campaigns have been benchmarked with mass size-resolved from SP2, showing a rather good agreement over Europe.
- The two versions of the model (GLOMAP-bin and GLOMAP-mode) have showed a good agreement over Europe and intramodel differences are less than model-observations differences.
- The main process over Europe for black carbon (41.9%) is the transfer from Aitken soluble BC to accumulation soluble BC due to cloud processes, but also ageing (9.9%) has a significant impact transferring BC (both in mass and number) from insoluble to soluble Aitken BC. The most efficient removal is due to the nucleation scavenging of the accumulation soluble mode (28.7%).
- Sensitivity runs to both emissions and ageing schemes have been performed, showing that for the single scattering albedo uncertainties in emissions have a stronger impact than uncertainties in microphysics. Sensitivities of the refractive index to SSA have been also performed showing that the differences are less than experimental errors.
- A new setup to take into account the mixing state of the black carbon has been implemented where the sulphate that condenses onto the BC particles is tracked as an additional tracer.

ACKNOWLEDGMENTS

This work is supported by the European Commission under the EUCAARI project and the Natural Environment Research Council ADIENT project. The authors would thank all groups and the Institutions within LONGREX and IMPACT campaigns for providing data.

FACTORS INFLUENCING ION-INDUCED NUCLEATION IN A BOREAL FOREST SITE, FINLAND

S. GAGNÉ[1], T. NIEMINEN[1], T. KURTÉN[1], T. PETÄJÄ[1], V.-M. KERMINEN[2], M. BOY[1], L. LAAKSO[3,1] and M. KULMALA[1]

[1]Department of Physics, University of Helsinki, P.O.Box 64, 00014Helsinki, Finland

[2]Finnish Meteorological Institute,P.O. Box 503, 00101 Helsinki, Finland

[3] School of Physical and Chemical Sciences, North-West University, Private Bag x6001, Potchefstroom 2520, Republic of South Africa.

Keywords: nucleation mechanisms, field measurements, Ion-DMPS, ion-induced nucleation.

INTRODUCTION

The Ion-DMPS (Mäkelä et al., 2003; Iida et al., 2006; Laakso et al., 2007) has been measuring in Hyytiälä, Finland since April 2005 until November 2008 (in this work the dataset stops on Jan 1 2008). This instrument allows us to determine the charging state of a new particle formation (NPF) event indicating the level of participation of ion-induced nucleation to the total particle formation. So-called *overcharged* days had higher charged particle concentrations than is expected at the steady-state and indicate a certain participation of ion-induced nucleation; *undercharged* days, on the other hand, have a similar or lower charged particle concentration than is expected at the steady-state and indicate no or very little participation of ion-induced nucleation.
During the selected period, 246 NPF events were found, 164 overcharged and 42 undercharged. These two categories are analyzed with respect to different meteorological parameters as well as charged and neutral particle concentration, formation rates, etc. in order to investigate which of these parameters influence the participation of ion-induced nucleation in a NPF event.

METHODS

In this paper, we analyze data from an Ion-DMPS as well as a Neutral and cluster Air Ion Spectrometer, NAIS (based on the AIS principle, Mirme et al., 2007), a Balance Scanning Mobility analyzer, BSMA (Tammet, 2006) and a Differential Mobility Analyzer, DMPS. Moreover, meteorological measurements are also used, including but not restricted to temperature and relative humidity. Modelled sulfuric acid is also used (SOSA, manuscript in preparation: Boy et al.) as well as condensation sink, solar radiation, radon decay and external radiation.
Two main ways of analysis were used. The main one consists of analyzing the daily cycle of a variable separately for overcharged and undercharged days. We use the formation rates and ion-induced fractions calculated from the NAIS as supporting data (because the data is only available for days in spring 2006 and 2007) and thus the size of the sample is rather limited.

CONCLUSIONS

One of the striking differences between overcharged and undercharged days are that overcharged days tend to happen on warmer (Fig. 1), dryer (lower relative humidity), and sunnier days than undercharged ones. Also the concentration of sulphuric acid is lower on overcharged days, suggesting that the threshold for the activation of electrically charged seeds is lower than for neutral seeds (also observed experimentally by Winkler et al. (2008)). The number concentration of nucleation mode particles is

higher on undercharged days (Fig. 2). Neutral nucleation seems to contribute larger concentrations of new particles, as was seen by Vana et al. (2006) on a smaller sample, with different instruments. This analysis allows us to speculate on how neutral and ion-induced mechanisms are influenced by the analyzed parameters.

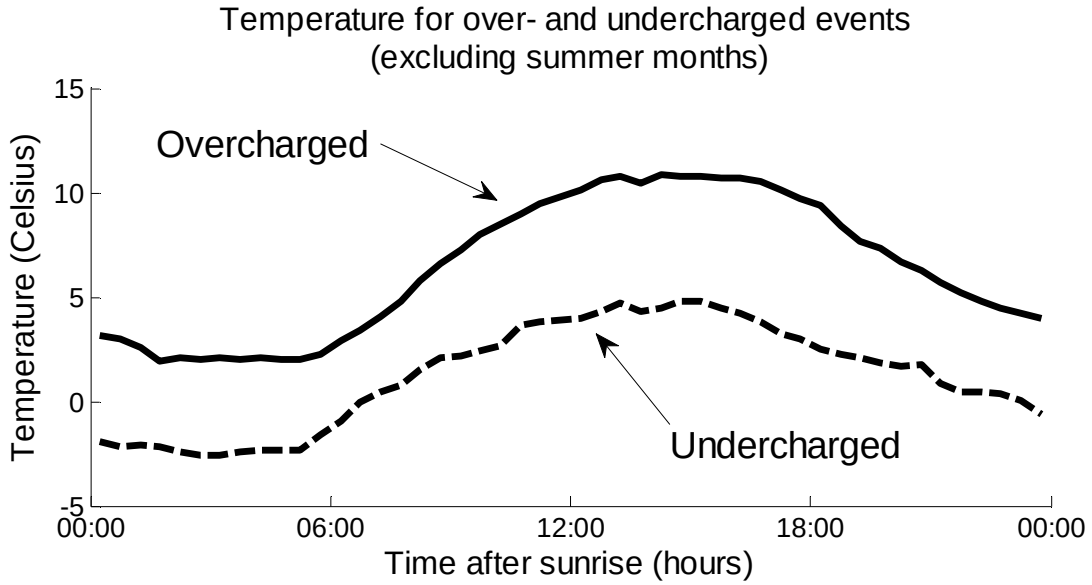

Figure 1. The median temperature, excluding summer months to avoid seasonal bias, for overcharged (full line) and undercharged (dashed line) days is presented as a function of the time after the sunrise.

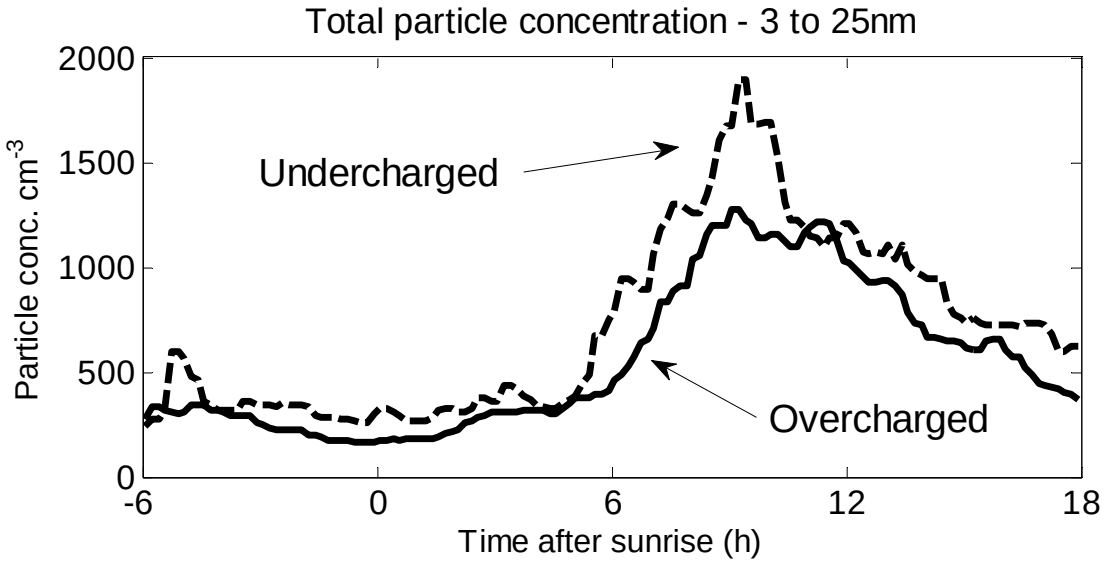

Figure 2. The median concentration (for all days) of nucleation mode particles as measured by a DMPS for overcharged (full line) and undercharged (dashed line) days is presented as a function of the time after the sunrise.

ACKNOWLEDGEMENTS

Erkki Siivola, Pekka Pihkala, Veijo Hiltunen, Heikki Laakso and Pasi Aalto are acknowledged for their work on building and maintaining the Ion-DMPS. Petri Keronen is acknowledged for providing meteorological data. This work was partly funded by the European Commission 6th Framework program project EUCAARI, contract no 036833-2 (EUCAARI).

REFERENCES

Iida, K., Stolzenburg, M., McMurry, P., Dunn, M., Smith, J., Eisele, F., and Keady, P. (2006). Contribution of ion-induced nucleation to new particle formation: Methodology and its application to atmospheric observations in Boulder, Colorado. *J. Geophys. Res*. 111, D23201, doi:10.1029/2006JD007167.

Laakso, L., Gagné, S., Petäjä, T., Hirsikko, A., Aalto, P., Kulmala, M., and Kerminen, V. (2007). Detecting charging state of ultra-fine particles: instrumental development and ambient measurements. *Atmos. Chem. Phys.*, 7, 1333–1345.

Mäkelä, J. M., Salm, J., Smirnov, V. V., Koponen, I., Paatero, J., and Pronin, A. A. (2003). Electrical charging state of fine and ultrafine particles in boreal forest air. J. Aerosol Sci., **32**, S149–150.

Mirme, A., Tamm, E., Mordas, G., Vana, M., Uin, J., Mirme, S., Bernotas, T., Laakso, L., Hirsikko, A., and Kulmala, M. (2007). A widerange multi-channel Air Ion Spectrometer, *Boreal Env. Res*., 12, 247–264.

Tammet, H. (2006). Continuous scanning of the mobility and size distribution of charged clusters and particles in atmospheric air and the balanced scanning mobility analyzer BSMA. *Atmos. Res.*, 82, 523–535.

Vana, M., Tamm, E., Hõrrak, U., Mirme, A., Tammet, H., Laakso, L., Aalto, P., and Kulmala, M. (2006). Charging state of atmospheric nanoparticles during the nucleation burst events. *Atmos. Res.*, 82, 536–546.

Winkler, P. M., Steiner, G., Virtala, A., Vehkamäki, H., Noppel, M., Lehtinen, K. E. J., Reischl, G. P.,Wagner, P. E., and Kulmala, M. (2008). Heterogeneous Nucleation Experiments Bridging the Scale from Molecular Ion Clusters to Nanoparticles. *Science*, 319, 1374, doi:10.1126/science.1149034.

CHEMICAL CHARACTERIZATION OF FINE AND COARSE AEROSOL IN DEVELOPING COUNTRIES

S. GILARDONI [1] , E. VIGNATI [1], P. ARTAXO [2], L. V. RIZZO [2], A. LOUREIRO [2], R. K. HOODA [3], T. S. PANWAR [3], L. LAAKSO [4, 5], J.P. BEUKES [4], P.G. VAN ZYL [4], H. LAAKSO [5] , V. VAKKARI [5], A. VIRKKULA [5] , J.J. PIENAAR [4]

[1]Institute for Environment and Sustainability, Joint Research Centre, Ispra, Italy.
[2]Instituto de Fisica, Universidade de Sao Paulo, Sao Paulo, Brazil
[3]Energy Environment Policy Division, The energy Resource Institute, New Delhi, India
[4]School of Physical and Chemical Sciences, North-West University, Potchefstroom, Republic of South Africa
[5]Department of Physics, University of Helsinki, Finland (lauri.laakso@helsinki.fi)

Keywords: Aerosol chemical composition, Developing countries, organic carbon, elemental carbon.

INTRODUCTION

The characterization of atmospheric aerosol in developing countries is one of the objectives of the EUCAARI project, and derives from the scarcity of continuous measurements in these regions. This work reports the results of chemical characterization of fine and coarse aerosols at Manaus (Brazil), Gual Pahari (India), and Elandsfontein (South Africa).

METHODS

Aerosol collection was performed with a Dichotomous Partisol sampler (Rupprecht & Patashnick Co., Inc). Fine particles (aerodynamic diameter below 2.5 μm) and coarse particles (aerodynamic diameter between 2.5 and 10 μm) were collected simultaneously on quartz filters. Aerosol masses were obtained from gravimetric analysis (relative humidity 20%). Water soluble ion concentrations (chloride, sulfate, nitrate, ammonium, sodium, calcium, potassium, and magnesium) were measured by ion chromatography. Elemental carbon (EC) and organic carbon (OC) were characterized using an EC/OC thermo-optical analyzer (Sunset Laboratory) (Birch and Cary, 1996). Equivalent black carbon (EBC) in Brazil was measured with a Smoke Stain Reflectometer (Diffusion System) (Andreae et al. 1984) that quantifies EBC deposited on filters from the reflectance of broad-band visible light.
During the first stage of the EUCAARI project in the developing countries, fine and coarse aerosol samples were collected in Brazil and India. The sampling site in Brazil was a mostly pristine rain forest site, 60 km north of Manaus, in the Central Amazonia (2.583° S, 60.033° W). Collection and physical characterization of aerosols were performed in collaboration with the Universidade de Sao Paulo (Brazil). In India the sampling was performed in an urban - background location (Gual Pahari 28.42° N, 77.09° E) at 10 km from New Delhi. Aerosol collection was performed by the personnel of The Energy Research Institute (TERI). Two sampling campaigns started in 2009 in South Africa and China and will end in 2010. At both sites one fine and one coarse aerosol samples are collected for 24 hours every 6 days. The South African sampling site (Elandsfontein) is located 200 km to the east of Johannesburg (23.26° S, 29.42° W). Sampling campaign started in March 2009 in collaboration with the North-West University, Potchefstroom Campus (South Africa). The sampling site in China is located at Wuqing (39.38° N, 117.02° E) Sampling, in collaboration with Peking University, started in August 2009.

RESULTS

The data here reported refers to the entire campaign in Brazil and India and to the first part of the campaign in South Africa. The average fine and coarse aerosol mass are reported in Table 1. At Manaus the chemical species identified during the present studies (carbonaceous aerosol and water soluble ions) reconstruct almost completely fine and coarse mass. At Gual Pahari the chemical analysis reconstructs completely the fine mass and 35% of the coarse mass. At Elandsfontein the percentage of reconstructed mass is 74% and 22% of fine and coarse aerosol, respectively. The lower value in the coarse mode is likely due to the contribution of dust. To quantify the contribution of dust at Elandsfontein additional aerosol samples will be collected on polycarbonate filter and analyzed by X-ray fluorescence (XRF).

	Fine - wet season	Coarse – wet season	Fine – dry season	Coarse – dry season
Manaus	2.5 (1.3)	8.0 (2.7)	4.2 (1.8)	6.9 (2.8)
Gual Pahari	38.2 (64.9)	39.9 (23.6)	100.5 (65.4)	43.3 (24.8)
Elandsfontein			18.8 (11.6)	21.7 (12.5)

Table 1. Fine and coarse aerosol mass concentration in μg m^{-3} (standard deviation between brackets).

Figure 1 shows the average composition of the fine and coarse mass at the three sites. In Manaus higher concentrations of sodium and chloride are observed in the coarse mode, likely due to marine sources. Sulfate, nitrate and ammonium are more abundant in the fine aerosols, where the ammonium concentration is usually enough to fully neutralize sulfate and nitrate. The higher concentration of sulfate in the fine fraction indicates gas-phase condensation processes. OC represents more than 50% of the fine mass and more than 75% of the coarse mass. The source of OC is mostly biogenic as confirmed by results of absolute principal component analysis and analysis of EC/OC thermo-optical data.

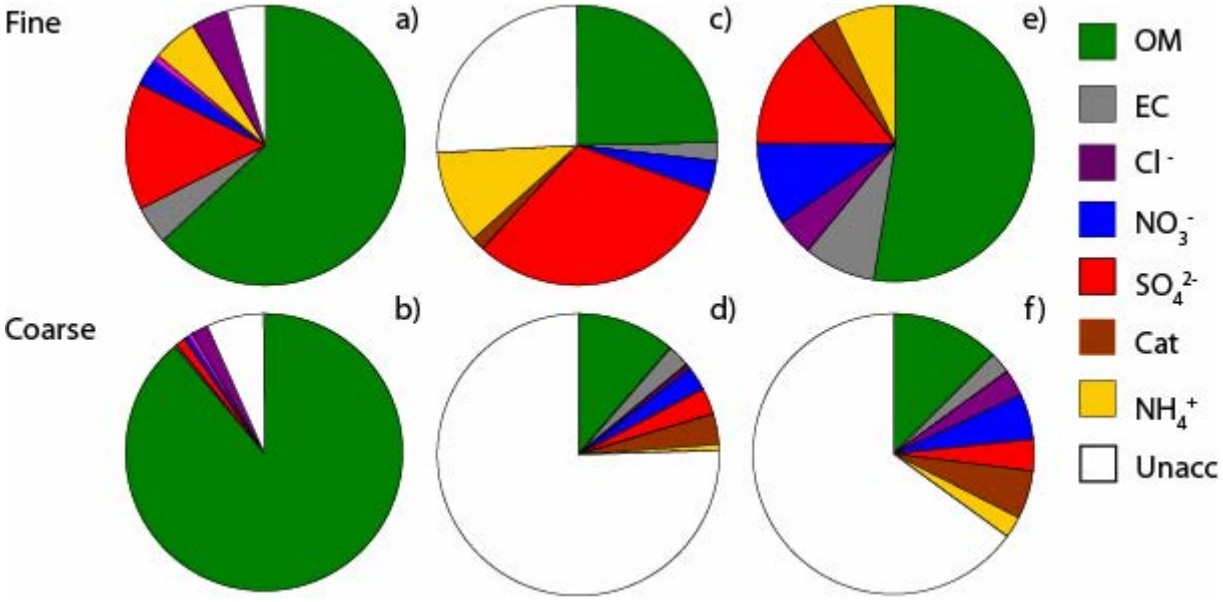

Figure 1. Average composition of reconstructed mass of fine and coarse aerosol at Manaus (a and b), Elandsfontein (c and d), and Gual Pahari (e and f). The pie charts report organic mass OM (green), elemental carbon EC (grey), chloride (purple), nitrate (blue), sulfate (red), sum of potassium, magnesium, calcium and sodium (brown), ammonium (yellow), and unaccounted mass (white).

In Elandsfontein ammonium sulfate and nitrate represent about 50% of fine mass. Aerosol masses affected by industrial sources are characterized by higher concentrations of nitrate and elemental carbon, while clean sector air masses show higher concentrations of sodium and chloride, indicating the influence of marine aerosol.

In Gual Pahari organic carbon represents more than 50% of the fine mass. Sulfate and nitrate are not able to fully neutralize ammonium, especially during the dry season when the concentration of ammonium is on average three times higher compared to the wet season; During the dry season chloride contributes to the neutralization of ammonium.

ACKNOWLEDGEMENTS

This work was supported by the European Commission EUCAARI project (grant N036833-2).
We would like to acknowledge all the personnel that worked for sample collection and gravimetric measurements at the four sites.

REFERENCES

Andreae M. O., et al. (1984), Long-range transport of soot carbon in the marine atmosphere, *Science of the Total Environment*, *36*, 73-80.

Birch, M. E., and R. A. Cary (1996), elemental carbon-based method for monitoring occupational exposures to particulate diesel exhaust, *Aerosol Science and Technology*, *25*(3), 221-241.

AEROSOL MICROPHYSICS DURING ANTICYCLONIC CONDITIONS OVER EUROPE DURING EUCAARI-LONGREX

T. HAMBURGER[1], A. MINIKIN[1], A. DÖRNBRACK[1], A. PETZOLD[1], H. RÜBA[1], H. SCHLAGER[1], M. SCHEIBE[1], A. IBRAHIM[1], H. COE[2], G. McMEEKING[2], W. T. MORGAN[2], A. STOHL[3], and R. KREJCI[4]

[1]Institut für Physik der Atmosphäre, DLR, Oberpfaffenhofen, 82234 Wessling, Germany.

[2]School of Earth, Atmospheric and Environmental Sciences, University of Manchester, Manchester M13 9PL, UK.

[3]Norwegian Institute for Air Research (NILU), P.O. Box 100, 2027 Kjeller, Norway.

[4]Department of Applied Environmental Science (ITM), Stockholm University, S 106 91 Stockholm, Sweden.

Keywords: Aerosol characterization, Aerosol evolution, Aerosol measurement, European pollution, Meteorology.

INTRODUCTION

Airborne measurements of tropospheric aerosol properties over Europe were conducted in May 2008 during the EUCAARI-LONGREX campaign, where LONGREX stands for “LONG Range EXperiment”. 15 research flights were performed with the DLR Falcon 20, of which most flights were coordinated with research flights performed by the FAAM BAe-146. Both aircrafts operated from Oberpfaffenhofen (48.08° N, 11.28° E). The flights of the FAAM BAe-146 were mainly conducted in the boundary layer and lower free troposphere, whereas the flights of the DLR Falcon 20 focussed on the free troposphere up to the tropopause level and on obtaining an extensive set of vertical profiles. The vertical profiles performed by the DLR Falcon 20 cover a large part of Central Europe. In-situ measurements of aerosol properties were also performed in the vertical tropospheric column over EUSAAR ground sites like Melpitz and Cabauw.

METHODS

DLR Falcon 20 aerosol data used for the analysis were measured by a set of Condensation Particle Counters (CPC), a thermodenuder at 250° C, two aerosol spectrometers by Grimm (Grimm Model 1.029 Optical Particle Counter), two further optical particle counters, the Passive Cavity Aerosol Spectrometer Probe (PCASP-100X) and the Forward Scattering Spectrometer Probe (FSSP-300) and one Particle Soot Absorption Photometer (PSAP). More detailed information about the instrumentation can be found in Petzold et al., 2007.

During the first part of the campaign a blocking anticyclone occurred over Central Europe with its core mainly situated over Denmark. This stable synoptic situation leads to accumulation of anthropogenic emissions in the continental boundary layer and westward transport of air masses across Northern Germany and South of England towards the Atlantic. Aerosol microphysical properties were measured in almost unpolluted air masses over the Baltic Sea advected from Scandinavia as well as in air masses within the anticyclone over Central Europe and the Atlantic.

CONCLUSIONS

Most measurements of accumulated and transported emissions showed a high fraction of non volatile particles within the total particle number concentration, up to almost 100 % in the boundary layer as shown in Figure 1. In contrast to this, the volatile fraction of the total volume of PM2.5 reaches 95 %. This indicates an internally mixed aerosol with a high load of condensed and accumulated volatile material with a non volatile core.

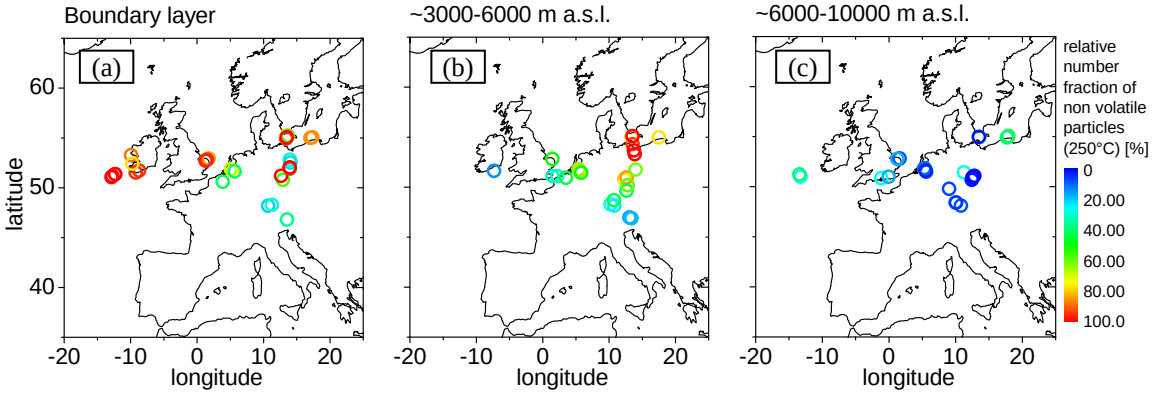

Figure 1. Airborne measurements of relative number fraction of non volatile particles (250°C) within the total particle number concentration. The colour indicates the relative number fraction in % from 0 (blue) to 100 (red). The measurements are sorted into three vertical intervals: inside the boundary layer (a), between approx. 3000-6000 m a.s.l. (b), and between approx. 6000-10000m a.s.l. (c).

The extensive data set obtained during EUCAARI-LONGREX within the stable synoptic situation over Europe combined with an analysis of the meteorological situation during air mass transport allows studies of aerosol microphysical properties during transformation and aging of anthropogenic emissions. These studies will also provide an important input to aerosol models. The main highlights of this analysis will be presented on the EUCAARI annual meeting 2009.

ACKNOWLEDGEMENTS

This work has been partly funded by EUCAARI (European Integrated project on Aerosol Cloud Climate and Air Quality interactions) No 036833-2. More information about EUCAARI-LONGREX can be found on http://www.pa.op.dlr.de/aerosol/eucaari2008/ .

REFERENCES

Petzold, A., B. Weinzierl, H. Huntrieser, A. Stohl, E. Real, J. Cozic, M. Fiebig, J. Hendricks, A. Lauer, K. Law, A. Roiger, H. Schlager, and E. Weingartner (2007). Perturbation of the European free troposphere aerosol by North American forest fire plumes during the ICARTT-ITOP Experiment in summer 2004, *Atmos. Chem. Phys.*, 7, 5105-5127.

NUCLEATION DURING THE 2009 EUCAARI CAMPAIGN IN THE PO VALLEY

Amar Hamed[1], Petri Vaattovaara[1], Pasi Miettinen[1], Petri Tiitta[1], Christian Plaß-Dülmer[2], Thomas Elste[2], Georg Stange[2], Stefano Decesari[3], Claudio Carbone[3], Maria Cristina Facchini[3], Jorma Joutsensaari[1], Ari Laaksonen[1,4]

[1]University of Kuopio, Department of Physics, P. O. Box 70211 Kuopio, Finland
[2]German Weather Service, Meteorological Observatory, Hohenpeissenberg, Germany
[3]CNR, Inst. Atmospheric Sciences and Climate, via Gobetti 101, I-40129, Bologna, Italy
[4]Finnish Meteorological Institute, Air Quality Research, P.O. Box 503, FI-00101 Helsinki, Finland

Keywords: nucleation rate, sulfuric acid concentrations, Po Valley.

INTRODUCTION

A field campaign was conducted at the polluted rural site, San Pietro Capofiume "SPC" in the PoValley, Italy from June 26th to July 12th 2009 in the frame of the EUCAARI (European integrated project on aerosol, cloud, climate, and air interactions) project. During this summer campaign, a large number of different quantities were measured; here we concentrate only on the measurements relevant to this study. Aerosol particle number size distributions have been measured continuously at the SPC station since March 2002 along with meteorological parameters and trace gases concentrations. The gas-phase sulfuric acid concentrations were measured for the first time in SPC station during this campaign (see accompanying poster by Plass-Dülmer et al.) which presented a good opportunity for us to examine the dependence of nucleation rate on sulfuric acid vapor concentrations in SPC measurement site.

METHODS

The particle formation events were identified and classified into different categories i.e., event and non-event days according to the particle number concentrations and the particle formation and growth rate. For nucleation event days, increase of the particle number concentrations in the nucleation mode showing clear growth of the new formed particles for several hours were observed. The classification method of nucleation events we followed here is based on the method described by Hamed et al. (2007).

The nucleation rate of critical clusters is a central quantity in this analysis and is estimated as the formation rate of 1 nm particles (J_1). Because critical clusters formed by atmospheric nucleation events cannot yet be measured (minimum detectable size about 3 nm), J_1 was extrapolated from the formation rate of 3 nm particles (J_3), which was obtained from measured particle size distributions. Particularly, we applied the method presented by Kerminen and Kulmala (2002) to get J_1 and time delay was taken into account for each nucleation day. The dependence of J_1 on $[H_2SO_4]$ concentrations was studied for each nucleation day individually and for all strong nucleation days as a whole.

RESULTS AND DISCUSSION

New particle formation days were selected according to the criteria that have been described earlier by Hamed et al., (2007). As a summary, the number of strong nucleation event days was 4 (29th and 30th of June and11th and 12th of July) and during 2 days were weak events (1st and 5th of July) while 7 days were classified as undefined days (2nd,3rd,4th,6th,8th and 9th of July). Days with no particle formation counted as 3 days (26th and 27th of June and 10th of July) (see fig 1.). We examined the correlations between concentrations of sulfuric acid vapor and the nucleation rate of newly formed particles measured during this campaign only for the strong nucleation days.

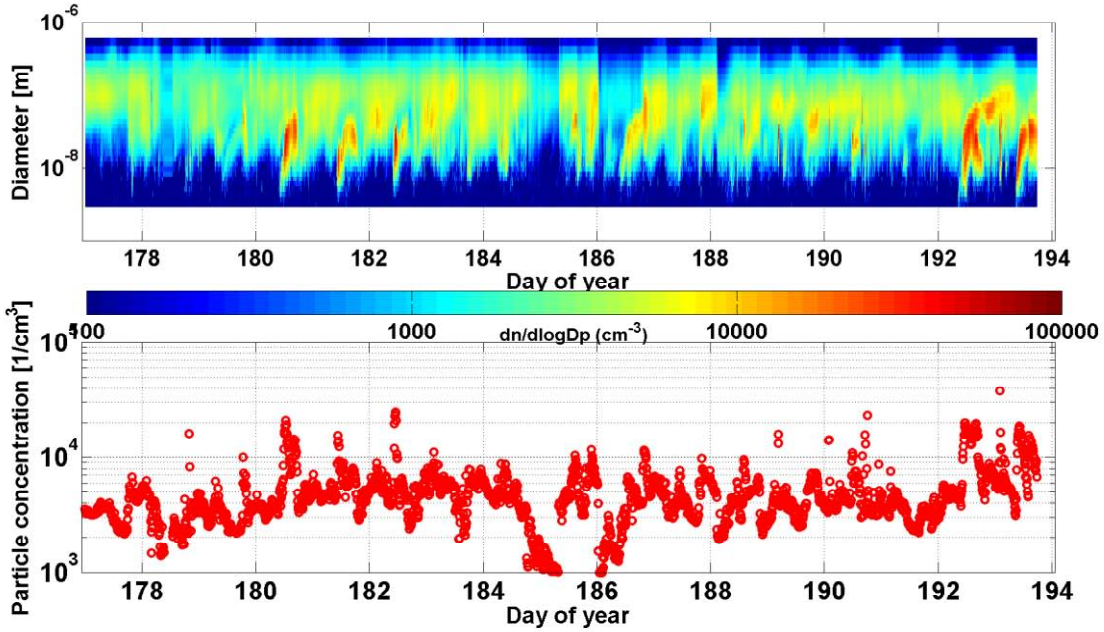

Figure 1. A surface plot of the particle size distribution data measured by DMPS system at SPC station during the whole EUCAARI campaign period (June 26th to July 12th 2009).

For our study the cumulative data set contained measured values of sulfuric acid and the estimated values of J_1 from the strong nucleation events observed at SPC. We examined the relationship between J_1 and H_2SO_4 only over the duration of the nucleation events as those times and the associated parameters most accurately characterize the nucleation process.

The dependence relationship always assume to follow a simple power law model for new particle formation where $J_1 = P\,[H_2SO_4]^n$ where P is the prefactor contains chemical and physical details of the nucleation process. It provides insight into the chemistry and physics of the nucleation mechanism (activation and kinetic mechanism, respectively); n is the nucleation exponent, its values ranges from 1and 2 in case of the activation (Sihto et al., 2006; Riipinen et al., 2007; Kulmala et al., 2006) and kinetic (McMurry and Friedlander, 1979; Kuang et al., 2008) mechanism for new particle formation, respectively. The activation model assumes that nucleation occurs through the activation of small clusters containing one H_2SO_4 molecule through one of several mechanisms including heterogeneous nucleation and heterogeneous chemical reactions. The kinetic model assumes that critical clusters are formed through bimolecular collisions of sulfuric acid containing cluster.

Figure 2 shows the logarithm of the nucleation rate J_1 (cm^{-3} s^{-1}) estimated from particle measurements versus logarithm of the sulfuric acid concentration at SPC site. The linear fitting of the data shows that the nucleation exponent n=2.2 ± 0.02 which is in agreement with the results obtained by Weber et al. (1996) and Kuang et al. (2009). The exponent n is close to 2 which mean the kinetic mechanism is more favorable during this SPC campaign period than the activation mechanism. According to the nucleation theorem for multicomponent systems (Oxtoby and Kashchiev, 1994) an exponent of 2 means the critical cluster are formed comprising two sulfuric acid molecules through a kinetically controlled nucleation process. Even though the same analysis applied to the individual days yielded similar slopes close to 2, we should keep in mind that only 4 strong nucleation days are not enough to generalize our conclusion so far.

More analysis is ongoing to study in more detail the composition of the nucleation mode particles and the role of the other gases on the formation of new particles.

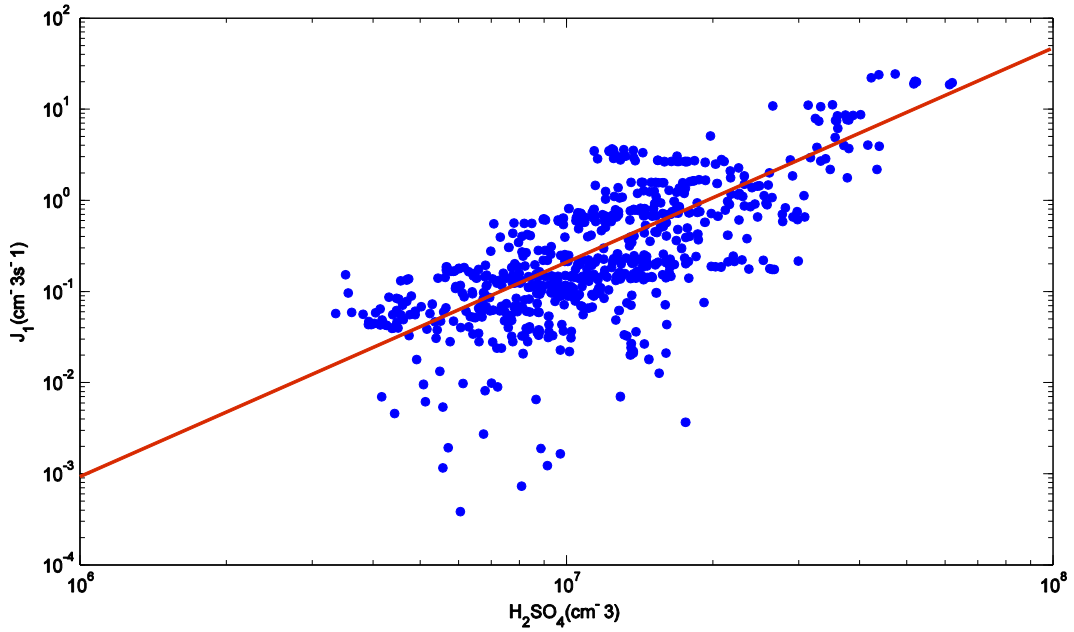

Figure 2. Logarithm of the nucleation rate J_1 (cm^{-3} s^{-1}) estimated from particle measurements versus logarithm of the sulfuric acid concentration. (Red line shows the linear fit, slope=2.2)

ACKNOWLEGMENTS

This work is funded by Magnus Ehrnrooth foundation. EUCAARI project and the Academy of Finland are acknowledged.

REFERENCES

Hamed, A., Joutsensaari, J., Mikkonen, S., Sogacheva, L., Dal Maso, M., Kulmala, M., Cavalli, F., Fuzzi, S., Facchini, M. C., Decesari, S., Mircea, M., Lehtinen, K. E. J. and Laaksonen, A. (2007), Nucleation and growth of new particles in Po Valley, Italy. Atmos. Chem. Phys., **7**, 355–376.

Kerminen, V., and M. Kulmala (2002), Analytical formulae connecting the ‘‘real’’ and the ‘‘apparent’’ nucleation rate and the nuclei number concentration for atmospheric nucleation events, J. Aerosol Sci., 33(4), 609–622.

Kuang, C., P. H. McMurry, A. V. McCormick, and F. L. Eisele (2008), Dependence of nucleation rates on sulfuric acid vapor concentration in diverse atmospheric locations, J. Geophys. Res., 113, D10209, doi:10.1029/2007JD009253.

Kulmala, M., K. Lehtinen, and A. Laaksonen (2006), Cluster activation theory as an explanation of the linear dependence between formation rate of 3 nm particles and sulphuric acid concentration, Atmos. Chem. Phys., 6, 787–793.

McMurry, P., and S. Friedlander (1979), New particle formation in the presence of an aerosol, Atmos. Environ., 13(12), 1635–1651.

Oxtoby, D., and D. Kashchiev (1994), A general relation between the nucleation work and the size of the nucleus in multicomponent nucleation, J. Chem. Phys., 100(10), 7665–7671.

Plass-Dulmer,C., Elste,T., Gilge, S., Stange,G., Decesari, S., (2009), Sulfuric acid and trace gas measurements in EUCAARI–SPC-2009. (Abstract submitted to EUCAARI Annual meeting, Stockholm 2009).

Riipinen, I., Sihto, S.-L., Kulmala, M., Arnold, F., Dal Maso, M., Birlmili, W., Saarnio, K., Teinilä, K., Kerminen, V-M., Laaksonen, A., and Lehtinen, K. E. J. (2007) , Connections between atmospheric sulphuric acid and new particle formation during QUEST III-IV campaigns in Hyytiälä and Heidelberg, Atmos. Chem. Phys., 7, 1899 –1914.

Sihto, S.-L., Kulmala, M., Kerminen, V.-M., Dal Maso, M., Petäjä, T., Riipinen, I., Korhonen, H., Arnold, F., Janson, R., Boy, M., Laaksonen, A., and Lehtinen, K. E. J. (2006), Atmospheric sulphuric acid and aerosol formation: implications from atmospheric measurements for nucleation and early growth mechanisms. Atmos. Chem. Phys., 6, 4079– 4091.

Weber, R., J. Marti, P. McMurry, F. Eisele, D. Tanner, and A. Jefferson (1996), Measured atmospheric new particle formation rates: Implications for nucleation mechanisms, Chem. Eng. Commun., 151(1), 53–64.

ARE BIOAEROSOLS IMPORTANT CONTRIBUTORS TO GLOBAL ATMOSPHERIC ICE NUCLEATION?

C. HOOSE[1], J. E. KRISTJÁNSSON[1], J.-P. CHEN[2], A. HAZRA[2]

[1] Department of Geosciences, University of Oslo, Norway
[2] National Taiwan University, Taiwan

Keywords: mixed-phase clouds, ice nucleation, bioaerosols

INTRODUCTION

Ice in tropospheric clouds is important for cloud radiative properties and precipitation formation, but its formation is neither theoretically fully understood nor empirically well constrained (Cantrell and Heymsfield, 2005). At temperatures between 0 and $-38°C$, aerosol particles are required as ice nuclei (IN) to initiate either freezing of supercooled cloud droplets or ice nucleation from the vapor phase. Various insoluble particles like mineral dust, soot, metallic particles, or primary biological particles can act as IN (Pruppacher and Klett, 1997). The dependence of heterogeneous ice nucleation on temperature, particle composition, size, coating and various other parameters has been the subject of numerous laboratory experiments (e.g. Welti et al., 2009). In general, it is found that some bacteria and the artificial IN silver iodide nucleate ice at the warmest temperatures, followed by other biogenic particles and mineral dust, and that combustion particles are relatively inefficient IN. Atmospheric in-situ observation of ice nucleation and the involved particles is very difficult. One possibility is to sample ice crystals and investigate the residual aerosol particles after evaporation. This can give information about the IN composition. The compilation of a large number of these data by Phillips et al. (2008) suggests that mineral dust is the dominant atmospheric IN. Additionally, a large portion of carbonaceous particles was found in ice crystals, but their exact composition (inorganic or organic) was not determined. Recently, Pratt et al. (2009) identified 33% of the ice crystal residual particles sampled in a wave cloud over Wyoming as biogenic. Prenni et al. (2009) found that chamber-measured IN in the Amazon basin were composed of mainly biological carbonaceous particles, and long-range transported dust. Further indication of the atmospheric relevance of biogenic particles for ice formation is given by the ubiquity of ice nucleation active bacteria in precipitation (Christner et al., 2008). Here we attempt to constrain the role of biogenic IN from a global modeling perspective.

MODEL DESCRIPTION

The aerosol-climate model CAM-Oslo is based on the Community Atmosphere Model CAM3 (Collins et al., 2006). It has been extended to include a detailed aerosol module (Seland et al., 2008) and a prognostic double-moment cloud microphysics scheme (Storelvmo et al., 2006; Hoose et al., 2009). The microphysical scheme for mixed-phase clouds (Storelvmo et al., 2008a,b) has now been modified by a new treatment of ice nucleation, see below. CAM-Oslo is coupled to the Community Land Model CLM2.

Primary biological particles are so far only crudely presented in global models. To study their importance for ice nucleation, bacteria, fungal spores and pollen are included in CAM-Oslo as passive tracers, which undergo advection, turbulent transport, sedimentation and wet deposition. Bioaerosol emissions depend strongly on the vegetation and soil characteristics, which can only

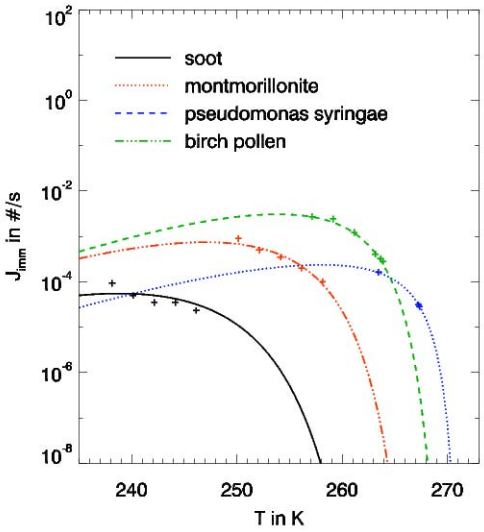

Figure 1: Immersion freezing parameterization for particles with a radius of 50 nm (soot), 750 nm (montmorillonite dust), 12.5 μm (birch pollen) and 500 nm (pseudomonas syringae bacteria). The crosses indicate freezing rates derived from measurements (Pitter and Pruppacher, 1973; DeMott, 1990; Diehl et al., 2002; Möhler et al., 2008).

be represented in a simplified way in global models. The emission parameterizations used here are based on Burrows et al. (2009) for bacteria, Heald and Spracklen (2009) for fungal spores and Jacobson and Streets (2009) for pollen.

As an extension of the CAM-Oslo model, an ice nucleation parameterization based on classical nucleation theory is formulated. Immersion and contact freezing as well as deposition nucleation are included. The necessary aerosol-related parameters are derived from laboratory experiments by the method of Chen et al. (2008). Mineral dust and soot are considered as possible ice nuclei, as well as bacteria, fungal spores and pollen. The immersion freezing parameterization is shown in Figure 1. Only those aerosol particles which are activated to cloud droplets can act as immersion nuclei.

PRELIMINARY RESULTS

Bioaerosol emission fluxes are shown in Figure 2. Bacteria, which are of the smallest size ($d = 1\,\mu$m), are emitted in the highest number concentrations. Fungi and pollen ($d = 5$ and $30\,\mu$m, respectively), are emitted in lower numbers, but with a higher total mass. All bioaerosols have maximum emissions in tropical regions with high vegetation density.

Note that only a small fraction of all bacteria and fungal spores is ice nucleation active (Hirano and Upper, 1995).

On global average, 82% of the simulated heterogeneous nucleation is initiated by a mineral dust particle, 18% by soot, and bioaerosols contribute only a fraction of 10^{-7} of all ice nucleation events. Immersion freezing is the dominant freezing mechanism, but for soot - which is often externally mixed and not activated to cloud droplets - contact freezing and deposition nucleation are also relevant. The zonal average immersion freezing rates are displayed in Figure 3.

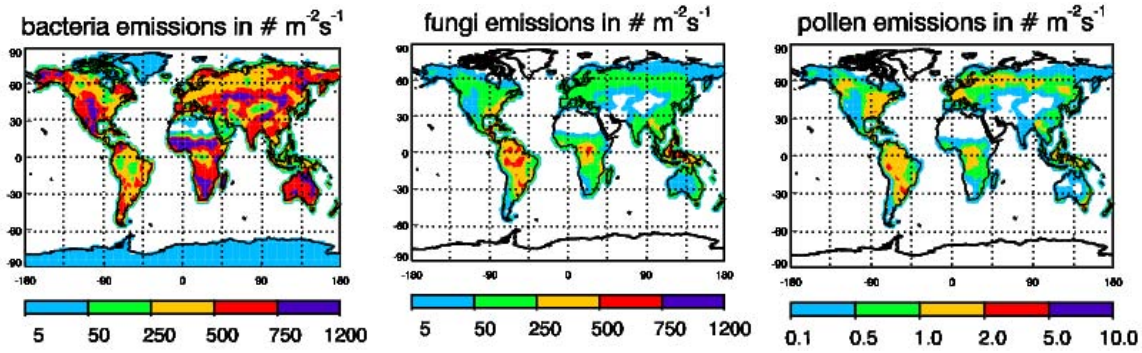

Figure 2: Annual mean bioaerosol number emission fluxes. Note the different scale for pollen.

CONCLUSIONS AND FUTURE WORK

With the currently available best estimates for bioaerosol emissions and their ice nucleation active fractions, their global contribution to heterogeneous ice nucleation is only marginal. Sensitivity studies have shown that even with very high estimates for their ice nucleation activity, their contribution remains minor compared to dust and soot. Nevertheless, they contribute at higher temperatures than other ice nuclei. Considerable uncertainties are linked to both the simulated aerosol concentrations and the ice nucleation parameterization, and further sensitivity studies are underway.

ACKNOWLEDGMENTS

This research is supported by the projects EUCAARI (European Integrated project No. 036833-2) and NorClim (Norwegian Research Council grant No. 178246), and computing time was provided through a grant from the Norwegian Research Council's program for Supercomputing.

REFERENCES

Burrows, S. M., Butler, T., Jöckel, P., Tost, H., Kerkweg, A., Pöschl, U., and Lawrence, M. G. (2009). Bacteria in the global atmosphere - Part 2: Modelling of emissions and transport between different ecosystems. *Atmos. Chem. Phys. Discussions*, 9(3):10829–10881.

Cantrell, W. and Heymsfield, A. (2005). Production of ice in tropospheric clouds: A review. *B. Am. Meteorol. Soc.*, 86(6):795–807.

Chen, J.-P., Hazra, A., and Levin, Z. (2008). Parameterizing ice nucleation rates using contact angle and activation energy derived from laboratory data. *Atmos. Chem. Phys.*, 8(24):7431–7449.

Christner, B. C., Morris, C. E., Foreman, C. M., Cai, R., and Sands, D. C. (2008). Ubiquity of biological ice nucleators in snowfall. *Science*, 319:1214.

Collins, W. D., Rasch, P. J., Boville, B. A., Hack, J. J., McCaa, J. R., Williamson, D. L., Briegleb, B. P., Bitz, C. M., Lin, S.-J., and Zhang, M. (2006). The formulation and atmospheric simulation of the Community Atmosphere Model Version 3 (CAM3). *J. Clim.*, 19(11):2144–2161.

DeMott, P. (1990). An exploratory study of ice nucleation by soot aerosols. *J. Appl. Meteorol.*, 29:1072–1079.

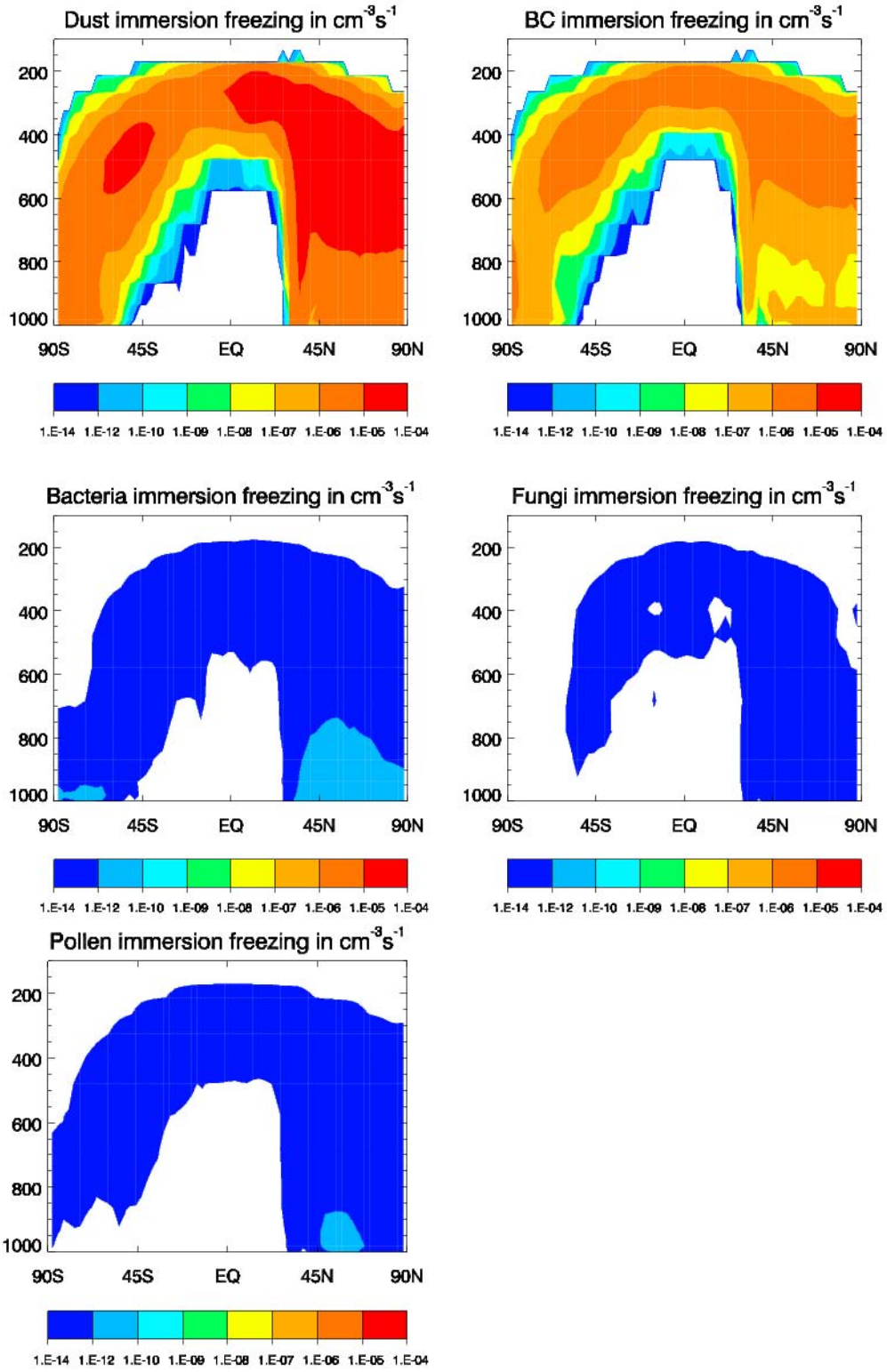

Figure 3: Zonal annual mean immersion freezing rates.

Diehl, K., Matthias-Maser, S., Mitra, S. K., and Jaenicke, R. (2002). The ice nucleating ability of pollen. Part II: Laboratory studies in immersion and contact freezing modes. *Atmos. Res.*, 61:125–133.

Heald, C. L. and Spracklen, D. V. (2009). Atmospheric budget of primary biological aerosol particles from fungal spores. *Geophys. Res. Lett.*, 36(L09806).

Hirano, S. S. and Upper, C. D. (1995). Ecology of ice nucleation-active bacteria. In Lee, R. E., Warren, G. J., and Gusta, L. V., editors, *Biological ice nucleation and its applications*, pages 41–61. The American Phytopathological Society, St. Paul, Minnesota, U.S.

Hoose, C., Kristjánsson, J. E., Iversen, T., Kirkevåg, A., Seland, Ø., and Gettelman, A. (2009). Constraining cloud droplet number concentration in GCMs suppresses the aerosol indirect effect. *Geophys. Res. Lett.*, 36(L12807).

Jacobson, M. Z. and Streets, D. G. (2009). Influence of future anthropogenic emissions on climate, natural emissions, and air quality. *J. Geophys. Res.*, 114(D08118).

Möhler, O., Georgakopoulos, D. G., Morris, C. E., Benz, S., Ebert, V., Hunsmann, S., Saathoff, H., Schnaiter, M., and Wagner, R. (2008). Heterogeneous ice nucleation activity of bacteria: new laboratory experiments at simulated cloud conditions. *Biogeosciences*, 5(5):1425–1435.

Phillips, V. T. J., DeMott, P. J., and Andronache, C. (2008). An empirical parameterization of heterogeneous ice nucleation for multiple chemical species of aerosol. *J. Atmos. Sci.*, 65(9):2757–2783.

Pitter, R. L. and Pruppacher, H. R. (1973). A wind tunnel investigation of freezing of small water drops falling at terminal velocity in air. *Q. J. Roy. Meteor. Soc.*, 99:540–550.

Pratt, K. A., DeMott, P. J., French, J. R., Wang, Z., Westphal, D. L., Heymsfield, A. J., Twohy, C. H., Prenni, A. J., and Prather, K. A. (2009). In situ detection of biological particles in cloud ice-crystals. *Nature Geoscience*, 2:398–401.

Prenni, A. J., Petters, M. D., Kreidenweis, S. M., Heald, C. L., Martin, S. T., Artaxo, P., Garland, R. M., Wollny, A. G., and Pöschl, U. (2009). Relative roles of biogenic emissions and Saharan dust as ice nuclei in the Amazon basin. *Nature Geoscience*, 2:402–405.

Pruppacher, H. R. and Klett, J. D. (1997). *Microphysics of Clouds and Precipitation*. Atmospheric and Oceanographic Sciences Library. Kluwer Academic Publishers, Dordrecht, The Netherlands.

Seland, Ø., Iversen, T., Kirkevåg, A., and Storelvmo, T. (2008). Aerosol-climate interactions in the CAM-Oslo atmospheric GCM and investigation of associated basic shortcomings. *Tellus*, 60A:459–491.

Storelvmo, T., Kristjánsson, J. E., Ghan, S. J., Kirkevåg, A., Seland, Ø., and Iversen, T. (2006). Predicting cloud droplet number concentration in Community Atmosphere Model (CAM)-Oslo. *J. Geophys. Res.*, 111(D24208).

Storelvmo, T., Kristjánsson, J. E., and Lohmann, U. (2008a). Aerosol influence on mixed-phase clouds in CAM-Oslo. *J. Atmos. Sci.*, 65:3214–3230.

Storelvmo, T., Kristjánsson, J. E., Lohmann, U., Iversen, T., Kirkevåg, A., and Seland, Ø. (2008b). Modeling of the Wegener-Bergeron-Findeisen process – implications for aerosol indirect effects. *Environ. Res. Lett.*, 3(045001).

Welti, A., Lüönd, F., Stetzer, O., and Lohmann, U. (2009). Influence of particle size on the ice nucleating ability of mineral dusts. *Atmos. Chem. Phys.*, 9(18):6705–6715.

LES MODELLING OF WARM CLOUDS USING A GPU

S. HORN[1]

[1] Leibniz Institute for Tropospheric Research, Permoserstr. 15, 04318 Leipzig, Germany.

Keywords: LES, Microphysics, Clouds, GPU.

INTRODUCTION

Large Eddy Simulations of warm cloud fields, especially the study of self organizing structures in such fields, require large model domains with very high resolution and small time steps. With that they are computational very expensive. With the invention of unified shaders in the market of graphical processing units, the most efficient computational devices of our time became available to the field of physical modelling. So we developed a new LES model using C++, OpenGL and GLSL. The model uses an explicit third order Runge Kutta scheme with time splitting methods to handle the acoustic modes and fast microphysical processes. In the beginning we used a simple one moment bulk microphysical scheme, which then was extented to warm cloud parametrisations based on the work of (Seifert and Beheng, 2006) to include drizzle and rain. At the moment the model is still under development and testing, using cases of the GEWEX Cloud System Study (GCSS). There are still some problems with the microphysical implementation, but first results are quite promising.

FIRST RESULTS

As the testbed for the microphysical parametrisation, some of the test cases of the GEWEX Cloud System Study (GCSS) were choosen. The one moment scheme was compared to the BOMEX (Siebesma et al, 2003) case and at the moment we use the RICO case to develop the drizzling implementation. Althrough not all processes are included yet, a timeline from the GPU model for the first hours of the RICO case is shown in Fig.1. The relative high cloud and rain droplet number concentrations may be explainable by missing accretion and rain self collection processes, which are not implemented yet.

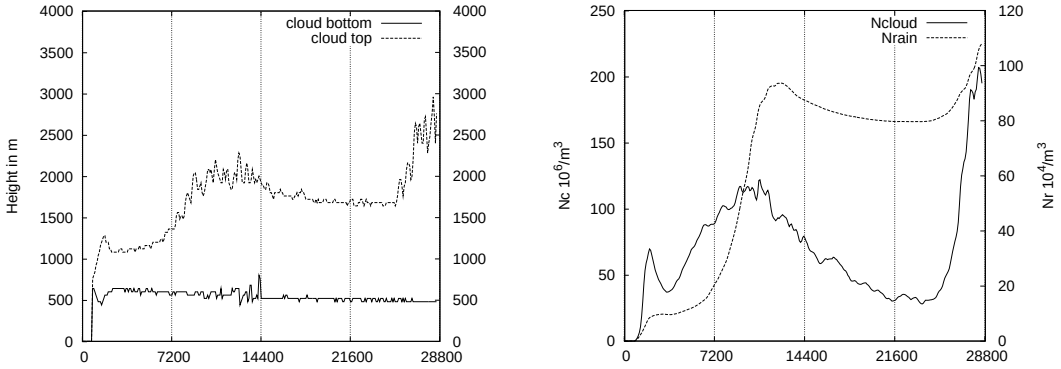

Figure 1: First 6 hours of the RICO case computed by with the GPU-Model.

PERFORMANCE

One of the main features of the new model is the computational perfomance, so it is possible to do calculations using a domain of 64x64x100 cells at a horizontal resolution of 100m and a vertical resolution of 40m with a timestep of 3s on an ordinary notebook using a *ATI Radeon HD 3650* graphics adapter in realtime. Using an actual gaming PC with an *ATI Radeon HD 4890* the 24 hours of the RICO test case are done within about 9 hours computation time. Using the new *ATI Radeon HD 5870* the computation time would halve to 4.5 hours.

Table 1: Comparison of different GPU's to an IBM Cluster node with 32 cores

Device	Peak Performance (precision)	Price	Power con.
nVidia Tesla C1060	0.93 TFLOPS (single)	1.150,00 EUR	0.160 kW
ATI HD 4890	1.2 TFLOPS (single)	182,00 EUR	0.190 kW
ATI HD 5870	2.16/0.57 TFLOPS (single/double)	360,00 EUR	0.188 kW
IBM System p5 575	0.11 TFLOPS (double)	about 50.000,00 EUR	41.6 kW

REFERENCES

Seifert A., and K. D. Beheng, 2006. A two-moment cloud microphysics parameterization for mixed-phase clouds. Part I: Model description. *Meteor. Atmos. Phys.*, **92**, 45-66.

Siebesma, A. P., C. S. Bretherton, A. Brown, A. Chlond, J. Cuxart, P. G. Duynkerke, H. Jiang, M. Khairoutdinov, D. C. Lewellen, C.-H. Moeng, E. Sanchez, Stevens, and D. E. Stevens, 2003. A large eddy simulation intercomparison study of shallow cumulus convection. *J. Atmos. Sci.*, **60**, 1201-1219.

CCN ACTIVATION DURING EUCAARI 2008 CAMPAIGN IN PO VALLEY

A. JAATINEN[1], P. TIITTA[1], P. MIETTINEN[1], P. VAATTOVAARA[1], A. KORTELAINEN[1], L. HAO[1], A. HAMED[1], S. DECESARI[2], T. RAATIKAINEN[3], S. ROMAKKANIEMI[1] and A. LAAKSONEN[1,3]

[1]University of Kuopio, Department of Physics, P.O. Box 1627, FI-70211 Kuopio, Finland.
[2]CNR, Inst. Atmospheric Sciences and Climate, Via Gobetti 101, I-40129 Bologna, Italy
[3]Finnish Meteorological Institute, P.O. Box 503, FI-00101 Helsinki, Finland.

Keywords: Q-AMS, CCN, NUCLEATION.

INTRODUCTION

New particle formation through nucleation is an important source of aerosol particles almost everywhere in the atmosphere (Kulmala *et al.*, 2004). The newly formed aerosols become climatically important if they are able to grow to sizes of 50 nm and larger. Particles in this size range can act as cloud condensation nuclei (CCN) and therefore they may contribute to the indirect aerosol effect, a series of proposed impacts that include increased cloud albedo due to increases in CCN concentrations (Twomey, 1991). The time needed for particles to grow this size depends inversely on the rate at which gases and aerosol are scavenged by background aerosol, and directly on the rate at which low volatility gases condense on newly formed particles. Once particles grow to a size where they can become CCN, their ability to activate into cloud droplets depends on their chemical composition, particle number concentration, and the water supersaturation of the surrounding air parcel. Composition affects CCN activity by determining the molecular weight of the solute, density, solubility, degree of dissociation, and surface tension (Quinn *et al*., 2008). In polluted regions with substantial amount of condensable species in the air, freshly formed particles often grow rapidly to sizes where they can act as CCN in spite of relatively high background aerosol concentrations.

In this work we have performed measurements in a rural, yet highly polluted area in the Po Valley, Italy, spring 2008, as a part of the EUCAARI (European integrated project on aerosol, cloud, climate, and air interactions) project, using a Quadrupole Aerosol Mass Spectrometer (Q-AMS) and Cloud Condensation Nuclei Counter (CCNC). In addition, DMPS (Differential Mobility Particle Sizer) data is used to classify the days into nucleation and non-nucleation days. We have focused on one new particle formation day to investigate the possible connections between the chemical composition and the cloud-forming ability of particles in this polluted area during and right after the particle formation process.

METHODS

Data sets of particle chemical composition, CCN concentrations and particle number size distributions from the San Pietro Capofiume measurement station in Northern Italy (44°39'N, 11°37'E, 10 m a.s.l.) were analyzed for the time period of ten days (4.4.2008 - 14.4.2008). San Pietro Capofiume (SPC) station is located about 30 km northeast from the city of Bologna, in the Po Valley. The station itself is in a sparsely inhabited area open to Adriatic Sea to the east side, but enclosed by densely populated areas, on its southern, western and northern sides and surrounded on these sides by mountains of Alps and Apennines. High levels of pollutants are therefore observed in this region (Hamed *et al.*, 2007).

The Aerodyne Quadrupole Aerosol Mass Spectrometer (Q-AMS) is a mass spectrometry-based system that provides size-resolved mass loadings of submicrometer non-refractory aerosols like NH_4^+, SO_4^{2-}, NO_3^- and particulate organic matter (POM). Here non-refractory means species detected via thermal

vaporization at about 600°C so mineral dust, sea salt or elemental carbon are not measured with the technique. Usually two measurement modes, mass spectrum (MS) and particle time of flight (PTOF) are applied. Full mass spectra of bulk aerosol are measured in MS mode, so the AMS is able to measure the average spectra for all sub-micrometer (PM1) aerosols every few minutes. Furthermore, information on aerosol sources can be extracted by using positive matrix factorization (PMF). Particle sizes are determined via flight times in the sizing chamber; the faster flight time means the smaller aerosol size. For more details see e.g. Jayne *et al*. (2000) and Ulbrich *et al.* (2009).

The DMT Cloud Condensation Nuclei Counter (DMT-CCNC) measures the concentration of CCN at a given supersaturation (SS). Details concerning the characteristics of the DMT-CCNC can be found in e.g. Roberts and Nenes (2005). In this study we selected two SS values, SS=0.4% and 0.6% and compared the concentration of activated particles to the total number concentration measured by a Condensation Particle Counter (CPC, TSI 3010) in order to get the average activated fraction (CCN/CN).

RESULTS AND DISCUSSION

During the ten day study period we observed three clear new particle formation days from which we have selected one for closer examination (Fig. 1). The new particle burst started around 10 a.m. (UTC+1) and lasted about 3 hours. Particle growth continued until about 4 p.m. with average growth rate of 6.8 nm h^{-1}. Even though there was no clear increase in the total particle number concentration during the event because of a substantial amount of background aerosols, a clear increase in the concentration of 3-10 nm was observed (Fig. 1, lower plot).

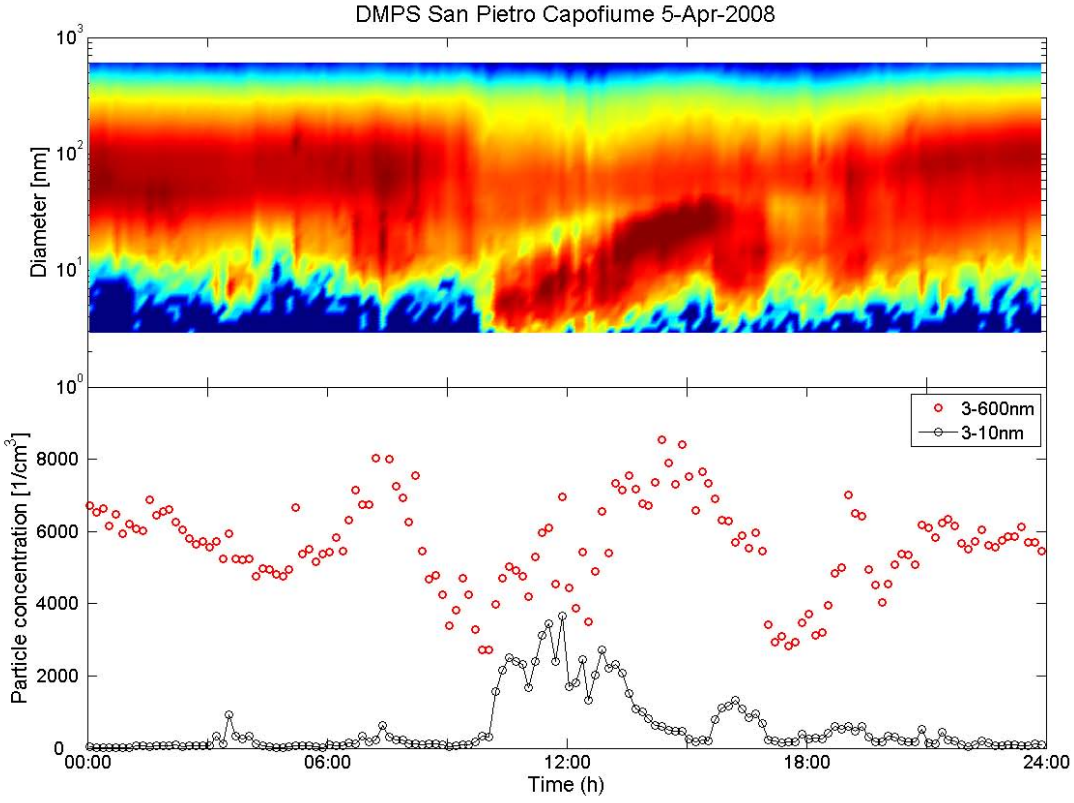

Figure 1. Diurnal pattern of particle size distribution and number concentrations during the selected particle formation day (5th April 2008). The lower plot shows total number concentration (open red circles) and the concentration of 3-10 nm particles (black line with black open circles) for the same day.

During the ten day measurement period, according to our preliminary results, the average activated fraction ranged from 10 % to 85% for the selected supersaturations depending on the day and on the particle size distribution. The lower supersaturation used (SS=0.4%) resulted in, on average, 30% smaller fraction of activated particles than the higher supersaturation (SS=0.6%).

Average PM1 mass concentrations for organics, nitrate, sulphate and ammonium during period 4.4 - 14.4.2008 were 4.0 μg/m^3, 2.7 μg/m^3, 1.4 μg/m^3 and 1.5 μg/m^3, respectively. Nitrate concentrations are typically high especially at night time in the Po Valley because of local sources and weak night time mixing. One obvious pollution period was observed during 8.4-11.4 with a peak nitrate concentration of 16 mg/m^3. The time-dependent organic mass spectrum was analyzed by PMF and two oxygenated organic aerosol (OOA) and a hydrocarbon-like organic aerosol (HOA) groups was identified. OOA1 is a non-volatile, highly oxidized, aged, long-range transported organic aerosol fraction. The less oxidized OOA2 is composed mainly of semi-volatile oxidation products of volatile organic vapours, and it is related to local sources. HOA is likely a combination of several combustion sources like diesel and gasoline vehicle emissions and actually have peak during morning rush hours 7 a.m. - 8 a.m. (Fig. 2). OOA2 concentration was dominating from 12 p.m. to 6. a.m. and decrease quickly with increasing vertical mixing and dilution (Fig. 2) when influence of local organic sources are weaker. Less volatile organics (OOA1) correlate with sulphate especially at daytime so they have probably similar sources.

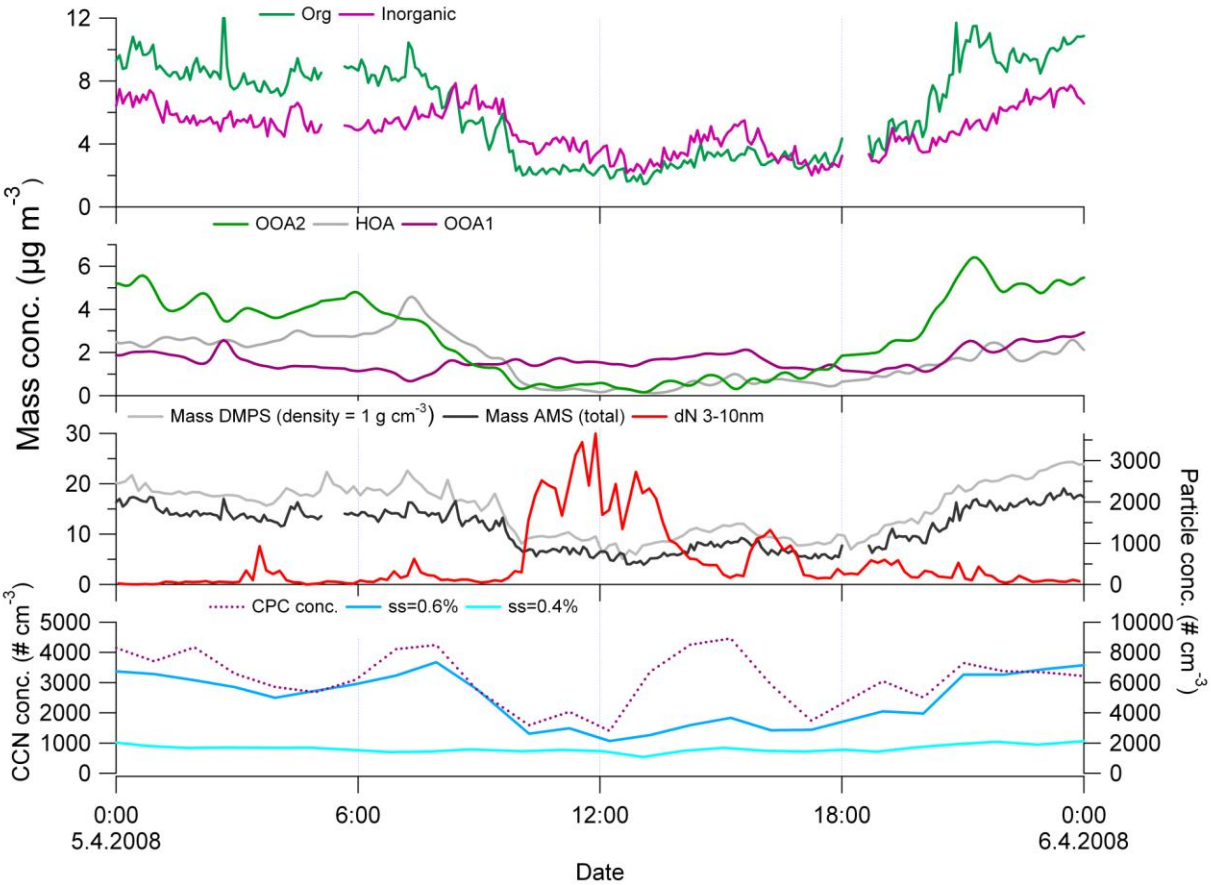

Figure 2. Q-AMS mass concentrations of total inorganics, and the three organic groups OOA1, OOA2, and HOA (two upper-most panels), comparison of DMPS and Q-AMS mass concentration (third panel) and CCN concentrations (lowest panel) for two supersaturations during the selected new particle formation event day.

The lowest panel of Figure 2 shows the CCN concentrations (left y-axis) for the supersaturations of 0.4 and 0.6%. In addition, the total particle number concentration given by the CPC is presented (right y-axis). Note that because of the 10 nm cut-off diameter of the TSI 3010 CPC used parallel with the

CCNC, the burst of the freshly formed particles are observed with some delay. With SS=0.4% CCN activation is quite constant throughout the day, except for the minor increase during evening, whilst with SS=0.6% CCN concentration correlates with OOA2 and HOA as both are clearly elevated during evening and night. During the daytime there is a small peak in the amount of inorganics after 3 p.m. This can be also seen as the increased number of SS=0.6% CCN, and although the newly formed particles have not grown to sizes able to activate in this SS, its likely that similar species condense both on newly formed particles and older particles in the accumulation mode.

In future analyses, we shall analyze AMS data to investigate how the size dependent composition of particles vary during the day, and how the estimated diameter of smallest activated particles depend on the composition of particles during and after the nucleation event.

ACKNOWLEDGEMENTS

EUCAARI and the Finnish Center of Excellence of Finnish Academy are acknowledged.

REFERENCES

Hamed, A. Joutsensaari, J., Mikkonen, S., Sogacheva, L., Dal Maso, M., Kulmala, M., Cavalli, F., Fuzzi, S., Facchini, M.C., Decesari, S., Mircea, M., Lehtinen, K.E.J., and Laaksonen, A. (2007). Nucleation and growth of new particles in Po Valley, Italy, *Atmos. Chem. Phys*., 7, 355-376.

Jayne, J.T., Leard, D.C., Zhang, X., Davidovits, P., Smith, K.A., Kolb, C.E., and Worsnop, D.R. (2000). Development of an Aerosol Mass Spectrometer for Size and Composition. Analysis of Submicron Particles, *Aerosol Science and Technology*, 33, 49-70.

Kulmala, M., Vehkamäki, H., Petäjä, T., Dal Maso, M., Lauri, A., Kerminen, V.-M., Birmili, W., and McMurry, P.H. (2004). Formation and growth rates of ultrafine atmospheric particles: a review of observations, *J. Aerosol Science*, 35, 143-176.

Quinn, P.K., Bates, T.S., Coffman D.J., and Covert D.S. (2008). Influence of particle size and chemistry on the cloud nucleating properties of aerosols, *Atmos. Chem. Phys*., 8, 1029-1042.

Roberts, G. C. and Nenes, A. (2005). A continuous-flow streamwise thermal gradient CCN chamber for atmospheric measurements, *Aerosol Sci. Tech*., 39, 206–221, 2005.

Twomey, S. (1991). Aerosols, clouds and radiation, *Atmos. Environ.*, 25A, 2435–2442.

Ulbrich, I.M., Canagaratna, M.R., Zhang, Q, Worsnop, D.R. and Jimenez J.L. (2009). Interpretation of Organic Components from Positive Matrix Factorization of Aerosol Mass Spectrometric Data, *Atmos. Chem. Phys*., 9(9), 2891-2918.

PRODUCT STUDIES OF FILTER AND DENUDER SAMPLES FROM THE SAPHIR CHAMBER (W.P. 1.2)

A. KAHNT[1], Y. IINUMA[1], T.F. MENTEL[2], R. FISSEHA[2], A. KIENDLER-SCHARR[2] and H. HERRMANN[1]

[1]Leibniz-Institut für Troposphärenforschung, Permoserstraße 15, D-04318, Leipzig, Germany.

[2]Institut für Chemie und Dynamik der Geosphäre ICG-2: Troposphäre, Forschungszentrum Jülich, D-52425 Jülich, Germany.

Keywords: SOA, AGING, MONOTERPENES, SESQUITERPENES.

INTRODUCTION

The work package 1.2 of the EUCAARI project aims to study the processes of aerosol formation from the oxidation of realistic and complex biogenic volatile compounds. The influence of different monoterpene precursors and the addition of sesquiterpenes were investigated during the EUCAARI 2008 campaign. The main focus of this study was the formation and aging of organic aerosol that were investigated in the SAPHIR outdoor chamber in Jülich.

METHODS

The reaction of boreal monoterpene mixtures was investigated in the SAPHIR chamber. In addition, the influence of additional ocimene and sesquiterpenes was studied (see Table 1). The oxidation experiments were carried out under atmospheric light intensity, HO_x and low NO_x conditions. The formation of the organic aerosol was studied during the first day and the aging of the produced aerosol was investigated the following day.

Table 1. Selected experimental conditions for the SAPHIR campaign 2008.

Experiment number	EUC08_1_1	EUC08_2_1	EUC08_4_1	EUC08_7_1	EUC08_7_2
Boreal Mix (□-pinene, □-pinene, limonene, 3-carene)	50ppb	50ppb	50ppb	100ppb	Photochemical aging of particles from EUC08_7_1
	with ocimene	without ocimene	-	-	
Sesquiterpenes (□-farnesene, caryophyllene)	-	-	5ppb	10ppb	
Filter number	3	5	9	15	16

The formed products were sampled using a denuder/PTFE filter sampling technique at the end of day one for the freshly generated aerosol and at the end of day two for the aged aerosol. In collaboration with the

different work package partners, particle properties such as aerosol hygroscopicity, volatility and product distribution were characterised.
The chemical analysis of this study focuses on the determination of acidic compounds in the particle-phase and carbonyl compounds in both particle- and gas-phases. The collected filter and denuder samples were extracted and subsequently derivatised with 2,4-dinitrophenylhydrazine (DNPH) for the latter purpose. The samples were analysed using HPLC/(-)ESI-TOFMS after purification by solid phase extraction. The acidic compounds were analysed from the filter samples using UPLC/(-)ESI-IMS-QTOFMS.

SUMMARY

In addition to known carbonyl compounds from monoterpene oxidation such as pinonaldehyde and endolim, previously unreported oxidation products were detected. These were tentatively identified as hydroxycarbonyl compounds with the molecular weight of 168 ($C_{10}H_{16}O_2$) and 154 ($C_9H_{14}O_2$).
Due to the possible accumulation of carbonyl compounds in the SAPHIR chamber during the campaign, no results of the aging experiments can be given for the gas-phase carbonyl compounds as significant levels of these compounds were found from the analysis of the “empty chamber” experiment samples. On the other hand, lower concentrations of acidic oxidation products are found after the photochemical aging except pinonic acid which shows almost the same or higher concentrations than the corresponding non-aging experiments. Pinic acid, which is believed to be a stable end product, is largely lost during the aging experiment. It has been suggested that the OH initiated oxidation of pinic acid can lead to recently identified "3-methyl-1,2,3-butanetricarboxylic acid" (MBTCA, Szmigielski et al., 2007) though only the trace amounts of MBTCA are detected in all samples, indicating the formation of different oxidation products.

ACKNOWLEDGEMENTS

This work was supported by the Europen Comission under grant 036833 (EUCAARI).

REFERENCES

Szmigielski, R., J. D. Surratt, Y. Gómez-González, P. Van der Veken, I. Kourtchev, R. Vermeylen, F. Blockhuys, M. Jaoui, T. E. Kleindienst, M. Lewandowski, J. H. Offenberg, E. O. Edney, J. H. Seinfeld, W. Maenhaut, and M. Claeys (2007), 3-methyl-1,2,3-butanetricarboxylic acid: An atmospheric tracer for terpene secondary organic aerosol, Geophys. Res. Lett., 34, L24811, doi:10.1029/2007GL031338.

Aerosol optical depth by MODIS and MISR

Scoring the performance of monthly level 3 products

S. Kinne

MPI-Meteorology, Hamburg

Abstract. A new scoring system is introduced to quantify the performance of MISR and MODIS satellite sensor retrieval products for aerosol optical depth (AOD). Based on comparisons to highly accurate ground-based sun-photometer data of AERONET here stratified into 25 regions and 12 month, scores for bias and variability are assigned. These regional and temporal sub-scores are then combined into single annual global overall scores. MODIS (.61) and MISR (.58) global annual scores are at the top of available multi-annual AOD data-sets. Both data-sets (based on multi-annual statistics) score even better than the usually well behaved multi-model median (.58). MODIS scores better over oceans and MISR scores better over land. Another aspect of this new scoring is the diagnostics, which allows tracing poor retrieval performance back to failure at temporal and spatial sub-scales. Such analysis for instance suggests that MODIS suffers from retrieval issues over continents in mid-latitudes during winter (possibly due to sub-pixel snow) and that MISR suffers from retrieval issue at high latitudes (certainly related to MISR's relatively poor temporal sampling). Differences in scores at these sub-scales allow the identification of regional and seasonal retrieval strengths and help in making more objective choices when picking one retrieval over another.

Key Words: satellite remote sensing, tropospheric aerosols

INTRODUCTION

Aerosol impacts on the hydrological cycle and consequently the Earth's climate remain uncertain. A major reason is that the influence of aerosol on properties of co-located clouds is poorly understood. It does not help that there are large uncertainties to spatially and temporally varying properties for aerosol amount and composition. These are modulated not just by natural variability (e.g. surface winds, wild-fires, volcanic eruption) but also by anthropogenic activity (fossil fuel burning, land-use change). Thus, the monitoring of aerosol global distributions from space has become an essential element in climate research. Aerosol dedicated data of multi-spectral MODIS and even a multi-directional MISR instruments on NASA's EOS platforms have been collected for almost ten years. Their solar reflectance data have been interpreted to provide global maps for aerosol column amount in terms of the mid-visible aerosol optical depth (AOD). However, even for cloud-free pixels in trace-gas poor solar sub-spectral bands, AOD estimates suffer from accuracy issues. Major reasons are a-priori assumptions to aerosol composition in the retrieval model and insufficiently accurate characterizations of the surface reflectance, which is a function of the viewing geometry and near-surface meteorological conditions. Thus, different AOD retrievals for the same location are rarely yield identical values. Recent studies have shown that simultaneous and co-located (successful) AOD retrievals of MODIS and MISR (from the same EOS Terra

platform) can be at times quite different (Liu and Mishchenko, 2008). This has put their usefulness for many applications in question. For a more general answer, monthly level 3 1x1 lat-lon gridded MODIS and MISR AOD products are assessed against quality data of the ground-based AERONET sun-photometer network (Holben et al., 1998). For these comparisons available local monthly statistics of all AERONET sites were combined onto a satellite data equivalent regular grid. Hereby, sites with better regional representation (T. Eck, private communication) were allowed to serve as reference for surrounding grid points. Separately for each region, available data-pairs (of satellite data and AERONET) were assessed on a (multi-annual) monthly basis in terms of bias, spatial variability and seasonality. After a brief introduction of the examined data-sets and the chosen regional stratification, the quantitative evaluation method is outlined. Regional monthly sub-scores as well as combined overall scores are established and compared among both products to convey general retrieval strengths and limitations.

DATA-SETS

The satellite AOD data-sets of interest are MISR and MODIS. The MISR data here refer to version 22 (Kahn et al., 2005), while the MODIS data refer to collection 5.1 (Levy at al., 2007). For better statistics monthly data of all available years are combined. The MISR data cover almost a decade (2000-2008) and MODIS data combine morning (2000-2006) and afternoon (2002-2006) data and deep-blue retrievals (Hsu et al., 2006) are included to extend land coverage of the standard algorithm to bright surfaces. Maps of annual AOD averages are presented in Figure 1.

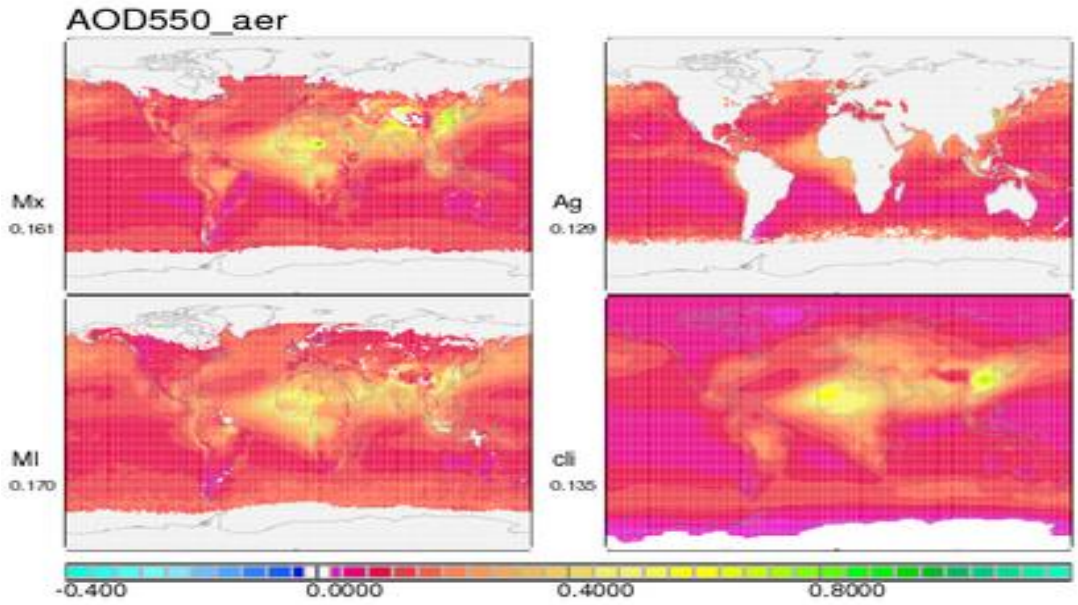

Figure 1. Annual multi-annual AOD values of MODIS (Mx), MISR (MI), AVHRR (Ag) and the climatology (cli) – values below the labels indicate the (annual) average of non-zero data points (no coverage by satellite data in polar regions, no land coverage by AVHRR)

For comparison purposes annual AOD averages of (2002-2004) AVHRR-GACP data (with ocean only coverage) and of a climatology are also presented in Figure 1. The climatology (Kinne, 2008) is based on characteristic (multi-model median) values by global modeling onto which quality data by AERONET are locally imposed.

To illustrate general biases the satellite data-sets are compared to the climatology. Differences maps are displayed in Figure 2. In place of the climatology the multi-model median is applied to illustrate the impact of AERONET statistics on suggestions by global modeling (indicating areas of deficiencies). Negative differences suggest underestimates and positive differences indicate overestimates.

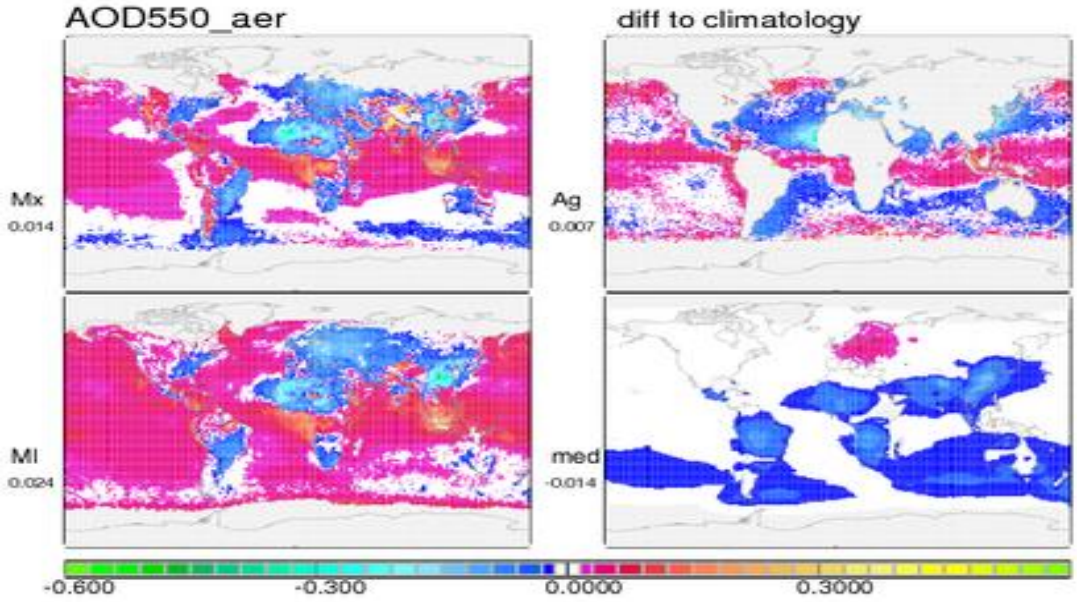

Figure 2. Annual multi-annual AOD differences of MODIS (Mx), MISR (MI), AVHRR (Ag) and the model median (med) with respect to the AERONET/model climatology – values below the labels indicate the global averages of non-zero data pairs

The AERONET modifications to the model median suggest that global modeling overestimates AOD over Europe (likely emission overestimate) and underestimate AOD over continental regions influenced by wildfires, over Asia and over Southern Oceans. If trusting the climatology, then MODIS and especially MISR overestimate AOD over ocean. AVHRR seems to do better over oceans, except for severe AOD underestimates in the dust-outflow region off Africa. Over continents MODIS and MISR underestimate AOD almost everywhere except for the central tropics. Larger AOD underestimates are found for regions dominated by dust (stronger for MISR) and urban pollution (stronger for MISR). Interestingly, the deviation patterns of MODIS and MISR are quite similar, so there is a suspicion, that the chosen reference could be in error. Thus, for a more solid evaluation, satellite data are (still statistically) only compared at the relatively few grid points with matches of satellite and AERONET monthly statistics. Hereby, these comparisons were combined on a regional basis.

REGIONAL STRATIFICATION

For the regional analysis, the globe was stratified into 25 regions of Figure 3.

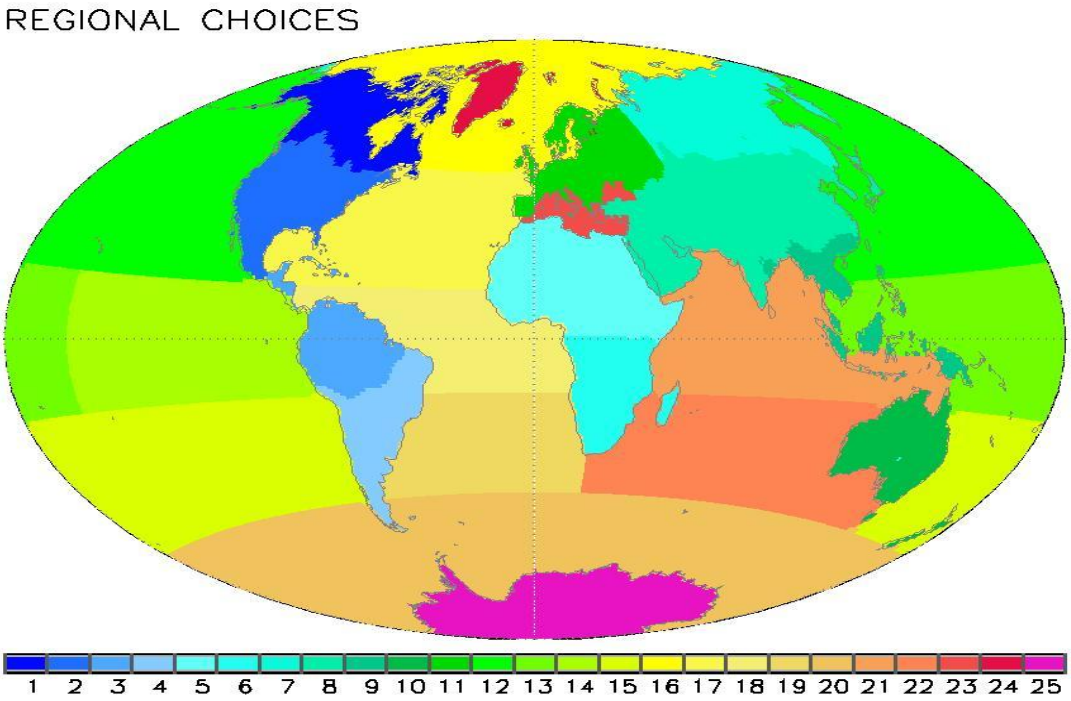

Figure 3 selected regional stratification based on TRANSCOM vegetation classes

Data pairs covered between 24% (continental USA) and 0% (Antartica) of the grid-points in each region. Due to no or too few data-pairs no evaluations were possible for Antarctica, the Arctic and the Southern Atlantic. Still questionable also might be scores based fewer than 40 matches. This affects mainly ocean regions in the tropics and in the southern hemisphere such as the Southern Oceans (~15), the tropical eastern Pacific (~20) and the southern Indian ocean (~35).

SCORING

A new scoring method has been developed for the evaluation of gridded data-sets. The overall goals of this quantifying scoring methods were

- *to assure robust scores, in the sense that they are resistant to single outliers*
- *to satisfy the need for capturing the overall performance by a single score*
- *to maintain diagnostic capabilities at spatial and temporal sub-grid scales.*

Thus, starting at selected temporal (e.g. daily or monthly) and spatial (e.g. Europe) sub-scales, test-data are compared to reference data. At these sub-scales, scores for bias and variability are determined. Then separately for bias and both temporal and spatial variability, local and seasonal scores are combined, first (via appropriate temporal weights) annually and then (via appropriate spatial weights) globally. Bias and both

variability scores can be combined (by multiplication) at each stage into an overall score. Similarly, a combination of global annual scores for bias and variability yield in one single score. To assure score robustness, solely outlier-resistant rank-based methods are employed. More details are given next.

The new method is based on error deductions **E** (0.0 = no error, 1.0 = maximum error) from a perfect score (1.0). These errors define sub-scores **S** (=1-**E**) for bias, for spatial and for temporal variability. The multiplication of the sub-scores yields an overall score $\mathbf{S_O}$, whereby the sign of the overall score carries the sign of the bias. ($\mathbf{S_O} = \mathbf{S_B}^* \mathbf{S_S}^* \mathbf{S_T} = \text{sign}(\mathbf{E_B})^* [1-|\mathbf{E_B}|]^* [1-\mathbf{E_S}]^* [1-\mathbf{E_T}]$).

For the bias error $\mathbf{E_B}$ [-1.0, 1.0] all (N) data-pair elements of both test and reference data are placed in one single array and ranked by value (e.g. rank=1 for the smallest value and rank=2*N for the largest value). Then the ranks belonging to the elements of the test-data and to the elements of the reference-data are separately summed. Then the two rank-sums are compared. If the two rank sums are equal or almost identical, no bias is indicated. However, if the rank-sums differ (strongly) a bias is identified. Hereby, the rank-sum difference is divided by their sum to assure that the bias error falls within -1.0 and +1.0 (the prescribed range).

$$\mathbf{E_B} = w * [(D_{SUM}-R_{SUM}) / (D_{SUM}+R_{SUM})]$$
$$\textit{with } w = \textit{min } (1.0, [_{RANGE}D+_{RANGE}R]/[_{MEDIAN}D+_{MEDIAN}R])$$

Note, a weight w is applied to reduce error-contributions, if variability is lacking. The variability is here estimated from the ratio between range and average. To make this variability estimate outlier resistant, the ratio of the inter-quartile range and the median-value was selected instead. If this ratio falls below 1.0, then the (rank-sum difference based) error is reduced with the ratio as weight. For the spatial variability error $\mathbf{E_S}$ [0.0, 1.0] and the temporal variability error $\mathbf{E_T}$ [0.0,1.0] rank correlations (ranking elements separately in each data-set by value and comparing ranks of all [test/reference] data pairs) are applied, such that the correlation error falls between 1.0 (correlated) and 0.0 (anti-correlated).

$$\mathbf{E_S} = w * [1-R_C] /2 \qquad \mathbf{E_T} = w * [1-R_C] /2$$
$$\textit{with } w = \textit{min } (1.0, [_{RANGE}D+_{RANGE}R]/[_{MEDIAN}D+_{MEDIAN}R])$$

Here R_C is the rank-correlation coefficient. As for the bias error again the variability weight w is applied to assure that errors at low variability are not overemphasized.

The scoring is started at the smallest temporal and spatial sub-scales. Based on these sub-scores, a single annual global score is achieved in two steps. In the first (temporal) averaging step, the sub-regional (w-weighted) rank-sums and spatial correlation errors are averaged in time to yield regional annual errors and scores. For the regional overall score sub-scores of bias and spatial variability are combined with a seasonality sub-score, which is based on the temporal correlation error, determined by correlating the ranks of (monthly) median values. Then, in a second (spatial) averaging step, annual global scores are achieved, by weighing regional scores with their associated surface area fraction.

RESULTS

The annual averaged performance of MODIS and MISR multi-annual AOD data versus AERONET multi-annual AOD data are ranked according to the overall score in Table 1, globally as well stratified into ocean and land region. For comparison purposes also scores of other data-sets are given. These includes the AVHRR-GACP performance over oceans, scores of two data-set associated with global modeling (the AeroCom model median, Kinne et. al. 2006 and an AERONET improved version termed 'aerosol climatology' Kinne, 2008) and scores of a remote sensing composite (where regionally best performing satellite data with respect to AERONET were combined, Kinne, 2009).

Table 1. AOD scores of test-data with respect to the AERONET reference in a multi-annual comparison. Aside from MODIS (modx_a) and MISR (misr_a), also the ocean (=global) score of AVHRR-GACP (gacp_K), the modeling associated median (med_a) and its AERONET tuned climatology (clim_a) as well as the a remote sening regional composite (best_a) are compared. The upper panel ranks global overall scores, the central table ranks overall scores limtited to oceans and the bottom ranks overall scores with respect to land. Also indicated are the associated sub-scores for seasonality (time), bias (bias) and spatial variability (space). In addition, statistical parameters of test-data median (med-d), reference median (med-r) at available matches, relative error (rel-err) and relative bias (rel-bias) are provided.

rank	global-score	time	bias	space	med-d	med-r	rel-err	rel-bias	label
1	0.6919	0.692	0.948	0.872	0.837	0.134	0.125	0.29E+00	0.14E+00	best_a
2	0.6424	0.642	0.932	0.828	0.833	0.137	0.123	0.37E+00	0.15E+00	clim_a
3	0.6086	0.609	0.924	0.828	0.795	0.147	0.125	0.39E+00	0.22E+00	modx_a
4	0.5866	0.587	0.916	0.801	0.799	0.155	0.124	0.47E+00	0.31E+00	misr_a
5	0.5691	0.569	0.868	0.813	0.806	0.119	0.123	0.44E+00	0.11E-01	medm_a

rank	ocean-score	time	bias	space	med-d	med-r	rel-err	rel-bias	label
1	0.6697	0.670	0.940	0.850	0.839	0.098	0.090	0.29E+00	0.16E+00	best_a
2	0.6137	0.614	0.923	0.800	0.831	0.099	0.087	0.40E+00	0.17E+00	clim_a
3	0.6079	0.608	0.921	0.805	0.821	0.118	0.089	0.39E+00	0.30E+00	modx_a
4	0.5729	0.573	0.865	0.802	0.826	0.086	0.087	0.45E+00	0.22E-01	medm_a
5	0.5652	0.565	0.908	0.770	0.808	0.136	0.088	0.51E+00	0.44E+00	misr_a
6	0.4757	0.476	0.808	0.843	0.698	0.106	0.090	0.51E+00	0.15E+00	gacp_K

rank	continent-score	time	bias	space	med-d	med-r	rel-err	rel-bias	label
1	0.7540	0.754	0.969	0.933	0.834	0.231	0.223	0.27E+00	0.75E-01	best_a
2	0.7245	0.725	0.955	0.904	0.839	0.242	0.223	0.31E+00	0.99E-01	clim_a
3	-0.6446	-0.645	0.938	-.887	0.775	0.207	0.224	0.36E+00	-.54E-01	misr_a
4	0.6048	0.605	0.932	0.894	0.725	0.224	0.225	0.39E+00	0.99E-02	modx_a
5	0.5561	0.556	0.878	0.845	0.749	0.209	0.223	0.41E+00	-.20E-01	medm_a

The remote sensing composite and the climatology perform best, but they also make use of AERONET data, which serve as reference. MISR and MODIS global annual scores are almost identical and slightly better than those of the median model. MODIS score higher than MISR over oceans, while MISR score better than MODIS over land. The bias sign indicates that both satellite data-sets have overall a positive bias. While MODIS overestimate over both oceans and land, MISR overestimates over oceans are partially compensated by underestimate over land. The errors associated with the overall scores among the six data-sets are compared in Figure 4.

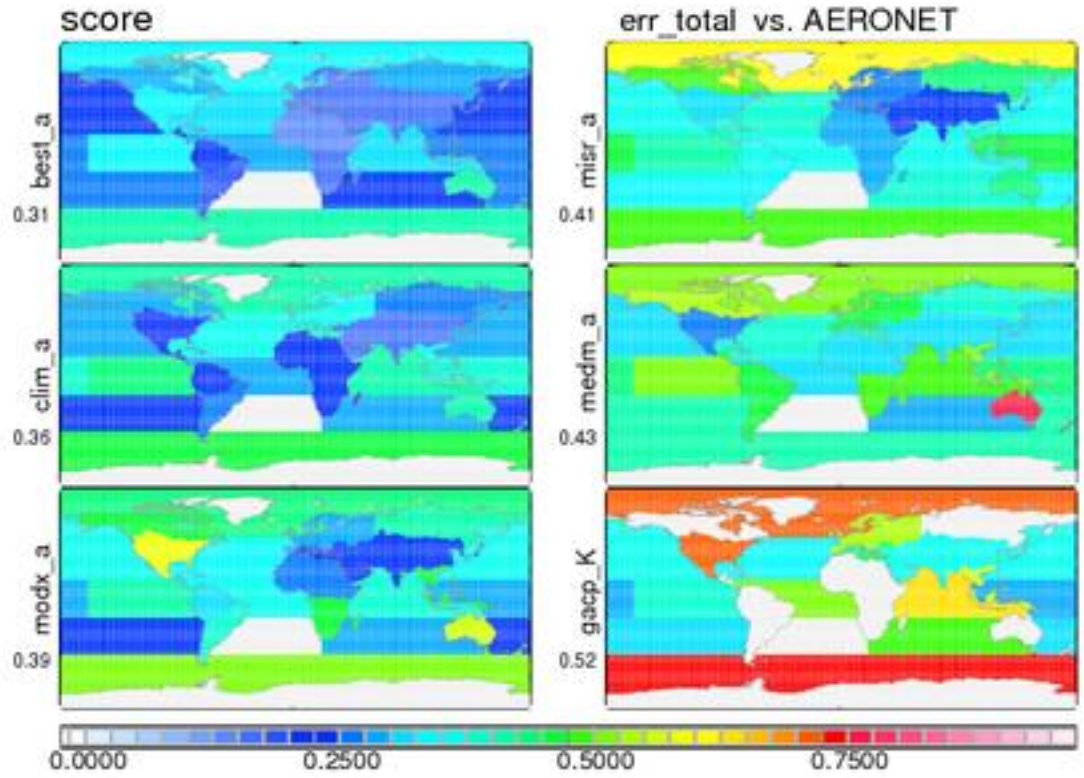

Figure 4 selected regional overall errors (error=1.0-score) for the six data-sets of Table 3.

The score in Figure 4 is represented by the deviation from a perfect score of 1.0, such that larger values indicate increased data-set deficiencies (compared to AERONET). For MODIS major problem areas are identified as the continental US and Australia. MISR does poorest over Arctic oceans. Generally the error in both data-sets increases towards polar altitudes. Better scores by both satellite data-sets are achieved over Europe, central Asia and Northern Africa.

Additional regional sub-scores and statistics of Figures 5 and 6 provide more scoring and performance detail for the MODIS and MISR data-sets. Both data-sets are usually biased high expect for South America, Africa, Europe and central Asia. The poor overall MODIS scores over the US and Australia is mainly caused by spatial variability. And the poor MISR score in the Arctic oceans is associated with errors in spatial variability and seasonality.

Inter-annual differences can be extracted from stratification into months. Monthly regional combined (bias and spatial variability) error totals for MODIS and MISR are presented in Figures 7 and 8. It is interesting to notice that these combined errors vary by season. For MODIS the US and Australia issues are mainly a winter-season problem (possibly a snow-cover issue), while for MISR the Arctic problem is strongest during summer (possibly a wildfire issue).

The difference scores for MODIS and MISR allow selections, in what region or season the one data-set should be picked over the other data-set. This can be easily demonstrated by exploring scoring differences in Figure 9 for annual averages and in Figure 10 for individual months.

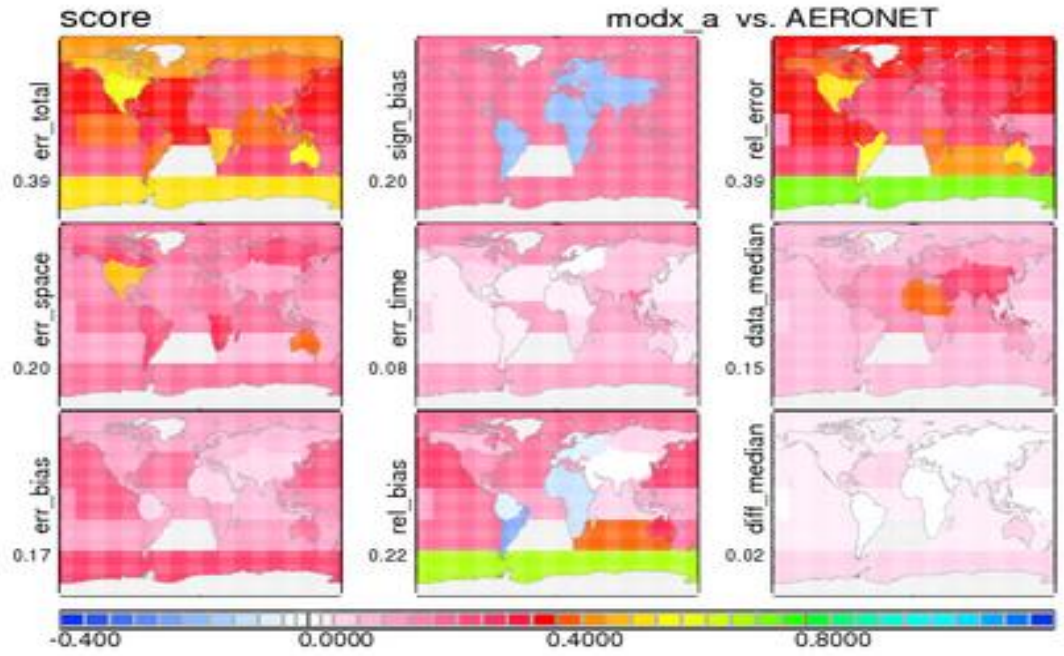

Figure 5. Annual regional errors and statistics for MODIS data. The central top panel displays the bias sign, while the lower right panel displays the median value difference for bias strength. Bias error in the lower left is combined with spatial variability error in the center left and the seasonality error in the center to yield the overall error which was already displayed in Figure 4. Other fields show the relative bias and the relative error as well as the data-set median values.

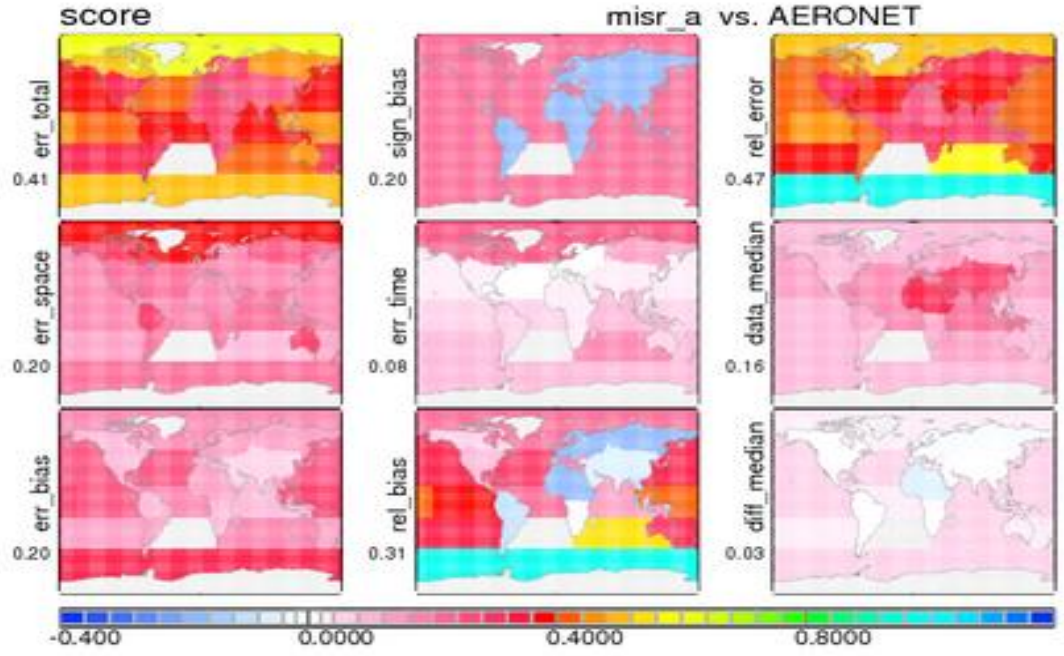

Figure 6. Annual regional errors and statistics for MISR AOD data (see Figure 5 captions)

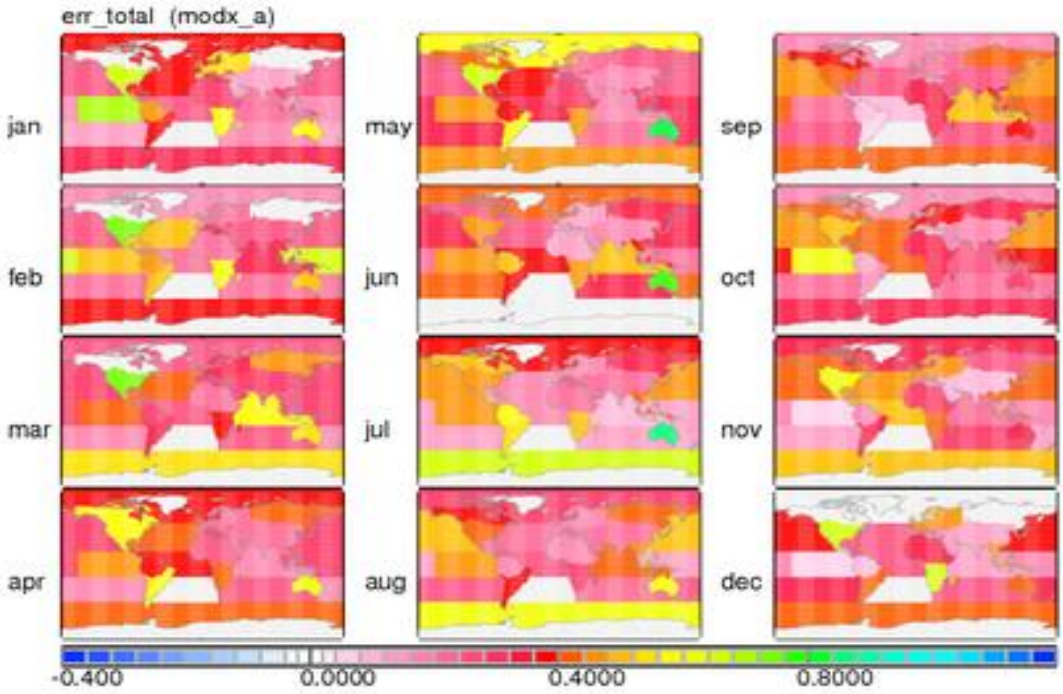

Figure 7. Monthly regional combined bias and spatial variability errors for MODIS AOD

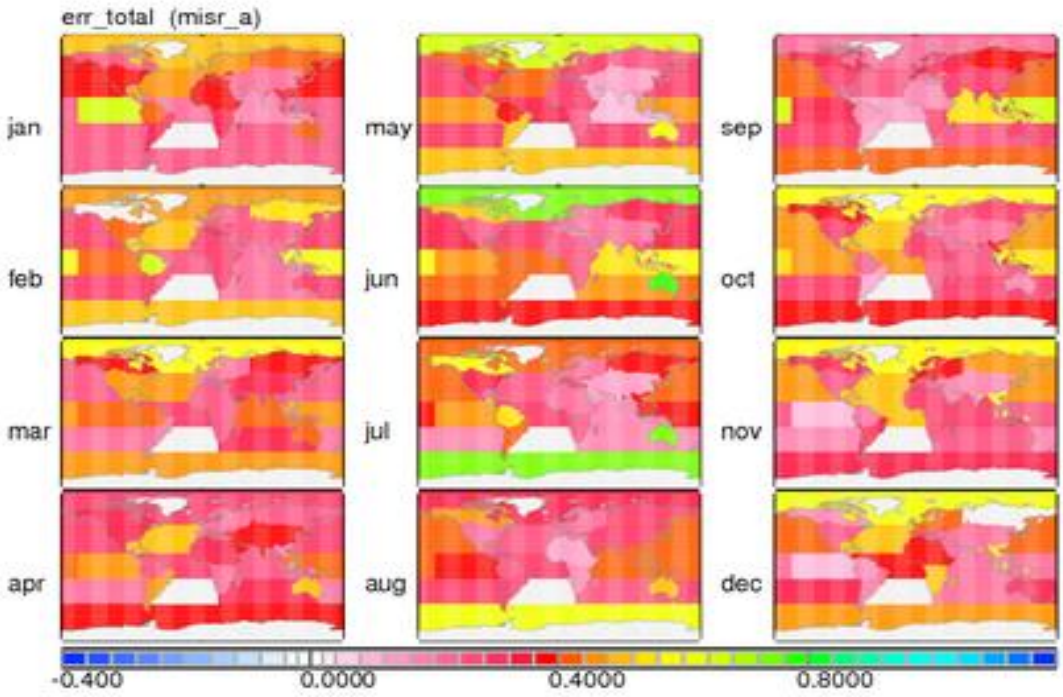

Figure 8. Monthly regional combined bias and spatial variability errors for MODIS AOD

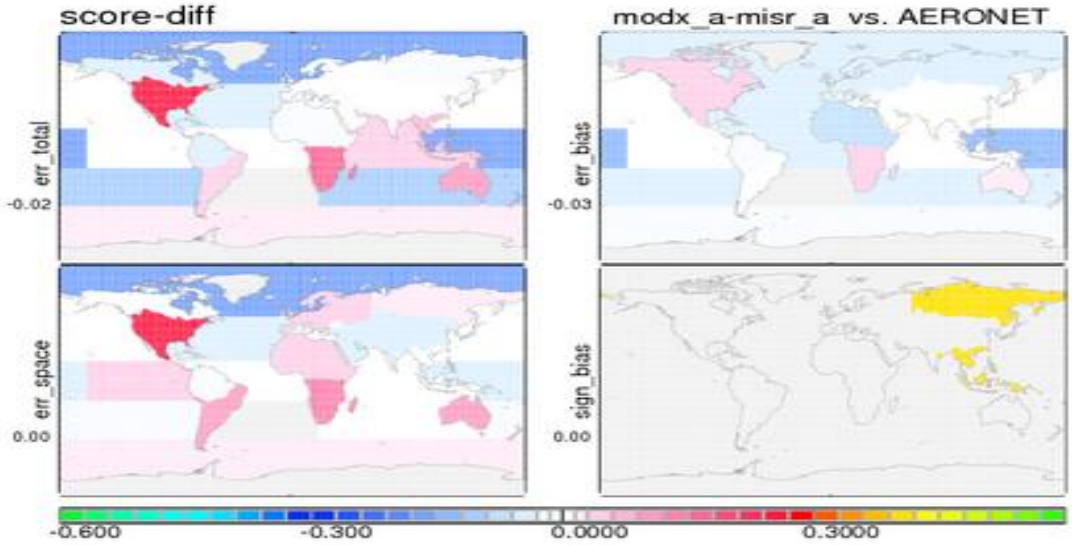

Figure 9. Annual regional (score associated) error differences between MODIS and MISR. Negative (blue) colors indicate a better performance by MODIS, whereas positive (red) values indicate a better performance by MISR. Investigated are overall score, spatial variability and bias. Also indicated are bias sign switch, from regional MISR underestimates to MODIS overestimates (indicated by the yellow color).

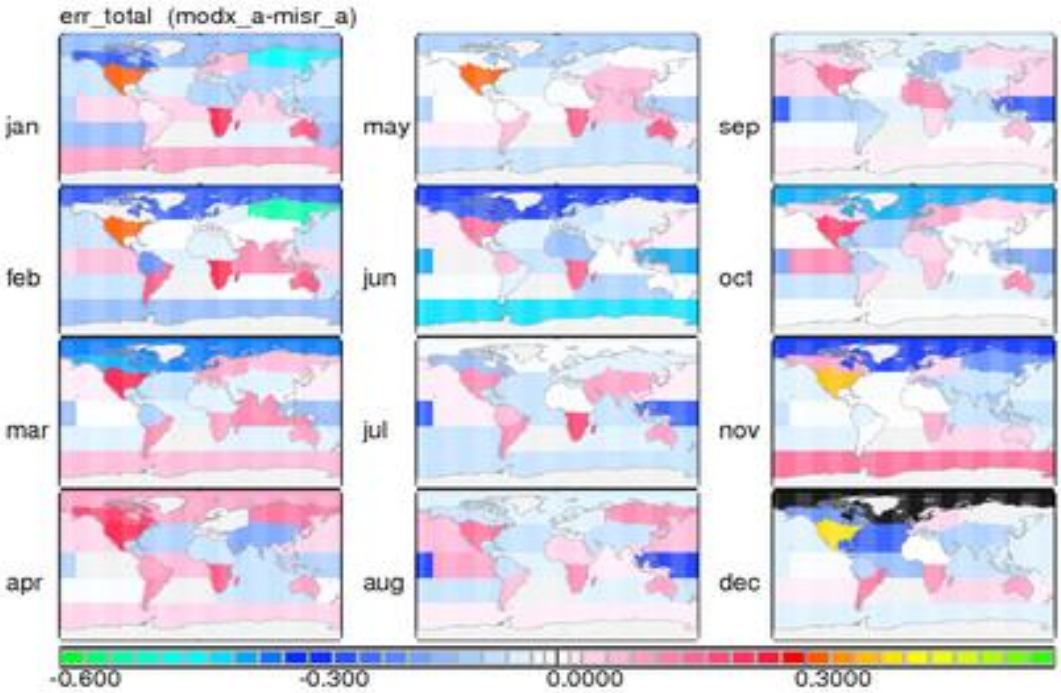

Figure 10. Monthly regional (overall score associated) error differences between MODIS and MISR. Negative (blue to black) colors indicate a better performance by MODIS, whereas positive (red) values indicate a better performance by MISR.

For current processing versions the annual averages MISR data seem preferable over continents, in particular for the US, Australia, Southern Africa and South America, whereas MODIS data are preferable over oceans, especially for the Arctic but also for tropical regions. This recommendation becomes more diverse though when looking at monthly scores. For instance in April the MISR score is preferable to that of MODIS against the general trend to choose MODIS for that region.

CONCLUSION

The evaluation demonstrated that both satellite AOD products of MODIS and MISR (even on a multi-annual basis) have a slightly better skill than the usually well-behaved model median data-set of global modeling. While global performance is quite similar, MISR performance is usually better over land and MODIS performance is better over oceans. Since the scoring system is based on individual scores at spatial and temporal sub-scales a more detailed error diagnostics is possible. For instance the stratification into regions and months suggests MODIS retrieval issues linked to contamination by sub-pixel snow and available aerosol models, while MISR retrieval issues are often linked to its poorer sampling possibly explaining boreal wildfires misrepresentations. For many regions, the presented scores may not necessarily be representative, because relatively few AERONET reference grid-points of often not sufficient to capture the overall regional performance. Still when using the aerosol climatology (whereby AERONET data are extended in space and time with data from global modeling) most individual sub-scores and tendencies of the examined satellite data-sets are reproduced. Certainly, a more detailed analysis based on statistics of overpass matches between satellite level2 retrievals and quality ground data is desirable and is needed for a better understanding of bias and uncertainties. And it should be done in the framework of a quantitative comprehensive scoring system, similar to the one suggested here, for more objective and temporal and spatially complete assessment.

Acknowledgements

The work was supported by EU-projects GEMS and EUCAARI. Efforts of many global modeling groups contributing to AeroCom exercises and the support of many remote sensing groups, in particular the AERONET group by providing input on site assessments for data quality and regional representation, is gratefully acknowledged.

References

Holben, B., T.Eck, I.Slutsker, D.Tanre, J.Buis, E.Vermote, J.Reagan, Y.Kaufman, T.Nakajima, F.Lavenau, I.Jankowiak and A.Smirnov, AERONET, a federated instrument network and data-archive for aerosol characterization, *Rem.Sens.Environ. 66*, 1-66, 1998.

Hsu C., S.-C. Tsay, M.D.King and J.R.Herman, Deep Blue retrievals of Asian aerosol properties during ACE-Asia *IEEE Trans. on geoscience and remote sensing, 44, NO. 11*, 2006.

Kahn, R., B. Gaitley, J. Martonchik, D. Diner, K. Crean, and B. Holben, MISR global aerosol optical depth validation based on two years of coincident AERONET observations, *J.Geophys. Res., doi:10:1029/2004JD004706*, 2005.

Kinne, S., Remote sensing data combinations-superior global maps for aerosol optical depth. *Satellite Aerosol Remote Sensing Over Land*, edited by A.Kokhanovsky and G. de Leeuw, Springer ISBN: 978-3-540-69396-3, 2009

Kinne, S, Climatologies of cloud related aerosols- part 1 particle number and size, *Clouds in the perturbed climate system*, edited by J.Heintzenberg and J.Charlson, ISBN: 978-0-262-01287-4, 2008.

.

Kinne S., M.Schulz, C.Textor, S.Guibert, S.Bauer, T.Berntsen, T.Berglen, O.Boucher, M.Chin, W.Collins, F.Dentener, T.Diehl, R.Easter, J.Feichter, D.Fillmore, S. Ghan, P.Ginoux, S.Gong, A.Grini, J.Hendricks, M.Herzog, L.Horowitz, I.Isaksen, T.Iversen, D.Koch, M.Krol, A.Lauer, J.F.Lamarque, G.Lesins, X.Liu, U.Lohmann, V.Montanaro, G.Myhre, J.Penner, G.Pitari, S.Reddy, O.Seland, P.Stier, T.Takemura, X.Tie, An AeroCom initial assessment – optical properties in aerosol component modules of global models, *ACP, 6*, 1-22, 2006.

Levy, R.C., L.A. Remer, S. Mattoo, E.F. Vermote, and Y.J. Kaufman, 2, Second-generation operational algorithm: Retrieval of aerosol properties over land from inversion of Moderate Resolution Imaging Spectroradiometer spectral reflectance, *J. Geophys. Res*., *112*, doi:10.1029/2006JD007811, 2007.

Liu, L., and M.I. Mishchenko, Toward unified satellite climatology of aerosol properties:Direct comparisons of advanced level 2 aerosol products, *J. Quant. Spectro. Rad. Transf, 109*, 2376-2385, 2008.

supporting material

additional material of this evaluation are available via anonymous ftp

1. scores

ftp://ftp-projects.zmaw.de *cd aerocom/assessment/aerosol/scores*

rank_yg_score	ranks global	annual scores
rank_yo_score	ranks ocean area combined	annual scores
rank_yg_score	ranks land area combined	annual scores
rank_ry_score	ranks regional (25 regions)	annual scores
rank_rm_score	ranks regional (25 regions)	monthly scores

2. plots

ftp://ftp-projects.zmaw.de *cd aerocom/assessment/aerosol/plots*

xc… absolute values map comparisons
xd… map differences to 'climatology'
yc… error (and statistics) of test-data with respect each (subdirectory-)
yd… error (and statistics) differences among data-sets
_s_ different errors for a satellite data-set
_c_ same error for different data-sets
…2month 2-series: ending-label indicates data for specific month
…3property 3-series: ending-name indicates data for specific property
…4 4-series: annual averages

the plots address errors (E=1-|S|) rather than scores S.
all plots display absolute values or changes to

overall error	(err_total)
spatial error	(err_space)
bias error	(err_bias)
bias sign	(sign_bias)

selected plots also address

relative bias	(rel_bias)
relative error	(rel_err)
test-data median	(data_median)

median diff. between test-data and reference data (diff_median).

FORMATION OF HUMIC-LIKE SUBSTANCES THROUGH TERPENE OXIDATION

G. KISS[1], N. TÖRŐ[2], V. DOMJÁN[2], A. HOFFER[1] R. FISSEHA[3], A. KIENDLER-SCHARR[3], T. BRAUERS[3] AND T.F. MENTEL[3]

[1]Air Chemistry Group of Hungarian Academy of Sciences, P. O. Box 158, H-8201 Veszprém, Hungary

[2]University of Pannonia, Dept. Earth and Env. Sci., P. O. Box 158, H-8201 Veszprém, Hungary

[3]Forschungszentrum Jülich, D-52425 Jülich, Germany

Keywords: TERPENES, OZONOLYSIS, LC-MS, HULIS

INTRODUCTION

Secondary aerosol formation from 5 monoterpenes (Ocimene, α-Pinene, β-Pinene, Limonene, Δ3-Carene) and 2 sesquiterpenes (β-Caryophyllene, α-Farnesene) under various conditions was studied in a series of experiments performed in the SAPHIR chamber at Forschungszentrum Jülich in June 2008. In these simulation experiments ozone concentration, relative humidity, temperature and light conditions varied. Aerosol microphysical characterization as well as aerosol mass spectrometry were performed on-line but filter sampling was also carried out for more detailed off-line chemical characterization. In most cases filter samples were collected in the first day of reaction then the aerosol particles aged in the chamber and filter samples were collected again on the second day. Reaction products were analyzed at University of Pannonia by electrospray ionization (ESI) and atmospheric pressure chemical ionization (APCI) mass spectrometry either directly or following HPLC separation. Results of ESI-MS are shown in this paper.

EXPERIMENTAL

Extraction of the filters

The targeted compounds (oxidation products of terpenes) have both hydrophobic (hydrocarbon) parts and hydrophilic parts (the oxygen containing functional groups). Therefore, acetone was chosen as an extracting solvent for its moderate polarity. After extraction the extracts were filtered through a 0.45 µm membrane filter (Millex LCR) and concentrated by a gentle nitrogen flow. Finally, the concentrated extracts were diluted with Milli-Q water-methanol mixture (1:1) prior to HPLC analysis.

HPLC-MS analyses

Phenomenex Luna C18(2)-HST column (L=100 mm, I.D.=3 mm, d_p=2,5 µm) was used with an eluent flow of 0.35 ml/min.) Gradient elution from 10% MeOH in acidified Milli-Q water to 100% MeOH in 10 minutes was applied. For direct injection ESI-MS analysis the following experimental setting was applied: Negative ionization mode, sample flow: 0.3 ml/h, nebulizer: 10 psi, dry gas: 4 l/min, dry temp.: 280 °C, scan: 50-500 m/z. For HPLC-ESI-MS nebulizer: 50 psi, dry gas: 10 l/min, dry temp.: 300 °C, scan: 50-500 m/z were set.

RESULTS

Direct ESI-MS analyses

Ions of a number of known oxidation products (e.g. pinic acic, caric acid, norlimonic acid, etc.) were found in the mass spectra, but in this paper unresolved complex compounds are in focus. In Figure 1a-c mass spectra obtained by direct ESI-MS in negative mode are shown for different mixtures of terpenes. In addition to the ions of known individual compounds (typically between m/z 150-220) periodic spectral lines ($\Delta m/z=14$) were also observed from approximately m/z 300 to 800 with maximum intensity around m/z 350 and 550. There was no obvious difference in the MS spectra of monoterpenes with or without ocimene (Figures 1a and 1b), however, the relative abundance of ions around m/z 500 increased when sesquiterpenes were also added (Figure 1c). The periodicity and the wide range of ions resembled those of humic-like substances found in rural aerosol although the maximum in ambient samples was around m/z 250-300 (Figure 1d). However, humic-like substances (HULIS) possess not only complex MS spectra but also characteristic UV and fluorescence (FL) properties. These features were also studied, UV and FL spectra are shown in Figures 2 and 3, respectively.

The UV spectrum of the terpene oxidation products showed monotonously decreasing absorbance from 200 to 400 nm, similarly to HULIS isolated from rural aerosol (Figure 2). The absorbance in the near visible range indicates the presence of polyconjugated structures that can be the consequence of oligomerisation reactions. In some of the filter extracts fluorescence was also observed. Excitation and emission wavelengths were iterated and the strongest emission was obtained when excitation with 271 nm was applied. The maximum in the emission spectrum was found at 403 nm, similarly to humic-like substances isolated from rural aerosol (Figure 3).

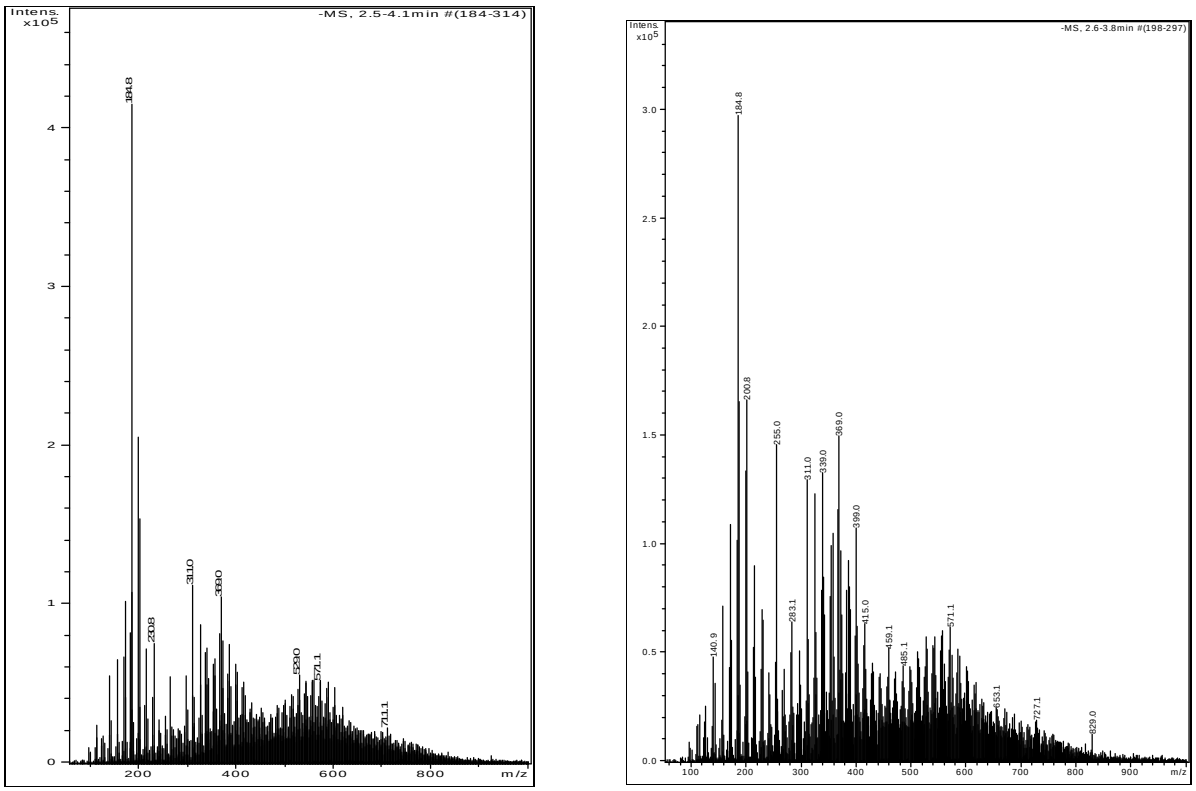

Figure 1 a (left panel): Direct ESI$^-$-MS spectrum of oxidation products of monoterpenes, and b (right panel): Direct ESI$^-$-MS spectrum of oxidation products of monoterpenes without ocimene

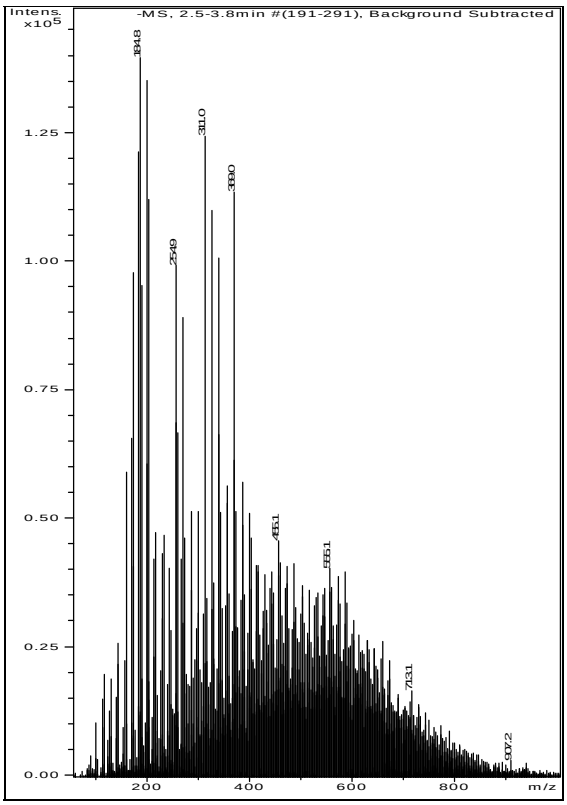

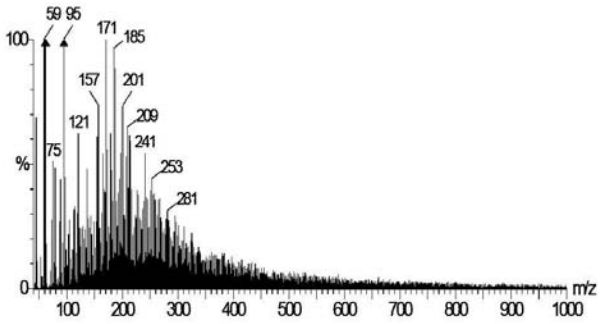

Figure 1 c (left panel): Direct ESI-MS spectrum of oxidation products of monoterpenes+sesquiterpenes, and d (right panel): Direct ESI-MS spectrum of HULIS isolated from rural aerosol sample

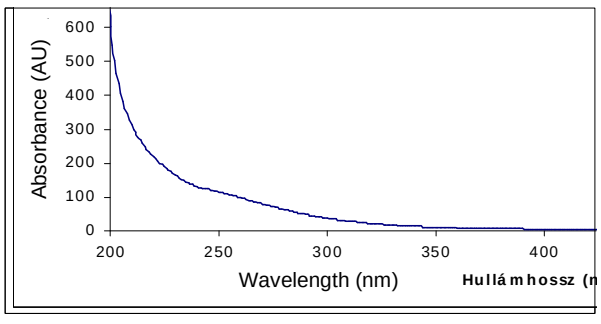

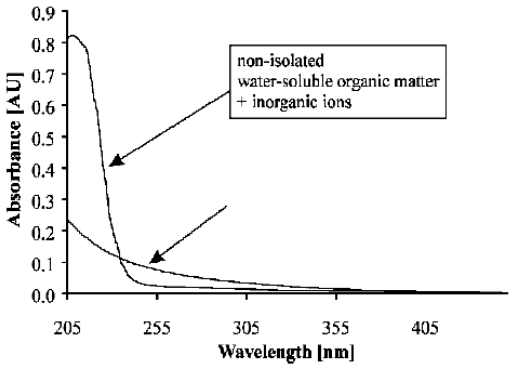

Figure 2 UV spectrum of a filter extract (left) and humic-like substances isolated from rural aerosol (right) (Kiss et.al, JGR, 2002)

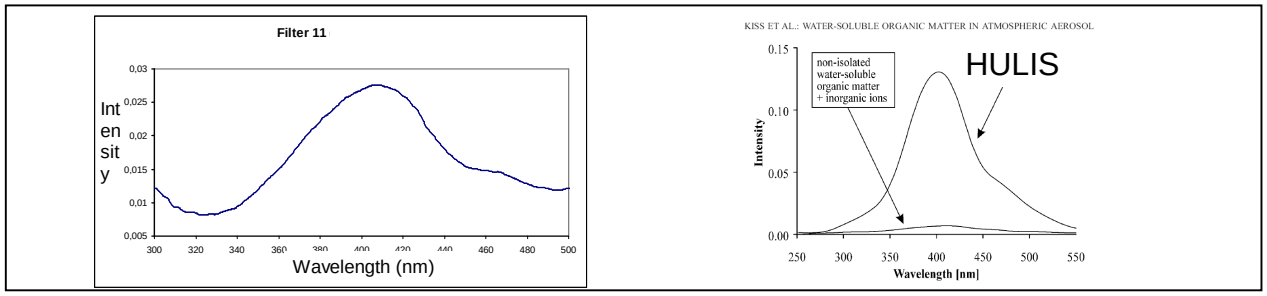

Figure 3 Fluorescence spectrum of a filter extract (left panel) and humic-like substances isolated from rural aerosol (right panel) (Kiss et.al, JGR, 2002)

CONCLUSIONS

On the basis of these results it can be concluded that in addition to known individual compounds (in most cases acids) complex mixture of oxidation products formed from monoterpenes and sesquiterpenes in the chamber experiments that resembled mass, UV and fluorescence properties of humic-like substances isolated from rural aerosol. Thus terpene emission can be an important source of humic-like substances which often account for 60% of the water-soluble organic carbon content of ambient aerosol. Furthermore, this phenomenon resolves to some extent the discrepancy between ambient SOA concentration and SOA formation observed in chamber experiments earlier (top down versus bottom up approach.)

ACKNOWLEDGEMENTS

This work was supported by the European Integrated project on Aerosol Cloud Climate and Air Quality Interactions (EUCAARI).

REFERENCES

Kiss, G., B. Varga, I. Galambos and I. Ganszky: “Characterization of water-soluble organic matter isolated from atmospheric fine aerosol”
Journal of Geophysical Research, 2002, Vol. 107, No. D21, art. no. 8339

IMPROVING THE PARAMETERIZATION OF IN-CLOUD UPDRAFT VELOCITY WITH THE AID OF EUCAARI-IMPACT DATA

C. HOOSE[1], J. E. KRISTJÁNSSON[1], S. ARABAS[2], H. PAWLOWSKA[2]

[1] Department of Geosciences, University of Oslo, Norway
[2] University of Warszaw, Poland

Keywords: cloud droplet activation, in-cloud turbulence

INTRODUCTION

In the global climate model CAM-Oslo, cloud droplet activation is calculated as a function of aerosol number, size and composition as well as of the vertical velocity w (Abdul-Razzak and Ghan, 2000; Storelvmo et al., 2006). In-cloud updrafts are not resolved in GCMs, and have to be parameterized. For this, a gaussian distribution of the vertical velocity around its grid-mean value is assumed. For the standard deviation of the gaussian distribution, σ_w, different formulations have been suggested in the literature (see below). Ideally, these formulations should account for wind shear, buoyancy generated at the surface or within clouds, radiative cooling at cloud top, solar heating, and entrainment. In reality, in models without turbulent kinetic energy schemes, simple expressions are used, which neglect cloud-generated turbulence.

PARAMETERIZATIONS FOR σ_w

In the previous CAM-Oslo version (Storelvmo et al., 2006), σ_w was parameterized after Ghan et al. (1997):

$$\sigma_w = \frac{\sqrt{2\pi}K}{\Delta z} \tag{1}$$

Δz is the layer thickness, and K the eddy diffusion coefficient for momentum. This parameterization has the disadvantage of being resolution-dependent.

Alternatively, the characteristic turbulent velocity w_{turb} given by Morrison and Gettelman (2008), which is employed in recent CAM-Oslo studies (Hoose et al., 2009), can be translated into σ_w using the relationship $w_{\mathrm{turb}} \approx 0.8\sigma_w$ (Fountoukis et al., 2007).

$$\sigma_w = 1.25 \cdot w_{\mathrm{turb}} = 1.25\frac{K}{l_c} \tag{2}$$

The mixing length l_c is set to a constant value of 30 m. This simplified assumption was improved by Wang and Penner (2009), who introduced a height-dependent mixing length $m_l(z)$.

$$\sigma_w = \frac{K}{m_l(z)} \tag{3}$$

Finally, a new approach is presented here. The CAM boundary layer scheme (Holtslag and Boville, 1993) provides the turbulent velocity scale w_t, from which K is derived. We add an empirical term to account for cloud-generated turbulence.

$$\sigma_w = w_t + C \cdot LWC \tag{4}$$

The constant C is set to $5 \cdot 10^5$ cm s^{-1}, for LWC (the liquid water content) given in kg kg^{-1}.

GLOBAL RESULTS AND COMPARISON TO EUCAARI-IMPACT DATA

In Figure 1 demonstrates the large differences between the four different parameterization schemes. The average values from different campaigns indicate that σ_w should range between 10 cm/s and about 1 m/s. Higher values are only observed in convective situations.

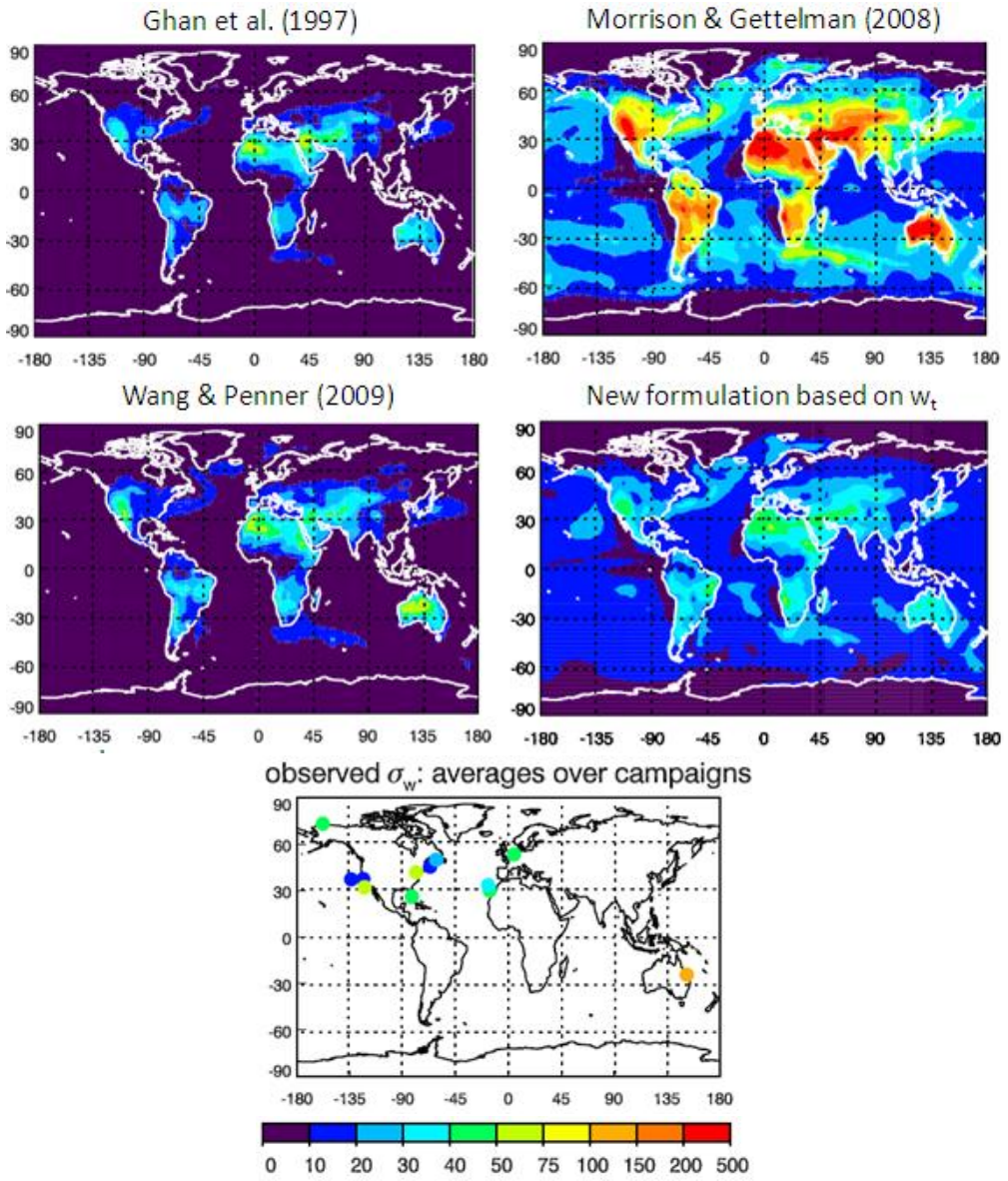

Figure 1: Annual average fields of σ_w in cm/s, parameterized after the four different approaches, for the lowest 2 km of the atmosphere. Below: Average values from different flight campaigns and ground-based measurements. The colorbar applies to all plots.

For the EUCAARI IMPACT campaign, vertically resolved profiles of σ_w are available from Wind-Cube ground-based measurements (Arabas et al., 2009). These are compared to the model results in Figure 2. The new empirical parameterization (equation 4) gives significantly improved results, especially at altitudes above 1 km and on cloudy days (not shown).

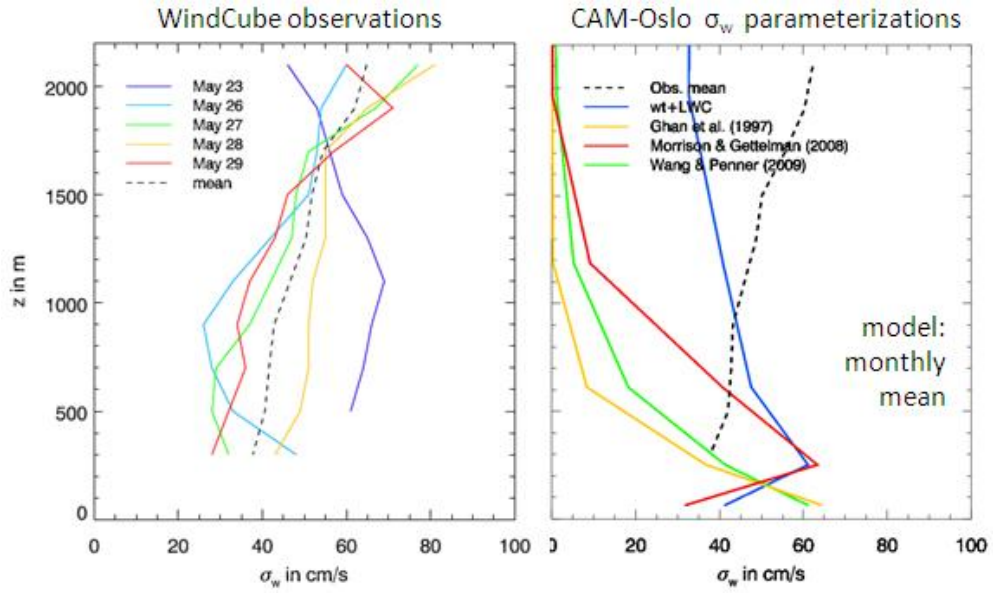

Figure 2: Average vertical profiles of σ_w for five days from the EUCAARI IMPACT campaign (Arabas et al., 2009), compared to monthly average profiles from the model with the four different parameterizations.

CONCLUSIONS AND FUTURE WORK

The new empirical formulation of σ_w, taking into account cloud-generated turbulence, has performed well for the EUCAARI-IMPACT campaign. Further comparisons to observations are planned, as well as theoretical considerations linking σ_w rather to the processes which generate turbulence (latent heat release, cloud-top cooling) than simply to the LWC.

In some situations, a gaussian probability distribution function is not a good approximation. For instance, marine stratocumulus clouds, in which turbulence is driven by cloud-top cooling, can exhibit positively skewed pdfs. Sensitivity studies with CAM-Oslo have shown that skewed distributions can reduce (positive skewness) or enhance (negative skewness) activation by 20%. However, the skewness of the updraft distribution function is even more difficult to parameterize than its width.

ACKNOWLEDGMENTS

This research is supported by the projects EUCAARI (European Integrated project No. 036833-2) and NorClim (Norwegian Research Council grant No. 178246), and computing time was provided through a grant from the Norwegian Research Council's program for Supercomputing.

REFERENCES

Abdul-Razzak, H. and Ghan, S. J. (2000). A parameterization of aerosol activation 2. Multiple aerosol types. *J. Geophys. Res.*, 105(D5):6837–6844.

Arabas, S., Baehr, C., Boquet, M., Bosveld, F., Dufournet, Y., Klein Baltink, H., Pawlowska, H., Siebert, H., and Unal, C. (2009). A comparison of selected vertical wind measurement techniques on basis of the EUCAARI IMPACT observations. *Geophys. Res. Abstracts*, 11(EGU2009-999).

Fountoukis, C., Nenes, A., Meskhidze, N., Bahreini, R., Conant, W. C., Jonsson, H., Murphy,

S., Sorooshian, A., Varutbangkul, V., Brechtel, F., Flagan, R. C., and Seinfeld, J. H. (2007). Aerosol-cloud drop concentration closure for clouds sampled during the International Consortium for Atmospheric Research on Transport and Transformation 2004 campaign. *J. Geophys. Res.*, 112(D10S30).

Ghan, S. J., Leung, L. R., Easter, R. C., and Abdul-Razzak, H. (1997). Prediction of cloud droplet number in a general circulation model. *J. Geophys. Res.*, 102(D18):21777–21794.

Holtslag, A. and Boville, B. (1993). Local versus nonlocal boundary-layer diffusion in a global climate model. *J. Clim.*, 6(10):1825–1842.

Hoose, C., Kristjánsson, J. E., Iversen, T., Kirkevåg, A., Seland, Ø., and Gettelman, A. (2009). Constraining cloud droplet number concentration in GCMs suppresses the aerosol indirect effect. *Geophys. Res. Lett.*, 36(L12807).

Morrison, H. and Gettelman, A. (2008). A new two-moment bulk stratiform cloud microphysics scheme in the Community Atmosphere Model, version 3 (CAM3). Part I: Description and numerical tests. *J. Clim.*, 21:3642–3659.

Storelvmo, T., Kristjánsson, J. E., Ghan, S. J., Kirkevåg, A., Seland, Ø., and Iversen, T. (2006). Predicting cloud droplet number concentration in Community Atmosphere Model (CAM)-Oslo. *J. Geophys. Res.*, 111(D24208).

Wang, M. and Penner, J. E. (2009). Aerosol indirect forcing in a global model with particle nucleation. *Atmos. Chem. Phys.*, 9(1):239–260.

2ND ION SPECTROMETER CALIBRATION AND INTERCOMPARISON WORKSHOP IN HELSINKI 25.5.-26.6.2009

K. LEHTIPALO[1], H. E. MANNINEN[1], S. GAGNÉ[1] , A. FRANCHIN[1], S. SCHOBESBERGER[1], and M. KULMALA[1]

[1]Department of Physics, University of Helsinki, P.O.Box 64, 00014 Helsinki, Finland

Keywords: ions, aerosol instrumentation.

INTRODUCTION

Ion spectrometers, like the Air Ion Spectrometer (AIS; Mirme *et al*. 2007) and its successor, the Neutral cluster and Air Ion Spectrometer (NAIS), have recently been extensively used for measuring the size distribution of atmospheric ions and particles. The mobility range of these instruments is 3.2-0.0013 $cm^2V^{-1}s^{-1}$ (~0.8-40 nm in mobility diameter). For detection of neutral particles the NAIS uses corona charging, which sets the lower size limit to about 2 nm depending on polarity and concentration (Asmi *et al*. 2009).

This workshop (WS) was a continuation to the 1st ion spectrometer calibration and intercomparison WS in Helsinki in January-February 2008 (Asmi *et al.* 2009). Between these two WSs the 12 instruments were employed for field measurements around the world as a part of the EUCAARI campaign (Kulmala *et al.* 2009). For interpreting the result of the campaign it is crucial to carefully calibrate and compare the performance of the instruments prior to and after the field measurement period.

METHODS

The WS started with cleaning the instruments, and checking and adjusting the flow rates. Then, the instruments' response to mobility and concentration was tested with three types of particles: electrospray-produced tetra-alkyl ammonium halides (TMAI- and THAB-ions) as mobility standards (Ude & Fernandez de la Mora, 2005), silver ions produced in a tube furnace and charged with an Am-241 source, and neutralized silver particles. The calibrations were done with two different set-ups: a Herrmann type high-resolution DMA for classification and a TSI-3068B electrometer for detection of mobility standards and silver ions up to 5 nm, and a Hauke-type DMA with an electrometer or a CPC (TSI 3025) for silver ions or particles between 3 and 40 nm.

Between the calibrations and during weekends all the instruments were measuring room air in a classroom. For comparison also a BSMA (0.03–3.2 $cm^2V^{-1}s^{-1}$; Tammet, 2006), a DMPS (10-1000 nm), and an ion-DMPS (Laakso *et al.* 2007) were measuring simultaneously.

CONCLUSIONS

Altogether 11 ion spectrometers were calibrated: 5 AISs and 6 NAISs. For most instruments the results does not significantly differ from the previous WS, although some working parameters had been changing during the 1-year field campaign.

The NAISs measured in general about 20% higher ion concentration in all size classes than the AISs, except at high concentrations. Negative ions were detected more accurately both in concentration and mobility than positive ones. The data analysis is still ongoing, and in future, we hope to use the results

for establishing calibration based transfer functions for calculating the size distribution instead of theoretical ones, which have been used so far.

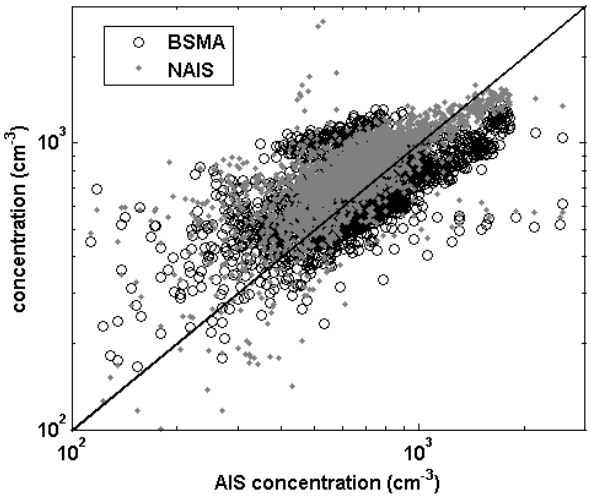

Figure 1.Concentration of negative ions (<7.5 nm) measured with the NAISs and the BSMA compared to the ions measured with the AISs.

ACKNOWLEDGEMENTS

The authors are grateful to all the people helping in the measurements. The work has been partially funded by the EUCAARI project (contract no 036833-2). K.L. acknowledges Maj and Tor Nessling foundation for financial support.

REFERENCES

Asmi, E., Sipilä, M., Manninen, H., Vanhanen, J., Lehtipalo, K., Gagné, S., Neitola, K., Mirme, A., Mirme, S., Tamm, E., Attoui, M., and Kulmala, M. (2009). Results of the first air ion spectrometer calibration and intercomparition workshop. *Atmos. Chem. Phys.*, 9, 141-154

Kulmala, M., Asmi, A., Lappalainen, H.K., Carslaw, K.S., Pöschl, U., Baltensperger, U., Hov, Ø., Benquier, J.-L., Pandis, S.N., Facchini, M.C., Hansson, H.-C., Wiedensohler, A., and O'Dowd, C.D. (2009). Introduction: European Integrated Project on Aerosol Cloud Climate and Air Quality interactions (EUCAARI) – integrating aerosol research from nano to global scales. *Atmos. Chem. Phys.*, 9, 2825-2841

Laakso, L., Gagné, S., Petäjä, T., Hirsikko, A., Aalto, P.P., Kulmala, M. and Keminen, V.-M. (2007). Detecting charging state of ultra-fine particles: instrumental development and ambient measurements. *Atmos. Chem. Phys.* 7, 1333-1345

Mirme, A., Tamm, E., Mordas, G., Vana, M., Uin, J., Mirme, S., Bernotas, T., Laakso, L., Hirsikko, A., Kulmala, M. (2007). A wide-range multi-channel Air Ions Spectrometer. *Boreal Env. Res.*, 12, 247-264

Tammet, H. (2006). Continuous scanning of the mobility and size distribution of charged clusters and nanometer particles in atmospheric air and the balanced scanning mobility analyzer BSMA. *Atmos. Res.*, 82, 523-535

Ude, S. & Fernandez de la Mora, J. (2005). Molecular Monodisperse Mobility and Mass Standards from Electrosprays of Tetra-alkyl Ammonium Halides. *J. Aerosol Sci.*, 36, 1224–1237

Ice Nucleation Ability of Mineral Dust Particles

Felix Lüönd, André Welti, Berko Sierau, Olaf Stetzer, and Ulrike Lohmann

ETH Zurich, Institute for Atmosperic and Climate Science, Zurich, Switzerland.

Keywords: ice nucleation, mineral dust, deposition freezing, immersion freezing, ZINC.

INTRODUCTION

The Zurich Ice Nucleation Chamber (ZINC) was used to explore ice nucleation of size selected mineral dust particles at temperatures between −20°C and −55°C. Four different mineral dust species have been tested: montmorillonite, kaolinite, illite and Arizona test dust (ATD). The selected particle diameters are 100 nm, 200 nm, 400 nm and 800 nm. Relative humidities with respect to ice (RH_i) required to activate 1% of the dust particles as ice nuclei (IN) are reported as a function of temperature. An explicit size dependence of the ice formation efficiency has been observed for all dust types.
Additionally, the recently developed Immersion Mode Cooling Chamber (IMCA) has been used as an extension of the ZINC in order to measure the ice nucleation efficiency of size selected kaolinite particles in the immersion mode. Particles with selected sizes of 200 nm, 400 nm and 800 nm have been activated as cloud condensation nuclei (CCN) in order to obtain droplets with single immersed particles. After continuous cooling of the droplets to the experimental temperature in ZINC, the frozen fraction of the droplets was measured with the newly developed depolarisation detector IODE (Ice Optical Detector; Nicolet *et al.*, 2008). In the investigated size range, kaolinite particles do not appear to be particularly efficient ice nuclei. Although not very strong, a size dependence of the freezing efficiency has been observed

METHODS

The experiments were carried out with the recently developed parallel plate continuous flow diffusion chamber ZINC. ZINC consists of two sections: the nucleation section where high RH_i can be generated, and the evaporation section. The evaporation section is held at ice saturation, so water droplets that might condense in the nucleation section when experimenting at relative humidities above water saturation, evaporate before reaching the optical particle counter (OPC). The design and functional details of ZINC are described by Stetzer *et al.* (2008).
Airborne mineral dust particles are generated with a fluidized bed aerosol generator, then size selected using a Differential Mobility Analyser (DMA), and subsequently analysed for their ice nucleating ability using the ZINC. The experimental setup of the immersion freezing experiments additionally includes the IMCA chamber - an extension which is mounted on top of the ZINC chamber. IMCA activates the particles into cloud droplets and continuously cools them to the experimental temperature maintained in ZINC which is set to a relative humidity close to water saturation. This prevents the droplets from evaporating before they freeze. At the end of ZINC, the IODE detector is used instead of an OPC to measure the frozen fraction of the droplets as a function of the experimental temperature.

RESULTS AND CONCLUSIONS

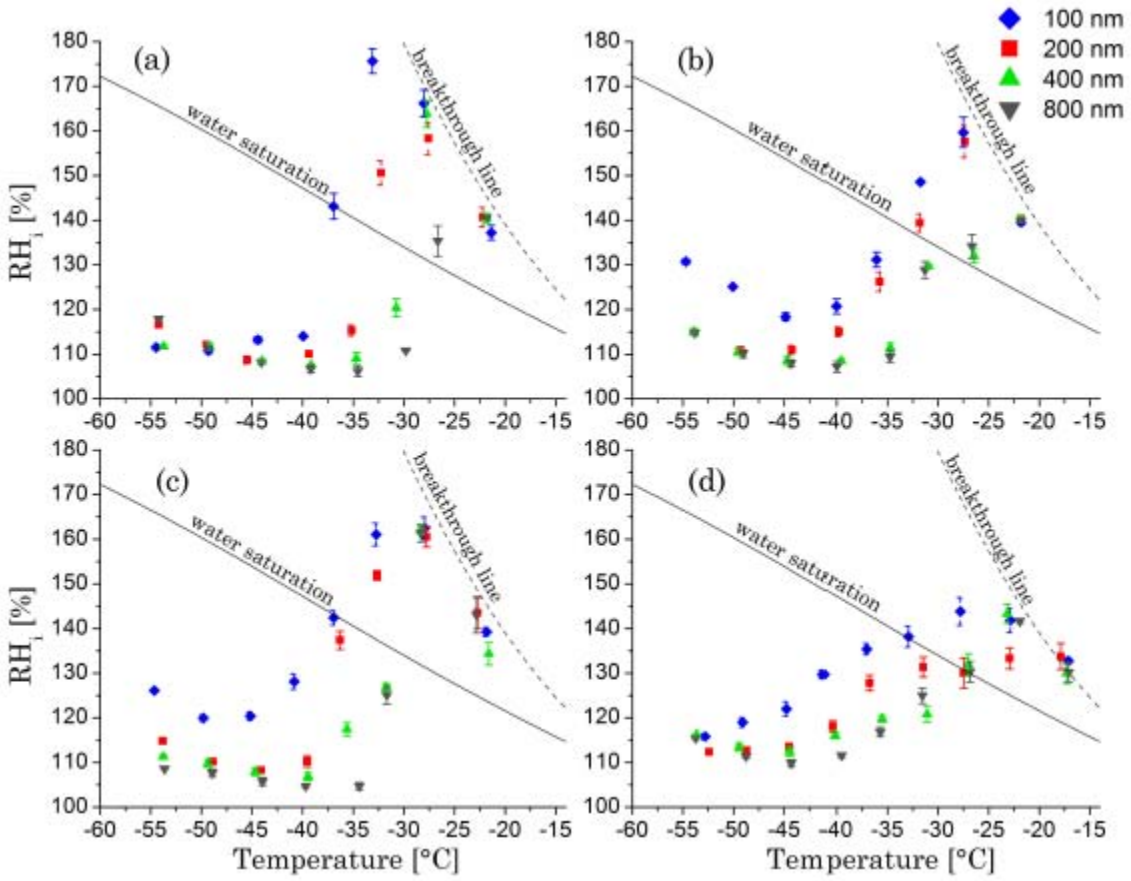

Figure 1. RH_i required for 1% activated fraction as a function of temperature of **(a)** montmorillonite, **(b)** kaolinite, **(c)** illite, **(d)** ATD for different particle sizes. The water saturation line is shown as a solid, black line. The breakthrough line marks the region where water drops condensed in the nucleation section, grow large enough to pass the evaporation section and thus are also detected by the OPC. Error bars represent the maxima and minima RH_i measured during a period of ±20 s around the detection of 1% activated fraction.

Montmorillonite, kaolinite, illite and ATD have been observed to act efficiently as IN. The larger the particle diameter of a dust aerosol, the more efficient the ice formation in deposition mode for the temperature range from −30°C to −55°C. The size effect is less pronounced at lower temperatures (Welti *et al*., 2009).

Ice nucleation in the immersion mode has been observed at temperatures where deposition nucleation has been reported to be active for the same kind of particles (Welti *et al*., 2009). In the present experimental runs, a concurrence between the deposition and the immersion mode can be seen in a significant reduction of ice crystals nucleated in the deposition mode upon increasing the supersaturation in the IMCA chamber. Although not very strong, a size dependence of the IN efficiency of the particles has been observed. The median freezing temperature increases from −35°C for 200 nm kaolinite particles to −33°C for 800 nm particles.The measured median freezing temperatures do not suggest kaolinite particles in this size range to be very efficient IN (Lüönd *et al*., 2009).

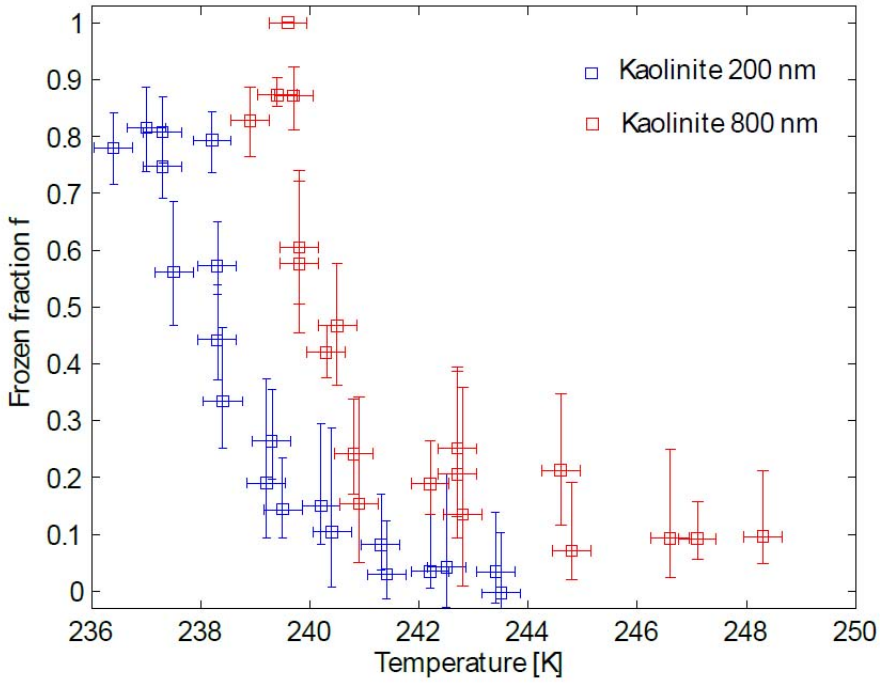

Figure 2. Frozen fraction *f* of droplets as a function of temperature for immersed 200 nm and 800nm kaolinite particles.

REFERENCES

Lüönd, F., Stetzer, O., and Lohmann, U.: Experimental study on the ice nucleation ability of size selected kaolinite particles in the immersion mode, submitted to J. Geophys. Res., 2009.

Nicolet, M., Stetzer, O., and Lohmann, U.: Single ice crystal measurements during nucleation experiments with the depolarization detector IODE, Atmos. Chem. Phys. Discuss., 8, 20965–21000, 2008.

Stetzer, O., Baschek, B., Lüönd, F., and Lohmann, U.: The Zurich Ice Nucleation Chamber (ZINC) – A new instrument to investigate atmospheric ice formation, Aerosol Sci. Technol., 42, 64–74, 2008.

Welti, A., Lüönd, F., Stetzer, O., and Lohmann, U.: Influence of particle size on the ice nucleating ability of mineral dusts, Atmos. Chem. Phys., 9, 6705–6715, 2009.

Benchmarking the GLOMAP-mode aerosol microphysics model against the more detailed GLOMAP-bin scheme in a chemistry transport model

G.W. MANN[1], K.S. CARSLAW[1], D.V. SPRACKLEN[1], D.A. RIDLEY[2], M.G. FRONTOSO[1], C. REDDINGTON[1]

[1] Institute for Climate and Atmospheric Science, School of Earth and Environment, University of Leeds, Leeds, West Yorkshire, LS2 9JT, United Kingdom.

[2] Department of Atmospheric Science. Colorado State University. Fort Collins, CO 80523-1371, U.S.A.

Keywords: aerosol, size, microphysics, evaluation.

INTRODUCTION

Successive IPCC climate assessment reports have identifed the particle size distribution as a critical factor in reducing uncertainties in simulated aerosol-climate interactions. However, computational constraints have hitherto limited most climate models participating in the reports to simulate aerosol in a simplified way, with schemes containing prognostic variables for mass only and determining number concentrations from an assumed fixed size distribution for prescribed aerosol types. However, simulated aerosol indirect effects on climate via changes in cloud albedo and lifetime are largely determined by changes in the *number* concentration of particles large enough to activate to cloud droplets (cloud condensation nucleii). Simulating processes such as aqueous sulphate production with the first generation mass-only schemes is problematic since the fixed size distribution means any increase in mass must be accompanied by an increase in number. Consequently, models using these schemes may be unrealistically perturbing cloud properties and precipitation rates in some regions with subsequent biases in the simulated climate.

This realisation has led to the development of so-called aerosol microphysics models, which transport particle number concentrations as well as mass, allowing particle growth to occur and composition to evolve in response to the controlling chemical and microphysical processes.

The most sophisticated of these schemes are the bin-resolved schemes which give a maximum degree of realism with the number and component mass concentrations in each bin transported and the particle size distribution evolving freely at the specified bin resolution. Although bin-resolved schemes have been included in regional models (e.g. (Jacobson, 1997)) and in global aerosol models (e.g. (Adams and Seinfeld, 2002)) for some time, two-moment bin schemes often have in excess of 100 aerosol tracers to advect, making them too expensive for multi-decadal simulations with current super-computing resource limits.

To address this, some global models include dynamically varying size with the cheaper modal aerosol dynamics approach (e.g. (Whitby and McMurry, 1997)). Here, the shape of the particle size distribution is parameterized as a series of log-normal modes, each covering particular regions of the particle radius range.

This latest generation of aerosol schemes require evaluation against a wider range of observational datasets. The international AEROCOM activity has a new "aerosol microphysics" working group to evaluate size-resolved number concentrations simulated by the models (http://www.igac.noaa.gov/newsletter/iga
The wide range of aerosol observations carried out within EUCAARI and at EUSAAR supersites will provide rich datsets which will directly inform this activity.

In this poster, we benchmark aerosol properties simulated by a 2-moment modal aerosol scheme (GLOMAP-mode) against those simulated by a 2-moment sectional scheme (GLOMAP-bin) and against observations. The two schemes are alternative configurations of the Global Model of Aerosol Processes (GLOMAP) aerosol model (Spracklen et al, 2005; Manktelow et al, 2007; Merikanto et al, 2009; Mann et al, in prep.). The work uses the bin-resolved scheme as a benchmark against which the modal scheme can be compared against. The findings from this work, and those of the AEROCOM aerosol microphysics working group, will help improve the realism and robustness of composition-climate model simulations.

METHODS

The GLOMAP aerosol microphysics model is an extension to the TOMCAT global 3-D off-line chemical transport model (CTM) (Chipperfield, 1999). Primary emissions, new particle formation, condensation, coagulation, cloud processing, dry deposition, sedimentation, nucleation scavenging and impaction svaenging are simulated in a size-resolved manner. The equations for these aerosol processes are solved in the aerosol microphysics module in an operator-split manner, while the gas phase chemistry and transport are dealt with by the host CTM. A spatial resolution of T42 (2.8 degrees latitude/longitude) is used in the paper with 31 vertical levels on a hybrid σ-pressure co-ordinate. The model is forced by ECMWF meteorogical analyses.

The original GLOMAP aerosol scheme (Spracklen et al, 2005) represents the aerosol size distribution using size sections (bins), with 20 bins spanning dry diameters from about 3 nm to 25 μm. Although initially only sulphate and sea-salt were included in a simple single-component approach, the model was extended to allow the simulation of several aerosol components in internally-mixed bins in a number of distributions (Spracklen et al, 2006; Spracklen et al, 2008a; Spracklen et al, 2008b). For this study, GLOMAP-bin is set-up as in (Merikanto et al, 2009), and the empirical "boundary layer nucleation" mechanism is switched off here.

The GLOMAP-mode scheme uses the same process descriptions as the original GLOMAP scheme but with a 2-moment modal aerosol dynamics scheme (e.g. (Whitby and McMurry, 1997)) rather than the bin-resolved approach. The scheme can represent any number of modes (with fixed standard deviation) and possible components, but here the model follows (Vignati et al, 2004) in carrying aerosol component masses and number concentrations in modes covering the nucleation (dry diameter $<$ 10nm), Aitken (10 to 100 nm), accumulation (100 nm to 1 μm) and coarse ($>$ 1 μm) size ranges. The larger three size modes have separate modes for fresh (non-hygroscopic) and aged (hygroscopic) giving 7 modes in total. GLOMAP-mode has already been used to study trends in sulphate aerosol since the 1980s (Manktelow et al, 2007) and the impact of DMS on CCN concentrations (Woodhouse et al, 2008). Here, the aerosol set-up is more extensive and includes sulphate, sea-salt, black carbon, organic carbon and dust. Note that dust is not included in the aerosol set-up for GLOMAP-bin.

CONCLUSIONS

An extensive evaluation effort of the modal GLOMAP-mode scheme against a wide range of in-situ and remote observations has been carried out (Mann et al, in prep.). In this poster we also show a benchmarking of the two-moment modal GLOMAP-mode scheme against the detailed two-moment sectional GLOMAP-bin scheme in the off-line chemistry transport model TOMCAT.

Surface speciated PM2.5 concentrations between the two schemes compare very closely for sulphate, black carbon and organic carbon. For sea-salt, GLOMAP-mode is biased high compared to GLOMAP-bin since the sedimentation of the largest particles is better handled in a sectional scheme. Nevertheless, sea-salt concentrations for the two schemes are mostly within a factor of

two. Condensation nucleii (total particle number) concentrations simulated by the two schemes are everywhere (globally) within 30% of each other except for in the Southern Ocean where GLOMAP-mode overestimates compared to GLOMAP-bin by up to a factor two. Surface CCN concentrations agree even more closely although GLOMAP-mode is slightly biased low by around 30% over the North Atlantic.

Figure a shows CCN concentrations calculated from the GLOMAP-mode size-resolved aerosol number concentrations against observations at a range of sites from various field campaigns and monitoring sites (shown in Figure c). Although there is considerable scatter, giving only a fairly weak correlation between model and observations, the normalised mean bias is quite low. Figure b shows CCN concentrations from GLOMAP-bin against those from GLOMAP-mode at the same sites which has a much stronger correlation, with GLOMAP-mode only biased very slightly low compared to GLOMAP-bin.

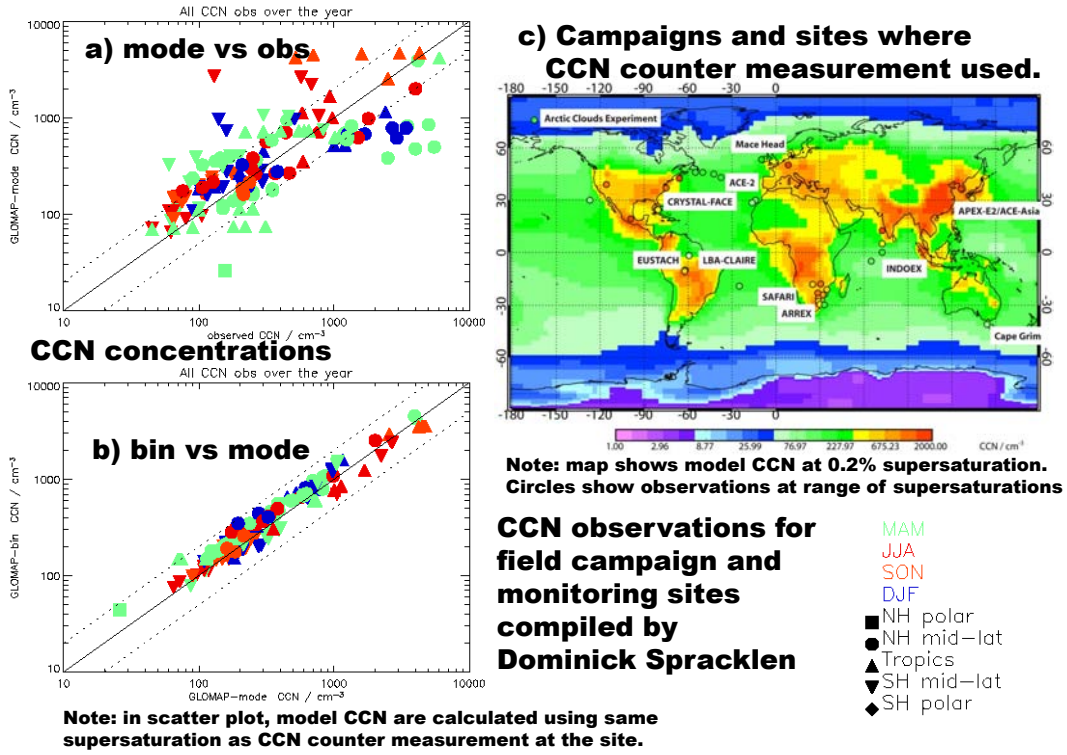

Figure 1: Comparison between CCN concentration as calculated by GLOMAP-mode and GLOMAP-bin, and as observed by CCN counter. a) GLOMAP-mode against observations, b) GLOMAP-bin against GLOMAP-mode c) GLOMAP-bin CCN map with observations over-plotted.

ACKNOWLEDGEMENTS

This work was supported by the National Centre for Atmospheric Science, the APPRAISE aerosol research programme, and several PhD studentships and research grants funded by the UK Natural Environment Research Council (NERC).

REFERENCES

Adams, P. J., and J. H. Seinfeld (2002). Predicting global aerosol size distributions in general circulation models *J. Geophys. Res.*, **vol. 107**, no. D19, doi:10.1029/2001JD001010.

Chipperfield, M. P. (1999). Multi-annual simulations with a three-dimensional chemical transport model. *J. Geophys. Res.*, **vol. 110**, doi:10.0129/2004JD005674.

Jacobson, M.Z. (1997). Development and application of a new air pollution modeling system – II. Aerosol module structure and design *Atmos. Env.*, **vol. 31**, no. 2, 131-144.

Manktelow, P. T., G. W. Mann, K. S. Carslaw et al (2007). Regional and global trends in sulfate aerosol since the 1980s. *Geophys. Res. Lett.*, **vol. 34**, doi:10.1029/2006GL028668.

Mann, G. W., K. S. Carslaw, D. V. Spracklen et al (in prep.). Description and evaluation of GLOMAP-MODE: A modal global aerosol microphysics model for the UKCA composition-climate model. *to be submitted to Geosci. Mod. Dev. Discuss.*.

Merikanto, J., D. V. Spracklen, G. W. Mann, et al (2009). Impact of nucleation on global CCN. *Atmos. Chem Phys. Discuss.*, **vol. 9**, 12999-13037.

Pringle, K. P., K. S. Carslaw, D. V. Spracklen et al (2009). The relationship between aerosol and cloud drop number concentrations in a global aerosol microphysics model *Atmos. Chem. Phys.*, **vol. 9**, 4131-4144.

Spracklen, D. V., K. J. Pringle, K. S. Carslaw et al (2005). A global off-line model of size-resolved aerosol microphysics: 1. Model development and prediction of aerosol properties *Atmos. Chem. Phys.*, **vol. 5**, 2227-2252.

Spracklen, D. V., K. S. Carslaw, M. Kulmala et al (2006). The contribution of boundary layer nucleation events to total particle concentrations on regional and global scales *Atmos. Chem. Phys.*, **vol. 6**, 5631-5648.

Spracklen, D. V., K. S. Carslaw, M. Kulmala et al (2008). Contribution of particle formation to global cloud condensation nuclei concentrations. *Geophys. Res. Lett.*, **vol. 35**, doi:10.1029/2007GL033038.

Spracklen, D. V., B. Bonn and K. S. Carslaw (2008). Boreal forests, aerosols and the impacts on clouds and climate. *Phil. Trans. R. Soc. A.*, **vol. 366**, 4613-4626..

Stier, P., J. Feichter, S. Kinne et al (2005). The aerosol-climate model ECHAM5-HAM *Atmos. Chem. Phys.*, **vol. 5**, 1125-1156.

Vignati, E., J. Wilson and P. Stier (2004) M7: An efficient size-resolved aerosol microphysics module for large-scale aerosol transport models *J. Geophys. Res.*, **vol. 109**, doi:10.1029/2003JD004485.

Whitby, E. R. and P. H. McMurry (1997). Modal aerosol dynamics modeling *Aer. Sci. Tech.*, **vol. 27**, 673-688.

Woodhouse, M. T., G. W. Mann and K. S. Carslaw (2008) The impact of oceanic iron fertilisation on cloud condensation nuclei *Atmos. Env.*, **vol. 42**, 5728-5730.

CLUSTER SPECTROMETERS IN LONG-TERM FIELD MEASUREMENTS

Hanna E. Manninen[1], Tuomo Nieminen[1], Eija Asmi[1], Stéphanie Gagné[1], Mikko Sipilä[1], Silja Häkkinen[1], Lauri Laakso[1], Marko Vana[1], Aadu Mirme[1], Sander Mirme[1], Urmas Hõrrak[1], Christian Plass-Dülmer[1], George Stange[1], Gyula Kiss[1], András Hoffer[1], Marcel Moerman[1], Marcel Brinkenberg[1], Giorgos N. Kouvarakis[1], Katerina Bougiatioti[1], Colin O'Dowd[1], Darius Ceburnis[1], Birgitta Svenningsson[1], Leone Tarozzi[1], Stefano Decesari[1], André Sonntag[1], Wolfram Birmili[1], Julien Boulon[1], Karine Sellegri[1], Ilona Riipinen[1], Veli-Matti Kerminen[1] and Markku Kulmala[1]

[1]Partner in the European Integrated project on Cloud Climate and Air Quality Interactions (EUCAARI), Project Office, Division of Atmospheric Sciences, University of Helsinki.

Keywords: Atmospheric aerosols, particle formation, ions, WP 1.1.

INTRODUCTION

The aim is to understand the initial steps of particle formation and sub subsequent growth better in different atmospheric environments by using continuous measurements in various field sites. We want to understand the role of new particle formation by nucleation and subsequent growth by condensation as particle source on global and regional scale. The ion spectrometers measure mobility distributions of charged aerosol particles and clusters. The neutral cluster spectrometer is also capable of measuring mobility distributions of sub-3 nm neutral and charged aerosol particles and clusters (Kulmala et al., 2007). As part of the EUCAARI campaign (European integrated project on aerosol cloud climate air quality interactions, see Kulmala et al., 2009) WP1.1, different types of ion spectrometers, have been operating in a total of 12 field sites around Europe (so-called EUCAARI sites). These field sites represent a wide variety of high and low altitude environments. The spectrometer data collection started during the EUCAARI Intensive Observation Period (IOP) on March 2008 and completed on the end of April 2009.

METHODS

The cluster spectrometer field measurements started in March 2008 during the EUCAARI Intensive Observation Period (IOP), and they were completed during April 2009. The longterm measurements with cluster spectrometers have been conducted in Hyytiälä and Pallas (Finland), Vavihill (Sweden), Mace Head (Ireland), Cabauw (The Netherlands), K-puszta (Hungary), Hohenpeissenberg and Melpitz (Germany), PoValley (Italy), Jungfraujoch (Schwitzerland), Puy de Dôme (France), Finokalia (Greece) and Rustenberg (South Africa). Each one of these stations has a particular environment. For example, there are stations at marine coastal sites and at continental sites and some have high background concentrations while some have low background concentrations etc. In addition, the A-NAIS (Airborne Neutral Air Ion Spectrometer) took part in the airborne measurements in an instrumented aircraft over the European field stations (Mirme et al., 2009).

The Air Ion Spectrometer (AIS; Mirme et al., 2007) is developed to measure the number size distribution of atmospheric nanometer-sized ions and charged particles in a diameter range 0.8-40 nm. The ion spectrometers have experienced several improvements, the most important being the development of the Neutral Air Ion Spectrometer (NAIS; Manninen et al., 2009). The NAIS is extended to additionally measure the neutral particle size distributions. The Balanced Scanning Mobility Analyzer (BSMA; Tammet, 2006) measures size distributions of ions and charged aerosol particles in a diameter range 0.8-7 nm. Before and after the field measurements the cluster spectrometers took part in a calibration and inter-comparison workshop in Helsinki to test the instrument operation under long-term measurements

(Asmi et al., 2009). Table 1 show which type of the cluster spectrometer was used in each field site and how long the measurements lasted.

Measurement site	Instrument	Measurement time	Duration (days)
Pallas	NAIS5 (UH/FMI)	23.4.08-7.4.09	349
Hyytiälä	BSMA1 (UH)	1.3.08-31.4.09	426
Vavihill	AIS5 (UL)	23.4.08-25.2.09	297
Cabauw	NAIS2 , AIS6 (UH)	16.4.08-31.3.09	296
Melpitz	NAIS4 (UT)	30.4.08-19.4.09	354
Mace Head	NAIS2 (UH)	13.6.08-7.5.09	328
K-Puszta	AIS1 (UH)	10.3.08-26.2.09	337
Finokalia	AIS3 (UH)	3.4.08-14.4.09	376
San Pietro Capofiume	BSMA3 (UH)	12.3.-31.10.08	215
Jungfraujoch	AIS7 (CNRS)	8.4.08-20.4.09	330
Puy de Dome	NAIS3 (CNRS)	2.4.08-5.5.09	398
Rustenburg, South Africa	AIS2 (SA)	1.3.08-1.3.09	365
Hohenpeissenberg	NAIS1 (UH)	6.3.08-26.2.09	357

Table 1. Long-term field measurements associated with EUCAARI project.

During the long-term EUCAARI field measurements using cluster spectrometers contains a total of ~1100 particle formation event days. The analysis of these days continues at the moment. In the future, this database will be integrated to regional and global scale climate models. To estimate regional aerosol source apportionment and long range transport also trajectory analysis will be included into the study.

RESULTS

New particle formation events have been seen on every one of the 13 EUCAARI site where cluster spectrometers was measuring. Typically the formation of sub-3 nm particles began around noon and the growth of the particles continued several hours towards the larger particle sizes. The monthly event distribution varies from one station to another, which was expected because the stations are influenced by different environments and are in different climates. In K-Puszta, Hungary, the number of new particle formation events was the highest amongst the studied stations. The most non-event days were seen in Finokalia, Greece, which is a Mediterranean coastal site. In Mace Head Ireland, particularly, many different types of event have been observed. Seasonal cycle of new particle formation event frequency was observed. According the monthly particle formation event distribution event frequency has maximum during the spring months and minimum during winter at most of the sites. Some of the sites have clear second maximum in particle formation event number during autumn.

ACKNOWLEDGEMENTS

This research has been funded by European Commission (6th Framework program project EUCAARI, Contract no. 036833-2). We thank all the researchers, technical staff and students who have taken part in the EUCAARI field measurements.

REFERENCES

Asmi, E., Sipilä, M., Manninen, H. E., Vanhanen, J., Lehtipalo, K., Gagné, S., Neitola, K., Mirme, A., Mirme, S., Tamm, E., Uin, J., Komsaare, K., Attoui, M., and Kulmala, M. (2009) Results of the first air ion spectrometer calibration and intercomparison workshop, *Atmos. Chem. Phys.*, 9, 141-154.

Kulmala M, Riipinen I, Sipilä M, Manninen H E, Petäjä T, Junninen H, Dal Maso M, Mordas G, Mirme A, Vana M, Hirsikko A, Laakso L, Harrison R M, Hanson I, Leung C, Lehtinen K E J, Kerminen, V-M (2007) Toward direct measurement of atmospheric nucleation. *Science* 318: 89-92.

Kulmala, M., Asmi, A., Lappalainen, H. K., Carslaw, K. S., Pöschl, U., Baltensperger, U., Hov, Ø., Brenquier, J.-L., Pandis, S. N., Facchini, M. C., Hansson, H.-C., Wiedensohler, A., and O'Dowd, C. D. (2009) Introduction: European Integrated Project on Aerosol Cloud Climate and Air Quality interactions (EUCAARI) – integrating aerosol research from nano to global scales, Atmos. Chem. Phys., 9, 2825-2841.

Manninen, H. E., Petäjä, T., Asmi, E., Riipinen, I., Nieminen, T., Mikkilä, J., Hõrrak, U., Mirme, A., Mirme, S., Laakso, L., Kerminen, V.-M. & Kulmala, M. (2009) Long-term fi eld measurements of charged and neutral clusters using Neutral cluster and Air Ion Spectrometer (NAIS). *Boreal Env. Res.* 14: 591–605.

Mirme A, Tamm E, Mordas G, Vana M, Uin J, Mirme S, Bernotas T, Laakso L, Hirsikko A, Kulmala M (2007) A widerange multi-channel Air Ion Spectrometer. *Boreal Environ. Res*. 12: 247–264.

Mirme, S., A. Mirme, A. Minikin, A. Petzold, U. Hõrrak, V. -M. Kerminen, and M. Kulmala (2009) Atmospheric sub-3 nm particles at high altitudes. *Atmos. Chem. Phys. Discuss.*, 9, 19435-19470.

Tammet, H. (2006) Continuous scanning of the mobility and size distribution of charged clusters and nanometer particles in atmospheric air and the Balanced Scanning Mobility Analyzer BSMA. *Atmos. Res.*, 82: 523–535.

HYGROSCOPIC PROPERTIES OF AEROSOL PARTICLES AT CABAUW FIELD STATION

J. MIKKILÄ[1], M. EHN[1], T. PETÄJÄ[1] and M. KULMALA[1]

[1]Department of Physics, University of Helsinki, FI-00014, Helsinki, Finland

Keywords: hygroscopicity, H-TDMA, field measurements.

INTRODUCTION

Hygroscopicity of an aerosol particle describes how it interacts with surrounding gas phase water vapor in different saturation ratios. The hygroscopic properties along with particle size determine the potential for the particles to act as cloud condensation nuclei (McFiggans *et al*. 2006). Hygroscopic particles are able to grow in size by absorbing water molecules even in sub-saturated conditions, which can be measured with a Hygroscopic Tandem Differential Mobility Analyzer (H-TDMA, Liu *et al*., 1978).

A simple way to describe the hygroscopicity of a particle is via a growth factor (*GF*), which is the ratio between the diameters of a particle measured in a certain saturation ratio (*D*) and the corresponding size in dry conditions (D_{dry}). When measuring the hygroscopicity of an aerosol population, a distribution of different growth factors is usually obtained instead of a single value (Swietlicki *et al.*, 2008). This is due the fact that hygroscopic properties are mainly governed by the chemical composition and the size of the particles.

METHODS

An H-TDMA is a device used for measuring aerosol particle hygroscopic properties. First aerosol particles are dried. Subsequently a dry size class of particles D_{dry} is selected using a Differential Mobility Analyzer (Winklmayr *et al*., 1991). Then the monodisperse particles are brought into controlled relative humidity (*RH*). The wet aerosol goes through DMA2, which scans a size range covering all possible D_{wet}. A corresponding concentration for each size fraction is monitored with a Condensation Particle Counter. A humidified size distribution for a certain D_{dry} is then obtained.

RESULTS AND CONCLUSIONS

The new version of University of Helsinki H-TDMA was deployed to monitor the hygroscopic properties of ambient aerosol particles at Cabauw field station in the Netherlands. Within the EUCAARI project (Kulmala *et al*. 2009) these measurements proceeded from 1 May 2008 onwards. The Cabauw site is surrounded by fields and small villages and further away by larger cities accompanied by motorways. At Cabauw the instrument was measuring continuously *GF* distributions of five different dry sizes (D_{dry} = 35, 50, 75, 110 and 165 nm) at *RH* of 90 % for one year.

The first results show significant variability in the average growth factors and in the growth factor probability distributions as a function of time of day and season as well as in different dry sizes (*figures* 1, 2). During the spring days growth factor distributions of dry size particles below accumulation mode seem to follow a diurnal pattern which is not present during the winter days. This might be explained by the condensation and evaporation of semi-volatile organic compounds. Variations in the nearly hydrophobic mode seem to be connected at least partly to the differences in the emissions of car traffic. Corresponding effect might be seen even in the morning minimum of the average growth factors (*figure* 2). A more hygroscopic mode is strongest in the winter and probably represents a more aged background

aerosol (*figure* 1). A bit surprisingly sea salt does not seem to have significant effect to the measured aerosol populations. As a summary of the results, a variable combination of a wide hygroscopic and a nearly hydrophobic mode was characteristic of the measured aerosol and thus the population was clearly externally mixed.

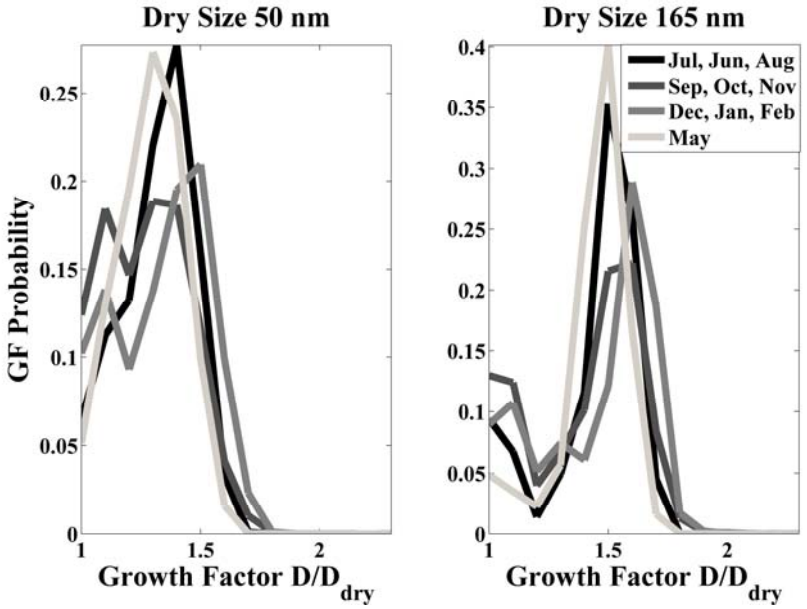

Figure 1. Average GF probability distributions of different seasons.

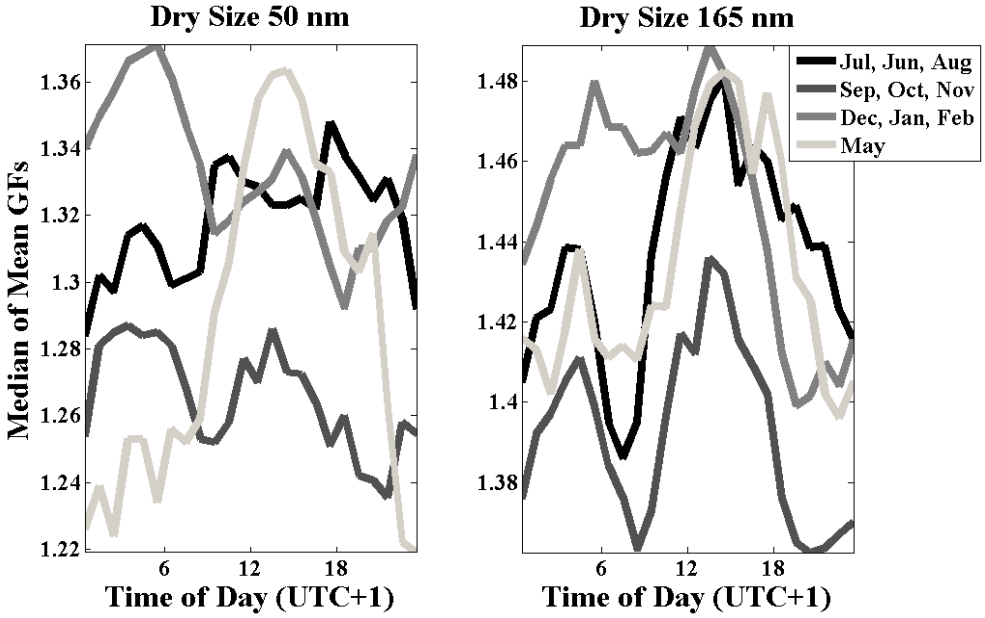

Figure 2. Hourly medians of mean GFs during different seasons.

ACKNOWLEDGEMENTS

The data processing was done with the help of TDMAinv Toolkit (Gysel *et al.*, 2009).

REFERENCES

Gysel, M., McFiggans, G. B. and Coe H. (2009), Inversion of tandem differential mobility analyser (TDMA) measurements, *J. Aerosol Sci*., 40, 134-151.

Kulmala, M. *et al*. (2009), Introduction: European Integrated Project on Aerosol Cloud Climate and Air Quality interactions (EUCAARI) – integrating aerosol research from nano to global scales, *Atmos. Chem. Phys*. 9, 2825-2841.

Liu, B. Y. H. *et al*. (1978), The Aerosol Mobility Chromatograph: A New Detector for Sulfuric Acid Aerosols, *Atmos. Environ.* 12, 99–104.

McFiggans, G. *et al.* (2006), The effect of physical and chemical aerosol properties on warm cloud droplet activation, *Atmos. Chem. Phys*. 6, 2593–2649.

Swietlicki, E. *et al*. (2008), Hygroscopic properties of submicrometer atmospheric aerosol particles measured with H-TDMA instruments in various environments—a review, *Tellus*, 60B, 432-469.

QUANTUM CHEMISTRY APPLIED TO ATMOSPHERIC RELEVANT SYSTEMS

I.K. ORTEGA, T. KURTÉN, H. VEHKAMÄKI, V. LOUKONEN, K. RUUSUVUORI, M. TOIVOLA, and M. KULMALA

Department of physics, P.O. Box 48, 00014 University of Helsinki, Finland

Keywords: Nucleation, clusters, quantum, mechanics.

INTRODUCTION

Atmospheric aerosols influence climate directly by scattering and absorbing radiation, and indirectly by acting as cloud condensation nuclei and affecting cloud properties. Unfortunately the role of atmospheric aerosols is still the forcing with the lowest level of scientific understanding, as reported in the newest report by the Intergovernmental Panel on Climate Change.

Gas-to-particle nucleation is an important source of new aerosol particles in the Earth's atmosphere. This phenomenon is observed almost everywhere around the world and has been the subject of intense studies in the last years (Kulmala et al. 2004), but the formation mechanism and the participating substances have not been resolved yet.

Due to the limitation of the experimental techniques detecting the composition of small molecular clusters present in the atmosphere, quantum mechanics methods have became a powerful tool to study the molecular mechanism behind new particle formation and composition of molecular cluster that are always present in the atmosphere

METHODS

We have recently developed a systematic multi-step method (Ortega et al. 2008).The method combines different theory levels, allowing the study of relatively large clusters (including big organic molecules and up to four sulphuric acid clusters). This method can be used to evaluate the possible role of different molecules in new particle formation but it can also provide useful input data for kinetic models and help to interpret experimental data.

CONCLUSIONS

We have perform a series of quantum mechanics calculation of different atmospherically relevant clusters, this include clusters formed by: sulphuric acid, ammonia, amines, organic acids and organosulphates.

We have calculated the formation energies of all this clusters, with the aim of identifying which are the best candidates to participate in nucleation events. We also have calculated different evaporation rates for all the clusters, this information can be used as input in different atmospheric models.

Summary of results.

-Ammonia does not enhance ion induce nucleation.

-Dimethyl amine enhances neutral and ion-induced sulphuric acid-water nucleation in the atmosphere more effectively than ammonia.

-Some organic acids forms really stable clusters with sulphuric acid, these clusters are good candidates to explain the pool of neutral clusters observed in the atmosphere.

-Organosulphates can activate charged sulphuric acid clusters, helping them to cross the nucleation barrier.

ACKNOWLEDGEMENTS

The authors thank the Scientific Computing Center (CSC) in Espoo, Finland for the computing time, and the Academy of Finland and Emil Aaltonen foundation for financial support.

REFERENCES

Kulmala, M., Vehkamäki, H., Petäjä, T., Dal Maso, M., Lauri, A., Kerminen V.M., Birmili, W. and McMurry, P. H. (2004). Formation and growth rates of ultrafine atmospheric particles: a review of observations *J. Aerosol. Sci*. 35 143

I.K. Ortega, T. Kurtén, H Vehkamäki and M. Kulmala (2008).The role of ammonia in ion induced nucleation. *Atmos. Chem. Phys.* 8 2859

TOWARDS ON-LINE 14C ANALYSIS OF CARBONACEOUS AEROSOL FRACTIONS

N. PERRON[1], S. SZIDAT[2], S. FAHRNI[1,2], M. RUFF[1,2,3], L. WACKER[3], A.S.H. PRÉVÔT[1], U. BALTENSPERGER[1]

[1]Paul Scherrer Institut (PSI), CH-5232 Villigen, Switzerland.

[2]Department of Chemistry and Biochemistry, University of Bern, Freiestrasse 3, CH-3012 Bern, Switzerland.

[3]Institute for Particle Physics, ETH Hönggerberg, CH-8093 Zürich, Switzerland.

Keywords: Radiocarbon, Acceleration Mass Spectrometer, source apportionment, thermo-optical EC/OC analyser.

INTRODUCTION

Atmospheric carbonaceous aerosol is traditionally divided into organic carbon (OC) and elemental carbon (EC). Their respective carbon amounts are usually analyzed by means of an OC/EC analyser and their fossil and non-fossil origins can be determined by radiocarbon analysis (Szidat *et al.*, 2007). So far, separation of OC and EC has been performed off-line by manual and time-consuming techniques (Szidat *et al.*, 2004). We present an on-line system that couples a commercial OC/EC analyser with the gas ion source (Ruff *et al.*, 2007) of the Accelerator Mass Spectrometer (AMS) MICADAS (Synal *et al.*, 2007) using its CO_2 feeding system (Ruff *et al.*, 2008). The performance achieved with reference materials and blanks are discussed to demonstrate the potential of this coupling for source apportionment of atmospheric carbonaceous particulate matter.

METHODS

A RT 3080 sunset thermo-optical OC/EC analyser was connected to the gas ion source of the small Acceleration Mass Spectrometer MICADAS using a gas interface developed by Ruff *et al.* (2008).

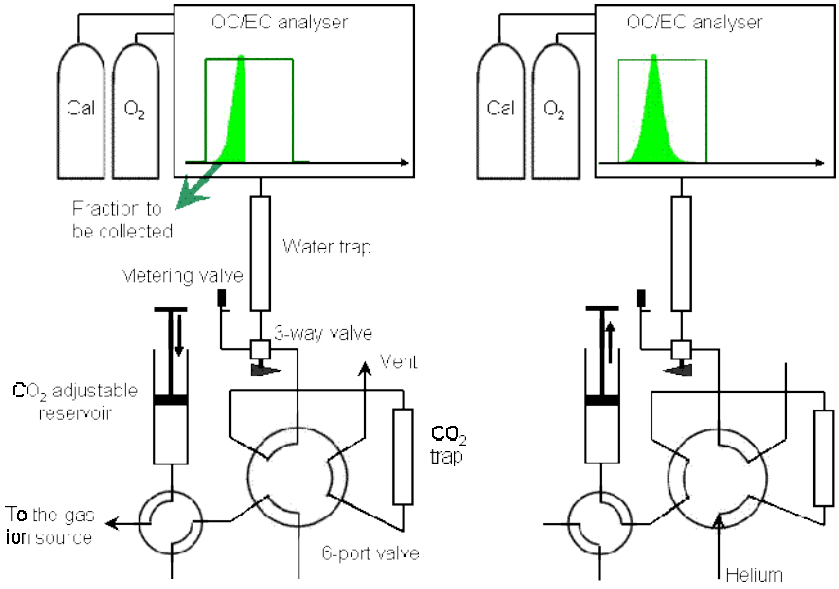

Figure 1. Coupling system between the OC/EC thermo-optical analyser and the gas interface, during CO_2 trapping (left) and during injection to the gas ion source (right).

The gas interface consisted of:

- a zeolite sieve to trap the CO_2 from the exhaust of the analyzer,
- a gas-tight syringe acting as an adjustable CO_2 reservoir and injecting the recovered CO_2 mixed with helium into the gas ion source,
- a 6-port valve connecting alternately the two former parts and isolating them from each other. This interface was run semi-automatically by a LabVIEW program.

In addition, we installed upstream of the interface:

- a $Mg(ClO_4)_2$ water trap,
- a 3-way valve to direct the instrument exhaust either to the interface or to an outlet equipped with a metering valve so as to keep a constant back pressure in the instrument.

The OC/EC analyzer was run under pure O_2, anticipating the use of a thermal EC/OC separation method that we are currently developing.

RESULTS

The first on-line coupling between an automatic thermo-optical OC/EC analyser and the MICADAS worked successfully. That shows that the existing gas ion source and gas interface using a zeolite trap can be adapted to different combustion devices for on-line ^{14}C analyses. Due probably to the use of quartz filters and resulting adsorption of volatile organic compounds on the filter fibres during the sample preparation, measurements of different standard materials had to be corrected for a blank contamination amounting to 2.0 μg carbon at 54 pmC, with 20% uncertainties for both parameters. After this correction, all but two of the ^{14}C signatures agreed within the 1-σ range with the nominal values of the corresponding reference materials.

CONCLUSIONS AND OUTLOOK

We exploited the flexibility of an AMS equipped with a gas ion source and a gas interface to successfully achieve the first coupling between the MICADAS and a commercial OC/EC analyzer. First on-line ^{14}C measurements of reference materials were performed and proved to be satisfying, although some contamination issues suggested that the system cleaning procedure can be further optimized. Future investigation will focus on adapting the thermal program of the OC/EC analyzer to real atmospheric filters in order to achieve on-line ^{14}C measurements of OC and EC, thus fostering the potential of radiocarbon for source apportionment of carbonaceous aerosol.

REFERENCES

S. Szidat, A. S. H. Prévôt, J. Sandradewi, M. R. Alfarra, H.-A. Synal, L. Wacker and U. Baltensperger (2007). Dominant impact of residential wood burning on particulate matter in Alpine valleys during winter, *Geophys. Res. Lett.* 34, L05820, doi:10.1029/2006GL028325.

S. Szidat, T.M. Jenk, H.W. Gäggeler, H.-A. Synal, I. Hajdas, G. Bonani and M. Saurer (2004). THEODORE, a two-step heating system for the EC/OC determination of radiocarbon (^{14}C) in the environment, *Nucl. Instrum. Methods Phys. Res., Sect. B, 223-224*, 829-836.

M. Ruff, L. Wacker, H.W. Gäggeler, M. Suter, H.-A. Synal and S. Szidat (2007). A gas ion source for radiocarbon measurements at 200 kV. *Radiocarbon* 49(2), 307-314.

H.-A. Synal, M. Stocker and M Suter (2007). MICADAS: A new compact radiocarbon AMS system. Nucl. *Instrum. Methods Phys. Res. B* 259(1):7-13.

M. Ruff, S. Fahrni, H.W. Gäggeler, M. Suter, H.-A. Synal, S. Szidat and L. Wacker (2008). Online radiocarbon measurements of small samples using elemental analyser and MICADAS gas ion source. *Radiocarbon*, submitted.

SULFURIC ACID AND TRACE GAS MEASUREMENTS IN EUCAARI-SPC-2009

C. PLASS-DÜLMER[1], T. ELSTE[1], S. GILGE[1], G. STANGE[1] , A. HAMED[2], and S. DECESARI[3]

[1]German Meteorological Service, Meteorological Observatory, 82383 Hohenpeissenberg, Germany
[2]University of Kuopio, Department of Physics, P. O. Box 70211 Kuopio, Finland
[3]CNR, Inst. Atmospheric Sciences and Climate, via Gobetti 101, I-40129, Bologna, Italy

Keywords: trace gas, aerosol precursor, sulphuric acid, Po Valley.

INTRODUCTION

As part of EUCAARI a field campaign was conducted in San Pietro Capofiume, Italy from June 26th to July 12th 2009. The field site is situated in rural eastern Po Valley about 30 km northeast from Bologna and 60 km west from the Adriatic Sea. Due to highly industrialized areas especially in the western Po valley and close to the coast, high pollution levels were expected during this campaign as also published by Hamed et al. (2007) and experienced during a previous EUCAARI-SPC-2008 campaign. During the 2008 campaign, a high frequency of nucleation events was observed. Accordingly, for SPC-2009 good conditions to study new particle formation in a polluted environment with very intensive photochemistry were expected. To better understand precursor – nucleation particle relations, the CIMS (chemical ionisation mass spectrometry) instrument by DWD (German Meteorological Service) capable of measuring gaseous sulphuric acid and OH-radical concentrations was operated at the site along with trace gas measurements of oxides of nitrogen and sulphur dioxide and a number of aerosol characterizing instruments including NAIS by University of Helsinki and DMPS by University of Kuopio (both Finland). While in this paper the trace gas situation and the balance of sulphuric acid during SPC-2009 are presented and discussed, in an accompanying poster the impact of sulphuric acid on new particle formation is presented (Hamed et al., 2009).

METHODS

Gaseous sulphuric acid and OH-radicals were measured by CIMS as previously described by Berresheim et al. (2000) and Rohrer and Berresheim (2006). The instrument was set up in a container and sampled air from a height of 3 m above ground, 0.5 m above the container. Basically, OH is chemically titrated by addition of SO_2 to yield H_2SO_4, H_2SO_4 is then selectively ionized by NO_3^- ions at atmospheric pressure, and the resulting ions are selectively transferred into a vacuum chamber. Here, water clusters are broken up and the HSO_4^- ions are analysed by mass spectrometry. The system has a sensitivity of $2\ 10^5$ molecules cm^{-3} and an estimated accuracy of 30%. Furthermore, during SPC-2009 SO_2 was measured by a fluorescence sensor (Thermo, TE 43 S), NO by chemiluminescence with O_3 (ECO-Physics CLD 770AL ppt), and NO_2 by photolytic conversion (ECO-Physics) and measurement as NO. Finally, photolysis frequencies of NO_2 and ozone to yield $J(O^1D)$ were measured by sets of up- and downward looking filter radiometers (MetCon).

RESULTS AND DISCUSSION

In Figure 1, the median diurnal profiles of the anthropogenic trace gases NO, NO_2, and SO_2, and of O_3 are shown. They depict clear dial cycles with generally different patterns for NO_x compounds, SO_2 and ozone. The anthropogenic NO_2 shows on average concentrations during daytime of mostly below 2 ppb which is rather low for a polluted site. After 18:00 mixing ratios increase again until 20:00 and afterwards increase slower to about 10 ppb at midnight. This reflects a typical dial variation with

enhanced mixing ratios at night due to anthropogenic emissions into a shallow boundary layer, and decreasing concentrations in the morning due to the rise of the mixed-layer. NO essentially follows this pattern on lower levels with 2 major discrepancies: during night concentrations steadily increase until the maximum of 3 ppb (median) is reached at around 7:00, and in the late afternoon and evening no increase is observed until 22:00. At night, the relaxed increase is due to titration by ozone, which yields NO2, but also consumes the ozone. When ozone is largely depleted after midnight, freshly emitted NO is no more titrated and starts to build up until to the early morning hours when photolysis of NO2 forms an additional strong source of NO. After that, NO and NO2 appear to be closely related (photo-stationary state). However, the ratio of NO/NO2 decreases during day time, pointing towards the build-up of peroxy-radicals after noon. The diurnal cycle of SO2 is almost inverted relative to NO2. At night, SO2 concentrations are low in the boundary layer mostly due to heterogeneous processes and low local sources. With the break-up of the nocturnal inversion at 8:00 it mixes into the boundary layer from above. Throughout the course of the day, concentrations decrease again probably due to photochemical removal. The pattern of ozone is governed by the dynamics of the mixed layer and loss processes during night due to titration by NO and deposition. Remarkably is the fairly constant level after noon indicating only marginal photochemical ozone production during sunlight hours. This is generally consistent with low ozone precursor concentrations (NO_x and VOC) and correspondingly low chemical turn-over at noon-time, again pointing to low pollution levels.

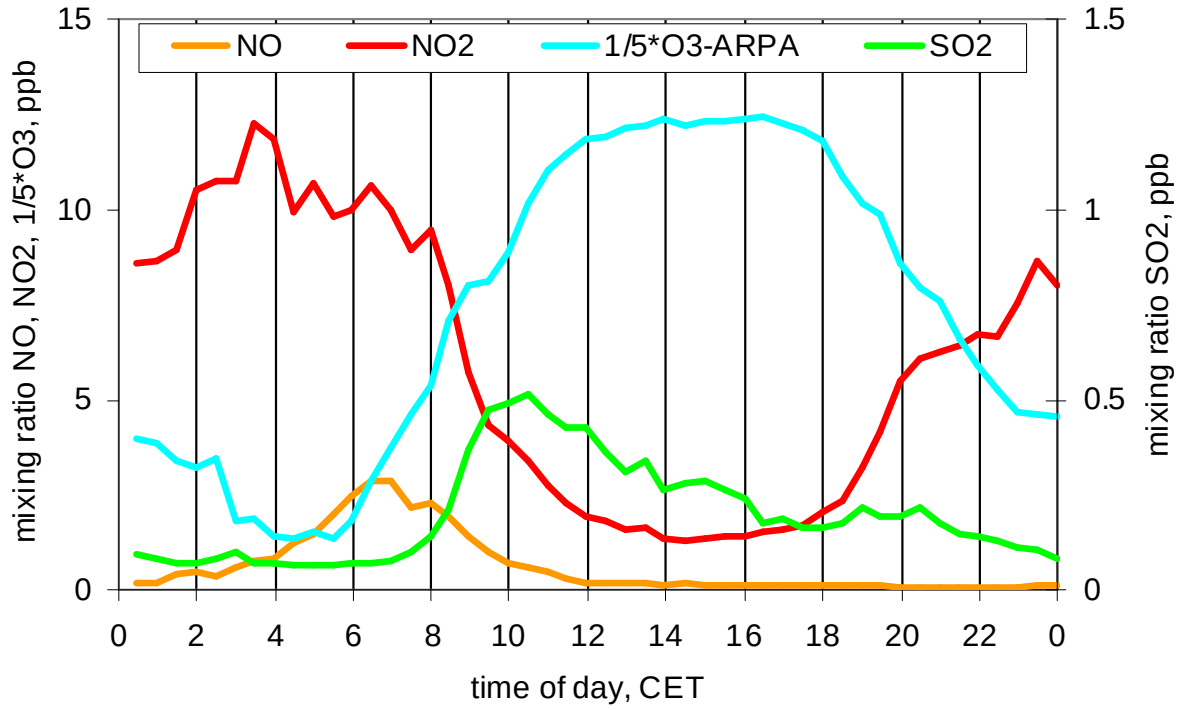

Figure 1. Median diurnal profiles of NO, NO_2, SO_2 and ozone during the EUCAARI-SPC-2009 campaign (ozone data from ARPA)

Time series of the concentrations of OH-radicals and sulphuric acid are shown in Figure 2. Daytime maximum concentrations of sulphuric acid are generally exceeding 1E7 molecules/cm³, occasionally they are above 3E7 molecules/cm³. At night, concentrations are mostly below 2E6 molecules/cm³. This extreme dial dynamic is due to the high photochemical production rates from reaction of OH radicals with SO_2 during day, and the short life-time of some 10 min towards condensation on pre-existing aerosol. At night, small production due to reactions of peroxy-radicals and criegee-biradicals with SO_2 are principally possible, however, due to the low SO_2 concentrations and the expected low concentrations of peroxy-radicals, they are assumed to play only a small role. Correspondingly, OH-radicals and SO_2 are

the major precursors for sulphuric acid during day-time. The time series of OH radicals again shows strong variations which can be mainly attributed to variations of $J(O^1D)$ (photolysis of ozone by UV-B light to yield electronically excited O-atoms), which is linked to both the primary production and recycling of OH radicals (Rohrer and Berresheim, 2006). Surprisingly, the time series of OH-radicals is more robust than that of sulphuric acid, although the life-time of OH radicals is much shorter and generally well below 1 s.

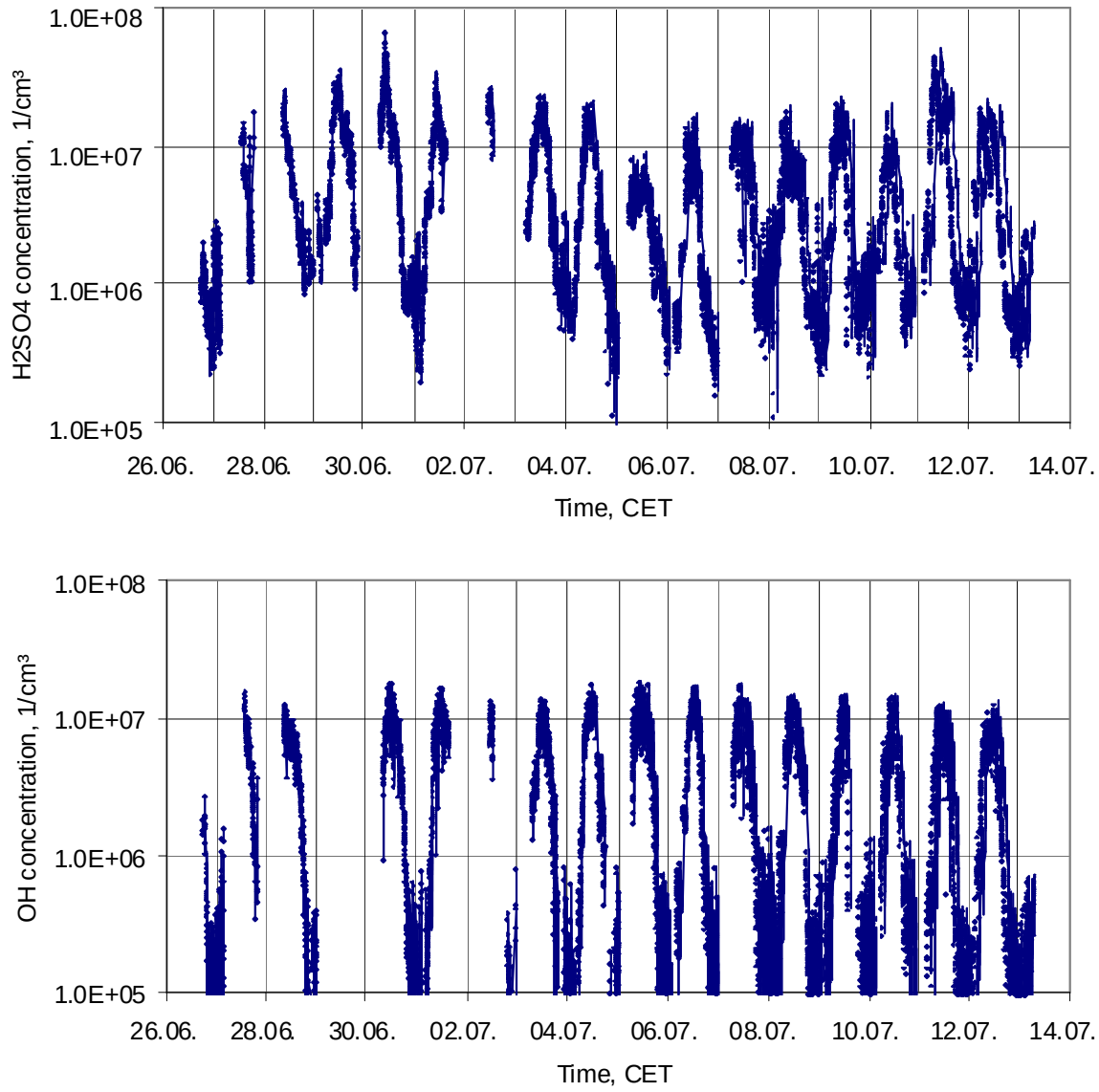

Figure 2. Time series of the concentrations of sulphuric acid and OH radicals during SPC-2009 (30-s values are presented by the dots)

The balance of sulphuric acid is determined by production (OH + SO_2) and loss (condensational sink on pre-existing aerosol). Accordingly, variations in the sulphuric acid are expected to be attributable to variations in either SO_2, or OH, or the condensational sink. Using estimates of the condensational sink from DMPS measurements (Hamed et al., accompanying poster), the balance for sulphuric acid during SPC-2009 will be presented and discussed.

ACKNOWLEDGEMENTS

We thank the CNR team and the staff at San Pietro Capofiume for the very good organisation and support in this field campaign, ARPA for providing ozone data. Financial support was given by the EUCAARI project.

REFERENCES

Berresheim, H., T. Elste, C. Plass-Dülmer, F.L. Eisele, and D.J. Tanner (2000) Chemical ionization mass spectrometer for long-term measurements of atmospheric OH and H_2SO_4, Int. J. Mass Spectrom., **202**, 91-109.

Hamed, A., Joutsensaari, J., Mikkonen, S., Sogacheva, L., Dal Maso, M., Kulmala, M., Cavalli, F., Fuzzi, S., Facchini, M. C., Decesari, S., Mircea, M., Lehtinen, K. E. J. and Laaksonen, A. (2007) Nucleation and growth of new particles in Po Valley, Italy. Atmos. Chem. Phys., **7**, 355–376.

Hamed, A., Petri Vaattovaara, Pasi Miettinen, Petri Tiitta, Christian Plaß-Dülmer, Thomas Elste, Georg Stange, Stefano Decesari, Claudio Carbone, Maria Cristina Facchini, Jorma Joutsensaari, Ari Laaksonen (2009) nucleation during the 2009 EUCAARI campaign in the Po valley, this issue.

Rohrer, F., and Berresheim, H. (2006) Strong correlation between levels of tropospheric hydroxyl radicals and solar ultraviolet radiation, Nature, **442**, 7099, 184–187, doi:10.1038/nature04924.

CLOUD DROPLET ACTIVATION OF MIXED SURFACTANT-SALT PARTICLES

N.L. PRISLE[1], T. RAATIKAINEN[2], A. LAAKSONEN[2,3], and M. BILDE[1]

[1] University of Copenhagen, Department of Chemistry, Universitetsparken 5, DK-2100, Copenhagen, Denmark.

[2]Finnish Meteorological Institute, Erik Palmenin Aukio 1, FI-00101, Helsinki, Finland.
[3]University of Kuopio, Department of Physics, P.O.B. 1627, FI-70211 Kuopio, Finland.

Keywords: surfactants, CCN, mixed organic-inorganic particles, Köhler theory.

INTRODUCTION

The aerosol cloud albedo effect constitutes the single largest uncertainty in assessing anthropogenic climate forcing (IPCC (2007)). Clouds form by condensation of water vapor onto the surfaces of atmospheric aerosol particles. Water soluble particle components may dissolve in the aqueous phase and form a solution droplet. The ability of particles to act as cloud condensation nuclei (CCN) therefore depends on their chemical composition, as well as their size. A threshold atmospheric water vapor content, or critical supersaturation, is required for particles to activate and grow into full-sized cloud drops. The equilibrium growth and activation of a small solution droplet can be described from Köhler theory (Köhler (1936)).

Surface active organic compounds (surfactants) have been identified in aerosol samples from many different environments (Mochida et al. (2007)). Surfactants preferentially concetrate in surface of aqueous solutions and can reduce solution surface tension. Reduced surface tension, compared to that of pure water, has been demonstrated in bulk samples of atmospheric cloud and fog water, and of dissolved atmospheric aerosol particles (Facchini et al. (2000)). We have previously studied the cloud droplet formation of single-component particles comprising organic surfactants and demonstrated the importance of a comprehensive account for surfactant properties in Köhler theory predictions (Prisle et al. (2008)).

Atmospheric aerosol particles are however generally mixtures of both organic and inorganic species (Murphy et al. (2006)). Here we therefore present the first study combining state-of-the-art laboratory experiments with comprehensive thermodynamic modeling, for particles comprising organic surfactants of high atmospheric relevance, mixed with inorganic salt.

METHODS

Critical supersaturations were measured for particles comprising organic surfactant mixed with sodium chlorinde (NaCl), using a static diffusion cloud condensation nucleus counter (Wyoming CCNC-100B). Investigated surfactants were the sodium salts of n-octanoic (C8, caprylic), n-decanoic (C10, capric) and n-dodecanoic (C12, lauric) acid, which have all been identified in the atmosphere (Mochida et al. (2003a,b)) together with sodium dodecyl sulfate (SDS). SDS has previously been used as a model compound for water-soluble atmospheric surfactants in cloud droplet formation studies (Li et al. (1998)).

Experimental results were modeled from Köhler theory employing three different representations of surfactant properties: (σ, p) using a concentration-dependent surface tension for the activating droplets and explicitly accounting for the effects of surfactant surface partitioning, (σ, b) disre-

garding surface partitioning and using a concentration-dependent surface tension for the droplets corresponding to a bulk aqueous solution of the same overall composition, and (σ_w) treating the surfactant as a generic solute and assuming the constant surface tension of pure water throughout droplet activation.

CONCLUSIONS

We confirm previous results for single-component organic surfactant particles, that experimental critical supersaturations are greatly underpredicted by using reduced surface tension in Köhler theory while ignoring the effects of surfactant surface partitioning (Prisle et al. (2008)). A comprehensive account for reduced surface tension and surfactant partitioning in activating droplets on the other hand predicts experimental critical supersaturations well. Treating the surfactant as a generic solute and assuming the constant surface tension of pure water can also lead to significant underpredictions of experimental critical supersaturations, most notably for particles containing the stronger surfactants. Nevertheless, for mixed particles comprising less than 50% by mass of surfactant, this representation provides a good first-order approximation of observed activation, which implies a significant simplification for representating surfactants in atmospheric models.

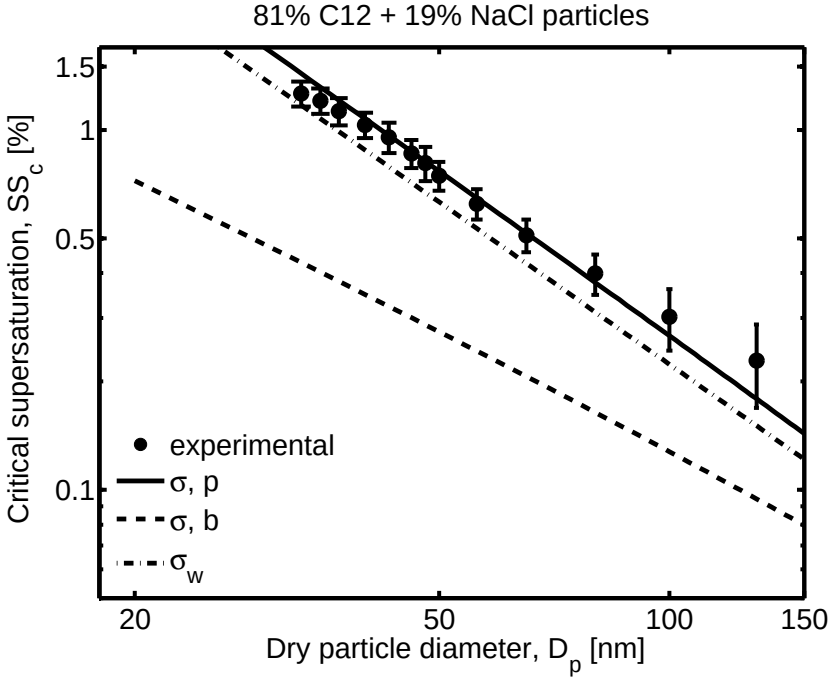

Figure 1: Experimental and modelled activation for mixed particles of C12 fatty acid salt and NaCl.

ACKNOWLEDGEMENTS

This work was supported by EUCAARI (European Integrated project on Aerosol Cloud Climate and Air Quality interactions) No 036833-2, the Danish Natural Science Research Council (Copenhagen Center for Atmospheric Research), and ACCENT Access to infrastructures.

REFERENCES

Facchini, M., Decesari, S., Mircea, M., Fuzzi, S., and Loglio, G. (2000). Surface Tension of Atmospheric Wet Aerosol and Cloud/Fog Droplets in Relation to their Organic Carbon Content and Chemical Composition. *Atmospheric Environment*, 34:4853–4857.

IPCC (2007). *Climate Change 2007, The Physical Science Basis, Contribution of Working Group I to the Fourth Assessment Report of the Intergovernmental Panel on Climate Change*. Cambridge University Press.

Köhler, H. (1936). The Nucleus in and the Growth of Hygroscopic Droplets. *Transactions of the Faraday Society*, 32:1152–1161.

Li, Z., Williams, A., and Rood, M. (1998). Influence of Soluble Surfactant Properties on the Activation of Aerosol Particles Containing Inorganic Solute. *Journal of the Atmospheric Sciences*, 55:1859–1866.

Mochida, M., Kawabata, A., Kawamura, K., Hatsushika, H., and Yamazaki, K. (2003a). Seasonal variation and origins of dicarboxylic acids in the marine atmosphere over the western North Pacific. *Journal of Geophysical Research-Atmospheres*, 108:(D6)4193.

Mochida, M., Kawamura, K., Umemoto, N., Kobayashi, M., Matsunaga, S., Lim, H.-J., Turpin, B., Bates, T., and Simoneit, B. (2003b). Spatial distributions of oxygenated organic compounds (dicarboxylic acids, fatty acids, and levoglucosan) in marine aerosols over the western Pacific and off the coast of East Asia: Continental outflow of organic aerosols during the ACE-Asia campaign. *Journal of Geophysical Research*, 108:D23S8638.

Mochida, M., Umemoto, N.and Kawamura, K., Lim, H. J., and Turpin, B. J. (2007). Bimodal size distributions of various organic acids and fatty acids in the marine atmosphere: Influence of anthropogenic aerosols, Asian dusts, and sea spray off the coast of East Asia. *Journal of Geophysical Research-Atmospheres*, 112:D15209.

Murphy, D. M., Cziczo, D. J., Froyd, K. D., Hudson, P. K., Matthew, B. M., Middlebrook, M., Peltier, R. E., Sullivan, A., Thomson, D. S., and Weber, R. J. (2006). Single-particle mass spectrometry of tropospheric aerosol particles. *Journal of Geophysical Research*, 111:D23S32.

Prisle, N. L., Raatikainen, T., Sorjamaa, R., Svenningsson, B., Laaksonen, A., and Bilde, M. (2008). Surfactant partitioning in cloud droplet activation: a study of C8, C10, C12 and C14 normal fatty acid sodium salts. *Tellus*, 60B:416–431.

LES SIMULATION OF A STRATOCUMULUS DIURNAL CYCLE

Vincent Puygrenier, Jean-Louis Brenguier, Frederic Burnet, Laurent Gomes, Odile Thouron

Météo France, Centre National de Recherches Météorologiques, Toulouse, France

INTRODUCTION

The meso-NH model was used to retrieve a stratocumulus diurnal cycle. A LES simulation was performed on a case study observed the 15th of May over the North Sea during the EUCAARI campaign. The measurements of the ATR-42 research aircraft, carried out twice during that day on the morning and the afternoon above the same area, were used to compare the simulated cloud fields to the observed ones.

The work were first devoted to simulate properly the cloud observed in the morning in order to asses the model ability to retrieve the midday cloud. Both observed datasets were used to control the realism of the simulated cloud in term of thermodynamical and microphysical properties.

MESO-NH MODEL AND LES SIMULATION SETUP

Meso-NH is a non-hydrostatic model (Lafore et al., 1998) which has been developed to simulate various atmospheric processes from the synoptic scale to turbulent eddies. The LES configuration chosen here uses a 3D turbulence scheme with a one and a half order closure, that is based on the prognostic turbulent kinetic energy and a diagnostic mixing length (Deardoff, 1980).

The simulation was performed with a two-moment bulk microphysical scheme based on the parameterization of Khairoutdinov and Kogan (2000), which was specifically designed for LES studies of warm stratocumulus clouds. The radiative transfer is computed using the European Centre for Medium-Range Weather Forecasts (ECMWF) operational model radiation code (Morcrette, 1991).

The simulated domain size is 10 km × 10 km × 3 km. Mesh size used is 50 m in both horizontal directions and 10 m to 100 m in vertical with maximal resolution in cloud and entrainment layer. Cyclic boundary conditions are performed. The simulation starts at 00:00 UTC the 15th of May and lasts 24 hours with a time step of 1s.

The simulation was initialized using vertical profiles of horizontal wind components measured by the ATR-42 research aircraft. The thermodynamical vertical profiles were determined in order to obtain the observed ones after 8 hours of simulation.

To limit the spin-up at the beginning of the simulation, a sub-saturated air with respect to liquid water was prescribed in the cloud boundary layer. The whole atmosphere temperature was cooled (~2,5 $K.h^{-1}$) using a Newtonian relaxation during the first 3 hours of the simulation to form progressively the cloud. According to ECMWF analysis, the sea surface temperature (*SST*) was set constant to 282 K during the simulation expected for the first 3 hours. Indeed, to avoid sub-cloud layer stabilization induced by the initial warming of the atmosphere, the *SST* was decreased linearly from 285.5 to 282 K.

The prescribed large-scale subsidence w_s varies proportionally with the altitude z in the cloud boundary layer. It was calculated as $w_s=-Dz$ with an horizontal divergence D of 6.10^{-6} s^{-1}. This divergence rate is close to the average value indicated in Neiburger (1960). Above the cloud boundary layer, the subsidence rate was determined in order to compensate the radiative cooling of the free atmosphere (w_s = $-2.25\ 10^{-3}$ $m.s^{-1}$).

The activation scheme of Cohard et al. (1998), based on a supersaturation diagnostic, is used in this simulation. This scheme allows to define the aerosol type and the number of activated cloud condensation nuclei (CCN). The activated CCN concentration was determined in order to simulate the observed cloud droplet number concentration (CDNC) considering CCN type as maritime aerosol (Cohard et al., 2000).

CLOUD MODEL VALIDATION

The morning cloud vertical and horizontal structure is well represented by the model in term of thermodynamical and microphysical properties. Both in the observations and the simulation, the median altitude of the cloud base is around 650 m and the median liquid water content (LWC) profile is close to the adiabatic one with a similar value of 0.5 $g.m^{-3}$ at the cloud top (Figure 3). The median temperature, vapor

mixing ratio and CDNC are not considered in this comparison since the observed values of these parameters were used to determine the initial conditions of the simulation.

In addition, figures 1 and 2 show that the main characteristics of the spatial variability are retrieved by the model with the same order of magnitude. For the thermodynamical parameters, the variability is different in the sub-cloud and cloud layer with a maximum encountered in the inversion zone. A large heterogeneity is also observed for the microphysical parameters at the cloud top and at the cloud base for the CDNC. In the cloud, the variation ranges of the potential temperature, the water vapor mixing ratio, the LWC and the CDNC can be estimated to 0.5 K, 0.2 $g.kg^{-1}$, 0.2-0.4 $g.m^{-3}$ and 20-30 cm^{-3} in the simulation and to 0.5 K, 0.4 $g.kg^{-1}$, 0.2-0.3 $g.m^{-3}$ and 30-40 cm^{-3} in the observations.

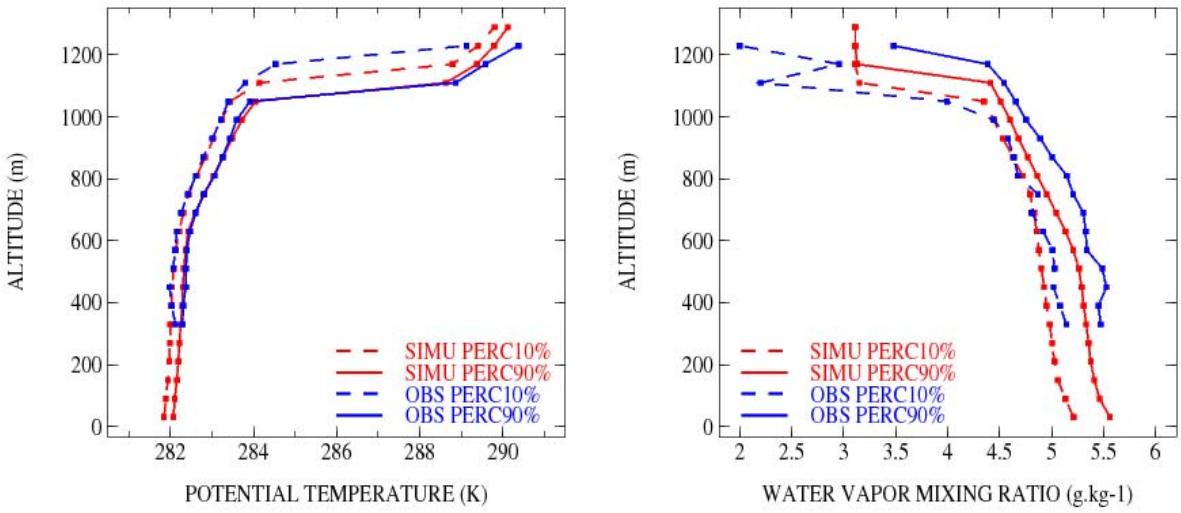

Figure 1: 10% and 90% percentiles vertical profiles of potential temperature (left panel) and water vapor mixing ratio (right panel) determined for the morning aircraft data (blue) and the instantaneous simulated field at 08:30 UTC (red).

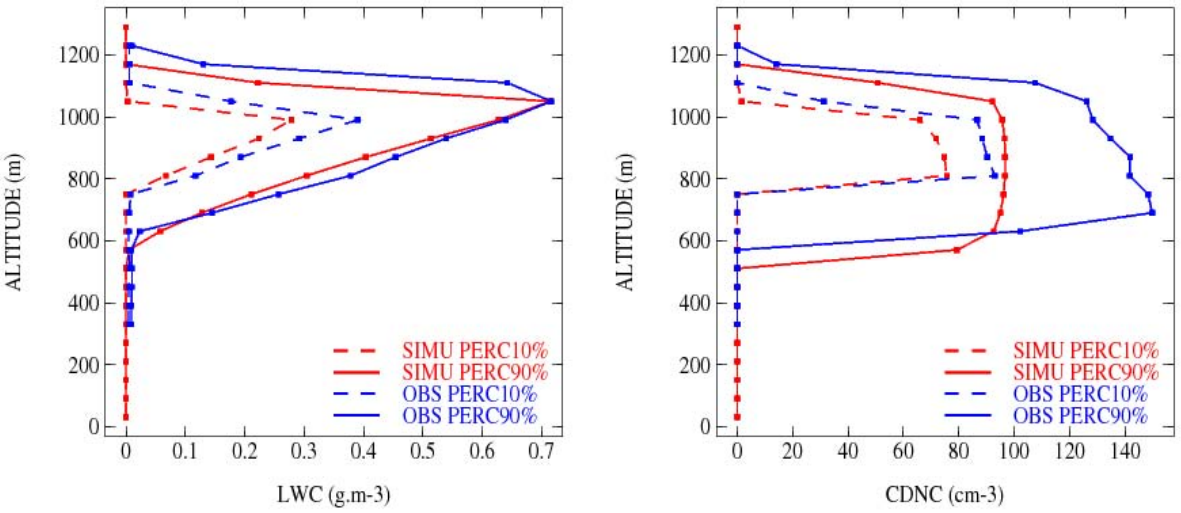

Figure 2: 10% and 90% percentiles vertical profiles of liquid water content LWC (left panel) and cloud droplet number concentration CNDC (right panel) determined for the morning aircraft data (blue) and the instantaneous simulated field at 08:30 UTC (red).

Since the thermodynamical and microphysical properties of the simulated cloud are realistic the morning, a comparison to the data collected the afternoon was undertaken. This comparison shows that the simulated cloud is distinct to the observed one. The median temperature in the boundary layer cloud is colder (~0.5 K) resulting in a lowest condensation level. Consequently, the median LWC is highest of about 0.15 g,m^{-3} at the cloud top and the median geometrical thickness is around 100 m deeper (Figures 4). Informations about the humidity in the cloud boundary layer are difficult to asses because the tendency between the morning and the afternoon is distinct from one instrument to another.

In addition, a CDNC decrease from 100-110 cm^{-3} to 60-70 cm^{-3} occurred between the morning and the afternoon as shown by the observations in the figures 3 and 4. This feature is not retrieved by the simulation and the median CDNC is unchanged at a value of 80-90 cm^{-3}. This drop can be estimated to about one third of the CDNC observed in the morning.

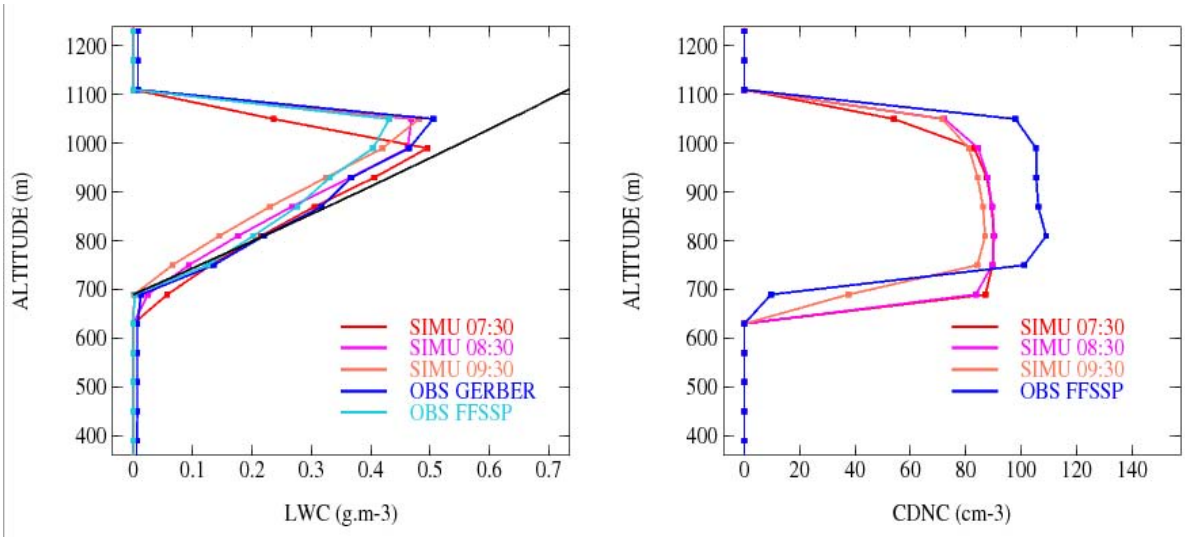

Figure 3: Median vertical profiles of the liquid water content LWC (left panel)and cloud droplet number concentration CDNC (right panel) determined for 3 instantaneous simulated fields at 07:30, 08:30 and 09:30 UTC and for the morning airborne measurements realized with the GERBER PVM and the Fast FSSP probes. The black line indicates the wet adiabatic.

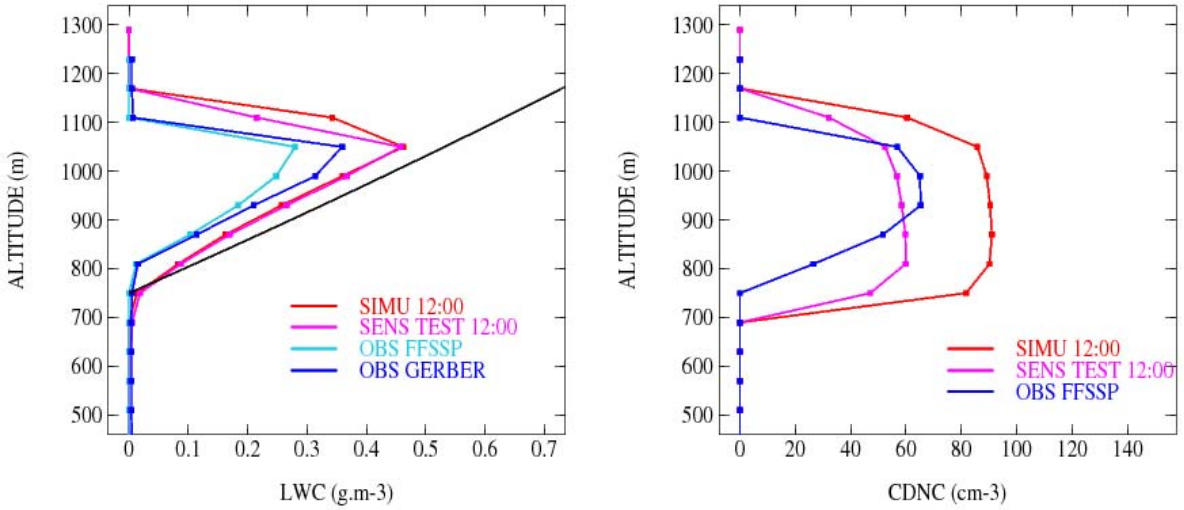

Figure 4: Median vertical profiles of the liquid water content LWC (left panel) and cloud droplet number concentration CDNC (left panel) determined for the simulated fields at 12:00 UTC, the sensibility test at 12:00 UTC and the midday aircraft measurements realized with the GERBER PVM and the Fast FSSP probes. The black line indicates the wet adiabatic.

To properly simulate the diurnal evolution of the stratocumulus, this modification of the mircrophysical properties have to be considered in the simulation. Indeed, the CDNC impacts the drizzle formation. A drop of CDNC leads to larger cloud droplet diameter and enhance the precipitation, hence the drizzle evaporation below the cloud base. This is known to play a key role in the dynamic of the stratocumulus diurnal cycle (Sandu et al., 2008).

Consequently, a sensitivity test have been performed to see the model response to a decrease of the CDNC in the cloud layer. But, no significant differences were obtained between the simulation and the sensitivity test as shown by the LWC comparison (Figure 4). Hence, accounted for the CDNC drop in the simulation did not modify the thermodynamical and microphysical properties of the simulated cloud.

This result indicates that the observed drop of CDNC does not affect the cloud boundary layer in the afternoon. The thinner cloud observed at midday and the model difficulty to retrieve it would be a consequence of large scale meteorological forcings. Indeed, they can affect even slightly the thermodynamical and dynamical properties of the atmosphere and lead to consequent change in the cloud boundary layer. For instance, a large-scale advection of dryer and warmer air during the late morning can enhance the drying of the cloud boundary layer through entrainment and lead to weaken the cloud depth.

CONCLUSION

The comparison of the LES simulation to the observed datasets shows that the model is able to retrieve realistic cloud fields. In the morning, the thermodynamical and microphysical structure of the simulated cloud corresponds to one of the observed cloud. The midday comparison exhibits that the model can not retrieve the observed thinner cloud due to large-scale phenomenons which were not taking into account in the simulation.

The first outgoing of this work would be to confirm this hypothesis testing model sensitivity to observed changes of large-scale forcings. Moreover, it would be interesting to test the realism of the simulated cloud in terms of optical properties. Satellite data and radiative measurements of this stratocumulus collected by the DLR Falcon 20 research aircraft might be used for the comparison.

REFERENCES

Cohard, J.M., J.P. Pinty and C. Bedos, 1998: Extending Twomey's analytical estimate of nucleated cloud dropplet concentrations from CC spectra. *J. Atmos. Sci*., **55**, 423-430.

Cohard, J.M., J.P. Pinty and K. Shure, 2000: On the parametrization of activation spectra from cloud condensation nuclei microphysical properties. *J. Geophys. Res*.,**105**,3767-3784.

Deardoff, J., 1980: Stratocumulus-capped mixed layers derived from a three dimensionnal model. *Bound.-Layer Meteor*., **18**, 495-527.

Khairoutdinov, M. and Y. Kogan, 2000: A new physics parameterization in a large-eddy simulation model of marin stratocumulus. *Mon. Wea. Rev*., **128**, 229-243.

Lafore, J.P. and Coauthors, 1998: The meso-NH atmospheric simulation system. Part I: adiabatic formulation and control simulations. *Ann. Geophys*., **16**, 90-109.

Morcrette, J.J. 1991: Radiation and cloud radiative properties in the European Centre for Medium Range Weather Forecasts forecasting system. *J. Geophys. Res*., **96**, 9121-9132.

Neiburger, M., 1960: The relation of air mass structure to the field of motion over the eastern north Pacific Ocean in summer. *Tellus*, **12**, 31-40,

Sandu, I., J.L., Brenguier, O., Geoffroy, O., Thouron and V. Masson, 2008: Aerosol impacts on the diurnal cycle of marine stratocumulus. *J. Atmos. Sci.*, **65**, 2705-2718.

GLOBAL MODEL SIMULATIONS OF PARTICLE NUMBER CONCENTRATIONS OVER EUROPE DURING THE EUCAARI INTENSIVE OBSERVATION PERIOD

C.L. REDDINGTON[1], M.G. FRONTOSO[1], K. CARSLAW[1], D. V. SPRACKLEN[1], A. MINIKIN[2], T. HAMBURGER[2], and H. COE[3]

[1]Institute for Climate & Atmospheric Science, School of Earth and Environment, University of Leeds, Leeds, LS2 9JT, United Kingdom

[2]Deutsches Zentrum für Luft- und Raumfahrt (DLR), Institut für Physik der Atmosphäre, Oberpfaffenhofen, Germany

[3]School of Earth, Atmospheric and Environmental Sciences, University of Manchester, Manchester, M13 9PL, United Kingdom

Keywords: Aerosol modelling, number concentration, nucleation.

INTRODUCTION

The alteration of the Earth's radiative balance by atmospheric aerosols is a major uncertainty in assessments and predictions of climate change on both global and regional scales (Forster *et al.*, 2007). To understand and quantify the impact of aerosol on climate it is important to understand how anthropogenic emissions alter the number size distribution of atmospheric aerosol on a range of temporal and spatial scales. Recent developments mean that global models like the Global Model of Aerosol Processes (GLOMAP) (Spracklen *et al.*, 2005) now include size-resolved aerosol microphysics schemes and represent particle number concentrations down to nanometre sizes. The budget of particle number over Europe is a major focus of the European Integrated Project on Aerosol Cloud Climate and Air Quality Interactions (EUCAARI). Within EUCAARI we aim to improve model parameterizations of aerosol processes and to quantify the relative contributions of secondary aerosol formation and primary emissions to total condensation nuclei (CN) concentrations over Europe. Here we use observations from the EUCAARI Intensive Observation Period to study the performance of GLOMAP over the European domain.

FIELD OBSERVATIONS

Over the EUCAARI Intensive Observation Period (IOP) in May 2008, extensive observations of European aerosol were made on a range of measurement platforms including research aircraft, ground-based field stations and satellites. The IOP included the Long Range Experiment (LONGREX) during which ambient aerosol was sampled over Europe by the DLR Falcon research aircraft providing particle number size distribution measurements from 14 separate flights. The CN number concentration data used in this study were obtained by the Condensation Particle Size Analyzer (CPSA) and Passive Cavity Aerosol Spectrometer Probe (PCASP) instruments onboard the aircraft. Observations of primary aerosol were also obtained by the Falcon aircraft by measuring the non-volatile particle fraction with a cut-off particle diameter (D_p) of 14nm.

The IOP also included spatially extensive surface-based measurements from the European Supersites for Atmospheric Aerosol Research (EUSAAR). EUSAAR consists of a network of high quality ground-based stations (supersites) that provide a range of atmospheric aerosol measurements in the boundary layer and free troposphere. Over the course of the campaign the Falcon and BAe-146 performed several

overpasses and vertical profiles over the ground stations located at Melpitz, Cabauw and Mace Head. EUSAAR measurements of aerosol number size distribution, used in this study for model validation, were made using various mobility particle sizer instruments (Scanning Mobility Particle Sizer, SMPS and Differential Mobility Particle Sizer, DMPS) classifying particles in different particle diameter ranges between ~ 3nm to ~ 1μm.

THE GLOBAL MODEL OF AEROSOL PROCESSES

The GLOMAP model simulates the evolution of size and composition resolved aerosols, and runs offline inside the TOMCAT global chemical transport model (Stockwell and Chipperfield, 1999). The aerosol particle types included in GLOMAP are sea spray, sulphate, black and organic carbon, and a simple scheme for secondary organic material based on monoterpene oxidation products. The aerosol size distribution is described using a two-moment sectional bin scheme with 20 size bins spanning 3nm to 25μm. Secondary particle formation in the free troposphere (FT) is treated using binary homogeneous nucleation of sulphuric acid and water (Kumala *et al*., 1998). Nucleation within the boundary layer (BL) is simulated using the activation mechanism, where the formation rate of 1nm clusters (j_1) is assumed to depend linearly on the gas-phase concentration of sulphuric acid ($[H_2SO_4]$) (Kumala *et al*., 2006), given by:

$$j_1 = A[H_2SO_4]; A = 2 \times 10^{-6}$$

where A is the empirical activation coefficient. To take into account scavenging losses of freshly nucleated clusters and condensable gases during growth, the production rate of detectable particles is controlled in GLOMAP by the cluster formation rate (j_1) and the pre-existing particle surface area. The following approximation from Kerminen and Kulmala (2002) is used to calculate the effective formation rate of observable 3nm-sized particles (j_3):

$$j_3 = j_1 \exp[-0.153 \frac{CS'}{GR}]$$

where *CS'* is the reduced condensation sink and *GR* is the growth rate of the 1nm clusters. In order to compare GLOMAP against the specific observations made during the IOP, the model was setup to provide output every hour over a European domain. All the results in the present work have a horizontal resolution of 2.8° x 2.8° and 20 vertical levels from surface to 10km.

RESULTS AND DISCUSSION

For the EUCAARI IOP, initial comparisons between GLOMAP and observations of CN number concentration in different particle size ranges have revealed a large model discrepancy within the BL. Figure 1 compares observed and modelled vertical profiles of CN number concentration (D_p > 10nm) averaged for all the DLR Falcon flights performed during LONGREX. For altitudes greater than ~3000m the modelled CN number concentration compares reasonably well to the observations, generally remaining within ~1σ. However, at lower altitudes (between the surface and ~2000m) GLOMAP is underestimating number concentrations of particles > 10nm by a factor of ~4. It is likely that the number concentrations of both primary and secondary particles need to be increased at these low altitudes to correct for the discrepancy in the model.

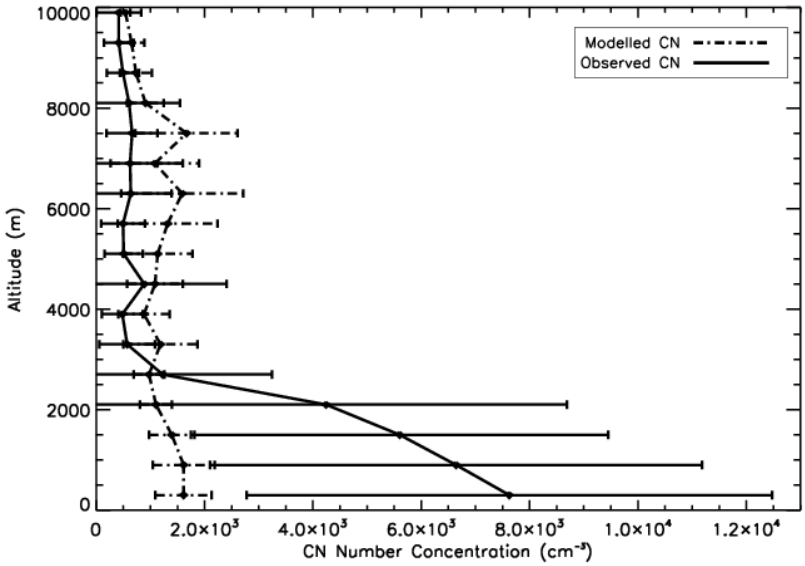

Figure 1. **A**verage vertical profile of modelled and observed CN number concentration (D_p > 10nm) for the EUCAARI-LONGREX campaign, May 2008. The modelled CN concentration was interpolated to the flight path of the Falcon aircraft and sectioned into altitude bins of 600m. The mean number concentration of each bin has been plotted with error bars showing the standard deviation of the mean.

A comparison between modelled and observed nucleation-mode (4 < D_p < 10nm) particle number concentration for the LONGREX field campaign is shown in Figure 2 (a). This comparison suggests that relatively few secondary particles are predicted by the model at low altitudes for this period, despite the inclusion of the BL nucleation scheme. An underestimation of nucleation-mode particles is also evident when the model is compared with EUSAAR ground-based measurements of CN number size distribution. The discrepancy in the model appears to be fairly consistent over different regions/environments in Europe. For example, modelled total CN number concentration is underestimated by a factor of ~ 5 for rural polluted region, Melpitz and by a factor of ~ 4 for remote boreal region, Hyytiala. These preliminary results suggest that either the nucleation rates in the BL need to be altered to increase secondary particle concentrations in the model, or that freshly nucleated particles are being scavenged too quickly after particle formation. Further investigation is needed to determine the reasons for the lack of nucleation-mode particles predicted by the model.

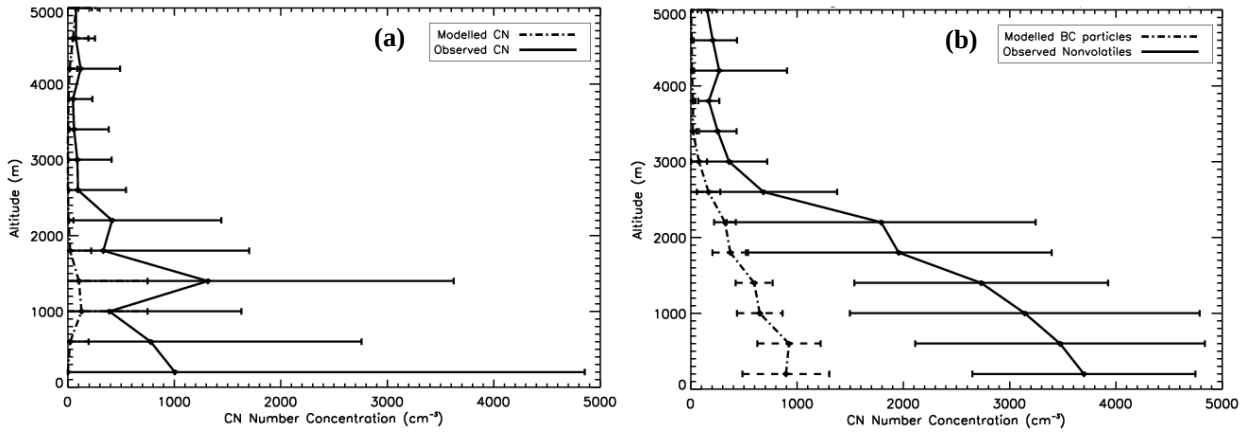

Figure 2. Campaign average vertical profiles of (a) modelled and observed nucleation-mode CN number concentrations (4 < D_p < 10nm) and (b) modelled BC and observed non-volatile particle number concentrations (D_p > 14nm). The modelled particle concentration was interpolated to the flight path of the Falcon aircraft and sectioned into altitude bins of 400m. The mean number concentration of each bin has been plotted with error bars showing the standard deviation of the mean.

To study primary aerosol emissions the set-up of GLOMAP has been modified, allowing the number concentration of black carbon (BC) particles to be tracked in the model. The measured non-volatile particle number from the DLR Falcon aircraft has been used to compare with the BC particle number concentration from GLOMAP. The non-volatile particle number is assumed to consist entirely of primary aerosol particles and, for comparison purposes, the composition of these particles is assumed to be that of BC (with mineral dust having a negligible contribution). Figure 2 (b) shows an average campaign vertical profile of modelled BC particle number concentration compared with the measured non-volatile concentration. These preliminary comparisons suggest that the model is under-predicting particle number concentrations of BC in the BL by a factor of ~4. Different BC emission schemes in the model have been investigated to find the best agreement with the observed non-volatile particle concentration, results from this study will be presented. Measurements of BC mass and size distribution from the SP2 instrument onboard the FAAM BAe-146 aircraft for the same period will also be taken into account ensuring that the model is not making compensating errors.

ACKNOWLEDGEMENTS

This work has been supported by funding from the European Integrated Project on Aerosol Cloud Climate and Air Quality Interactions (EUCAARI). The authors would like to thank the FAAM and DLR flight teams and all EUSAAR instrument P.I.'s for providing data.

REFERENCES

Kerminen, V.-M., and M. Kulmala (2002). Analytical formulae connecting the "real" and the "apparent" nucleation rate and the nuclei number concentration for atmospheric nucleation events, *J. Aerosol Sci.* 33, 609.

Kulmala, M., A. Laaksonen, and L. Pirjola (1998). Parameterizations for sulfuric acid/water nucleation rates, *J. Geophys. Res.-Atmos.* 103(D7), 8301.

Kulmala, M., K.E.J Lehtinen, and A. Laaksonen (2006). Cluster activation theory as an explanation of the linear dependence between formation rate of 3 nm particles and sulfuric acid concentration, *Atmos. Chem. Phys.* 6, 787.

Spracklen, D. V., K.J. Pringle, K.S. Carslaw, M.P. Chipperfield, and G.W. Mann (2005). A global off-line model of size-resolved aerosol microphysics: I. Model development and prediction of aerosol properties, *Atmos. Chem. Phys.* 5, 2227.

Stockwell, D. Z. and M.P. Chipperfield (1999). A tropospheric chemical transport model: Development and validation of the model transport schemes, *J. Geophys. Res,* 125, 1747.

.

LONG TERM MEASUREMENTS OF AEROSOL PROPERTIES IN A PRISTINE SITE IN AMAZÔNIA

Luciana V. Rizzo[1], Paulo Artaxo[1], Kenia Wiedemann[1], Alfred Wiedensohler[2], Thomas Müller[2], Erik Swietlicki[3], Pontus Roldin[3], Erik Nilsson[3]

[1] University of São Paulo, Brazil
[2] Leibniz Institute for Tropospheric Research, Germany
[3] University of Lund, Sweden

Keywords: biogenic aerosol, scattering, absorption, size distribution

INTRODUCTION

As a part of EUCAARI, a long term experiment has been conducted in a pristine area in the Amazon forest. As cooperation between the University of São Paulo (Brazil), the IFT-Leipzig (Germany), the Lund University (Sweden) and the State University of Amazonas (Brazil), measurements of aerosol optical properties (scattering, absorption), size distribution and elemental composition have been made since February 2008. This long term experiment is planned to be held for two years.

EXPERIMENTAL

Field measurements of aerosol properties have been taken since February 2008 at the Cuieiras forest reservation, 60 km NNW of Manaus in Central Amazonia. The site is relatively undisturbed, as the prevailing trade winds blow over vast expanses of intact tropical forest before reaching the measurement tower (TT34). Inlet lines run from the measurement level (45m, ~10 m above tree height) to a ground-based lab, climatically controlled. A drier on the inlet line keeps low relative humidity levels (30-40%). Aerosol scattering coefficients have been measured with a TSI-3563-Nephelometer. Aerosol absorption have been double measured by two different equipment: 7-lambda Aethalometer (Magee Scientific) and MAAP-CARUSSO. The main difference between these two absorption instruments is that MAAP measures not only absorption through a filter, but also measures the angular reflection to account for filter-particle interactions. Two fine mode aerosol spectrometer systems (10-300nm) have been used: a TSI-3936-SMPS and a lab-made DMPS developed at Lund University. Coarse mode number size distributions have been interchangeably measured with an OPC-Grimm (300nm-20μm) and an OPC-Lasair (300nm-5μm). Number concentrations have been measured with a TSI-3785-CPC optical particle counter. Stacked Filter Units (SFU) have been used to collect fine mode (D_p < 2.0 μm) and coarse mode (D_p > 2.0 mm) aerosols during daytime (7 am to 5 pm) and nighttime (5pm to 7 am) periods. Nuclepore filters have been analysed for particulate mass, equivalent black carbon and elemental composition.

PRELIMINARY RESULTS

Several aerosol properties have been continuously measured at the Cuieiras forest site. The time series of aerosol scattering coefficient is illustrated at Figure 1, showing a clear seasonal pattern, with higher scattering coefficients observed during the dry season (Jul-Oct), at the onset of the biomass burning period, in comparison to the wet season (Nov-Jun). From wet to dry season, average aerosol scattering coefficients increased from 10 Mm^{-1} to 100 Mm^{-1}. The forest site is preserved, in the sense that no biomass burning occurs in the reservation. Although, measurements have shown that

the site is occasionally affected by regional transport of polluted air masses, either from biomass burning or urban plumes.

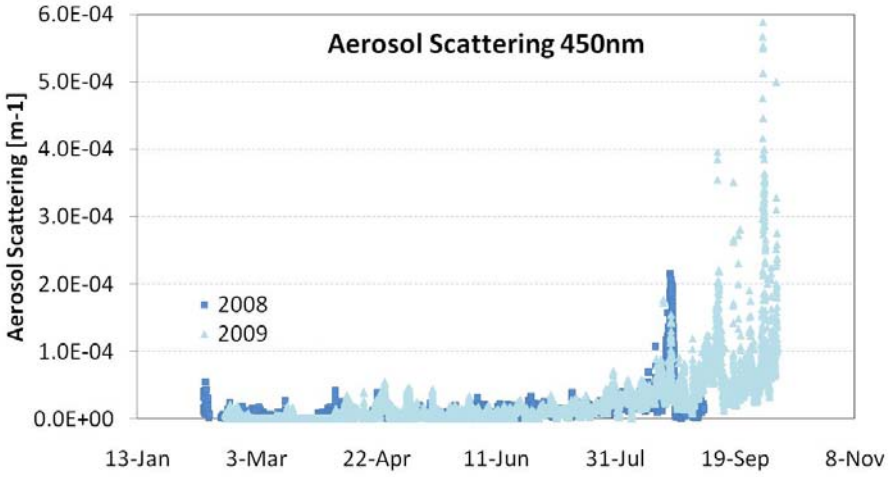

Figure 1: Time series of aerosol scattering coefficient (450nm).

Observed aerosol absorption coefficients were frequently below the detection limit of the instruments (Aethalometer: 2Mm^{-1} at 450nm; MAAP: 1 Mm^{-1} at 637nm), specially during the wet season. This is consistent with the absence of local biomass burning aerosol sources. Figure 2 shows the average absorption spectrum calculated for the wet season, measured with the Aethalometer. It is important to highlight that the absolute magnitude of absorption shown in Figure 2 may be overestimated by a factor 2-5, due to multiple scattering effects within the Aethalometer filter matrix. Despite the imprecision concerning the absorption magnitude, the Aethalometer provide an accurate measurement of the spectral dependency of aerosol absorption. The negative slope of the absorption log-log plot is known as the Angstrom exponent. Soot carbon particles, formed during combustion processes, are expected to exhibit an Angstrom exponent of 1.0 (black dashed line on Fig. 2). The average absorption spectrum during the wet season shows a sharp increase in absorption towards lower wavelengths (450nm). It indicates the presence of non-soot absorbing aerosols, often denominated “brown carbon”, possibly including dust, humic-like substances and biogenic aerosols.

Aerosol number size distributions were continuously measured with a SMPS system (10-400nm), and occasional measurements of coarse-mode size distribution were taken with an OPC-Grimm particle counter (300nm-20μm). Figure 3a shows the combined SMPS-OPC aerosol number size distributions determined for the wet season of 2008 (Feb-Mar) and for the dry season of 2009 (Jul-Aug). Only a few nucleation events were observed during the whole experiment, which is reflected by the absence of a nucleation mode at the calculated averages. However, the Aitken mode has been present in most of observed aerosol size distributions, suggesting that new particle formation may be occurring somewhere else above or below the canopy. Aerosol volume size distributions were derived from measured number size distributions assuming spherical particles. Coarse mode particles, possibly from biogenic origin, dominate the volume size spectra, either at dry or wet season. Figure 3b shows the average diurnal cycle calculated for the volume ratio between coarse (CPM) and fine particle mode (FPM). The volume ratio between coarse and fine mode increases greatly at night, suggesting a nocturnal release of biogenic particles as a result of the ecosystem natural metabolism.

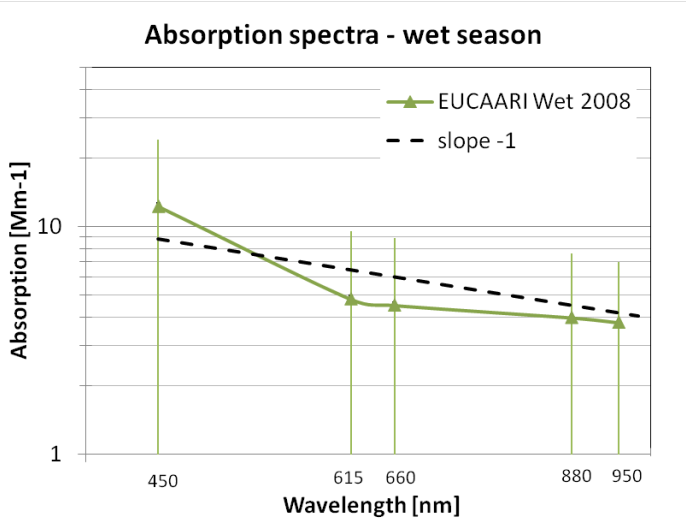

Figure 2: Average aerosol absorption spectra for the 2008 wet season (Feb-Jun). The absolute magnitude of absorption may be overestimated by a factor 2-5, due to multiple scattering effects within the Aethalometer filter matrix.

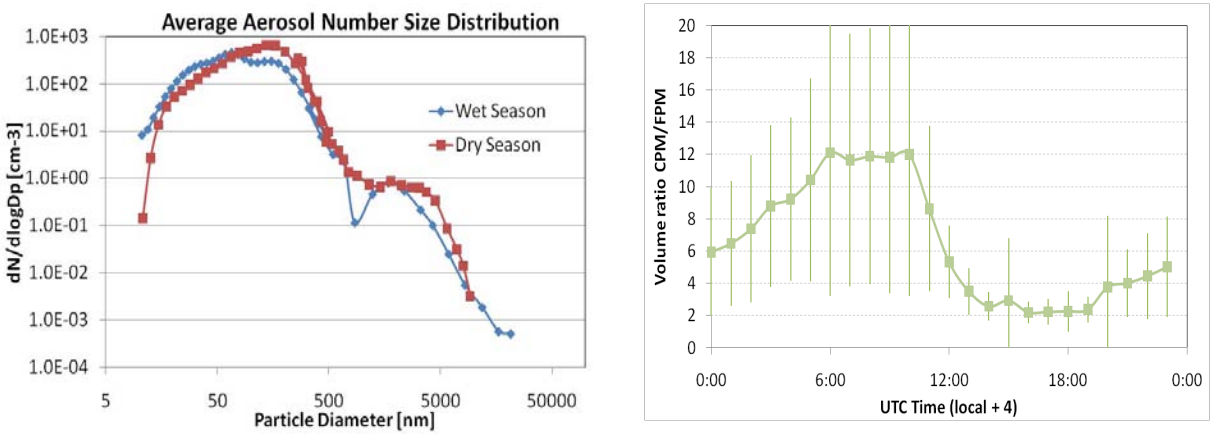

Figure 3: a) Average aerosol number size distribution for the wet season (2008 Feb-Mar) and for the dry season (2009 Jul-Aug). b) Average diurnal cycle calculated for the volume ratio between coarse and fine particle mode, derived from measured number size distributions.

It is important to emphasize that the results presented here are still preliminary. In upcoming analysis, single scattering albedo will be calculated from observed scattering and absorption coefficients, using a Mie model to correct for the contribution of coarse mode particles. In situ measurements of aerosol properties will be compared to atmospheric column observations (LIDAR, sun-photometers) and remote observations (satellites). This analysis will provide a detailed description of the optical properties of natural Amazonian aerosol, as well as a better comprehension of its potential influence over regional and global climate.

AIRBORNE MEASUREMENTS OF AEROSOLS IN THE BOUNDARY LAYER AND LOWER TROPOSPHERE OVER SOUTHERN FINLAND

S. SCHOBESBERGER[1], A. VIRKKULA[1], T. POHJA[1], P.P. AALTO[1], E. SIIVOLA[1], A. FRANCHIN[1], T. PETÄJÄ[1] and M. KULMALA[1]

[1]Division of Atmospheric Sciences and Geophysics, Department of Physics, University of Helsinki, P.O. Box 64, FI-00014 Helsinki, Finland.

Keywords: AIRBORNE, NEW PARTICLE FORMATION, BIOMASS BURNING, PLUME.

INTRODUCTION

The Europe-wide measurement network within the "European Integrated project on Aerosol Cloud Climate and Air Quality Interactions" (EUCAARI) project consist mainly of ground-based measurement stations distributed around Europe (Kulmala *et al.*, 2008). However, airborne measurements were performed as part of the project in the form of measurement flights using the DLR's (German Aerospace Center) Dassault Falcon 20 aircraft. The Falcon is a twin jet engine powered airplane, capable of reaching relatively high speeds (> 800 km/h) and altitudes (> 12 km). The majority of those flights where conducted above the mixing boundary layer at high altitudes, while covering areas 1000 to 4000 km across (e.g. Mirme *et al.*, 2009).

This abstract reports results on preliminary analysis of the first measurements conducted using a modified Cessna aeroplane as a platform. This aircraft was loaded with a suite of aerosol instruments to provide an overview of particle data over regional scale supported by ground based measurements at SMEAR II in Hyytiälä in the boreal forest of southern Finland (Hari and Kulmala, 2005). The flights were conducted at generally lower altitudes (up to 4 km) and lower speeds (< 200 km/h), allowing for a higher spatial and temporal resolution. In addition, a detailed analysis of aerosol plumes, originating mainly from industrial facilities and biomass burnings could be accomplished.

EXPERIMENTAL SETUP

The aircraft that was used in the measurements presented here is a modified Cessna FR172F – a light airplane, powered by a single engine (piston) and normally seating four people. The rear seats as well as the co-pilot's controls had been removed to accommodate the bulk of the scientific equipment. Majority of the instruments were located in a rack behind the pilot's and co-pilot's seat, and were supplied with sample air collected from an external inlet. This inlet was mounted on the airplane's right wing, so that it faced the undisturbed air ahead of the wing. Figure 1 shows a picture of the inlet, taken from the cockpit during flight. The inlet's design was adapted from the University of Hawai'i shrouded solid diffuser inlet design presented by McNaughton *et al.* (2007) for use aboard a DC-8 aircraft for airborne aerosol sampling. Our inlet was a downsized version of it, suiting the lower cruise speed of the Cessna.

The sample air was passed on to the instruments inside the aircraft through stainless steel tubing. Sample air not taken by the instruments was passed outside the aircraft again where it exited through a Venturi tube. The forward movement of the flying airplane together with the Venturi tube provided the sample air flow, which was controlled by a flow meter (TSI 4000 series) and a manually operated valve. A schematic flow diagram is depicted in figure 2, giving also an overview of the instruments implemented in the rack inside the aircraft: A CO_2/H_2O analyzer (LI-COR LI-840), two TSI 3772 condensation particle counters (CPCs) for cut-off sizes of 10 and 6 nm respectively, one TSI 3776 CPC tuned and calibrated for a cut-off size of 3 nm, a triple wavelength (467, 530, and 660 nm) particle/soot absorption photometer (PSAP; Radiance Research), and a nephelometer (Radiance Research Model 903) using a wavelength of 545 nm. The two TSI 3772 CPCs, the LI-840, as well as the PSAP required an external

vacuum that was provided by a vacuum pump (Thomas 107CDC20/12). The TSI 3772 CPCs are designed for maximum particle concentrations of 10^4 cm^{-3}, hence a dilution unit with a dilution factor of 1:10 could be optionally implemented in the sample line for those two instruments.

Figure 1. Photograph of the inlet mounted on the right wing during flight. The stainless steel sampling tube runs back under the wing and then along the wing strut towards the cabin where it enters from underneath. The aluminium cover tube that houses the temperature/relative humidity sensor can be seen under the inlet, with cables being passed along the sampling tube towards the inside of the airplane.

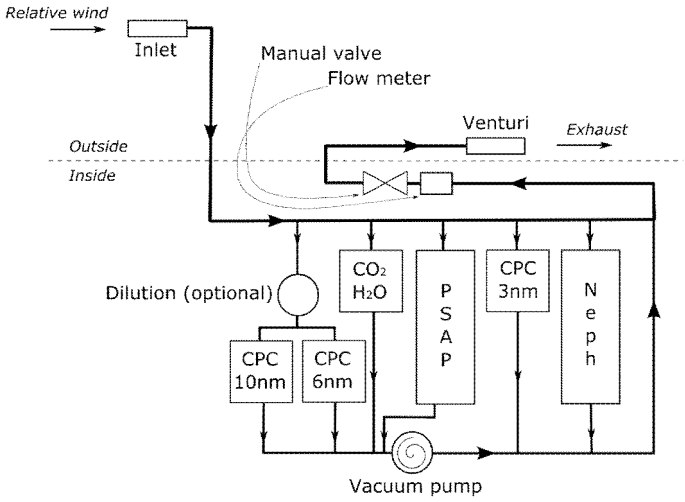

Figure 2. Schematic depiction of the flow system used on the measurement airplane, plus an overview of the instruments located inside the airplane. In this diagram the airplane would fly to the left, with the inlet mounted under the airplane's right wing. The dashed line represents the side wall of the cabin.

A GPS receiver was used onboard to track the airplane's latitude, longitude, and altitude at a time resolution of one second. Data from all instruments was collected by a computer that was built into the rack and could be accessed remotely from the front seats by laptop. This allowed for a continuous surveillance of the instruments during the flights. Also, the equipment includes a combined temperature/relative humidity sensor (Rotronic HygroClip-S) mounted on the airplane's right wing in an aluminium cover tube. It can be seen in figure 1 underneath the sample air inlet.
Electrical power (12 V DC) was provided by two rechargeable batteries, attached to the instrument rack.
Throughout 2009, all flights with the described setup were flown from and to Tampere-Pirkkala Airport (ICAO-Code EFTP) in southern Finland. First test flights were conducted in spring 2009 and confirmed that measurements work as planned. From May 7, 2009, to September 21, 2009, a total of 18 measurement flights have then been flown. The total area covered reaches from the west coast of Finland around Pori to the lake of Päijänne to the east. To the north the flights reached up to 62.5° of latitude, to the south down to 61° of latitude.
Several flights aimed at supplementing data collected on the ground – in particular at the SMEAR II station in Hyytiälä, situated in the boreal forest 60 km northeast of Tampere-Pirkkala Airport, where

(amongst other things) extensive measurements on ambient aerosol are taken continuously. These flights were flown in the form of series of climbs up to 4 km above mean sea level (AMSL) and subsequent descents to as low as possible and allowed (about 100 m above ground level minimum in remote areas) in the area around the ground station. This yielded both horizontal and vertical profiles of the measured parameters. During September 21 and 22, four such flights were conducted within 24 hours – also during night time – in order to observe diurnal and regional variations in the boundary layer and lower troposphere aerosol.
Flights were also conducted into and around the plumes emitted by industrial facilities (e.g. power plants) and from road works, and a series of flights investigated extensively the plumes of a controlled biomass burning experiment in Hyytiälä on June 26, 2009.

RESULTS & DISCUSSION

An exemplary particle number concentration profile during an afternoon flight on September 21, 2009 is presented in Fig. 3. On that day, a new particle formation event was observed at ground level at the SMEAR II station in Hyytiälä. The data collected during the flight suggests convincingly that the new particle formation is also occurring in the whole boundary layer, as well as several hundred meters above it, over an area 30 to 50 km west of Hyytiälä.

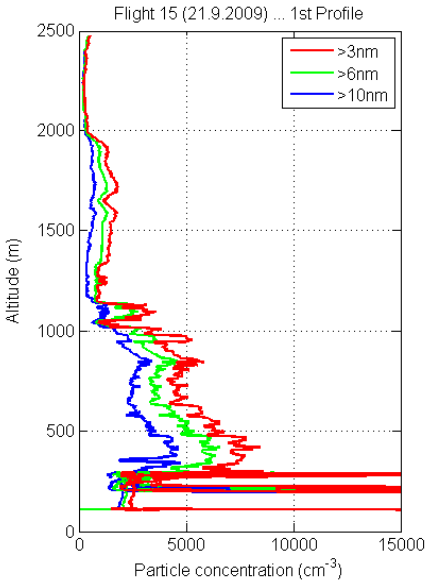

Figure 3. The figure shows a vertical profile of particle concentrations as measured by the three CPCs with three different cut-off sizes during the afternoon of September 21 during the first climb. Altitude is given as height above mean sea level (AMSL). Very high concentrations close to the ground level originate from airplane exhaust. Upon the initial climb-out, the city of Tampere was overflown at a height of 200 to 300 m. Then a continuous climb to north-northwest was initiated over lake Nenäjärvi, about 10 km north of Tampere city center. Note that significant amounts of particles between 3-10 nm in size were detected, suggestive of an ongoing new particle formation event. The concentrations are considerably higher in the mixed boundary layer than above in the free troposphere (> 1000 m).

During the 18 flights, a set of vertical profiles in the Southern Finland were conducted. The data suggest that new particle formation is occurring throughout the boundary layer, which agrees with conclusions drawn from the earlier airborne measurements (O'Dowd *et al.*, 2009) around Hyytiälä. It is also evident from the data that this kind of new particle formation is a regional rather than a local phenomenon, as has been reported earlier, e.g. by Hussein *et al.* (2009). Using the current results, we will be able to retrieve information on the temporal distribution of the events.

Our data also indicates regions of high nanoparticle concentrations in the vicinity of clouds as well as in the entrainment zone. Occassional high concentration regions occurred at various altitudes within a confined altitude range. Further data analysis is needed to elucidate the extent of this phenomenon.

Measurements in low altitude plumes from industrial facilities yielded maximal particle concentrations in the order of $> 10^5$ cm^{-3}, plumes from road works up to 10^4 cm^{-3}. The plumes from the controlled biomass burning experiments during the morning of June 26 revealed peak particle concentrations of $> 10^6$ cm^{-3}, accompanied by CO_2 concentrations up to 25% above background levels, and scattering and absorption coefficient values up to several thousand Mm^{-1}. The analysis of all data from plumes is still work in progress, and more detailed results will be available soon. Flights over the biomass burning site were also made at later times during the day of the burning, and the day after, to provide information on the evolution of the plumes. The analysis is still ongoing. Hence, all results presented here are of preliminary nature, as for instance diffusion losses (though by estimate small) are not yet taken into account, and minor problems with some of the instruments during certain flights need to be addressed.

CONCLUSIONS

The first 18 measurement flights showed that the measurement setup used onboard the Cessna airplane works well in general, but also exposed minor problems that have to be addressed. Several types of plumes could be successfully analyzed in terms of particle concentrations, optical aerosol properties, and CO_2 concentrations. Due to calibrating the three CPCs to different cut-off sizes, limited information was obtained also on particle size distributions. Additionally, a set of vertical profiles was recorded – mostly over boreal forest areas around the measurement station in Hyytiälä in southern Finland. This way, new particle formation could be observed at large ranges of latitude, longitude, and altitude.

The analysis of the collected data is still ongoing, and results at this time are preliminary. Improvements on the existing setup for possible future flights will be discussed. For instance, the possibility of implementing a differential mobility analyzing instrumentation to the existing setup, would allow for obtaining more detailed information on particle size distributions in the future. Another valuable addition could be the implementation of instruments analyzing atmospheric ions.

ACKNOWLEDGEMENTS

This work was supported by the European Commission 6th Framework program project EUCAARI, contract no 036833-2.

REFERENCES

Hari, P. and Kulmala, M. (2005). Station for measuring ecosystem-atmosphere relations (SMEAR II), *Boreal Env. Res.* 10, 5, 315-322.

Hussein, T. *et al.* (2009). Time span and spatial scale of regional new particle formation events over Finland and Southern Sweden, *Atmos. Chem. Phys.* 9, 4699–4716.

Kulmala, M. *et al.* (2008). Introduction: European Integrated project on Aerosol Cloud Climate and Air Quality interactions (EUCAARI) – integrating aerosol research from nano to global scales, *Atmos. Chem. Phys. Discuss.* 8, 19415-19455.

McNaughton, C.S. *et al.* (2007). Results from the DC-8 Inlet Characterization Experiment (DICE): Airborne Versus Surface Sampling of Mineral Dust and Sea Salt Aerosols, *Aerosol Science and Technology* 41, 136–159.

Mirme, S. *et al.* (2009). Atmospheric sub-3nm particles at high altitudes, *Atmos. Chem. Phys. Discuss.* 9, 19435–19470.

O'Dowd, C.D. *et al.* (2009). Airborne measurements of nucleation mode particles II: boreal forest nucleation events, *Atmos. Chem. Phys.* 9, 937–944.

Kinetic double-layer model of aerosol surface chemistry and gas-particle interactions (K2-SURF): Degradation of polycyclic aromatic hydrocarbons exposed to O_3, NO_2, H_2O, OH and NO_3

Manabu Shiraiwa, Rebecca M Garland and Ulrich Pöschl

Max Planck Institute for Chemistry, Department of Biogeochemistry
J.J. Becherweg 27/29, D55128, Mainz, Germany

Key words: Kinetic model, heterogeneous reaction, uptake, PAH

We present a kinetic double-layer surface model (K2-SURF) (Fig. 1) that describes the degradation of polycyclic aromatic hydrocarbons (PAHs) on aerosol particles exposed to ozone, nitrogen dioxide, water vapor, hydroxyl and nitrate radicals [Shiraiwa et al. 2009]. The model is based on multiple experimental studies of PAH degradation and on the PRA framework (Pöschl-Rudich-Ammann, 2007) for aerosol and cloud surface chemistry and gas-particle interactions.

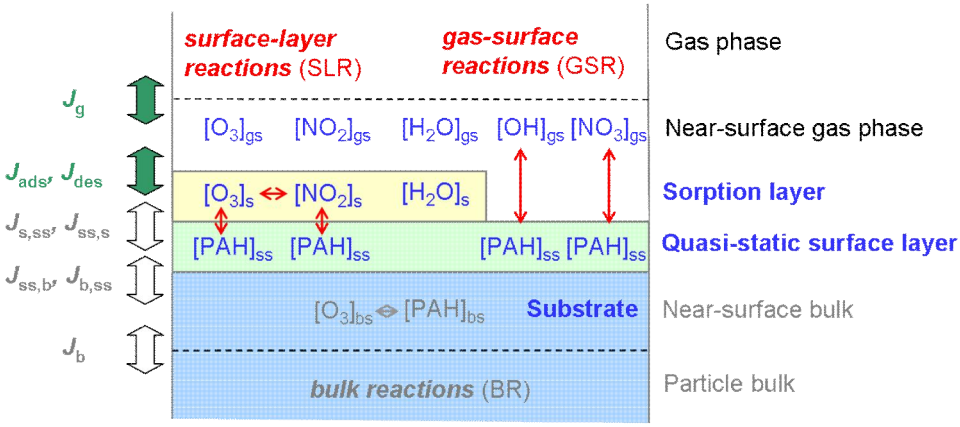

Figure 1. Schematic illustration of the kinetic double-layer surface model (K2-SURF). Compartments and transport fluxes for volatile species (O_3, H_2O, NO_2, OH and NO_3) and non-volatile species (PAHs).

For a wide range of substrates, including solid and liquid organic and inorganic substances (soot, silica, sodium chloride, octanol/decanol, organic acids, etc.), the concentration- and time-dependence of the heterogeneous reaction between PAHs and O_3 can be efficiently described

with a Langmuir-Hinshelwood-type mechanism. Depending on the substrate material, the effective Langmuir adsorption constants for O_3 vary over three orders of magnitude ($K_{ads,O3} \approx 10^{-15}$ - 10^{-13} cm^3), and the second-order rate coefficients for the surface layer reaction of O_3 with different PAH vary over two orders of magnitude ($k_{SLR,PAH,O3} \approx 10^{-18}$ - 10^{-17} cm^2 s^{-1}). The available data indicate that the Langmuir adsorption constants for NO_2 are similar to those of O_3, while those of H_2O are several orders of magnitude smaller ($K_{ads,H2O} \approx 10^{-18}$ - 10^{-17} cm^3). The desorption lifetimes and adsorption enthalpies inferred from the effective adsorption coefficients suggest chemisorption of NO_2 and O_3 - possibly in the form of O atoms - and physisorption of H_2O.

The K2-SURF model enables the calculation of ozone uptake coefficients, γ_{O3}, and of PAH concentrations in the quasi-static particle surface layer. Competitive adsorption and chemical transformation of the surface (aging) lead to a strong non-linear dependence of γ_{O3} on time and gas phase composition, with different characteristics under dilute atmospheric and concentrated laboratory conditions. Under typical ambient conditions, the ozone uptake coefficients of PAH-coated aerosol particles are expected to be in the range of 10^{-6} - 10^{-5}.

At ambient temperatures, NO_2 alone does not efficiently degrade PAHs, but it was found to accelerate the degradation of PAHs exposed to O_3. The accelerating effect can be attributed to highly reactive NO_3 radicals formed in the gas phase or on the surface (Fig. 2). Estimated second-order rate coefficients for O_3-NO_2 and PAH-NO_3 surface layer reactions are in the range of 10^{-17} – 10^{-16} cm^2 s^{-1} and 10^{-15} – 10^{-12} cm^2 s^{-1}, respectively.

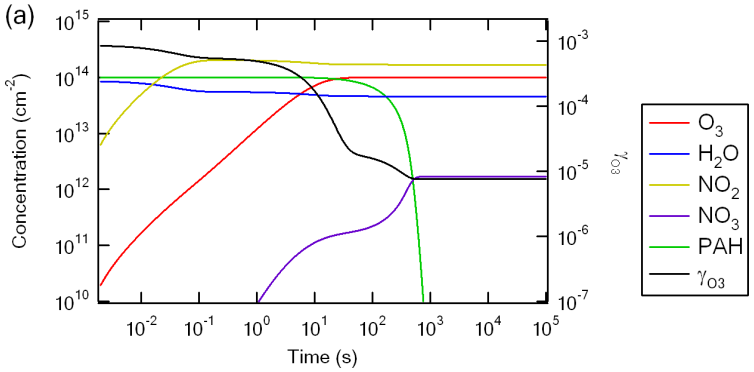

Figure 2. Temporal evolution of the surface concentrations of PAHs and volatile species on soot, and of the ozone uptake coefficient (γ_{O3}) at 100 ppb O_3, 500 ppb NO_2 and 25% RH. Surface reaction of O_3 with NO_2 leads to formation of NO_3 radical on the surface.

The chemical half-life of PAH is expected to range from a few minutes on the surface of soot to multiple hours on organic and inorganic solid particles and days on liquid particles, as shown in Fig.3. On soot, the degradation of particle-bound PAHs in the atmosphere appears to be dominated by a surface layer reaction with adsorbed ozone. On other substrates, it is likely dominated by gas-surface reactions with OH or NO_3 radicals (Eley-Rideal-type mechanism).

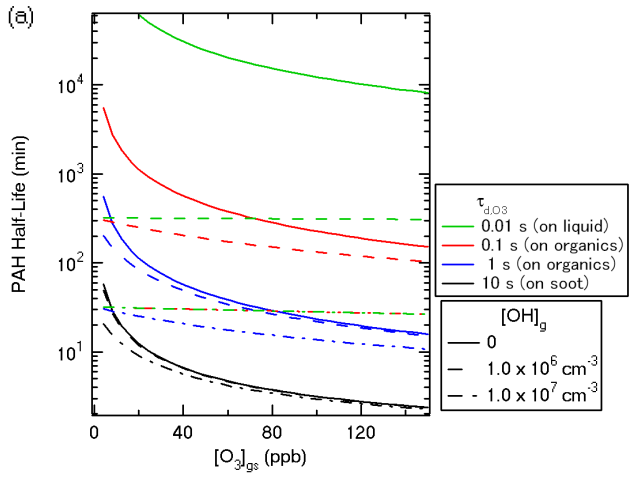

Figure 3. Chemical half-life of PAHs on different substrates (soot, solid organic, liquid) as a function of gas phase ozone concentration at 25% RH assuming OH concentrations of 0 (solid lines), 1.0×10^6 cm^{-3} (dashed lines), and 1.0×10^7 cm^{-3} (dotted lines). The desorption lifetime of O_3 ($\tau_{d,O3}$) was set to 10 s (soot), 1 or 0.1 s (solid organic), and 0.01 s (liquid), respectively.

To our knowledge, K2-SURF is the first atmospheric process model describing multiple types of parallel and sequential surface reactions between multiple gaseous and particle-bound chemical species. It illustrates how the general equations of the PRA framework can be simplified and adapted for specific reaction systems, and we suggest that it may serve as a basis for the development of a general master mechanism of aerosol and cloud surface chemistry.

References.

Pöschl, U., Y. Rudich and M. Ammann (2007). "Kinetic model framework for aerosol and cloud surface chemistry and gas-particle interactions - Part 1: General equations, parameters, and terminology." Atmospheric Chemistry and Physics 7(23): 5989-6023.

Shiraiwa, M., R. M. Garland and U. Pöschl (2009). "Kinetic double-layer model of aerosol surface chemistry and gas-particle interactions (K2-SURF): degradation of polycyclic aromatic hydrocarbons exposed to O_3, NO_2, H_2O, OH and NO_3." Atmos. Chem. Phys. Discuss. **9**(5): 18021-18063.

Explicit entrainment parameterisation in the global climate model ECHAM5-HAM

C. Siegenthaler – Le Drian, P. Spichtinger and U. Lohmann

Institute for atmospheric and climate science, ETH-Zurich, Switzerland.

Keywords: GCM, cloud top entrainment.

Introduction

The complex interactions affecting cloud lifetime and LWP are not really captured in different global climate models (GCM). A recent climate model intercomparison showed an overestimation of the positive correlation of LWP with AOD by a factor of two compared to MODIS data for almost all models participating (Quaas *et al.*, 2009). As the author suggest, a proper interaction of the boundary layer dynamics, particularly the inclusion of cloud top entrainment may be an improvement.

ECHAM5 uses a turbulent kinetic energy (TKE)-scheme, which simulates the cloud top fluxes in function of the local turbulence. It reproduces relatively well the clear convective and stratocumulus-topped boundary layers in a quite high resolution model (Duynkerke and Driedonks, 1987). Nevertheless, a study of the turbulent scheme of ECHAM4, showed that its performance diminishes when the resolution decreases, the different fluxes and TKE being not represented satisfactory in the resolution L31 (31 vertical levels) (Lenderink *et al.*, 2000). We thus replace the TKE diffusion by an explicit entrainment closure at the top of the boundary layer clouds.

We use the new version of the Hamburg general circulation model ECHAM5 (Roeckner *et al.*, 2003) coupled to the double moment modal aerosol microphysics scheme HAM (Stier *et al.*, 2005). The cloud scheme in ECHAM5 that is used for this study includes the double-moment cloud microphysics scheme for cloud droplets and ice crystals (Lohmann *et al.*, 2007).

The new version of the boundary layer in ECHAM5 which includes a parametrisation of cloud-top entrainment in the stratocumulus regions is called ENTR. The version with diffusion on moist conserved variables (MCO) is considered as a reference version. The standard version (with turbulent diffusion on non-conserved variables) is called STD.

Results

Diurnal cycle in SCM study

The simulation is based on observations taken during the second flight of ASTEX Lagrangian Experiment campaign.

The results of the different SCM simulations are quite different. The highest values of TKE in ENTR are more in the range of measurements (between 0.1 and 0.5 ms^{-1} (de Roode and Duynkerke, 1997)) than the huge values in STD and CMO. Moreover the highest values of TKE in STD are in a narrow time interval before midnight, thought the values are more constant during the night for ENTR. Furthermore the strong increase of TKE during night takes place at the base of the cloud in STD, but it should be at the top of the cloud due to radiative cooling in typical stratocumulus. This feature is reproduced nicely in ENTR. Finally the diurnal cycle simulated in cloud cover or

equivalantely in cloud water is much more representative of observed subtropical stratocumulus in ENTR than in STD. On the other hand, the TKE is not well distributed vertically, probably due to a defficiency in turbulent transport of TKE.

GPCI

The same constraints were used as described during the GCSS/WGNE Pacific Cross-section Intercomparison (Teixeira *et al.*, 2009) but for the summer 2000 to conduct simulations along a Pacific Ocean cross-section, from the stratocumulus region off the coast of California to the deep convection region.

In general, all the versions produce quite realistic cross-sections, we simulate an upgoing inversion marquing the transition. The most interesting information is that the entrainment parametrisation leads to an enhanced Hadley circulation because of enhanced triggering of convection, which follows from an enhanced latent heat flux due to a dryer surface layer in shallow cumulus regions. ENTR shows a transition from shallow cumulus to stratocumulus more comparable to the observations in terms of cloud cover, but less clouds in stratocumulus regions, which is worse agreement to observations.

ACKNOWLEDGEMENTS

This work was supported by the EU project EUCAARI.

References

de Roode, S. R. and Duynkerke, P. G. (1997). Observed Lagrangian transition of stratocumulus into cumulus during ASTEX: Mean state and turbulence structure. *J. Atm. Sci.*, 54(17):2157–2173.

Duynkerke, P. G. and Driedonks, A. G. M. (1987). A model for the turbulent structure of the stratocumulus topped atmospheric boundary layer. *J. Atmos. Sci*, 44:43–64.

Lenderink, G., Van Meijgaard, E., and Holtslag, A. M. (2000). Evaluation of the ECHAM4 cloud-turbulence scheme for stratocumulus. *Meteorologische Zeitschrift*, 9(1):0041–47.

Lohmann, U., Stier, P., Hoose, C. *et al.* (2007). Cloud microphysics and aerosol indirect effects in the global climate model ECHAM5-HAM. *Atmos. Chem. Phys.*, 7:3425–3446.

Quaas, J., Ming, Y., Menon, S. *et al.* (2009). Aerosol indirect effects – general circulation model intercomparison and evaluation with satellite data. *Atm. Chem. Phys. Discuss.*, 9:12731–12779.

Roeckner, E., Bäuml, G., Bonaventura, L. *et al.* (2003). The atmospheric general circulation modell echam5, part I: Model description. Technical Report 349, Max-Planck-Institute for Meteorology, Hamburg,Germany.

Stier, P., Feichter, J., Kinne, S. *et al.* (2005). The aerosol-climate model ECHAM5-HAM. *Atmos. Chem. Phys.*, 5:1125–1156.

Teixeira, J., Cardoso, S., Bonazzola, M. *et al.* (2009). Tropical and sub-tropical cloud transitions in weather and climate prediction models: the GCSS/WGNE pacific cross-section intercomparison (GPCI). Submitted to J. Climate.

INTERPRETATION OF THE NUCLEATION EXPERIMENTS DEPEND ON THE PERFORMANCE OF THE PARTICLE DETECTOR

M. SIPILÄ[1], T. NIEMINEN[1], T. PETÄJÄ[1] and M. KULMALA[1]

[1]Department of Physics, PO. Box 64, 00014 University of Helsinki, Finland.

Keywords: NUCLEATION, SULPHURIC ACID, CONDENSATION PARTICLE COUNTER

INTRODUCTION

Atmospheric new particle formation represents a global phenomenon observed in numerous locations (Kulmala et al., 2004) and sulphuric acid has shown to be strongly connected in this process (Sihto et al., 2007). However, laboratory experiments on sulphuric acid nucleation have systematically failed to reproduce ambient observations (e.g. Viisanen et al. 1997, Berndt et al. 2005, Young et al., 2008) yielding too low nucleation rates (J) and wrong dependence of nucleation rate on sulphuric acid concentration – i.e. "slope": $d(\ln J)/d(\ln[H_2SO_4])$. Growth rate of the freshly nucleated particle due to sulphuric acid condensation is extremely small in close ambient concentrations of sulphuric acid ([H2SO4] < 10^8 molec. cm^{-3}, Lehtinen and Kulmala, 2003). Therefore relatively long time is needed to grow the particles to sizes where they can be counted. In most flow tube experiments the residence time has been reasonably short – of the order of seconds or minutes and CPCs used to detect particles have had their lowest detection limits lying between 3 and 20 nm depending on the experiment.

The aim of this study is to explore the effects of non-ideal particle counting to flow tube nucleation experiments. We apply nucleation and growth modelling and take into account the size dependent counting efficiency curves of the detector to simulate the reality behind the apparent behaviour of J as a function of sulphuric acid concentration.

METHODS

To test the concept, the nucleation was described as a linear function of sulphuric acid ("slope"=1):

$$J_{1nm} = 10^{-6}[H_2SO_4]^1 \; cm^{-3}s^{-1} \; .$$

Particle growth was modelled using a simplified description for the sulphuric acid concentration dependent growth rate:

$$GR = 4 \cdot 10^{-11}[H_2SO_4] \; nm \; s^{-1}cm^3 \; .$$

Three different particle detectors were simulated. The ideal CPC was able to count all the particles whereas the two others had simulated detection efficiency (E) curves using a function of form:

$$E = 1 - \exp\left(a - \frac{D_p}{b}\right).$$

The cut-off sizes (i.e. the size, when half of the particles are accounted for) were 3 and 10 nm simulating TSI models 3025 and 3010 which are commonly used CPC types in the nucleation experiments. Wall losses of sulphuric acid or particles are not accounted for in this preliminary model.

CONCLUSIONS

Example of the simulation is shown in Figure 1. Nucleation followed by a growth time of 100s was assumed. The ideal CPC detection efficiency was unity for all particle sizes and it reproduces the assumptions well. Two other CPCs have 50%-cut-off sizes of 3 and 10 nm. Onset (J=1) sulphuric acid concentration was affected by 2-3 orders of magnitude and slope shifted from 1 to even 15 with 10 nm CPC. This behaviour has not accounted for in many H2SO4 – H2O nucleation studies. The conclusion by e.g. Young et al. (2008) that the detected nucleation rate at 2.5 nm equals to real nucleation rate is only true when all particles have grown above 2.5nm. This is typically not the case in the experiments performed in sulphuric acid concentrations below 10^9 molec cm^{-3}.

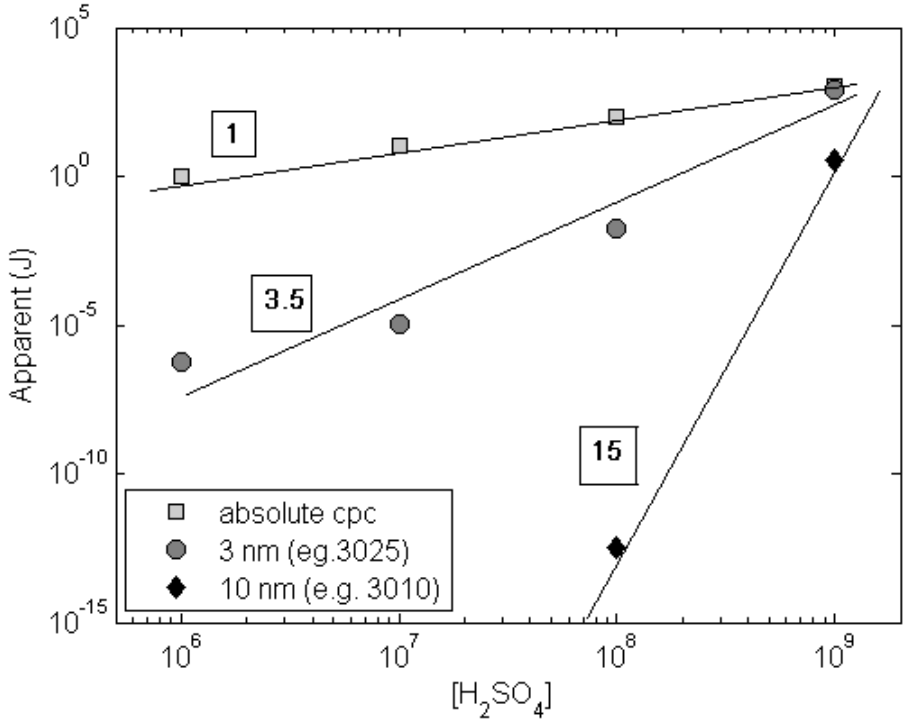

Figure 1. A choice of detector can potentially have a huge effect on the experimental results if the size dependent detection efficiency is not accounted for.

REFERENCES

Berndt, T., Böge, O., Stratmann, F., Heintzenberg, J., Kulmala, M. Rapid Formation of Sulfuric Acid Particles at Near-Atmospheric Conditions, *Science*, **207**, 698-700 (2005).

Kulmala, M., et al. Formation and growth rates of ultrafine atmospheric particles: a review of observations, *J. Aerosol Sci.*, **35**, 143-176 (2004).

Lehtinen K.E.J., Kulmala, M. A model for particle formation and growth in the atmosphere with molecular resolution in size, *Atmos. Chem. Phys.*, **3**, 251-257 (2003).

Sihto, S.-L., et al. Atmospheric sulphuric acid and aerosol formation: Implications from atmospheric measurements for nucleation and early growth mechanisms, *Atmos. Chem. Phys.*, **6**, 4079-4091 (2006).

Viisanen, Y., Kulmala, M., Laaksonen, A. Experiments on gas-liquid nucleation of sulphuric acid and water, *J. Chem. Phys.*, **107**, 920-926 (1997).

Young, L.-H., et al. Laboratory studies of H2SO4/H2O binary homogeneous nucleation from the SO2+OH reaction: evaluation of the experimental setup and preliminary results, *Atmos. Chem. Phys.*, **8**, 4997-5016 (2008).

EXPLAINING GLOBAL SURFACE AEROSOL CONCENTRATIONS IN TERMS OF PRIMARY EMISSIONS AND PARTICLE FORMATION

D.V. SPRACKLEN[1], K.S. CARSLAW[1] and J. MERIKANTO[1]

[1]Institute for Climate and Atmospheric Science, University of Leeds, Leeds, LS2 9JT, UK.

Keywords: New particle formation, nucleation, particle number concentration.

We use observations of total particle number concentration (CN) at 36 worldwide ocean and continental sites (see Figure 1) and a global aerosol model (GLOMAP) to quantify the primary and secondary sources of particle number. Emissions of primary particles can reasonably reproduce the spatial pattern of observed CN (R^2=0.51; see Figure 2) but not the observed seasonal cycle (R^2=0.1). The modelled CN concentration in the free troposphere is biased low (normalised mean bias, NMB=-88%) unless a secondary source of particles is included, for example from binary homogeneous nucleation of sulfuric acid and water (NMB=-25%). Simulated CN concentrations in the continental boundary layer (BL) are also biased low (NMB=-74%) unless anthropogenic primary particles are emitted at small sizes or an empirical BL particle formation mechanism based on sulfuric acid is included. We find that the seasonal CN cycle observed at continental BL sites is better simulated by including a BL particle formation mechanism (R^2=0.3) than by increasing the number emission from primary anthropogenic sources (R^2=0.18). Using sensitivity tests we derive optimum nucleation rate coefficients for this mechanism, which agree with values derived from detailed case studies at individual sites.

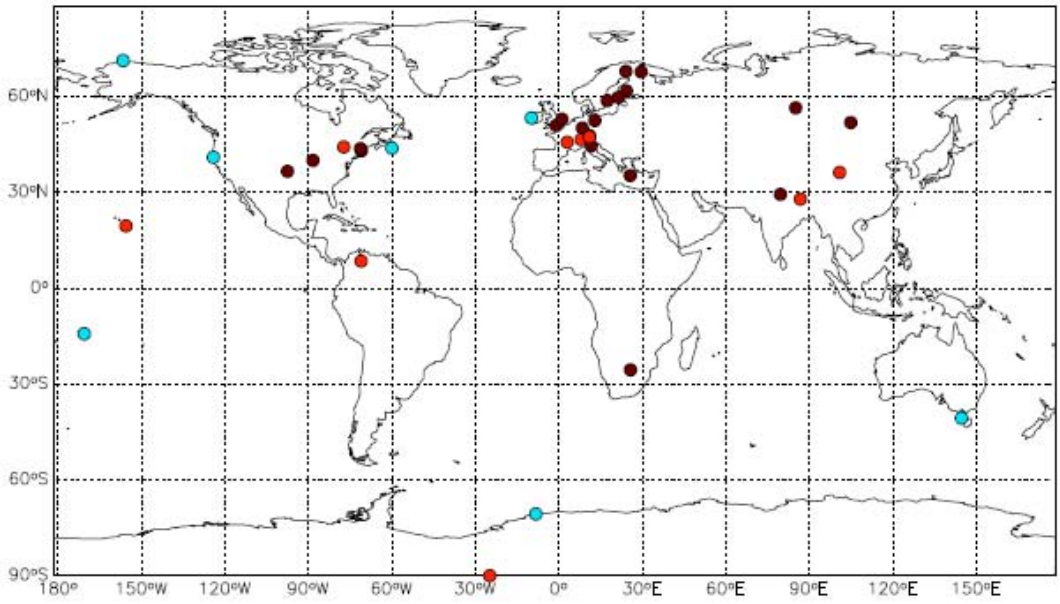

Fig. 1. Location of observation sites used in this analysis: FT (red), MBL (blue), continental BL (brown).

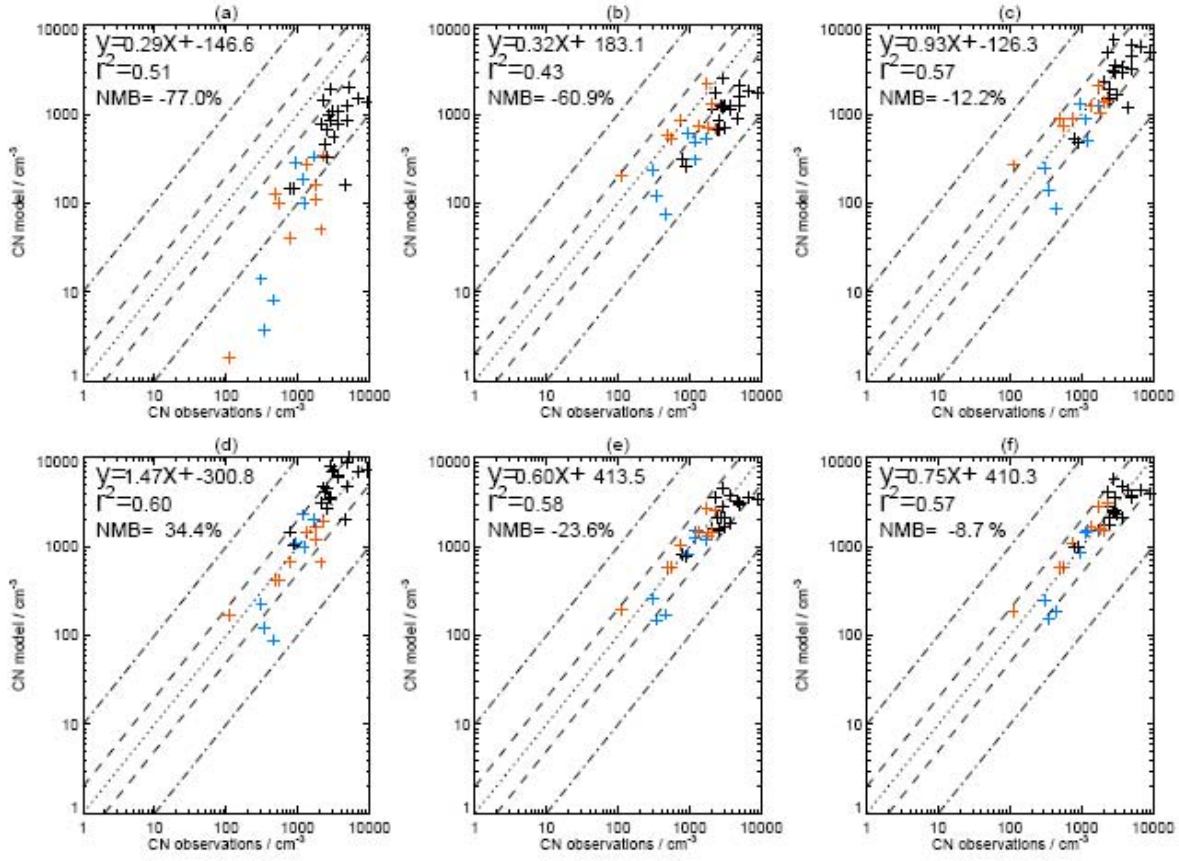

Fig. 2. Scatterplot of simulated (GLOMAP) versus observed annual mean CN concentrations for the sites shown in Figure 1. Sites are classified as FT (red), MBL (blue) and continental BL (black). The different model simulations are (a) Primary emissions only, (b) Primary emissions and binary homogeneous nucleation, (c) BHN and primary EC/OC number emission increased by a factor of 8, (d) BHN and increased primary sulfate number emission, (e) Primary emissions, BHN and activation particle formation restricted to the BL (formation rate of 1-nm particles, $J1=k[H_2SO_4]$), (e) Primary emissions, BHN and kinetic particle formation restricted to the BL ($J1=k[H_2SO_4]^2$). The regression equation for the reduced major axis linear regression, Pearson correlation coefficients (R^2) and normalised mean bias (NMB) are shown. The dotted line represents the 1:1 relation and the dashed lines factor of 2 and 10 deviations.

ACKNOWLEDGEMENTS

This work was supported through EUCARRI, NERC APPRAISE and NERC AEROFORM NE/D01395X/1. We acknowledge the UK Air Quality Archive (http://www.airquality.co.uk/), EU CREATE (http://tarantula.nilu.no/projects/ccc/create/), Global Atmospheric Watch World Data Centre for Aerosols (http://tarantula.nilu.no/projects/ccc/create/), Atmospheric Investigation, Regional, Modeling, Analysis and Prediction (AIRMAP) program (www.airmap.unh.edu), British Atmospheric Data Centre (http://badc.nerc.ac.uk/home/), U.S. Department of Energy, Atmospheric Radiation Measurements program (ARM) and European Supersites for Atmospheric Research (EBAS) (http://ebas.nilu.no) for provision of data.

Developing reduced complexity parameterisations to calculate gas/particle partitioning in large scale models

D.O.Topping[1,2], G.B.McFiggans[1], M. Barley[1], D. Lowe[1]

[1]School of Earth, Atmospheric and Environmental Science, University of Manchester, Manchester, M13 9PL, UK

[2]National Centre for Atmospheric Science, UK..

Keywords: Thermodynamics, Gas/Particle partitioning, Organic aerosol.

1.INTRODUCTION

Gas to particle mass transfer of semi-volatile components, driven by a difference in equilibrium and actual partial pressures above an aerosol particle, is an important factor in determining the evolving chemical composition of the particle and is necessary for predicting aerosol loading and composition. The equilibrium pressure is dictated by composition dependent properties such as dissociation constants, pure component vapour pressures and activity coefficients in solution. Unfortunately, not only are properties such as pure component vapour pressures uncertain (see Booth et al poster: ASSESSING VAPOUR PRESSURE ESTIMATION METHODS AND THEIR IMPACT USING KNUDSEN EFFUSION MASS SPECTROMETRY (KEMS)), but activity coefficients are very detailed numerical models of complex behaviour. This prohibitive computational expense must be avoided via a reduction in numerical complexity. Also, whilst explicit hydrocarbon oxidation mechanisms that track many thousands of degradation products of volatile organic compounds (VOC) have been developed, aerosol schemes in large-scale models neglect the majority of chemical components predicted to occur in the organic mixture and will continue to do so in the future. Reduction mechanisms that neglect compositional information are widely used to derive those parameters deemed important for climatic and health impacts. However, it is possible to make detailed predictions of the range of organic components expected to condense to atmospheric aerosol by combining a gas/particle partitioning model with a detailed gas phase chemical mechanism. Provided they are of sufficient skill, these predictions can be used as the basis for process and composition complexity reduction whilst retaining mechanistic understanding. In this report we present a compound selection methodology and then illustrate the potential to extend the hybrid Partial Derivative Fitted Taylor Expansion (PD-FiTE) of Topping et al (2009) in which parameterisations for calculating the equilibrium vapour pressure of the semi-volatile inorganic gases, HNO_3, HCl and NH_3, above an aqueous aerosol have already been published.

2. OVERVIEW

2.2 A methodology for the selection of compounds used to represent secondary organic aerosol

Any of the thousands of organic species present in the atmosphere can potentially condense and contribute to the mass of the aerosol. To gain further insights into the range of organic components expected to condense to atmospheric aerosol in this study we present a compound selection methodology which combines a partitioning model (Barley et al 2009) and vapour pressure estimation technique with a detailed gas phase chemical mechanism. As an example, we combine this methodology with the Master Chemical Mechanism (or MCM) to predict the formation of organic aerosol (OA) from the chemical composition of parcels of air arriving at Writtle, Essex, during two days in August 2003 (Johnson et al 2006a,b, Utembe et al 2005). In this work we have used the same output of the MCM for the air parcel arriving at 18:00 on August 6th as that used by Johnson et al. (2006a, 2006b) to simulate the formation of secondary organic aerosol (SOA). However, we have significantly reworked the calculation of the vapour pressures for all the MCM components; explicitly included the condensation of water in the calculations and assumed that any acid-anhydrides present will undergo hydrolysis to the corresponding

acids. We have investigated the condensation of OA over 75 different combinations of temperature (3 levels), %RH(3 levels) and total organic aerosol (5 levels) to get a more complete picture of how the OA composition varies under different conditions. Using a modified MCM scenario with very low anthropogenic inputs we have done a similar exercise to find the predominant biogenic components in SOA. From this analysis the top 10 biogenic and the top 3 anthropogenic SOA components were identified for use in further modelling studies.

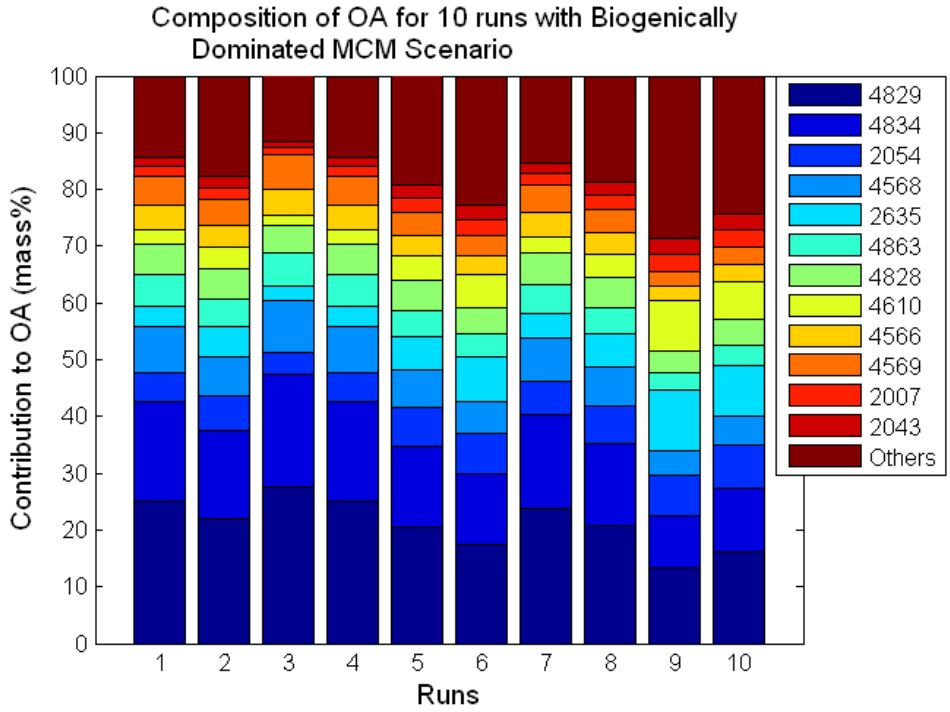

Figure 1. Example predicted composition of organic aerosol across 10 runs, with compounds identified by MCM code (4829=pinic acid) in terms of mass%.

2.1 A novel reduced complexity thermodynamic framework

The hybrid Partial Derivative Fitted Taylor Expansion (PD-FiTE) (Topping et al 2009) is a reduced complexity thermodynamic model for calculating activity coefficients in solution. This approach uses optimised model parameters describing the interaction between different inorganic ions resulting in comparable computational performance with existing reduced methods, whilst remaining accurate. Comparisons with the most accurate inorganic activity coefficient model (E-AIM) available indicate that PD-FiTE performs well over the parameterisation space of the system H^+-NH_4^+-Na^+-SO_4^{2-}-HSO_4^--NO_3^--Cl^- at 298.15K. The linear additive framework allows the inclusion of further species, including the ability to describe the interaction between inorganic/organic components if appropriate data exists. Coupling PD-FiTE to a coupled box model of gaseous chemistry and aerosol microphysics in a test case investigating marine aerosol passing through a polluted environment demonstrates its robustness and ability to capture fine details of important phenomena such as the outgassing of HCl in response to HNO_3 uptake by sea-salt particles. Including organics within PD-FiTE is possible using a modular approach whereby interactions between inorganic and organic compounds are currently ignored. Whilst attempts have been made to formulate detailed coupled thermodynamic models for atmospheric purposes, an interim assessment concluded that a neglective approach which renders the inorganic and organic components uncoupled is preferable (Tong et al 2008). There remain significant difficulties with coupled schemes, most notably including a lack of experimental data from which important interaction parameters can be derived. Because of this, various thermodynamic models use a flexible approach. The approach presented here can incorporate individual treatment of each fraction individually, but can also

exploit data from mixed inorganic / organic systems. This is due to the method of finding 'optimum' interaction parameters akin to semi-empirical models. Both reduced complexity modules within PD-FiTE have been derived using models employed within 'full complexity' thermodynamic frameworks. Two interim conclusions regarding the comparison between organic PD-FiTE and E-AIM for the calculations of vapour pressures can be taken as follows: 1) As the relative humidity approaches 99% both models begin to converge, which is to be expected as the aqueous solution become more 'ideal' and interactions between solutes decreases. 2) As the concentration of solute '1' becomes relatively small in the same system, then the activity coefficient of solute '1' predicted with PD-FiTE begins to deviate increasingly from E-AIM.

ACKNOWLEDGEMENTS

This work was supported by the National Centre for Atmospheric Science (UK).

REFERENCES

Barley, M.H., Topping, D. O., Jenkin, M.E. and McFiggans, G. (2009), Sensitivities of the absorptive partitioning model of secondary organic aerosol formation to the inclusion of water, Atmospheric Chemistry and Physics, 9:2919-2932.

Johnson, D., et al. (2006a), Simulating the detailed chemical composition of secondary organic aerosol formed on a regional scale during the TORCH 2003 campaign in the southern UK, *Atmospheric Chemistry and Physics*, *6*, 419-431.

Johnson, D., et al. (2006b), Simulating regional scale secondary organic aerosol formation during the TORCH 2003 campaign in the southern UK, *Atmospheric Chemistry and Physics*, *6*, 403-418.

Tong, C. H., S. L. Clegg, and J. H. Seinfeld (2008), Comparison of activity coefficient models for atmospheric aerosols containing mixtures of electrolytes, organics, and water, *Atmospheric Environment*, *42*, 5459-5482.

Topping, D., D. Lowe, and G. McFiggans (2009), Partial Derivative Fitted Taylor Expansion: An efficient method for calculating gas-liquid equilibria in atmospheric aerosol particles: 1. Inorganic compounds, *Journal of Geophysical Research-Atmospheres*, *114*,

Utembe, S. R., et al. (2005), Modelling the ambient distribution of organic compounds during the August 2003 ozone episode in the southern UK, *Faraday Discussions*, *130*, 311-326.

PARTICLE SIZE MAGNIFIER FOR DETECTION OF SUB - 2 NM AEROSOL PARTICLES

J. VANHANEN[1], J. MIKKILÄ[1], M. SIPILÄ[1,2] and M. KULMALA[1]

[1]Department of Physics, University of Helsinki, PO Box 64 FI-00014, Helsinki, Finland

[2]Helsinki Institute of Physics, PO Box 64 FI-00014, Helsinki, Finland

Keywords: CPC, PSM, MOBILITY STANDARD.

INTRODUCTION

Condensation particle counters are widely used to detect airborne nanoparticles (McMurry, 2000). The main principle is to introduce aerosol particles to a highly saturated vapour, in order to condensate the working fluid on the aerosol particles. Particles are grown to optical sizes and counted with optical particle counter. High saturation ratio can be attained for example by cooling of saturated air containing the aerosol particles, by rapid expansion of the sample - vapour mixture or by turbulent mixing.

The main principle of a particle size magnifier (PSM) is to mix turbulently cooled air stream containing the sample aerosol particles with heated clean air stream saturated with the working fluid. This way a high saturation ratio can be achieved. Particles having critical saturation ratio smaller than the attained saturation ratio will activate and grow by condensation.

In order to measure the smallest aerosol particles of just 1 nm in diameter a high saturation ratio is needed. Iida *et al.* 2009 concluded that by using working fluid having low vapour pressure and high surface tension, a high saturation ratio is achieved without homogeneous nucleation. From their modelling study they concluded that diethylene glycol and oleic acid are the best non-toxic working fluids for CPCs. Diethylene glycol was used as a working fluid in this study. Because diethylene glycol has such a low vapour pressure, the particles cannot be easily grown to optical sizes. This is why an external CPC (TSI-3010) has to be used to grow particles further and to count them.

CALIBRATION RESULTS

The PSM was calibrated by using mobility standards (Ude and Fernández de la Mora, 2005) and silver nanoparticles. Mobility standards are relatively large positively charged molecules (tetra-alkyl ammonium halide salts) that can be used as condensation nuclei with known mobility (and mobility equivalent diameter d). Detection efficiency of the PSM is presented in figure 1 for mobility standards (MS) (Tetraheptyl ammoinium bromide (monomer d = 1.47nm and dimer d = 1.78nm) and tetramethyl ammonium iodine (monomer d = 1.05nm)) and for both negatively and positively charged silver nanoparticles. Also detection efficiencies for commercial CPCs for negatively charged silver particles are shown in the figure. Cut-off size of the PSM is below 2 nm and the cut-off sizes of the TSI-3776 and TSI-3786 are 3.2 and 3.4nm, respectively. Below 2 nm detection efficiencies of commercial CPCs are less than 5%. The solid line in the figure 1 represents the theoretically calculated losses inside the inlet and the mixing section of the PSM due to turbulence and diffusion (Gormley, P. G., and Kennedy, M., 1949).

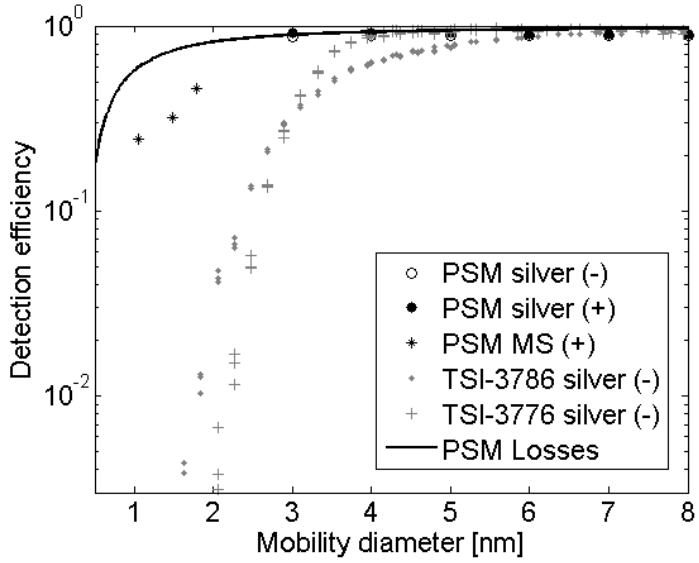

Figure 1. Detection efficiency of the PSM and commercial CPCs as a function of mobility equivalent diameter.

PSM can also be used as a size spectrometer by scanning the flow ratio between the flow through the saturator and the total flow after the mixing. Figure 2 shows the activated fraction (detection efficiency scaled to unity) as a function of the mixing ratio for different mobility standards. Mobility standards activate at different mixing ratios, depending on the size of the molecule down to 1.5nm. For TMAI monomer the onset mixing ratio is slightly lower than for the THAB, although TMAI monomer has higher mobility. This can be due to some chemical parameter for example wettability or solubility of the particle by the working fluid. Other suggestion is that for the smallest aerosol particles the onset of heterogeneous nucleation is dominated by the charge of the particle over the size of the particle.

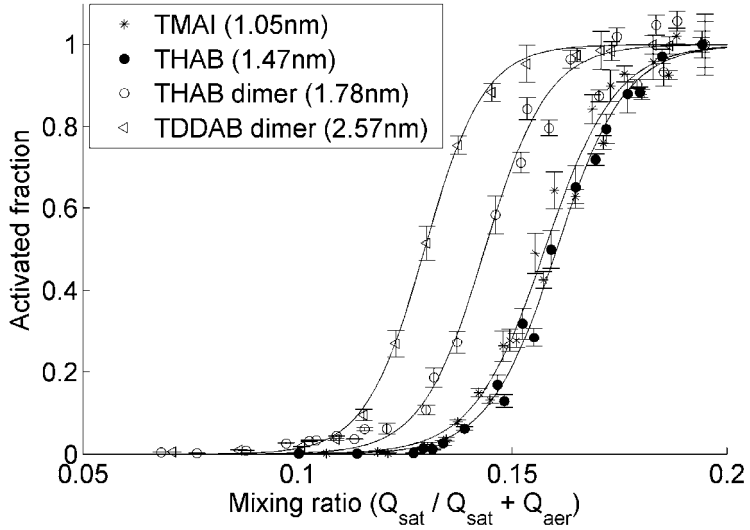

Figure 2. Activated fraction as a function of the mixing-ratio for mobility standards. The mobility equivalent diameter inside the parentheses.

CONCLUSIONS

A new portable particle size magnifier was developed and constructed for detection of aerosol particles down to ~1 nm in mobility equivalent diameter. Laboratory calibrations showed that for charged mobility standards of different tetra-alkyl ammonium halides with mobility diameters of 1.05, 1.47 and 1.78 nm the instrument's detection efficiencies were 25, 32 and 46%, respectively. Calibration results also indicate that the PSM can be used as a size spectrometer for nanometer sized aerosol particles down to ~1.5 nm.

REFERENCES

McMurry, P. H. (2000). The history of condensation nucleus counters. *Aerosol Sci. Technol.* 33, 297-322.

Iida, K. et al. (2009). Effect of working fluid on sub-2 nm particle detection with a laminar flow ultrafine condensation particle counter. *Aerosol Sci. Technol.*, 43, 82-96.

Ude, S., and Fernández de la Mora (2005). Molecular monodisperse mobility and mass standards from electrosprays of tetra-alkyl ammonium halides. *J. Aerosol Sci.*, 36, 1224-1237.

Gormley, P. G., and Kennedy, M.: Diffusion from a Stream Flowing through a Cylindrical Tube, *Proc. Royal Irish Acad.* 52(A):163–169, 1949.

THE PRESCRIBED BURNING EXPERIMENT IN HYYTIÄLÄ IN JUNE 2009

A. VIRKKULA[1], J. LEVULA[2], T.POHJA, G. DE LEEUW[1,3], , D. M. SCHULTZ[1,3], C. B. CLEMENTS[4], J. KUKKONEN[2], L.PIRJOLA[5], AND M. KULMALA[1]

[1]University of Helsinki, Department of Physics, Helsinki, Finland
[2]Hyytiälä Forestry Field Station, Hyytiälä, Finland
[3]Finnish Meteorological Institute, Helsinki, Finland
[4]Department of Meteorology, San José State University, San José, CA, USA
[5]Metropolia University of Applied Sciences, Department of Technology, Helsinki, Finland

Keywords: Biomass burning, Forest fire, Dispersion, Hyytiälä.

BACKGROUND

Wildland fires have many serious negative impacts on health, safety, regional economies and global climate. On the other hand, controlled burning has been used for centuries in Finnish forests, earlier to produce crops and later, since the 1920's to promote the regeneration of forests. To combine the research of the atmospheric and forest economical effects of fire a prescribed burning experiment was conducted near the SMEAR II station in Hyytiälä as part of the EUCAARI project in June 2009. The experiment was also an important part of another project, the Integrated Monitoring and Modelling System for Wildland Fires (IS4FIRES).

OBJECTIVES

The overall general goal was to provide data for estimating the effect of natural forest fires in air quality and climate. Even though the fire was not large in global scale, it was well-characterized: the amount of biomass burned was estimated and therefore the results may be scaled to larger areas. More detailed goals were to measure the aerosol chemical composition and physical characteristics such as size, hygroscopic properties, light absorption and scattering coefficient; the concentration of gaseous compounds such as carbon dioxide emitted; the chemical and physical processes, such as nucleation and growth of aerosols and gas-phase chemical processes. The objective of the IS4FIRES is to develop an Integrated Monitoring and Modelling System (IS) for wildland fires. This includes detection of fires using satellite remote sensing, modelling both the fire spread and the atmospheric dispersion of the fire plume, and to determine the source areas using a combination of ground-based air quality measurements and a long-range transport modelling system. For the forest science the experiment provides data on recovery of forest after burning. This study requires long-term measurements of soil properties and vegetation before and after the burning.

ACTION

The experiment was conducted in the morning of 26.6.2009. The burned area was approximately 0.8 ha and the amount of burned organic material about 45 tons. In addition to SMEAR II's measurements there were meteorological and ecological measurements on and around the site. One of the goals was to measure the smoke dispersion both horizontally and vertically. Ground-level dispersion was measured both by using the research van, "Sniffer", and by walking in the forest with portable particle counters at different distances from the burning area. Vertical and horizontal dispersion were measured with instruments installed in a Cessna 172.

Airborne in-situ measurements with a C-ToF aerosol mass spectrometer during EUCAARI/IMPACT (May 2008)

R. Weigel[1,2], S. Crumeyrolle[1], W. Morgan[3], J. Allan[3], L. Gomes[4], J.-M. Pichon[1], David Picard[1], H. Coe[3], A. Schwarzenböck[1], K. Sellegri[1], P. Laj[5]

[1]Laboratoire de Météorologie-Physique, University of Clermont-Ferrand, France
[2]now Institute for Physics of the Atmosphere, University of Mainz, Germany
[3]Centre for Atmospheric Science, University of Manchester, United Kingdom
[4]CNRS Metéo-France/CNRM/GMEI/MNPCA, Toulouse, France
[5]Laboratoire de Glaciologie et Geophysique de l'Environnement, University of Grenoble, France

Keywords: airborne C-ToF AMS measurements, aerosol chemical composition, boundary layer and lower free troposphere

INTRODUCTION

An Aerodyne Time-of-Flight Aerosol Mass Spectrometer (cToF-AMS, Jayne et al., 2000; Drewnick et al., 2005; Canagaratna et al., 2007) was used onboard the French ATR-42 to measure aerosol chemical composition during EUCAARI/IMPACT. For studies described herein an isokinetic and isoaxial (auto-positioned) aerosol inlet has been used. This was developed by Meteo France and described for the first time by Crumeyrolle et al. (2008). A Pressure Controlled Inlet (PCI) was implemented upstream of the aerodynamic lens (Zhang et al., 2002, 2004) similarly to Bahreini et al. (2008) to maintain the pressure at a constant value independent of flight altitudes. The AMS operated in two modes, Mass Spectrometer (MS) and Particle Time-of-flight (PToF) mode, finishing a full MS-PToF measurement cycle every 25 seconds. Aerosol studies with the AMS generally aim at both the aerosol chemical composition and size resolved aerosol information. This study is focusing on the MS measurements. The meteorological situation during the first 12 days over central Europe was dominated by a stable anticyclone affecting a blocking of fresh air mass transport into the ATR-42 operation section. In total 5 flights up to 3.5 km altitude, within the boundary layer and the lower free troposphere, have been performed during the period of predominant anticyclonic situation between May 5 and 11 (1st clear-sky period). Two further flights have been performed on May 28 and 29, after cyclone-driven air mass exchange.

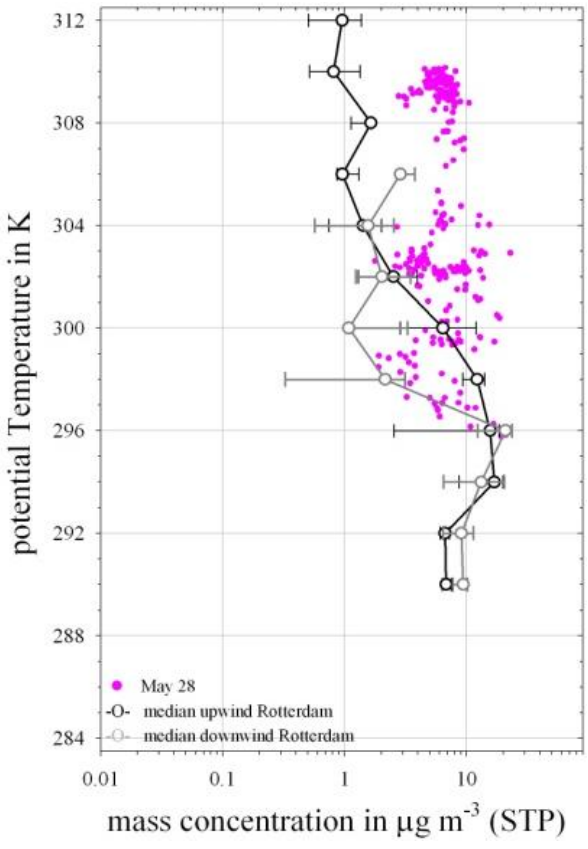

Figure 1: Vertical profile of total mass concentration versus potential temperature. Median profiles (with 25- and 75- percentile) of measurements upwind (black) and downwind (gray) Rotterdam together with one single flight on May 28 (pink).

RESULTS

One flight (May 09) was used for a AMS comparison with an instrument of the same type (operated by the University of Manchester) on board the FAAM BAe-146 during a wing-to-wing manoeuvre for about 35 minutes at altitudes of 1.2 km and 2.7 km (asl). Results generally show good agreement within 20 % between both AMSs, serving as one instrumental proof for the French AMS. Further discussion will be provided.

As the predominant wind direction during the clear-sky period was Easterly the vertical profiles (potential Temperature Θ as ordinate) of the total mass concentration (TMC) (as median with 25- and 75-percentile) from AMS measurements upwind (black – 2 flights) and downwind (gray – 4 flights) of Rotterdam are compared (figure). Within the boundary layer (< 296 K) the total aerosol mass concentration (both Nitrate-rich and Organics-dominated) does not differ significantly and reflect the anthropogenic (industrial) influence. Between 296 K and 302 K the TMCs show differences of up to one order of magnitude. Here, in both cases Sulphate is the dominating aerosol component. Pink dots show the TMC of a single flight (May 28) when the air mass transport, a singular event during the clear-sky period, came from South (within 24 hours from Sardinia, Corsica, North Italy into the air space of measurement). May 28 particularly shows a vertically well mixed distribution above 296 K. Here,

Sulphate is the dominant aerosol component exceeding the Sulphate content of up- and downwind Rotterdam by a factor of five. Further comparisons will be discussed.

ACKNOWLEDGEMENTS

We are thankful to J. Jayne, A. Trimborn from Aerodyne Research for their preparatory work. We thank G. Momboisse and T. Bourrianne from Meteo France, particularly for the necessary "filters". Also A. Bourdon, E. Matthieu, H. Bellec, J. - C. Etienne and M. Cluzeau as well as the rest of Safire and the ATR-42 crew are gratefully acknowledged. This work was supported by the European Integrated project on Aerosol Cloud Climate and Air Quality Interactions (EUCAARI, N° 036833-2) - a project within EU sixth framework program.

REFERENCES

Bahreini, R., E.J. Dunlea, B.M. Matthew, C. Simons, K.S. Docherty, P.F. DeCarlo, J.L. Jimenez, C.A. Brock, and A.M. Middlebrook. Design and Operation of a Pressure Controlled Inlet for Airborne Sampling with an Aerodynamic Aerosol Lens. Aerosol Science and Technology, 42(6)465–471, 2008.

Canagaratna, M.R., J.T. Jayne, J.L. Jimenez, J.D. Allan, M.R. Alfarra, Q. Zhang, T.B. Onasch, F. Drewnick, H. Coe, A. Middlebrook, A. Delia, L.R. Williams, A.M. Trimborn, M.J. Northway, P.F. DeCarlo, C.E. Kolb, P. Davidovits, D.R. Worsnop, Chemical and Microphysical Characterization of Ambient Aerosols with the Aerodyne Aerosol Mass Spectrometer, Mass Spectrometry Reviews, 26, 185– 222, 2007

Crumeyrolle,S., L. Gomes, P. Tulet, A. Matsuki, A. Schwarzenboeck, and K. Crahan; Increase of the aerosol hygroscopicity by cloud processing in a mesoscale convective system: a case study from the AMMA campaign; Atmos. Chem. Phys., 8, 6907-6924, 2008.

Drewnick, F., S.S. Hings, P.F. DeCarlo, J.T. Jayne, M. Gonin, K. Fuhrer, S. Weimer, J.L. Jimenez, K.L. Demerjian, S. Borrmann, D.R. Worsnop. A new Time-of-Flight Aerosol Mass Spectrometer (ToF-AMS) – Instrument Description and First Field Deployment, Aerosol Science and Technology, 39:637–658, 2005

Jayne J. T., D. C. Leard, X. Zhang, P. Davidovits, K. A. Smith, C. E. Kolb, D. R. Worsnop, Development of an Aerosol Mass Spectrometer for Size and Composition Analysis of Submicron Particles, Aerosol Science and Technology, 33:49-70, 2000.

Zhang, X., K.A. Smith, D.R. Worsnop, J.L. Jimenez, J.T. Jayne, and C.E. Kolb, A Numerical Characterization of Particle Beam Collimation by an Aerodynamic Lens-Nozzle System. Part I: An Individual Lens or Nozzle, Aerosol Science and Technology, 36: 617–631 (2002)

Zhang, X., K.A. Smith, D.R. Worsnop, J.L. Jimenez, J.T. Jayne, C.E. Kolb, J. Morris, and P. Davidovits, Numerical Characterization of Particle Beam Collimation: Part II Integrated Aerodynamic Lens-Nozzle System, Aerosol Science and Technology, 38(6): 619-638, 2004

EVAPORATION OF MULTICOMPONENT DROPLETS

A.A. ZARDINI[1], I. RIIPINEN[2], I.K. KOPONEN[3], M. KULMALA[2] and M. BILDE[1]

[1]Department of Chemistry, University of Copenhagen, DK-2100, Denmark

[2]Department of Physics, University of Helsinki, F-00014, Finland

[3]National Research Center for the Working Environment, DK-2100 Copenhagen, Denmark

Keywords: ORGANIC AEROSOLS, EVAPORATION, AEROSOL THERMODYNAMICS

INTRODUCTION

A large fraction of the atmospheric organic aerosol is water soluble and semi volatile, hence taking up water and partitioning between the condensed and the gaseous phases. Atmospheric particles are mixtures of water and organic as well as inorganic molecules and to understand phase equilibrium thermodynamics of organic molecules it is crucial to understand the mutual interactions between inorganics, organics, and water in multicomponent particles.

METHODS

We have used the modified TDMA system described in Bilde et al. (2003), Riipinen et al., 2006 and Koponen et al. (2007) to study the evaporation of multicomponent droplets made of an organic semi volatile compound (succinic acid), a non volatile inorganic salt (sodium chloride or ammonium sulfate) and water. Table 1 gives an overview of our experimental conditions

Table 1. Experimental conditions of the evaporation measurements of sodium chloride (SC), ammonium sulfate (AS), and succinic acid (SA). Forg is the organic to inorganic salt molar fraction.

Mixture	RH%	F_{org}	T (C°)
AS+SA	40- 80	0.5-0.9	21
SC+SA	65- 75	0.33-0.9	21

Two modelling approaches were combined to investigate evaporation of the ternary solution droplets: A phase equilibrium model (The Extended Aerosol Inorganic Model, E-AIM) was used for calculating the initial and final equilibrium composition of the droplets and the gas-to-particle partitioning of succinic acid. The temporal evolution of the droplets size was predicted with a semi-ternary evaporation model, where only water and succinic acid, were allowed to evaporate from the droplets and the salt (NaCl) was considered as an inert compound with respect to evaporation. This model is an extension of binary condensation models (see Vesala et al. (1997) and Riipinen et al. (2006) for details).

CONCLUSIONS

Evaporation of the studied ternary solution droplets could be predicted sufficiently well with the evaporation model using activity coefficients calculated with the equilibrium model, especially for large organic content.
The observed evaporation is systematically slower than the model predictions for low organic molar fraction. This is an indication that the kinetics of evaporation may play an important role for a detailed description of both particles formation and growth processes, and for the organic aerosol burdens in the atmosphere.

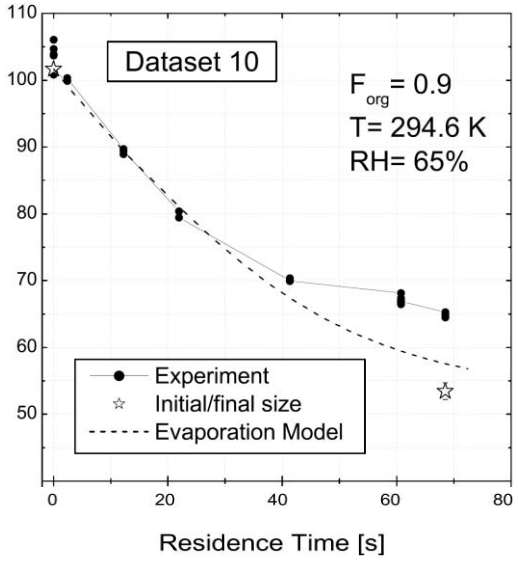

Figure 1. Comparison between experimental and modelled evaporation of aqueous droplets containing sodium chloride and succinic acid.

ACKNOWLEDGEMENTS

This work was supported by: EUCAARI (European Integrated project on Aerosol Cloud Climate and Air Quality interactions) No 036833-2, the Danish Natural Science Research Council, and The Carlsberg Foundation.

REFERENCES

Bilde, M., *et al.* (2003). Even-odd alternation of evaporation rates and vapor pressures of C3-C9 dicarboxylic acid aerosols. *Environ. Sci. Tech.*, 37, 1371-1378.

Clegg, S.L. and J.H. Seinfeld (2006). Thermodynamic Models of Aqueous Solutions Containing Inorganic Electrolytes and Dicarboxylic Acids at 298.15 K. 2. Systems Including Dissociation Equilibria. *J. Phys. Chem. A*, 110, 5718.

E-AIM, Extended AIM Aerosol Thermodynamics Model: A community model for calculating gas/liquid/solid partitioning in aerosol systems containing inorganic and organic components and water, and solute and solvent activities in aqueous solutions and liquid mixtures. Clegg, S. L., Brimblecombe, P., and Wexler, A. S. *URL: http://www.aim.env.uea.ac.uk/aim/aim.php*, last access on September 24, 2009.

Koponen, I.K. *et al.* (2007). Thermodynamic Properties of Malonic, Succinic, and Glutaric Acids: Evaporation Rates and Saturation Vapor Pressures. *Environ. Sci. Tech.*, 41, 3926-3922.

Kulmala, M. and T. Vesala, (1991). Condensation in the continuum regime. *J. Aerosol Sci.*, 22, 3, 337–346.

Riipinen, I., *et al.* (2006). A method for determining thermophysical properties of organic material in aqueous solutions: Succinic acid. *Atmos. Res.*, 82 579–590.

Vesala, T., Kulmala, M., Rudolf, R., Vrtala, A., & Wagner, P. E. (1997). Models for condensational growth and evaporation of binary aerosol particles. *Journal of Aerosol Science*, 28, 565–598.